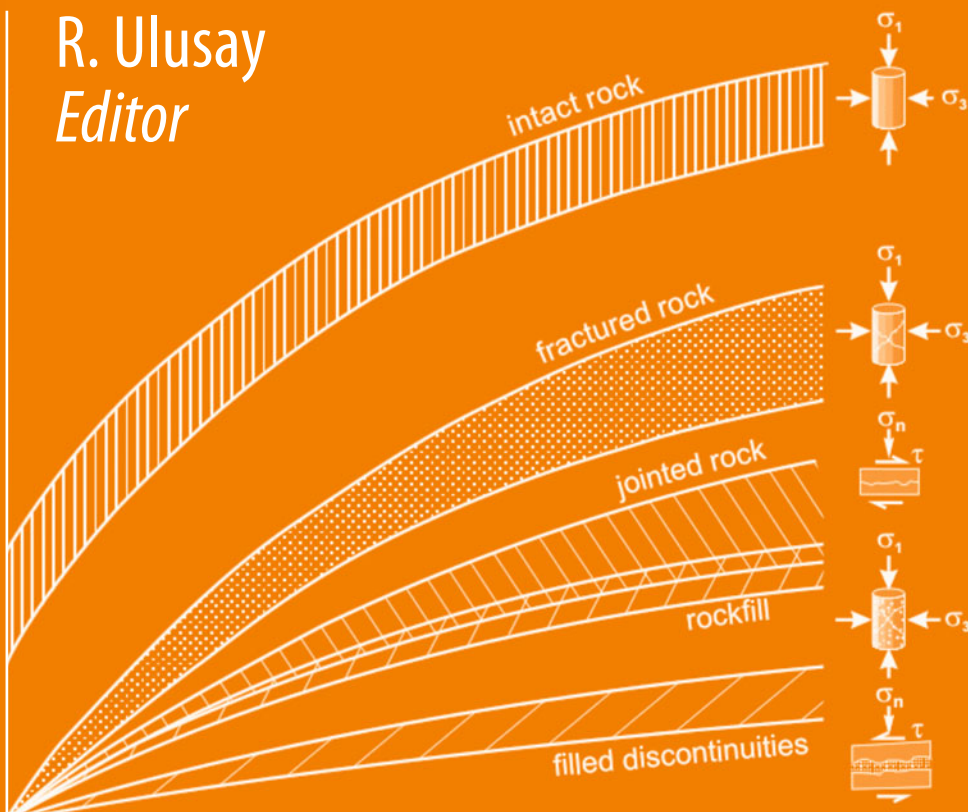


R. Ulusay
Editor



The ISRM Suggested Methods for Rock Characterization, Testing and Monitoring: 2007–2014



ISRM

 Springer

The ISRM Suggested Methods for Rock
Characterization, Testing and Monitoring:
2007–2014

R. Ulusay
Editor

The ISRM Suggested Methods for Rock Characterization, Testing and Monitoring: 2007–2014



ISRM

International Society for Rock Mechanics
Commission on Testing Methods

 Springer

Editor
R. Ulusay
Department of Geological Engineering
Hacettepe University
Ankara
Turkey

ISBN 978-3-319-07712-3 ISBN 978-3-319-07713-0 (eBook)
DOI 10.1007/978-3-319-07713-0
Springer Cham Heidelberg New York Dordrecht London

Library of Congress Control Number: 2014941508

© Springer International Publishing Switzerland 2015

The Suggested Methods have been reprinted from issues of the International Journal of Rock Mechanics and Mining Sciences and Rock Mechanics and Rock Engineering with permission from Elsevier and Springer Verlag, respectively.

This work is subject to copyright. All rights are reserved by the Publisher, whether the whole or part of the material is concerned, specifically the rights of translation, reprinting, reuse of illustrations, recitation, broadcasting, reproduction on microfilms or in any other physical way, and transmission or information storage and retrieval, electronic adaptation, computer software, or by similar or dissimilar methodology now known or hereafter developed. Exempted from this legal reservation are brief excerpts in connection with reviews or scholarly analysis or material supplied specifically for the purpose of being entered and executed on a computer system, for exclusive use by the purchaser of the work. Duplication of this publication or parts thereof is permitted only under the provisions of the Copyright Law of the Publisher's location, in its current version, and permission for use must always be obtained from Springer. Permissions for use may be obtained through RightsLink at the Copyright Clearance Center. Violations are liable to prosecution under the respective Copyright Law.

The use of general descriptive names, registered names, trademarks, service marks, etc. in this publication does not imply, even in the absence of a specific statement, that such names are exempt from the relevant protective laws and regulations and therefore free for general use.

While the advice and information in this book are believed to be true and accurate at the date of publication, neither the authors nor the editors nor the publisher can accept any legal responsibility for any errors or omissions that may be made. The publisher makes no warranty, express or implied, with respect to the material contained herein.

Cover Illustration: The figure on the front cover of this ORANGE BOOK emphasizes the general non-linearity of shear strength envelopes for intact rock, for stress-induced fractures, and for rock joints—the latter showing great similarity to rock fill due to common, highly stressed asperities and contact points. A combination of triaxial and direct shear tests is illustrated as if at the same scale. The reality may be widely different sample sizes. Although non-linear behavior has been a focus of rock mechanics developments for the last half century, it remains convenient to consider an approximately 'linear' behavior when the range of stress is limited. Thus the Coulomb and Mohr-Coulomb criteria continue to be utilized in shear test interpretation, despite the availability of non-linear alternatives. When interpreted in a strictly correct manner, only intact rock displays true cohesive and tensile strength, and could be extrapolated into the tensile sector of this diagram. The critical viewer will note the superposition of several different stress levels, as the five illustrated 'samples' are seldom tested over the same range of stress. Missing from the test samples is their aggregate: the rock mass, which may have at least four of the symbolic samples contributing to its shear strength, each at different magnitudes of strain. (*Figure modified from Barton, 2006. Drawing: R. Abrahão.*)

Printed on acid-free paper

Springer is part of Springer Science+Business Media (www.springer.com)

Foreword

The International Society for Rock Mechanics (ISRM) is continuing to grow year by year. At the time of writing in early 2014, the Society has more than 7,000 individual members from 54 countries, together with close to 150 corporate members. Moreover, there has been a continuously increasing ISRM membership over the last 10 years. Commensurate with these statistics, there has been a corresponding increase in the Society's activities—not least of which has been the work of the Testing Methods Commission which produces the ISRM Suggested Methods. These documents provide guidance to readers on characterisation, testing and monitoring for a wide range of rock mechanics and rock engineering applications.

The ISRM Testing Methods Commission is led by Prof. Resat Ulusay. In order to produce each Suggested Method, a Working Group is established with its own Chairman and Members who have expertise in the particular subject being considered. The draft Suggested Method thus generated is then subjected to rigorous review, a process which includes the ISRM Board members. The Suggested Method is then published as an individual item: in earlier years, this was in the *International Journal of Rock Mechanics and Mining Sciences*; and, more recently, in the *Rock Mechanics and Rock Engineering Journal*.

In order to provide access to all the Suggested Methods in one volume, the ISRM Blue Book was published in 2007 (by the ISRM via the Turkish National Group) and contains the complete set of Suggested Methods from 1974 to 2006 inclusive. Since that time, and as a result of the enthusiasm and dedicated work of Prof. Ulusay and his colleagues, many more Suggested Methods have been generated—leading to this Orange Book, published by Springer Science, which contains the ISRM Suggested Methods generated from 2007 to 2014, as well as some related articles.

It is with great pleasure and with gratitude to the industrious and pertinacious Prof. Ulusay, together with everyone who has been involved in the production of the Suggested Methods, that we introduce this ISRM Orange Book. We know that the contents will be of great assistance to the rock mechanics and rock engineering community. Thus, we hope that this Orange Book volume will be as successful as its Blue Book predecessor.

John A. Hudson, ISRM President, 2007–2011

Xia-Ting Feng, ISRM President, 2011–2015

Preface

One of the main areas of interest for civil, mining and geological engineers is “rock engineering”. After the establishment of the International Society for Rock Mechanics (ISRM) in 1962, led by Prof. Leopold Müller from Salzburg (Austria), important contributions to rock mechanics and rock engineering have been provided by worldwide efforts over the last 52 years. The main products of ISRM’s work have been generated by its internal Commissions as appointed by the ISRM President and the Commission Presidents. These Commissions are designed to develop practical solutions, methods and data for the wide spectrum of rock engineering problems. Starting with the need to develop a common terminology for the properties of rock material and rock masses and the tests by which they are measured, a Commission on Standardisation of Laboratory and Field Tests (now the ISRM Commission on Testing Methods) was established at the time of the first ISRM Congress, held in Lisbon in 1966.

The tests are published as “Suggested Methods” (SMs)—a term which has been carefully chosen: these are not standards *per se*; they are explanations of recommended procedures to follow in the various areas of rock characterisation, testing and monitoring. If practitioners and researchers have not been involved with a particular subject before and it is described in an ISRM SM, they will find the guidance to be most helpful. The SMs can be used as standards on a particular project if required, but they are intended more as guidance. The methods provide a definitive procedure for the identification, measurement and evaluation of one or more qualities, characteristics or properties of rocks or rock masses and they produce test results.

The ISRM SMs, thus produced by the ISRM Commission on Testing Methods, are developed and established within the consensus principles of the ISRM and approved according to a strict set of ISRM procedures and regulations. When a proposal for a method is accepted by the Commission, a draft document is written by a Working Group (WG) and sent to at least three experts for review. Following revision and further comments by the Commission members, the final document is approved by the ISRM Board as an ISRM SM and submitted to a journal for publication without further review. Since 1974, the ISRM Commission on Testing Methods has generated a succession of SMs covering a wide range of subjects. One SM was published in “Rock Mechanics” (at present “Rock Mechanics and Rock Engineering—RMRE”) of Springer Verlag in 1977, while the remaining ones were published in the “International Journal of Rock Mechanics and Mining Sciences—IJRMMS” of Pergamon Press (an imprint of Elsevier) until 2012. In 2012, RMRE started to publish the ISRM SMs.

The first collection of the ISRM SMs was organised by Profs. Richard Bieniawski and John Franklin and issued in 1981 as the ISRM “Yellow Book” which was edited by Prof. Ted Brown and published by Pergamon Press. Professor John A. Hudson was the President of the ISRM Commission on Testing Methods between 1987 and 2006 until he was elected as the ISRM President for the period 2007–2011. During his Commission Presidential tenure, he continued with the production of the SMs and their publication in the IJRMMS, and initiated a system where the documents were produced more in the form of papers—so that the authors

would receive full citation recognition of their efforts. This development was most successful and the number of new ISRM SMs has steadily increased after 1981.

After his election to the Presidency of the ISRM for the period 2007–2011, Prof. Hudson asked Prof. Ulusay if he would take over the Testing Methods Commission, which he did in 2006. With the 1981 Yellow Book becoming out of print, a new collection containing the complete set of ISRM SMs, from 1974 to 2007, became necessary. In 2007, a book, called the ISRM “Blue Book”, which includes the complete set of 40 SMs generated between 1974 and 2006, was edited by Profs. Resat Ulusay and John A. Hudson and published by the ISRM Turkish National Group. This book was well received and many copies have been distributed worldwide.

However, since 2006, and under the overall leadership of Prof. Ulusay, the ISRM Commission on Testing Methods has established 21 new Working Groups (WGs) for developing new and revised/upgraded ISRM SMs. Between 2006 and 2014, 16 WGs have produced a total of 21 new or upgraded ISRM SMs, which have been approved by the ISRM Board as ISRM SMs. It is also possible for new SMs to be developed through cooperation of two ISRM Commissions. An example of this is the new SMs entitled “SMs for Determining the Dynamic Strength Parameters and Mode-I Fracture Toughness of Rock Materials”—which is a product of the ISRM Commission on Rock Dynamics and the ISRM Commission on Testing Methods.

The current book, called the ISRM “Orange Book”, now contains a total of 21 separate new and upgraded ISRM SMs that have been generated between 2009 and 2014, and is being published as a supplementary volume to the 2007 “Blue Book”. The SMs are collated here in four parts, namely: “Laboratory Testing”, “Field Testing”, “Monitoring” and “Failure Criteria”. Tests and measurements carried out in the laboratory and field have been categorised into two separate sub-divisions. Although some index tests, such as the “Schmidt Hammer Test” and “Needle Penetration Test”, can be performed either in the laboratory or in the field using portable laboratory equipment, they are considered in Part I (Laboratory Testing). It should be noted that the 1975 version of the “SM for Laboratory Determination of the Shear Strength of Rock Joints”, and 1978 versions of the SMs concerning “Schmidt Hammer Test” and “Sound Velocity by Ultrasonic Pulse Transmission Technique” were revised in 2013, 2009 and 2013, respectively, so only the updated versions of these SMs have been included in this compilation. In Part II (Field Testing), the tests concerning rock mass displacements, observations on rock fractures and *in situ* properties of rock masses, and establishing a model for the *in situ* stress at a given site (the latter being a supplementary SM for the series of *in situ* stress measurement techniques published in the Blue Book) are included. Part III (Monitoring) includes only a new method for monitoring rock displacements using the Global Positioning System (GPS).

In the application of rock mechanics to rock engineering design, one of the most important issues is the failure of rock: while the failure of rocks is highly desirable during the excavation process, it should of course be avoided or at least controlled in structural rock mechanics applications. For this reason, the failure of rock has been one of the most important research subjects since the formation of the ISRM. However, over the years, it has become difficult to decide which failure criterion can/should be used in specific situations. The ISRM Commission on Testing Methods set out to prepare SMs for Failure Criteria to provide guidance on the nature and characteristics of six existing failure criteria and to suggest circumstances when they could be employed. It is not appropriate for the ISRM to dictate which criteria should be used because rock engineering circumstances can vary: rather, the intention of these SMs is to inform readers about the background, formulation, related experimental data, advantages and limitations, plus recommendations concerning the six criteria. These SMs, which are included in Part IV (Failure Criteria), will assist readers in understanding the nature of each of the failure criteria and hence enable them to make more informed and hence appropriate choices concerning which criterion to utilise in any given circumstance.

The Orange Book also includes two supplementary, but non-SM, documents. One of them is entitled “3D Laser Scanning Techniques for Application to Rock Mechanics and Rock Engineering” by Quanhong Feng and Kennert Röshoff. The 3-D laser techniques have been used in many engineering fields over the last 20 years and show great promise for characterising rock surfaces. The original development of the document commenced in 2007 and was conducted during the 2007–2011 ISRM Presidential period of Prof. Hudson through the Swedish National Group of ISRM. The motivation for the work was to produce a comprehensive report explaining the techniques and advantages of laser scanning for rock mechanics/rock engineering use. Thus, the ISRM Commission on Testing Methods considered that a report concentrating on the description of the laser scanning capabilities, plus the actual and potential rock mechanics applications, would be of great benefit to the ISRM members and the rock engineering community at large and so it is included in the Orange Book as a supplementary document.

The other supplementary document is titled “The Present and Future of Rock Testing: Highlighting the ISRM Suggested Methods”. This document was presented by the Editor of this book at the 7th Asian Rock Mechanics Symposium (ARMS7) in 2012 in Seoul, Korea, as a Keynote Lecture. Following the permission given by the ARMS7 Organising Committee, the tables in the paper are updated to reflect the latest situation of the ISRM Suggested Methods and the slightly revised version of the paper is included in this book. The members of the ISRM Commission on Testing Methods enthusiastically supported the suggestion from one of its members that the Editor’s Keynote paper on the Commission’s work should be included as the first item in the Orange Book in order to provide the historical and current contexts for the production of the Suggested Methods.

New and revised ISRM SMs will continue to be published individually in the journal RMRE as they become available. I believe that feedback and contributions from users are essential for the development of new SMs and updating of the current SMs. Those who can suggest improvements to the published SMs or wish to recommend new techniques or instruments for publication in an SM form are urged to send full details of their proposals to Prof. R. Ulusay, President of the ISRM Commission on Testing Methods, at “resat@hacettepe.edu.tr”.

The publication of this Orange Book could not have been possible without the kind help, efforts, contributions and cooperation of several colleagues. I should like to kindly acknowledge the generous efforts and contributions of all those who have participated and assisted (Chairmen and Members of the Working Groups) in the preparation of the SMs from 2007 to 2014, which numbers many tens of experts. The names of the contributors to each published SM are listed on the title page in each case. Many thanks go to all the contributing experts for their kind reviews and constructive suggestions for the improvement of the SMs before their approval.

I give heartfelt thanks to: the Commission members; Profs. John A. Hudson and Xia-Ting Feng (not only as the Commission members, but also as the past (2007–2011) and present (2011–2015) ISRM Presidents, respectively), Prof. Sergio Fontoura, Dr. Eda de Quadros, Prof. Hasan Gercek, Prof. Ove Stephansson, Prof. Yuzo Obara, Dr. Robert J. Fowell, Dr. Nuno Grossman, Dr. Don Banks (passed away in 2013), Prof. Frederic Pellet, Dr. Chulwhan Park and Dr. Jose Muralha for their enthusiasm, support and kind contributions since 2006. Dr. Luis Lamas (ISRM Secretariat) and all ISRM Board members (2007–2011, 2011–2015) are also kindly acknowledged for their sincere support and constructive comments on the SMs during the approval stages.

In addition, I greatly appreciate Dr. Nick Barton’s kindness for permission to use his original figure on the cover page of the book and his brief explanation of the figure and for his colleague Ricardo Abrahao from Brazil for his fine drawing of the figure. I am also extremely grateful to Prof. Giovanni Barla, the Editor of RMRE journal, for his enthusiasm, kind cooperation and efforts to ensure rapid publication of the ISRM SMs in the journal since 2012, together with his help in the publication of this Orange Book through Springer Verlag.

Drs. Quanhong Feng and Kennert Röshoff are acknowledged for their kind preparation of their detailed report on laser scanning which is included in the book.

Elsevier is kindly acknowledged for allowing the ISRM to reproduce the two SMs in this printed form and I am sure that its generosity will be appreciated not only by the ISRM members but also by the whole rock mechanics and rock engineering community at large.

March 2014

R. Ulusay

Contents

The Present and Future of Rock Testing: Highlighting the ISRM Suggested Methods	1
Resat Ulusay	
Part I Laboratory Testing	
ISRM Suggested Method for Determination of the Schmidt Hammer Rebound Hardness: Revised Version	25
Adnan Aydin	
Suggested Methods for Determining the Dynamic Strength Parameters and Mode-I Fracture Toughness of Rock Materials	35
Y. X. Zhou, K. Xia, X. B. Li, H. B. Li, G. W. Ma, J. Zhao, Z. L. Zhou and F. Dai	
ISRM Suggested Method for the Determination of Mode II Fracture Toughness.	45
Tobias Backers and Ove Stephansson	
ISRM Suggested Method for Reporting Rock Laboratory Test Data in Electronic Format.	57
Hong Zheng, Xia-Ting Feng, Zuyu Chen, J. A. Hudson and Yujie Wang	
Upgraded ISRM Suggested Method for Determining Sound Velocity by Ultrasonic Pulse Transmission Technique	95
Adnan Aydin	
ISRM Suggested Method for Determining the Abrasivity of Rock by the CERCHAR Abrasivity Test.	101
Michael Alber, Olgay Yaralı, Filip Dahl, Amund Bruland, Heiko Käsling, Theodore N. Michalakopoulos, Marilena Cardu, Paul Hagan, Hamit Aydın and Ahmet Özarslan	
ISRM-Suggested Method for Determining the Mode I Static Fracture Toughness Using Semi-Circular Bend Specimen	107
M. D. Kuruppu, Y. Obara, M. R. Ayatollahi, K. P. Chong and T. Funatsu	
ISRM Suggested Methods for Determining the Creep Characteristics of Rock	115
Ömer Aydan, Takashi Ito, Ugur Özbay, M. Kwasniewski, K. Shariar, T. Okuno, A. Özgenoğlu, D. F. Malan and T. Okada	

ISRM Suggested Method for Laboratory Determination of the Shear Strength of Rock Joints: Revised Version	131
José Muralha, Giovanni Grasselli, Bryan Tatone, Manfred Blümel, Panayiotis Chryssanthakis and Jiang Yujing	
ISRM Suggested Method for the Needle Penetration Test	143
Resat Ulusay, Ömer Aydan, Zeynal A. Erguler, Dominique J. M. Ngan-Tillard, Takafumi Seiki, Wim Verwaal, Yasuhito Sasaki and Akira Sato	
Part II Field Testing	
ISRM Suggested Method for Rock Fractures Observations Using a Borehole Digital Optical Televiewer	159
S. J. Li, Xia-Ting Feng, C. Y. Wang and J. A. Hudson	
ISRM Suggested Method for Measuring Rock Mass Displacement Using a Sliding Micrometer	169
S. J. Li, Xia-Ting Feng and J. A. Hudson	
ISRM Suggested Method for Step-Rate Injection Method for Fracture In-Situ Properties (SIMFIP): Using a 3-Components Borehole Deformation Sensor	179
Yves Guglielmi, Frederic Cappa, Hervé Lançon, Jean Bernard Janowczyk, Jonny Rutqvist, C. F. Tsang and J. S. Y. Wang	
ISRM Suggested Methods for Rock Stress Estimation—Part 5: Establishing a Model for the In Situ Stress at a Given Site	187
Ove Stephansson and Arno Zang	
Part III Monitoring	
ISRM Suggested Method for Monitoring Rock Displacements Using the Global Positioning System (GPS)	205
Norikazu Shimizu, Shinichiro Nakashima and Tomohiro Masunari	
Part IV Failure Criteria	
Suggested Methods for Rock Failure Criteria: General Introduction	223
R. Ulusay and J. A. Hudson	
Introduction to Suggested Methods for Failure Criteria	225
Bezalel Haimson and Antonio Bobet	
Mohr–Coulomb Failure Criterion	227
Joseph F. Labuz and Arno Zang	
The Hoek–Brown Failure Criterion	233
Erik Eberhardt	

Three-Dimensional Failure Criteria Based on the Hoek–Brown Criterion	241
Stephen Priest	
Drucker–Prager Criterion	247
Leandro R. Alejano and Antonio Bobet	
Lade and Modified Lade 3D Rock Strength Criteria.	253
Sergio A. B. da Fontoura	
A Failure Criterion for Rocks Based on True Triaxial Testing	259
Chandong Chang and Bezalel Haimson	
Part V Additional Article on Rock Characterization	
A Survey of 3D Laser Scanning Techniques for Application to Rock Mechanics and Rock Engineering	265
Quanhong Feng and Kennert Röshoff	

The Present and Future of Rock Testing: Highlighting the ISRM Suggested Methods

Resat Ulusay

1 Introduction

The term “Rock Mechanics” refers to the basic science of mechanics applied to rocks, whilst the term “Rock Engineering” refers to any engineering activity involving rocks (Hudson and Harrison 2000). The application of mechanics on a large scale to a pre-stressed, naturally occurring material is the main factor distinguishing rock mechanics from other engineering disciplines. Although, as early as 1773, Coulomb included results of tests on rocks collected from France in his paper (Coulomb 1776; Heyman 1972), the subject of rock mechanics started in the 1950s from a rock physics base and gradually became a discipline in its own right during the 1960s. Rock mechanics was born as a new discipline in 1962 in Salzburg, Austria, mainly by the efforts of Professor Leopold Müller and he officially endorsed at the first congress of the International Society for Rock Mechanics (ISRM) in 1966.

Since the formation of the ISRM, there have been many developments and technological advances in both rock mechanics and rock engineering. Nevertheless, the subject remains essentially concerned with rock modelling behaviour, whether as a research subject or to support the design of structures to be built on or in rock masses. The models developed depend critically on the input parameters, such as boundary conditions (i.e. in situ stresses), rock material and rock mass properties. As seen from Fig. 1, site

investigations and laboratory and field tests provide important inputs for rock modelling and rock engineering design approaches. Therefore, determination of rock properties both in the laboratory and for in situ and monitoring of rock behaviour and rock structures, provides some of the main important areas of interest in rock mechanics and rock engineering, which are commonly applied to engineering for civil, mining and petroleum purposes.

The knowledge of a material’s ability to safely sustain a load (or indeed a displacement) before breaking has been of paramount importance to man ever since structures were first built. It is difficult to conceive that the qualitative ranking of softwoods, hardwoods and stone were unknown in the Neolithic time, and the earlier civilizations such as Turanian, Indian, Chinese, Greek, Egyptian and Roman civilizations clearly had an understanding of material strength perhaps purely based on experiences initially.

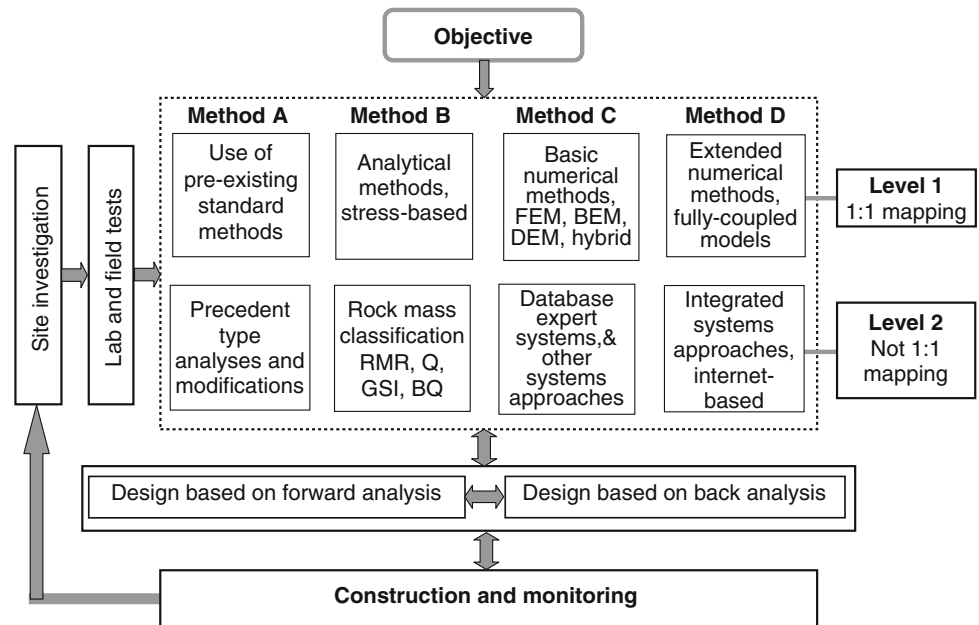
Mechanical testing of materials has been carried out since about 1500 and testing machines have been in existence since the early 18th century (Timeshenko 1953; Gray 1988). In the 1920s, Josef Stini was probably the first to emphasise the importance of structural discontinuities as related to the engineering behaviour of rock masses. Other notable scientists and engineers from a variety of disciplines, such as von Karman (1911), King (1912), Griggs (1936), Ide (1936), and Terzaghi (1946) worked on the failure of rock materials. In 1921, Griffith proposed his theory of brittle material failure and in 1931 Bucky started using a centrifuge to study the failure of mine models under simulated gravity loading. However, after the formal development of rock mechanics as an engineering discipline in the early 1960s, better understanding of the importance of rock mechanics in engineering practice, increasing demands from rock engineering studies and rapid advances in technology resulted in development of a number of laboratory rock testing methods.

In addition, recognition of the fact that test results from a small specimen of rock cannot be directly applied to solve all rock engineering problems (unlike the case of soils,

This supplementary document was presented by the Editor of this book in ARMS7 Symposium held in Seoul, Korea, in 2012, as keynote lecture. Based on the permission by the ARMS7 Organizing Committee, the tables in the paper are updated to reflect the latest situation of the ISRM Suggested Methods and its slightly revised version is included in this book.

R. Ulusay (✉)
Department of Geological Engineering, Hacettepe University,
06800, Beytepe, Ankara, Turkey
e-mail: resat@hacettepe.edu.tr

Fig. 1 Flowchart of rock mechanics modelling and rock engineering design approaches (Feng and Hudson 2011)



excepting rockfills), focused attentions on the development of in situ tests and monitoring techniques in rock mechanics. During this period, the efforts by the Commissions established by the ISRM also contributed to the development of experimental methods in rock mechanics and rock engineering by motivating the researchers. Accordingly, since 1974, the ISRM Commission on Testing Methods has spent considerable effort in developing a succession of ISRM Suggested Methods (SMs) for different aspects of rock mechanics through the contribution of a number of Working Groups.

In the first part of this paper, a brief history of both laboratory and in situ rock testing and monitoring techniques, and the main near-future trends associated with experimental methods in rock mechanics are introduced. The emphasis in the second part of the paper is on providing brief information about the tasks of the ISRM Commission on Testing Methods, general principles followed in developing the ISRM SMs, the stages followed in their evaluation and recent progresses related to the ISRM SMs. Because of limitations of space, the references given for the advances listed in the following part of the paper are intended to provide examples of the significant contributions made to the various topics or techniques being discussed and are not intended to be either fully exhaustive or definitive.

2 Historical Background: From the Past to the Present

Interest in materials had began and mechanical testing procedures possibly have been developed thousands of years ago during one of the eras when large-scale wood and

stone structures were being built. Mankind has been utilizing rocks in different forms since early times. The earlier uses involve the natural caves and cliffs for accommodation and protecting people against their enemies. They also utilized rocks as excavation tools and creating flames through friction of rock. Although some of them were initially accidental findings, they later improved their knowledge and know what type of rocks can be used. The positive science, which constitutes the basics of rock mechanics and rock engineering of the modern time, is said to have been started following the Renaissance period. However, it is quite arguable who were the pioneers of mechanical laws governing solids and fluids and their testing and monitoring techniques in view of huge engineered structures related to rock built in the lands of Turan, China, India, Middle East (Sumerians, Iranian, Akadian, Urartu etc.), Egypt, Central America, Peru as well as Roman and old Greek lands and some of which were built more than thousands years ago with a high precision of modern days. There are many historical remains related to rocks from various civilizations all over the world such as Sumerians (originally from Central Asia), Turanian, Anatolian, Egyptian, Indian, Chinese, Peruvian, Maya, Aztecs, Iranian, Roman and Greek. Mankind built underground structures in past, and some examples can be still found in the Cappadocia region of Turkey (2000 BC–500 AD) as underground or semi-underground cities, and tombs of pharaohs in Thebes of Egypt (3000–2300 BC), Ajanta and Ellora caves (started to be built in 200 BC) in India and Kızıl Cave and Bezelik excavated in reddish sandstone during 420–589 AD in East Turkistan (Uyгурistan), Kandovan underground caves in Azerbaijan. Karez in Turkistan, Qanats in Iran are the well-known irrigation tunnels built in many arid regions of the



Fig. 2 Examples of man-made historical underground structures: **a** Çat (Cappadocia, Turkey), **b** Bezelik (East Turkistan), **c** Tebes (Egypt), **d** Ajanta Caves (India) (after Aydan 2012a)

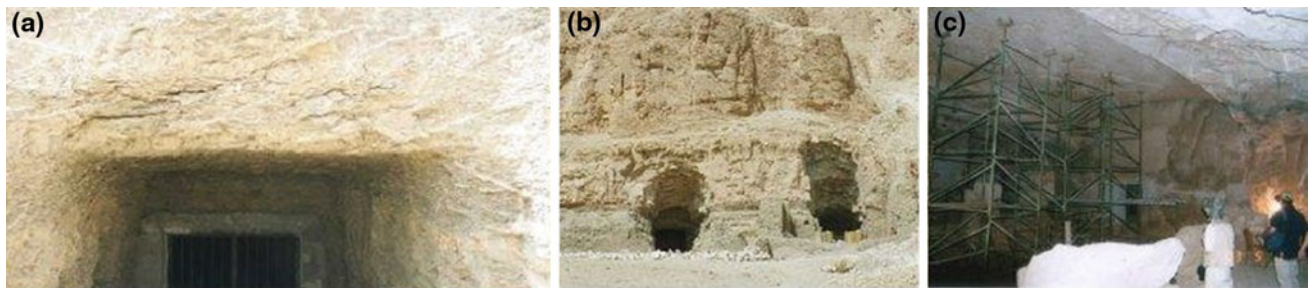


Fig. 3 Progress of opening excavation techniques in old Egypt: **a** shale, **b** roof limestone and sidewall shale, **c** limestone (after Aydan and Genis 2004; Hamada et al. 2004)

world (Fig. 2). Karez network started to be built in 206 BC is about 5,000 km long with 1,100 wells in Turfan in East Turkistan. The excavations were even carried in very hard rocks such as basalts. The underground excavations in the Capadocia region are very extensive and reaching to a depth of 80 m below the ground surface with amazing natural ventilation systems (Aydan and Ulusay 2003).

One can easily notice the progress of understanding short- and long-term characteristics of rocks in the King, Queen and West valleys by the builders of underground Pharaoh tombs in Luxor area in Egypt (Aydan and Genis 2004). They first selected soft shale formation for siting the underground tombs at earlier stages in view of available excavation tools at that time. Since shale easily deteriorates, the tombs should had been suffering from some stability problems in the roof as seen in Fig. 3a. For this reason, they probably had chosen later the limestone as the roof layer while sidewalls and floor was within the shale layer

(Fig. 3b). However, the limestone layer just above the shale formation (transition zone) is highly jointed, they should had again experienced the roof stability problems for large span excavations as seen in Fig. 3c. The advance in excavation techniques and tools and better knowledge of rock characteristics with time should had lead the tomb builders to choose the soft-limestone layer for siting the underground tombs. In some underground tombs, the builders seem that they had designed and built the tombs by following the geometry of the soft limestone layer. The orientation of chambers and their dimensions, the number of pillars and their sizes should had been done according to some computations as no randomness is observed in the in situ investigations at all (Aydan and Genis 2004; Hamada et al. 2004). Some underground mining activities existed in Anatolia as early as 3000 BC. The Göltepe tin underground mines near Toros (Taurus) mountains are found to be at least 5000 years old (Kaptan 1992).

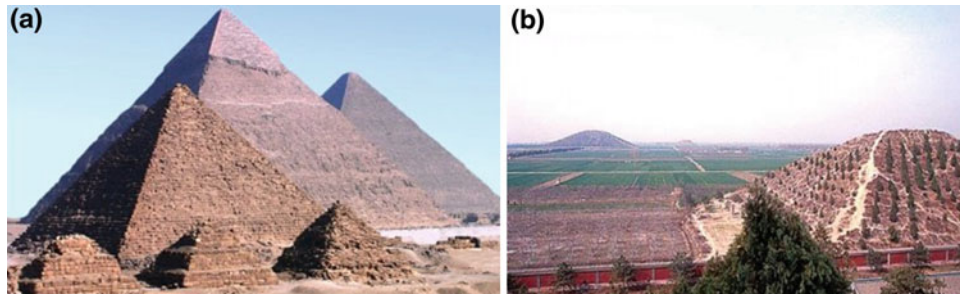


Fig. 4 a Pyramids in Giza (Egypt), b Turkish pyramids near Xianyang, China (<http://www.panoramio.com/photo/>)



Fig. 5 Underground quarries in a Egypt (Qurna) and Anatolia (b. Bazda and, c. Kusini) (Kulaksiz and Aydan 2010; Aydan and Kumsar 2005)

Pyramids made of huge rock blocks to achieve both structural stability under both static and dynamic loading conditions for thousands years and those in Egypt are well known worldwide (Fig. 4a). However, some pyramids have been recently unearthed in Peru, Mexico, Bosnia and present China. The pyramids near Xianyang (Fig. 4b) in present China were constructed by Proto-Turks (Proto-Uygurs) about 3000 BC, which makes them oldest pyramids of the world and it confirms the hypothesis that pyramids in Egypt built by people who migrated from Central Asia due to climate change and dried inland seas such as Taklamakan and Gobi Deserts. Besides the good mechanical interlocking of rock blocks, there are caverns within these pyramids. The roof of these caverns consists of beams of hard rock (mainly granite) with blocks in sidewalls put together to form to create inverted V-shape or trapez shape arches (like Sumerian arches). Of course, the beams were dimensioned in a way that they can resist tensile stresses induced by bending due to surcharge loads for thousands years.

As seen in Fig. 5, one can find also some ancient underground quarries in Anatolia and Thebes (Kulaksiz and Aydan 2010, Aydan and Kumsar 2005). Amenophis III Quarry at Qurna of Thebes region of Egypt, limestone mining started probably 3350–3500 years ago. Bazda Quarry at Harran, Urfa region of Turkey probably was opened 4000 years ago by Sumerians (Kulaksiz and Aydan 2010). At Qurna, there are lines and inscriptions, which explain daily progress records and indicator of calculating

the payments of excavations workers. The observations are compared with theoretical estimation according to the stability evaluation methods based on bending and arching action of beam with the consideration of rock mass strength evaluations and the results for Qurna and Bazda are consistent with the bending and arching action evaluations of beams.

Aphrodisias is one of the antique cities built by using the marble blocks excavated from the marble quarries nearby. The first school for sculptures and artifacts of marble in history was established in Aphrodisias in Karia, which is one of great Anatolian civilizations (Erim 1986). Quarries are usually bounded by fracture zones such as normal faults (Kumsar et al. 2003). It seems that the quarrymen of Aphrodisias had a good and advanced knowledge of how to utilize the structural discontinuities to their advantage for excavation and extraction of marble blocks as well as to initiate the quarrying operations (Fig. 6). Bedding or schistosity planes are used as the bottom surface of blocks since they can be easily separated from the layer below. This further implies that the quarrymen did also have the knowledge of anisotropy of tensile strength of rocks. It is also interesting to note that Sumerians found that they can increase the strength of clay bricks by straw fibers and firing them and can create open spaces by utilizing inverted V or U shape arches.

These achievements can not be simply intuitive and an experience only and there is no doubt that there are some mechanics and mathematics behind in their achievements,

Fig. 6 Rock column or block extraction techniques in Egypt and Anatolia: **a** slots around the unfinished obelisk in Aswan (Egypt) (Hamada et al. 2004), **b** slots around a marble block in Aphrodisias (Turkey) (Kumsar et al. 2003)



which need further through investigations to understand our ancestors achievements in rock mechanics and rock engineering. All these earlier civilizations have precise unit systems for measuring physical quantities, angles and time, which are the most fundamental elements of testing and monitoring in the past and modern days.

In the general context of material science, the earliest recorded evidence of a written standard, or specification, dates back to the 4th Century BC. However, it should be noted dates may be much earlier in view of achievements of Sumerians. The “Stele of Eleusis” (Fig. 7) is a stone tablet inscribed with the specification of the composition of bronze spigots used for keying together the stone blocks for constructing columns in Greek buildings. This stele is important since it clearly implies that (a) the Greeks at that time understood the importance of the relation between the composition of the alloy and its mechanical properties and (b) it is the first reference to the use of turning of a metallic component on a lathe to achieve the desired dimensions (Varoufakis 1940; after Loveday et al. 2004). When the pyramids and temples were constructed, the strength of stone had probably been considered by the Egyptians and Greeks and other civilizations, but no records have been found so far in western sources. Da Vinci (ca. 1500) tested the tensile strength of wire and his note “Testing the Strength of Iron Wires of Various Lengths” is the first recorded mechanical testing. He also studied the strength of columns and the influence of the width and length on the strength of beam.

During the 16th and 17th centuries some experiments on mechanical properties of materials were carried out with simple testing apparatus. Galileo (1638) presented the first serious mathematical treatment of the elastic strength of a material in a structure subjected to bending (Loveday et al. 2004). This is illustrated in the well known drawing that appeared in his ‘Discorsi e Dimostrazioni Matematiche’ published in Leiden (Fig. 8), as discussed by Todhunter and Pearson (1886). Mariotte (1740) extended Galileo’s work



Fig. 7 4th Century BC Stele of Eleusis (ISO Bulletin 1987)

and investigated the tensile strength of wood, paper and metal, and of beams with built-in and simply supported ends. During this period, the concept that a simple relation exists between the applied load and elastic (recoverable) deformation of a material was published in 1678 by Hooke. Young (1773-1829) is associated with the measurement of the modulus of elasticity of materials although most modern day research workers would not recognise the description that he used to express the relation between stress and

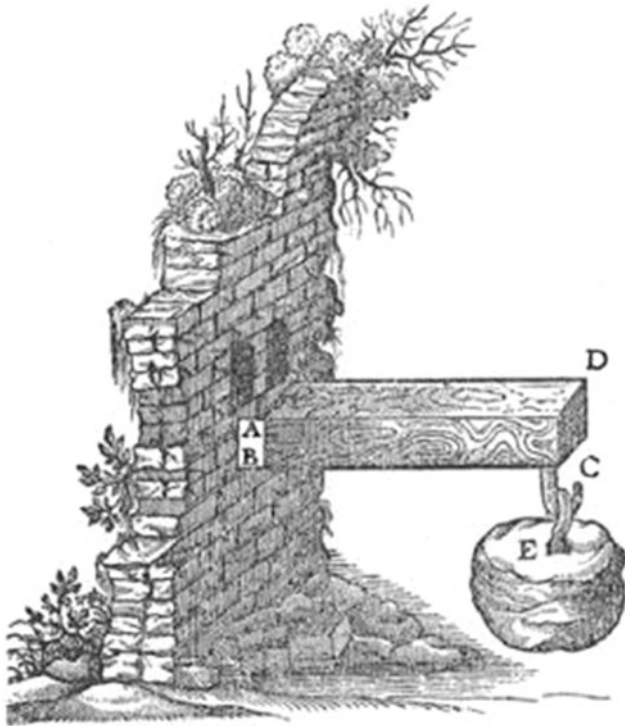


Fig. 8 Galileo's bending test (Galileo 1638)

strain: "A modulus of the elasticity of any substance is a column of the same substance capable of producing a pressure on its base which is the weight causing a certain degree of compression as the length of the substance is to the diminution of its length." (Loveday et al. 2004). One of the earliest machines used for the systematic measurement of tensile strength was developed by a Dutch physicist von Musschenbroek (1729) at the University of Leiden. In this machine, specimens were held at each end by special gripping devices and load was applied by a system of hooks (Fig. 9). The basic concept of a 'steel-yard' used to apply a load to the sample has subsequently been used in the design of many tensile testing machines.

The first rock mechanics experimental studies were performed by Gauthey, who built a testing machine using the lever system and measured the compressive strength of cubic specimens, in about 1770 for the design of the pillars for the Sainte Genevieve Church in Paris. Gauthey noted that the compressive strength of longer specimens was lower than the cube strength (Hudson et al. 1972). The systematic assessment of the strength of materials at high temperatures using the machine shown in Fig. 10 was an important contribution by Fairbairn (1856). Loads up to 446 kN could be applied to the test pieces by the lever system of this machine (Loveday 1982). David Kirkaldy also made an important contribution to the determination of the strength of materials by designing and building a large horizontal hydraulic testing machine in order to undertake testing to

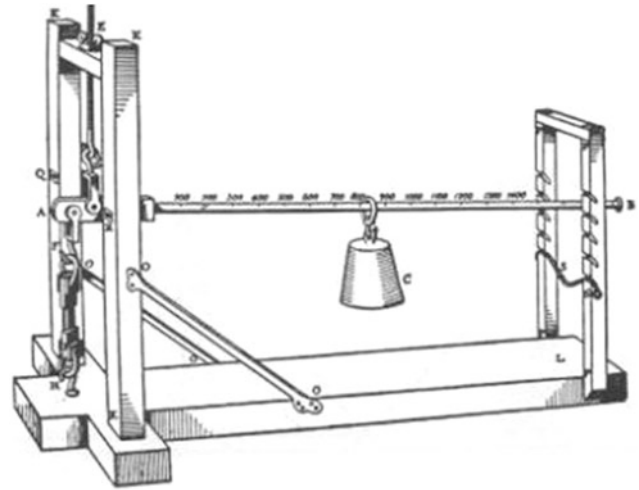


Fig. 9 Petrus van Musschenbroek lever testing machine (after Loveday et al. 2004)

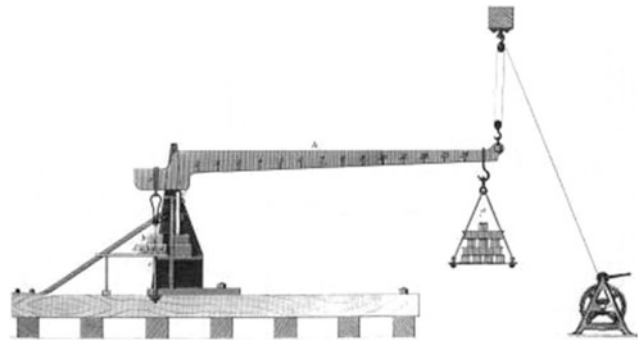


Fig. 10 Fairbairn's tensile testing machine used for temperature tensile testing (after Loveday et al. 2004)

uniform standards (Smith 1982). This machine was used in the first commercial testing laboratory of Kirkcaldy in London and it was capable of testing compression specimens up to 21.5 ft long and 32 in. square and tension specimens up to about 25 ft long (Fig. 11). The real motivation to design and build testing machines was provided in the latter part of the 18th century and early 19th century when stone and cast iron bridges were being built and chain cables were developed for ships (Gibbons 1935). A typical testing machine of the 1880s is shown in Fig. 12.

During the early part of the 20th century, interesting works on the failure of rock materials was conducted by von Karman (1911) and King (1912) in Europe and Griggs (1936) and Handin (1953) in the US, respectively, playing pioneering roles in the development of high pressure loading testing machines. In experimental rock mechanics, important developments were performed between 1945 and 1960, based on laboratory large-scaled experimental works by Mogi (1959), the studies on friction of discontinuities by

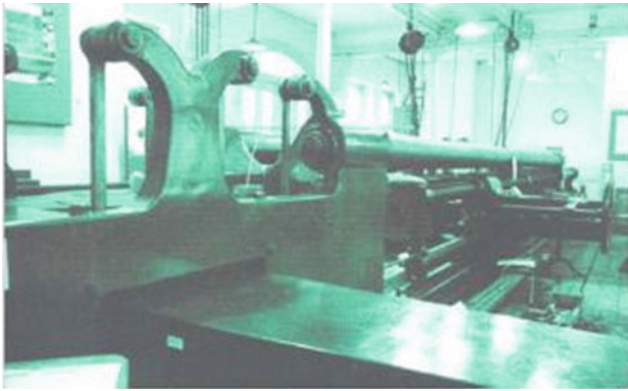


Fig. 11 Kirkcaldy's 300 ton horizontal high hydraulic testing machine in Southwark, London (after Loveday et al. 2004)

Jaeger (1959, 1960) and large-scale triaxial tests performed by Blanks and McHenry (1945), and Golder and Akroyd (1954). In addition, studies by Rocha et al. (1955) and John (1962) motivated a more common use of large scale field shear testing of rock discontinuities in many parts of the world. In the absence of modern fracture mechanics theory and scaling laws, Prof. Fernando L.L.B. Carneiro from Brasil, had tried to establish a correlation between compressive strength and flexural tensile strength. A challenging engineering problem inspired Carneiro to develop a new test method that is known as the Brazilian test (Fairbairn and Ulm 2002). The method was presented in September 1943, at the 5th meeting of the Brazilian Association for Technical Rules (Carneiro 1943) (Fig. 13).

Another important advance in rock testing was the development of stiff and servo-controlled testing machines (Fig. 14a). Until 1966, load-displacement measuring was terminated just after the peak strength had been reached, because the rock specimens failed explosively. This explosive failure was thought to be an inherent characteristic of the rock. In 1966, it was recognised that the stiffness of the testing machine (relative to the slope of the post-peak load-displacement curve) determined whether failure of the specimen is stable or unstable. As shown in Fig. 14b, a soft machine causes sudden failure by the violent release of stored strain energy, i.e. by the testing system itself. In their state of the art review, Hudson et al. (1972) indicated that the advantage of developing stiff testing machines was first suggested by Spaeth (1935). Then laboratory tests on machine stiffness and rock failure and the development of such machines were continued by several investigators (i.e. Cook 1965; Bieniawski 1966; Waversik and Fairhurst 1970; Hudson et al. 1971; Martin 1997).

After the establishment of the ISRM Commission on Testing Methods in 1966, a number of laboratory and field testing methods and monitoring techniques to be used in rock engineering were developed and/or improved with the

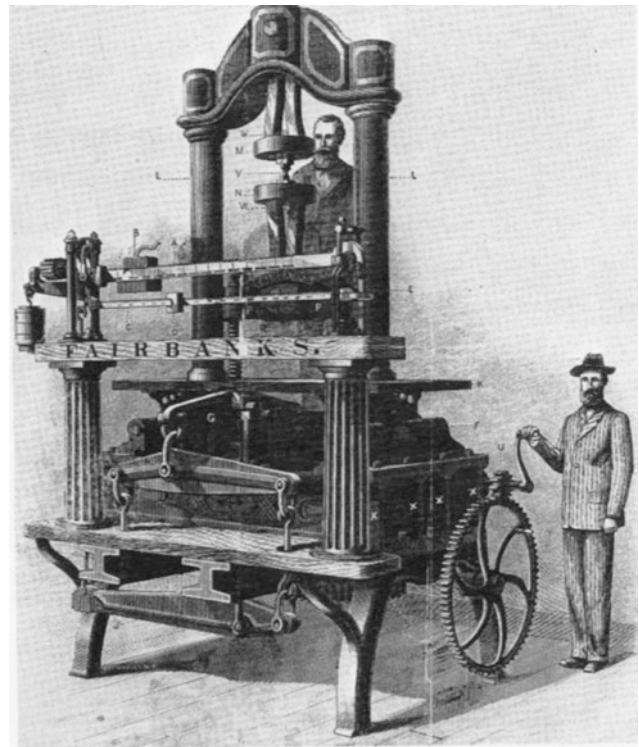


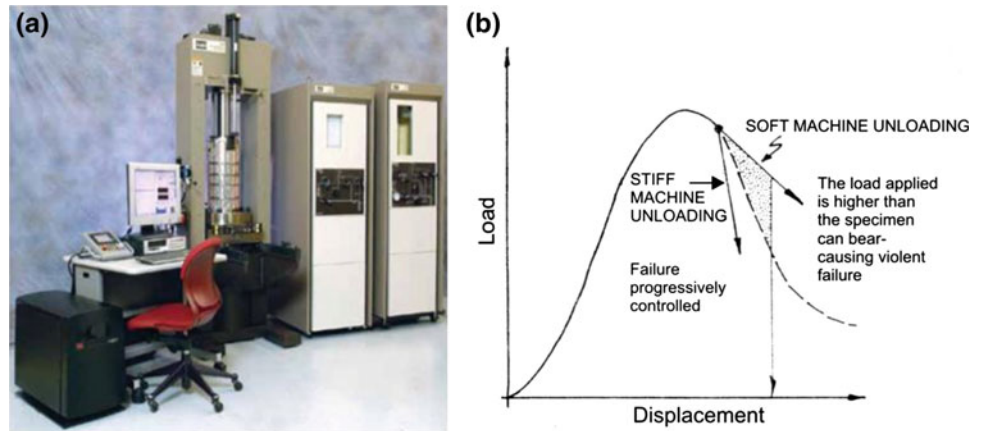
Fig. 12 Testing machine of the 1880s (after Abbott 1884)



Fig. 13 Prof. Carneiro at the laboratory preparing a sample for the Brazilian test (after Fairbairn and Ulm 2002)

efforts of the Commission, its Working Groups and cooperations between other ISRM Commissions (ISRM 1981, 2007), based on the previous experiences and new developments in technology. These methods are given in Sect. 4.5. In this period, in addition to stiff testing machines, the use of computerised methods of test control and automatic test data collection and analysis also became popular and some experimental contributions were made on the determination of shear strength and deformability characteristics, including creep behaviour of discontinuities and

Fig. 14 a A stiff and servo-controlled testing system (MTS 2012) b comparison of load-displacement curves obtained from stiff and soft machines (arranged from Hudson 1989)



shear zones under desired effective in situ states of stress (Barla et al. 2007).

In the past, particularly depending on the researches on solid materials performed by Inglis (1913) and Griffith (1921), the principles of fracture mechanics have been applied successfully for predicting initiation and propagation of fractures and to design engineering structures in metal and metallic materials. Then the principles of rock fracture mechanics have been adopted from fracture mechanics developed for man-made materials. Rock fracture mechanics dates back to the mid 1960 and its application to rock burst problems and collapses in deep gold mines of South Africa (Bieniawski 1967). Fracture mechanics of rocks have been presented in three text books by Paterson (1978), Atkinson (1987) and Whittaker et al. (1992). It is applied to (i) hydraulic fracture propagation, (ii) rock fragmentation by cutting action and due to blasting, (iii) analysis of rock burst, and (iv) rock slope engineering problems. Mode I (extension and opening) and Mode II (shear and sliding) fracturing are most important in rock mechanics and rock engineering (Stephansson 2001). Mode I fracture mechanics is more frequently studied and the related fracture properties have been standardized, such as the ISRM SM for Determining the Fracture Toughness of Rock (ISRM, 2007). More recently, the experimental procedure for Mode II was also developed and accepted as an ISRM SM (Backers and Stephansson 2012).

Determination of the thermal properties of rock including thermal conductivity, heat capacity, thermal diffusivity etc. has become increasingly important with the widespread interest in building of underground structures such as tunnels, metro stations, repositories for spent nuclear fuel, storage of natural gas and underground energy storage. Furthermore, worldwide investigations related to using geothermal energy require knowledge about the thermal behavior of rock/fluid/stress system.

In addition to laboratory methods for rock mechanics, particularly after the establishment of the ISRM, in situ tests and monitoring of rock structures were considered to also

have vital importance in rock engineering applications and they gained an increasing popularity both in research and practice. From the second half of the 20th century to the present, important contributions were made to the development and improvement of the field methods. One of the groups considered in field tests includes the tests used for determining in situ deformability of rock masses, such as plate loading, flat jack and dilatometer tests which have been included in the ISRM SMs (ISRM 1981, 2007).

The other group of field methods commonly applied in rock engineering practice is geophysical techniques. The main emphasis of geophysical surveys in the formative years was for petroleum and mineral exploration. From these surveys, technology continually developed and is developing that allows geophysical techniques to play an important role in modern science. From the 1950s until the present time geophysical methods have enjoyed an increasing role in geotechnical projects, and now are used in an almost routine manner to provide information on site parameters, such as in situ dynamic properties, cathodic protection design values, depth to and condition of rock that in some instances are not obtainable by other methods. Since 1981 a number of geophysical methods were accepted as ISRM SMs (ISRM 1981, 2007) and now are being commonly used in practice. In the last two decades, seismic imaging has an increasing popularity particularly as it relates to rock-burst investigations (Young 1993).

Knowledge of the virgin stress field is very important in many problems dealing with rocks in civil, mining and petroleum engineering as well as in geology, geophysics and seismology. The need for understanding of in situ stresses in rocks has been recognised by engineers and geologists for a long time, and many methods to measure these stresses have been proposed since the early 1930s. One of the earliest measurements of in situ stresses using surface relief methods was reported by Lieurance (1933, 1939) from the US Bureau of Reclamation in Denver. These methods consisted of disturbing the stress equilibrium with some mechanical device and measuring the resulting



Fig. 15 In situ stress measurement using flat-jack in the 1970s in France (after Hoek 1974)

deformations. Professor Pierre Habib, who was the 4th President of ISRM, was involved in the development and application of the flat jack method (Fig. 15) as early as 1950 (Habib 1950; Mayer et al. 1951; Habib and Marchand 1952), and this method was also used to measure the in situ moduli of rock masses (Habib 1950), as were dynamic methods (Brown and Robertshaw 1953; Evison 1953). After the 1960s a wide range of methods of rock stress measurement had been investigated and developed, and they are reviewed in the books written by Amadei and Stephansson (1997) and most recently by Zang and Stephansson (2010). The stress relief technique, which is also known as the overcoring technique, is based on the assumption that rock behaves elastically. Due to technical and practical difficulties, hydraulic fracturing methods, which can be used at considerable depths, were developed. As observed in the field, the boreholes drilled for in situ stress measurements sometimes starts to fail as the depth increases. For such situations, the borehole breakout method can be useful supplement.

These methods, such as hydraulic fracturing, the CCBO technique, overcoring methods, the flat jack method and other issues considered in situ stress measurements were also accepted as ISRM SMs and published by the ISRM (ISRM 2007; Sugawara and Obara 1999; Hudson et al. 2003; Sjöberg et al. 2003; Haimson and Cornet 2003; Christiansson and Hudson 2003; and most recently Stephansson and Zang 2012). In addition, some in situ stress inference methods using laboratory experiments have also been developed. The

acoustic emission (AE) method is one of the well-known methods of this kind. Although some supplementary studies to compare stresses inferred from the AE method applied to oriented samples under uniaxial loading and those of well known in situ stress determination methods (Tuncay and Ulusay 2008) are necessary, it may be a practical tool for engineers in years to come (Tuncay et al. 2002; Lehtonen et al. 2012).

Monitoring of rock deformations, stresses in rock and blast vibrations is important for assessing the stability of rock structures, such as slopes, tunnels, dams, foundations etc. To confirm the validity of the design during/after construction and to assist in answering specific questions concerning a project. Monitoring of performance of excavations in rock had been carried out for many years before the establishment of the ISRM in 1962 and had become an integral part of rock engineering practice through the observational method (Brown, 2011). Early monitoring used mechanical and optical, and then electronical and electro-optical techniques (i.e. Franklin and Denton 1973; Kovari et al. 1979; Dunicliff 1988; Brady and Brown 2004).

In order to achieve successful monitoring, various instruments and systems, such as extensometers, inclinometers and tiltmeters for movement monitoring, hydraulic cells for pressure monitoring and blast vibration monitoring techniques have been developed and were accepted as ISRM SMs (ISRM 1981, 2007). Most recently, the Global Positioning System (GPS) (Fig. 16) has an important potential to contribute through 3D displacement monitoring over an extensive area with high accuracy in real time, and has become an attractive monitoring tool in rock engineering. With the aid of this system; 3D displacements can be measured with millimetre accuracy, and the methods for reducing the influence of tropospheric delays and overhead obstacles have been established, so these measurements will be helpful for rock engineers to understand the unknown mechanisms of complex rock behaviour (Shimizu et al. 2011). In addition, and particularly for open pit mining, laser scanning (LiDAR), radar and satellite imaging techniques and systems are now also used to monitor slope movements (e.g. Hawley et al. 2009; Sakurai et al. 2009; Herrera et al. 2010).

3 Near Future Trends in Rock Testing and Monitoring

Experimental rock mechanics has a very wide scope ranging from laboratory tests to field tests and monitoring of rock structures. There are some issues requiring further investigations and a need for further developments in experimental methods which may lead to new ISRM SMs.

Fig. 16 GPS displacement monitoring system (after Shimizu et al. 2011)

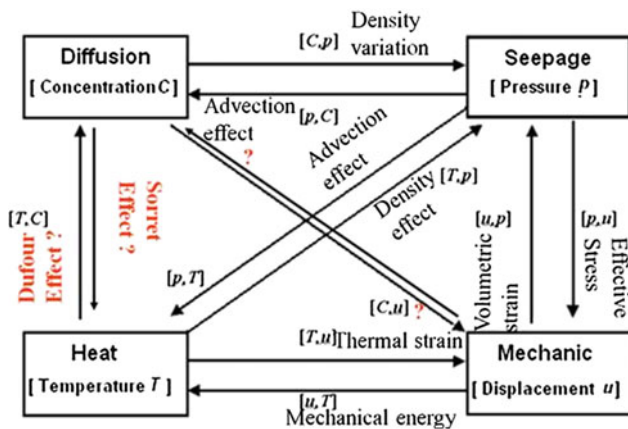
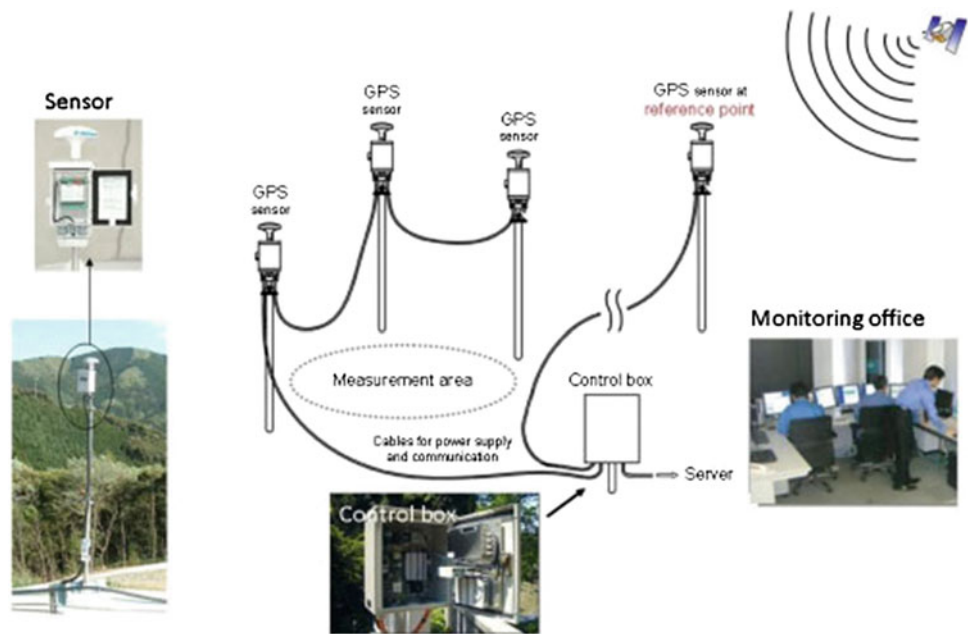


Fig. 17 The concept of the coupling of the governing equations when modelling the high-level nuclear waste disposal problem (slightly modified from Aydan 2008)

A brief summary on these is given in the following paragraphs.

Radioactive nuclear waste disposal and geothermal energy extraction are typical examples of thermo-hydro-mechanical phenomena in geo-engineering. In particular, the nuclear waste disposal issue is one of hot topics in countries utilising nuclear energy and/or having nuclear weaponry. The design time frame ranges from 10,000 to 1,000,000 years. The constitutive law parameters among coupling of diffusion $[C]$, heat flow $[T]$ and seepage $[p]$ are generally unknown and further experimental studies are required to obtain the actual values of Dufour and Soret coefficients for a meaningful assessment of fully coupled thermo-hydro-diffusion phenomena (Aydan 2008) (Fig. 17).

Due to the additional 4th dimension of time, dynamics has been a more challenging topic to understand and to apply. It remains, at least in the discipline of rock mechanics, a relatively virgin territory, where research and knowledge are limited. Although new dynamic laboratory test methods using Hopkinson bar, which were also accepted by ISRM as SMs (Zhou et al. 2012), have been developed, there are many issues in rock dynamics requiring further investigations; these have been summarised by Zhao (2011) in the most recently published book entitled “Advances in Rock Dynamics and Applications”. Among them, as experimental studies, new trends are related to the shear strength of rock joints under dynamic loads (in order to understand the rate effects on shear strength and dilation), and exploration of the mechanical and physical causes of the rate effects on the rock strength and failure pattern etc.

Since stress is a tensorial quantity requiring six independent components, estimation of rock stress is one of the most important and problematic issues in rock engineering due to the considerable variation in the rock stress at all scales (caused inter alia by various types of fracturing). As emphasised by Hudson (2008, 2011) and Bieniawski (2008), although there are some rock stress measurement techniques recommended, the development of a method of rapidly and reliably estimating the six components of the rock stress tensor at a given location is an important need. Also, although the AE method is being used to estimate rock stress, further studies to compare stresses inferred from this method applied suitably on oriented samples under uniaxial loading and those of well-known in situ stress determination methods together with a SM for AE measurement are still urgent needs.

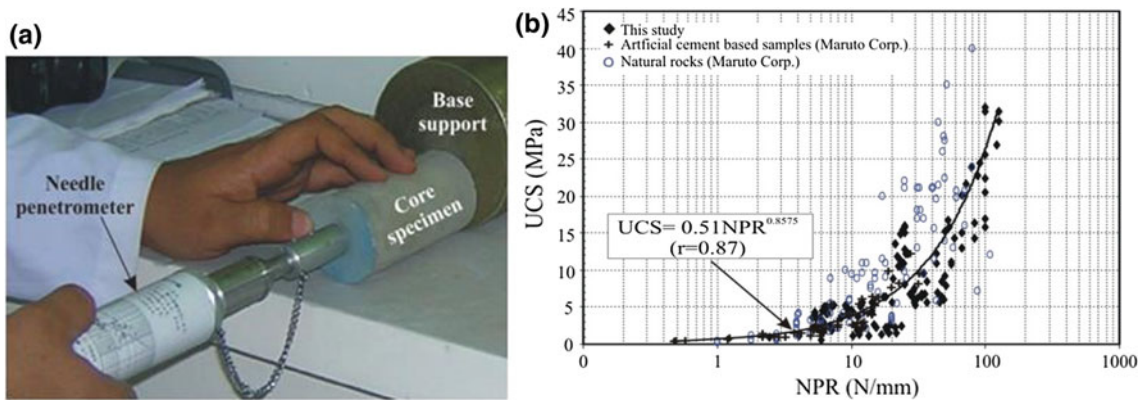


Fig. 18 a Needle penetration test, b relation between the needle penetration resistance and uniaxial compressive strength (Erguler and Ulusay 2007)

The preparation of smaller samples from weak and soft rocks even for some index tests is also difficult. In addition, sampling from historical sites, monuments and buildings for strength determinations in rock engineering studies is generally discouraged. Also, the degradation of the surrounding rock due to various causes may increase and sampling for laboratory tests becomes difficult. Therefore, the use of non-destructive techniques has been receiving great attention in recent years. To overcome these difficulties, for example, a portable light-weight testing non-destructive device (Fig. 18), called the needle penetrometer, has been developed in Japan and its application in rock engineering has been investigated by several researchers (i.e. Erguler and Ulusay 2007; Aydan et al. 2008; Aydan 2012b; Ngan-Tillard et al. 2012). It has found that the needle penetration resistance determined from this test is a useful index for the estimation of some rock properties (Aydan 2012b). It is a practical test and can be applied both in the laboratory and field. However, this method still needs a standard or a SM. Similarly, rock reinforcement and support elements such as rockbolts, rock anchors and steel ribs may deteriorate or corrode, and concrete linings may crack due to shrinkage, cyclic loading etc. (Aydan 2008). Due to this, developments are still necessary in relation to testing equipments for non-destructive tests.

By considering the increasing interest in TBMs and deep borings, some improvements on the determination of excavability and drillability parameters and the associated preparation of ISRM SMs for them are also some of the near future expectations which may assist considerably in the effort of predicting TBM excavability.

One of the important steps in a rock engineering project is site characterisation of rock exposures, which is required to collect the input data for further analysis, design and numerical modelling. The quality and quantity of the site characterization data play an important role in the subsequent use of the results. Traditional methods are now still

used in most of the rock engineering projects, however; they have some drawbacks in terms of capturing enough data for further analysis, which then affects the results for the whole project. The most well-known drawback in traditional methods is that too much personal work is involved in the in situ data acquisition procedure, which is time-consuming, not accurate enough, sometimes difficult, and can be dangerous when reaching the rock faces physically (Feng et al. 2011).

One of the efforts for improving site characterisation data with new techniques is the use of 3D terrestrial laser scanning techniques which have been developed since the late 1990s. These techniques have been used in many engineering fields over the last twenty years and show great promise for characterising rock surfaces. Although any standard or SM for these techniques is not available yet, the studies summarised by Feng et al. (2011) indicate that 3D terrestrial laser scanning techniques have a great potential in rock engineering applications, such as for fracture mapping, identification of rock types, detecting water leakage, monitoring of rock mass deformations, and the associated documentation and visualisation (Fig. 19). Some limits with the current techniques are reported by Feng et al. (2011), such as colour scanning which is limited to having good illumination, difficulties related to processing the large amount of scanning data at high resolution and particularly the lack of software development for application to rock mechanics. The solution of these aspects and the further developments will play an important role in the production of useful SMs on 3D terrestrial laser scanning techniques.

A number of geophysical methods are available to be used in rock engineering. However, newer sophisticated instrumentation with increased measurement sensitivities will permit geophysical techniques to play an increasingly important role in rock engineering. There is need to obtain more rock property information, particularly on the geometry and mechanical properties of rock fractures. More

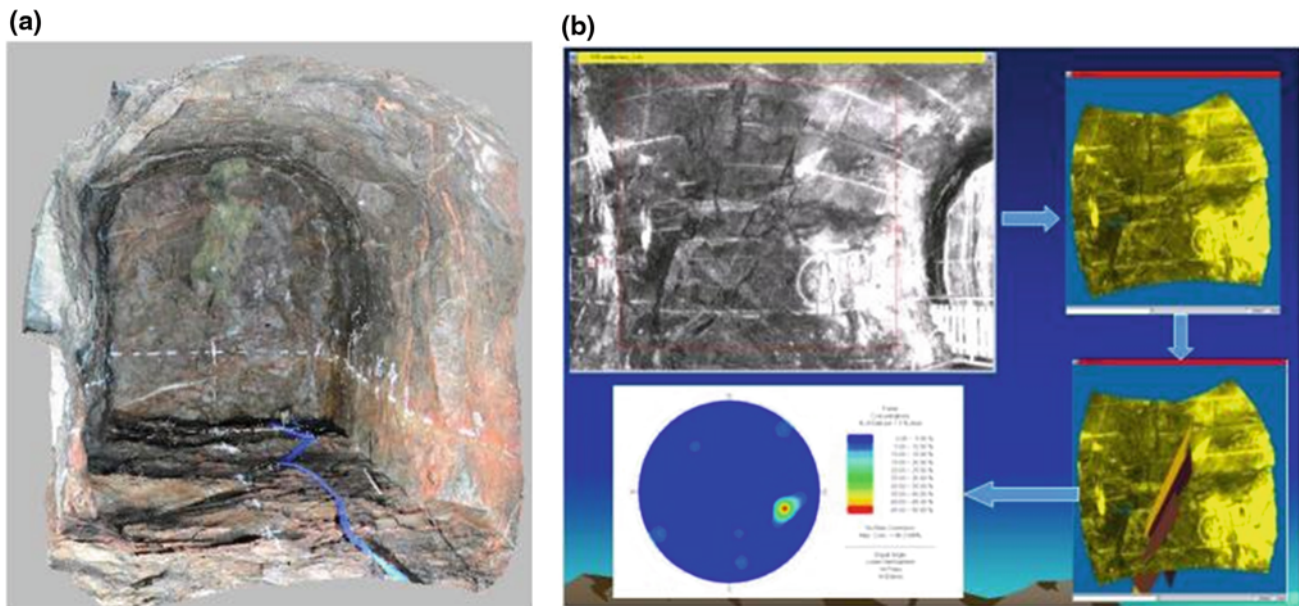


Fig. 19 Some applications of 3D laser scanning techniques: **a** 3D colour model of scanning in a tunnel, **b** semi-automatic fracture mapping (Feng et al. 2011)

emphasis will be given on geophysical methods in site investigation through rapidly developing seismic techniques, especially tomography and associated 3D visualisation methods. As emphasised by the ISRM Commission on Geophysics (Matsuoka, 2011), because CCS is becoming one of the key technologies for the reduction of CO₂ emission in the atmosphere, rock mechanics is expected to contribute to the procedures. Geophysics is also expected to play a central role for monitoring and verifying CO₂ movement in the ground. Although geophysics has been applied already to several CCS fields, there still remain many challenges to be solved in the future. Monitoring geophysics is also developing.

As a result of extracting oil from deeper and more difficult geological settings, the use of rock mechanics in petroleum engineering has become increasingly important since the 1970s (e.g. Roegiers 1999). In terms of rock testing, the factors are mainly the measurement of in situ stresses, particularly shale and sandstone characterisation and petroleum engineering related laboratory tests such as the thermo-hydro-mechanical behaviour of shales (ARMA 2012-Workshop on Petroleum Geomechanics Testing). Boring and testing issues including coring guidelines and best practices, minimising core damage, identifying core damage, sample preparation and handling, “best-practice” testing protocols, index testing, non-standard tests (e.g. creep, high temperature, high pressure, reactive fluids, fractured rock) and the use of analogue materials will be the important developments expected in the near future.

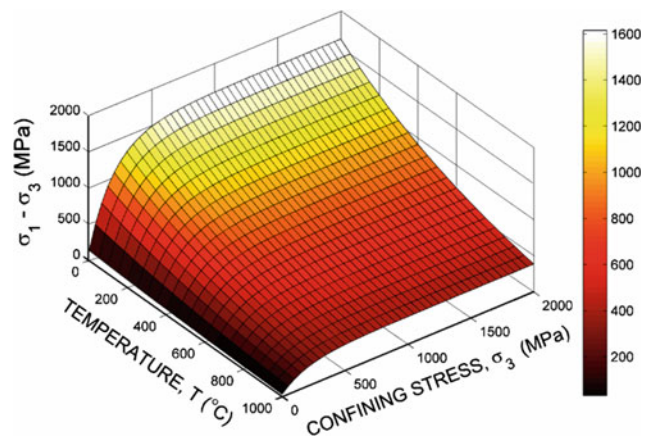


Fig. 20 A three-dimensional representation of Aydan (1995)'s failure criterion for the experimental results of Hirth and Tullis (1994)

In geomechanics, there is almost no yield (failure) criterion incorporating the effect of temperature on the yield (failure) properties of rocks although there has been some experimental researches (e.g. Hirth and Tullis 1994). The criterion proposed by Aydan (1995) is the only criterion known to the author and it was used to study the stress state of the earth. This yield (failure) criterion was applied to experimental results which are shown in Fig. 20. There is a need to focus attention on this issue and to consider the effect of rate dependency and the effect of saturation for some rocks on yield criteria.

Rock spalling is also an important aspect in rock engineering, particularly in underground studies and in the preservation of man-made historical underground openings. As emphasized by the ISRM Commission on Rock Spalling (Diederichs 2008), the focus is mainly on spalling in hard and low porosity rocks. In terms of experimental rock mechanics, the near future primary tasks are providing guidelines for laboratory procedures to detect damage thresholds and suggesting field observations using the televiewer, core discing etc. which can be used during investigations to assess spalling potential. The exact mechanism of spalling in foliated rocks also needs clarification.

One of the important gaps appearing among the ISRM SMs is the methods for determination of the hydraulic properties of intact rocks, discontinuities and rock masses both at laboratory and field scales. Based on current experiences on this issue, the gap may be filled relatively soon. In addition, long-term maintenance and preservation of man-made historical and modern rock structures as well as waste disposal sites become important issues in geo-engineering. Although they are well-known issues, quantitative evaluation methods are still lacking. Important issues are how to evaluate the weathering and degradation rates and effect of variations in water content on rocks with minerals or particles susceptible to water, and to incorporate these in the stability assessments (i.e. Aydan 2003; Aydan et al. 2005; Ulusay and Aydan 2011). Available methods such as slake durability, drying and wetting, freezing and thawing, and swelling tests are insufficient to provide experimental data for constitutive and mechanical modelling. Therefore, the development of new experimental techniques to solve this problem is urgently needed.

Summary tables of the information required for the rock mechanics modelling used to support rock engineering design are given in Feng and Hudson (2011).

4 ISRM Suggested Methods and Recent Advances

4.1 ISRM Commission on Testing Methods

- (a) After the formation of the ISRM in 1962 in Salzburg, some Commissions on different aspects of rock mechanics and rock engineering were established by the ISRM. One of these Commission is the Commission on Testing Methods which was established in 1966 at the time of the 1st ISRM Congress as the “Commission on Standardisation of Laboratory and

Field Tests”. In 1979, its name was changed to “Commission on Testing Methods” at the 4th ISRM Congress held in Switzerland. This commission was chaired by Dr. Don Deere (1966–1972), Prof. Z.T. Bieniawski and Dr. John Franklin (1972–1979), Dr. John Franklin (1979–1987) and Prof. John A. Hudson (1987–2006). Since 2006, the Commission has been chaired by the author of this paper.

- (b) The objectives of the ISRM Commission on Testing Methods are
- (i) to generate and publish SMs for testing or measuring properties of rocks and rock masses, as well as for monitoring the performance of rock engineering structures,
 - (ii) to raise or upgrade the existing SMs based on recent developments and publish them in book form,
 - (iii) to solicit and invite researchers to develop new methods, procedures or equipment for tests, measurements and the monitoring required for rock mechanics and laboratory or field studies, and
 - (iv) to encourage collaboration of those who practice in rock mechanics testing. The commission also cooperates with other ISRM Commissions for the development of new SMs as was most recently successfully done with the ISRM Commission on Rock Dynamics.
- (c) Since 1974, through the Commission, the ISRM has generated a succession of SMs covering a wide range of subjects. The first collection of the ISRM SMs was edited by Prof. Ted Brown and published by Pergamon Press in 1981. Because this book, affectionally known as the “Yellow Book” (Fig. 21a), is out of print and many new SMs have been produced since then, a book, called the “Blue Book” (Fig. 21b), which includes complete set of SMs from 1974 to 2006, was edited by Professors Resat Ulusay and John A. Hudson and published by the ISRM Turkish National Group (TNG) in 2007. The ‘Blue Book’ is available from the ISRM Secretariat and ISRM TNG.

4.2 What Is an ISRM SM

The term ‘Suggested Method’ has been carefully chosen: these are not standards per se; they are explanations of recommended procedures to follow in the various aspects of rock characterisation, testing and monitoring. An “ISRM SM” is a document that has been developed and established

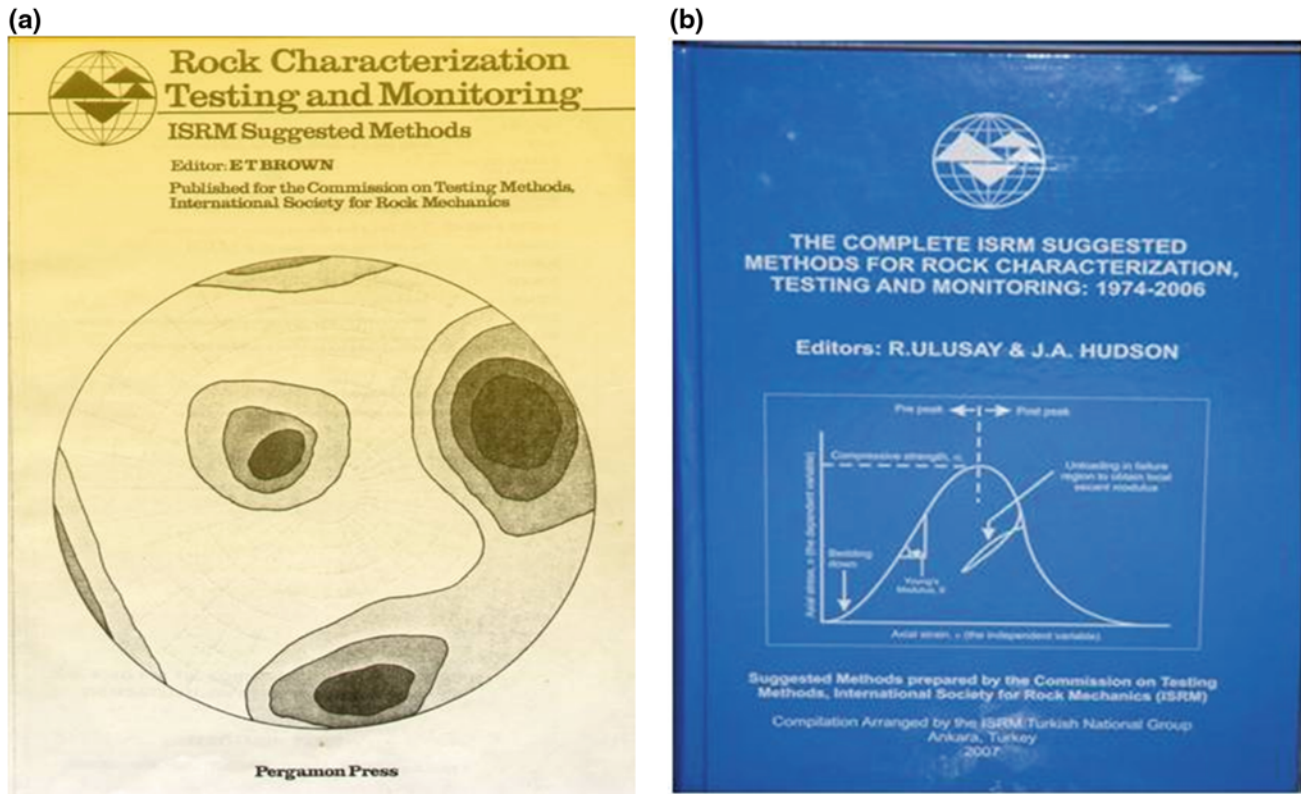


Fig. 21 a Yellow Book (ISRM 1981) and b Blue Book (ISRM 2007)

within the consensus principles of the ISRM and that meets the approval requirements of the ISRM procedures and regulations. If someone has not been involved with a particular subject before and if this subject is part of a Suggested Method, they will find the guidance to be most helpful. For example, rock stress estimation is not an easy task and anyone involved in measuring rock stresses should not take on the task lightly. The four SMs concerning rock stress estimation cover the understanding of rock stress, overcoring, hydraulic fracturing, and quality assurance. In other words, the two main stress measurement methods of overcoring and hydraulic fracturing are bracketed, firstly by ensuring that the reader is aware of the rock stress pitfalls, and secondly by ensuring that the necessary quality checks have been highlighted. The Suggested Methods can be used as standards on a particular project if required for contractual reasons, but they are intended more as guidance.

The purpose of the ISRM SMs is therefore to offer guidance for rock characterisation procedures, laboratory and field testing and monitoring in rock engineering. These methods provide a definitive procedure for the identification, measurement and evaluation of one or more qualities, characteristics or properties of rocks or rock systems that produce a test result.

4.3 Guideline for Developing ISRM SMs and the Procedure Followed for Their Evaluation

The following guideline is recommended by the ISRM Commission on Testing Methods to the volunteers and invited Working Groups (WG) who intend to develop new or to upgrade the current ISRM SMs.

1. The SM, which will be proposed, must be directly related to rock mechanics and rock engineering. It can be a laboratory or field testing method or a monitoring technique.
2. The proposed method should have been experienced at different laboratories or under different site conditions by different investigators and its results should have acceptable levels of repeatability and reproducibility. Also, the testing device or equipment should be clearly described or commercially available.
3. The effects of the testing device, specimen dimensions, environmental conditions etc. On the rock property, which will be determined or measured, should have been investigated in necessary detail and clearly defined.
4. Before the proposal of the SM is submitted to the ISRM Commission on Testing Methods, some papers and/or

reports on the proposed method should have been published.

5. In addition to the proposal of a new method, methods which can be an alternative to the current ISRM SMs or upgraded versions of the current ISRM SMs may also be recommended.
6. A proposal should be prepared by a WG which is established by a Chairman or Co-chairmen and consist of investigators who are studying the same or similar method from different countries.
7. A proposal for a SM, which will be submitted to the Commission, should include the followings:
 - a. Scope (aim of the method and its necessity in rock mechanics and/or rock engineering and technical benefits expected from the method)
 - b. Content of the method (testing procedure) and some information on the test device to be used
 - c. List of WG members (with their correspondence addresses and e-mails); and
 - d. Work plan and date of submission of the draft document to the Commission.

The proposals should be submitted to the President of the Commission by the Chairmen of the WGs. The general content of an ISRM SM is given below:

1. Introduction
2. Scope
3. Apparatus
4. Procedure : (a) Specimen preparation (for laboratory tests), (b) testing
5. Calculations
6. Presentation of results
7. Notes and recommendations (if necessary)
8. Acknowledgements (if necessary)
9. References

The procedure followed by the Commission on Testing Methods and the ISRM for the evaluation and approval of a proposed SM is given in the flow-chart in Fig. 22. Based on this procedure, in case of acceptance of any SM and its approval by the Commission and ISRM Board, respectively, the manuscript is submitted to an international journal on rock mechanics for publication without further review. Until 2012, the SMs approved by the ISRM Board as ISRM SMs were published in the “International Journal of Rock Mechanics & Mining Sciences (IJRMMS)”. Since 2012, they are being published in “Rock Mechanics & Rock Engineering (RMRE)”.

4.4 How the ISRM SMs Should Be Referenced

Following Dr. Don’s initial work in the late 1960s and early 1970s in establishing the groundwork and priorities for the topics to be covered, the production of the majority of the

early SMs was managed by Prof. Z.T. Bieniawski and Dr. J.A. Franklin who arranged WGs to produce successive drafts of each SM. The final versions were then published in the IJRMMS. These earlier SMs did not have authors as such, although the WG members were acknowledged. In 1987, Prof. J.A. Hudson took over the Presidency of the Commission and initiated a system where the documents were produced more in the form of papers, so that the authors would receive full citation recognition of their efforts. Up to now all ISRM SMs have been referenced as ISRM (1981) or with the names of their authors. In order to give full credit to the authors of the SMs and also to indicate that these methods have been approved by the ISRM as ISRM SMs, it is recommended that both the authors of the SMs and the name of the ISRM Book, which includes these SMs, should be referred to in the text as given below (Note that all ISRM SMs published between 1974 and 2006 have been included in the Blue Book (ISRM 2007)). For example, “ISRM SM for Rock Stress Estimation: Part-3”, the following referencing style is recommended to be used in the text and figure and table captions, and in the List of References:

Referencing style in the text: “.....(Haimson and Cornet 2003; ISRM 2007).....”

Referencing style in the list of references:

“Haimson, B., Cornet, F.H., 2003. ISRM Suggested Methods for rock stress estimation—Part 3: hydraulic fracturing (HF) and/or hydraulic testing of pre-existing fractures (HTPF). *Int. J. Rock Mech. & Min. Sci.*, 40, 1011–1020.”

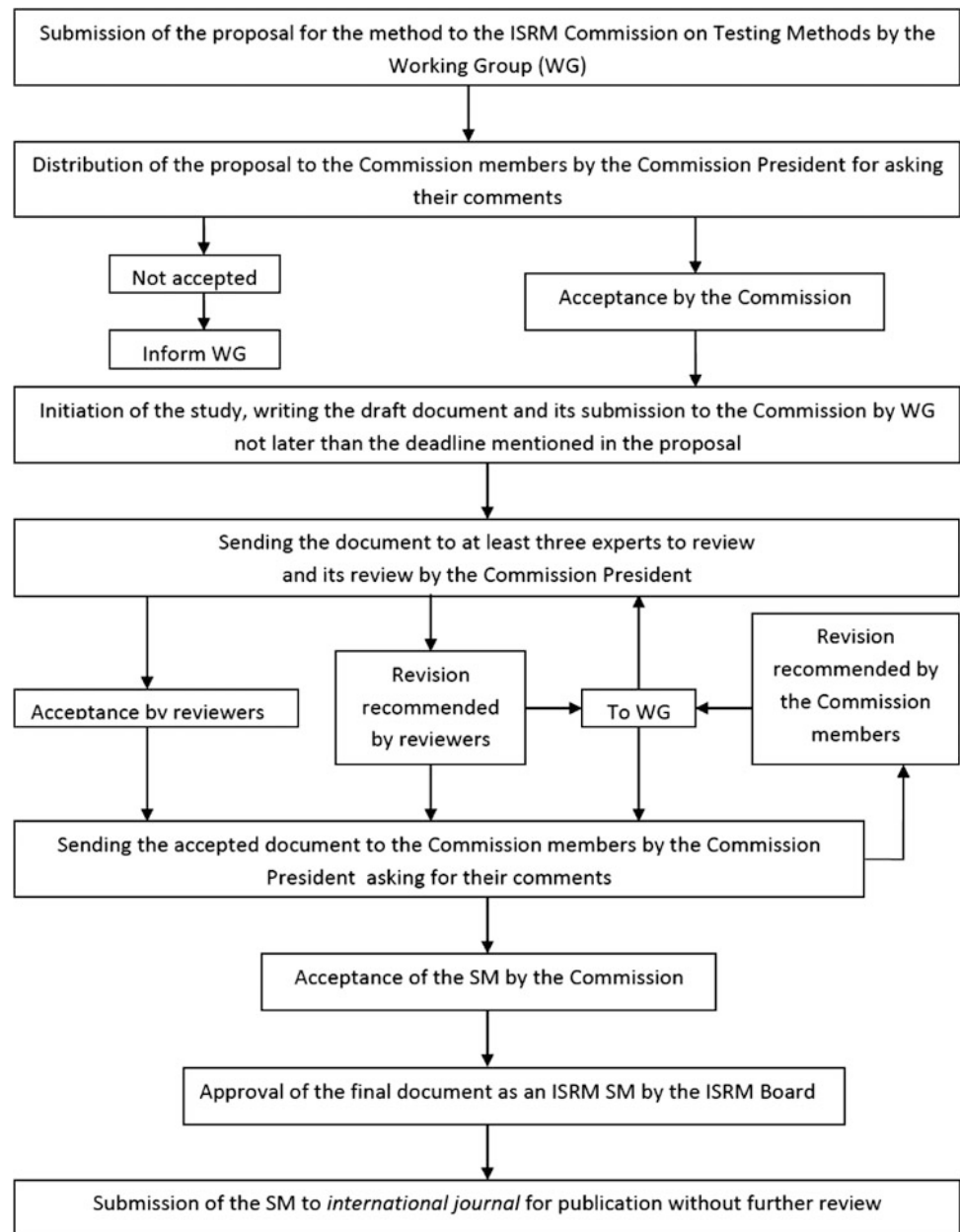
“ISRM, 2007. *The Complete ISRM Suggested Methods for Rock Characterization, Testing and Monitoring: 1974–2006. Suggested Methods Prepared by the Commission on Testing Methods, International Society for Rock Mechanics, R. Ulusay & J.A. Hudson (eds.), Compilation Arranged by the ISRM Turkish National Group, Ankara, Turkey, 628 p.*”

The old SMs of which the authors are not cited should be referenced as “ISRM (2007)”

4.5 Current ISRM SMs and Most Recent Attempts

From 1974 to the present the ISRM has generated 62 SMs. The SMs are classified into four groups, namely: Site Characterisation, Laboratory Testing, Field Testing and Monitoring. The SMs involving the description of discontinuities and geophysical logging of boreholes are included in the Site Characterisation group. Although some index tests, such as the Point Load Test and Schmidt Hammer Test, can be performed either in the laboratory or in the field using portable laboratory equipment, all index and

Fig. 22 Flowchart showing the procedure for application, developing and approval of the ISRM SMs



mechanical tests, along with the petrographic description of rocks, are considered in the “Laboratory Testing” group. Note that the 1975 version of the SM for shear strength of rock joints, and 1978 versions of the SMs concerning tri-axial compressive strength testing, the measurement of Shore hardness, Schmidt hammer test and sound velocity test were revised in 2014, 1983, 2006, 2009 and 2014, respectively. In the “Field Testing” group, the tests are divided into five sub-groups: Deformability Tests, In situ Stress Measurements, Geophysical Testing, Other Tests, and Bolting and Anchoring Tests. The Monitoring group includes the methods for monitoring of movements, pressures and blast vibrations occurring in rock structures and

rock masses. These methods are listed in Table 1 in chronological order. In addition, the ISRM SMs books (Yellow Book, 1981; Blue Book, 2007; Orange Book, 2014), which include these methods, are also mentioned in this table.

Since 2006, twenty one new WGs were established by the ISRM Commission on Testing Methods to develop new and/or revised/upgraded ISRM SMs. Sixteen WGs produced twenty one new and/or upgraded ISRM SMs. These SMs were approved by the ISRM and first published in the journals and then in the ISRM Orange Book. One of these new SMs, entitled “SMs for Determining the Dynamic Strength Parameters and Mode-I Fracture Toughness of Rock Materials” is a product of the ISRM Commission on

Table 1 List of all the ISRM Suggested Methods published between 1974 and 2014 (In chronological order)

SM for Determining Shear Strength ^{a, b} —1974
SM for Rockbolt Testing ^{a, b} —1974
SM for Determining Water Content—Porosity—Density—Absorption and Related Properties and Swelling and Slake-Durability Index Properties ^{a, b} —1977
SM for Monitoring Rock Movements Using Inclinometers and Tiltmeters ^{a, b} —1977
SM for Determining Sound Velocity ^{a, b} —1978
SM for Determining Tensile Strength of Rock Materials ^{a, b} —1978
SM for Determining Hardness and Abrasiveness of Rocks ^{a, b} —1978
SM for Determining the Strength of Rock Materials in Triaxial Compression ^{a, b} —1978
SM for Monitoring Rock Movements Using Borehole Extensometers ^{a, b} —1978
SM for Petrographic Description of Rocks ^{a, b} —1978
SM for Quantitative Description of Discontinuities in Rock Masses ^{a, b} —1978
SM for Determining in Situ Deformability of Rock ^{a, b} —1979
SM for Determining the Uniaxial Compressive Strength and Deformability of Rock Materials ^{a, b} —1979
SM for Pressure Monitoring Using Hydraulic Cells ^{a, b} —1980
SM for Geophysical Logging of Boreholes ^{a, b} —1981
SM for Determining the Strength of Rock Materials in Triaxial Compression: Revised Version ^b —1983
SM for Surface Monitoring of Movements across Discontinuities ^b —1984
SM for Determining Point Load Strength ^b —1985
SM for Rock Anchorage Testing ^b —1985
SM for Deformability Determination Using a Large Flat Jack Technique ^b —1986
SM for Deformability Determination Using a Flexible Dilatometer ^b —1987
SM for Rock Stress Determination ^b —1987
SM for Determining the Fracture Toughness of Rock ^b —1988
SM for Seismic Testing Within and Between Boreholes ^b —1988
SM for Laboratory Testing of Argillaceous Swelling Rocks ^b —1989
SM for Large Scale Sampling and Triaxial Testing of Jointed Rock ^b —1989
SM for Blast Vibration Monitoring ^b —1992
SM for Rapid Field Identification of Swelling and Slaking Rocks ^b —1994
SM for Determining Mode I Fracture Toughness Using Cracked Chevron Notched Brazilian Disc ^b —1995
SM for Deformability Determination Using a Stiff Dilatometer ^b —1996
SM for Determining the Indentation Hardness Index of Rock Materials ^b —1998
SM for Complete Stress-Strain Curve for Intact Rock in Uniaxial Compression ^b —1999
SM for in Situ Stress Measurement Using the Compact Conical-Ended Borehole Overcoring Technique ^b —1999
SM for Laboratory Testing of Swelling Rocks ^b —1999
SM for Determining Block Punch Strength Index ^b —2001
SM for Rock Stress Estimation—Part 1: Strategy for Rock Stress Estimation ^b —2003
SM for Rock Stress Estimation—Part 2: Overcoring Methods ^b —2003
SM for Rock Stress Estimation—Part 3: Hydraulic Fracturing (HF) and/or hydraulic testing of pre-existing fractures (HTPF) ^b —2003
SM for Rock Stress Estimation—Part 4: Quality Control of Rock Stress Estimation ^b —2003
SM for Land Geophysics in Rock Engineering ^b —2004
SM for Determining the Shore Hardness Value for Rock ^b —2006 (updated version)
SM for Determination of the Schmidt Hammer Rebound Hardness: Revised version ^c —2009
SMs for Determining the Dynamic Strength Parameters and Mode I Fracture Toughness of Rock Materials ^c —2012
SM for the Determination of Mode II Fracture Toughness ^c —2012

(continued)

Table 1 (continued)

SM for Determining Shear Strength ^{a, b} —1974
SM for Rock Stress Estimation—Part 5: Establishing a Model for the In situ Stress at a Given Site ^c —2012
SMs for Rock Failure Criteria (Six failure criteria) ^c —2012:
a. SM for Mohr-Coulomb Failure Criterion ^c
b. SM for the Hoek-Brown Failure Criterion ^c
c. SM for 3D Hoek-Brown Failure Criterion ^c
d. SM for Drucker-Prager Failure Criterion ^c
e. SM for Lade and Modified Lade 3D Rock Strength Criteria ^c
f. SM for a Failure Criterion for Rocks Based on True Triaxial Testing ^c
SM for Measuring Rock Mass Displacement Using a Sliding Micrometer ^c —2013
SM for Rock Fractures Observations Using a Borehole Digital Optical Televiwer ^c —2013
SM for Determining the Mode-I Static Fracture Toughness Using Semi-Circular Bend Specimen ^c —2014
SM for Reporting Rock Laboratory Test Data in Electronic Format ^c —2014
SM for Determining Sound Velocity by Ultrasonic Pulse: Upgraded Version ^c —2014
SM for Determining the Creep Characteristics of Rock Materials ^c —2014
SM for Monitoring Rock Displacements Using Global Positioning System ^c —2014
SM for Laboratory Determination of the Shear Strength of Rock Joints: Revised Version ^c —2014
SM for Determining the Abrasivity of Rock by the Cerchar Abrasivity Test ^c —2014
SM for Step-Rate Injection Method for Fracture In-situ Properties (SIMFIP): Using a 3-Components Borehole Deformation ^c —2014
SM for the Needle Penetration Test ^c —2014

^a Published in ISRM (1981, Yellow Book)

^b Published in ISRM (2007, Blue Book)

^c Published in ISRM (2014, Orange Book)

Table 2 The new ISRM SMs under preparation by the WGs established in 2013

1. SM for Determining Thermal Properties of Rock Samples
2. SM for Laboratory Acoustic Emission Monitoring
3. SM for Uniaxial-Strain Compressibility Testing for Reservoir Geomechanics
4. SM for the Lugeon Test
5. SM for In Situ Microseismicity Monitoring of the Rock Mass Fracturing Process

Rock Dynamics based on the co-operation between that Commission and the ISRM Commission on Testing Methods. The new five WGs, which were established in 2013, are preparing the new SMs given in Table 2. The “SM for Uniaxial-Strain Compressibility Testing for Reservoir Geomechanics” (Table 2), which is under preparation, will be the product of the ISRM Commission on Petroleum Geomechanics based on the co-operation between that Commission and ISRM Commission on Testing Methods.

The Orange Book also includes two supplementary but non-SM documents, such as “3D Laser Scanning Techniques for Application to Rock Mechanics and Rock Engineering” and this paper.

In the near future and based on current experiences and experimental studies, the ISRM Commission on Testing Methods expects the production of new ISRM SMs which

will be developed by various WGs and/or based on the co-operation with the commission and other ISRM Commissions. These are listed below.

- Based on the co-operation between the Commission on Testing Methods and some other ISRM Commissions, the development of new SMs on rock dynamics, petroleum geomechanics (SMs for geomechanical testing of the mudstone cap rock above injection, for block testing with polyaxial stresses and fluid flow-coupling etc.) and rock spalling (such as guidelines for laboratory procedures to detect damage thresholds, suggested field observations to be used during investigations for assessing spalling conditions etc.) are anticipated.
- SMs for rock mass excavability tests.
- SMs for 3D laser scanning techniques for application to rock engineering.

d. Although some tests, such as slake durability, freezing and thawing, drying and wetting and swelling tests, are insufficient to provide experimental data for constitutive and mechanical modelling, they are useful for the assessment of rocks during material selection. By considering that ISRM SMs for freezing and thawing, and drying and wetting tests are still not available, the development of SMs for these two tests based on co-operation with the ISRM Commission on Soft Rocks will be useful.

5 Conclusions

Since the establishment of the International Society for Rock Mechanics (ISRM) in the 1960s, there have been important scientific developments and technological advances both in rock mechanics and rock engineering. In particular, modelling of rock behaviour, design methodologies for rock structures and rock testing methods are the main issues in these developments and advances. The models developed depend considerably on the input parameters such as boundary conditions and material and rock mass properties. For this reason, the importance of experimental investigations and the determination of engineering properties of rocks will continue as an integral part of rock mechanics and rock engineering applications in the future.

Developments in the laboratory and in situ testing and monitoring methods in rock dynamics, petroleum geomechanics, new non-destructive testing methods, tests for the determination of the thermo-hydro-mechanical behaviour of rocks, methodologies for detecting rock spalling, and application of 3D laser scanning techniques and GPS methods for rock characterisation and displacement measurements seem to be the most popular areas of interest in terms of experimental rock mechanics. Depending on these developments and future co-operation between the ISRM Commissions, it is expected that valuable contributions through the production of new and upgraded ISRM Suggested Methods will continue with increasing speed.

Acknowledgements The author would like to thank the ARMS7 Organizing Committee for their kind invitation to him to give this keynote lecture and kind permission given for the publication of this paper in the Orange Book, specifically Dr. Chul-whan Park (member of the ISRM Commission on Testing Methods and Vice-Chairmen of ARMS7), Prof. Seokwon Jeon (Vice-Chairmen of ARMS7) and Dr. Kong Chang Han (President of the Korean Society for Rock Mechanics). In addition, the author specifically wishes to thank Professors Ömer Aydan (Japan), John A. Hudson (UK) and Hasan Gercek (Turkey) who enhanced some ideas expressed in this paper and provided some documents. Professor Hudson also provided editorial assistance.

References

- Abbot AV (1884) *Testing Machines: Their History, Construction and Use*. Van Nostrand, New York.
- Amadei B, Stephansson O (1997) *Rock Stress and Its Measurement*. Kluwer, Dordrecht.
- ARMA (2012) Workshop on Petroleum Geomechanics Testing. <http://www.arma.org/conference/2012/Chicago.aspx>.
- Atkinson BK (ed.) (1987) *Fracture mechanics of rock*. Academic Press, London.
- Aydan Ö (1995) The stress state of the earth and the earth's crust due to the gravitational pull. *Proceedings of the 35th US Rock Mechanics Symposium, Lake Tahoe*, pp 237–243.
- Aydan Ö (2003) The moisture migration characteristics of clay-bearing geo-materials and the variations of their physical and mechanical properties with water content. *Proceedings of the 2nd Asian Conference on Saturated Soils (UNSAT-ASIA 2003)*, Osaka, pp 383–388.
- Aydan Ö (2008) New directions of rock mechanics and rock engineering: Geomechanics and geoengineering. *Proceedings of the Asian Rock Mechanics Symposium (ARMS5)*, A Majdi and A Ghazvinian (eds.), Tehran, Vol. 1, pp 3–21.
- Aydan Ö (2012a) *Historical rock mechanics and rock engineering*. Tokai University, Japan, Unpublished Notes, 9 p.
- Aydan Ö (2012b) The inference of physico-mechanical properties of soft rocks and the evaluation of the effect of water content and weathering on their mechanical properties from needle penetration tests. *Proceedings of the 46th US Rock Mechanics/Geomechanics Symposium, Chicago, ARMA 12–639* (on CD).
- Aydan Ö, Ulusay R (2003) Geotechnical and geo-environmental characteristics of man-made underground structures in Cappadocia, Turkey. *Engineering Geology* 69: 245–272.
- Aydan Ö, Geniş M (2004) Properties of surrounding rock and the stability of openings of the rock tomb of Amenhotep III (Egypt). *Proceedings of 7th Regional Conference of Rock Mechanics, A Ceylanoglu and B Erdem (eds.)*, Cumhuriyet University, Sivas, pp 191–202 (in Turkish).
- Aydan Ö, Kumsar H (2005) Investigation of the Kusini antique underground marble quarry in view of engineering geology and rock engineering. *Bulletin of Engineering Geology* 20: 41–60 (in Turkish).
- Aydan Ö, Daido M, Ito T, Tano H, Kawamoto T (2005) Instability of abandoned lignite mines and the assessment of their stability in long term and during earthquakes. *4th Asian Rock Mechanics Symposium, Singapore, Paper No. A0355* (on CD).
- Aydan Ö, Watanabe S, Tokashiki N (2008) The inference of mechanical properties of rocks from penetration tests. *Proceedings of the Asian Rock Mechanics Symposium (ARMS5)*, A Majdi and A Ghazvinian (eds.), Tehran, Vol. 1, pp 213–220.
- Barla G, Barla M, Camusso M, Martinotti ME (2007) Setting up a new direct shear testing apparatus. In: L Ribeiro e Sousa, C Olalla, NF Grossmann (eds.), *Proceedings of 11th Congress of International Society for Rock Mechanics, Lisbon*, Taylor & Francis, pp 415–418.
- Backers T, Stephansson O (2012) ISRM Suggested Method for the determination of mode II fracture toughness. *Rock Mechanics and Rock Engineering* 45: 1011–1022.
- Bieniawski ZT (1966) Mechanism of rock fracture in compression. *S. Afr. Counc. Sci. Ind. Res., Mech. Eng. Inst., Res. Rep.* 459.
- Bieniawski ZT (1967) Mechanism of brittle fracture of rock. Thesis, University of Pretoria, Pretoria.
- Bieniawski ZT (2008) Reflections on new horizons in rock mechanics design: Theory, education and practice. *Proceedings of the 5th*

- Asian Rock Mechanics Symposium (ARMS5), A Majdi and A Ghazvinian (eds.), Tehran, Vol. 1, pp 37–50.
- Blanks RF, McHenry D (1945) Large triaxial testing machine built by Bureau of Reclamation, *Engineering News Record* 135(6): 171–172.
- Brady BHG, Brown ET (2004) *Rock Mechanics for Underground Mining*. 3rd ed., Kluwer, Dordrecht.
- Brown ET (2011) Fifty years of the ISRM and associated progress in rock mechanics. *Proceedings of the 12th International Congress on Rock Mechanics*, Q Qian and Y Zhou (eds.), Beijing, CRC Press, pp 29–45.
- Brown PD, Robertshaw J (1953) The in situ measurement of Young's modulus for rock by a dynamic method. *Géotechnique* 3(7): 283–286.
- Christiansson R, Hudson JA (2003) ISRM suggested methods for rock stress estimation-Part 4: quality control of rock stress estimation. *International Journal of Rock Mechanics & Mining Sciences* 40: 1021–1025.
- Cook NGW (1965) The failure of rock. *International Journal of Rock Mechanics & Mining Sciences* 2 (4): 389–403.
- Coulomb CA (1776) *Essai sur une application des regles de maximis et minimis a quelques problemes de statique, relatifs a l'architecture*. *Memoires de Mathematique & de Physique* 7: 343–382.
- Carneiro F L L B (1943) A new method to determine the tensile strength of concrete. *Proceedings of the 5th Meeting of the Brazilian Association for Technical Rules, Section 3*, 126–129 (in Portuguese).
- Diederichs M (2008) ISRM Rock Spalling Commission: Report for 2008. *ISRM News Journal* 11: 50–51.
- Dunnicliff J (1988) *Geotechnical Instrumentation for Monitoring Field Performance*. John Wiley, New York.
- Erguler ZA, Ulusay R (2007) Estimation of uniaxial compressive strength of clay-bearing weak rocks using needle penetration resistance. *Proceedings of the 11th Congress of the International Society for Rock Mechanics*, L Sousa, C Olalla and NF Grossman (eds.), Lisbon, Taylor & Francis, London, Vol. 1, pp 265–268.
- Erim KT (1986) *Aphrodisias, City of Venus Aphrodite*. Muller, Blund and White, USA.
- Evison FF (1953) The seismic determination of Young's modulus and Poisson's ratio for rocks in situ. *Géotechnique* 6 (3): 118–123.
- Fairbairn W (1856) On the tensile strength of wrought iron at various temperatures. *Brit. Assn. Annual Rep.*, pp 405–422.
- Fairbairn EMR, Ulm FJ (2002) A tribute to Fernando LLB Carneiro (1913–2001), engineer and scientist who invented the Brazilian test. *Materials and Structures* 35: 195–196.
- Feng Q, Wang G, Röshoff K (2011), Investigation of 3D terrestrial laser scanning techniques for potential application to rock mechanics. *Proceedings of the 12th International Congress on Rock Mechanics*, Q Qian and Y Zhou (eds.), Beijing, CRC Press, pp 963–968.
- Feng XT, Hudson JA (2011) *Rock Engineering Design*. CRC Press, Taylor & Francis, London.
- Franklin JA, Denton PE (1973) The monitoring of rock slopes. *Quarterly Journal of Engineering Geology* 6 (3–4): 259–286.
- Galileo G (1638) *Two New Sciences*. Elsevier, Leiden, English Translation by H Crew and A de Salvio, Macmillan, New York.
- Gibbons CH (1935) *Materials Testing Machines*. Instruments Publishing Company, Pittsburgh, Pa.
- Golder HQ, Akroyd TNW (1954) An apparatus for triaxial compression tests at high pressures. *Géotechnique* 4 (4): 131–136.
- Gray TGF (1988) Tensile testing, Chp. 1. In: *Mechanical Testing*, Book 445. Pub Inst. of Metals, London, pp 1–42.
- Griffith AA (1921) The phenomena of rupture and flow in solids. *Phil. Trans. Royal Soc. London* A221: 163–197.
- Griggs DT (1936) Deformation of rocks under high confining pressures. *Journal of Geology* 44: 541–577.
- Habib P (1950) Détermination du module d'élasticité des roches en place. *Annales de l'Institut Technique du Bâtiment et des Travaux Publics* 145: 27–35.
- Habib P, Marchand R (1952) Mesures des pressions de terrains par l'essai de vérin plat. *Suppléments aux Annales de l'Institut Technique du Bâtiment et des Travaux Publics, Série Sols et Foundations* 58: 967–971.
- Haimson B, Cornet FH (2003) ISRM suggested methods for rock stress estimation-Part 3: hydraulic fracturing (FH) and/or hydraulic testing of pre-existing fractures (HTPF). *International Journal of Rock Mechanics & Mining Sciences* 40: 1011–1020.
- Hamada M, Aydan Ö, Tano H (2004) *Rock Mechanical Investigation: Environmental and Rock Mechanical Investigations for the Conservation Project in the Royal Tomb of Amenophis III. Conservation of the wall paintings in the Royal Tomb of Amenophis III, First and Second Phases Report*. UNESCO and Institute of Egyptology, Waseda University, pp 83–138.
- Handin J (1953) An application of high pressure geophysics: experimental rock mechanics. *Transactions American Society of Mechanical Engineers* 75: 315–324.
- Hawley M, Marisett S, Beale G, Stacey P (2009) Performance assessment and monitoring. In: J Read & P Stacey (eds), *Guidelines for Open Pit Slope Design*, CSIRO Publishing, Melbourne, pp 327–379.
- Herrera G, Tomás R, Vicente F, Lopez-Sanchez JM, Mallorquí JJ, Mulas J (2010) Mapping ground movements in open pit mining areas using differential SAR interferometry. *International Journal of Rock Mechanics & Mining Sciences* 47(7): 1114–1125.
- Heyman J (1972) *Coulomb's Memoir on Statics*. Cambridge at the University Press.
- Hirth G, Tullis J (1994) The brittle-plastic transition in experimentally deformed quartz aggregates. *Journal of Geophysical Research* 99: 11731–11747.
- Hoek E (1974) The design of rock slopes and foundations. *General Report for 3rd Congress of the International Society for Rock Mechanics*, Denver (<http://www.rocksolid.com/hoek/references/H1974a.pdf>)
- Hudson JA (1989) *Rock Mechanics Principles in Engineering Practice*. Butterworths, London.
- Hudson JA (2008) The future for rock mechanics and the ISRM. *Proceedings of the Asian Rock Mechanics Symposium (ARMS5)*, A Majdi and A Ghazvinian (eds.), Tehran, Vol. 1, pp 105–118.
- Hudson JA (2011) The next 50 years of the ISRM and anticipated future progress in rock mechanics. *Proceedings of the 12th International Congress on Rock Mechanics*, Q Qian and Y Zhou (eds.), Beijing, CRC Press, pp 47–55.
- Hudson JA, Harrison JP (2000) *Engineering Rock Mechanics*. Pergamon, Amsterdam.
- Hudson JA, Brown ET, Fairhurst C (1971) Optimizing the control of rock failure in servo-controlled laboratory tests. *Rock Mechanics* 3: 217–224.
- Hudson JA, Crouch SL, Fairhurst C (1972) Soft, stiff and servo-controlled testing machines: A review with reference to rock failure. *Engineering Geology* 6: 155–189.
- Hudson JA, Cornet FH, Christiansson R (2003) ISRM suggested methods for rock stress estimation-Part 1: Strategy for rock stress estimation. *International Journal of Rock Mechanics & Mining Sciences* 40: 991–998.
- Ide JM (1936) Comparison of statically and dynamically determined Young's modulus of rock. *Proceedings of National Academy of Sciences*, 22: 81–92.
- Inglis CE (1913) Stresses in a plate due to presence of cracks and sharp corners. *Transactions of the Institute of Naval Architects* 55: 219–241.
- ISO Bulletin (1987) ELOT Price goes to ISO. *ISO Bulletin*, April 1987.

- ISRM (1981) Rock Characterization, Testing and Monitoring. ISRM Suggested Methods. ET Brown (ed.), Pergamon Press.
- ISRM (2007) The Complete ISRM Suggested Methods for Rock Characterization, Testing and Monitoring: 1974-2006. R Ulusay and JA Hudson (eds.), Suggested Methods Prepared by the Commission on Testing Methods, International Society for Rock Mechanics, Compilation Arranged by the ISRM Turkish National Group, Ankara, Turkey.
- Jaeger JC (1959) The frictional properties of joints in rock. *Geofisica Pura e Applicata* 43 (Part 2): 148–158.
- Jaeger JC (1960) Shear fracture of anisotropic rocks. *Geological Magazine* 97: 65–72.
- John KW (1962) An approach to rock mechanics. *Journal of Soil Mechanics & Foundation Division, ASCE* 88(SM4): 1–30.
- Kaptan E (1992) Tin and ancient underground tin mining in Anatolia. *Jeoloji Mühendisliği (Geological Engineering)* 40: 15–19 (in Turkish).
- King LV (1912) On the limiting strength of rocks under conditions of stress existing in the earth's interior. *J. Geol.* 20: 119–138.
- Kovari K, Amstad C, Köppel J (1979) New developments in the instrumentation of underground openings. In: AC Maevis and WA Hustrulid (eds.), *Proc. 1979 Rapid Excavation & Tunneling Conf.*, New York, A.I.M.E., pp 817–837.
- Kulaksiz S, Aydan Ö (2010) Characteristics of ancient underground quarries Turkey and Egypt and their comparison. *Proceedings of the 22nd World Mining Congress and Expo, S Eskikaya (ed.)*, Istanbul, Vol. 2, pp 607–614.
- Kumsar H, Çelik SB, Aydan, Ö, Ulusay, R (2003) Aprodias: Anatolian antique city of building and sculptural stones. *Proceedings of International Symposium on Industrial Minerals and Building Stones-IMBS'2003*, E Yuzer, H Ergin and A Tugrul (eds.), Istanbul, Turkey, pp 301–309.
- Lehtonen A, Cosgrove JW, Hudson JA, Johansson E (2012) An examination of in situ rock stress estimation using the Kaiser effect. *Engineering Geology* 124: 424–437.
- Lieurance RS (1933) Stresses in foundation at Boulder (Hoover) dam. US Bureau of Reclamation Technical Memorandum No. 346.
- Lieurance RS (1939) Boulder canyon project final report: Part V Technical investigation). *Bull.* 4: 265–268.
- Loveday MS (1982) High temperature and time dependent mechanical testing: an historical introduction- Chapter 1. In: *Measurement of high temperature mechanical properties of materials*, MS Loveday, MF Day, BF Dyson (eds.), Pub. HMSO, London, pp 1–12.
- Loveday MS, Gray T, Aegerter J (2004) Tensile Testing of Metallic Materials: A Review, Tenstand- Work Package 1-Final Report (http://resource.npl.co.uk/docs/science_technology/materials/measurement_techniques/tenstand/test_method_review.pdf)
- Mariotte E (1740) *Collected works*. The Hague.
- Martin CD (1997) The effect of cohesion loss and stress path on brittle rock strength. *Canadian Geotechnical Journal* 34 (5): 698–725.
- Matsuoka T (2011) Annual report of the ISRM Geophysics Commission. *ISRM News Journal* 14: p 54.
- Mayer A, Habib P, Marchand R (1951) Mesure en place des pressions de terrains. *Proc. Conf. Int. sur les Pressions de Terrains et le Soutènement dans les Chantiers d'Exploration*, Liège, pp 217–221.
- Mogi K (1959) Experimental study of deformation and fracture of marble (1): On the fluctuation of compressive strength of marble and relation to the rate of stress application. *Bulletin of Earthquake Research Institute, University of Tokyo* 37: 155–170.
- MTS (2012) Civil engineering testing solutions for materials, structures and components. http://www.mts.com/ucm/groups/public/documents/library/dev_002182.pdf
- Ngan-Tillard DJM, Engin HK, Vervaal W, Mulder A, Ulusay R, Erguler ZA (2012) Evaluation of micro-structural damage caused by Needle Penetration testing. *Bulletin of Engineering Geology and the Environment* 71: 487–498.
- Paterson MS (1978) *Experimental Rock Deformation—The Brittle Field*. Springer Verlag, Berlin.
- Rocha M, Serafim JL, Silveira A, Neto JR (1955) Deformability of foundation rocks. *Proceedings of 5th Congress on Large Dams*, Paris, R75, 3, pp 531–559.
- Roegiers J-C (1999) The importance of rock mechanics to the petroleum industry. In: G Vouille and P Berest (eds.), *Proc. 9th Congress of International Society for Rock Mechanics*, Paris, Balkema, Vol. 3, pp 1525–1549.
- Sakurai S, Farazmand A, Adachi K (2009) Assessment of the stability of slopes from surface displacements measured by GPS in an open pit mine. In: G Deák and ZG Agioutantis (eds.), *Sustainable Exploitation of Natural Resources*, Proc. 3rd Int. Seminar ECO-MINING—Europe in 21st Century, Milos Island, Greece, pp 239–248.
- Shimizu N, Masunari T, Iwasaki T (2011) GPS displacement monitoring system for the precise measuring of rock movements. *Proceedings of the 12th International Congress on Rock Mechanics*, Q Qian and Y Zhou (eds.), Beijing, CRC Press, pp 1117–1120.
- Sjöberg J, Christiansson R, Hudson JA (2003) ISRM suggested method for rock stress estimation-Part 2: overcoring methods. *International Journal of Rock Mechanics & Mining Sciences* 40: 999–1010.
- Smith D (1982) David Kirkaldy (1820–1897) and engineering materials testing. *Newcomen Society Eng. & Tech. Trans.* 52: 49–65.
- Spaeth W (1935) Einfluss der federung der Zerreißmaschine auf das spannungs-Denhungs-Schaubild. *Arch. Eisenhüttenwesen* 6: 277–283.
- Stephansson O (2001) What can fracture mechanics do for us? *Proceedings of the ISRM Regional Symposium EUROCK2011: Rock Mechanics a Challenge for Society*, Helsinki, Balkema, pp 21–25.
- Stephansson O, Zang A (2012) ISRM suggested methods for rock stress estimation—Part 5: Establishing a model for in situ stress at a given site. *Rock Mechanics and Rock Engineering* 45: 955–969.
- Sugawara K, Obara Y (1999) ISRM suggested method for in situ stress measurement using the compact conical-ended borehole overcoring (CCBO) technique. *International Journal of Rock Mechanics & Mining Sciences* 36: 307–322.
- Terzaghi K (1946) Rock defects and loads on tunnel supports. In: *Rock Tunneling with Steel Supports*, RV Proctor and TL White (eds.), 1, pp 17–99. Youngstown, OH, Commercial Shearing and Stamping Company.
- Timeshenko SP (1953) *History of Strength of Materials*. McGraw-Hill, New York.
- Todhunter I, Pearson K (1886) *A history of the theory of elasticity and the strength of materials from Galilei to the present time*. Cambridge University Press, Vol. 1, pp 1–6.
- Tuncay E, Ulusay R (2008) Relation between Kaiser effect levels and pre-stresses applied in the laboratory. *International Journal of Rock Mechanics and Mining Sciences* 45: 524–537.
- Tuncay E, Ulusay R, Watanabe H, Tano H, Yüzer E, Aydan Ö (2002) Acoustic emission (AE) technique: A preliminary investigation on the determination of in situ stress by AE technique in Turkey. *Yerbilimleri/Earthsciences* 25: 83–98 (in Turkish).
- Ulusay R, Aydan Ö (2011) Issues on short- and long-term stability of historical and modern man-made cavities in the Cappadocia Region of Turkey. *Proceedings of First Asian and 9th Iranian Tunnelling Symposium*, Tehran (on CD).
- Varoufakis GJ (1940) *Materials testing in classical Greece*. Technical Specifications of the 4th Century BC by Hellenic Organisation for Standardization.

- von Karman Th (1911) Festigkeitsversuche unter allseitigem Druck. *Zeit d Ver Deutscher Ing* 55: 1749–1757.
- von Musschenbroek P (1729) *Introductio ad cohaerentiam corporum firmorum*, Referenced in *Materials Testing Machines* (CH Gibbons), Instrument Publishing Company, Pittsburgh.
- Wawersik WR, Fairhurst C (1970) A study of brittle rock fracture in laboratory compression experiments. *International Journal of Rock Mechanics & Mining Sciences* 7 (5): 561–575.
- Whittaker BN, Singh RN, Sun G (1992) *Rock Fracture Mechanics: Principles, Design and Applications*. *Developments in Geotechnical Engineering*, 71, Elsevier, Amsterdam.
- Young RP (1993) Seismic methods applied to rock mechanics, *ISRM News Journal*, 1 (3), 4–18.
- Zang A, Stephansson O (2010) *Stress Field of the Earth's Crust*. Springer Verlag.
- Zhao J (2011) An overview of some recent progress in rock dynamics research: Chp. 2. In: *Advances in Rock Dynamics and Applications*, Y Zhou and J Zhao (eds.), CRC Press, pp 5–33.
- Zhou YX, Xia K, Li XB, Li HB, Ma GW, Zhao J, Zhou ZL, Dai F (2012) Suggested methods for determining the dynamic strength parameters and mode-I fracture toughness of rock materials, *International Journal of Rock Mechanics & Mining Sciences* 49: 105–112.

Part I

Laboratory Testing

ISRM Suggested Method for Determination of the Schmidt Hammer Rebound Hardness: Revised Version

Adnan Aydin

1 Introduction

With its portable, simple and affordable attributes, the Schmidt hammer (SH) is an ideal index apparatus, which underlies its increasing popularity and expanding range of applications. The SH rebound hardness value (R) is perhaps the most frequently used index in rock mechanics practice for estimating the uniaxial compressive strength (UCS) and the modulus of elasticity (E) of intact rock both in laboratory conditions and in situ. The SH is also widely used for estimating the UCS of discontinuity walls and assessing the workability, excavatability and boreability of rocks by mechanical means (cutting, polishing, milling, crushing and fragmentation processes in quarrying, drilling and tunneling).

In the three decades since the earlier ISRM suggested method for conducting the SH test was published [1], researchers have sought to establish correlations between the SH rebound values (R) and the UCS and E for different rock types. A critical review of the basic issues was recently conducted by Aydin and Basu [2], which considered the influence of hammer type, the direction of hammer impact, specimen requirements, weathering, moisture content and testing, data gathering/reduction and analysis procedures. Understanding the operation of the apparatus and the

mechanisms and modes of indentation upon hammer impact are crucial in addressing these issues, determining how the data scatter can be reduced, and settling upon an acceptable or expected degree of scatter.

With this notion, this revised suggested method aims to clarify and improve the current SH testing methodology and identifies areas where further research is needed, in particular customizing the energy level and plunger diameter and curvature to suit groups of rocks with radically different microstructures.

2 Scope

This revised suggested method focuses on the use of the SH to determine the rebound hardness of rock surfaces both in laboratory conditions and in situ with an emphasis on the use of this hardness value as an index of the UCS and E of rock materials. This revised suggested method supersedes the portion of the earlier ISRM document [1] that dealt with the SH test.

3 Apparatus

3.1 Operational Principle

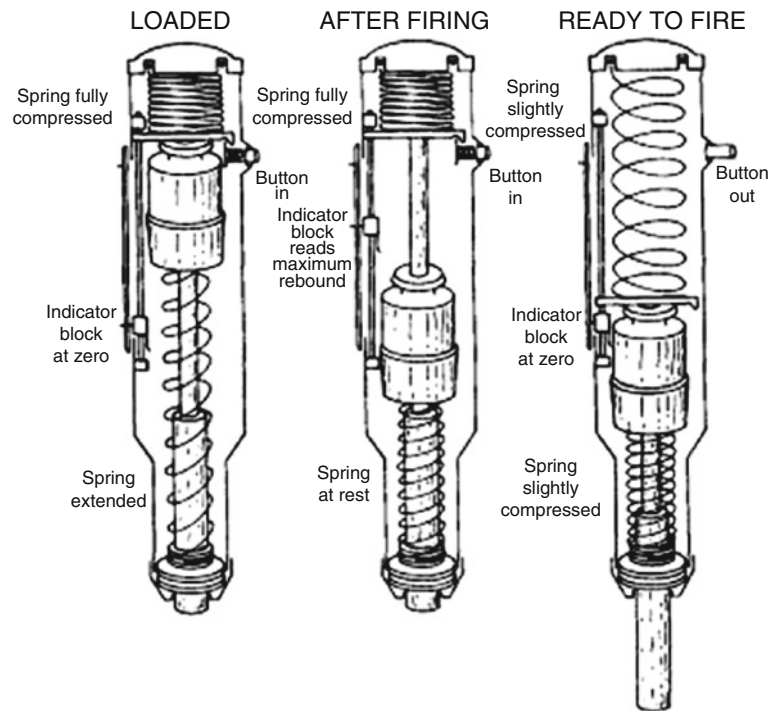
The SH consists of a spring-loaded piston which is released when the plunger is pressed against a surface (Fig. 1). The impact of the piston onto the plunger transfers the energy to the material. The extent to which this energy is recovered depends on the hardness (or impact penetration/damage resistance) of the material, which is expressed as a percentage of the maximum stretched length of the key spring before the release of the piston to its length after the rebound [2].

Please send any written comments on this "ISRM Suggested Method" to Prof. Resat Ulusay, President of ISRM Commission on Testing Methods (resat@hacettepe.edu.tr).

Reprinted from International Journal of Rock Mechanics & Mining Sciences, 46, A. Aydin, ISRM Suggested Method for Determination of the Schmidt Hammer Rebound Hardness: Revised Version, 627–634, 2009, with permission from Elsevier.

A. Aydin (✉)
Department of Geology and Geological Engineering,
The University of Mississippi University, Oxford,
MS 38677, USA
e-mail: aaydin@olemiss.edu

Fig. 1 Working principle of a Schmidt hammer [3]



3.2 Hammer Type, Test Range and Calibration

The earlier ISRM suggested method [1] endorsed the use of only the L-type SH. However, for a given plunger tip diameter and radius of curvature, the impact energy of the SH determines its range of applicability. Accordingly, this limitation should be kept in mind in selecting the hammer type. For instance, the standard L- and N-type hammers, with respective impact energies of 0.735 and 2.207 N m, should be used with caution when the *UCS* of the rock material or discontinuity wall is outside the range of 20–150 MPa, where sensitivity decreases and data scatter increases. The N-type hammer is less sensitive to surface irregularities, and should be preferred in field applications; while the L-type hammer has greater sensitivity in the lower range and gives better results when testing weak, porous and weathered rocks.

The use of different hammer types results in datasets which may not be readily correlated. Although the standard L- and N-type hammers were shown to have demonstrably high correlation coefficients, these correlations may not be equally convincing across the entire *UCS* range because, they are based on the assumption that both types of hammers produce similar modes of indentation at every point of impact [2]. Furthermore, higher impact energy of N-type hammer (corresponding to probing a larger volume of material by a deeper and wider penetration) should reduce scatter in rebound values compared to L-type hammers [2].

SH are supplied with calibration anvils with vertically guided impact points made of steel as hard as that of the

plunger tip (usually Brinell 500 or Rockwell 52 C). It is essential to verify that the hammers maintain their standard rebound values before and after field investigations. In correlation studies, two consistent readings within the predetermined range of rebound from the anvil should be taken before and after testing each specimen. A drift in the calibrated rebound values may suggest that the key spring is losing its stiffness and should ideally be replaced. If this is not possible, a correction factor (*CF*) for the hammer should be calculated [1] and applied to all readings to account for the loss of stiffness:

$$CF = \frac{\text{specified standard value of the anvil}}{\text{average of ten readings on the anvil}} \quad (1)$$

4 Procedure

4.1 Specimen Requirements

Specimens should be intact (free of visible cracks), petrographically uniform and representative of the rock mass domain (identified from cores or exposures) being characterized. Test surfaces, especially under the plunger tip (impact points), should be smooth and free of dust and particles. In the field, a medium-grained abrasive stone can be used for local smoothing of rough surfaces in hard rock.

Fine sandpaper can be used to smooth the surfaces of cores and block specimens, especially when drilling or sawing

produces visible ridges. Cores and blocks should be air dried or saturated before testing. When this is not possible, the degree of moistness of the surface and the specimen as a whole should be recorded as wet, moist or damp.

Cores should be of at least NX size (≥ 54.7 mm) for the L-type hammer and preferably T2 size (≥ 84 mm) for the N-type. Block specimens should be at least 100 mm thick at the point of impact. It is essential that impact energy is not dissipated in the form of wave scatter or cracking because the impact points are too close to the specimen boundaries. In order to provide similar degrees of confinement in all directions, impact points should be one radius away from the nearest end of core specimens and half the thickness away from block boundaries.

Length of cores and surface area of blocks should be large enough to accommodate these suggestions; for example, if a 2 cm spacing of impact points is chosen, a core length of 43.5 cm (for NX size) or a block surface area of 268 cm² (for 10 cm thickness) is required to gather 20 readings.

The test is generally nondestructive for rocks of at least moderate strength (>80 MPa), and the same sample can be used for the determination of the *UCS* and *E*. However, potential microcracking, grain crushing and pore collapse in friable, porous and weathered rocks necessitate use of different samples.

4.2 Test Requirements

4.2.1 Relative Direction of Impact

Unless the hammer impact direction remains roughly perpendicular to the tested surface, there is a danger of frictional sliding of the plunger tip, material removal by chipping and a partial transfer of energy to and from the hammer. It is therefore essential that the hammer be held at a right angle to the tested surface using a guide tube similar to that used by Aydin and Basu [2], to ensure that the deviation does not exceed $\pm 5^\circ$ [1]. It is suggested that a standard guide tube be manufactured and supplied with the SH.

4.2.2 Normalization of Rebound Values with Reference to Horizontal Impact Direction

The analytical normalization function defining the equivalent rebound value in the horizontal direction has been presented recently by Basu and Aydin [4]. This formulation enables testing in any direction (Fig. 2), especially for in-situ applications (e.g. testing oblique discontinuity surfaces and circular tunnel walls), provided that the direction is accurately recorded. It is suggested that a mechanical or digital angle measuring device be supplied as an attachment by the manufacturers of the Schmidt hammers.

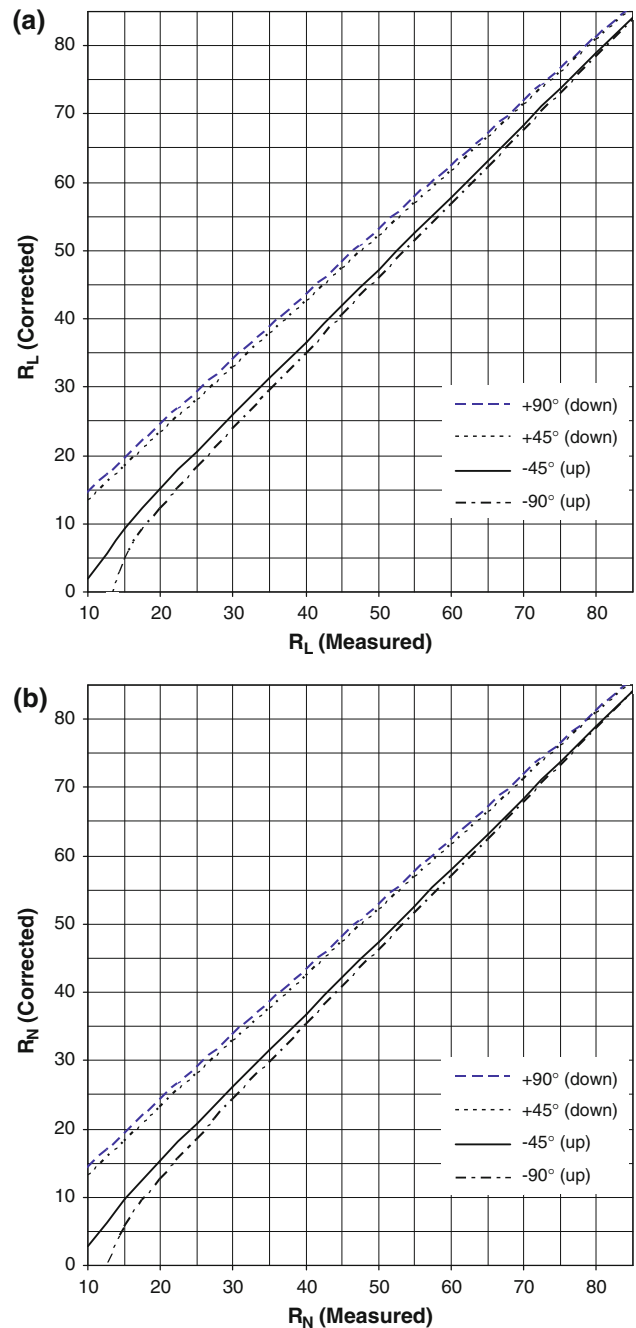


Fig. 2 Normalization of rebound values obtained by **a** L- and **b** N-type Schmidt hammers at selected angles [4] (Positive and negative angles refer to the downward and upward positions of the SH, respectively)

4.2.3 Specimen–Steel Base–Ground Interface

Specimens should be securely clamped to a steel base (with a minimum weight of 20 kg for the L-type hammer and 40 kg for the N-type hammer) located on firm, flat ground. Core specimens should be placed in an arc-shaped machined slot as shown in Fig. 3. V-shaped slots should be avoided particularly in weak rocks because the unsupported

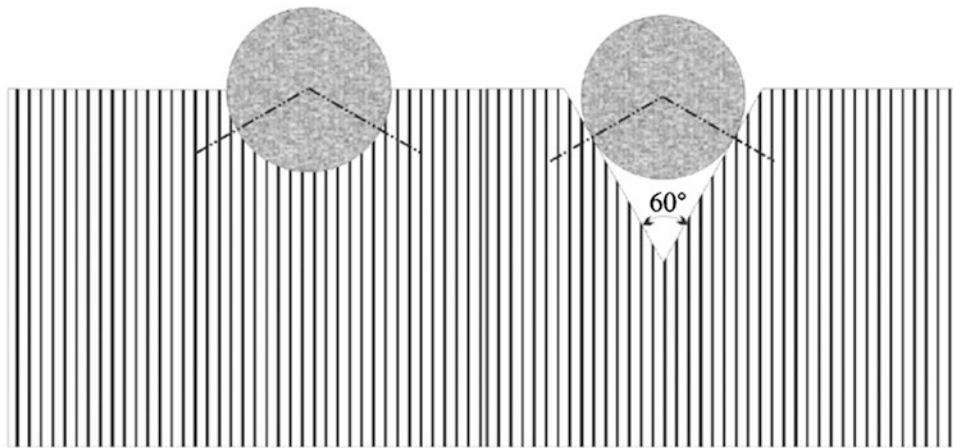


Fig. 3 Cross sections of steel-base blocks with the arc- and V-shaped machined slots in which NX size (54.7 mm) core specimens are seated. (While the use of V-shaped slots is discouraged, if used, the slots

should have the specified angle to ensure identical seating positions for different diameter specimens. Also note that an arc angle of 120° is sufficient for similar lateral confinement as in V-shaped slots.)

section of the core surface falls directly below the impact point, effectively changing the loading configuration and potentially reducing rebound value.

4.3 Data Gathering and Reduction

For data gathering, 20 rebound values, as recommended by the earlier ISRM suggested method [1], should be recorded from single impacts separated by at least a plunger diameter (to be adjusted according to the extent of impact crater and radial cracks). On the other hand, the test may be stopped when any ten subsequent readings differ only by four (corresponding to SH repeatability range of ± 2).

When sufficient quantities of microstructurally uniform specimens are not available and the rock is isotropic, several sets of readings can be taken from different faces of the blocks or along any four straight lines by rotating the core axis 90° at a time. Should this be the case, the set of readings should be given in the corresponding order and any consistent reduction from the first set of measurements (e.g., due to impact-induced cracking) should be carefully monitored.

As the *UCS* and *E* values of a material are strongly influenced by the density, distribution and connectivity of its weak microstructural elements, low and high rebound readings are equally necessary to reflect the nature of heterogeneity and potential spread in the values of mechanical properties. Therefore, no reading should be discarded, and the *mean* (arithmetic average), *median* (middle value), *mode* (most repeating value) and *range* of the readings should be presented to fully express the variations in the surface hardness. Digital images of the test area before and after each impact will provide a more meaningful base for the analysis of these statistics and eliminate the need for recording detailed description of damage features such as

grain crushing, pore collapse, radial and lateral cracking. An in-depth analysis of the *UCS* or *E* versus *R* correlations is presented in Appendix A.

In field applications, the operator should also record the approximate dimensions of tested blocks (the depth being the length of the block free of visible cracks or thin soft layers in the impact direction), their nature (e.g., discontinuity wall, blasted or mechanically broken block), any small scale roughnesses (asperities) of the original surface and how the impact points were smoothed.

5 Influencing Factors

5.1 Relative Strength of Coarse Grains Versus Matrix

The size and distribution of grains and the relative strength of the matrix has a considerable influence on the degree of scatter of rebound values [2]. When a surface contains grains with sizes comparable to the plunger tip diameter, the readings from these grains may significantly deviate from the average, depending on their strength relative to the matrix or dominant grain size. In such cases, impact points should be selected to obtain rebound values from individual coarse-grains and matrix separately. Averaging the rebound values of these components may result in an erroneous determination of hardness.

5.2 Weathering and Moisture Content

Microstructural changes induced by weathering result in different response mechanisms, especially in crystalline igneous rocks, and significantly different rebound values.

Differential weathering of different rock forming minerals enhances heterogeneity at grain scale, which in coarse-grained rocks results in a large scatter of rebound values. It is therefore crucial that samples are uniform in terms of overall weathering degree and detailed petrographic description.

When test samples or individual surfaces display variable degrees of weathering, the decrease in rebound value from the first to the second impact at the same point may be taken as a mechanical index of weathering, as demonstrated by Aydin and Basu [2].

Moisture content of the rock within the zone of influence of impact may considerably affect the rebound values depending on its microstructural character. Moisture facilitates inter-grain sliding and leads to softening of grains and loose skeletal bonding (plasma) holding the grains together. These mechanisms are most effective in weathered, porous, loosely cemented and/or mud rocks but may also be significant in fresh crystalline rocks with abundant intra-grain microcracks. When the purpose of the SH tests is to derive correlations between UCS and/or E and rebound values, all tests should be carried out at the same moisture content. However, low permeability rocks should preferably be tested at dry state due to the difficulty in achieving uniform saturation. It should also be noted that the influence of moisture on elastic surfaces is greatest at a depth equal to about half of the contact radius beneath the contact point where the yielding starts (refer to Appendix A for the relevant aspects of Hertzian theory).

5.3 Anisotropy

Planes of anisotropy in laminated and schistose rocks such as shale, slate, phyllite and schist control the response to impact and loading. The rebound values are strongly reduced when the impact direction is normal to such planes as they absorb impact energy whereas the UCS and E values steeply decrease at oblique angles of anisotropy. Therefore, the use of SH in such rocks is not recommended unless intact slabs thicker than 10 cm and free of such features are available. In any case, the direction of hammer impact with reference to such features should be recorded and correlations with the UCS and E should be attempted only for the same direction of loading.

5.4 Field Versus Laboratory Testing

Because of the difficulty of determining the presence of cracks and other discontinuities directly under the impact points and of clamping the blocks to a firm base in the field, the possibility of vertical deformation and vibration at such interfaces when testing laminated, exfoliated, weathered or

closely fractured rocks directly on the exposed surfaces should be avoided. In rocks such as coal, shale and slate, testing over lamination walls may produce a narrow range of rebound values due to their uniform and naturally smooth nature, but also significantly low values due to these interfaces. However, in most cases, the degree of scatter will increase and the average magnitude of rebound values will decrease in field testing. On the other hand, laboratory tests suffer from limited dimensions of the core and block specimens. The influence of specimen geometry, boundary distance (defining lateral confinement) and small-scale roughness on the rebound values needs to be investigated using uniform synthetic materials of different hardness and elastic-plastic properties.

5.5 Testing Discontinuity Walls

ISRM [5] states that “The Schmidt test is one of the few tests ... which takes into account the mechanical strength of the thin band of weathered wall material close to a discontinuity surface”. The SH presents a unique means of estimating the UCS of the discontinuity walls, and thus, calculating their shear strength in situ [5]. In spite of this, testing procedures for discontinuity walls have not been well-defined due to the difficulty of assigning relative contributions of the natural discontinuity wall features to their shear strength. Small asperities (especially on freshly exposed joints), thin bands of weathering (of joints in shallow and exposed rock masses), coating and filling materials (of hydrothermal and superficial origin), and thin loose slabs (especially in shear zones and exfoliated surfaces) are common features of discontinuity walls that influence the rebound values and the shear strength in different proportions. As these features are generally non uniform across the surface, a wide range of rebound values should be expected. Determining and presenting this scatter is therefore crucial for the subsequent interpretation of the possible range of the shear strength.

In general, to preserve the loose thin layers, discontinuity walls (unlike intact rock) should not be polished. On the other hand, small asperities might cause a significant reduction in the rebound values but do not substantially contribute to the shear strength of clean freshly exposed non planar joints. Accordingly, such joint walls should be lightly polished to eliminate these small scale weak projections. It is, however, most sensible and straightforward to gather two sets of data before and after polishing the discontinuity surfaces that enables calculation of the upper and lower bound values of their shear strength. The data reduction procedure recommended for intact rock (Sect. 4.3) should be followed to obtain representative rebound values of discontinuity walls.

6 Further Improvements

Contact mechanics theory and experiments show that plunger diameter and shape significantly influence the rebound values in metals. Static indentation experiments by Momber [6] confirmed that large diameter and blunt indenters promote elastic response in rocks. Although present correlations claim significant success in predicting the *UCS* and *E*, it is essential that rock response to impact and static loading takes place in the same domain, i.e. elastic or elastoplastic. Differences in this response may be responsible for some seemingly erratic scatters (an aspect which is worth investigating with a view to determining the appropriate plunger tip radius to provide guidelines for the manufacturers).

The modulus of elasticity (*E*), Poisson's ratio (ν) of the plunger material and the radius of curvature of the plunger tip (*r*) should be provided by the manufacturers to enable delineation of the contact radius (*a*) depth of indentation (δ) and mean pressure (p_m) under the contact point. These parameters in turn enable theoretical estimation of the rebound value at which the yield initiate from the ratio of work done to the impact energy (input) of a given hammer type. The tip radius (*r*) required for the onset of yield at a given indenter-rock system modulus (*E*^{*}) can also be estimated. As the purpose is to limit the response of rock to the elastic domain, SH should be flexibly designed to enable the piston mass and/or the stiffness or the stretch of the key spring to be changed to control the impact energy.

Field applications in particular require an angle measuring device while testing core specimens requires a standard steel base with an arc-shaped machined slot (for seating of core specimens) and clamps to secure the specimens (core or slab type specimens).

The initially smooth and hemispherical plunger tips become rough with repeated impacts and gradually lose their curvature. This deterioration modifies the initial contact area and may result in a decrease of rebound values on rock surfaces but may not cause noticeable changes in the anvil. Therefore, potential influence of plunger tip deterioration on rebound values from rock surfaces needs to be investigated.

The potential influence of specimen shape and size on rebound values has not been systematically investigated in rocks due to practically endless variations in their microstructural nature, and hence, difficulty of isolating any pattern that may exist. It is suggested that influence of specimen shape and size be investigated using uniform rock types and equivalent synthetic materials and establish correction factors if necessary.

7 Reporting of the Results

The test report should include the following information:

- (a) Lithological description of the rock (preferably in the order of strength, color, texture/fabric, weathering/alteration, ROCK NAME with grain size as prefix).
- (b) Geographic location and depth of sampling or *in-situ* rock faces.
- (c) Date of sampling or excavation and testing, and storage conditions or climate (i.e. exposure to temperature extremes, humidity, etc.).
- (d) Specimen or face number.
- (e) Specimen type (core, saw-cut block, large field block, excavation face, natural exposure).
- (f) Method of excavation or block production (e.g. blasting, ripping, mechanical splitting, boring)
- (g) Dimensions of specimens or exposure surfaces.
- (h) Sample moisture during testing (water content % or in descriptive terms such as dry, moist, damp).
- (i) Hammer type (L-, N- or another type).
- (j) Use and nature of clamping and steel base support.
- (k) Orientation of hammer axis (impact direction) with reference to horizontal (in degrees, downward being +90° and upward -90°).
- (l) Orientation of hammer axis with reference to intact rock anisotropy features (e.g. lamination, foliation, schistosity, lineation).
- (m) Histogram of 20 rebound readings (normalized to horizontal impact direction and ordered in descending value), and the mean, median, mode and range statistics (the mean values should be rounded off to the nearest integer).
- (n) Photographs (or description) of impact points before and after damage.

Acknowledgments The revised suggested method was based on a study supported by a grant from the Research Grants Council of the Hong Kong Special Administrative Region, China (Project No. HKU 7143/06E). The author would like to thank Resat Ulusay for his encouragement, and Don Banks for his meticulous review of the paper.

Appendix A: *UCS* and *E* Versus Rebound Value Correlations in the Light of Indentation Mechanisms

As the number of studies proposing new correlations estimating the uniaxial compressive strength (*UCS*) and the modulus of elasticity (*E*) of intact rock based on the SH rebound hardness determination are rapidly increasing, it is important for the users of these correlations to be aware of the

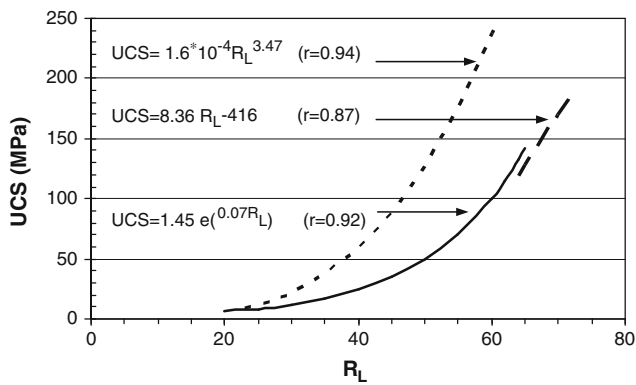


Fig. A.1 Comparison of predictions of the uniaxial compressive strength (UCS) of granites based on their rebound hardness values (R_L) using the L-type hammer. (Dotted [7]—Grade I–IV; dashed [8]—Grade I; solid [2]—Grade I–IV)

fact that high correlation coefficients presented in these studies do not necessarily guarantee better point estimates. Contrary to common assumption, the scatter in the original datasets of these correlations may be such that correlation coefficients for smaller ranges of rebound values may actually be lower than those for wider ranges. It should also be noted that the type of correlation functions varies with the range for which the correlations are established. This appendix is aimed to provide an insight into the nature of these correlations in the light of indentation mechanisms and help users to select appropriate functions and interpret them for their particular cases.

Three correlation functions (Fig. A.1) were selected from the literature to facilitate this discussion. All three functions were derived for variably weathered granites using the L-type hammer. Striking differences in these correlations (Fig. A.1) may be partly due to different testing, data gathering and reduction procedures adopted in these studies as well as different microstructures of the granites tested. For example, Hong Kong granites [2] had noticeably high microcrack densities even at fresh state resulting in lower UCS values than those of hydrothermally altered granites of Southwest England [7].

Interestingly, the linear correlation proposed in [8] for a wide variety of fresh to slightly weathered granitic rocks from Turkey is quite consistent with the trends of the other correlations in the same UCS range. Thus at the outer ends of the rock weathering spectrum (Grade I–IV) when the microstructures are relatively uniform, linear correlations may be expected. The fact that most of the linear correlations were proposed for coal [2] proves the role of microstructural consistency as well as surface smoothness in shaping these correlations.

The presence of two different linear correlation domains joined with a transitional domain suggests that indentations mechanisms change as rock microstructure is altered through weathering processes. Understanding how these

mechanisms operate or how different microstructures control these mechanisms are crucial in selecting most appropriate data gathering and reduction methods and improving plunger tip shape and diameter in order to develop better correlations with well-delineated ranges of applicability.

Momber [6] applied classical Hertzian contact mechanics theory [9] to explain different modes of indentation of four rock types (granite, rhyolite, limestone and schist) by two spherical indenters (1.0 and 5.0 mm in diameter) at contact forces between 0.1 and 2.45 kN using a classical Rockwell hardness tester. He observed that elastic response (formation of an array of ring cracks or Hertzian cracks surrounding a damaged core zone) is limited to granite and rhyolite, whereas limestone and schist displayed plastic response. Indentation of limestone surface was in the form of collapse (sink-in) due to its porous structure and that of schist was in the form of pile-up (characterized by wall formation around periphery of the plunger tip, presumably due to sliding along the schistosity planes). However, according to Hertzian theory, yielding starts at a depth equal to about half of the contact radius beneath the contact point, and thus most of the deformation may be hidden in the elastic-to-plastic transition domain. Static hardness tests might also result in different indentation modes than impact tests. For example, grain crushing and fragmentation is a common occurrence under impact, especially when grains are coarse and/or weak, and plastic flow (pile-up) behavior is not observed unless the material is highly viscoelastic.

Taking such differences into account, it is now possible to interpret the nonlinear nature of most UCS versus R correlations more systematically. Looking at Fig. A.1 again, it becomes obvious that in the lower end of the weathering spectrum, where rock porosity substantially increased due to leaching and feldspar grains are at least partly weakened by pseudomorphic replacement by clay [10], indentation is mainly through the collapse of the pore space and grain crushing. In the upper end of the spectrum, the linear response is caused by the domination of an elastic-brittle response at the grain scale. The degree of scatter is also expected to be lesser in the elastic domain. In the transitional region, the response to hammer impact is mixed (elastoplastic) and the scatter is bound to be much larger than both domains.

A.1 Guidelines for the Correlations

From the preceding discussion, it becomes obvious that correlations should ideally be established for a given rock type whose response falls within a single response domain. Nonlinear correlations simply indicate significant microstructural changes in that seemingly identical rock type. This is well-illustrated in Fig. A.1 for weathering-induced

microstructural changes in granite. When the aim is to derive a generic correlation function involving a large group of rock types (e.g. carbonates, mudrocks) it is essential to ensure that there are no large gaps across the entire range and all distinct microstructural varieties of each rock type are represented.

In terms of data gathering and reduction procedures, it also becomes evident that averaging single impact readings is the only rational approach. Note that data gathering procedures based on multiple (or repeated) impact at a single point alter the original microstructure of the test surface resulting in the loss of invaluable information.

The UCS or E versus R correlations should be established using the mean rebound value using the entire set of measurements. The structure of each rebound value data set reflects the nature of surface heterogeneity and it is not immediately obvious which microstructural element or feature (corresponding to average, median or most repeated rebound value) controls or dominates UCS and E of the corresponding rock. Therefore, median and mode (with the number of repetition) values should also be plotted along the range bars on the correlation graphs to facilitate interpretation of overall significance of the correlation and potential variability in UCS and E values of each sample.

On the other hand, the UCS and E of a given rock type are highly sensitive to slight changes in its microstructural state (e.g. degree and style of weathering, density and orientation of microcracks, grain size distribution, mineralogy). However, a systematic analysis of the potentially large variability in these basic mechanical properties is not always feasible due to the difficulties of laboratory testing (justifying the search for indirect predictions using index tests). As a result, in establishing correlations (especially those involving a mixture of rock types), only a few UCS or E values are often available to represent full range of variability in each rock type. This important limitation in constraining potential scatter in UCS and E values can be partly offset by careful evaluation of the variability in rebound values, which should be depicted on the correlation plots by range bars. The reliability of the correlation coefficient and variance can also be better evaluated in this context.

For the identification of weathering grade in granites, Aydin and Basu [2] showed that changes in rebound values between first and second impact provide the best correlation. This procedure is supported in the light of the indentation mechanisms discussed above.

In order to capture overall trends among different rock types or across the weathering spectrum of a given rock type, one of the following pairs of generalized expressions can be used to establish the UCS and E versus rebound value (R) correlations [2]:

$$UCS = ae^{bR}, \quad E_t = ce^{dR} \quad (A.1)$$

$$UCS = aR^b, \quad E_t = cR^d \quad (A.2)$$

where a , b , c and d are positive constants that depend on the rock type. However, as a final note on the validity of generalizing expressions for a mixture of rocks or for a given rock across the weathering spectrum, Aydin and Basu [2] cautioned that these correlations are valid "assuming similar style and sequence of microstructural changes". This is probably the key consideration in selecting appropriate functions for estimating point values of the UCS and E , and hence, such generalized expressions are not recommended for use in practice when more specific expressions becomes available for the corresponding rock microstructures.

It was demonstrated that when the SH tests are conducted using the recommendations outlined in this suggested method, the rebound values (R) obtained by using standard L- and N-type Schmidt hammers are almost perfectly correlated with a very limited scatter for the range of $R_L > 30$ or $R_N > 40$ [2]:

$$R_N = 1.0646 R_L + 6.3673 (r = 0.99) \quad (A.3)$$

Note, however, that this relationship has been derived on granitic core samples with relatively smooth surfaces in laboratory conditions and the degree of correlation and data scatter may be expected to deteriorate in case of field applications and testing weak porous rocks due to the differences in the impact energies.

References

1. ISRM. Suggested methods for determining hardness and abrasiveness of rocks. In: Brown ET editor. Rock characterization, testing and monitoring: ISRM suggested Methods. Oxford: Pergamon; 1981. p. 95–6.
2. Aydin A, Basu A. The Schmidt hammer in rock material characterization. Eng Geol 2005;81:1–14.
3. McCarroll D. The Schmidt hammer as a measure of degree of rock surface weathering and terrain age. In: Beck C editor. Dating in exposed and surface contexts. Albuquerque: Univ New Mexico Press; 1994. p. 29–45.
4. Basu A, Aydin A. A method for normalization of Schmidt hammer rebound values. Int J Rock Mech Min Sci 2004;41:1211–4.
5. ISRM. Suggested methods for the quantitative description of discontinuities in rock masses. In: Brown ET editor. Rock characterization, testing and monitoring: ISRM suggested Methods. Oxford: Pergamon; 1981. p. 3–52.
6. Momber AW. Deformation and fracture of rocks loaded with spherical indenters. Int J Fract 2004;125:263–79.
7. Dearman WR, Irfan TY. Assessment of the degree of weathering in granite using petrographic and physical index tests. In: Proceeding of the international symposium on deterioration and

- protection of stone monuments. Paris: Unesco; 1978. p. 1–35 (paper 2.3).
8. Tugrul A, Zarif IH. Correlation of mineralogical and textural characteristics with engineering properties of selected granitic rocks from Turkey. *Eng Geol* 1999;51:303–17.
 9. Johnson KL. *Contact mechanics*. Cambridge: Cambridge Univ Press; 1985.
 10. Aydin A, Duzgoren-Aydin NS. Indices for scaling and predicting weathering-induced changes in rock properties. *Env Eng Geosci* 2002; 8:121–35.

Suggested Methods for Determining the Dynamic Strength Parameters and Mode-I Fracture Toughness of Rock Materials

Y. X. Zhou, K. Xia, X. B. Li, H. B. Li, G. W. Ma, J. Zhao, Z. L. Zhou, and F. Dai

1 Introduction

The properties of rocks under dynamic loading are important for the study of a whole range of rock mechanics and rock engineering problems, including blasting, protective design, explosives storage, rock bursts and seismic events. The propagation of dynamic stress waves in the ground, response of rock tunnels to dynamic load, dynamic support design and damage assessment all require a good understanding of the behavior of rocks under dynamic loading.

Please send all written comments on these ISRM Suggested Methods to Prof. R. Ulusay, President of the ISRM Commission on Testing Methods, Hacettepe University, Geological Engineering Department, 06800 Beytepe, Ankara, Turkey at resat@hacettepe.edu.tr.

Reprinted from International Journal of Rock Mechanics and Mining Sciences, 49, Y. X. Zhou, K. Xia, X. B. Li, H. B. Li, G. W. Ma, J. Zhao, Z. L. Zhou, F. Dai, Suggested Methods for Determining the Dynamic Strength Parameters and Mode-I Fracture Toughness of Rock Materials, 105–112, 2012, with permission from Elsevier.

Y. X. Zhou
Defence Science and Technology Agency, Singapore, Singapore

K. Xia (✉) · F. Dai
Department of Civil Engineering, University of Toronto, Room GB 314A, 35 St. George Street, Toronto, ON M5S 1A4, Canada
e-mail: kaiwen@ecf.utoronto.ca; kaiwen.xia@utoronto.ca

X. B. Li · Z. L. Zhou
School of Resources and Safety Engineering, Central South University, Changsha, China

H. B. Li
Institute of Rock and Soil Mechanics, The Chinese Academy of Sciences, Wuhan, China

G. W. Ma
School of Civil and Resource Engineering, University of Western Australia, Crawley, Australia

J. Zhao
Laboratory for Rock Mechanics, Ecole Polytechnique Federale de Lausanne, Lausanne, Switzerland

Due to the transient nature of dynamic loading, the dynamic tests of rock material are very different from static tests.

The Suggested Methods for Determining Dynamic Strength Parameters and Mode I Fracture Toughness of Rock Materials were prepared by the International Society for Rock Mechanics (ISRM) Commission on Rock Dynamics, chaired by Yingxin Zhou (Coordinators: Yingxin Zhou, Kaiwen Xia and Xibing Li; Contributing authors: H.B. Li, G.W. Ma, J. Zhao, Z.L. Zhou and F. Dai).

The ISRM Commission on Rock Dynamics was established in 2008. One of its terms of references was to develop suggested methods for the dynamic testing of rocks. The commission organized a workshop on rock dynamics at the Swiss Federal Institute of Technology at Lausanne (EPFL) in June 2009, where the commission agreed on the work plan for drafting the Standard Method (SM) for rock dynamic testing. A second workshop was held at the Institute of Rock and Soil Mechanics, Chinese Academy of Sciences, in Wuhan, China, in December 2010, where the drafted SM was discussed and finalized after extensive consultations with members of the ISRM Commission on Testing Methods. The coordinators acknowledge the valuable comments and reviews by the members of the ISRM Commission on Testing Methods chaired by Prof. Resat Ulusay. Prof. Guruswami Ravichandran and Prof. Weinong Chen are acknowledged for their constructive and valuable comments to this work.

2 Part 1: Suggested Method for Determining the Dynamic Uniaxial Compressive Strength of Rock Materials with SHPB

2.1 Scope

This test method is intended to measure the dynamic uniaxial compressive strength of a rock specimen in the form of a cylindrical shape. The test is mainly intended for dynamic strength classification and characterization of intact rocks.

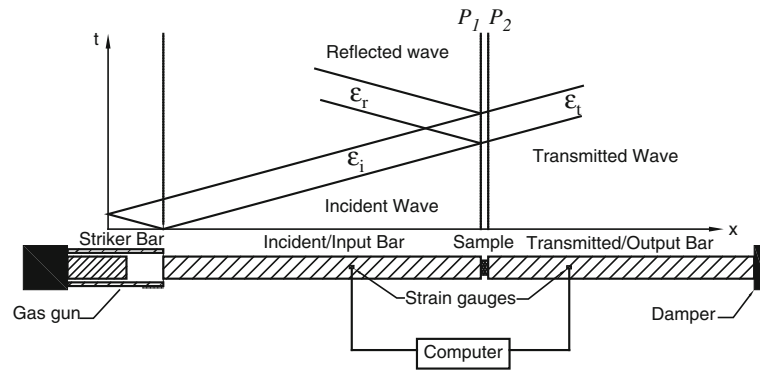


Fig. 1 Schematics of SHPB (ϵ denotes strain, and the subscripts i , r and t refer to the *incident*, *reflected* and *transmitted* waves, respectively. P_1 and P_2 are the dynamic force on the incident bar-sample interface and transmitted bar-sample interface, respectively)

2.2 Apparatus

- (a) A standard Split Hopkinson Pressure Bar (SHPB), as shown in Fig. 1, consists of a striker bar, an input bar, an output bar, a damper, a gas gun and a data acquisition unit [1–3]. The bars are made of high-strength steels. The specimen is sandwiched between the input and output bars. The impact of the striker bar on the incident bar produces an incident wave (ϵ_i). The interaction of the incident wave with the sample results in a reflected wave (ϵ_r) and a transmitted wave (ϵ_t). These waves are recorded by the strain gauges mounted on the incident bar and transmitted bar.
- (b) The diameter of the bars should be slightly larger than the diameter of the rock specimen. The length for input/output bar should be at least 30 times of the bar diameter to satisfy the one dimensional stress wave propagation theory. The length of the striker bar is chosen to vary the duration of the loading pulse.
- (c) In conventional SHPB experiments for metals, the incident wave generated by the direct impact of the striker on the incident bar is of a rectangular shape with high frequency oscillation. At the initial stage of the loading, the dynamic forces are unbalanced. To achieve dynamic force balance, a cone-shaped striker can be used to generate a ramped (half sine) incident wave. Figure 2 shows a striker bar works in a 50 mm diameter SHPB system [4].
- (d) An alternative choice to generate a ramped loading pulse is to use pulse-shaper [1]. The pulse-shaper technique is relatively easy to implement and applicable to different material bars. The pulse-shaper is a small thin disk made of soft material, such as pure copper, rubber or paper. It is placed on the impact end of the incident bar. During tests, the striker impacts the pulse-shaper before the incident bar, thus generating a non-dispersive ramp pulse propagating into the

incident bar and thus facilitating the dynamic force balance of the specimen. The dynamic force balance validates the static stress analysis in the specimen. Materials and dimensions of the pulse shaper should be carefully chosen before tests and depicted in the final report of the results [5].

- (e) A pair of strain gauges should be glued diametrically at the middle section of the input bar and the output bar to measure the incident wave, the reflected wave and the transmitted wave. High precision dynamic strain gauge with length around 2 mm is recommended.
- (f) The data acquisition rate should be around 2 millions points per second and the bandwidth of the recording system should be around 100 kHz. The data precision should be around 10 bit.

2.3 Specimen Description

Specimens should be cored from the same rock block with no visible geological weakness. Specimens should be intact, petrographically uniform and representative of the rock mass domain being characterized. The diameter of the specimen should be close to 50 mm or at least 10 times the average grain size in the rock. The length to diameter ratios of 1:1 and 0.5:1 are recommended for small and large samples, respectively [5].

2.4 Procedure

Grinding machine should be used to ensure that ends of the specimen are smooth and parallel [6]. The ends of the specimen shall be flat to 0.02 mm and shall not depart from perpendicularity to the axis of the specimen by more than 0.001 rad or 0.025 mm in 25 mm.

The side surface of the specimen shall be smooth and free of abrupt irregularities and straight to within 0.02 mm

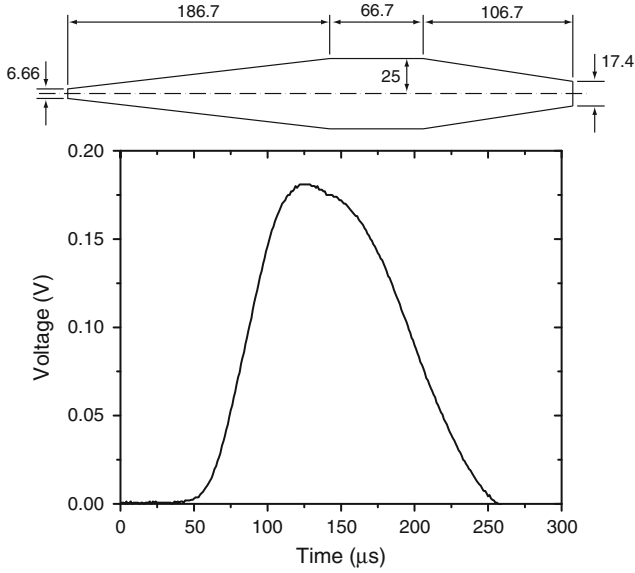


Fig. 2 Geometry of a cone-shaped striker (unit in mm) and the incident stress wave produced

over the full length of the specimen. Ultrasonic velocity should be measured to choose specimen with similar velocity for the same group. The number of specimens per sample tested should be determined from practical considerations, but normally 30 tests are recommended to cover a wide dynamic loading range.

2.5 Calculation

With captured signals, incident, reflected and transmitted waves can be extracted, as shown in Fig. 3. The point of failure is identified in the reflected wave, where the sudden increase of the signal occurs. This increase is due to the failure and thus the loss of load-bearing capacity of the specimen [7].

Using incident, reflected and transmitted waves, the stress, strain and strain rate of specimen can be derived as

$$\sigma(t) = \frac{AE}{2A_s} [\varepsilon_i(t) + \varepsilon_r(t) + \varepsilon_t(t)] \quad (1)$$

$$\varepsilon(t) = \frac{C}{L_s} \int_0^t [\varepsilon_i(t) - \varepsilon_r(t) - \varepsilon_t(t)] dt \quad (2)$$

$$\dot{\varepsilon}(t) = \frac{C}{L_s} [\dot{\varepsilon}_i(t) - \dot{\varepsilon}_r(t) - \dot{\varepsilon}_t(t)] \quad (3)$$

In these equations, $\sigma(t)$ is the axial compressive stress of the sample, A is the cross sectional area of the bar, E is the Young's modulus of the elastic bars, C is the 1D elastic bar

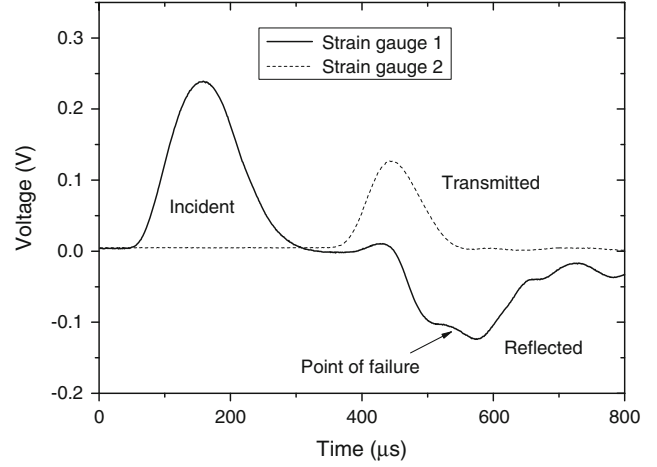


Fig. 3 Incident, reflected and waves transmitted captured in a typical test

wave speed and A_s and L_s are the cross-sectional area and length of the specimen, respectively. ε denotes strain, and the subscripts i , r and t refer to the incident, reflected and transmitted waves, respectively.

Furthermore, the dynamic forces on the incident bar-sample interface (P_1) and the transmitted bar-sample interface (P_2) are

$$P_1 = AE(\varepsilon_i + \varepsilon_r), \quad P_2 = AE\varepsilon_t \quad (4)$$

Equations (1)–(3) are derived based on the following assumptions:

- Propagation of elastic waves through the input and output bars can be described by one-dimensional stress wave theory. This can be fulfilled approximately with the suggested bar dimensions.
- Specimen reaches stress equilibrium before failure. This can be checked by comparing the stress histories at the two ends of the specimen (i.e., $P_1 \approx P_2$ or $\varepsilon_i + \varepsilon_r \approx \varepsilon_t$, as in Fig. 4a).
- Friction and axial inertia effects on the specimen can be ignored. This can be approximately satisfied with the suggested system and testing procedures [5].

An approximate uniform deformation of the rock sample is a prerequisite of a valid dynamic uniaxial compression test [5]. To meet this requirement, the dynamic stresses on both ends of the sample should be roughly identical. This can be checked by comparing the stress histories on both ends of the sample during the dynamic tests. Figure 4a illustrates the dynamic stress balance on both ends of the sample for the typical test shown in Fig. 3. It is clear that in this test, the uniformity of the dynamic stress across the sample has been achieved and thus the axial inertial effect has been reduced to a negligible level. With dynamic stress balance, the stress–strain curve of rocks can be obtained (Fig. 4b) using Eqs. (1–3).

Fig. 4 **a** Dynamic stress balance (In: Incident wave, Re: Reflected wave, Tr: Transmitted wave), **b** determination of loading rate

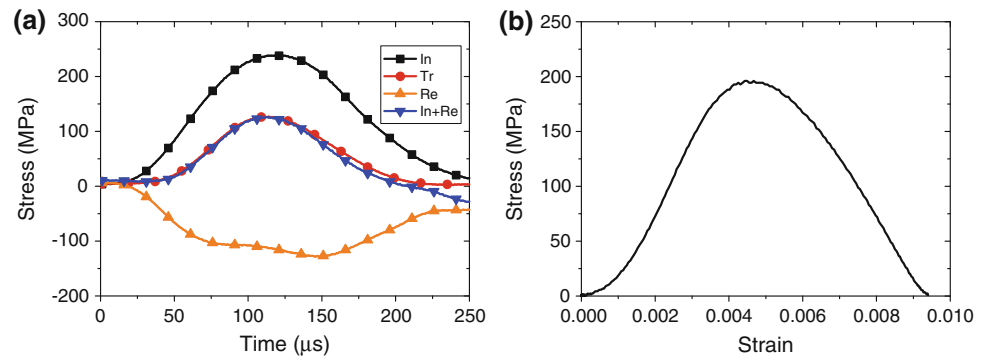
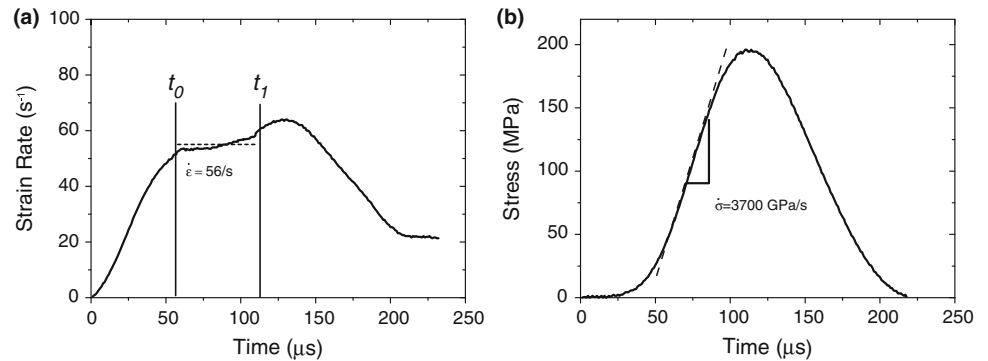


Fig. 5 Determination of **a** the strain rate and **b** the loading rate for the dynamic compressive test (The vertical line in **a** indicates the point of failure)



The dynamic loading of a test is usually characterized by the strain rate. The strain rate history is determined using Eq. (3) as shown in Fig. 5a. The time for the sample to reach a stress equilibrium state is about three times of the round-trip of stress wave in the sample and this time is denoted as t_0 . The failure time instance is t_1 . The strain rate for the test is thus the average strain rate level between t_0 and t_1 . The failure time can be determined as the peak load (Fig. 4a) or as the sudden jump of the strain rate [7]. The sample may reach the stress equilibrium before the constant strain rate, it is thus better to pick the flat region of the curve before the failure point (Fig. 5a). Alternatively, the dynamic loading can also be characterized using the loading rate (Fig. 5b), which is the slope of the curve before the failure point. The loading history shown in Fig. 5b is calculated using Eq. (1). Theoretically, the ratio of the loading rate to the strain rate is the Young's modulus. These two representations of the dynamic loading of the test are thus equivalent as shown in Fig. 5.

The maximum value from Eq. (1) (or the peak value of the stress in Fig. 4b) is the dynamic uniaxial compressive strength of the specimen at average strain rate or loading rate as determined (Fig. 5).

2.6 Reporting of Results

The test report should include the following information:

- Lithologic description of the rock (rock type, color, texture, grain size, weathering and other available information from observation).

- Specimen number and basic parameter of the specimen (diameter, length, seismic wave velocity, density, etc.).
- Test scheme including specimen groups and number of specimen in each group.
- Test signals including incident, reflected and transmitted waves.
- Mode of failure or failure degree of the specimen.
- Stress–strain curve, strain rate and loading histories of the test.
- Dynamic uniaxial compressive strength for each specimen and corresponding strain rate (or loading rate).

3 Part 2: Suggested Method for Determining Dynamic Indirect Tensile Strength of Rock Materials by the Brazil Test

3.1 Scope

This method of test is intended to measure the dynamic tensile strength of the prepared rock specimens indirectly by the Brazil test. The method is intended to extend the ISRM suggested method for determining the static indirect tensile strength by the Brazil test to its dynamic counterpart [5, 8]. The dynamic load is induced by the split Hopkinson pressure bar (SHPB). The test is mainly intended for dynamic strength classification and characterization of intact rocks.

3.2 Apparatus

- An SHPB is used to exert the dynamic load to the disk sample (Fig. 1). The length of the striker bar is chosen to vary the duration of the loading pulse. Based on the one dimensional stress wave theory, the dynamic forces on the incident bar- sample interface (P_1) and the transmitted bar-sample interface (P_2) can be calculated using Eq. (4).
- It is critical to ensure force balance (i.e., $P_1 \approx P_2$) during the dynamic test. The pulse shaper technique is relatively easy to implement and applicable to different material bars. During tests, the striker impacts the pulse shaper before the incident bar, thus generating a non-dispersive ramp pulse propagating into the incident bar and thus facilitating the dynamic force balance of the specimen. The dynamic force balance validates the static stress analysis in the specimen.
- In the static test by the Brazil test suggested by the ISRM, two special steel loading jaws are designed to achieve an arc of contact of approximate 10° at failure of the disk sample [9]. In addition, two adhesive paper strips are used to wrap the sample disk up on its periphery. In dynamic tests using SHPB, these designs will interfere with the wave propagation and thus introduce errors in the results. Given a properly aligned SHPB system, the disk specimen is recommended to be placed between the bars directly [5].

3.3 Specimen Description

The geometry of the Brazil test specimen is shown in Fig. 6. The specimen diameter should be related to the average grain size in the rock by a ratio of at least 10:1 or should be close to 50 mm, and the thickness should be approximately equal to the specimen radius. Smaller specimens are preferred to achieve the dynamic force balance and higher loading rates.

3.4 Procedure

- The test specimens should be cut and prepared using clean water. The cylindrical surfaces should be free from obvious tool marks and any irregularities across the thickness of the specimen should not exceed 0.025 mm. End faces shall be flat to 0.25 mm and parallel to within 0.25° .
- Specimen orientation shall be known and the water content should be controlled or measured and reported in accordance with the ISRM Suggested Method for Determination of Water Content of a Rock Sample [10].

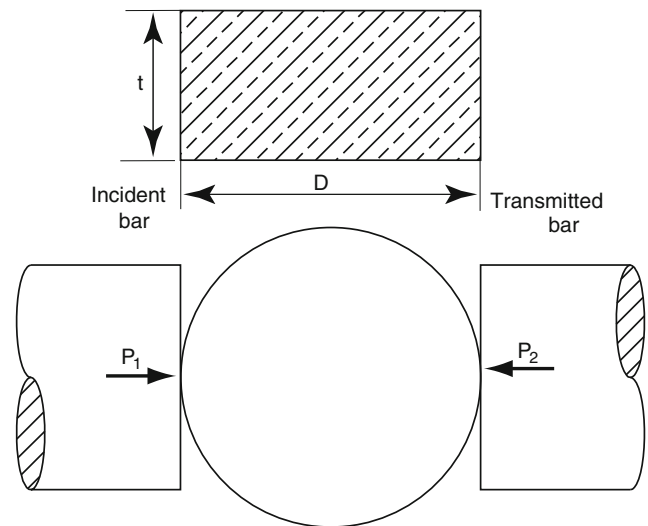


Fig. 6 Schematics of the disk specimen for the Brazil test in a split Hopkinson pressure bar (SHPB) system (D : diameter of the specimen, t : thickness of the specimen. P_1 and P_2 are the dynamic forces on both ends of the sample)

- Load on the specimen shall be applied using an SHPB system where the pulse-shaper technique is used to ensure the dynamic force balance. The loading rate is controlled by varying the impact velocity of the striker bar and the material and the geometry of the pulses shaper.
- The data acquisition rate should be around 2 millions points per second and the bandwidth of the recording system should be around 100 kHz. The data precision should be around 10 bit.
- The number of specimens per sample tested should be determined from the practical considerations, but normally thirty tests are recommended to cover a wide dynamic loading range.

3.5 Calculation

- Verification of the dynamic force balance: Using Eq. (4), the dynamic forces applied on both ends of the sample can be determined. A typical test featuring the dynamic force balance is illustrated in Fig. 7.
- Determination of the tensile stress history at the specimen center: If the dynamic force balance is achieved, the resultant tensile stress at the sample center, $\sigma(\tau)$ can be determined as

$$\sigma(\tau) = 0.636P(\tau)/(Dt) \quad (5)$$

In Eq. (5), τ is the time, $\sigma(\tau)$ is the resultant tensile stress at the sample center, $P(\tau)$ is the loading history, which is determined following standard SHPB data

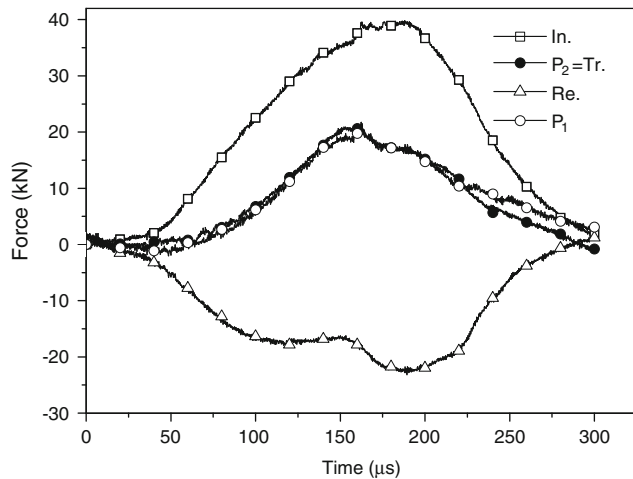


Fig. 7 Dynamic force balance (In: *Incident wave*, Re: *Reflected wave*, Tr: *Transmitted wave*, P_1 : the dynamic force on the incident bar-sample interface and P_2 : the dynamic force the transmitted bar-sample interface)

reduction scheme. D and t are the diameter and thickness of the disk, respectively.

- (c) Determination of the tensile strength: For the static Brazilian test, the tensile strength σ_t is determined as the peak value of $\sigma(\tau)$. This method applies also for the dynamic test because the dynamic force balance has been achieved. The dynamic tensile strength is determined as the peak-load using Eq. (5).
- (d) Determination of the loading rate: The loading rate of the test is determined as the slope of the tensile stress history before the failure onset (Fig. 8). For the case shown in the figure, the loading rate is 1689 GPa/s and the dynamic tensile strength is 40.9 MPa.

3.6 Reporting of Results

- (a) Lithologic description of the rock.
- (b) Orientation of the axis of loading with respect to specimen anisotropy (e.g. bedding planes, foliation. etc.).
- (c) Source of sample, including geographic location, depth and orientation, dates and method of sampling and storage history and environment.
- (d) Seismic wave speeds of the specimen measured using ultrasonic method.
- (e) Number of specimens tested.
- (f) Specimen diameter and thickness.
- (g) Water content and degree of saturation at the time of test.
- (h) Date of testing and details of the testing machine.
- (i) Mode of failure.

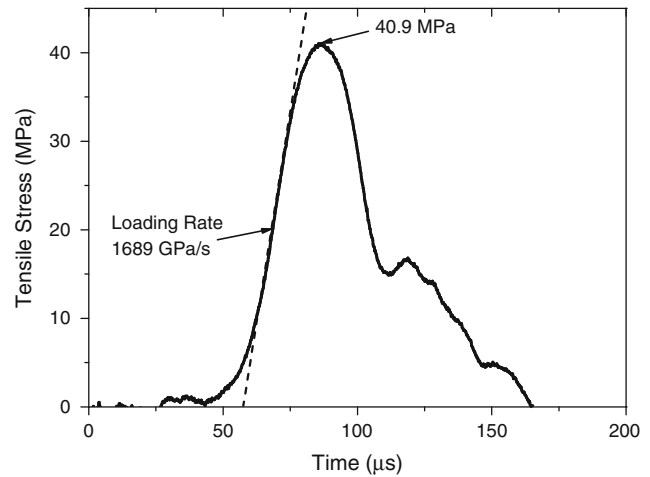


Fig. 8 Tensile stress history

- (j) Any other observations or available physical data such as specific gravity, porosity and permeability, citing the method of determination for each.
- (k) The check for dynamic force balance for each specimen.
- (l) The dynamic loading history of each test and the loading rate.
- (m) The dynamic tensile strength plotted as a function of the loading rate.

4 Part 3: Suggested Method for Determining Dynamic Mode I Fracture Toughness of Rock Materials

4.1 Scope

This method of test is intended to measure the dynamic fracture toughness of a rock sample using the notched semicircular bend (NSCB) specimen [11]. The test is mainly intended for the classification and characterization of intact rock with respect to its resistance to the crack propagation. The dynamic fracture toughness also serves as an index for rock fragmentation processes involving drilling, crushing and tunnel boring or for the analysis of fracturing in rock blasting.

4.2 Apparatus

- (a) SHPB is used to exert the dynamic load to the sample (Fig. 1). The dynamic forces on the incident bar-sample interface (P_1) and the transmitted bar-sample interface (P_2) can be determined using Eq. (4).

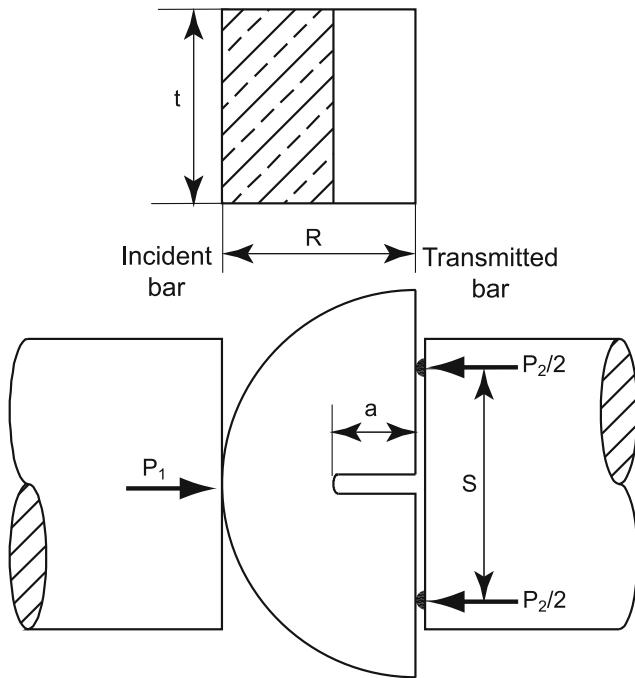


Fig. 9 Schematics of the notched semi-circular bend (NSCB) specimen in the split Hopkinson pressure bar (SHPB) system (R : radius of the specimen, t : thickness of the sample, a : notch length, S : distance between the two supporting pins. P_1 and P_2 are the dynamic forces on both ends of the sample)

(b) It is critical to ensure force balance (i.e., $P_1 \approx P_2$) during the dynamic test. The pulse-shaper technique should be used to generalize a non-dispersive ramp loading pulse to the test, which facilitates the dynamic force balance of the specimen. The dynamic force balance guarantees quasi-static stress analysis of the specimen [11].

4.3 Specimen Description

- (a) The geometry of the NSCB specimen is shown in Fig. 9. The apex of the NSCB specimen is in contact with the incident bar and the diametrical end of the specimen is supported by two pins mounted on the transmitted bar. The specimen diameter should be related to the average grain size in the rock by a ratio of at least 10:1 or should be close to 50 mm, and the thickness should be approximately equal to the specimen radius. Smaller specimens are preferred to achieve the dynamic force balance and higher loading rates.
- (b) All the dimensions of the geometry should be converted into dimensionless with the specimen radius R and diameter $D = 2R$ as: $\alpha_a = a/R$, $\alpha_t = t/R$, $\alpha_S = S/D$. a is the notch length.

4.4 Procedure

- The test specimens should be cut and prepared using clean water. The cylindrical surfaces should be free from obvious tool marks and any irregularities across the thickness of the specimen should not exceed 0.025 mm. End faces shall be flat to 0.25 mm and square and parallel to within 0.25° .
- Specimen orientation shall be known and the water content controlled or measured and reported in accordance with the suggested method for determination of water content of a rock sample [10].
- The disk is then split along the diameter into two semicircular samples. A notch is machined subsequently to the semi-circular sample using a rotary diamond-impregnated saw from the center of the original disk and perpendicular to the diametrical cut. A diamond wire saw should be used to further sharpen the notch-tip into a crack-tip. The radius of the fabricated crack-tip should be less than the average grain size of the rock material.
- Load on the specimen shall be applied using an SHPB system where the pulse-shaper technique is used to ensure the dynamic force balance. The loading rate is controlled by varying the impact velocity of the striker bar and the geometry and material of the pulse-shaper.
- The data acquisition rate should be around 2 millions points per second and the bandwidth of the recording system should be around 100 kHz. The data precision should be around 10 bit.
- The achievable loading rate has a lower bound where the NSCB specimen can be barely broken and a high bound where the initial failure occurs from one of its contacts with the supporting pins, not from the tip of the notch.
- The number of specimens per sample tested should be determined from practical considerations, but normally thirty tests are recommended to cover a wide dynamic loading range.

4.5 Calculation

- Verification of the dynamic force balance: It is a must to ensure that the dynamic forces applied on both sides of the sample are approximately balanced during the entire dynamic loading period. One typical example of dynamic force balance check is illustrated in Fig. 10. Using Eq. (4), the dynamic forces applied on both ends of the sample can be determined.
- Determination of the dynamic fracture toughness: The history of mode-I stress intensity factor (SIF) $K_I(t)$ in

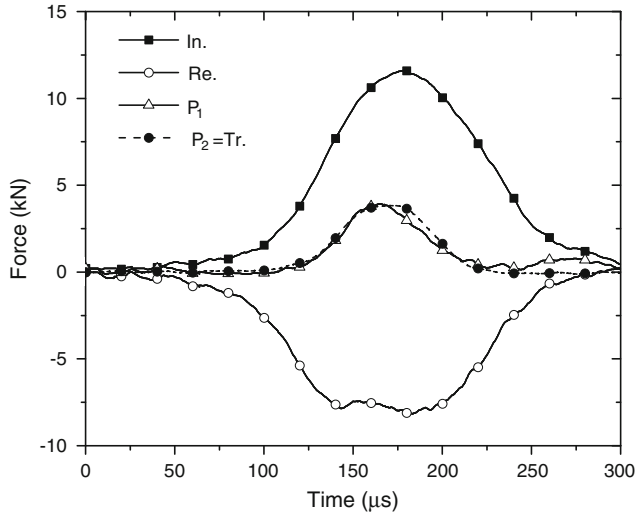


Fig. 10 Dynamic force balance (In: Incident wave, Re: Reflected wave, Tr: Transmitted wave, P_1 : the dynamic force on the incident bar-sample interface, P_2 : the dynamic force on the transmitted bar-sample interface)

current NSCB specimen can be determined by the following formula:

$$K_I(t) = \frac{P(t)S}{tR^{3/2}} Y(\alpha_a) \quad (6)$$

where R is the radius of the specimen, t is the thickness of the sample, S is the distance between the two supporting pins and $P(t)$ is the loading history. $Y(\alpha_a)$ is a dimensionless function depending on crack geometry and can be calibrated numerically.

The supporting span α_S around 0.55 is recommended. For $0.15 < \alpha_a < 0.5$, $Y(\alpha_a)$ can be determined using the following equations:

$$Y(\alpha_a) = 0.5037 + 3.4409\alpha_a - 8.0792\alpha_a^2 + 16.489\alpha_a^3 (\alpha_S = 0.50) \quad (7a)$$

$$Y(\alpha_a) = 0.4670 + 3.9094\alpha_a - 8.7634\alpha_a^2 + 16.845\alpha_a^3 (\alpha_S = 0.55) \quad (7b)$$

$$Y(\alpha_a) = 0.4444 + 4.2198\alpha_a - 9.1101\alpha_a^2 + 16.952\alpha_a^3 (\alpha_S = 0.60) \quad (7c)$$

For other values of α_S , numerical analysis is needed to determine $Y(\alpha_a)$. A typical stress intensity factor history from a dynamic NSCB test is shown in Fig. 11. The dynamic fracture toughness K_{IC} is obtained from the peak value of $K_I(t)$, provided that the dynamic

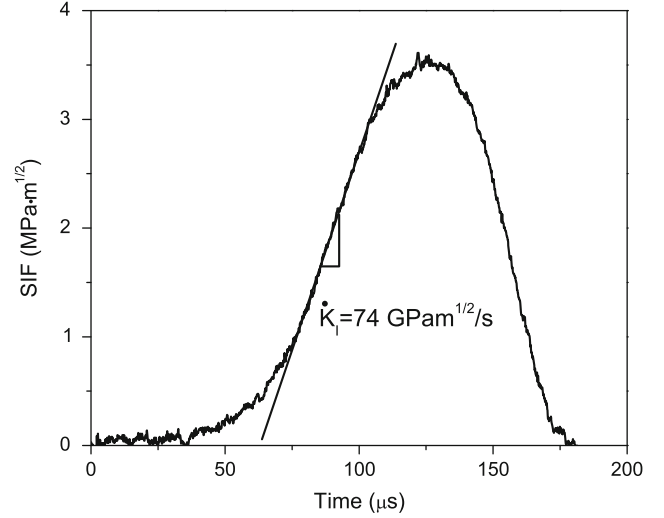


Fig. 11 Evolution of SIF obtained from a dynamic NSCB test

force balance has been achieved at both ends of the sample.

- (c) Determination of the dynamic loading rate: The rock dynamic fracture toughness depends on the loading rate. The loading rate is measured as the pre-peak slope of the SIF history curve (Fig. 11). The loading rate for the test as shown in the figure is determined as $74 \text{ GPa}\cdot\text{m}^{1/2}/\text{s}$.

4.6 Reporting of Results

- Lithologic description of the rock.
- Orientation of the axis of loading with respect to specimen anisotropy (e.g. bedding planes, foliation, etc.).
- Source of sample, including geographic location, depth and orientation, dates and method of sampling and storage history and environment.
- Seismic wave speeds of the specimen measured using ultrasonic method.
- Number of specimens tested.
- Specimen diameter and height.
- Water content and degree of saturation at the time of test.
- Test duration and stress rate.
- Date of testing and type of testing machine.
- Mode of failure.
- Any other observations or available physical data such as specific gravity, porosity and permeability, citing the method of determination for each.
- The check for dynamic force balance and detection of failure onset for each specimen.
- The dynamic loading history of each specimen in the sample and the loading rate.

- (n) The dynamic fracture toughness plotted as a function of the loading rate.

5 Notes and Recommendations

Three testing methods for determining dynamic rock compressive strength, dynamic rock indirect tensile strength and dynamic rock fracture toughness (mode I) were proposed. The suggested dynamic compression and tension testing methods are directly expanded from the ISRM suggested methods for measuring the static uniaxial compressive strength of rocks [6] and the tensile strength of rocks by the Brazilian tests [9].

For the fracture toughness measurement of brittle rocks, core-based samples are preferred, because they can be easily obtained from natural rock blocks. As a result, the developed standard method of fracture toughness tests on metals [12] and ceramics [13] are rarely utilized. ISRM recommended two methods with three types of core-based specimens for determining the fracture toughness of rocks: Chevron bend (CB) and short rod (SR) specimens in 1988 [14] and cracked chevron notched Brazilian disk (CCNBD) specimen in 1995 [15].

It is noted that each of the three suggested fracture samples has a pre-fabricated chevron notch; and the critical crack is not pre-fabricated but formed in the process of crack propagation. The complexity of the three dimensional crack as well as its influence to the dynamic wave propagation is far from being explored. Further, in the SR test, the accuracy of the measurement suffers significantly from the friction between the driving wedge and the notch corner of the sample [16]. In contrast, the NSCB [17, 18] sample configuration has a simple two dimensional crack with less disturbance on the stress wave propagation during the dynamic loading, which facilitates dynamic stress balance in the sample. Indeed, the reliability of this sample configuration on the fracture tests of rocks has been critically validated [11]. Because the sample fabrication procedure and data reduction equations developed for the dynamic NSCB method can be used for static NSCB tests without modification, it is recommended that the NSCB method be also considered as one of the suggested methods by ISRM for measuring static fracture toughness.

There are other important dynamic mechanical properties for rocks. It is recommended that dynamic testing methods for other rock dynamic properties, such as dynamic shear strength, dynamic flexural strength and dynamic frictional properties be developed. Furthermore, because rocks are normally under tectonic stress in their natural states, it is thus important to determine the effects of pre-stresses on the dynamic properties of rocks. Because the primary difference

between the dynamic tests and the static tests is the loading device, it is thus recommended that any dynamic testing method developed also be considered as the corresponding ISRM static testing suggested method so that a direct comparison of the static and dynamic properties can be made.

References

1. Chen W, Song B. Split Hopkinson (Kolsky). Bar: Springer; 2011.
2. Li XB, Lok TS, Zhao J, Zhao PJ. Oscillation elimination in the Hopkinson bar apparatus and resultant complete dynamic stress-strain curves for rocks. *Int. J. Rock Mech. Min. Sci.* 2000;37:1055–60.
3. Ma GW, Wu W. Suggested methods for determining the dynamic properties of rock materials. Report no 5. DSTA-NTU Underground Technology and Rock Engineering Program; 2010.
4. Li XB, Zhou ZL. Large diameter SHPB tests with special shape striker. *ISRM News J.* 2009;12:76–9.
5. Dai F, Huang S, Xia K, Tan Z. Some fundamental issues in dynamic compression and tension tests of rocks using split Hopkinson pressure bar. *Rock Mech. Rock Eng.* 2010;43:657–66.
6. Bieniawski ZT, Bernede MJ. Suggested methods for determining the uniaxial compressive strength and deformability of rock materials. in: Ulusay R, Hudson JA, editors. *The complete ISRM suggested methods for rock characterization, testing and monitoring; 1974–2006.* Ankara, Turkey: ISRM Turkish National Group; 2007. p. 151–6.
7. Xia K, Nasser MHB, Mohanty B, Lu F, Chen R, Luo SN. Effects of micro-structures on dynamic compression of Barre granite. *Int. J. Rock Mech. Min. Sci.* 2008;45:879–87.
8. Dai F, Xia K. Tensile strength anisotropy of Barre granite. *Pure Appl. Geophys.* 2010;167:1419–32.
9. Bieniawski ZT, Hawkes I. Suggested methods for determining tensile strength of rock materials. in: Ulusay R, Hudson JA, editors. *The complete ISRM suggested methods for rock characterization, testing and monitoring; 1974–2006.* Ankara, Turkey: ISRM Turkish National Group; 2007. p. 177–83.
10. Franklin JA, Vogler UW, Szlavlin J, Edmond JM, Bieniawski ZT. Suggested methods for determining water-content, porosity, density, absorption and related properties and swelling and slake-durability index properties. in: Ulusay R, Hudson JA, editors. *The complete ISRM suggested methods for rock characterization, testing and monitoring; 1974–2006.* Ankara, Turkey: ISRM Turkish National Group; 2007. p. 83–8.
11. Dai F, Chen R, Xia K. A semi-circular bend technique for determining dynamic fracture toughness. *Exp. Mech.* 2010;50:783–91.
12. ASTM Standard E399-09. Standard test method for linear-elastic plane-strain fracture toughness K_{IC} of metallic materials. ASTM International; 2009.
13. ASTM Standard C1421-01b. Standard test methods for determination of fracture toughness of advanced ceramics at ambient temperature. ASTM International; 2007.
14. Ouchterlony F. Suggested methods for determining the fracture toughness of rock. in: Ulusay R, Hudson JA, editors. *The complete ISRM suggested methods for rock characterization, testing and monitoring; 1974–2006.* Ankara, Turkey: ISRM Turkish National Group; 2007. p. 231–58.
15. Fowell RJ, Hudson JA, Xu C, Chen Jf. Suggested method for determining mode-I fracture-toughness using cracked chevron-

- notched Brazilian disc (CCNBD) specimens. in: Ulusay R, Hudson JA, editors. The complete ISRM suggested methods for rock characterization, testing and monitoring; 1974–2006. Ankara, Turkey: ISRM Turkish National Group; 2007. p. 259–68.
16. Zhang ZX, Kou SQ, Yu J, Yu Y, Jiang LG, Lindqvist PA. Effects of loading rate on rock fracture. *Int. J. Rock Mech. Min. Sci.* 1999;36:597–611.
 17. Chong KP, Kuruppu MD. New specimen for fracture-toughness determination for rock and other materials. *Int. J. Fract.* 1984;26:R59–62.
 18. Lim IL, Johnston IW, Choi SK, Boland JN. Fracture testing of a soft rock with semicircular specimens under 3-point bending 1. Mode-I. *Int. J. Rock Mech. Min. Sci.* 1994;31:185–97.

ISRM Suggested Method for the Determination of Mode II Fracture Toughness

Tobias Backers and Ove Stephansson

1 Introduction

Fracture is a failure mechanism of brittle materials that is of great importance for the performance of structures. Rapid and violent failures of large-scale geotechnical, mining or civil engineering structures cause significant safety hazards, material damage, and interruption to or even cessation of mining or building activities. Ability to recognise pre-failure rock mass behaviour may result in predicting or averting the potential for geotechnical and geological failures (Szwedzicki 2003). Rock fracture mechanics is one approach to resolve this task.

Rock fracture mechanics can be employed not only to improve safety, but also to enhance the performance and profitability of rock engineering structures. Examples are the geological disposal of radioactive waste, terrestrial sequestration of carbon dioxide to ease prejudicial effects on the environment, efficient underground storage of oil, gas or air, enhanced recovery of hydrocarbons, geothermal energy extraction, and underground constructions at increasing overburden pressure for infrastructure or transport. For these geomechanical applications the stress states

are mostly compressive, therefore, shearing is an important failure mechanism in rock materials.

The stress and displacement field around a crack tip during shearing results from the application of uniform shear loadings at infinity. In this so-called Mode II loading in fracture mechanics, the crack faces slide relative to each other and displacements of the crack surfaces are in the crack plane and perpendicular to the crack front. The crack initiation takes place when the crack tip stress intensity factor K_{II} reaches a critical value, called the Mode II plain strain fracture toughness K_{IIC} . The value of K_{II} depends on the external loading, the geometry of the specimen and crack dimension. The fracture toughness K_{IIC} , sometimes called critical stress intensity factor, is a material parameter depending on the type of rock material and its physical boundary conditions, such as confining pressure and temperature.

Whittaker et al. (1992) have presented an overview of different methods for determination of Mode II fracture toughness. Some more recent methods have been proposed by e.g. Chang et al. (2002), Hakami and Stephansson (1990), Ko and Kemeny (2006), Rao et al. (2003). Only Rao et al. (2003) performed experiments on Short Beam Compression specimens with application of confining pressure that is independent of the vertical load, but the method is under discussion as it frequently delivers $K_{IC} > K_{IIC}$ (Whittaker et al. 1992; Watkins and Liu 1985).

The important influence of confining pressure on Mode II fracture toughness can only be determined by methods that can independently apply a normal load to the fracture plane. It has been stated by several researchers that under conditions of overall compression Mode II fracture, propagation is most likely (Melin 1986; Lawn 1993). This was experimentally confirmed by Bobet and Einstein (1998) who demonstrated that macroscopic wing fractures (Mode I) can be suppressed by applying confining pressure, i.e. normal stress. Confining pressure had to be applicable to the specimen to be able to

Please send all written comments on these ISRM Suggested Methods to Prof R. Ulusay, President of the ISRM Commission on Testing Methods, Hacettepe University, Geological Engineering Department, 06800 Beytepe, Ankara, Turkey at resat@hacettepe.edu.tr.

Originally published as an article in the journal *Rock Mechanics and Rock Engineering*, 45, T. Backers, O. Stephansson, ISRM Suggested Method for the Determination of Mode II Fracture Toughness, 1011–1022, 2012.

T. Backers (✉) · O. Stephansson
Geomecon GmbH, August-Bebel-Strasse 27, 14482
Potsdam, Germany
e-mail: tobias.backers@geomecon.de

O. Stephansson
Helmholtz-Zentrum Potsdam GFZ German Research Centre
for Geosciences, Telegrafenberg, 14473 Potsdam, Germany

suppress macroscopic tensile fracturing. The Punch-Through Shear with Confining Pressure (PTS/CP) experiment (Backers 2005; Backers et al. 2002a, b, 2004) allows measuring K_{IIC} at different confining pressures. A modified version of PTS/CP test of rectangular samples under biaxial loading was presented by Lee (2007).

In Mode I loading the crack is subjected to a normal stress, the crack surfaces separate symmetrically and the crack front propagates in direction of the crack plane. Three ISRM Suggested Methods for determining Mode I fracture toughness K have been presented (Ouchterlony 1988; Fowell et al. 1995). Fracturing in rock structures commonly occurs under mixed mode I–II loading where crack faces undergo both opening and sliding displacements and where pure Mode I stress and pure Mode II stress intensity are the limiting cases of mixed mode I–II loading. To solve common rock engineering problems with a fracture mechanics approach both fracture toughnesses K_{IC} and K_{IIC} are needed.

The suggested method for K_{IIC} fracture toughness determination makes use of the PTS/CP experiment, where specimens from K_{IC} testing (Chevron Bend test Ouchterlony 1988) can be used to obtain fracture toughness data for both Mode I and Mode II analysis.

It may be discussed if the concept of *mode of fracturing* is applicable to rock material. Rock is, in general, a multi-component material. Hence, when a fracture propagates through the material, it may not follow a straight trace but is influenced by grain boundaries, cracks, flaws and other discontinuities. From a mathematical point of view, in which the concept of the *mode of fracturing* was developed, a pure mode of fracture can only be achieved if the fracture propagates in a straight continuous plane within a given homogeneous stress field. Therefore, any deviation of the propagation direction of the fracture within the applied stress field introduces some mixed mode kind of fracturing.

Moreover, the fracture follows the given fabric and the fabric itself will introduce stress fluctuations that superimposes to the applied stress field (Dyskin 1999). In addition, the fracture generated will itself introduce cracks in its surrounding and build up a zone of mixed mode micro-cracking, the so-called fracture process zone. Hence, for a granular material the differentiation into the *mode of fracturing* is not possible on the microscale.

From analysis of acoustic emission recording in laboratory experiments it has been clearly shown that at Mode I and Mode II loading conditions, where the macroscopic fracture follows the direction of Mode I and Mode II, respectively, the micromechanical breakdown involves both tensile as well as shear cracking (e.g. Backers et al. 2005; Stanchits et al. 2003). Therefore, neither under pure Mode I nor Mode II loading conditions is the crack propagation pure tensile or pure shear; fracturing in rock material which always involves a mixed mode on the microscale.

In the context of laboratory based fracture toughness testing the *mode of fracturing* is here understood from a macroscopic point of view, at which the fracture propagation is in the direction of Mode I or Mode II. Further, as fracture toughness depends on boundary conditions, the term *material property* is not applicable.

2 Scope

The laboratory experiment is intended to directly measure the Mode II (in-plane shear) fracture toughness of rock material. The geometry of the test specimen is designed to use standard core material (NX size or 50 mm diameter) and to deploy the remaining halves from Mode I (tensile) fracture toughness testing by the Chevron Bend method [ISRM Suggested Method (Ouchterlony 1988)]. The experimental set-up allows the Mode II fracture toughness to be measured at different levels of confining pressure. The test is called the PTS/CP experiment.

3 Specimen Preparation

1. For any specimen preparation treatment appropriate high precision (preferably diamond stud) tools should be used. During specimen preparation, caution has to be taken to limit the micromechanical damage of the specimen. Micromechanical damage may influence the fracture propagation and cause reduced magnitude of fracture toughness. Cautious specimen preparation should involve slow drilling, cutting and grinding operations to limit vibrations and heat generation. If no cooling agent can be used in the process of specimen preparation, special caution has to be taken to limit the temperature increase due to specimen preparation.
2. The specimens should be right circular cylinders having a height L to diameter D ratio of 1:1 and a diameter D equal to 50 mm (Fig. 1). The end surfaces should be flat to 0.01 mm and shall not depart from perpendicularity to the longitudinal axis of the specimen by more than 0.5° .
3. The mantle surface of the specimen cylinder should be smooth, free of abrupt irregularities and straight to within 0.5 mm over the full length of the specimen. Such irregularities might act as stress concentrators.
4. A circular notch of diameter $ID = 0.5D = 25 \pm 0.2$ mm and depth $a = 0.1D = 5 \pm 0.2$ mm is to be inserted into one end surface of the cylindrical specimen and a circular notch of diameter $ID = 0.5D = 25 \pm 0.2$ mm and depth $b = 0.6D = 30 \pm 0.2$ mm shall be manufactured into the other end surface (Fig. 1). Hence, the intact rock portion is of length $IP = L - a - b = 15$ mm. The axis

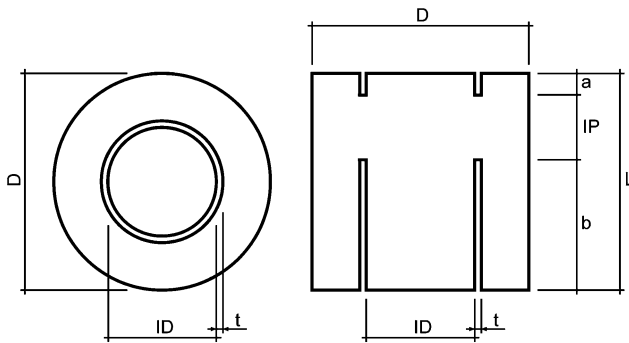


Fig. 1 Specimen geometry and dimensions of the Punch-Through Shear with Confining Pressure experiment

of the circular notches has to be aligned with the cylinder axis of the specimen. The sinking of the notches may be performed preferably by a computerised numerical control (CNC) milling machine or alternatively an appropriate hollow drill bit. The width of the notches shall be $t = 1.5 \pm 0.2$ mm. The bottom of the notches should have a small curvature.

5. The dimensions of the specimen should be measured to the nearest 0.1 mm. The specimen diameter should be measured by averaging two diameters measured at right angles at at-least two levels. The notch depths should be reported by averaging three measurements at angles of 120° . The specimen height should be determined by averaging three measurements at angles of 120° .
6. The specimen should be stored after specimen preparation for an appropriate time interval at sufficient conditions to achieve the desired moisture condition and history. The conditions of storage, moisture adjustment or drying shall be reported.
7. The minimum information on each specimen shall include dimensions, specimen preparation routines, special observations made during specimen preparation, moisture content, and macroscopic description of the surface.

4 Experimental Set-Up

1. The specimen is placed on top of a bottom support that has a central cut out CO of diameter $ID + 2t < CO < ID + 5$ mm and depth $CD \approx 0.1D$ (Fig. 2). The specimen end surface with the notch of length b faces downwards.
2. A load stamp assembly is placed on top of the specimen that should contain a load piston of diameter $LO = ID$ and shall provide a sealing of the specimen from a possible confining pressure liquid (Fig. 2).

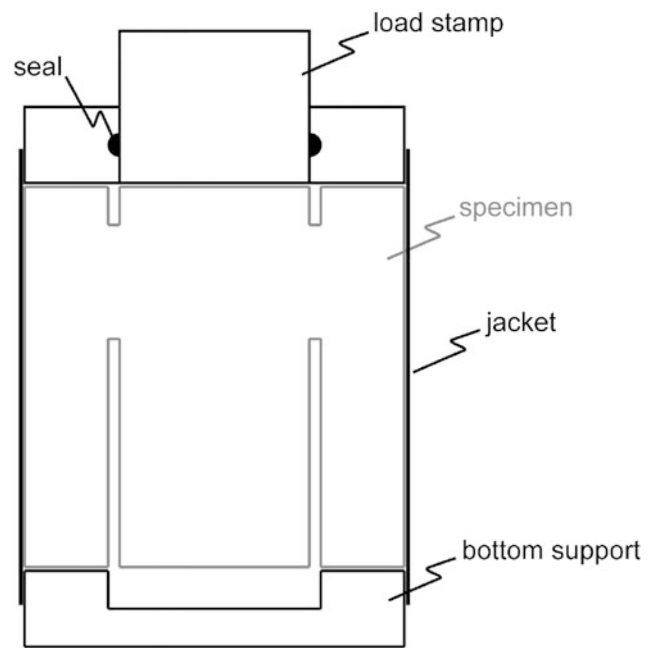


Fig. 2 Principle set-up of the Punch-Through Shear with Confining Pressure experiment

3. The whole assembly may be covered by a jacket that seals the specimen from the confining pressure medium.
4. The assembly consisting of specimen, loading devices and jacket is placed into a loading frame of sufficient capacity and equipped with a system to apply a confining pressure that can be independently controlled. The load piston of the system should be travelled into contact with the load stamp of the installed assembly; no axial load should be applied at this stage. Thereafter, the confining pressure system should be filled with confining pressure medium.

No guidelines on how to insert the specimen assembly into the loading frame or confining pressure device are given in detail, as very different systems are available. It must be assured that the workflow can be followed with the used loading equipment.

5 Testing Procedure

1. The minimum information collected during experiment is the applied confining pressure P_C and peak load F_{max} . However, it is advisable to continuously record the axial deformation δ (accuracy $\Delta\delta = 0.001$ mm), the axial load F_{ax} (accuracy $\Delta F_{ax} = 0.05$ kN) and the confining pressure (accuracy $\Delta P_C = 0.05$ MPa) during the experiment. The rate of data acquisition should be

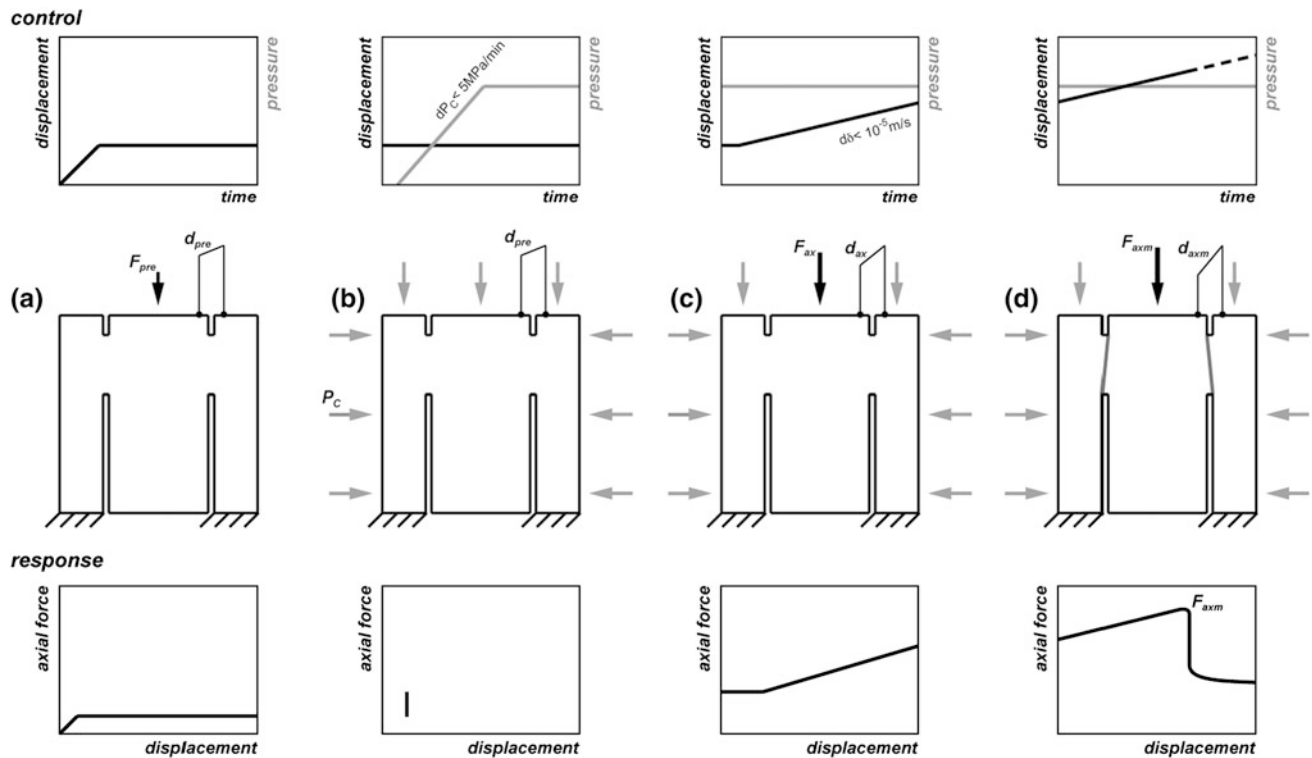


Fig. 3 Loading scheme and response of the Punch-Through Shear with Confining Pressure PTS/CP experiment

appropriate to detect the maximum load achieved; a rate of four data sets per second (s) may be found sufficient for the suggested axial displacement rate.

2. A small pre-load F_{pre} is applied to the experimental set-up. The pre-load F_{pre} should be large enough to firmly stabilise the assembly, but sufficiently small as to not introduce any damage to the specimen (Fig. 3a).
3. The confining pressure P_C is applied subsequently (Fig. 3b). The confining pressure will act on the mantle surface and on the top surface of the specimen. On reaching the desired level of confining pressure, P_C should be kept constant. A servo-controlled system is recommended.
4. The axial displacement is increased at a constant rate of $d\delta = 0.2 \text{ mm/min}$ ($3.3 \times 10^{-6} \text{ m/s}$) (Fig. 3c) resulting in an increase of the axial load. The other boundary conditions are kept constant.
5. At peak load a fracture propagates between the notches (Fig. 3d). The experiment may be terminated after driving the test to the post-peak.
6. The number of specimens per sample tested should be determined by practical considerations, but a minimum of five specimens is recommended. A sample in the sense of experiments consists of all specimens tested at the same boundary conditions.

6 Calculations

The Mode II fracture toughness may be evaluated from the peak load F_{max} achieved during testing by

$$K_{IIC} = 7.74 \times 10^{-2} F_{max} - 1.80 \times 10^{-3} P_C, \quad (1)$$

where K_{IIC} is in $\text{MPa}\sqrt{\text{m}}$, F_{max} is given in kN, and P_C is given in MPa. The formula is valid for the suggested geometry only, i.e., if $L = D = 50 \text{ mm}$, $ID = 25 \text{ mm}$, $a = 5 \text{ mm}$ and $b = 30 \text{ mm}$.

7 Reporting of Results

The report of each experiment should at least include the following:

1. Source of specimen as precisely as possible; location and orientation.
2. Lithological description of the rock type including grain size.
3. Details of the methods used for specimen preparation, dimensions of the prepared specimen, special observations made during specimen preparation, and macroscopic description of the specimen surface.

Table 1 Values for Mode I and Mode II fracture toughness of various rocks

Rock		K_{IC}	K_{IIC} (low P)	K_{IIC} (high P)	K_{IIC}/K_{IC}
Ävrö granite, medium grained	Sweden	3.8	4.7	11.5	1.2/3.0
Aue granite, coarse grained	Germany	1.6	4.2	10.5	2.6/6.6
Mizunami granite, medium grained	Japan	2.4	4.2	10.9	1.5/3.8
Seoul granite, finegrained	Korea	1.6	4.0	–	2.5/–
Carrara marble	Italy	2.4	3.1	6.7	1.3/2.8
Flechtingen sandstone, finegrained	Germany	1.2	2.1	5.3	1.8/4.4
Bentheim sandstone, finegrained	Germany	0.9	–	–	–/–
Ruedersdorf limestone, mudstone	Germany	1.1	3.1	4.2	2.8/3.8

4. Orientation of the loading axis with respect to the specimen anisotropy, bedding planes, etc.
5. History and environment of test specimen storage or treatment (temperature, drying, saturation, etc.).
6. Specimen condition at time of test (saturation degree, fluid/gas content, temperature, etc.).
7. Details of experiment including history, confining pressure, loading rate, etc.
8. A record of the peak load.
9. Individual test plots showing confining pressure, axial stress and axial displacement versus time. If there is major stress drops during loading, the test should be considered invalid.
10. The calculated value of the Mode II fracture toughness; if known, along with the Mode I fracture toughness and the ratio of K_{IIC}/K_{IC} .
11. Description of the specimen after testing, especially description of the macroscopic visible fractures. If there are fractures other than the vertical connection of the notches on stopping the test at peak load, the test may be discarded.
The report of a series of samples should contain the following:
12. The average value of each sample of experiments including a representative measure of the scatter.
13. A plot showing the Mode II fracture toughness of each sample as a function of confining pressure.
14. The ratio of K_{IIC}/K_{IC} if the Mode I fracture toughness was determined, e.g. by the Chevron Bend experiment [ISRM Suggested Method (Ouchterlony 1988)].

8 Typical Values

Table 1 gives some examples of Mode I and Mode II fracture toughness values for different rocks. The Mode I fracture toughness was determined using the ISRM Suggested Method, Chevron Bend Method (Ouchterlony 1988) and the Mode II fracture toughness was determined by to the above procedure.

9 Notes and Recommendations

The following notes and recommendations shall support and explain the details of the suggested method. For further details on the reported results and information, please refer to the given references.

9.1 Evaluation Procedure

It is suggested that K_{IIC} is estimated by a technique based on a displacement extrapolation technique (DET) as frequently used in literature, e.g. Lim et al. (1993). The displacement formulations are based on Irwin's crack tip displacement equations (Whittaker et al. 1992). In Cartesian coordinates, the displacements are given by

$$u = \frac{K_I}{4G} \sqrt{\frac{r}{2\pi}} \left[(2k-1) \cos \frac{\theta}{2} - \cos \frac{3\theta}{2} \right] + \frac{K_{II}}{4G} \sqrt{\frac{r}{2\pi}} \left[(2k+3) \sin \frac{\theta}{2} + \sin \frac{3\theta}{2} \right] \quad (2)$$

$$v = \frac{K_I}{4G} \sqrt{\frac{r}{2\pi}} \left[(2k+1) \sin \frac{\theta}{2} - \sin \frac{3\theta}{2} \right] + \frac{K_{II}}{4G} \sqrt{\frac{r}{2\pi}} \left[-(2k-3) \cos \frac{\theta}{2} - \cos \frac{3\theta}{2} \right], \quad (3)$$

where u is the displacement in shear direction, v is the displacement perpendicular to u , G is the shear modulus, $k = 3-4\nu$, with ν being Poisson's ratio, r is the distance from the crack tip, and θ is the angle from the shear direction. In the case of $\theta = \pm 180^\circ$, i.e. on the notch faces, Eqs. (2) and (3) become

$$u = \frac{K_{II}}{4G} \sqrt{\frac{r}{2\pi}} [2k+2] \quad (4)$$

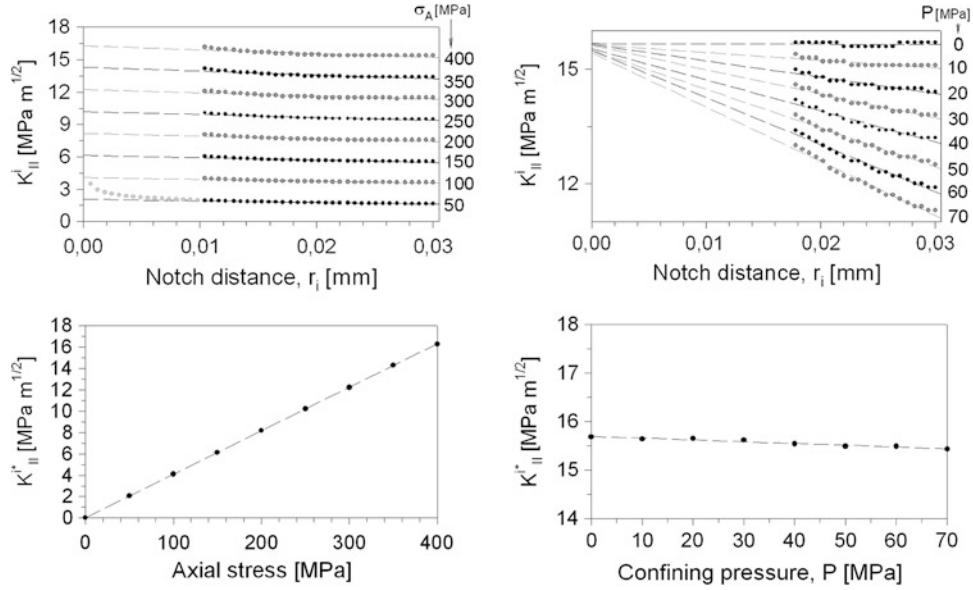


Fig. 4 Displacement extrapolation technique. The displacements for the calculation of K_{II}^i were determined by 2D FEM using the standard PTS/CP geometry. (Top left) from a K_{II}^i versus r_i plot the curve is

$$v = \frac{K_I}{4G} \sqrt{\frac{r}{2\pi} [2k + 2]}. \quad (5)$$

Thus, K_I and K_{II} can be determined separately by the x - and y -direction displacements. In the case of K_{II} , u is measured at the nodal points of the upper and lower notch faces, i.e. $\theta = \pm 180^\circ$, thus

$$u_i^+ = \frac{K_{II}^i}{2G} \sqrt{\frac{r_i}{2\pi} [k + 1]}, \quad \text{at } \theta = +180^\circ \quad (6)$$

$$u_i^- = \frac{K_{II}^i}{2G} \sqrt{\frac{r_i}{2\pi} [k + 1]}, \quad \text{at } \theta = -180^\circ. \quad (7)$$

The relative y -direction displacement of the corresponding nodes is

$$\Delta u = u_i^+ - u_i^- = \frac{K_{II}^i}{G} \sqrt{\frac{r_i}{2\pi} [k + 1]} \quad (8)$$

and consequently K_{II}^i is defined by

$$K_{II}^i = \frac{G}{k + 1} \sqrt{\frac{2\pi}{r_i}} \Delta u_i. \quad (9)$$

The K_{II}^i at given boundary stresses for different r_i are determined and plotted as functions of the distance from the notch tip. For the linear part of that function, a linear regression extrapolates K_{II}^i to the notch tip, i.e. $r = 0$ and K_{II}^{i*} .

extrapolated to the K_{II}^i axis providing a linear correlation between axial stress σ_A and axis intercept K_{II}^{i*} (top right). (Bottom) The same procedure provides a correlation between confining pressure P and K_{II}^i

For the suggested geometry, the corresponding relations are determined on the bottom notch. The influence of axial loading, σ_A , and confining pressure, P_C , are evaluated (Fig. 4).

Some other methods can be used to evaluate K_{IIC} from the PTS/CP experiment; some of those are explained and discussed in Backers (2005). Here, the values obtained by the DET method used here are compared to the J -integral approach (Rice 1968). In the case of the PTS/CP method it becomes

$$J \approx \frac{1}{2} \Delta u \Delta \tau \quad (10)$$

where Δu is the shear displacement in the notch plane and $\Delta \tau$ the drop of average shear stress from peak to residual shear stress across the fracture faces. Δu and $\Delta \tau$ can be obtained from the post peak part of the shear stress versus strain diagram (see Hakami 1988 for details).

The Energy Release rate obtained by the J -integral analysis of a limestone sample ($P_C = 5$ MPa, $\sigma_A = 87.2$ MPa) is $J \approx 4 \times 10^4$ J/m² or $K_{IIC} \approx 3.1$ MPa m^{1/2}. In comparison, the DET method provides $K_{IIC} = 3.3$ MPa m^{1/2}. The J -integral method requires that small scale yielding is evident to be able to assume equivalence to K_{IIC} , and additional fracturing in the specimens, as sometimes obtained, limits the evaluation capability of the method.

The advantage of the suggested method to determine K_{IIC} is that only the peak load needs to be recorded. For e.g., a J -integral approach a full load and displacement recording would be necessary.

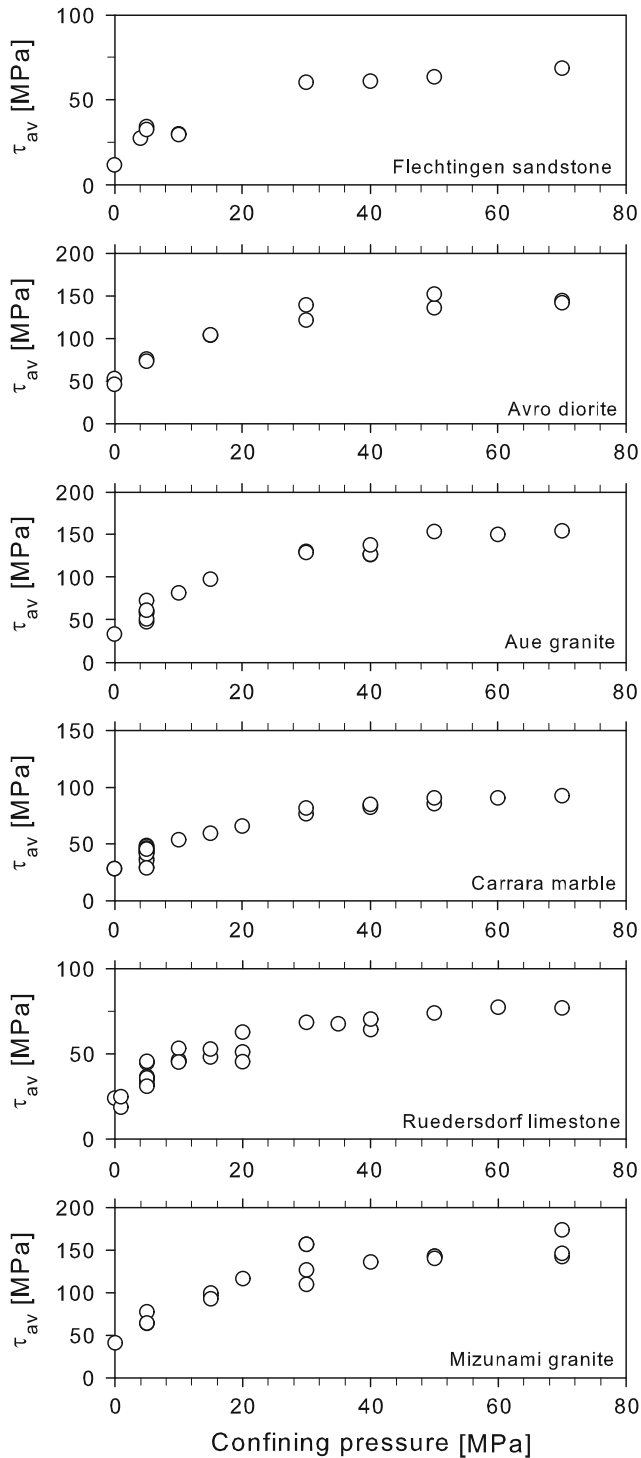


Fig. 5 Influence of confining pressure, P_C , on and τ_{av} (the shear stress is not an interpreted value and therefore presented here. K_{IIC} and τ_{av} are linked by a factor only and hence the trends are the same), $\tau = F_{max} (\pi \times ID \times IP)^{-1}$, for different rock types. (Recalculated data after Backers 2005; Backers et al. 2002b)

The given formulation is valid only for the suggested geometry and deviations from the ideal configuration will result in inaccurate values of K_{IIC} . Further, at low confining

pressures wing fractures may be introduced in the specimen altering the stress fields. This alteration is not accounted for in the equation.

9.2 Influence of Confining Pressure

The shear stress ($\tau = F_{max}(\pi \times ID \times IP)^{-1}$) (intact rock portion $IP = L - a - b$) at failure is reported to increase with confining pressure for various rock types. Figure 5 summarises selected data from Backers (2005) and Backers et al. (2002b). The PTS/CP test data shows results for experiments performed at confining pressures, P_C , up to 70 MPa.

The reported shear stress at failure increases non-linearly with confining pressure. As K_{IIC} is linearly linked to the shear stress at failure, K_{IIC} shows similar behaviour. Due to the observations from microstructural analyses (Backers et al. 2002a), the increase of shear stress and fracture toughness may be interpreted as a bi-linear relation. At low confining pressures the average shear stress between the notches, τ_{av} , steeply increases with P_C , while at high P_C the τ_{av} necessary for fracture propagation increases moderately with increase in confining pressure. The transition from steep to shallow slope is around 25–35 MPa. Alternatively, one might consider a square root rise to a maximum value. However, that would imply constant fracture toughness at very high P_C and no frictional influence.

From microstructural analyses, it has been reported that at low confining pressures wing fractures, i.e. tensile fractures, are initiated at the bottom notch inner tip at about 30 % of the peak load. The wing fractures are typically not initiated at confining pressures $P_C > 30$ MPa. Also, the signature (shape and crack content) of the fracture process zone changes with the increase of confining pressure up to about 30 MPa, but not above, indicating a change of micromechanism. A discussion of these features can be found in Backers et al. (2002a, b).

9.3 Discussion of Loading History

The PTS/CP experiment has the unique ability to independently apply an external shear load and a normal stress perpendicular to the plane of shear loading. In principle, some other methods do have the possibility to vary the confining pressure, but not independently to an external shear load (i.e. triaxial compression test (Hakami and Stephansson 1990) and compression shear cube test

$${}^1 K_{IIC} = 7.74 \times 10^{-2} F_{max} - 1.80 \times 10^{-3} P_C = 7.74 \times 10^{-2} \tau \times \pi \times ID \times IP - 1.80 \times 10^{-3} P_C.$$

(Jumikis 1979). The very important influence of overall compression (confinement) on Mode II loading induced fracturing (Melin 1986; Lawn 1993) can be adequately studied by the Punch-Through Shear test only.

Due to the geometry and the suggested loading layout of the test, the specimen is not loaded purely isostatically on application of the confining pressure. A shear load is introduced in the plane between the notches. The ratio of confining pressure to shear stress, $\kappa = P_C/\tau$, is constant during application of confining pressure.

After application of confining pressure, the inner cylinder is punched down in displacement control. The ratio of confining pressure to shear stress, $\kappa = P_C/\tau$, will, therefore, decrease on punching down the inner cylinder. It was shown numerically by Melin (1986) that at high ratios of κ Mode II is preferred. Lower ratios will cause preferred initiation of Mode I fracture. When P_C is high enough K_{II} will reach K_{IIC} before τ has reached the level at which Mode I is preferred. κ is decreased in the PTS/CP experimental procedure, hence Mode II is preferred if P_C is sufficiently high. In other methods (e.g. Rao et al. 2003; Jumikis 1979), Mode II loading is applied by adjusting the loading angle and confining pressure also depends on the loading angle. Hence, κ is governed by the limited loading angle to achieve Mode II loading and then is kept constant with simultaneous increase of shear stress and confining pressure.

9.4 Discussion of Displacement Rate

It has been shown for a selection of rock types that the displacement rate has minor influence on the peak strength (Backers 2005). In a testing series the displacement rate was varied between 3.3×10^{-7} and 1.7×10^{-3} m/s at constant confining pressure for various rock types (Fig. 6). The tested rock types have homogeneous mineralogical composition and grain size. For an inhomogeneous, coarse grained granite it was reported that the fracture initiation stress increases at higher displacement rates. The suggested displacement rate of 3.3×10^{-6} m/s allows performance of the test within reasonable time without effects of the operational condition such as subcritical crack growth weakening effects. It should be noted that there is evidence to expect an influence by this subcritical crack growth mechanism on individual rock types, and this possibility should be considered in the planning of a testing campaign (c.f. Sect. 9.8).

9.5 Discussion of Geometry

The circular geometry of the PTS/CP experiment is superior to a rectangular geometry in terms of structural stability as

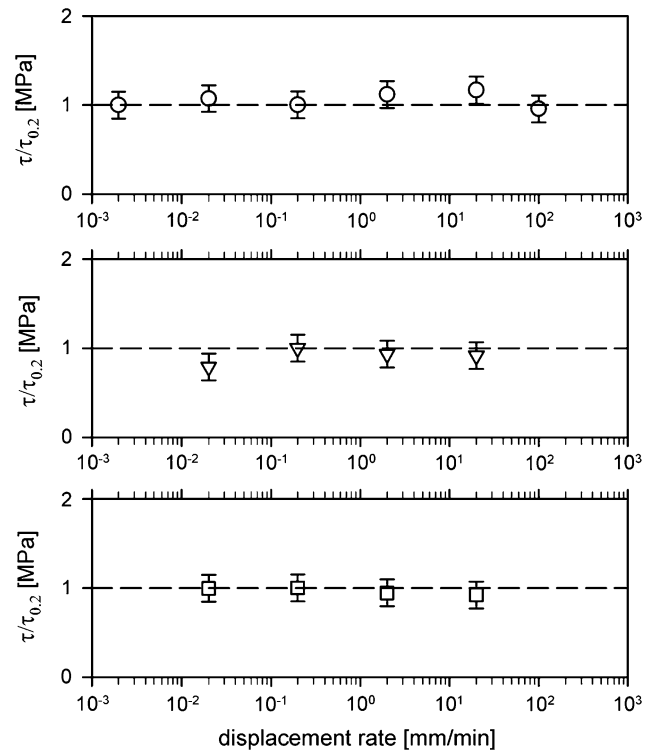


Fig. 6 Shear stress on notch plane at fracture initiation versus displacement rate at constant confining pressure of 5 MPa for a selection of rock types [the shear stress at fracture initiation is normalised with the shear stress at 0.2 mm/min. *Top* Carrara marble; *middle* Flechtingen sandstone; *bottom* Ruedersdorf limestone]

is mostly favoured in several Mode II testing methods. The tubular (hollow-cylindrical) layout of the PTS/CP test in the notch regions is able to withstand high confining pressures due to the tangential stresses; no sign of specimen failure is reported up to 120 MPa for limestone (Backers et al. 2004). A geometry with straight notches can be studied at low confining pressures only, as bending stresses introduced by the confining pressure would cause failure.

9.5.1 Influence of Notch Depth

Variation of the notch depth yielded a region of constant shear stress in the plane between the notches for $10 \text{ mm} < IP < 20 \text{ mm}$ (Fig. 7). The upper notch depth, a , is fixed to 5 mm at specimen height $L = 50 \text{ mm}$ and the lower notch depth, b , is varied. The average shear stress on the cylindrical plane between the notches remains almost constant for Ruedersdorf limestone and Carrara marble, but increases for small IP for Aue granite. It is constant between IPs of approximately 10 and 20 mm for the three rock types. The suggested IP of 15 mm lies within the constant regime for all tested rock types.

Variation of rock ligament between the notches, IP, illustrates a plateau of τ_{av} for a certain range of IP (Fig. 7). Similar results are reported by Yoon et al. (Yoon and Jeon

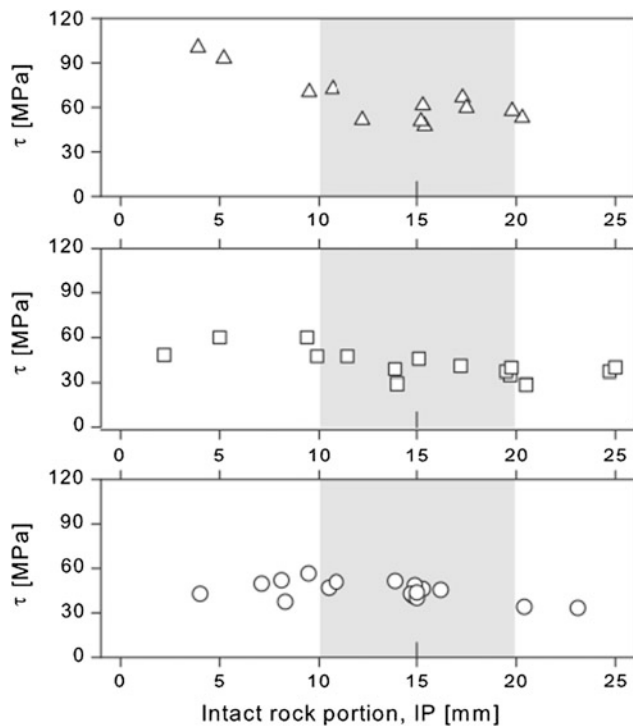


Fig. 7 Shear stress on notch plane at fracture initiation versus intact rock portion IP [The average shear stress on the cylindrical plane between the notches remains almost constant for Ruedersdorf limestone and Carrara marble, but increases for small IP for Aue granite. It is constant between IPs of approximately 10 and 20 mm for the three rock types. ($L = 50$ mm, $D = 50$ mm, $a \approx 5$ mm, $P_C = 5$ MPa). *Top* Aue granite; *middle* Ruedersdorf limestone; *bottom* Carrara marble. Recalculated data from Backers (2005)]

2003) for Daejeon granite. They report constant K_{IIC} for IP of about 17 to 40 mm. Numerical analyses performed by Watkins (1983) on samples with similar, but cubic geometry give evidence of constant stress intensity factor in Mode II for IP/ L ratios of 0.3–0.5 (IP = 15–25 mm in case of PTS/CP geometry) for experimental Mode II fracture toughness determination of mortar without confining pressure.

For small ligament lengths the notches are expected to influence each other by coalescence and interaction of the initial process zones before actual fracture propagation takes place at peak load; a decrease of shear stress necessary for fracture propagation is expected at small IP. The initial fracture process zone was shown by means of acoustic emission to be few millimetres in length (~ 2 – 3 mm for Mizunami granite; (Backers 2005; Stanchits et al. 2003). If the process zones of the top and bottom notches interact at low IP, as is suggested by acoustic emission, coalescence/overlap of the fracture process zones should result in a magnified loss of strength. This is only vaguely supported by the shape of the stress versus IP plot at low IP in Fig. 7 for Ruedersdorf limestone and Carrara marble. The elevated average shear stress necessary for fracture growth in Aue

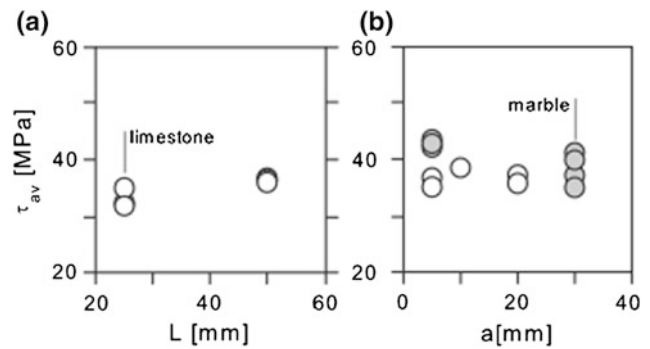


Fig. 8 **a** Influence of symmetrical and unsymmetrical sample geometry. τ_{av} is similar for symmetrical ($L = 25$ mm) and unsymmetrical ($L = 50$ mm) Ruedersdorf limestone samples. ($a = 5$ mm, $D = 50$ mm, $P_C = 5$ MPa). **b** Influence of the upper notch length, a , on τ_{av} of Carrara marble and Ruedersdorf limestone (white circles) and Carrara marble (grey circles). [Results for upper notch depth $a = 5$ and 30 mm with similar IP are given. There is no evidence for a significant influence of the notch depth on τ_{av} . ($L = 50$ mm, $D = 50$ mm, $P_C = 5$ MPa). Recalculated data from Backers (2005)]

granite (Fig. 7) might be explained by the comparably large grains (average is 1 mm, but up to 5 mm are included). At small IP only few grains are located between the notches and hence coalescence might be aggravated by inter- as well as intragranular crack propagation accompanied by interlocking and crack arrest.

9.5.2 Influence of Asymmetric Specimen Geometry

The proposed depth of the notches is non-symmetrical; this is to avoid compressive failure of the upper part of the inner cylinder during axial loading.

To verify an influence of the asymmetry on the test results, tests on samples of $L = 25$ mm with $a = b = 5$ mm, that is, with a similar length of IP as for the suggested geometry, are performed. τ_{av} is the same within sample-to-sample scatter for both the suggested ($L = 50$ mm) and short ($L = 25$ mm) geometries (Fig. 8). This also suggests that samples of $L = 25$ mm may be used if sample material is slender. Nevertheless, larger specimens are easier to handle and specimen preparation is more secure.

To investigate the influence of notch length, tests were performed with $a = 30$ mm and $b = 5$ mm, i.e. with the (suggested) specimen turned upside down, and compared to testing of samples with suggested set-up (Fig. 8). No evidence for a noteworthy influence of the notch depth on τ_{av} is reported (Backers 2005). During this series of testing, compressive failure of the top of the inner cylinder was frequently observed for specimens with $a = 30$ mm.

An unsymmetrical shape of the sample, i.e. notch depth $a \neq b$, and sample height, L , is shown to have a minor influence on the obtained τ_{av} . Hence, the contribution of bending of the unsupported outer ring to the Mode II fracture process is either negligible or non-existing.

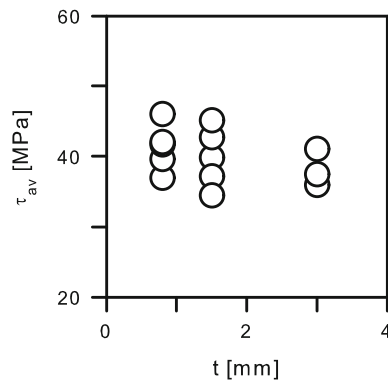


Fig. 9 Influence of the notch width, t , on τ_{av} for Carrara marble. [The shear stress at failure remains similar for the tested t . ($L = 50$ mm, $D = 50$ mm, $a \approx 5$ mm, $ID \approx 25$ mm, $IP \approx 15$ mm). Reprocessed data from Backers (2005)]

9.5.3 Influence of Notch Diameter and Sample Diameter

It should be noted that the Mode II fracture toughness as derived from the PTS/CP experiment may be sensitive to the sample diameter D and notch diameter ID (Backers 2005). It was reported that τ_{av} decreases with increasing ID at constant D for one large grained rock type. In addition, from selected experiments it is suggested that an increase of D increases τ_{av} at given ID . The effect appears to depend on grain size, but has only been studied at low confining pressure up to $P_C = 5$ MPa.

9.5.4 Influence of Notch Width

Experiments with notch widths, t , of 0.8, 1.5 and 3.0 mm were carried out on Carrara marble (Backers 2005). The 0.8 mm notch was manufactured using a CNC milling machine, the 1.5 mm notch was prepared using a standard drill bit, and the 3.0 mm notch was created by two drill bits with overlapping diameters. Results from this series of experiments are given in Fig. 9. The differences in τ_{av} show no clear trend for the tested t . Slight variation of τ_{av} may apply due to the different methods to introduce the notches. Further, in a wider notch more grains are intersected at the bottommost of the notch, and hence more grain boundaries might be preferably oriented for local failure. The notch width ($t = 1.5$ mm) for the method was recommended as it may be produced with conventional hollow drill bits.

9.6 Discussion of Fracture Generation

The fracture generation was studied on a variety of specimens and rock types and under varying boundary conditions. Fracture development and characteristics were described using macroscopic observations, thin section analysis, SEM, and analysis of acoustic emission recordings.

Figure 10 summarises the typical fracture characteristics as observed in several studies. At low confining pressures, typically $P_C < 30$ MPa, at about 30 % of the peak load a wing shaped fracture develops from the bottom notch inner tip (Fig. 10a). During propagation it turns towards the centre of the specimen until it is oriented almost vertically and then stops. Frequently, it stops even before aligning itself parallel to the displacement direction. The length of the wing fracture decreases with increasing confining pressure. At about 60 % of the peak load at the top notch a fracture was frequently observed propagating from the dilatant tip of the notch to the mantle surface of the specimen (Fig. 10b). Upon further loading these fractures remain stable. At peak load a fracture starts from the bottom notch and propagates to connect to the top notch (Fig. 10c). At fracture propagation the load versus displacement data shows negative slope indicating disintegration.

The reported formation of the bottom wing fracture (~ 30 % peak load) and upper horizontal fracture (~ 60 % peak load) are not detectable in the stress versus displacement data, hence the energy consumption of those is assumed to be minor.

Increased confining pressure, typically $P_C > 30$ MPa, the wing shaped fractures are not initiated. The negative stress intensity at the level of loading is sufficient to suppress tensile macroscopic fracture. Only the fracture connecting the notches develops at increased confining pressures.

In contrast to the wing shaped fracture, which is usually a very distinct feature highlighting only a single crack line separating mostly grains boundaries, the fracture that develops at peak load shows a wide fracture process zone. In a study of the influence of the confining pressure on the characteristic of the process zone of the shear fracture it was observed that the width of the zone is considerably reduced with increase of confining pressure (Backers et al. 2002a). The applied normal load to the fracture trace alters the local stress redistribution and the fractures initiated in the process zone rotate to align with the main fracture trace. Further, less crack surface is initiated leading to a smaller fracture process zone width. These changes in characteristics were most prominent at $P_C < 30$ MPa. Above this confining pressure the reported changes were minor.

The changes in appearance of the fracture evolution and its characteristics with confining pressure may be related to a change in slope in the shear strength/Mode II fracture toughness versus confining pressure data, c.f. Fig. 5.

Application of confining pressure superimposes a negative ² K_I and this results in shorter wing fractures that stop before being aligned with the major principle stress. No

² A negative K_I describes a state of compression.

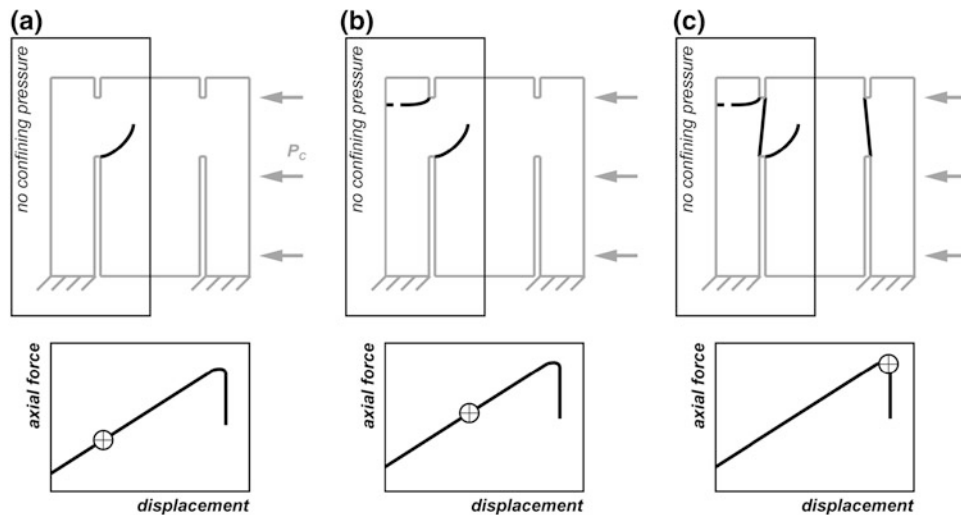


Fig. 10 Fracture evolution in the PTS/CP experiment. *Top* fracture evolution for $P_C = 0.1$ MPa (*left side of individual sketch*) and $P_C > 30$ MPa (*right side of individual sketch*). [The axial force vs.

displacement data is given at the *bottom* and displays the position of the *top* drawings in the loading path. **a** 30 % of peak load, **b** 60 % of peak load, **c** peak load]

wing fractures are initiated at the notches in samples subjected to confining pressures >30 MPa. According to Melin (1986) pure macroscopic shear fracture growth occurs if the level of confining pressure is high enough so that all tensile stresses at the fracture tips vanish or even become compressive. The stresses at the bottom notch in PTS/CP testing at higher confining pressures are consequently below a critical level to allow macroscopic wing fracture initiation. Suppression of Mode I fracturing above a certain level of confining pressure was experimentally proven by Bobet and Einstein (1998) and is consistent with the observations for the PTS/CP experiment.

9.7 Influence of Temperature

In a series of experiments on a Korean granite the influence of temperature on Mode II fracture toughness was studied by Meier et al. (2009). 53 specimens were tested at temperatures ranging from -75 to 250 °C and using the Punch-Through Shear with Confining Pressure experiment (Fig. 11). Variation of temperature has an impact upon the average shear strength granite within the applied temperature range. The shear stress at failure shows elevated values at sub-zero temperatures; it is anticipated that the water phase of the air dry specimens forms ice and the toughness of the ice adds to the toughness of the rock. As the water is frozen below 0 °C and the properties do not vary significantly, and τ_{av} remains constant for that interval, the hypothesis of the superposition of rock and ice toughness is assumed valid. Around the freezing point the values drop down to remain constant for up to 100 °C. Presumably above temperatures of 100 °C τ_{av} is slightly increasing

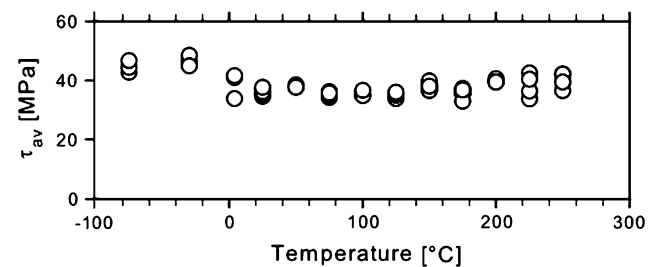


Fig. 11 τ_{av} at different temperatures at ambient pressure conditions ($P_C = 0.1$ MPa) for a Korean granite

again; the increase is due to crack propagation into newly formed arrester positions (i.e. microcracks in orthogonal directions to the main travel direction).

9.8 Subcritical Crack Growth

The PTS/CP experiment was also employed to determine the subcritical crack growth parameters as defined in Charles' law (Backers et al. 2006). The study applied static loading at different fractions of the peak load and measured the time-to-failure. From a weakest link theory (Wilkins 1980, 1987) the subcritical parameters may be derived.

Acknowledgments Erik Rybacki, Georg Dresen (both Helmholtz-Centre Potsdam—GFZ German Research Centre for Geosciences, Germany) and Tobias Meier (then Geomecon GmbH) were involved in certain aspects of the development of the testing procedure, the discussion of results, and the review of this contribution. John Napier, John Kemeny, Chulwhan Park, Resat Ulusay and an anonymous reviewer gave valuable comments, which helped improve the manuscript. The early versions of the method were developed in

collaboration with Technical University of Berlin, Germany, and Royal Institute of Technology KTH Stockholm, Sweden. The main body of work was conducted at Helmholtz-Centre Potsdam—GFZ German Research Centre for Geosciences, Germany. The work on some aspects as reported in the appendix was carried out partly in the context of a GeoFrames GmbH (now Geomecon GmbH) research and development project supported by the European Union, European Fund for Regional Development, program ‘Investment to Future’, Period 2007–2013. Calvin Seward (Geomecon GmbH) gave the manuscript a final language reading. The contributions of the different individuals and institutions are greatly acknowledged.

References

- Backers T (2005) Fracture toughness determination and micromechanics of rock under mode I and mode II loading. University of Potsdam, Potsdam
- Backers T et al (2002a) Fractography of rock from the new punch-through shear test, in structural integrity and fracture. In: Dyskin AV, Hu X, Sahouryeh E (eds) *The International Conference on structural integrity and fracture*, Perth, Australia
- Backers T, Stephansson O, Rybacki E (2002b) Rock fracture toughness testing in Mode II—punch-through shear test. *Int J Rock Mech Min Sci* 39(6):755–769
- Backers T et al (2004) New data on Mode II fracture toughness of rock from the punch-through shear test. *Int J Rock Mech Min Sci* 41(3):351–352
- Backers T, Stanchits S, Dresen G (2005) Tensile fracture propagation and acoustic emission activity in sandstone: the effect of loading rate. *Int J Rock Mech Min Sci* 42(7–8):1094–1101
- Backers T, Antikainen J, Rinne M (2006) Time dependent fracture growth in intact crystalline rock: laboratory procedures and results. In: *GeoProc2006—2nd International Conference on coupled T-H-M-C processes in geosystems: fundamentals, modelling, experiments, applications*, Nanjing, China
- Bobet A, Einstein HH (1998) Fracture coalescence in rock-type materials under uniaxial and biaxial compression. *Int J Rock Mech Min Sci* 35(7):863–888
- Chang SH, Lee CI, Jeon S (2002) Measurement of rock fracture toughness under modes I and II and mixed-mode conditions by using disc-type specimens. *Eng Geol* 66(1–2):79–97
- Dyskin AV (1999) On the role of stress fluctuations in brittle fracture. *Int J Fract* 100(1):29–53
- Fowell RJ et al (1995) Suggested method for determining Mode-I fracture-toughness using cracked chevron-notched Brazilian disc (Ccnbd) specimens. *Int J Rock Mech Min Sci Geomech Abstr* 32(1):57–64
- Hakami H (1988) Post-failure behaviour of brittle rock. Division of Rock Mechanics, Lulea University of Technology, Sweden
- Hakami H, Stephansson O (1990) Shear fracture energy of Stripa granite—results of controlled triaxial testing. *Eng Fract Mech* 35:855–865
- Jumikis AR (1979) *Rock Mechanics*. Trans Tech Publications (series on rock and soil mechanics), Clausthal, p 356. ISBN:0878490264
- Ko TY, Kemeny J (2006) Determination of Mode II stress intensity factor using short beam compression test. In: *4th Asian Rock Mechanics Symposium*, Singapore
- Lawn BR (1993) *Fracture of Brittle Solids*. Cambridge University Press, Cambridge
- Lee JS (2007) Time-dependent crack growth in brittle rocks and field applications to geological hazards. The University of Arizona, USA
- Lim IL, Johnston IW, Choi SK (1993) Stress Intensity Factors for Semicircular Specimens under 3-Point Bending. *Eng Fract Mech* 44(3):363–382
- Meier T, Backers T, Stephansson O (2009) The influence of temperature on Mode II fracture toughness using the Punch-Through Shear with Confining Pressure experiment. In: Diederichs M, Grasselli G (eds) *ROCKENG09: Proceedings of the 3rd CANUS Rock Mechanics Symposium*, Toronto, Canada
- Melin S (1986) When does a crack grow under mode II conditions? *Int J Fract* 30:103–114
- Ouchterlony F (1988) Suggested Methods for Determining the Fracture Toughness of Rock. *Int J Rock Mech Min Sci Geomech Abstr* 25(2):71–96
- Rao QH et al (2003) Shear fracture (Mode II) of brittle rock. *Int J Rock Mech Min Sci* 40(3):355–375
- Rice JR (1968) A path independent integral and the approximate analysis of strain concentration by notches and cracks. *J Appl Mech* 35:379–386
- Stanchits S et al (2003) Comparison of acoustic emission events and micromechanics of granite under Mode I and Mode II loading. In: Makurat A, Curri P (eds) *EUROConference on rock physics and geomechanics—micromechanics, flow and chemical reactions*. Delft, The Netherlands
- Szwedzicki T (2003) Quality assurance in mine ground control management. *Int J Rock Mech Min Sci* 40(4):565–572
- Watkins J (1983) Fracture toughness test for soll-cement samples in mode II. *Int J Fract* 23(4):R135–R138
- Watkins J, Liu KLW (1985) A finite element study of the short beam test specimen under mode II loading. *Int J Cem Compos Lightweight Concrete* 7(1):39–47
- Whittaker BN, Singh RN, Sun G (1992) *Rock fracture mechanics—principles, design and applications*. Elsevier Science Publisher, Amsterdam
- Wilkins BJS (1980) Slow crack growth and delayed failure of granite. *Int J Rock Mech Min Sci Geomech Abstr* 17(6):365–369
- Wilkins BJS (1987) The long-term strength of plutonic rock. *Int J Rock Mech Min Sci Geomech Abstr* 24(6):379–380
- Yoon J, Jeon S (2003) An experimental study on Mode II fracture toughness determination of rock. *J Korean Soc Rock Mech* 13(1):64–75

ISRM Suggested Method for Reporting Rock Laboratory Test Data in Electronic Format

Hong Zheng, Xia-Ting Feng, Zuyu Chen, J. A. Hudson, and Yujie Wang

1 Introduction

The ISRM Suggested Methods for rock characterization, testing and monitoring have been widely established and included in the Blue Book (ISRM 2007). A following book on the new and updated ISRM Suggested Methods, released between 2007 and 2013, will be published soon in the ISRM Book Series. This will be called the Orange Book. However, the reports of testing results using these ISRM Suggested Methods are individually somewhat different, because they have different contents. The output format of the test data from different testing machines also varies considerably.

It should be noted that usually the reporting of testing results is currently only retained by the tester or published in journal or conference papers. Thus, it is not easy to use and compare the testing results for the same rock type from different sites or indeed different rock types (Toll and Cubitt

2003; Toll 2007, 2008; Weaver et al. 2008). Therefore, it is important to develop an approach leading to a digital standardised format for the storage and reporting of rock testing results for the same rock type and for different rock types conducted worldwide (Exadaktylos et al. 2007; Chen 2009; Zheng et al. 2010; Li et al. 2012). In order to use the format across the world, a Web style is required (AGS 1999, 2004, 2005; Swift et al. 2004; see the Websites for GADML, eEarth, XMML, GeoSciML, NEES, RockLab, Rockware, DIGGS). This should be suitable not only for the existing ISRM Suggested Methods but also for new and upgraded ISRM Suggested Methods. Also, it should be independent of any specific language environment and sufficiently extendable to satisfy the requirements of new ISRM Suggested Methods incorporating different items and parameters. In this way, such reporting will be useful for data integration and comparative analysis of remote data resources and improving the reliability and accuracy of complex engineering problem solving methods.

Hence, the purpose of the ISRM Suggested Method (SM) for reporting rock laboratory test data in electronic format is to provide a method for the reporting of results for the ISRM Suggested Methods for rock laboratory tests in a digitally standardised format. Such a report could include one or more of the following:

1. The original testing data and results obtained from different testing machines as guided by an ISRM Suggested Method (for example, the ISRM Suggested Method for determination of the uniaxial compressive strength of rock materials) which is stored in a standard electronic format.
2. A group of laboratory tests for the same rock type at the same project site (for example, a report for testing results for the uniaxial compressive strength of several specimens of marble at the Jinping II hydropower station site in China) which is stored and reported in a standard electronic format with local and Web output.

Please send any written comments on this ISRM Suggested Method to Prof. Resat Ulusay, President of the ISRM Commission on Testing Methods, Hacettepe University, Department of Geological Engineering, 06800 Beytepe, Ankara, Turkey.

Originally published as an article in the journal *Rock Mechanics and Rock Engineering*, 47, X. Zheng, X.-T. Feng, Z. Chen, J.A. Hudson, Y. Wang, ISRM Suggested Method for Reporting Rock Laboratory Test Data in Electronic Format, 221–254, 2014.

H. Zheng · X.-T. Feng (✉)
State Key Laboratory of Geomechanics and Geotechnical Engineering, Institute of Rock and Soil Mechanics, Chinese Academy of Sciences, Wuhan, 430071, Hubei, China
e-mail: xtfeng@whrsm.ac.cn; xia.ting.feng@gmail.com

Z. Chen · Y. Wang
China Institute for Water Resources and Hydropower Research, Beijing 100038, China

J. A. Hudson
Department of Earth Science and Engineering, Imperial College, London, SW7 2AZ, UK

3. The results of laboratory tests for the same rock type at different project sites (for example, reports of testing results for different marble stratum types following the same ISRM Suggested Method). These would be stored and reported in a standard electronic format with local and Web output.
4. The results of laboratory tests for different rock types at different/or the same project sites (for example, reporting of testing results for Jinping marble, Longyou sandstone, Inada granite, etc., following the corresponding ISRM Suggested Methods, stored and reported in a standard electronic format with local and Web output).

With a standard electronic format, users in different locations in the world can upload the information and can store their own testing data, including tables, photographs and figures, on the Web file. Researchers and engineers around the world can look at the testing results through the Web. In this way, testing results for the same rock type from the project, the same rock type from different project sites, and different rock types from the same or different project sites can be compared. Thus, the reporting of testing results can be shared worldwide.

As a first step, the electronic formats for reporting of the ISRM Suggested Methods for rock laboratory tests have been developed. This strategy can later be extended to all ISRM Suggested Methods for rock characterization and monitoring.

2 Standardisation of the Reporting Structure of the ISRM Suggested Methods for Rock Laboratory Testing

In order to develop a series of electronic formats for all ISRM Suggested Methods for rock laboratory testing, the basic features of the Suggested Methods have firstly been analysed. Each Suggested Method for laboratory testing includes five categories, i.e. “Scope”, “Apparatus”, “Procedures”, “Calculations” and “Reporting of Results”. However, the different Suggested Methods for laboratory testing have different parameters for each category (Table 1). A standardisation method is required to describe the contents of each category. Also, the category “Reporting of Testing” includes four sub-categories, i.e., description of the test equipment, description of the test object, description of the test process and description of the test results. The latter category for a group of testing results on the same rock type includes a description of general information which is a description of the testing equipment, rock and specimens, and a description of the specific information, which is a description of testing results for a set of specimens. The descriptions for these sub-categories and

their general and individual information vary within the Suggested Methods. Therefore, three-step strategies are developed to standardise overall testing reports and the testing result format (Fig. 1). The first step is the standardisation of the five categories. The second step is the standardisation of four sub-categories for the category “Reporting of Results”. The third step is to standardise the testing result format for the sub-category “Description of the Test Results”.

The details for the three steps are further developed and shown in Fig. 2. The standardisation of contents for the first four categories, shown in Fig. 2, is performed via the overall standardisation strategy. The four sub-categories for the category “Reporting of Results” are further detailed in Fig. 2. The apparatus type and description of rock in the field can be considered as general information, indicating that the same rock type is tested in the same equipment. The description of testing specimens, testing process and testing results varies and can be considered as individual specific information.

According to the developed standardisation method, an overall structure tree of the data structure document has been constructed, as shown in Fig. 3. This includes ‘parent nodes’ such as “Apparatus Information”, “Rock Information”, “Sample Source” and “Specimen”; ‘middle nodes’ such as “Specimen Size”, “Failure Pattern” and “Result Parameters”; and ‘children nodes’ such as “Apparatus Name”,..., “Number of Specimen”, “Specimen No.”, “Diameter”, “Height”, “Ends Flatness”,..., “Loading Rate”, “Failure Type”, “Failure Photo” “Tested by”,..., “Remarks”.

The parent node “Specimen” as a repeated node can be repeatedly used according to the number of specimens. For example, if five specimens are to be used for the same tests, it will be repeated five times to represent “Specimen 1”, “Specimen 2”, “Specimen 3”, “Specimen 4” and “Specimen 5” successively.

The middle node “Geographic Location” can be explicitly represented by its three children nodes, such as “X-coordinate”, “Y-coordinate”, and “Z-coordinate”, which are established by users to distinguish the sample source. In detail, the “X-coordinate” and “Y-coordinate” are the projection plane coordinates of the sample source with respect to the same project site; the “Z-coordinate” means the depth of the sample source. If the user wishes to use the conventional drill hole survey notation, it can be represented by the drill hole ID and its down-hole position in metres.

The middle node, “Result Parameters”, can be subdivided into several children nodes according to the number of parameters in the testing results. For example, for the report of testing results for triaxial compression, the result parameters include “triaxial compressive strength” as

Table 1 Basic features of the ISRM Suggested Methods for laboratory testing

Name of testing method	Scope and introduction	Apparatus	Procedures	Calculations	Reporting of results
Determining point load strength index	Test purpose, use instructions, requirements and limitations of the test object and apparatus	The components of apparatus: loading system, load measuring system, distance measuring system	Specimen selection and preparation, calibration, the diametral test, the axial test, the block and irregular lump tests; anisotropic rock	Uncorrected point load strength index, size correction, mean value calculation, Point load strength anisotropy index	The sample number, source location and rock type, and the nature and in situ orientation of any planes of anisotropy or weakness. The water content of the rock at the time. The loading directions; failure load; distance between the two platen contact points; uncorrected point load strength index; corrected point load strength index
Determining the indentation hardness index of rock materials	Use instructions, requirements and limitations of test object and apparatus	The components of apparatus: loading system; load measuring system; penetration measuring system	Specimen preparation; storage environment; load rate; indentation process	The peak load; the corresponding penetration; the indentation hardness index	Source of sample; lithologic description of the rock; number of specimens tested; orientation of the axis of loading with respect to specimen anisotropy; specimen diameter and height; water content and degree of saturation at time of test; test duration and load rate; the mode of failure; the peak load; the corresponding penetration, the indentation hardness index with the average results for each rock sample
Determining the block punch strength index	Test purpose, use instructions, requirements of test object and apparatus	The components of apparatus; punching block; base support; Ram	Specimen preparation; testing	Uncorrected block punch strength index; size-corrected block punch strength index; strength index in the strongest direction	Lithological description of the rock; orientation of the axis of loading with respect to specimen anisotropy; the sample number, source location, sampling depth; number of specimens tested; water content at time of test; date of testing; failure pattern; specimen diameter and height; Failure load; corrected block punch strength index; strength index in the strongest direction

(continued)

Table 1 (continued)

Name of testing method	Scope and introduction	Apparatus	Procedures	Calculations	Reporting of results
Determining the uniaxial compressive strength and deformability of rock material	Test purpose, Use instructions, requirements and limitations of test object and apparatus	The components of the apparatus and the function of each system	Specimen preparation; loading rate	Uniaxial compressive strength; axial strain; diametric strain; compressive stress; axial Young's modulus; Poisson's ratio; volumetric strain	Lithologic description of the rock; orientation of the axis of loading with respect to specimen anisotropy; source of sample; number of specimens tested; specimen diameter and height; water content and degree of saturation at time of test; test duration and loading rate; date of testing and type of testing machine; mode of failure; any other observations or available physical data; uniaxial compressive strength; values of applied load, stress and strain; Young's modulus; Poisson's ratio; method of determination of Young's modulus and at what axial stress level or levels determined
Determining the strength of rock materials in triaxial compression	Test purpose, use instructions, requirements of test object and apparatus	General testing equipment; loading device; triaxial cell; device for applying confining pressure; equipment for measuring and recording	Specimen preparation; the different procedures of three types (individual test, multiple failure state test, continuous failure state test)	Axial stress; peak strength; residual strength; internal friction angle; cohesion	Source of sample; lithological description of the rock; methods of specimen preparation, also the history and environment of test specimen storage; Orientation of the axis of loading with respect to specimen anisotropy; water content and degree of saturation at time of test; description of testing machine; data of testing; specimen diameter and height; test duration and stress and displacement rates; mode of failure; confining pressure and axial strength; Internal friction angle; cohesion; any other observations

(continued)

Table 1 (continued)

Name of testing method	Scope and introduction	Apparatus	Procedures	Calculations	Reporting of results
Determining shear strength	Test purpose, use instructions, requirements of test object and apparatus	Equipment for taking specimens of rock; equipment for mounting the specimen; testing equipment	Specimen preparation; consolidation; shearing	Peak strength; normal displacement; shear displacement; normal stress; shear stress	Data of testing; type of apparatus; methods of drilling and testing; geological description of the intact rock, sheared surface, filling and debris preferably accompanied by relevant index test data; source of sample; size of specimen; test duration; peak and residual shear strength; normal displacement; shear displacement; normal stress; shear stress; shear strength parameters
Determining tensile strength of rock materials	Test purpose, use instructions, requirements of test object and apparatus	The components of the apparatus and the function of each system	Specimen preparation; storage environment; load rate	For direct tensile strength tests: the maximum load; tensile strength For indirect tensile strength tests: the load at failure; diameter; thickness; tensile strength	Lithological description of the rock; orientation of the axis of loading with respect to specimen anisotropy; source of sample; number of specimens tested; specimen diameter and height; water content and degree of saturation at time of test; test duration and load rate; data of testing; type of apparatus; mode of failure; any other observations; tensile strength
Laboratory testing of swelling rocks	Test purpose, use instructions, requirements of test object and apparatus	The components of the apparatus and the function of each system	Sampling; storage environment; specimen preparation; loading temperature; load rate	The area of cross-section; axial stress; compensated swelling strain; non-compensated swelling strain	A unique identification of the sample and of each individual specimen; date and method of sampling; method of sealing and storage; method of specimen preparation for testing; orientation of the axis of loading with respect to specimen anisotropy; dimensions of the test specimen; density, water content, grain density and degree of saturation of the test specimen before and after the swelling test; test temperature; applied seating-load; specification of water used for immersion; axial stress; axial swelling strain; total compensated swelling strain

(continued)

Table 1 (continued)

Name of testing method	Scope and introduction	Apparatus	Procedures	Calculations	Reporting of results
Complete stress-strain curve for intact rock in uniaxial compression	Test purpose, use instructions, requirements of test object and apparatus	The component of apparatus: loading system, hydraulics, Spherically seated platen and specimen platen; control system; Strain measurement transducer; data acquisition	Specimen preparation; the testing procedure of specimens that generally exhibit ductile behaviour and specimens that generally exhibit brittle behaviour	Axial strain; diametric strain; compressive stress; circumferential strain; Young's modulus(Tangent Young's modulus; average Young's modulus; secant Young's modulus); Poisson's ratio; volumetric strain	Lithologic description of the rock; orientation of the axis of loading with respect to specimen anisotropy; source of sample; number of specimens tested; specimen diameter and height; water content and degree of saturation at time of test; test duration and load rate; date of testing and type of testing machine; mode of failure; any other observations or available physical data; values of applied load, stress and strain; pre-peak Young's modulus; Poisson's ratio; method of determination of pre-peak Young's modulus and at what axial stress level or levels determined
Determining the fracture toughness of rock	Test purpose, use instructions, requirements of test object and apparatus	The component of apparatus: specimen preparation equipment; testing machine and load fixtures; specimen alignment aids; displacement measuring equipment; recording	Specimen selection and preparation; calibration; setting up; testing	Loading rate; slope values; fracture toughness; correction of fracture toughness for non-linearity; additional quantities; Young's modulus; Poisson's ratio; total work of fracture	Sample number; source location and rock type and the nature and in situ orientation of any planes of anisotropy or weakness; core axis with respect to in site geology and structures and in case of sub-samples, the direction of loading; storage history and environment, water content and degree of saturation at the time of testing; Index properties obtained by other types of testing and physical data; specimen dimensions; level of testing and the appropriate loading rate; maximum load; the load at the evaluation point; the fracture toughness; auxiliary parameters

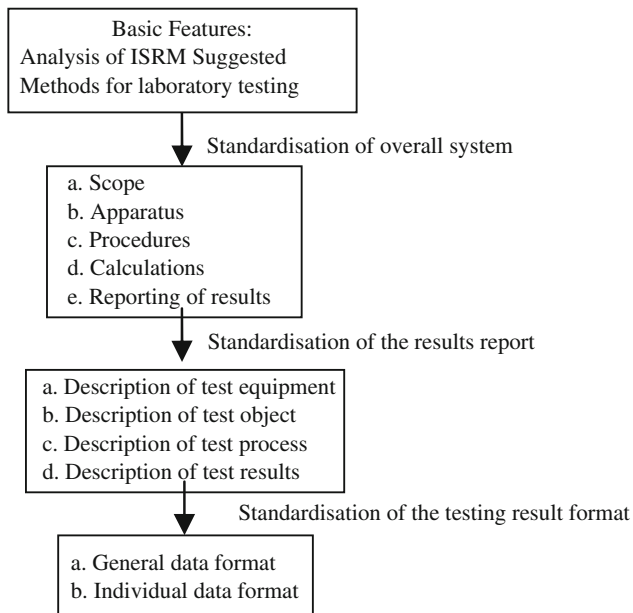


Fig. 1 Standardisation steps for the ISRM suggested methods for laboratory rock testing

“Parameter 01”, “Confining Pressure” as “Parameter 02”, “Internal friction angle” as “Parameter 03”, and “Cohesion” for “Parameter 04”. However, for uniaxial compressive tests, it includes “Uniaxial Compressive Strength” as “Parameter 01”, “Young’s modulus” as “Parameter 02”, “Poisson’s ratio” as “Parameter 03”, “Modulus Method” as “Parameter 04” and “Axial Level” as “Parameter 05”.

Moreover, the middle node “Original Testing Data” and “Other Observations” can also be sub-divided into several children nodes which are truncated here for brevity. “Original Testing Data” is used to store the testing data of each specimen. And its children nodes are different for each of the Suggested Methods for laboratory testing. For example, the middle node “Original Testing Data” includes “Time”, “Pressure”, “Axial Strain”, “Lateral Strain” and “Stress” for uniaxial compression testing. However, it includes “Time” and “Value of strain” for creep testing. And “Other Observations” is used for extending nodes. Some information could be included in this middle node, such as “SEM image”, “CT image”, “Microseismic events distribution map”, “Microseismic data”, etc.

The overall structure tree shown in Fig. 3 and includes the items in the existing Suggested Methods (ISRM 2007). This may need to be extended or modified according to the content of future new Suggested Methods. However, it is easy to implement such modifications.

3 Digitisation of the Reporting Structure for the ISRM Suggested Methods for Rock Laboratory Testing

The data structure shown in Fig. 3 needs to be digitised. The digitisation of the data structure includes three types of documents: data structure document, data storage document and data display document. This has the key features shown in Fig. 4, as in the following list:

- The data structure document, categories and nodes should be capable of being extendable.
- It should be easy to store and find data in the nodes with large memory and good compression.
- Data storage should be divorced from the environment. This means that a language environment should not be necessary to access data.
- Data types should be customisable. The users should be able to define their own data types.
- There should be data display flexibility.
- The data should be able to be shared and transmitted by network.

With the application of network language technology in the Extensible Markup Language, three types of documents including data structure document (XSD), data storage document (XML) and data display document (XSL), are developed to digitise the data structure in Fig. 3.

3.1 The Data Structure Document

The basic digitised data structure can be defined according to the structure in Fig. 3. It has different digitised data structures for each type of node.

All root nodes, parent nodes and middle nodes are of “complex type” because they have their own children nodes. The digitised data structures for these three nodes can be defined as the structure of the “complex type” which includes each secondary node as “element ref”. For instance, the root node “Test” has its secondary nodes—such as “Apparatus Information”, “Rock Information”, “Sample Source” and “Specimen”. The repeated node “Specimen” is marked as ‘maxOccurs = unbounded’. Therefore, the digitised data structure for the root node “Test” in Fig. 3 can be defined in Appendix 1.

The children nodes can be in the value type of “selection”, “decimal” or “string”. The digitised data structures of children nodes are defined in Appendixes 2, 3 and 4, respectively. For example, the children nodes whose value is selected, i.e., “Failure Type”, can be defined in Appendix 2. The children nodes, which are decimal, for example, “Diameter”, can be defined in Appendix 3. The children

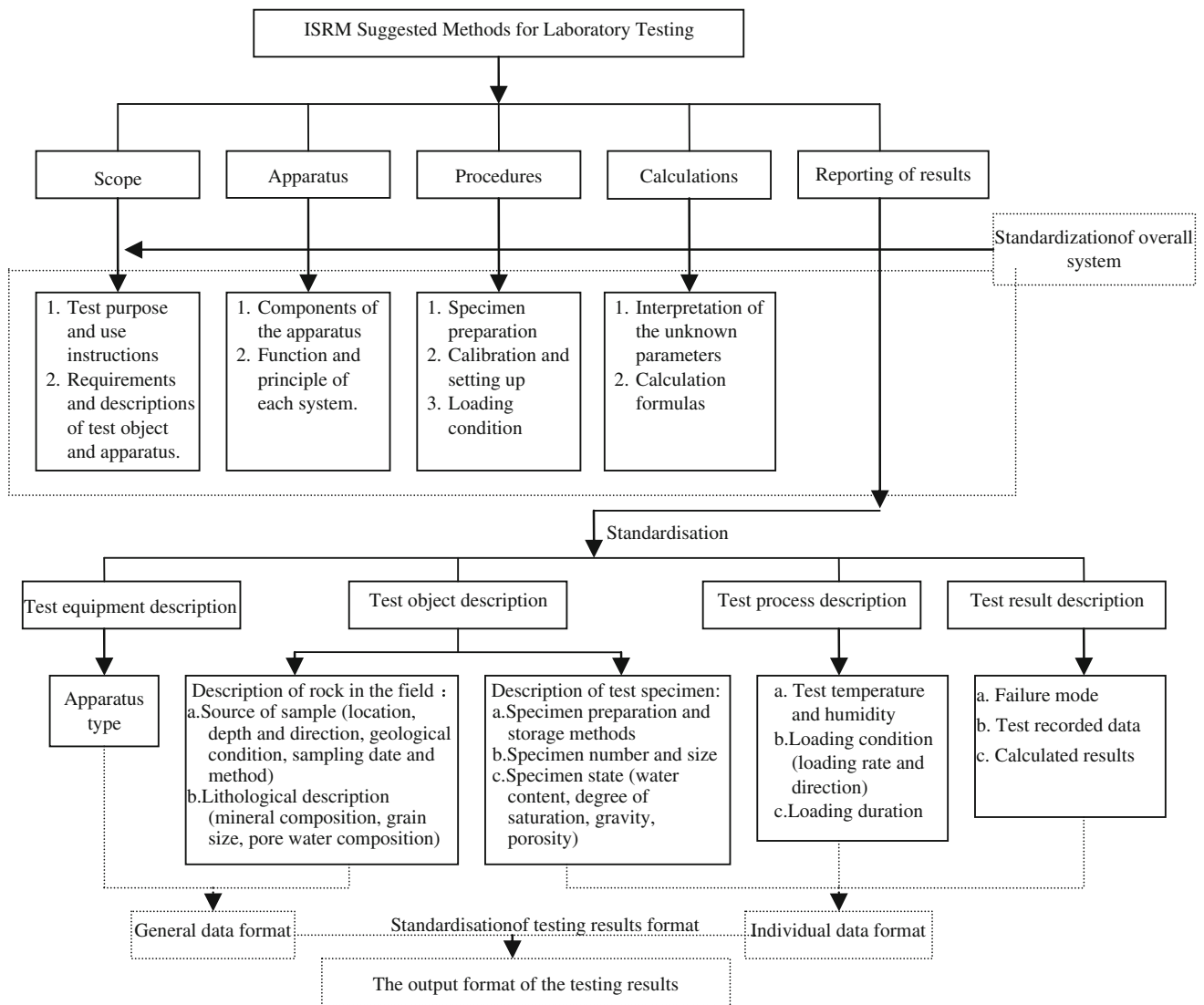


Fig. 2 The standard items for the ISRM suggested methods for laboratory testing

nodes which are a string, for example, “Apparatus Name”, can be defined in Appendix 4.

There is a data structure document for each ISRM Suggested Method. The data structure document for UCS testing, for example, can be named as “UCS.xsd”.

3.2 The Data Storage Document

The data storage document is to define the storage format of the data having the structure in Fig. 3. It should have the following advantages:

1. Good compression to enable the storage of a large number of test data.
2. Convenience for the integration of structured test data with different sources.

3. Ability for updates through this digital format. If any part of the data changes, the document can be automatically updated without resending the entire structured data.

XML, as a digital format, is very effective for these requirements (Bowman 1998; Wang 2001; Durant 2003; Nance and Hay 2005; Byron and Lysandros 2006; Caronna 2006; Chandler et al. 2006; Madria et al. 2008; Bardet and Zand 2009). According to the data structure in Fig. 3, the data can be stored in their own nodes. For example, for the data for the node $\langle \text{SpecimenNo} \rangle$, the datum “1” is stored as $\langle \text{SpecimenNo} \rangle 1 \langle / \text{SpecimenNo} \rangle$. It is a text format which is independent of the language (see an example in Appendix 5).

The testing results can be input by using the user interface (see Fig. 5 for input interface, an example for uniaxial compressive strength tests, UCS). Photographs of specimen

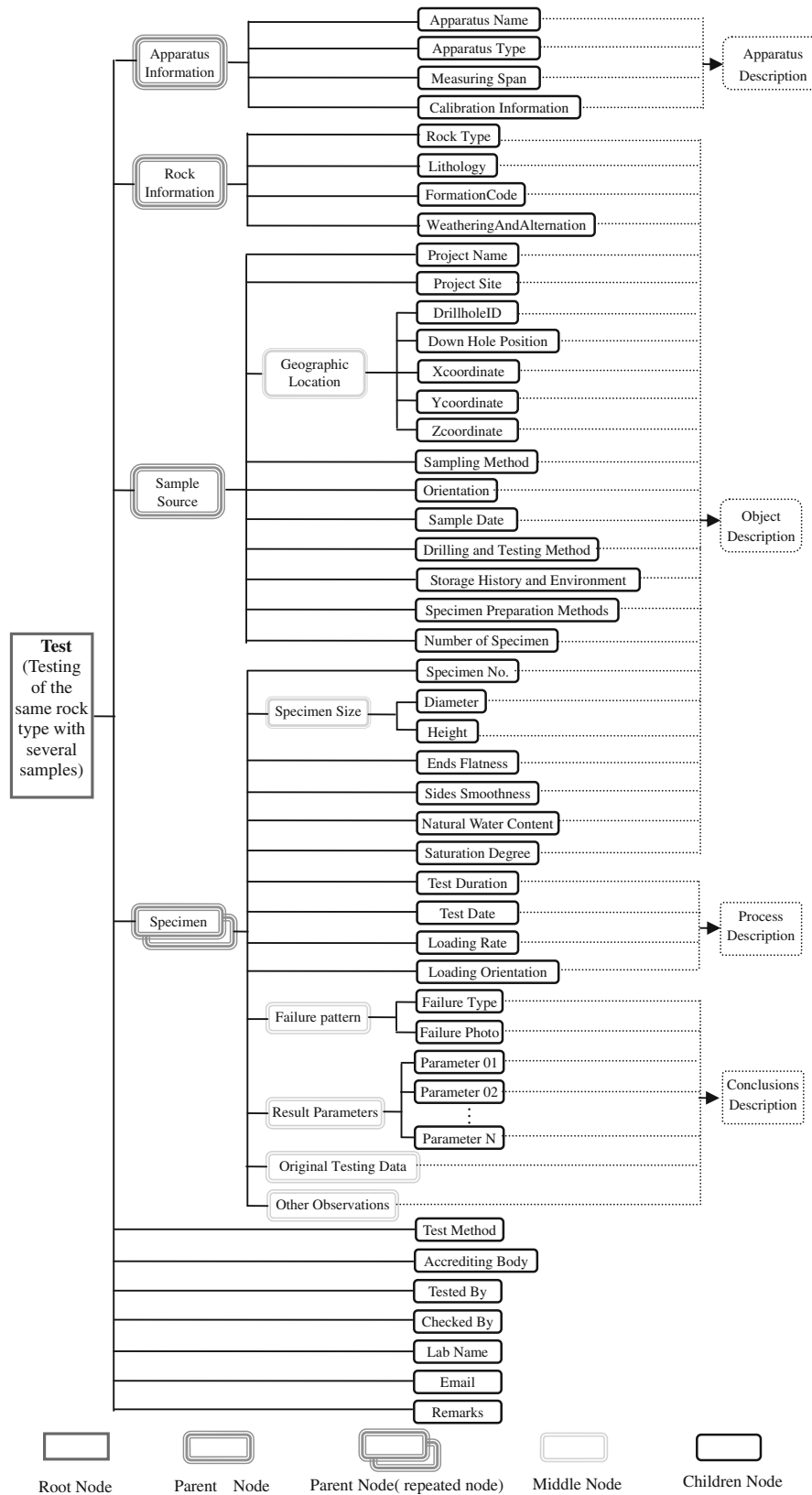


Fig. 3 The overall structure tree in the data structure document

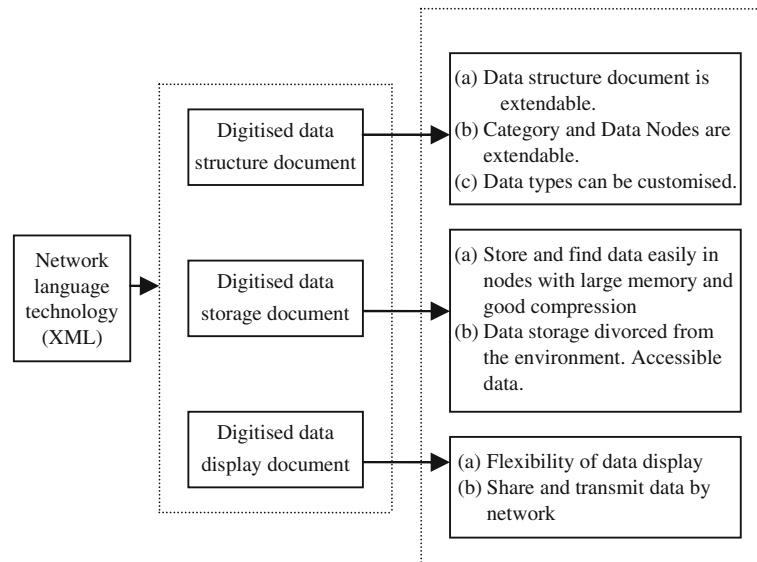


Fig. 4 Digitisation of the ISRM suggested methods for rock laboratory testing

Electronic Format for UCS Test

ISRM Suggested Method for UCS Test in Electronic Format

Input test information

Apparatus Information

Apparatus Name: Materials testing system Measuring Span: Axial force capacities 2600 kN, Maximum travel range for axial extensometer: -4 to +4(mm), 1

Apparatus Type: MTS 815.04 Calibration Information: Axial force: 0.5% of full scale range, Maximum non-linearity for axial extensometer.

Rock Information

Rock Type: sandstone Formation Code: J3

Lithology: Contains quartz, feldspar, mica and a small amount of accessory

Weathering and Alteration: moderate weathering, no alternation

Sample Source

Project Name: Historic preservation for Longyou grottoes

Project Site: Longyou Sampling Method: Drill hole sampling

Orientation: North by West Sample Date: 2010-01-01

Number of Specimen: 5 Note: Geographic Location could be defined in two ways. Choose one fit you.

Geographic Location:

Coordinate System Drillhole Survey Notation

X-coordinate(m): Drillhole ID: 327-16A

Y-coordinate(m): Down-hole position(m): 24.55

Z-coordinate(m):

Information for Each Specimen

Specimen No. 1 Height(mm): 100

Diameter(mm): 50 Sides Smoothness(mm): 0.30

Ends Flatness(mm): 0.02 Saturation Degree: 0.021

Water Content: 0.021 Test Duration(Hour): 0.15

Loading Rate(MPa/s): 0.5 Loading Orientation: 90

Test Date: 2010-02-01 UCS(MPa): 0.9075

Young's Modulus(GPa): 36.0141 Failure Type: Shear

Poisson's Ratio: 0.3262 Modulus Method: Tangent Modulus

At what Axial stress level to determine the modulus: 0.5

Additional information

Attach the original data? Attach the picture?

Yes No Yes No

Add

Fig. 5 An example of the interface for user input

failure and testing curves, etc. can be uploaded and added in the report of testing results (see Fig. 6 as an example). Moreover, the type of the attached pictures can be chosen in

the user interface (Fig. 7). The recorded data may have different formats according to the testing system. The original testing data recorded by the testing system for each

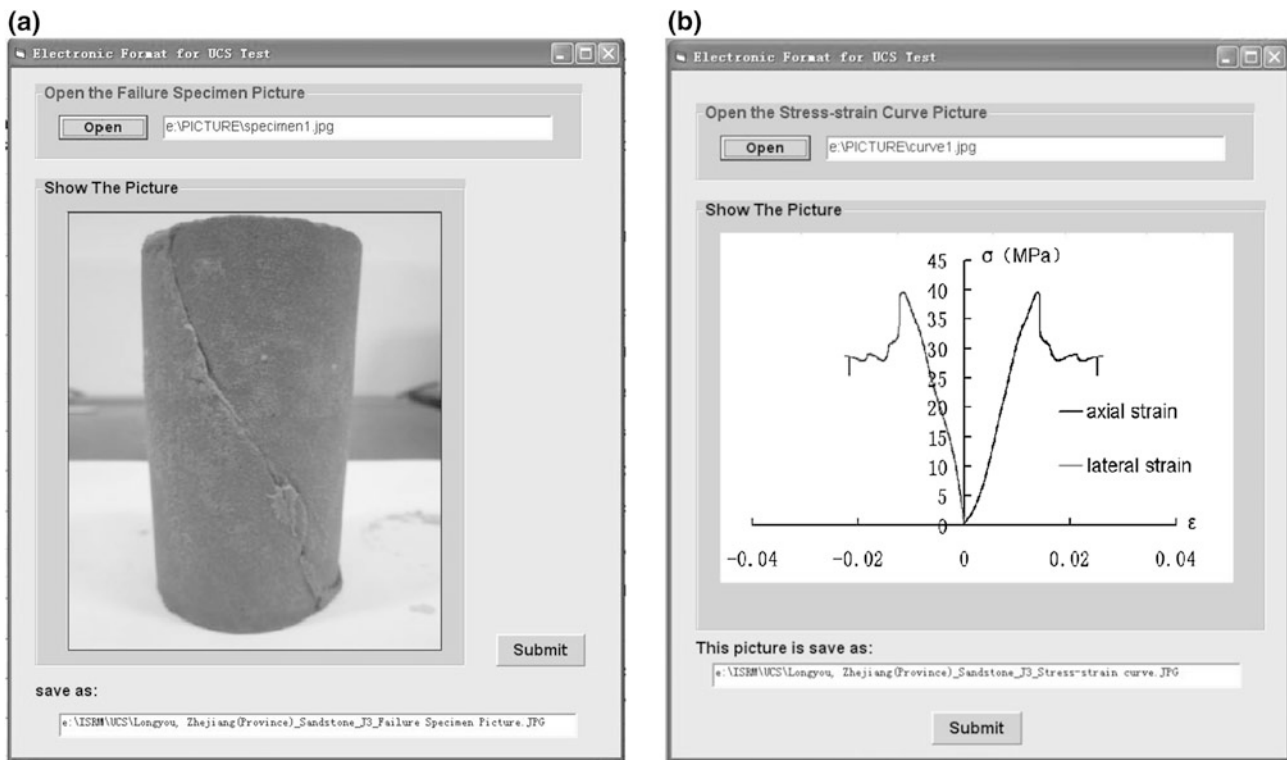


Fig. 6 An example of uploading of **a** failure specimen picture and **b** stress–strain curve

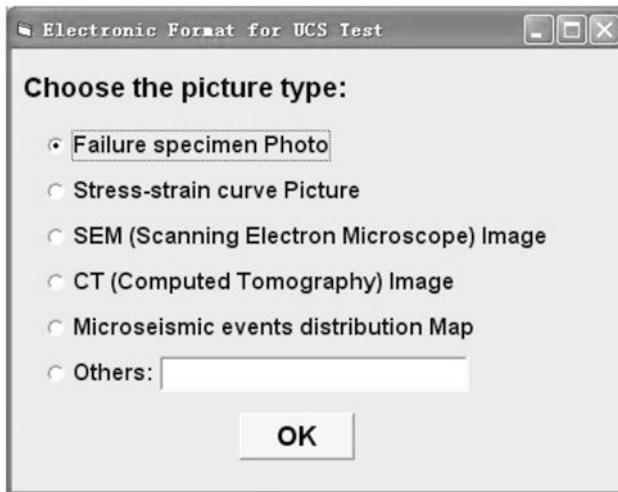


Fig. 7 The choose window for the attached picture

rock specimen can also be transferred into the standard format shown by children nodes of the middle node “OriginalTestingData” and stored as an attached node. The calculation equations included in the Suggested Method can be also displayed to obtain the testing results (see Fig. 8 for an example of calculation of the UCS).

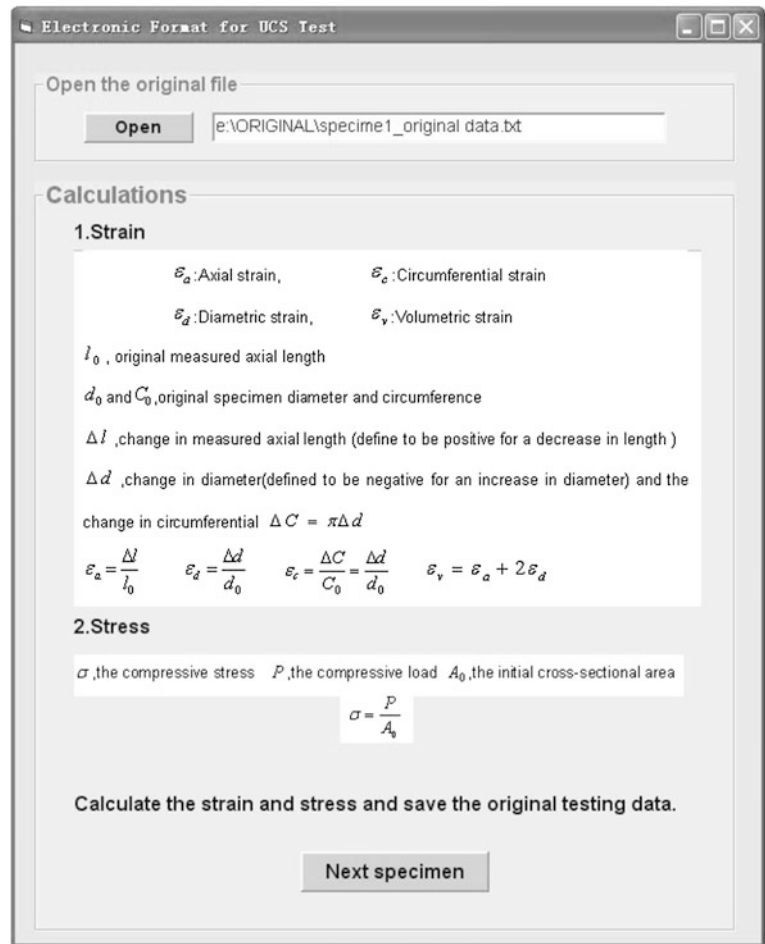
The testing results are stored in the user’s name, i.e., the name of the rock type with project site, formation code and testing method. For example, the determination of the UCS

testing for sandstone of late Jurassic, J3, at Longyong Grottoes, the data storage document can be named as “Longyong_Sandstone_J3_UCS.xml”.

3.3 The Data Display Document

The purpose of the data display document is to define the display format of the data described by the data structure document and the storage document. XSL, Extensible Style sheet Language, can be used to present the XML data in a readable format. Each test parameter’s unit could be specified in this data display document (XSL). The data are displayed in a tabular format. The photographs and testing curves can also be included by inserting the data for the attached nodes. The data of the node “Specimen” are displayed in rows of the number of the specimens, one row for the testing results of each specimen. The data display document is defined in the corresponding file “.xsl”, for example, “xxx_xxx_xxx_UCS.xsl” for the data display document of the testing result report in the UCS test and “xxx_xxx_xxx_(Original)UCS.xsl” for the data display document of the original test data in the UCS test. Moreover, its flexibility in display patterns allows bespoke design by referring to the user’s requirement. The testing results report can be stored at the users’ local computer (Fig. 9a) and uploaded on the ISRM Website (Fig. 9b) to enable data

Fig. 8 An example of the calculation equations for the recorded test data leading to the actual test results



sharing around the world. The reporting of the testing results can include photographs and curves (Fig. 10). The original testing data can also be displayed, e.g., for specimen 1 in Fig. 11.

4 Notes and Recommendations for the Electronic Formats for Different ISRM Suggested Methods

Based on the standardisation and digitisation methods mentioned above, each ISRM Suggested Method has its own data structure and its own three files, including the data structure document with “.xsd”, data storage document with “.xml”, and data display document with “.xsl”. The data structure for a given ISRM Suggested Method can be generated by modifying Fig. 3 according to its data items. The corresponding three files, including the data structure document, the data storage document and the data display document, can be changed accordingly. For example, the data structure and three files, UCS.xsd, UCS.xml, and UCS.xsl, for reporting of UCS testing have been established in Appendix 5.

A code has been developed to perform the process of the electronic format for storage and reporting of the testing data and results for the existing ISRM Suggested Methods for rock laboratory tests, including uniaxial compressive strength, shear strength, triaxial compressive strength, point load strength index, and tensile strength, etc. The original testing data from the Suggested Methods recorded from the testing system can be transferred into the standard format. The testing results can be calculated by using the equations and methods given in the ISRM Suggested Methods. The testing results can be stored automatically from the calculation, uploading of the calculated results or with input from the interface. The reporting of the testing results can be displayed on a personal computer or through the Web.

The procedure is outlined for practical implementation as follows (by taking reporting of Longyou sandstone UCS as an example).

Step 1: Run the code LabTestElectronicformat.exe.

Step 2: Click the ISRM Suggested Method for testing, e.g., UCS (Fig. 12).

Step 3: Designate the storage path for the digitised files and create the data structure document for testing, e.g., UCS (see Fig. 13).

(a)

The screenshot shows an Excel spreadsheet with the following data:

The Uniaxial Compressive Test of Rock Materials																				
Apparatus Name:		Materials testing system										Apparatus Type:		MTS 815.04						
Measuring Span:		Axial force capacities 2600 kN, Maximum travel range for axial extensometer -4 to +4(mm), Maximum chordal travel range for circumferential extensometer -2.5 to +12.5mm																		
Calibration Information:		Axial force 0.5% of full scale range, Maximum non-linearity for axial extensometer: 0.15% of range, Maximum non-linearity for circumferential extensometer: 0.30% of range																		
Rock Type:		sandstone		Lithology:		Contains quartz, feldspar, mica and a small amount of accessory minerals and composed by chlorite, gypsum														
Weathering And Alteration:		moderate weathering, no alternation										Geographic Location (x,y,z in local coordinates)								
Project Site:		Longyou					Drillhole_ID:		DHPosition(m):											
Project Name:		Historic preservation for Longyou grottoes					X-coordinate(m):		143.75	Y-coordinate(m):		22.52	Z-coordinate(m):		131.42					
Orientation:		North by West		Formation Code:		J3		Number of Specimen:					5							
Sample Date:		2010-01-01		Sampling Method:		Drill hole sampling					Remark:					All the data is unreal just for example				
Tested by :		HongZheng		Lab Name:		State Key Laboratory of Geomechanics and Geotechnical Engineering					Email:					hongzhengjirm@gmail.com				
Test Method:		ISRM Suggested Method for the Uniaxial Com					Accrediting Body:		UKAS 0000					Checked By:		Tom				
Specimen No	Specimen Size		Ends Flatness (mm)	Sides Smoothness (mm)	Water content (%)	Saturation Degree (%)	Test Duration (Hour)	Test Date	Loading Orientation	Loading Rate (MPa/s)	Failure Pattern	UCS (MPa)	Young's Modulus (GPa)	Poisson's Ratio	Modulus Method	Axial stress level to determine the modulus (%)				
	Diameter (mm)	Average Height (mm)																		
1	50.0	100.0	0.02	0.30	2.1	2.1	0.15	2010-02-01	90.0	0.5	Shear	17.5	3614.1	0.32	Tangent Modulus	50.0				
2	50.0	100.0	0.02	0.30	2.1	2.1	0.15	2010-02-02	90.0	0.5	Shear	13.3	3806.1	0.37	Tangent Modulus	50.0				
3	50.0	100.0	0.02	0.30	2.1	2.1	0.15	2010-02-03	90.0	0.5	Shear	18.7	3428.5	0.33	Tangent Modulus	50.0				
4	50.0	100.0	0.02	0.30	2.1	2.1	0.15	2010-02-04	90.0	0.5	Shear	13.8	2964.9	0.31	Tangent Modulus	50.0				
5	50.0	100.0	0.02	0.30	2.1	2.1	0.15	2010-02-05	90.0	0.5	Shear	16.8	2861.4	0.29	Tangent Modulus	50.0				

(b)

The screenshot shows a web browser displaying the following structured report:

The Uniaxial Compressive Test Of Rock Materials

Apparatus Information

Apparatus Name: Materials testing system | Apparatus Type: MTS 815.04
 Measuring Span: Axial force capacities 2600 kN, Maximum travel range for axial extensometer -4 to +4(mm); Maximum chordal travel range for circumferential extensometer -2.5 to +12.5mm
 Calibration Information: Axial force 0.5% of full scale range, Maximum non-linearity for axial extensometer: 0.15% of range; Maximum non-linearity for circumferential extensometer: 0.30% of range

Rock Information

Rock Type: sandstone | Lithology: Contains quartz, feldspar, mica and a small amount of accessory minerals and composed by chlorite, gypsum.
 Formation Code: J3 | Alteration and Weathering: moderate weathering, no alternation

Sample Source

Project Site: Longyou | Geographic Location: X=143.75, Y=22.52, Z=131.42, Drillhole_ID: DHPosition(m):
 Project Name: Historic preservation for Longyou grottoes
 Orientation: North by West | Number of Specimen: 5 | Sample Date: 2010-01-01 | Sampling Method: Drill hole sampling
 Remark: All the data is unreal just for example

Specimen No	Specimen Size		Ends Flatness (mm)	Sides Smoothness (mm)	Water Content (%)	Saturation Degree(%)	Test Duration (Hour)	TestDate	Loading Orientation (deg)	Loading Rate (MPa/s)	Failure Pattern	UCS (MPa)	Young's Modulus (GPa)	Poisson's Ratio	Type of modulus of elasticity	Axial stress level to determine the modulus (%)
	Diameter (mm)	Height (mm)														
1	50.0	100.0	0.02	0.30	2.1	2.1	0.15	2010-02-01	90.0	0.5	Shear	17.5	3614.1	0.32	Tangent Modulus	50.0
2	50.0	100.0	0.02	0.30	2.1	2.1	0.15	2010-02-02	90.0	0.5	Shear	13.3	3806.1	0.37	Tangent Modulus	50.0
3	50.0	100.0	0.02	0.30	2.1	2.1	0.15	2010-02-03	90.0	0.5	Shear	18.7	3428.5	0.33	Tangent Modulus	50.0
4	50.0	100.0	0.02	0.30	2.1	2.1	0.15	2010-02-04	90.0	0.5	Shear	13.8	2964.9	0.31	Tangent Modulus	50.0

Fig. 9 An example of reporting of testing results in the format of a local computer and b the Web

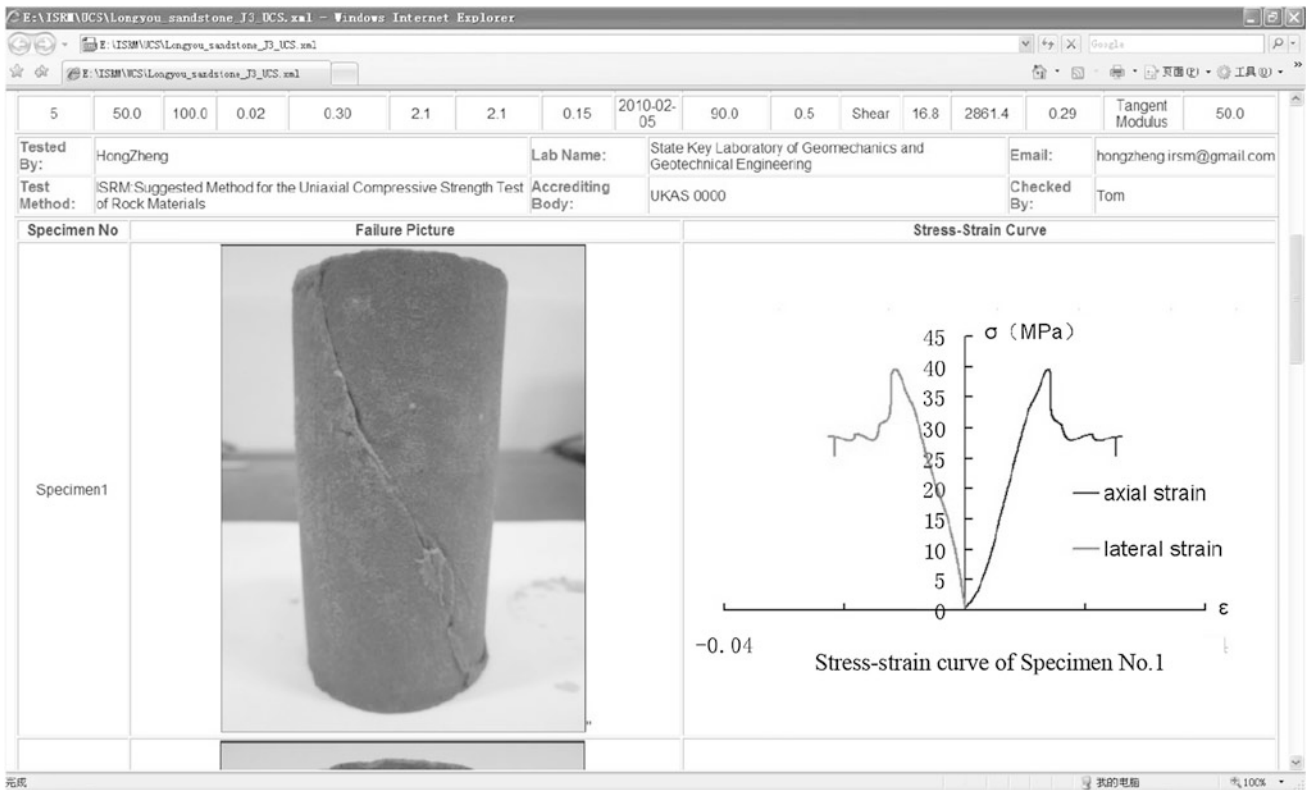


Fig. 10 Reporting of the testing results including photograph and figures

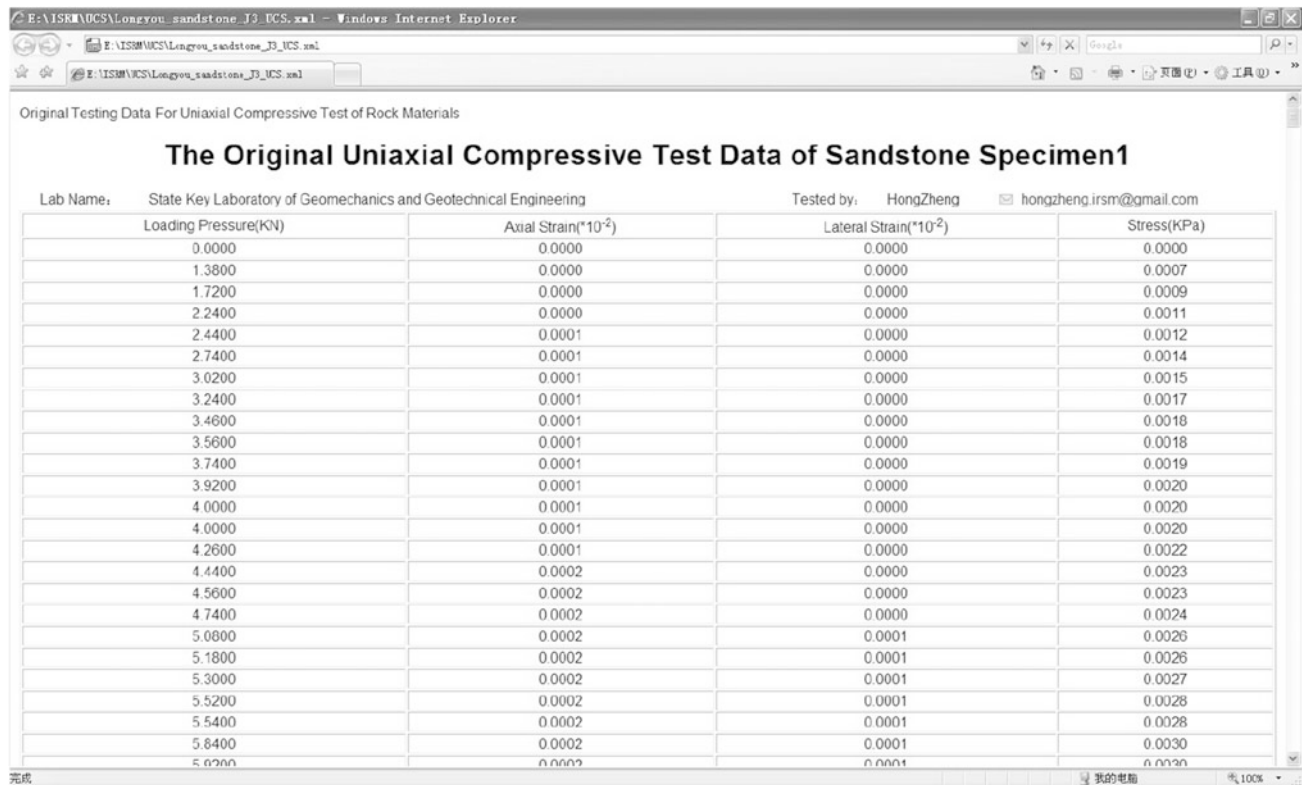


Fig. 11 An example of the display of the original test data

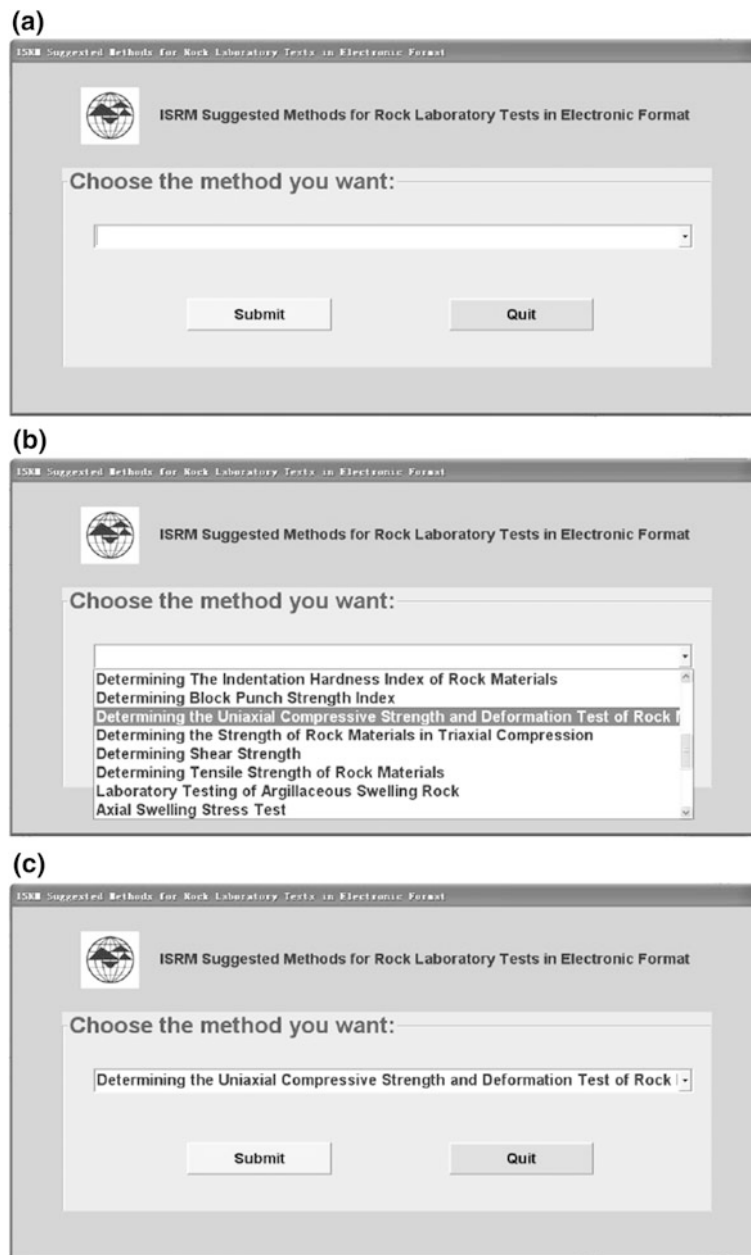


Fig. 12 Interface for selection of the ISRM suggested methods

- Step 4: Perform a standard process of electronic format.
1. Select input mode of the testing results by using input interface or uploading the test result file obtained by the software of the testing system. For the former, the testing results for each specimen are inputted one by one (see Fig. 5). For the latter, the data structure in the existing Excel file shall follow the standard format suggested in this method and matching the data structures (see Fig. 9a). Upload the photographs of failure mode and stress–strain curve of each specimen by clicking the corresponding boxes and files (see Figs. 6, 7).
 2. Upload the original data file by clicking the box (see Fig. 8). The data structure in the existing file shall follow the standard format suggested in this method. For some testing systems, there may be some calculations—for example, for UCS testing, calculating stress and strain. The system provides this function (see Fig. 8).
 3. Input the file name of the testing results given by the user with the format of “ProjectSite_Rocktype_FormationCode” (Fig. 14). For example, Longyou_sandstone_J3_UCS.xml for the testing results for sandstone

Fig. 13 Interface for designating the storage path for the digitised files and creating the data structure document for testing

Fig. 14 Input of file names and display type of the testing report and original data

of late Jurassic, J3, at Longyou Grottoes. All the testing results, plus the original testing data for each specimen, are stored as standard electronic format “.xml”.

4. Input the data display file names for the testing results report and the original testing data (see Fig. 14), e.g., Longyou_sandstone-J3_UCS.xml for the testing results report and Longyou_sandstone_J3_ (Original)UCS.xml for the original testing data.

Step 5: Output the testing report at the local computer by clicking the box “Local display” and at the Web by clicking the box “Web” (see Fig. 14). Output the original data file at the local computer by clicking the box “Local display” and at the Web by clicking the box “Web” (see Fig. 14). If the testing report and the original testing data are displayed in the local computer, they will be transferred into the excel format and displayed in this format (see Fig. 9a).

With the procedure outlined above, the users do not need to be experts in XML. The electronic formats for updated or new ISRM Suggested Methods for rock laboratory tests can be obtained by modifying the three documents mentioned above. The corresponding codes with interfaces can be developed accordingly.

5 Postscript

There may exist compatibility/uniformity problems between the proposed SM for reporting rock laboratory test data in electronic format with some existing formats for the electronic data transfer of site investigation data which some countries have or are adopting, for example, the AGS, MZGS BTA, AGS4NZ v1.0 (New Zealand), AGS(SG), etc. Nevertheless, the laboratory test data are just a part of the full site investigation data. In order to have the compatibility with the existing electronic transfer formats, e.g., AGS4NZ v1.0 (New Zealand), AGS(SG), and BCA, etc., the SM can also give the output of the testing results in the

format used in these formats. As an example, it shows the additional format for the output for UCS in Appendix 5.4. Input the file name of the compatible format file for AGS4NZ v1.0 (New Zealand) (see Fig. 14), e.g., Long-you_sandstone-J3_(AGS4NZ).txt. The ISRM will be further addressing this issue with the intention of producing a future document on the subject for other existing electronic transfer formats.

Acknowledgments The reviewers, especially Dr. Antonio Samaniego and Professors Hasan Gercek and Seokwon Jeon and Prof. Resat Ulusay, President of ISRM Commission on Testing Methods, Dr. Beck David, Dr. Yingxin Zhou, and Dr. Luis Lamas provided most helpful comments which enabled us to improve the manuscript. They are all appreciated.

Appendix 1

The digital data structure for the “complex type” nodes including root nodes, parent nodes and middle nodes in Fig. 3

```
<xs:element name="Name of a root node, a parent node or a middle node">
  <xs:complexType>
    <xs:sequence>
      <xs:element ref="name of its secondary node 1"/>
      ...
      <xs:element ref="name of its secondary node n"/>
    </xs:sequence>
  </xs:complexType>
</xs:element>
```

For example, the root node “Test” can be defined as follows:

```
<xs:element name="Test">
  <xs:complexType>
    <xs:sequence>
      <xs:element ref="ApparatusInformation"/>
      <xs:element ref="RockInformation"/>
      <xs:element ref="SampleSource"/>
      <xs:element ref="Specimen" maxOccurs="unbounded"/>
    </xs:sequence>
  </xs:complexType>
</xs:element>
```

This part can be modified or extended according to changes of the “complex type” nodes in Fig. 3.

Appendix 2

The digital data structure for the children nodes of “selection” type

```
<xs:element name="Name of a children node in selection type">
  <xs:simpleType>
    <xs:restriction base="xs:string">
      <xs:enumeration value="Option 1"/>
      ...
      <xs:enumeration value="Option n"/>
    </xs:restriction>
  </xs:simpleType>
</xs:element>
```

For example, the children node “Failure Type” can be defined as follows

```
<xs:element name="FailureType">
  <xs:simpleType>
    <xs:restriction base="xs:string">
      <xs:enumeration value="Shear"/>
      <xs:enumeration value="Axial Cleavage"/>
      <xs:enumeration value="Other"/>
    </xs:restriction>
  </xs:simpleType>
</xs:element>
```

This part can be modified or extended according to the change of ‘children nodes’ in Fig. 3.

Appendix 3

The digital data structure for the children node of “decimal” type

```
<xs:element name="Name of a children node in decimal type">
  <xs:simpleType>
    <xs:restriction base="xs:decimal">
      <xs:fractionDigits value="?" /> → Restrict the maximal decimal digits
    </xs:restriction>
  </xs:simpleType>
</xs:element>
```

For example, the children node “Diameter” can be defined as follows

```
<xs:element name="Diameter">
  <xs:simpleType>
    <xs:restriction base="xs:decimal">
      <xs:fractionDigits value="4"/>
    </xs:restriction>
  </xs:simpleType>
</xs:element>
```

Appendix 4

The digital data structure for the children nodes of “string” type

```
<xs:element name="Name of a children node in string type" type="xs:string"/>
```

For example, the children node “Apparatus Name” can be defined as follows

```
<xs:element name="ApparatusName" type="xs:string"/>
```

Appendix 5

The data structure with its children nodes description and the structure of three digitised documents for determining the uniaxial compressive strength and deformability of rock material.

nodes and defining the children nodes. In this structure tree, the children nodes of the middle node “Result Parameters” are defined as “Uniaxial Compressive Strength”, “Young’s modulus”, “Poisson’s ratio”, “Modulus Method” and “Axial Level”. For the middle node “Original Testing Data”, its children nodes include “Time”, “Pressure”, “Axial Strain”, “Lateral Strain” and “Stress”.

5.1 The Data Structure

According to the overall structure tree in Fig. 3, the data structure for UCS test is built up as follows by filtering

5.2 Description of the Children Nodes in the Data Structure

See Table 2.

Table 2 Description of the children nodes in the data structure

Children node name	Suggested unit/type	Description	Example
Apparatus type	String	Type of testing machine	MTS 815.04
Apparatus name	String	Name of testing machine	Materials testing system
Measuring span	String	Testing measuring span for force capacity, axial extensometer and circumferential extensometer	Axial force capacities 2,600 kN; Maximum travel range for axial extensometer: -4 to +4(mm); Maximum chordal travel range for circumferential extensometer: -2.5 to +12.5 mm
Calibration information	String	Calibration accuracy for force capacity, axial extensometer and circumferential extensometer	Axial force: 0.5 % of full scale range; maximum non-linearity for axial extensometer: 0.15 % of range; maximum non-linearity for circumferential extensometer: 0.30 % of range
Rock type	String	Rock type	Sandstone

(continued)

Table 2 (continued)

Children node name	Suggested unit/type		Description	Example
Apparatus type		String	Type of testing machine	MTS 815.04
Lithology		String	Petrographic description of rocks, including the sample's texture, fracturing, alteration, matrix, degree of weathering, structure, etc.	Contains quartz, feldspar, mica and a small amount of accessory minerals and composited by chlorite, gypsum
Formation code		String	Formation code in geologic age	J3 (Late Jurassic)
Weathering and alteration		String	Describe the weathering and alteration condition of sample	Moderate weathering; no alternation
Project name		String	Project title	Historic preservation for Longyou grottoes
Project site		String	Location of the project	Longyou
X-coordinate	m	Decimal (fraction digits: 2)	X-coordinate to describe the geographic location of sampling site	143.76
Y-coordinate	m	Decimal (fraction digits: 2)	Y-coordinate to describe the geographic location of sampling site	22.52
Z-coordinate	m	Decimal (fraction digits: 2)	Depth to top of sample	131.42
Drill hole _ID		String	Sample unique global identifier	327-16A
DH position	m	Decimal (fraction digits: 2)	Down-hole position of drill hole	24.55
Orientation		String	Sample orientation	North by West
Sample date	yyyy-mm-dd	Data	Sampling date	2009-04-09
Sampling method		String (enumeration)	Sampling method	Drill hole sampling
Number of specimens		Integer	The number of specimens in test	5
Specimen number		Integer	Specimen number	1
Diameter	mm	Decimal (fraction digits: 1)	Specimen diameter	50.0
Height	mm	Decimal (fraction digits: 1)	Specimen height	100.0
Ends flatness	mm	Decimal (fraction digits: 2)	The flatness of ends of specimen	0.02
Sides flatness	mm	Decimal (fraction digits: 2)	The flatness of ends of specimen	0.30
Water content	%	Decimal (fraction digits: 1)	Water content of specimen tested	2.1
Saturation deg	%	Decimal (fraction digits: 1)	Saturation deg of specimen tested	2.1
Test duration	Hour	Decimal (fraction digits: 2)	Test duration	0.15

(continued)

Table 2 (continued)

Children node name	Suggested unit/type		Description	Example
Apparatus type		String	Type of testing machine	MTS 815.04
Test date	yyyy-mm-dd	Date	Test date	2010-02-01
Loading orientation	deg	Decimal (fraction digits: 1)	Orientation of the axis of loading with respect to specimen anisotropy	90.0
Loading rate	MPa/s	Decimal (fraction digits: 1)	Loading stress rate	0.5
Failure type		String (enumeration)	Mode of failure	Shear
UCS	MPa	Decimal (fraction digits: 1)	Uniaxial compressive strength	16.8
Young's modulus	GPa	Decimal (fraction digits: 1)	Young's modulus	36.2
Poisson's ratio		Decimal (fraction digits: 2)	Poisson's ratio	0.33
Modulus method		String (enumeration)	Method of determining Young's modulus	Tangent modulus
Axial level	%	Decimal (fraction digits: 1)	Stress level at which modulus has been measured	50 %
Time	s	Decimal (fraction digits: 1)	Time in original test data	76.5
Pressure	KN	Decimal (fraction digits: 4)	Pressure in original test data	24.880201
Axial strain	10–5 mm/mm	Decimal (fraction digits: 4)	Axial strain in original test data	2.0581676
Lateral strain	10–5 mm/mm	Decimal (fraction digits: 4)	Lateral strain in original test data	–4.610667
Stress	MPa	Decimal (fraction digits: 4)	Stress in original test data	1.678518
Test method		String	Test method	ISRM Suggested Method for the uniaxial compressive strength test of rock materials
Accrediting body		String	Accrediting body and reference number (when appropriate)	UKAS 0000
Checked by		String	The checker of the tests	C. Einstein
Tested by		String	The tester of the tests	Tom Yao
Lab name		String	Name of testing laboratory/organisation	SKLGM
Email		String	Email address of responsible person	hongzheng@gmail.com
Remark		String	Remarks	Specimen tested outside required 2.5–3.0 diameter to length ratio

5.3 Three Digitised Documents

1. The structure of the data structure document (*UCS.xsd*):

The structure of the data structure document, UCS.xsd, can be generated by combining the format of Appendices 1, 2, 3 and 4 by following the structure of Appendix 5.1 above. It is described as follows.

```
<?xml version="1.0" encoding="UTF-8" standalone="yes"?>
<!--W3C Schema generated by XMLSpy v2005 rel. 3 U (http://www.altova.com)-->
<xs:schema xmlns:xs="http://www.w3.org/2001/XMLSchema"
elementFormDefault="qualified">
  <xs:annotation>
    <xs:documentation>XML Schema is for the Uniaxial Compressive Strength Test of
Rock Materials.
</xs:documentation>
</xs:annotation>
<xs:element name="ApparatusName" type="xs:string"/>
<xs:element name="ApparatusType" type="xs:string"/>
<xs:element name="MeasuringSpan" type="xs:string"/>
<xs:element name="CalibrationInformation" type="xs:string"/>
<xs:element name="RockType" type="xs:string"/>
<xs:element name="Lithology" type="xs:string"/>
<xs:element name="FormationCode" type="xs:string"/>
<xs:element name="WeatheringAndAlteration" type="xs:string"/>
<xs:element name="ProjectName" type="xs:string"/>
<xs:element name="ProjectSite" type="xs:string"/>
<xs:element name="SampleDate" type="xs:date"/>
<xs:element name="Orientation" type="xs:string"/>
<xs:element name="SamplingMethod" type="xs:string"/>
<xs:element name="TestDate" type="xs:date"/>
<xs:element name="FailurePhoto" type="xs:string"/>
<xs:element name="TestMethod" type="xs:string"/>
<xs:element name="AccreditingBody" type="xs:string"/>
<xs:element name="CheckedBy" type="xs:string"/>
<xs:element name="TestedBy" type="xs:string"/>
<xs:element name="LabName" type="xs:string"/>
<xs:element name="Email" type="xs:string"/>
<xs:element name="Remark" type="xs:string"/>
<xs:element name="SpecimenNo" type="xs:integer"/>
<xs:element name="NumberOfSpecimen" type="xs:integer"/>
<xs:element name="Drillhole_ID" type="xs:integer"/>
<xs:element name="DHPosition" type="xs:integer"/>
<xs:element name="ModulusMethod">
  <xs:simpleType>
    <xs:restriction base="xs:string">
      <xs:enumeration value="Tangent Modulus"/>
      <xs:enumeration value="Average Modulus"/>
      <xs:enumeration value="Secant Modulus"/>
    </xs:restriction>
  </xs:simpleType>
</xs:element>
</xs:schema>
```



```

    </xs:simpleType>
  </xs:element>
  <xs:element name="FailureType">
    <xs:simpleType>
      <xs:restriction base="xs:string">
        <xs:enumeration value="Shear"/>
        <xs:enumeration value="Axial Cleavage"/>
        <xs:enumeration value="Other"/>
      </xs:restriction>
    </xs:simpleType>
  </xs:element>
  <xs:element name="Xcoordinate">
    <xs:simpleType>
      <xs:restriction base="xs:decimal">
        <xs:fractionDigits value="2"/>
      </xs:restriction>
    </xs:simpleType>
  </xs:element>
  <xs:element name="Ycoordinate">
    <xs:simpleType>
      <xs:restriction base="xs:decimal">
        <xs:fractionDigits value="2"/>
      </xs:restriction>
    </xs:simpleType>
  </xs:element>
  <xs:element name="Zcoordinate">
    <xs:simpleType>
      <xs:restriction base="xs:decimal">
        <xs:fractionDigits value="2"/>
      </xs:restriction>
    </xs:simpleType>
  </xs:element>
  <xs:element name="Time">
    <xs:simpleType>
      <xs:restriction base="xs:decimal">
        <xs:fractionDigits value="1"/>
      </xs:restriction>
    </xs:simpleType>
  </xs:element>
  <xs:element name="EndsFlatness">
    <xs:simpleType>
      <xs:restriction base="xs:decimal">
        <xs:fractionDigits value="2"/>
      </xs:restriction>
    </xs:simpleType>
  </xs:element>
  <xs:element name="SidesSmoothness">
    <xs:simpleType>
      <xs:restriction base="xs:decimal">
        <xs:fractionDigits value="2"/>
      </xs:restriction>
    </xs:simpleType>
  </xs:element>
  <xs:element name="TestDuration">
    <xs:simpleType>
      <xs:restriction base="xs:decimal">
        <xs:fractionDigits value="2"/>
      </xs:restriction>
    </xs:simpleType>
  </xs:element>
  <xs:element name="LoadingRate">
    <xs:simpleType>
      <xs:restriction base="xs:decimal">
        <xs:fractionDigits value="1"/>
      </xs:restriction>
    </xs:simpleType>
  </xs:element>
  <xs:element name="AxialLevel">
    <xs:simpleType>
      <xs:restriction base="xs:decimal">
        <xs:fractionDigits value="1"/>
      </xs:restriction>
    </xs:simpleType>
  </xs:element>
  <xs:element name="LoadingOrientation">
    <xs:simpleType>
      <xs:restriction base="xs:decimal">
        <xs:fractionDigits value="1"/>
      </xs:restriction>
    </xs:simpleType>
  </xs:element>
  <xs:element name="WaterContent">
    <xs:simpleType>
      <xs:restriction base="xs:decimal">
        <xs:fractionDigits value="1"/>
      </xs:restriction>
    </xs:simpleType>
  </xs:element>
  <xs:element name="SaturationDegree">
    <xs:simpleType>
      <xs:restriction base="xs:decimal">
        <xs:fractionDigits value="1"/>
      </xs:restriction>
    </xs:simpleType>
  </xs:element>

```

```

</xs:element>
<xs:element name="Diameter">
  <xs:simpleType>
    <xs:restriction base="xs:decimal">
      <xs:fractionDigits value="1"/>
    </xs:restriction>
  </xs:simpleType>
</xs:element>
<xs:element name="Height">
  <xs:simpleType>
    <xs:restriction base="xs:decimal">
      <xs:fractionDigits value="1"/>
    </xs:restriction>
  </xs:simpleType>
</xs:element>
<xs:element name="UCS">
  <xs:simpleType>
    <xs:restriction base="xs:decimal">
      <xs:fractionDigits value="1"/>
    </xs:restriction>
  </xs:simpleType>
</xs:element>
<xs:element name="YoungsModulus">
  <xs:simpleType>
    <xs:restriction base="xs:decimal">
      <xs:fractionDigits value="1"/>
    </xs:restriction>
  </xs:simpleType>
</xs:element>
<xs:element name="PoissonsRatio">
  <xs:simpleType>
    <xs:restriction base="xs:decimal">
      <xs:fractionDigits value="2"/>
    </xs:restriction>
  </xs:simpleType>
</xs:element>
<xs:element name="Pressure">
  <xs:simpleType>
    <xs:restriction base="xs:decimal">
      <xs:fractionDigits value="4"/>
    </xs:restriction>
  </xs:simpleType>
</xs:element>
<xs:element name="AxialStrain">
  <xs:simpleType>
    <xs:restriction base="xs:decimal">
      <xs:fractionDigits value="4"/>
    </xs:restriction>
  </xs:simpleType>
</xs:element>
</xs:restriction>
</xs:simpleType>
</xs:element>
<xs:element name="LateralStrain">
  <xs:simpleType>
    <xs:restriction base="xs:decimal">
      <xs:fractionDigits value="4"/>
    </xs:restriction>
  </xs:simpleType>
</xs:element>
<xs:element name="Stress">
  <xs:simpleType>
    <xs:restriction base="xs:decimal">
      <xs:fractionDigits value="4"/>
    </xs:restriction>
  </xs:simpleType>
</xs:element>
<xs:element name="GeographicLocation">
  <xs:complexType>
    <xs:sequence>
      <xs:element ref="Xcoordinate" minOccurs="0"/>
      <xs:element ref="Ycoordinate" minOccurs="0"/>
      <xs:element ref="Zcoordinate" minOccurs="0"/>
      <xs:element ref="Drillhole_ID" minOccurs="0"/>
      <xs:element ref="DHPosition" minOccurs="0"/>
    </xs:sequence>
  </xs:complexType>
</xs:element>
<xs:element name="FailurePattern">
  <xs:complexType>
    <xs:sequence>
      <xs:element ref="FailureType"/>
      <xs:element ref="FailurePhoto"/>
    </xs:sequence>
  </xs:complexType>
</xs:element>
<xs:element name="SpecimenSize">
  <xs:complexType>
    <xs:sequence>
      <xs:element ref="Diameter"/>
      <xs:element ref="Height"/>
    </xs:sequence>
  </xs:complexType>
</xs:element>
<xs:element name="ApparatusInformation">
  <xs:complexType>
    <xs:sequence>

```

```

        <xs:element ref="ApparatusType"/>
        <xs:element ref="ApparatusName"/>
        <xs:element ref="MeasuringSpan"/>
        <xs:element ref="CalibrationInformation"/>
    </xs:sequence>
</xs:complexType>
</xs:element>
<xs:element name="RockInformation">
    <xs:complexType>
        <xs:sequence>
            <xs:element ref="RockType"/>
            <xs:element ref="Lithology"/>
            <xs:element ref="FormationCode"/>
            <xs:element ref="WeatheringAndAlteration"/>
        </xs:sequence>
    </xs:complexType>
</xs:element>
<xs:element name="SampleSource">
    <xs:complexType>
        <xs:sequence>
            <xs:element ref="ProjectName"/>
            <xs:element ref="ProjectSite"/>
            <xs:element ref="GeographicLocation"/>
            <xs:element ref="Orientation"/>
            <xs:element ref="SampleDate"/>
            <xs:element ref="SamplingMethod"/>
            <xs:element ref="NumberOfSpecimen"/>
        </xs:sequence>
    </xs:complexType>
</xs:element>
<xs:element name="ResultParameters">
    <xs:complexType>
        <xs:sequence>
            <xs:element ref="UCS"/>
            <xs:element ref="YoungsModulus"/>
            <xs:element ref="PoissonsRatio"/>
            <xs:element ref="ModulusMethod"/>
            <xs:element ref="AxialLevel"/>
        </xs:sequence>
    </xs:complexType>
</xs:element>
<xs:element name="OriginalTestData">
    <xs:complexType>
        <xs:sequence>
            <xs:element ref="Time"/>
            <xs:element ref="Pressure"/>
            <xs:element ref="AxialStrain"/>
            <xs:element ref="LateralStrain"/>
            <xs:element ref="Stress"/>
        </xs:sequence>
    </xs:complexType>
</xs:element>
<xs:element name="Specimen">
    <xs:complexType>
        <xs:sequence>
            <xs:element ref="SpecimenNo"/>
            <xs:element ref="SpecimenSize"/>
            <xs:element ref="EndsFlatness"/>
            <xs:element ref="SidesSmoothness"/>
            <xs:element ref="WaterContent"/>
            <xs:element ref="SaturationDegree"/>
            <xs:element ref="TestDuration"/>
            <xs:element ref="TestDate"/>
            <xs:element ref="LoadingOrientation"/>
            <xs:element ref="LoadingRate"/>
            <xs:element ref="FailurePattern"/>
            <xs:element ref="ResultParameters"/>
            <xs:element ref="OriginalTestData" minOccurs="0"/>
        </xs:sequence>
    </xs:complexType>
</xs:element>
<xs:element name="Test">
    <xs:complexType>
        <xs:sequence>
            <xs:element ref="ApparatusInformation"/>
            <xs:element ref="RockInformation"/>
            <xs:element ref="SampleSource"/>
            <xs:element ref="Specimen" maxOccurs="unbounded"/>
            <xs:element ref="TestMethod"/>
            <xs:element ref="AccreditingBody"/>
            <xs:element ref="CheckedBy"/>
            <xs:element ref="TestedBy"/>
            <xs:element ref="LabName"/>
            <xs:element ref="Email"/>
            <xs:element ref="Remark"/>
        </xs:sequence>
    </xs:complexType>
</xs:element>
</xs:schema>

```

(2) The data storage document for UCS (UCS.xml)

Generally, according to the sequence of the children nodes from top to down shown in Fig. 15, the data storage document is structured as follows

```

<Name of root node>
  <Name of parent node 1>
    <Name of middle node 1>
      <Name of children node 1> Value of children node <Name of children node 1 >
      ...
      <Name of children node m> Value of children node <Name of children node m>
    </Name of middle node 1>
    ...
    <Name of middle node n>
      <Name of children node 1> Value of children node <Name of children node 1 >
      ...
      <Name of children node p> Value of children node <Name of children node p>
    </Name of middle node n>
  </Name of parent node 1>
</Name of root node>

```

Accordingly, the data storage document for UCS of a specimen of Longyou Sandstone is defined as:

```

<?xml version="1.0" standalone="yes"?>
<?xml-stylesheet type="text/xsl" href="Longyou_sandstone_J3_UCS.xsl"?>
<Test>
  <ApparatusInformation>
    <ApparatusType>MTS 815.04</ApparatusType>
    <ApparatusName>Materials testing system</ApparatusName>
    <MeasuringSpan>Axial force capacities 2600 kN; Maximum travel range for axial
    extensometer:-4 to +4(mm); Maximum chordal travel range for circumferential extensometer:
    -2.5 to +12.5mm</MeasuringSpan>
    <CalibrationInformation>Axial force:0.5% of full scale range; Maximum non-linearity
    for axial extensometer: 0.15% of range; Maximum non-linearity for circumferential extensometer:
    0.30% of range</CalibrationInformation>
  </ApparatusInformation>
  <RockInformation>
    <RockType>sandstone</RockType>
    <Lithology>Contains quartz, feldspar, mica and a small amount of accessory minerals
    and composited by chlorite, gypsum.</Lithology>
    <FormationCode>J3</FormationCode>
    <WeatheringAndAlteration>moderate weathering;no
    alternation</WeatheringAndAlteration>
  </RockInformation>
  <SampleSource>
    <ProjectName>Historic preservation for Longyou grottoes</ProjectName>
    <ProjectSite>Longyou</ProjectSite>
    <GeographicLocation>

```

```

    <Xcoordinate>143.76</Xcoordinate>
    <Ycoordinate>22.52</Ycoordinate>
    <Zcoordinate>131.42</Zcoordinate>
</GeographicLocation>
<Orientation>North by West</Orientation>
<SampleDate>2010-01-01</SampleDate>
<SamplingMethod>Drill hole sampling</SamplingMethod>
<NumberOfSpecimen>5</NumberOfSpecimen>
</SampleSource>
<Specimen>
  <SpecimenNo>1</SpecimenNo>
  <SpecimenSize>
    <Diameter>50.0</Diameter>
    <Height>100.0</Height>
  </SpecimenSize>
  <EndsFlatness>0.02</EndsFlatness>
  <SidesSmoothness>0.30</SidesSmoothness>
  <WaterContent>2.1</WaterContent>
  <SaturationDegree>2.1</SaturationDegree>
  <TestDuration>0.15</TestDuration>
  <TestDate>2010-02-01</TestDate>
  <LoadingOrientation>90.0</LoadingOrientation>
  <LoadingRate>0.5</LoadingRate>
  <FailurePattern>
    <FailureType>Shear</FailureType>
  </FailurePattern>
  <ResultParameters>
    <UCS>17.5</UCS>
    <YoungsModulus>3614.1</YoungsModulus>
    <PoissonsRatio>0.32</PoissonsRatio>
    <ModulusMethod>Tangent Modulus</ModulusMethod>
    <AxialLevel>50.0</AxialLevel>
  </ResultParameters>
  <OriginalTestData>
    <Pressure>0.0000</Pressure>
    <AxialStrain>0.0000</AxialStrain>
    <LateralStrain>0.0000</LateralStrain>
    <Stress>0.0000</Stress>
  </OriginalTestData>
  <OriginalTestData>
    <Pressure>1.3800</Pressure>
    <AxialStrain>0.0020</AxialStrain>
    <LateralStrain>0.0005</LateralStrain>
    <Stress>4392.6800</Stress>
  </OriginalTestData>
  <OriginalTestData>
    <Pressure>1.7200</Pressure>
    <AxialStrain>0.0030</AxialStrain>
    <LateralStrain>0.0004</LateralStrain>
    <Stress>5474.9350</Stress>
  </OriginalTestData>
  ... ..
</Specimen>
<Specimen>
  <SpecimenNo>2</SpecimenNo>
  <SpecimenSize>
    <Diameter>50.0</Diameter>
    <Height>100.0</Height>
  </SpecimenSize>
  <EndsFlatness>0.02</EndsFlatness>
  <SidesSmoothness>0.30</SidesSmoothness>
  <WaterContent>2.1</WaterContent>
  <SaturationDegree>2.1</SaturationDegree>
  <TestDuration>0.15</TestDuration>
  <TestDate>2010-02-02</TestDate>
  <LoadingOrientation>90.0</LoadingOrientation>
  <LoadingRate>0.5</LoadingRate>
  <FailurePattern>
    <FailureType>Shear</FailureType>
  </FailurePattern>
  <ResultParameters>
    <UCS>13.3</UCS>
    <YoungsModulus>3806.1</YoungsModulus>
    <PoissonsRatio>0.37</PoissonsRatio>
    <ModulusMethod>Tangent Modulus</ModulusMethod>
    <AxialLevel>50.0</AxialLevel>
  </ResultParameters>
</Specimen>
<Specimen>
  <SpecimenNo>3</SpecimenNo>
  <SpecimenSize>
    <Diameter>50.0</Diameter>
    <Height>100.0</Height>
  </SpecimenSize>
  <EndsFlatness>0.02</EndsFlatness>
  <SidesSmoothness>0.30</SidesSmoothness>
  <WaterContent>2.1</WaterContent>
  <SaturationDegree>2.1</SaturationDegree>

```

```

<TestDuration>0.15</TestDuration>
<TestDate>2010-02-03</TestDate>
<LoadingOrientation>90.0</LoadingOrientation>
<LoadingRate>0.5</LoadingRate>
<FailurePattern>
  <FailureType>Shear</FailureType>
</FailurePattern>
<ResultParameters>
  <UCS>18.7</UCS>
  <YoungsModulus>3428.5</YoungsModulus>
  <PoissonsRatio>0.33</PoissonsRatio>
  <ModulusMethod>Tangent Modulus</ModulusMethod>
  <AxialLevel>50.0</AxialLevel>
</ResultParameters>
</Specimen>
<Specimen>
  <SpecimenNo>4</SpecimenNo>
  <SpecimenSize>
    <Diameter>50.0</Diameter>
    <Height>100.0</Height>
  </SpecimenSize>
  <EndsFlatness>0.02</EndsFlatness>
  <SidesSmoothness>0.30</SidesSmoothness>
  <WaterContent>2.1</WaterContent>
  <SaturationDegree>2.1</SaturationDegree>
  <TestDuration>0.15</TestDuration>
  <TestDate>2010-02-04</TestDate>
  <LoadingOrientation>90.0</LoadingOrientation>
  <LoadingRate>0.5</LoadingRate>
  <FailurePattern>
    <FailureType>Shear</FailureType>
  </FailurePattern>
  <ResultParameters>
    <UCS>13.8</UCS>
    <YoungsModulus>2964.9</YoungsModulus>
    <PoissonsRatio>0.31</PoissonsRatio>
    <ModulusMethod>Tangent Modulus</ModulusMethod>
    <AxialLevel>50.0</AxialLevel>
  </ResultParameters>
</Specimen>
<Specimen>
  <SpecimenNo>5</SpecimenNo>
  <SpecimenSize>
    <Diameter>50.0</Diameter>
    <Height>100.0</Height>
  </SpecimenSize>
  <EndsFlatness>0.02</EndsFlatness>

```

```

<SidesSmoothness>0.30</SidesSmoothness>
<WaterContent>2.1</WaterContent>
<SaturationDegree>2.1</SaturationDegree>
<TestDuration>0.15</TestDuration>
<TestDate>2010-02-05</TestDate>
<LoadingOrientation>90.0</LoadingOrientation>
<LoadingRate>0.5</LoadingRate>
<FailurePattern>
  <FailureType>Shear</FailureType>
</FailurePattern>
<ResultParameters>
  <UCS>16.8</UCS>
  <YoungsModulus>2861.4</YoungsModulus>
  <PoissonsRatio>0.29</PoissonsRatio>
  <ModulusMethod>Tangent Modulus</ModulusMethod>
  <AxialLevel>50.0</AxialLevel>
</ResultParameters>
</Specimen>
<TestMethod>ISRM:Suggested Method for the Uniaxial Compressive Strength Test of Rock
Materials</TestMethod>
<AccreditingBody>UKAS 0000</AccreditingBody>
<CheckedBy>Tom</CheckedBy>
<TestedBy>HongZheng</TestedBy>
<LabName>State Key Laboratory of Geomechanics and Geotechnical
Engineering</LabName>
<Email>hongzheng.irms@gmail.com</Email>
<Remark>All the data is unreal,just for example.</Remark>
</Test>

```

(3) The data display document for UCS (UCS.xml):

The data display document is structured as the format of the tabling of the testing results including pictures. According to the sequence of the children nodes from top to

bottom shown in Fig. 15, the data display document is arranged tabling row by row. For each row of the data, it is structured as follows

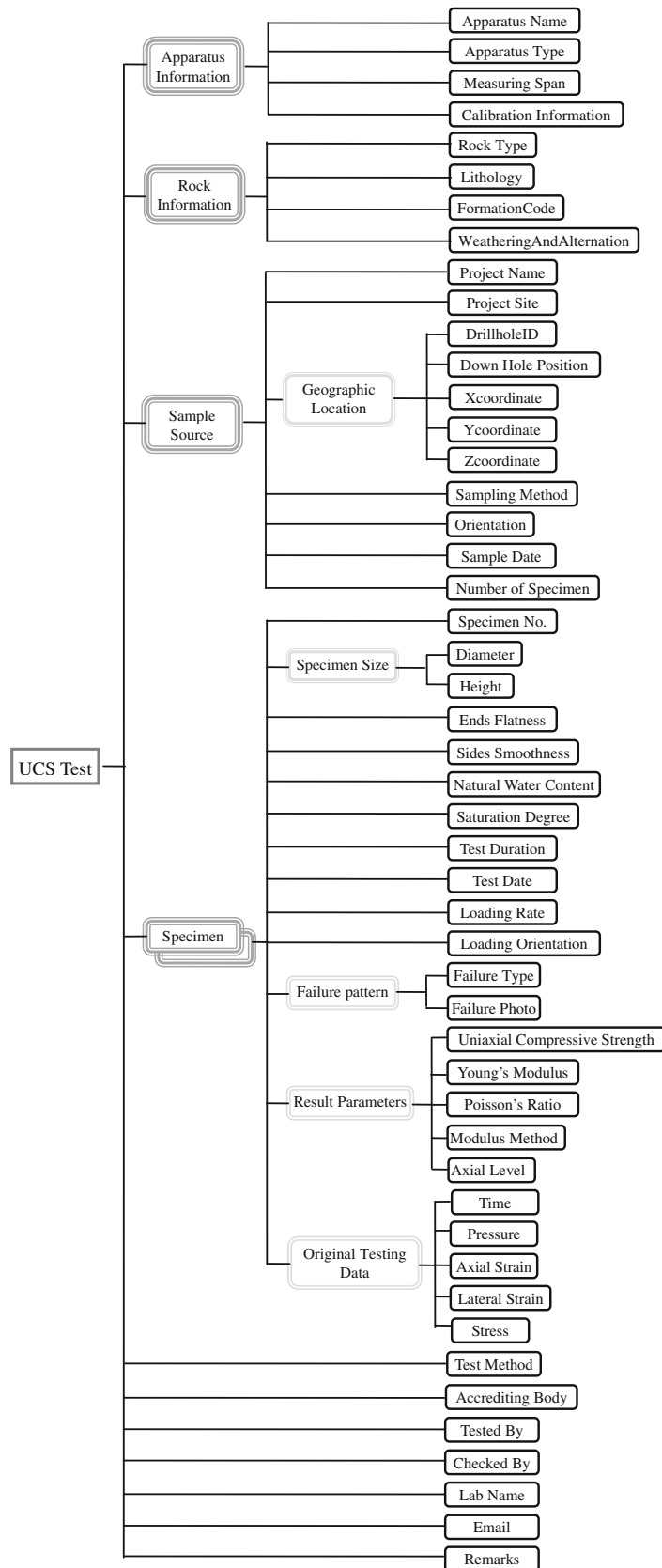


Fig. 15 The data structure for determining the uniaxial compressive strength and deformability of rock material


```

<tr>
<td colspan="length" style="Font format specification "> Name of children node i:</td>
<td colspan="length"><xsl:value-of select=Value of the children node i/></td>
...
<td colspan="length" style="Font format specification "> Name of children node j:</td>
<td colspan="length"><xsl:value-of select= Value of children node j /></td>
</tr>

```

The format for display two pictures is written by

```

<tr>
<td width="value of width" bgcolor="value of back ground color">
<center> //picture is located at the center
</center>
</td>
<td width="value of width">
<center>

</center>
</td>
<td width="value of width">
<center>

</center>
</td>
</tr>

```

The data display document for UCS tests in UCS.xml is accordingly described as follows

```

<?xml version="1.0" encoding="GB2312"?>
<xsl:stylesheet version="1.0" xmlns:xsl="http://www.w3.org/1999/XSL/Transform">
<xsl:template match="/">
<html>
<head style="font-family: arial">Format For Uniaxial Compressive Test of Rock Materials
</head>
<body style="font-family: arial">
<center>
<H1>The Uniaxial Compressive Test Of Rock Materials</H1>
</center>
<table width="100%" border="1" bgcolor="#ffffcc">
<tr>
<td colspan="50" style="font-weight: bold; color:#FF9900; font-size: 22"><center>Apparatus
Information</center></td>

```

```

</tr>
<tr>
<td colspan="8" style="font-weight: bold; color:#FF9900">Apparatus Name:</td>
<td colspan="22"><xsl:value-of select="Test/ApparatusInformation/ApparatusName"/></td>
<td colspan="6" style="font-weight: bold; color:#FF9900">Apparatus Type:</td>
<td colspan="14"><xsl:value-of select="Test/ApparatusInformation/ApparatusType"/></td>
</tr>
<tr>
<td colspan="8" style="font-weight: bold; color:#FF9900">Measuring Span:</td>
<td colspan="42"><xsl:value-of select="Test/ApparatusInformation/MeasuringSpan"/></td>
</tr>
<tr>
<td colspan="8" style="font-weight: bold; color:#FF9900">CalibrationInformation:</td>
<td colspan="42"><xsl:value-of
select="Test/ApparatusInformation/CalibrationInformation"/></td>
</tr>
</table>
<table width="100%" border="1" bgcolor="#ffccff">
<tr>
<td colspan="50" style="font-weight: bold; color:#cc0099; font-size: 22"><center>Rock
Information</center></td>
</tr>
<tr>
<td colspan="8" style="font-weight: bold; color:#cc0099">Rock Type:</td>
<td colspan="8"><xsl:value-of select="Test/RockInformation/RockType"/></td>
<td colspan="12" style="font-weight: bold; color:#cc0099">Lithology:</td>
<td colspan="22"><xsl:value-of select="Test/RockInformation/Lithology"/></td>
</tr>
<tr>
<td colspan="8" style="font-weight: bold; color:#cc0099">Formation Code:</td>
<td colspan="8"><xsl:value-of select="Test/RockInformation/FormationCode"/></td>
<td colspan="12" style="font-weight: bold; color:#cc0099">Alteration and Weathering:</td>
<td colspan="22"><xsl:value-of
select="Test/RockInformation/WeatheringAndAlteration"/></td>
</tr>
</table>
<table width="100%" border="1" bgcolor="#E0FFFF">
<tr>
<td colspan="100" style="font-weight: bold; color:#006600; font-size: 22"><center>Sample
Source</center></td>
</tr>
<tr>
<td colspan="5" style="font-weight: bold; color:#006600">Project Site:</td>
<td colspan="10"><xsl:value-of select="Test/SampleSource/ProjectSite"/></td>
<td colspan="85" style="font-weight: bold; color:#006600"
bgcolor="#CCFFCC"><center>Geographic Location</center></td>
</tr>

```

```

<tr>
<td colspan="5" style="font-weight: bold; color:#006600">Project Name:</td>
<td colspan="10"><xsl:value-of select="Test/SampleSource/ProjectName"/></td>
<td colspan="5" style="font-weight: bold; color:#006600"
bgcolor="#CCFFCC">X-coordinate(m):</td>
<td colspan="5" bgcolor="#CCFFCC"><xsl:value-of
select="Test/SampleSource/GeographicLocation/Xcoordinate"/></td>
<td colspan="5" style="font-weight: bold; color:#006600"
bgcolor="#CCFFCC">Y-coordinate(m):</td>
<td colspan="5" bgcolor="#CCFFCC"><xsl:value-of
select="Test/SampleSource/GeographicLocation/Ycoordinate"/></td>
<td colspan="5" style="font-weight: bold; color:#006600"
bgcolor="#CCFFCC">Z-coordinate(m):</td>
<td colspan="5" bgcolor="#CCFFCC"><xsl:value-of
select="Test/SampleSource/GeographicLocation/Zcoordinate"/></td>
<td colspan="5" style="font-weight: bold; color:#006600"
bgcolor="#CCFFCC">Drillhole_ID:</td>
<td colspan="23" bgcolor="#CCFFCC"><xsl:value-of
select="Test/SampleSource/GeographicLocation/Drillhole_ID"/></td>
<td colspan="5" style="font-weight: bold; color:#006600"
bgcolor="#CCFFCC">DHPosition(m):</td>
<td colspan="23" bgcolor="#CCFFCC"><xsl:value-of
select="Test/SampleSource/GeographicLocation/DHPosition"/></td>
</tr>
<tr>
<td colspan="5" style="font-weight: bold; color:#006600">Orientation:</td>
<td colspan="10"><xsl:value-of select="Test/SampleSource/Orientation"/></td>
<td colspan="10" style="font-weight: bold; color:#006600">Number of Specimen:</td>
<td colspan="5"><xsl:value-of select="Test/SampleSource/NumberOfSpecimen"/></td>
<td colspan="10" style="font-weight: bold; color:#006600">Sample Date:</td>
<td colspan="10"><xsl:value-of select="Test/SampleSource/SampleDate"/></td>
<td colspan="10" style="font-weight: bold; color:#006600">Sampling Method:</td>
<td colspan="40"><xsl:value-of select="Test/SampleSource/SamplingMethod"/></td>
</tr>
<tr>
<td colspan="5" style="font-weight: bold; color:#006600">Remark:</td>
<td colspan="95"><xsl:value-of select="Test/Remark"/></td>
</tr>
</table>
<table width="100%" border="1">
<tr>
<td rowspan="2" colspan="3" style="font-weight: bold; color:#330099"><center>Specimen
No</center></td>
<td colspan="4" style="font-weight: bold; color:#330099"><center>Specimen
Size</center></td>
<td rowspan="2" colspan="3" style="font-weight: bold; color:#330099"><center>Ends

```

```

Flatness (mm)</center></td>
<td rowspan="2" colspan="4" style="font-weight: bold; color:#330099"><center>Sides
Smoothness (mm)</center></td>
<td rowspan="2" colspan="2" style="font-weight: bold; color:#330099"><center>Water
Content(%</center></td>
<td rowspan="2" colspan="3" style="font-weight: bold; color:#330099"><center>Saturation
Degree(%</center></td>
<td rowspan="2" colspan="3" style="font-weight: bold; color:#330099"><center>Test
Duration(Hour)</center></td>
<td rowspan="2" colspan="4" style="font-weight: bold;
color:#330099"><center>TestDate</center></td>
<td rowspan="2" colspan="4" style="font-weight: bold; color:#330099"><center>Loading
Orientation(deg)</center></td>
<td rowspan="2" colspan="3" style="font-weight: bold; color:#330099"><center>Loading
Rate(MPa/s)</center></td>
<td rowspan="2" colspan="2" style="font-weight: bold; color:#330099"><center>Failure
Pattern</center></td>
<td rowspan="2" colspan="2" style="font-weight: bold;
color:#330099"><center>UCS(MPa)</center></td>
<td rowspan="2" colspan="3" style="font-weight: bold; color:#330099"><center>Young's
Modulus (GPa)</center></td>
<td rowspan="2" colspan="3" style="font-weight: bold; color:#330099"><center>Poisson's
Ratio</center></td>
<td rowspan="2" colspan="3" style="font-weight: bold; color:#330099"><center>Type of
modulus of elasticity</center></td>
<td rowspan="2" colspan="4" style="font-weight: bold; color:#330099"><center>Axial stress
level to determine the modulus(%</center></td>
</tr>
<tr>
<td colspan="2" style="font-weight: bold;
color:#330099"><center>Diameter(mm)</center></td>
<td colspan="2" style="font-weight: bold;
color:#330099"><center>Height(mm)</center></td>
</tr>
<xsl:for-each select="Test/Specimen">
<tr>
<td colspan="3"><center><xsl:value-of select="SpecimenNo"/></center></td>
<td colspan="2"><center><xsl:value-of select="SpecimenSize/Diameter"/></center></td>
<td colspan="2"><center><xsl:value-of select="SpecimenSize/Height"/></center></td>
<td colspan="3"><center><xsl:value-of select="EndsFlatness"/></center></td>
<td colspan="4"><center><xsl:value-of select="SidesSmoothness"/></center></td>
<td colspan="2"><center><xsl:value-of select="WaterContent"/></center></td>
<td colspan="3"><center><xsl:value-of select="SaturationDegree"/></center></td>
<td colspan="3"><center><xsl:value-of select="TestDuration"/></center></td>
<td colspan="4"><center><xsl:value-of select="TestDate"/></center></td>
<td colspan="4"><center><xsl:value-of select="LoadingOrientation"/></center></td>
<td colspan="3"><center><xsl:value-of select="LoadingRate"/></center></td>

```

```

<td colspan="2"><center><xsl:value-of select="FailurePattern"/></center></td>
<td colspan="2"><center><xsl:value-of select="ResultParameters/UCS"/></center></td>
<td colspan="3"><center><xsl:value-of
select="ResultParameters/YoungsModulus"/></center></td>
<td colspan="3"><center><xsl:value-of
select="ResultParameters/PoissonsRatio"/></center></td>
<td colspan="3"><center><xsl:value-of
select="ResultParameters/ModulusMethod"/></center></td>
<td colspan="4"><center><xsl:value-of
select="ResultParameters/AxialLevel"/></center></td>
</tr>
</xsl:for-each>
</table>
<table width="100%" border="1">
<tr>
<td colspan="10" style="font-weight: bold; color:#b22222">Tested By:</td>
<td colspan="23"><xsl:value-of select="Test/TestedBy"/></td>
<td colspan="10" style="font-weight: bold; color:#b22222">Lab Name:</td>
<td colspan="23"><xsl:value-of select="Test/LabName"/></td>
<td colspan="10" style="font-weight: bold; color:#b22222">Email:</td>
<td colspan="23"><xsl:value-of select="Test/Email"/></td>
</tr>
<tr>
<td colspan="10" style="font-weight: bold; color:#b22222">Test Method:</td>
<td colspan="23"><xsl:value-of select="Test/TestMethod"/></td>
<td colspan="10" style="font-weight: bold; color:#b22222">Accrediting Body:</td>
<td colspan="23"><xsl:value-of select="Test/AccreditingBody"/></td>
<td colspan="10" style="font-weight: bold; color:#b22222">Checked By:</td>
<td colspan="23"><xsl:value-of select="Test/CheckedBy"/></td>
</tr>
</table>
<table width="100%" border="1">
<tr>
<td style="font-weight: bold; color:#330099"><center>Specimen No</center></td>
<td style="font-weight: bold; color:#330099"><center>Failure Picture</center></td>
<td style="font-weight: bold; color:#330099"><center>Stress-Strain Curve</center></td>
</tr>
<tr>
<td width="10%">
<center>
</center>
</td>
<td width="45%">
<center>

</center>
</td>

```

```
<td width="45%">
<center>
</center>
</td>
</tr>
<tr><td width="10%">
<center>
</center>
</td>
<td width="45%">
<center>
"
</center>
</td>
<td width="45%">
<center>
</center>
</td>
</tr>
<tr><td width="10%">
<center>
</center>
</td>
<td width="45%">
<center>

</center>
</td>
<td width="45%">
<center>
</center>
</td>
</tr>
<tr><td width="10%">
<center>
</center>
</td>
<td width="45%">
<center>

</center>
</td>
<td width="45%">
<center>
</center>
</td>
</tr>
```

```

<tr><td width="10%">
<center>
</center>
</td>
<td width="45%">
<center>

</center>
</td>
<td width="45%">
<center>
</center>
</td>
</tr>
</table>
</body>
</html>
</xsl:template>
</xsl:stylesheet>

```

5.4 The Compatibility of the Output Format in the SM with AGS4NZ v1.0 (New Zealand)

In order to have the compatibility with the AGS4NZ v1.0 (New Zealand), the SM can also give the output of the

testing results in the format used in the AGS4NZ v1.0 (New Zealand). It is showing as follows:

For The Group "PROJ", the data output format is as follows

```

"GROUP","PROJ"
"HEADING","PROJ_NAME","PROJ_LOC"
"UNIT","",""
"TYPE","X","X"
"DATA","Historic preservation for Longyou grottoes","Longyou"

```

For The Group "RUCS", the data output format is as follows

```

"GROUP","RUCS"
"HEADING","LOCA_ID","SAMP_TOP","SAMP_TYPE","SPEC_REF","SPEC_DESC","SPEC_PREP","RUCS_SDIA","RUCS_LEN","RUCS_MC","RUCS_DURN","RUCS_STRA","RUCS_UCS","RUCS_MODE","RUCS_CS_E","RUCS_MU","RUCS_ESTR","RUCS_ETYP","RUCS_MACH","RUCS_REM","RUCS_METH","RUCS_LAB","RUCS_CRED","TEST_STAT"
"UNIT","ID","2DP","PA","ID","X","X","1DP","1DP","1DP","T","1DP","3FS","X","3FS","2DP","X","PA","X","X","X","X","X"
"DATA","327-16A","24.55","U","1","sandstone","Prepared according to client instructions","50.0","100.0","2.1","09:00","0.5","17.5","Shear","3614.1","0.32","0-50%UCS, 8.75MPa","Tangent","MTS 815.04","All the data is unreal, just for example.","ISRM: Suggested Method for the Uniaxial Compressive Strength Test of Rock Materials","SKLGT","UKAS 0000","checked"

```

References

- AGS (1999) Electronic transfer of geotechnical and geoenvironmental data, 3rd edn. Association of Geotechnical and Geoenvironmental Specialists, Beckenham, Kent. <http://www.ags.org.uk/>
- AGS (2004) Electronic transfer of geotechnical and geoenvironmental data, 3.1 edn. Association of Geotechnical and Geoenvironmental Specialists
- AGS (2005) Electronic transfer of geotechnical and geoenvironmental data using XML data format. Association of Geotechnical and Geoenvironmental Specialists, Beckenham, Kent. <http://www.ags.org.uk/agsml/AGSMLAugust2005Report.pdf>
- Bardet JP, Zand A (2009) Spatial modeling of geotechnical information using GML. *Trans GIS* 13(1):125–165
- Bowman D (1998) Civil engineering data meets GIS. *J Comput Civil Eng* 12:5–7
- Byron A, Lysandros T (2006) The potential of XML encoding in geomatics converting raster images to XML and SVG. *Comput Geosci* 32:184–194
- Caronna S (2006) Implementing XML for geotechnical databases, geo-engineering data: representation and standardization. DIGGS
- Chandler RJ, Quinn PM, Beaumont AJ, Evans DJ, Toll DG (2006) Combining the power of AGS and XML: AGSML the data format for the future. In: *Proceedings of GeoCongress 2006: Geotechnical Engineering in the information technology age*, Atlanta, USA, ASCE, Reston, pp 112–117
- Chen ZY (2009) Standardization and digitization of the ISRM suggested methods on rock mechanics tests, SINOROCK2009, Hong Kong, 18–21 May 2009
- Durant JR (2003) Importing XML maps, XML lists, and dynamic chart sources in Excel 2003, Microsoft Office Excel 2003, [http://msdn.microsoft.com/en-us/library/aa203727\(v=office.11\).aspx](http://msdn.microsoft.com/en-us/library/aa203727(v=office.11).aspx)
- Exadaktylos G, Liolios P, Barakos G (2007) Some new developments on the representation and standardization of rock mechanics data: From the laboratory to the full scale project, Specialized Session S02, 11th ISRM Congress
- ISRM (2007) The complete ISRM Suggested Methods for rock characterization, testing and monitoring: 1974–2006. In: Ulusay R, Hudson JA (eds) *Suggested Methods prepared by the Commission on Testing Methods*, International Society for Rock Mechanics, compilation arranged by the ISRM Turkish National Group, Kozan Ofset, Ankara, Turkey
- Li X, Wang G, Zhu H (2012) A data model for exchanging and sharing ISRM rock mechanics test data. *Electron J Geotech Eng (EJGE)* 17 (Bund. D): 377–401
- Madria S, Passi K, Bhowmick S (2008) An XML schema integration and query mechanism system. *Data Knowl Eng* 65(2):266–303
- Nance KL, Hay B (2005) Automatic transformations between geosciences standards using XML. *Comput Geosci* 31:1165–1174
- Swift J, Bobbitt J, Roblee C, Futrelle J, Tiwana S, Peters A, Castro J, Ali M, Nasir F, Javed A, Khan Y, Stepp C (2004) *Cosmos/Peer Lifelines Geotechnical Virtual Data Center*, COSMOS Workshop 1, 15 October 2004. www.cosmoseq.org/Projects/GSMA/Presentation/GSMA2004
- Toll DG (2007) Geo-Engineering Data: representation and standardization. *Electron J Geotech Eng*. <http://www.ejge.com/2007/Ppr0699/Ppr0699.htm>
- Toll DG (2008) International Data Exchange: the future for geo-engineering. In: *The 12th international conference of International Association for Computer Methods and Advances in Geomechanics (IACMAG)1–6 October 2008*
- Toll DG, Cubitt AC (2003) Representing geotechnical entities on the World Wide Web. *Adv Eng Softw* 34(11–12):729–736
- Wang GR (2001) XML data management technology. Electronic Industry Press, Beijing
- Weaver SD, Lefchik T, Hoit M, Beach K (2008) Geo-environmental and geotechnical data exchange: setting the standard. In: *Proceedings of GeoCongress 2008*. New Orleans
- Zheng H, Feng X-T, Chen Z (2010) Standardization and digitization for ISRM suggested methods of rock mechanics laboratory tests. *Chin J Rock Mech Eng* 29(12):2456–2468

Upgraded ISRM Suggested Method for Determining Sound Velocity by Ultrasonic Pulse Transmission Technique

Adnan Aydin

1 Introduction

Ultrasonic testing is one of the most widely used non-destructive testing methods for rock material characterization (Lama and Vutukuri 1978). The method is based on the generation, transmission and reception of small-amplitude wave trains of adjustable pulse length and ultrasonic pulse frequencies.

Wave propagation can be considered as transfer or passage of strain energy through a medium (e.g., Eringen 1980; Jaeger et al. 2007). In routine material testing, microstructural characteristics (encompassing mineralogy, size and shape distribution of voids and grains and their relative arrangements) of the medium determine the rate of energy dissipation, uniquely modify the frequency spectrum and define the velocities of different propagation modes, e.g., compressional and shear. Therefore, the wave velocities and their amplitude-frequency spectra are related to the material's physical and mechanical properties that are also strongly related to the microstructural characteristics. This relationship constitutes the basis of ultrasonic tests, but also poses great challenges for improvement of its precision and offers opportunities for a wider range of applications.

Please send any written comments on this ISRM Suggested Method to Prof. Resat Ulusay, President of the ISRM Commission on Testing Methods, Hacettepe University, Department of Geological Engineering, 06800 Beytepe, Ankara, Turkey.

Originally published as an article in the journal *Rock Mechanics and Rock Engineering*, 47, A. Aydin, Upgraded ISRM Suggested Method for Determining Sound Velocity by Ultrasonic Pulse Transmission Technique, 255–259, 2014

A. Aydin (✉)
Geology and Geological Engineering Department,
The University of Mississippi, University,
MS, USA
e-mail: aaydin@olemiss.edu

2 Scope

The original suggested methods (Rummel and Van Heerden 1978; ISRM 2007) consist of three different approaches for the laboratory determination of sound velocity. These approaches utilize waves generated at different frequency ranges and require different specimen shapes, testing and analysis procedures. This upgraded suggested method covers the first two approaches, the so-called high (100 kHz–2 MHz) and low (2–30 kHz) frequency ultrasonic pulse techniques, while the resonant approach will be presented in a companion suggested method. This upgrade (a) unifies the two ultrasonic approaches by a generalized scheme applicable to any specimen shape/size at any frequency within the ultrasonic range (>20 kHz), (b) emphasizes the peculiarities and particulars of rocks as ultrasonic test materials, and (c) suggests possible modifications/adjustments in test procedures and specimen preparation to account for the special microstructural features encountered in common rock types.

In the pulse method of ultrasonic testing, generating sound wave trains and detecting their propagation through solids can be achieved by a single transducer (pulse-echo technique) or by a pair of transducers (pitch-catch technique). The pulse-echo technique is designed for locating flaws forming seismic impedance contrasts within the host material. The pitch-catch technique can be used in three different configurations of transducer pairs depending on the accessibility of test surfaces (Fig. 1). This suggested method concentrates on the issues pertaining to the direct-transmission configuration of the pitch-catch technique, and thus the influences of the near field length and beam spread on transducer selection and test procedures are not discussed. Note that the direct-transmission configuration is preferred to the others because the direction and length of path along which the wave-front travels is known with greater certainty and that the test results are not influenced by possible damage or deterioration of specimen surface and/or edges.

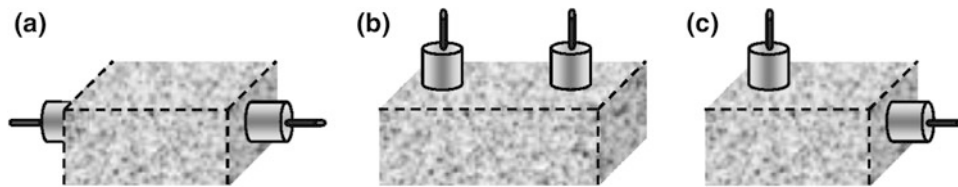


Fig. 1 Basic configurations of transducer pairs (transmitter–receiver) used in pitch-catch technique: **a** direct (through) transmission; **b** indirect (surface) transmission; and **c** semi-direct (edge) transmission

Ultrasonic P-wave velocity (V_P) and S-wave velocity (V_S) are customarily used in establishing predictive correlations (mainly with porosity, strength and static modulus) and in determining dynamic elastic constants. The ultrasonic test system as a non-destructive tool should also be used routinely for examination of uniformity/integrity and anisotropy of other test specimens to reduce or explain scatters in rock mechanics test results. This examination can be conducted by determining the velocity over a grid-pattern on large surfaces or by velocity profiling along one or more traverses on narrower surfaces. Rectangular blocks provide an opportunity for determining the principal axes of velocity anisotropy on rock specimens with banded, laminated, foliated, phyllitic, schistose and similar orientated fabric that may impart directional dependencies to strength and deformation resistance. Oriented cylindrical cores and sphere-shaped specimens, where available, may also be used for this purpose.

3 Apparatus

Ultrasonic test systems have substantially benefitted from the technological advances in the past three decades. There are now many commercially available advanced test system alternatives with digital waveform display, processing and storage capabilities. It is no longer possible or necessary to include such a vast amount of easily accessible information in testing standards for specific materials. However, a typical layout of essential ultrasonic testing system components is shown in Fig. 2 as a preliminary guideline. These components include a signal generator to trigger timer to mark the beginning of each excitation pulse interval, an arrival timer in the form of a threshold trigger and/or an oscilloscope for visual analysis of the waveform, amplifiers and filters for signal enhancement, and a data acquisition unit interfacing with the apparatus. Two separate transmitter–receiver transducer pairs are needed for the determination of P- and S-wave velocities. Each (piezo-electric) transducer pair may have a nominal frequency between 20 kHz and 2 MHz, but the 50–500 kHz range is recommended for practical purposes.

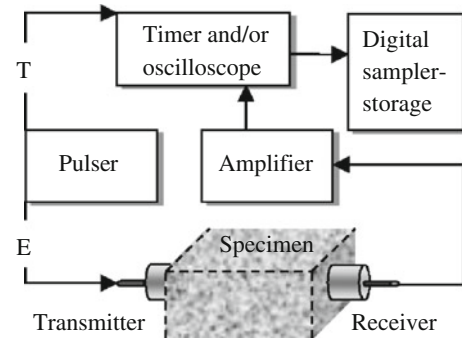


Fig. 2 A simplified layout of basic components of an ultrasonic apparatus. (E transmitter excitation signal, T timer trigger signal)

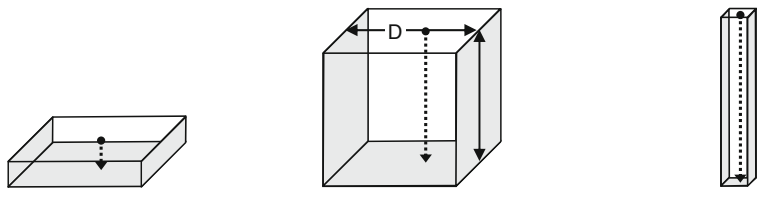
4 Sample Preparation

When testing rock materials, it should be remembered that in situ microstructures are inevitably altered in varying degrees during recovery, transport, storage and preparation, but this can be minimized using right tools and procedures and exercising care in all stages. The direct-transmission transducer configuration requires test specimens with smooth (using fine sandpaper), flat (specified by a maximum gap size between specimen surface and standard straightedge, which accommodates 0.025 mm thick feeler gage) and parallel (<math><1\text{ mm}/100\text{ mm}</math> of wave travel path length) faces. Each specimen dimension (as specified later in Fig. 3) should be measured at several points with a precision of $\pm 0.01\text{ mm}$.

5 Test Procedure

Ultrasonic test procedure for pitch-catch configurations is quite straightforward especially if analysis of frequency spectrum is not to be conducted. Determination of V_P and V_S of a test specimen requires measurement of two basic variables: the length of wave travel path L (taken as the shortest distance between transmitter and receiver transducers) and the length of travel time of each wave type (t_P and t_S). The latter corresponds to identification of P- and S-wave arrivals on the oscilloscope traces. There are,

Fig. 3 Three distinct specimen shapes with corresponding limiting dimensions and velocity expressions



SLAB	BLOCK	BAR
$L/D \leq 0.1$	$L/D \approx 1$	$L/D \geq 10$
$\lambda \leq 0.1 D$	$\lambda \leq 0.1 D$	$\lambda \geq 5 D$
$L \geq 10 d_g$		
$V_p = \sqrt{\frac{E_d}{\rho} \frac{1}{(1 + \nu_d)(1 - \nu_d)}}$	$V_p = \sqrt{\frac{E_d}{\rho} \frac{(1 - \nu_d)}{(1 - 2\nu_d)(1 + \nu_d)}}$	$V_p = \sqrt{\frac{E_d}{\rho}}$
$V_s = \sqrt{\frac{G_d}{\rho}} = \sqrt{\frac{E_d}{\rho} \frac{1}{2(1 + \nu_d)}}$		
$\nu_d = 1 - 2 \frac{V_s^2}{V_p^2}$	$\nu_d = \frac{V_s^2 - 0.5 V_p^2}{V_s^2 - V_p^2}$	$\nu_d = 0.5 \frac{V_p^2}{V_s^2} - 1$

d_g : average grain size (equivalent spherical diameter)

however, a number of important issues that influence the test results as highlighted below:

- (a) A thorough description of microstructural composition (especially any discrete features or boundaries that are likely to create significant acoustic mismatch).
- (b) Specimens can be tested *dry* or *fully saturated* or *in situ moisture content*. Procedures to achieve and maintain these conditions as provided in the relevant suggested methods should be followed (ISRM 2007).
- (c) As each specimen may be tested in more than a single direction, include a sketch or a photograph showing orientation of each travel path with reference to the specimen's planar fabric (bedding planes, laminations, schistosity, etc.) or to long axes of elongated or lenticular features (clasts, fragments, inclusions, fossils, etc.).
- (d) A thin layer of coupling medium should be used to ensure efficient and uniform energy transfer from/to the transducers. There are a large variety of options (including phenyl salicylate, high-vacuum grease, glycerin, putty, Vaseline, oil) but a high viscosity medium (e.g., epoxy resin) is needed if S-wave velocity is to be measured.
- (e) The transducers should be positioned and aligned to produce an acoustic axis (center beam) that is normal to both faces.
- (f) In direct-transmission test configuration, a custom-made benchtop load frame with an in-built low-capacity load transducer can be used for coaxial positioning of the transducers and for maintaining a small coupling stress (~ 10 kPa) for a given transducer diameter.
- (g) Note that the minimum coupling stress at which wave travel times stabilize may vary substantially with rock type and the degree of microstructural damage. Also beware of the possibility of internal shearing or exfoliation of specimens with strong anisotropy when loaded oblique or normal, respectively, to anisotropy planes. In anisotropic and weak rocks, when applying seating/coupling load, observe any changes in the velocities at 5–10 N load increments and report such variations. For small diameter transducers, observe any settlement into the specimens and report any changes in travel path length (0.1 mm/100 mm) upon the application of the seating load.
- (h) The measured wave travel time through a specimen may need to be corrected for a small amount of system response delay time. The system delay correction needs to be readjusted each time a new transducer pair is used. This delay can be determined (Rummel and Van Heerden 1978; ISRM 2007): (a) by placing the transmitting and receiving transducers in direct contact with each other and measuring the travel time at zero length; and (b) by measuring the travel time on a number of standard specimens of different lengths and extending the best-fit line to the time-distance data pairs to zero length (recommended for S-wave transducers).
- (i) A reference bar with a known velocity or a reference spacer with a known transit time should be used to regularly monitor any drift in the measured values.

- (j) When the transducers are coupled manually by hand, the travel times should be measured for at least three times applying different pressures, and if possible, the received waveform should be recorded for about 10 pulse intervals.

6 Calculations

The velocities of P- and S-waves are determined from $V_P = L/t_P$ and $V_S = L/t_S$, where L is the travel path length and t_P and t_S are travel times for P- and S-waves, respectively. The approximate analytical solutions that link the velocity of sound wave propagation through isotropic and homogeneous solids to the elastic constants (White 1983; Jaeger et al. 2007) are based on two fundamental assumptions. It is important to understand these to select the most appropriate model for utilization of wave velocity (V_P and V_S) and to interpret/calibrate the differences in test results from different specimens and/or transducers. These assumptions are explained below and illustrated in Fig. 3:

1. The first assumption establishes the effects of boundary interference via specimen's minimum dimension (D) (twice the shortest distance from the transducer center to the specimen boundary) relative to specimen's length (L) (shape factor) and to the wavelength (λ) at a given transducer frequency (f). For the direct-transmission configuration, three distinct shapes (and corresponding wave propagation patterns) can be identified for rectangular (slab, block and bar) and cylindrical (disk, block and rod) specimens.
2. The second assumption defines the scale at which a material can be tested to ensure representative and reproducible results. For granular materials, in which variations in grain compositions, grain boundary types and pores form the dominant features of microstructure, this scale can be expressed in terms of the number of grains along the wave propagation path, which is equal to the specimen's length (L) in the direct-transmission configuration.

Figure 3 also provides the analytical solutions that should be selected carefully for each specimen and test condition expecting that these assumptions will not be met in most practical cases.

For purposes of predicting the dynamic elastic constants, standard rock mechanics test specimens (D 50–60 mm and L/D 2–2.5) can be classified as a block-bar specimen, where the measured velocity will be closer to that of a bar at high frequency and vice versa. There are, however, a few tests (e.g., indirect tension, block punch) that require slab- or disk-like specimens with L/D ratios of less than 1.

If the block specimen (approximating infinite medium conditions) is taken as a reference, the velocity of P-waves can be shown to decrease in both slab and bar specimens as a function of the Poisson's ratio (ν), revealing a relative order of magnitudes of $V_{P-Block} > V_{P-Slab} > V_{P-Bar}$. For example, for a rock material with $\nu = 0.30$, slab- and bar-like specimens may produce up to 10 and 14 % lower velocities than a block specimen of the same material, respectively.

Once V_P and V_S are determined for a specimen, the dynamic (ultrasonic-based) Poisson's ratio (ν_d) can be calculated as shown in the last row of Fig. 3. The Poisson's ratio value can then be used to predict the dynamic Young's (E_d) and shear (G_d) moduli based on the measured or predicted value of the specimen's density. Note that the values of these dynamic elastic constants are expected to differ from the static ones derived from actual loading experiments.

7 Reporting of Results

The report should include the following information:

- (a) Lithological description of the test specimens (preferably in the order of strength, color, texture/fabric, weathering/alteration, rock name with grain size as prefix).
- (b) Geographic location of source area and coordinates of sampling points.
- (c) Geological setting (formation name, proximity or association with geological features, e.g., faults, shear zones, dykes, lenses, narrow valleys, high cliffs).
- (d) Sample recovery and in situ conditions (drilling/coring techniques; method of quarry production; weathering and fracturing degrees in the sampling intervals/exposures).
- (e) Specimens (length and conditions of storage; preparation procedures including method of drying or saturation; smoothness and parallelity of opposite faces; microstructural descriptions of grain and void structures).
- (f) Physical properties (density, porosity and water content) and static elastic constants (e.g., E_s and ν_s).
- (g) Test system (manufacturer and model number or complete technical specifications of the system and the transducers; calibration date and method).
- (h) Test procedure (date and method of transducer calibration; transducer configurations and alignment; transducer-specimen coupling medium; means (manual or mechanical) and level of seating/coupling force).
- (i) Specimen shape and dimensions; position and length of each travel path on specimen surfaces; minimum lateral dimension for each position.

- (j) Relative orientation of travel path (acoustic axis) to nearby geological features and to intact rock anisotropy (e.g., lamination, foliation, schistosity, lineation).
- (k) P- and S-wave velocities recorded at each transducer position and along each travel path orientation; mean and standard deviation of velocity variations within and among specimens.
- (l) Predicted values of dynamic elastic constants and the selected velocity model (Fig. 3).

8 Notes and Recommendations

8.1 Terminology

The term “sound” is often used to refer to mechanical (body and surface) waves that can travel through any medium and at any frequency. “Sound” as used in the title of this suggested method specifically denotes body waves propagating through rock materials at ultrasonic frequencies.

P- and S-waves are both body waves, which can be generated at the boundary or the interior of a medium and propagate through that medium (i.e., unlike surface waves that are confined to a boundary zone). P- and S-waves are often defined by different pairs of terms highlighting different aspects of their propagation: (1) irrotational–equivoluminal (nature of elemental deformation); (2) longitudinal–transverse (particle displacement direction); (3) compressional and/or dilatational–shear (particle displacement mechanics); and (4) Primary–Secondary (arrival order).

8.2 Limitations for Sample Dimensions

As discussed in “Calculations” section, this test can be performed practically on any specimen without limitations on shape or dimensions. The only limitation that may be imposed relates to the possibility of excessive weakening of signal strength due to attenuation of wave energy if the travel length is too long. Because rock materials exhibit a wide range of attenuation coefficients for different lithologies, weathering states and along different directions, the maximum travel length (penetration depth) at which a clearly distinguishable waveform and/or a stable signal can be recorded is variable. For a given specimen, the coefficient of attenuation due to scattering is strongly dependent on the transducer frequency, which favors a shorter specimen length when using high frequency transducers.

8.3 Representation of Field Conditions in Laboratory Testing

It should be borne in mind that predicting in situ properties based on laboratory test results is complicated due to inadequate representation of field conditions. In situ stress and its anisotropy, pore fluid type and pressure, and saturation degree alter the microstructure of rock materials and hence its wave propagation characteristics in many different ways. Discussion of specialized tests and experimental setup to simulate such field conditions are beyond the scope of this suggested method.

8.4 Calculation of Elastic Constants in Transversely Anisotropic Rocks

Most common form of anisotropy in rock materials is the transverse or polar type imparted by unidirectional compaction during burial of sedimentary rocks, development foliation in metamorphic rocks, etc. Determination of elastic constants and quantification of anisotropy is possible from measurement of P- and S-wave velocities normal, parallel and at an angle of exactly 45° to the plane of anisotropy (Thomsen 1986). Considering that testing at the inclined angle may not often be possible in practice, the users are encouraged to determine the velocities in the normal and parallel directions, which will help determine four of the five elastic moduli of transversely isotropic rock materials, as well as quantify the degree of their P- and S-wave velocity anisotropies.

References

- Eringen AC (1980) *Mechanics of Continua*, 2nd edn. R.E. Krieger, New York
- ISRM (2007) *The Complete ISRM Suggested Methods for Rock Characterization, Testing and Monitoring: 1974–2006*. In: R. Ulusay and J.A. Hudson (eds.), *Suggested Methods Prepared by the Commission on Testing Methods, International Society for Rock Mechanics*, Compilation Arranged by the ISRM Turkish National Group, Ankara
- Jaeger JC, Cook NGW, Zimmerman RW (2007) *Fundamentals of rock mechanics*, 4th edn. Blackwell, Singapore, 475 p
- Lama RD, Vutukuri VS (1978) *Handbook on mechanical properties of rocks*, vol II. Trans Tech, Herzberg
- Rummel F, Van Heerden WL (1978) Suggested methods for determining sound velocity. *Int J Rock Mech Min Sci Geomech Abstr* 15(2):53–58
- Thomsen L (1986) Weak elastic anisotropy. *Geophysics* 51(10): 1954–1966
- White JE (1983) *Underground sound: applications of seismic waves*. Elsevier, New York

ISRM Suggested Method for Determining the Abrasivity of Rock by the CERCHAR Abrasivity Test

Michael Alber, Olgay Yaralı, Filip Dahl, Amund Bruland, Heiko Käsling, Theodore N. Michalakopoulos, Marilena Cardu, Paul Hagan, Hamit Aydın, and Ahmet Özarslan

1 Introduction

Rock abrasivity plays an important role in characterizing a rock material for excavation purposes. Abrasion can be defined as the wearing or tearing away of particles from the surface, i.e. it is a process causing removal or displacement

Please send any written comments on this ISRM Suggested Method to Prof. Resat Ulusay, President of the ISRM Commission on Testing Methods, Hacettepe University, Department of Geological Engineering, 06800 Beytepe, Ankara, Turkey.

Originally published as an article in the journal *Rock Mechanics and Rock Engineering*, 47, M. Alber, O. Yaralı, F. Dahl, A. Bruland, H. Käsling, T. N. Michalakopoulos, M. Cardu, P. Hagan, H. Aydın, A. Özarslan, ISRM Suggested Method for Determining the Abrasivity of Rock by the CERCHAR Abrasivity Test, 261–266, 2014.

M. Alber (✉)
Engineering Geology/Rock Engineering, Ruhr-University
Bochum, 44780, Bochum, Germany
e-mail: michael.alber@rub.de

O. Yaralı · H. Aydın · A. Özarslan
Mining Engineering Department-67, Bülent Ecevit University,
100 Zonguldak, Turkey

F. Dahl · A. Bruland
Building and Infrastructure, Rock Engineering, SINTEF,
7465 Trondheim, Norway

H. Käsling
Engineering Geology, Technical University Munich, Arcisstr. 21,
80333 Munich, Germany

T. N. Michalakopoulos
Department of Mining Engineering, National Technical
University of Athens, Zographou Campus, 15780, Athens, Greece

M. Cardu
Department of Environment, Land and Infrastructure
Engineering, Politecnico di Torino, DITAG, 24 Corso Duca degli
Abruzzi, CAP 10129 Turin, Italy

P. Hagan
School of Mining Engineering, The University of New South
Wales, Sydney, Australia

of material at a solid surface, which will lead to wear, especially on tools that are used in mining, drilling, and tunneling applications. The CERCHAR Abrasivity Test is a method to determine an index called CERCHAR Abrasivity Index (CAI) for the rock's abrasivity.

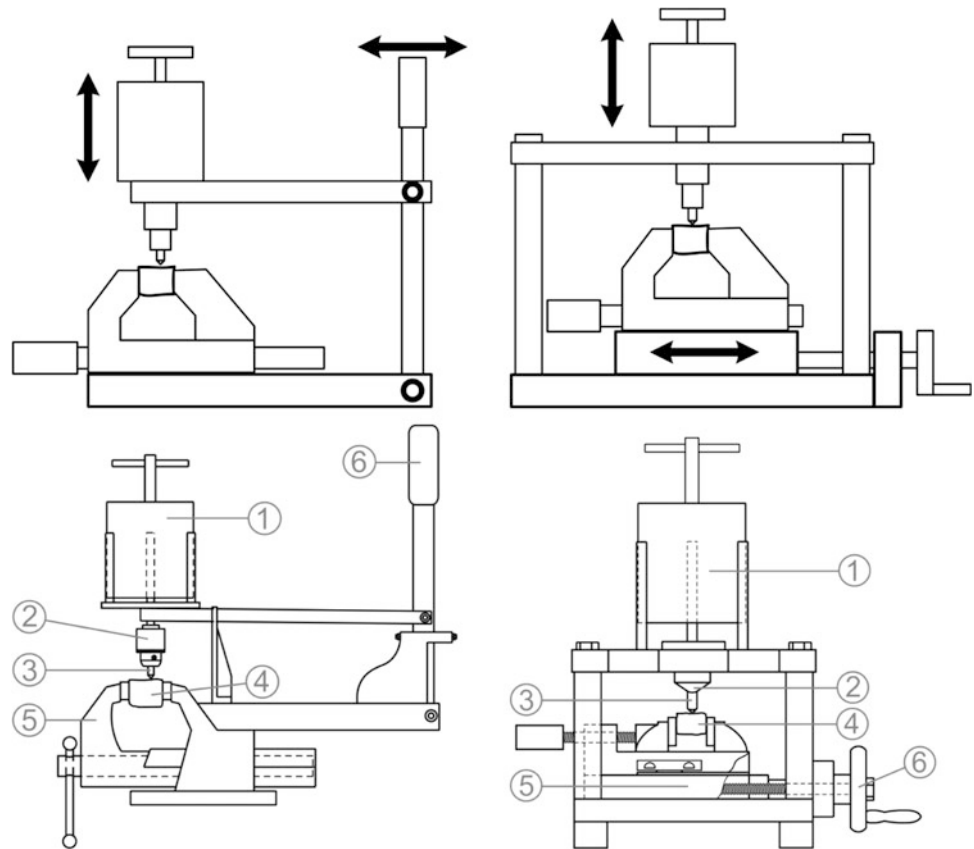
The test was originally developed by the Laboratoire du Centre d'Études et Recherches des Charbonnages (CERCHAR) de France for coal mining applications (Cerchar 1986). Two standards exist for this test method: the French standard AFNOR NF P 94-430-1 (2000) and ASTM D7625-10 (2010). The test is widely used in research and practice. There are essentially two designs of testing apparatus: the original design as developed at the CERCHAR Centre (Valantin 1973) and a modified design as reported by West (1989). While the designs are similar there are some important differences as well as ambiguities in test conditions that include equipment actuation, material properties of the stylus and sample preparation as summarized by Plinninger et al. (2003).

2 Scope

The CERCHAR Abrasivity Test is intended as an index test for classifying the abrasivity of a rock material. The test measures the wear on the tip of a steel stylus having a Rockwell Hardness of HRC 55.

A rock specimen, disc-shaped or irregular, is firmly held in the test apparatus. The stylus is lowered carefully onto the rock surface. While under a normal force of 70 N, the stylus is moved a total distance of 10.0 mm across the rock. The wear surface of the stylus tip is measured under a microscope to an accuracy of 0.01 mm. The CAI is a dimensionless unit value and is calculated by multiplying the wear surface stated in units of 0.01 mm by 10. For example, if the wear flat of a stylus tip was measured as being 0.25 mm, the corresponding value of CAI should be reported as 2.5.

Fig. 1 Basic mechanisms as well as exemplary sketches of the two main forms of test apparatus in use. *Left* Type 1, original design CERCHAR-type testing apparatus. *Right* Type 2, the modified CERCHAR apparatus as reported by West (1989). 1 mass, 2 pin chuck/guide, 3 stylus, 4 specimen, 5 vice, 6 lever/hand crank



3 Apparatus

3.1 Basic Mechanisms

There are two fundamentally different mechanisms to actuate the relative movement between the stylus and rock surface. In the original CERCHAR design, both the stylus and deadweight are made to move across the stationary rock surface. In the case of the West design, the rock samples moved under a stationary stylus. Figure 1 schematically depicts the method of actuation in the two designs. The main features in the design of the two test apparatus and the nomenclature for these apparatus are also offered. A consequence of the difference in design is a near tenfold difference in test duration between the fast lever actuation with the CERCHAR design compared to the slow screw feed actuation with the West design.

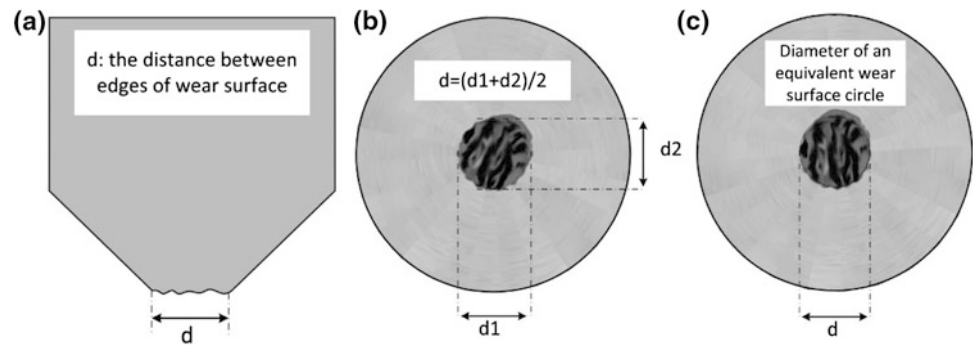
Both machines use a rigid vice to firmly clamp the rock sample. It is important to ensure that the apparatus is sufficiently stiff to minimize any lateral movement during a test. The static force of 70 N is the result of a deadweight placed on top of the stylus. The stylus should be carefully lowered onto the rock surface. The stylus should be placed normal to the surface of the rock specimen. The test

duration involving displacement of the stylus by 10 mm should be completed within 1 ± 0.5 s with Type 1 apparatus and 10 ± 2 s with Type 2 apparatus.

3.2 Stylus

The stylus should be manufactured of a standard chrome–vanadium alloyed cold-work tool steel (such as Material Nr. 1.2210 as specified for example in DIN 115CrV3; AFNOR 100C3; UNI 107CrV3KU; AISI L2, respectively) tempered to the desired hardness. It is strongly recommended to employ only styli tempered to Rockwell hardness $HRC 55 \pm 1$. Provisions for different stylus hardness are given below. As the hardness values of the steel styli achieved during heat treatment can vary, the actual hardness of each stylus must be measured and recorded on at least one occasion prior to first use. A stylus having hardness beyond the tolerance limits of $HRC \pm 1$ must not be used. The diameter of the stylus should be at least 6 mm and its length shall be such that the visible part of the stylus between the pin chuck/guide and rock surface during a test is at least 15 mm. The tip of a stylus shall have a conical angle of 90° . A worn stylus should be re-sharpened and the tip angle checked under a microscope before use in a further test.

Fig. 2 Measurement by side-view (a) and top view (b, c). The methods shown in (a) and (b) are recommended for optical measurements and (c) for digital measurements



3.3 Force

The static force acting on the stylus should be 70 N.

3.4 Grinder

Each used stylus should be re-sharpened using a standard abrasive stone wheel. The grinding wheel should have fine grit to avoid leaving rough ground surfaces at the stylus tip. The use of a suitable cooling-fluid, that will prevent any change in stylus hardness as a result grinding, is mandatory.

3.5 Test Specimen

The rock sample may be either disc-shaped or irregular in shape. Test on a fresh, fractured rock surface is recommended. Rough surfaces may be obtained by Brazilian Testing on rock discs or by firm hammer blows on a rock core or rock sample, respectively. Alternatively, sawn-cut surface may be prepared by a water-cooled diamond saw blade. The testing surface should be cleared from debris or loose grains. The specimen can either be saturated, having the natural water content, air dried or oven dried. The path of the stylus on the rock surface should be free of visible pores. There is no limitation with respect to the grain size. However, for rocks having grain size greater than 2 mm, a larger number of tests should be considered. A test path may be dominated by a large mineral grain, and therefore, five single scratches may not represent the full mineral composition of the rock specimen. The size of the rock surface should be sufficient to permit five test scratches that are at least 5 mm from the edge of the rock surface. Each test should be 5 mm apart.

Anisotropic rocks, as expressed by for example bedding, gradation, banding, schistosity, etc., should be given special attention with respect to scratch directions. Scratches perpendicular to the anisotropic feature as well as on the surface of the anisotropic feature are suggested. The location and direction of testing in any sample should be selected to

represent the dominant mineralogy and texture of the rock sample observed in macroscopic samples.

4 Test Procedure

Prior to a test, the stylus should be inspected under a microscope. The apparatus should be checked for proper functionality. The sample should be clamped firmly in the vice while observing the desired scratching direction. The rock surface should be, to the extent possible, horizontal. The stylus should be carefully lowered onto the rock surface to avoid any damage to the tip of the stylus. The stylus should be positioned so it is vertical and perpendicular to the rock surface. The length of a test scratch in the rock sample must be exactly 10.0 mm. Depending on the apparatus design, the testing duration should be either 1 s with Type 1 or 10 s with Type 2 apparatus, respectively (Fig. 1). During the test there should be constant contact between the stylus and the rock surface. Otherwise, there is likely to be an erroneous result and the test must be repeated with a new stylus.

After testing, the stylus is carefully lifted from the rock surface and the stylus removed. Measurements of the tip wear flat are made as specified in Sect. 5.

A minimum of five test replications must be made on the rock surface, each time by a new or re-sharpened stylus.

5 Stylus Wear Measurement

The length or diameter of the wear flat, d , shall be based on optical and digital methods using a microscope having a minimum magnification of $25\times$. The measuring resolution should be at least ± 0.005 mm with readings reported to the nearest 0.01 mm. Measurements may be executed by side- or top-view settings as shown in Fig. 2.

Measurements by side view are however strongly recommended. When testing a fresh, fractured rock surface, especially in harder rock types, the wear flat can often exhibit

Fig. 3 Side view of a correct tip wear flat measurement (a) and what could be regarded as an overestimation of the wear flat by a top-view measurement method (b)

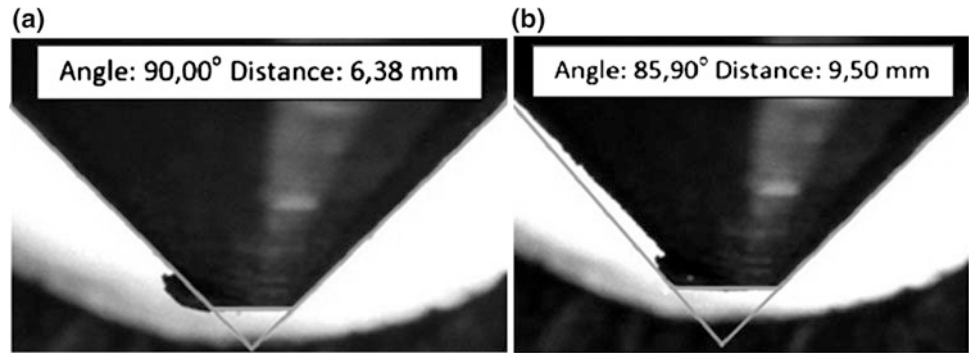
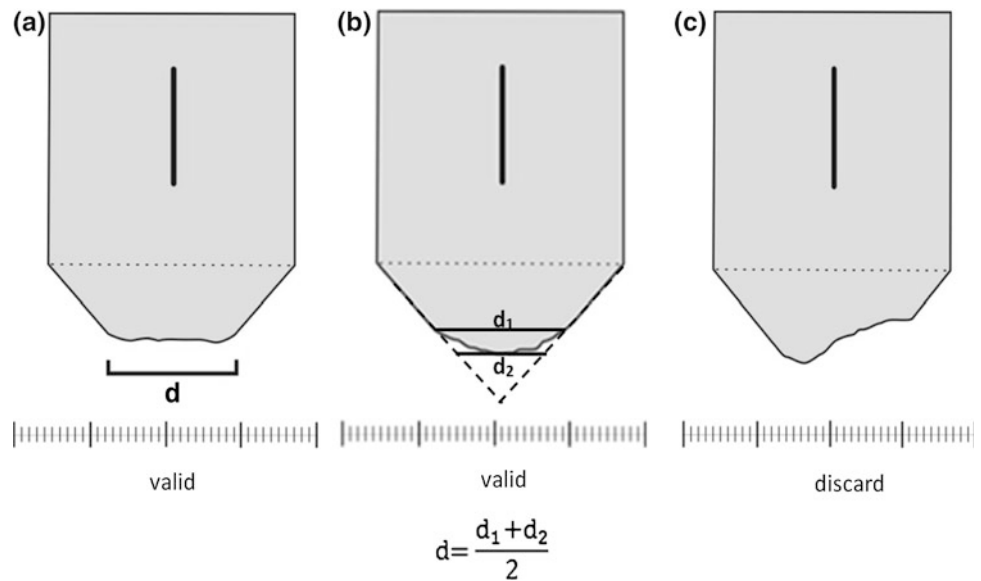


Fig. 4 Standard worn profiles (a, b) and the corresponding length of wear surface, c an example of a non-standard profile in which case no measurement should be recorded



a non-symmetrical shape with splinters or burrs of steel that stretch beyond the wear flat (as shown in Fig. 3). This can affect measurements by making it difficult to determine the true diameter of the wear flat by top-view measurements. A correct determination of the start and end points of the wear flat, as stated by Rostami et al. (2005), is crucial to the accuracy of the test which might otherwise contribute to large variations between different operators and laboratories.

The profile of the worn surface may, in some instances, make the estimation of the measurement difficult. Hence only measurements obtained from certain standard surface profiles should be used, examples of these standard profiles are shown in Fig. 4a, b. No measurement should be recorded and the test repeated in the case of any non-standard worn profile such as shown in Fig. 4c.

When using the side-view method, it is suggested the stylus should be placed in a V-notch holder or jig and four measurements shall be made each at 90° rotation. The measurements should be taken parallel and perpendicular to the direction of scratching.

Two measurements should be performed when using the top-view method as shown in Fig. 2b. When digital equipment is used, one measurement from the top will suffice (Fig. 2c).

6 Calculations

For each measurement of the wear flat, d , the CAI is calculated by the formula given in Eq. (1)

$$\text{CAI} = d \times 10 \quad (1)$$

where d is the wear tip surface measured to an accuracy of 0.01 mm.

The dimensionless CAI value is reported as the arithmetic mean of five or more test replications together with the standard deviation (Table 1).

Whenever a stylus hardness other than the recommended hardness of $\text{HRC } 55 \pm 1$ is used, the symbol notation adopted when reporting the CAI shall be $\text{CAI}_{(x)}$, where the

Table 1 Example of CERCHAR Abrasivity testing with five test replications with four measurements of the wear flat by side view of each test pin

Test No.	1	2	3	4	5
Pin Hardness (HRC)	55	55	55	55	55
Measurement d_1 (mm)	0.40	0.42	0.42	0.40	0.39
Measurement d_2 (mm)	0.41	0.44	0.40	0.41	0.38
Measurement d_3 (mm)	0.40	0.42	0.41	0.40	0.39
Measurement d_4 (mm)	0.42	0.41	0.41	0.44	0.39
Mean reading d_M (mm)	0.41	0.42	0.41	0.41	0.39
Mean pin wear (mm)					0.41
CERCHAR-Abrasivity-Index (CAI) (-)					4.1
Standard deviation of CAI					0.11

Table 2 Classification of CAI

Mean CAI	Classification
0.1–0.4	Extremely low
0.5–0.9	Very low
1.0–1.9	Low
2.0–2.9	Medium
3.0–3.9	High
4.0–4.9	Very high
≥ 5	Extremely high

subscript x denotes the value of hardness in units of Rockwell hardness HRC. The symbol CAI shall only apply to “as measured” values of wear flat on a stylus having a hardness of $HRC 55 \pm 1$. Values for the CAI using a stylus hardness other than HRC 55 can be converted using the method as suggested by Michalakopoulos et al. (2006) or Jacobs and Hagan (2009), the latter been shown below.

If the length or diameter of wear flat on a stylus of a given hardness is known then the equivalent calculated value of CAI or CAI' at the standard stylus hardness of HRC 55 can be calculated as follows (Jacobs and Hagan 2009)

$$CAI' = 0.415 CAI_{(x)} / (1 - 0.0107x) \quad (2)$$

where $CAI_{(x)}$ is measured as the value of CAI using a stylus having a hardness of HRC x .

7 Tests on Saw-Cut Surfaces

In special cases, the CERCHAR test may be executed on a saw-cut rock surface. The influence of a saw-cut surface on the CAI' value may be accounted for by correcting the wear tip flat length, d_s , from test on saw-cut surface using Eq. 3 after Käsling and Thuro (2010):

$$d = 1.14 d_s \quad (3)$$

Equation (3) should not be used for hard and very highly abrasive rocks.

8 Classification

The abrasivity classification system is given in Table 2. This classification system is based on the “as measured” CAI or equivalent calculated CAI' based on stylus having a Rockwell Hardness HRC 55 and a rough rock surface. The classification system must not be used for other values of stylus hardness.

9 Reporting

A report on a CERCHAR test shall include the following information:

- Source of sample(s), sampling date, method of preserving sample(s) during transport
- Testing date
- Storage/testing environment (saturated, as received, air dried, oven dried)
- Rock type (if known)
- Maximum grain size
- Planes of weakness or anisotropy (bedding, schistosity, etc.)
- Direction of scratching with respect to planes of weakness or anisotropy
- Surface condition (rough, saw-cut)
- Rockwell hardness HRC of stylus
- Type of apparatus (Type 1, Type 2)
- Measurement method (side view, top view, optical, digital)
- Each “as measured” value of CAI, mean and standard deviation, and where appropriate the equivalent values for CAI' (Table 1)
- Classification based on criteria shown in Table 2.

Acknowledgments A 3-day workshop of the WG members at Bülent Ecevit University, Zonguldak, Turkey was made possible by financial support of the Bülent Ecevit University, Zonguldak, Turkey and TUBITAK (The Scientific and Technological Research Council of Turkey) Grant No. 110M579. Input from H. Copur (Technical University Istanbul, Turkey) is gratefully acknowledged. We acknowledge the useful and constructive comments of the reviewers Prof. Bilgin (Istanbul Technical University, Turkey), Prof. Nilsen (NTNU Trondheim, Norway), Prof. Thuro (Technical University Munich, Germany), Dr. Plinninger (Dr. Plinninger Geotechnik, Bernried, Germany) and Prof. Rostami (Pennsylvania State University, USA).

References

- AFNOR (2000) Détermination du pouvoir abrasif d'une roche—Partie 1: Essai de rayure avec une pointe (NF P 94-430-1), Paris
- ASTM (2010) Standard test method for laboratory determination of abrasiveness of rock using the CERCHAR method. Designation: D7625-10
- Cerchar—Centre d'Études et des Recherches des Charbonnages de France (1986) The Cerchar abrasivity index. Verneuil
- Jacobs N, Hagan P (2009) The effect of stylus hardness and some test parameters on the Cerchar Abrasivity Index. In: Proceedings of 43rd US rock mechanics symposium, June 28–July 1, Asheville, NC, USA
- Käsling H, Thuro K (2010) Determining rock abrasivity in the laboratory. In: Zhao, Labiouse, Dudt, Mathier (eds) Rock mechanics in civil and environmental engineering—Proc EUROCK 2010. Taylor & Francis, London, pp 425–428
- Michalakopoulos TN, Anagnostou VG, Bassanou ME, Panagiotou GN (2006) The influence of steel styli hardness on Cerchar abrasiveness index value. *Int J Rock Mech Min Sci* 43:321–327
- Plinninger R, Käsling H, Thuro K, Spaun G (2003) Testing conditions and geomechanical properties influencing the Cerchar abrasiveness index (CAI) value. *Int J Rock Mech Min Sci* 40:259–263
- Rostami J, Özdemir L, Bruland A, Dahl F (2005) Review of issues related to Cerchar abrasivity testing and their implications on geotechnical investigations and cutter cost estimates. In: Rapid Excavation and Tunnelling Conference, Seattle, WA, USA, pp 15–29
- Valantin A (1973) Examen des différents procédés classiques de détermination de la nocivité des roches vis-à-vis de l'abattage mécanique. Exposé Présenté Aux Journées d'information Techniques de Creusement, les 28–29 Novembre 1973, Luxembourg, pp 133–140
- West G (1989) Rock abrasiveness testing for tunnelling. *Int J Rock Mech Min Sci* 26:151–160

ISRM-Suggested Method for Determining the Mode I Static Fracture Toughness Using Semi-Circular Bend Specimen

M. D. Kuruppu, Y. Obara, M. R. Ayatollahi, K. P. Chong, and T. Funatsu

1 Introduction

Rock fracture mechanics can be used to identify and predict the imminent failure of rock mass structures thereby providing guidelines to improve the stability and the safety of these structures. Another application is for the exploitation of mineral resources by adopting techniques such as mechanical mining, blasting and hydraulic fracturing. In fracture processes which are not associated with high strain rates, the mode I plane-strain static fracture toughness gives the critical value of the stress intensity factor leading to the onset of crack growth in that mode (Liu 1983). Some of the applications of fracture toughness include index of fragmentation processes like those used in tunnel boring, a

modelling parameter in processes such as rock cutting and hydraulic fracturing and for the stability analysis of civil, mining and earthen structures (Whittaker et al. 1992).

A number of standard methods have been proposed to determine the mode I fracture toughness of rock. They include those based on short rod (SR) specimen, chevron bend (CB) specimen and cracked chevron notched Brazilian disk (CCNBD) specimen (ISRM 2007). The semi-circular bend (SCB) specimen has been widely used for fracture toughness determination of geomaterials owing to inherent favourable properties such as its simplicity, minimal requirement of machining and the convenience of testing that can be accomplished by applying three-point compressive loading using a common laboratory load frame (Chong and Kuruppu 1984; Chong et al. 1987; Lim et al. 1993, 1994; Ayatollahi and Aliha 2007; Aliha et al. 2012; Karfakis and Akram 1993; Obara et al. 2006, 2007a, b, 2009; Molenaar et al. 2002). As geomaterials are weak in tension, fracture tests should preferably be conducted with compressive loading in such a way that tensile fractures are induced. The CB and CCNBD specimens used for the standard methods as well as the SCB specimen satisfy those requirements. Use of more than one type of specimen is regarded as appropriate when it is required to measure the fracture toughness of anisotropic materials in different material directions of a rock sample (Chong et al. 1987). An ISRM-suggested method for mode I static fracture toughness determination of rock and other geomaterials using SCB specimen is herein presented.

Originally published as an article in the journal *Rock Mechanics and Rock Engineering*, 47, M.D. Kuruppu, Y. Obara, M.R. Ayatollahi, K.P. Chong, T. Funatsu, ISRM-Suggested Method for Determining the Mode I Static Fracture Toughness Using Semi-Circular Bend Specimen, 267–274, 2014.

M. D. Kuruppu (✉)
Curtin University, Locked Bag 30, Kalgoorlie, WA 6433,
Australia
e-mail: M.Kuruppu@curtin.edu.au

Y. Obara
Graduate School of Science and Technology, Kumamoto
University, 2-39-1 Kurokami, Kumamoto, 860-8555, Japan

M. R. Ayatollahi
School of Mechanical Engineering, Iran University of Science
and Technology, Narmak, 16846, Tehran, Iran

K. P. Chong
National Institute of Standards and Technology, Stop 8615,
Gaithersburg, MD 20899, USA

K. P. Chong
Department of Mechanical Engineering, George Washington
University, Washington DC, 20052, USA

T. Funatsu
Institute for Geo-Resources and Environment, AIST, Central 7 1-
1-1 Higashi, Tsukuba, Ibaraki 305-8567, Japan

2 Scope

This test method is intended to measure the mode I static fracture toughness K_{Ic} under slow and steady loading where dynamic effects are negligible. However, another suggested method developed by the ISRM should be followed if the loading rate is high, as in the case of explosive fragmentation of rock (Zhou et al. 2012). The geometry of the test specimen is designed to use standard core material. A minimum

specimen diameter D_{\min} is suggested to be used in order to satisfy the minimum size requirement as explained in Sect. 7. If the rock material is known to be anisotropic, the core axis should be oriented either parallel or perpendicular to any anisotropic feature, such as a bedding plane. If required, the remaining material from mode I fracture toughness tests performed using CB and SR methods can be used to find fracture toughness in orthogonal directions (Chong et al. 1987). For example, for sedimentary rocks that exhibit transversely isotropic material properties, a combination of tests performed using SR, CB, CCNBD and/or SCB specimen with cores taken perpendicular and parallel to bedding planes, will give the complete information of fracture toughness. Alternatively, SCB specimens themselves can be made from cores such that the notch directions are either aligned or perpendicular to the bedding planes.

The advantages of using the SCB specimens are (a) material requirement per specimen is small, (b) machining is relatively simple and (c) only the maximum compressive load is required to determine the fracture toughness.

3 Specimen Preparation

The circular disks required to make the SCB specimen are prepared by sawing or slicing standard rock cores using a high-precision diamond tool. The geometry of the SCB specimen is shown in Fig. 1. The specimen diameter ($D = 2R$) should be related to the average grain size in the rock by a ratio of at least 10:1 or should be at least 76 mm and the minimum specimen thickness shall be the larger of $0.4D$ or 30 mm. Caution should be exercised to minimise the micromechanical damage of the specimens as it can affect the fracture toughness. Water or other coolant should be used while machining, in order to avoid heat damage that can alter the fracture toughness. Slow drilling is recommended in case that the cores are drilled from a large rock sample.

Each of the circular disks should be sawn into two halves which may be carried out using the same cutting tool used to make the circular disks. The final operation of introducing a notch should be performed using a thin cutting blade of thickness $\leq 1.5 \pm 0.2$ mm, or preferably, using a diamond-impregnated fine wire saw that will produce a straight notch of the required length. The radius of the notch tip should be less than the average grain size of the rock material. The notch length should be such that $0.4 \leq a/R \leq 0.6$.

The plane surface along the thickness direction should be flat to 0.01 mm. The plane of the notch shall not depart from perpendicularity to the plane surface in the thickness direction by more than 0.5° . The dimensions of the test specimen are given in Table 1.

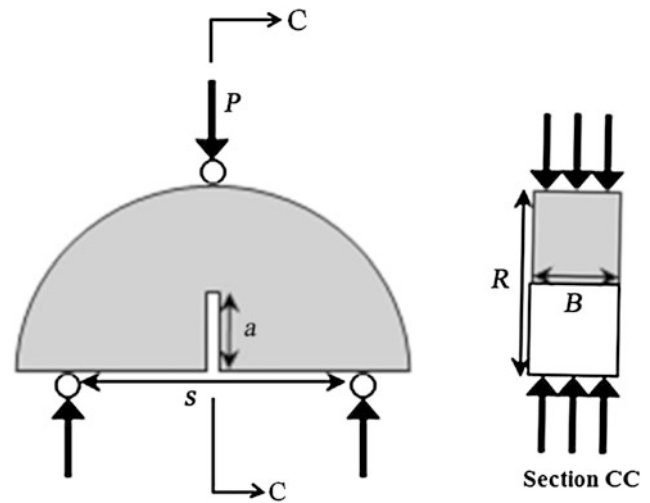


Fig. 1 SCB specimen geometry and schematic loading arrangement (R radius of the specimen, B thickness, a notch length, s distance between the two supporting cylindrical rollers, P monotonically increasing compressive load applied at the central loading roller of the three-point bend loading)

When slicing a core, the plane of the resulting disks should not deviate from the perpendicularity to the core axis by more than 0.5° .

When cutting a disk into two halves to form two semi-circular disks, care must be given not to deviate the cutting plane from a diametral plane by more than 0.2 mm. Also, the perpendicularity to the plane of the disk should be assured to be within 0.5° .

The specimens must be marked with a reference that gives the details of its orientation with respect to any directions of material anisotropy (e.g. inclination of the notch plane to bedding planes). Specimens of the same sample should have identical notch orientation.

The notch length should be measured as an average taken on both the semi-circular planar surfaces which are perpendicular to the core axis. The two readings should be within 2 % of each other.

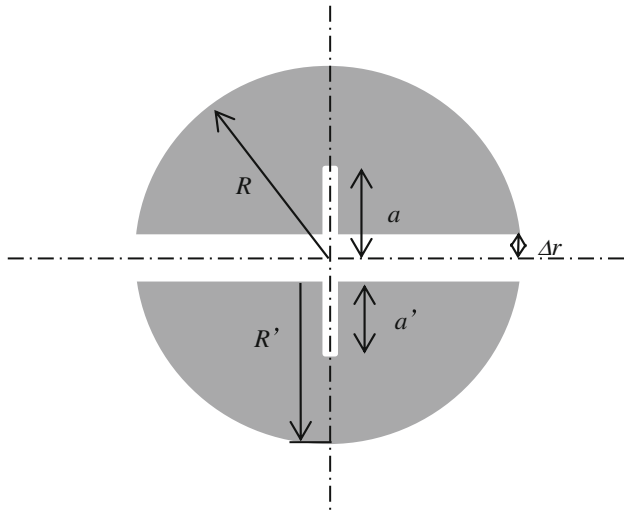
The thickness should be uniform and shall not deviate by more than 0.2 mm.

The dimensions of the specimens should be measured to the nearest 0.1 mm. The required dimensions are the radius R , the thickness B and the notch length a .

If the thickness of the saw blade used to cut the disks into semi-circular specimens is greater than $0.05D$, where D is the disk diameter, then the values of the measured radius R' and the measured notch length a' should be corrected as shown in Fig. 2 (i.e. the corrected radius $R = R' + \Delta r$ and corrected notch length $a = a' + \Delta r$). Note that the radius measurement shall be taken aligned with the notch direction.

Table 1 Recommended geometrical dimensions of SCB specimen (see Fig. 1)

Descriptions	Values or range
Diameter (D)	Larger of $10\times$ grain size or 76 mm
Thickness (B)	Larger of $0.4D$ or 30 mm
Crack length (a)	$0.4 \leq \frac{a}{R} (= \beta) \leq 0.6$
Span length (s)	$0.5 \leq \frac{s}{2R} \leq 0.8$

**Fig. 2** Correction for a , R when the thickness of the saw blade is not negligible (i.e. $2\Delta r \geq 0.05D$, where Δr is the half thickness of the saw blade used for cutting)

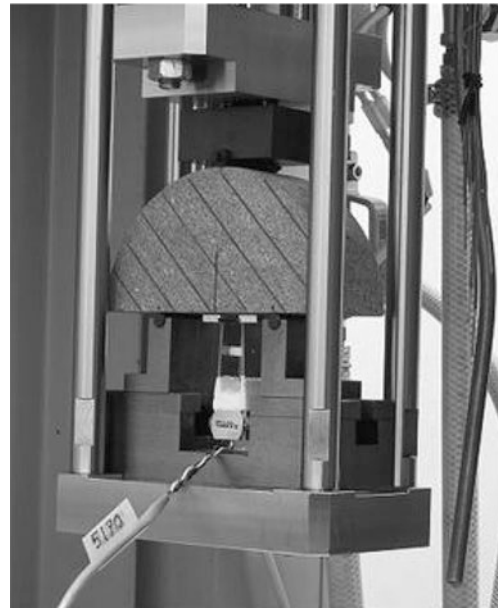
The specimen should be stored after specimen preparation for an appropriate period of time that is sufficient to achieve the desired conditions (e.g. moisture content). The conditions of storage, moisture adjustment or drying, as well as any macroscopically noticeable features of the specimen surfaces, shall be reported with fracture toughness results.

The tensile strength of the material should be known (or measured) (ISRM 2007).

4 Experimental Setup

The test should be performed using a standard compressive or universal test frame commonly available in most rock mechanics laboratories. While a servo-hydraulic test system is preferable, a mechanically driven compressive testing machine may be adequate if the capacity and the precision of the load measurement is as given below. The load frame should be equipped with a system to record the load, the axial displacement and any other measuring signal of interest.

The load application is performed via a conventional three-point bend fixture. The specimen is to be placed on the two bottom loading cylindrical rollers which are kept

**Fig. 3** SCB specimen loading fixture

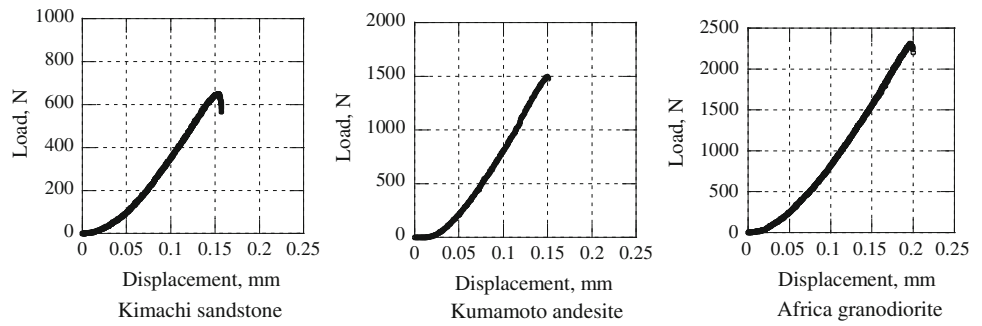
apart at a predetermined distance commensurate with the size of the specimen as shown in Fig. 3. The rollers shall be placed on the bottom loading plate so that they can rotate and move apart slightly when the specimen is loaded, thus permitting roller contact at supports offering no frictional resistance. A suitable span length should be selected within the range of span (s) to diameter ratio (D), s/D of $0.5 \leq s/D \leq 0.8$. The parallel positioning of the two bottom support rollers should be ensured. It may help to mark the positions of the two bottom support rollers on either side of the semi-circular faces of the specimen prior to its positioning on the support rollers. These positions should be drawn symmetrical to the plane of the notch. A top loading cylindrical roller is attached to the top loading plate so that the load application occurs symmetrically between the two bottom support rollers. A suitable recess made on the top loading plate may be required to hold the roller in position.

The diameter of the rollers should be chosen in relation to the specimen diameter. A ratio of 1:20 is recommended (i.e. 10 mm diameter rollers are used for testing 200 mm diameter specimens). However, the minimum diameter of the rollers used for testing specimens <100 mm diameter should be 5 mm.

Alignment of the notch plane with the loading direction should be carefully controlled.

The load frame should be equipped with a load cell having a resolution of 0.01 kN or greater. A linear variable displacement transducer (LVDT) set up between the top and bottom loading roller positions is the preferred arrangement for measuring the displacement. Crack opening displacement measurement by a clip gauge is also useful (Karfakis and Akram 1993). A successful test is usually associated with a

Fig. 4 Typical load versus displacement plots showing the critical fracture point



monotonically increasing and continuous load–displacement graph. Moreover, the load versus displacement behaviour reveals the degree of nonlinearity of the rock material.

If testing is required to be performed at conditions other than the ambient, then the specimen may be kept inside an environment chamber that will provide those conditions. For example, moisture content measured by water vapour pressure may be set at a predetermined level and maintained until reaching saturation under that condition (Obara et al. 2010). Temperature may be set at a predetermined level and maintained until the specimen is heated uniformly (Funatsu et al. 2004; Kuruppu and Seto 2001). They may be controlled independently from the axial load application that would perform the three-point bend loading of the specimen.

5 Testing Procedure

The minimum data required during testing is the peak load P_{\max} and any other environmental conditions, if applicable. However, a continuous measurement of the load and the displacement between the top and bottom loading roller positions during the test is recommended in order to verify that the load has increased continuously with increasing displacement until reaching the point of fracture as shown in Fig. 4 (Kataoka et al. 2010, 2011). It is appropriate to gather data at a rate of four data sets per second if digital data acquisition is used.

The testing should be done at a constant displacement rate of not greater than 0.2 mm/min to avoid any dynamic effect (Backers and Stephansson 2012; Khan and Al-Shayea 2000). Data acquisition should begin prior to closing the gap between the specimen and the top loading roller and continue until the specimen fails completely.

When the gap is closed and a small load is applied, the test may be stopped momentarily to check the alignment of support/loading rollers and that they are in touch with the specimen along the entire thickness of the specimen.

After the test is completed, the two parts of the broken specimen should be kept for further observation of failure mode. The results shall be considered invalid if the plane of the cracked ligament deviates from the notch plane by more than $0.05D$.

The number of specimens tested per sample should be determined by practical considerations. A minimum of five specimens are recommended. All specimens of the sample ought to be tested subjected to the same conditions.

6 Calculations

Mode I fracture toughness K_{Ic} shall be determined using the observed peak load P_{\max} such that:

$$K_{Ic} = Y' \frac{P_{\max} \sqrt{\pi a}}{2RB} \quad (1)$$

where,

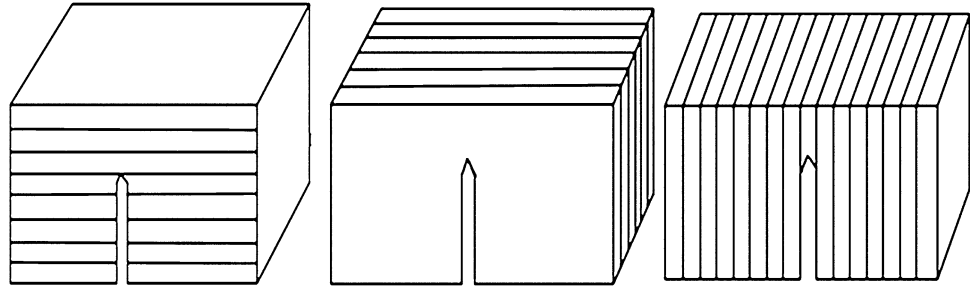
$$Y' = -1.297 + 9.516(s/2R) - (0.47 + 16.457(s/2R))\beta + (1.071 + 34.401(s/2R))\beta^2 \quad (2)$$

and $\beta = a/R$. Equation (2) gives the non-dimensional stress intensity factor Y' derived using the finite element method while assuming plane-strain conditions. Further details about the numerical analyses performed for deriving Eq. (2) can be found in the Appendix. Table 2 gives some of the values calculated for Y' . Equation (2) is valid for $\beta \geq 0.2$. However, a relatively deep notch is required for the bending effect to produce a strong mode I stress field near the tip of the notch. Hence, a normalised length β in the range $0.4 \leq \beta \leq 0.6$ is recommended to be used.

The suggested range of $s/2R$ is $0.5 \leq s/2R \leq 0.8$. For testing strong materials, it is preferable to use a value approaching 0.8. However, this may not be practical for specimens made of weak geomaterials in which case a value at the lower end of the range should be used.

Table 2 Non-dimensional stress intensity factor Y'

$s/2R$	$\beta = 0.4$	$\beta = 0.5$	$\beta = 0.6$
0.5	2.905	3.679	4.819
0.6	3.748	4.668	6.022
0.7	4.592	5.657	7.224
0.8	5.436	6.645	8.427

Fig. 5 Principal crack orientations with respect to bedding planes (*left to right* arrester, divider and, short transverse configurations)

Some of the previously published suggested methods are meant to determine two levels of fracture toughness of rock. Level I is based on the maximum failure load and level II further incorporates a nonlinearity correction to take any non-linear material behaviour into account. However, this suggested method only addresses level I fracture toughness.

As described in Sect. 2 the SCB specimen can be used to determine the fracture toughness of sedimentary rock in which major planes of anisotropy can be found. Those rocks mostly exhibit transversely isotropic properties. For complete characterization, specimens with their notches aligned in three mutually perpendicular directions should be tested (Fig. 5). One possibility is to use three sets of SCB specimens having the notches oriented in each of the arrester, divider and short transverse directions. However, it may be more practical to use a combination of fracture toughness test specimens. While it is up to the user to decide which combination of specimens is to be employed, one combination is to use the straight edge cracked round bar in bending (SECRBB), SCB and centrally cracked Brazilian disk (CCBD) specimens made with their notches aligned to form divider, arrester and short transverse configurations, respectively. These specimens must be made with cores taken in the direction of bedding planes.

7 Size Effects

As geomaterials tend to form relatively large process zones prior to fracture, certain minimum specimen sizes need to be satisfied to achieve the requirements for linear elastic fracture

mechanics, according to which the concept of K_{Ic} is defined. The process zone is largely affected by the grain size of the material; those consisting of relatively small grains have small size requirements and vice versa (Ouchterlony 1990; Kuruppu and Chong 2012; Bazant 1984).

Chong et al. (1987) suggested the following size requirement for the SCB specimen:

$$D \geq 2.0 \left(\frac{K_{Ic}}{\sigma_t} \right)^2 \quad (3)$$

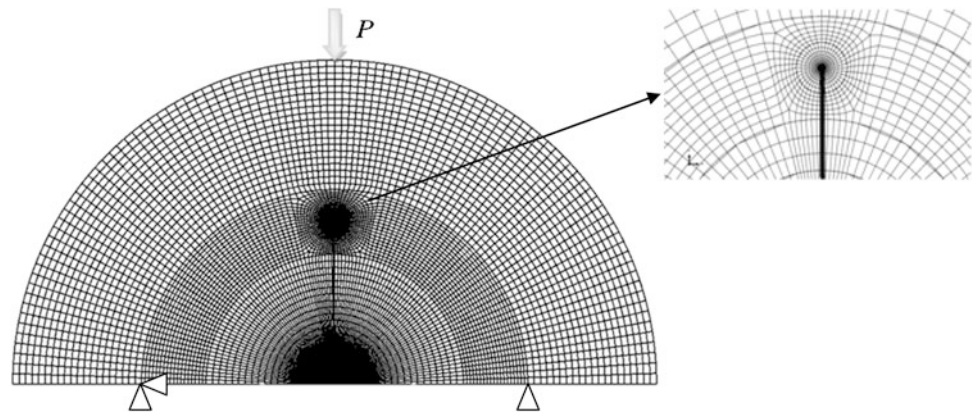
where σ_t is the tensile strength of the material. However, this may be a conservative estimate as the size requirements applicable for chevron notched CB and SR specimens are much lower (Ouchterlony 1989). No definitive size requirement can be given for SCB specimens. One way to determine the size requirement for a particular material is by comparing K_{Ic} values deduced using a number of specimens of different diameters D . The smallest specimen diameter D_{min} , that generates K_{Ic} value consistent with larger diameter specimens, will be the minimum size required to give a valid fracture toughness test.

8 Reporting of Results

The report should include the following:

1. Source of specimens as precisely as possible (e.g. material, location, date and orientation).
2. Lithological description of the rock type including grain size.

Fig. 6 A sample mesh pattern used for simulating the SCB specimen



3. Dimensions of the specimens. Any particular observations about macroscopic appearance of the specimen surface.
4. If applicable, the orientation of the notch with respect to the specimen anisotropy (e.g. direction of bedding planes, etc.).
5. History and environment of test specimen storage (e.g. temperature, water vapour pressure).
6. Conditions at the time of test (e.g. temperature, water vapour pressure).
7. Details of the test equipment and test procedure used, particularly if the method employed deviated from the suggested method and the reasons for such deviation.
8. Record of all signals measured, loading rate and any other relevant parameters not included in this list.
9. The calculated value of fracture toughness of each specimen.
10. Description of the broken specimens after testing. If there are fractures other than the near-symmetric split of the specimens then the results of those specimens will not be valid.
11. The average value of mode I fracture toughness of each sample disregarding any invalid results. Statement of any associated environmental conditions.

Acknowledgments The authors thankfully acknowledge the guidance and encouragement given by Prof. Resat Ulusay, President of the ISRM commission on testing methods, and other commission members in order to develop this suggested method.

Appendix: Details of Numerical Analysis Used for Deriving Eq. (2)

The SCB specimens of different crack lengths were simulated and analyzed using eight-node plane-strain elements in the finite element code Abaqus Unified FEA (2012). The loading, the boundary conditions and a typical finite element mesh used for the simulations are shown in Fig. 6.

Singular elements with nodes at quarter-point positions were used for the first ring of elements around the crack tip. In the circular partitions surrounding the crack tip where the contour integrals are calculated, the mesh was biased toward the crack tip. The stress intensity factors K_I were extracted directly from ABAQUS which makes use of the J -integral method to compute the stress intensity factors. The numerical results showed that there was negligible variation in the J -integral values calculated for successive contours surrounding the crack tip.

Using a fixed arbitrary load P , the stress intensity factor K_I was determined for each set of β and $\frac{s}{2R}$, and the non-dimensional stress intensity factor Y' was calculated from

$$Y'(\beta, \frac{s}{2R}) = \frac{2RBK_I}{P\sqrt{\pi a}} \quad (\text{A1})$$

then Eq. (2) was derived by fitting a second order polynomial to the numerical results obtained for Y' . Tutluoglu and Keles (2011) recently reported limited numerical results for Y' in the SCB specimen. As shown in Table 3, very good agreement exists between the present results and those reported by Tutluoglu and Keles (2011). Table 3 can also be considered as validation for the finite element results obtained in this study, particularly for the ranges $0.4 \leq \beta \leq 0.6$ and $0.5 \leq s/2R \leq 0.8$, as suggested in Sect. 6.

It is noteworthy that a number of investigators have presented mode I stress intensity factors of the SCB specimen (Chong et al. 1987; Lim et al. 1994; Basham 1989). For instance, Lim et al. (1994) extracted the stress intensity factors of the SCB specimen from finite element analysis and suggested a fifth order polynomial for Y' as.

$$Y' = \frac{s}{2R} (2.91 + 54.39\beta - 391.4\beta^2 + 1210.6\beta^3 - 1650\beta^4 + 875.9\beta^5) \quad (\text{A2})$$

Table 3 Numerical values of Y' , present results compared with those of Tutluoglu and Keles (2011)

$\beta = a/R$	$s/2R$	Present results	Tutluoglu and Keles (2011)
0.3	0.5	2.495	2.538
0.5	0.5	3.679	3.550
0.67	0.5	5.835	6.209

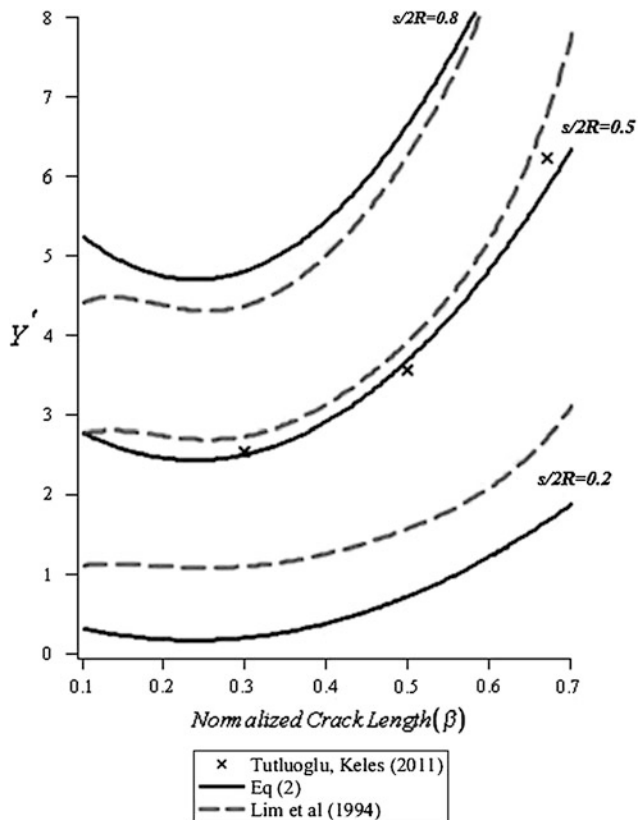


Fig. 7 The curves plotted based on Eqs. (2) and (A2)

Figure 7 shows a comparison between the curves plotted based on Eqs. (2) and (A2) for different values of β and $\frac{s}{2R}$. Significant discrepancies can be seen between these two sets of results.

Having checked our finite element results by different mesh designs and element numbers, we concluded that the observed discrepancy can be due to less accurate method used by Lim et al. (1994) for determining the stress intensity factors of the SCB specimen. The displacement/stress extrapolation method employed by Lim et al. was a common technique in the 1990s for deriving stress intensity factors from finite element results. But, later more accurate methods were proposed like the contour integral techniques (e.g. J -integral method). It is now well established that the numerical errors in the region of high stress gradient around the crack tip affects the J -integral method much less than the displacement/stress extrapolation technique.

References

- Abaqus Unified FEA (2012) Dassault systems
- Aliha MRM, Sistaninia M, Smith DJ, Pavier MJ, Ayatollahi MR (2012) Geometry effects and statistical analysis of mode I fracture in Guiting limestone. *Int J Rock Mech Min Sci* 51:128–135
- Ayatollahi MR, Aliha MRM (2007) Wide range data for crack tip parameters in two disc-type specimens under mixed mode loading. *Comput Mater Sci* 38:660–670
- Backers T, Stephansson O (2012) ISRM suggested method for the determination of mode II fracture toughness. *Rock Mech Rock Engng* 45:1011–1022
- Basham KD (1989) Nonlinear fracture mechanics using semi-circular specimens and tension softening behaviour. PhD dissertation, Department of Civil Engineering, The University of Wyoming, USA
- Bazant ZP (1984) Size effect in blunt fracture: concrete, rock, metal. *J Engng Mech Div ASCE* 110:518–535
- Chong KP, Kuruppu MD (1984) New specimen for fracture toughness determination of rock and other materials. *Int J Fract* 26:R59–R62
- Chong KP, Kuruppu MD, Kuzmaul JS (1987) Fracture toughness determination of layered materials. *Eng Fract Mech* 28:43–54
- Funatsu T, Seto M, Shimada H, Matsui K, Kuruppu M (2004) Combined effects of increasing temperature and pressure on the fracture toughness of clay bearing rocks. *Int J Rock Mech Min Sci* 41:927–938
- ISRM (2007) The complete ISRM suggested methods for rock characterization, testing and monitoring: 1974–2006. In: Ulusay R, Hudson JA (eds) Suggested methods prepared by the commission on testing methods, International Society for Rock Mechanics, compilation arranged by the ISRM Turkish National Group. Kozan Ofset, Ankara
- Karfakis MG, Akram M (1993) Effects of chemical solutions on rock fracturing. *Int J Rock Mech Min Sci Geomech Abstr* 30(7):1253–1259
- Kataoka M, Obara Y, Yoshinaga T, Kuruppu M (2010) Fracture toughness of rock under water vapour pressure. In: Proceedings of the ISRM International Symposium on Rock Mechanics and 6th Asian Rock Mechanics Symposium, New Delhi, Paper No. 12 (on CD)
- Kataoka M, Obara Y, Kuruppu M (2011) Estimation of fracture toughness of anisotropic rocks by SCB test and visualization of fracture by means of X-ray CT. In: Qian Q, Zhou Y (eds) Proceedings of the ISRM 12th International Congress on Rock Mechanics, Beijing, pp 667–670
- Khan K, Al-Shayea NA (2000) Effect of specimen geometry and testing method on mixed mode I–II fracture toughness of a limestone rock from Saudi Arabia. *Rock Mech Rock Engng* 33(3):179–206
- Kuruppu MD, Chong KP (2012) Fracture toughness testing of brittle materials using semi-circular bend (SCB) specimen. *Eng Fract Mech* 91:133–150
- Kuruppu MD, Seto M (2001) Determination of fracture toughness of rock under in situ conditions using semi-circular specimen. In: Proceedings of ICF10, 10th International Conference on Fracture, Hawaii, pp 651 (abstracts vol)
- Lim IL, Johnston IW, Choi SK (1993) Stress intensity factors for semi-circular specimens under three-point bending. *Eng Fract Mech* 44(3):363–382

- Lim IL, Johnston IW, Choi SK, Boland JN (1994) Fracture testing of a soft rock with semi-circular specimens under three-point loading, part I-mode I. *Int J Rock Mech Min Sci* 31:185–197
- Liu HW (1983) On the fundamental basis of fracture mechanics. *Eng Fract Mech* 17:425–438
- Molenar AAA, Scarpas A, Liu X, Erkens SMJG (2002) Semi-circular bending test; simple but useful? *J Assoc Asph Paving Technol* 71:794–815
- Obara Y, Sasaki K, Matusyama T, Yoshinaga T (2006) Influence of water vapour pressure of surrounding environment on fracture toughness of rock. In: *Proceedings of ARMS 2006, Asian Rock Mechanics Symposium, Singapore, 7th chapter (on CD)*
- Obara Y, Sasaki K, Yoshinaga T (2007a) Estimation of fracture toughness of rocks under water vapour pressure by semi-circular bend (SCB) test. *J of MMIJ* 123:145–151
- Obara Y, Sasaki K, Yoshinaga T (2007b) Influence of water vapour pressure of surrounding environment on fracture toughness and crack velocity of rocks. In: *Proceedings of 11th congress of ISRM, Vol 1, Lisbon, pp 51–54*
- Obara Y, Yoshinaga T, Hirata A (2009) Fracture toughness in mode I and II of rock under water vapour pressure. In: Vrkljan I (ed) *Proceedings of ISRM regional symposium EUROCK, Cavtat, pp 333–338*
- Obara Y, Kuruppu M, Kataoka M (2010) Determination of fracture toughness of anisotropic rocks under water vapour pressure by semi-circular bend test. In: Topal E, Kuruppu MD (eds) *Proceedings of mine planning and equipment selection, The Australasian Institute of Mining and Metallurgy, Victoria, Australia, pp 599–610*
- Ouchterlony F (1989) Fracture toughness testing of rock with core based specimens, the development of an ISRM standard. In: Mihashi H, Takahashi H (eds) *Fracture toughness and fracture energy. A. A. Balkema, Rotterdam, The Netherlands, pp 231–251*
- Ouchterlony F (1990) Fracture toughness testing of rock with core based specimens. *Eng Fract Mech* 35:351–366
- Tutluoglu L, Keles C (2011) Mode I fracture toughness determination with straight notched disk bending method. *Int J Rock Mech Min Sci* 48:1248–1261
- Whittaker BN, Singh RN, Sun G (1992) *Rock fracture mechanics—principles, design and applications. Elsevier Sci Publisher, Amsterdam*
- Zhou YX, Xia K, Li XB, Li HB, Ma GW, Zhao J, Zhou ZL, Dai F (2012) Suggested methods for determining the dynamic strength parameters and mode-I fracture toughness of rock materials. *Int J Rock Mech Min Sci* 49:105–112

ISRM Suggested Methods for Determining the Creep Characteristics of Rock

Ömer Aydan, Takashi Ito, Ugur Özbay, M. Kwasniewski, K. Shariar, T. Okuno, A. Özgenoğlu, D. F. Malan, and T. Okada

1 Introduction

It is important to note that creep is only one aspect of the time-dependent behavior of rocks. In Fig. 1, three cases are illustrated with respect to the complete stress–strain curve: creep, i.e., increasing strain when the stress is held constant; stress relaxation, i.e., decreasing stress when the strain is held constant; and a combination of both, when the rock unloads along a chosen unloading path. This ISRM suggested method deals only with the case of creep, which is particularly relevant for cases where the applied load or stress is kept constant.

Creep tests have also been carried out on soft rocks such as tuff, shale, lignite, and sandstone, medium-hard rocks such as marble, limestone, and rock salt, and hard rocks

such as granite and andesite (i.e., Akagi 1976; Akai et al. 1979, 1984; Ito and Akagi 2001; Berest et al. 2005; Doktan 1983; Passaris 1979; Serata et al. 1968; Wawersik 1983; Okubo et al. 1991, 1993; Masuda et al. 1987, 1988; Ishizuka et al. 1993; Lockner and Byerlee 1977; Boukharov et al. 1995; Fabre and Pellet 2006; Aydan et al. 1995; Chan 1997; Cristescu and Hunsche 1998; Hunsche 1992; Hunsche and Hampel 1999; Ito et al. 1999; Mottahed and Szeki 1982; Perzyna 1966; Slizowski and Lankof 2003; Yang et al. 1999). These experiments were mostly carried out under compressive loading conditions.

There are few studies on rocks using creep tests under a tensile loading regime (Ito and Sasajima 1980, 1987; Ito et al. 2008; Aydan et al. 2011). In particular, shallow underground openings may be subjected to a sustained tensile stress regime, which requires the creep behavior of rocks under such conditions.

Please send any written comments on this ISRM suggested method to Prof. Resat Ulusay, President of the ISRM Commission on Testing Methods, Hacettepe University, Department of Geological Engineering, 06800 Beytepe, Ankara, Turkey.

Originally published as an article in the journal *Rock Mechanics and Rock Engineering*, 47, Ö. Aydan, T. Ito, U. Özbay, M. Kwasniewski, K. Shariar, T. Okuno, A. Özgenoğlu, D.F. Malan, T. Okada, *ISRM Suggested Methods for Determining the Creep Characteristics of Rock*, 275–290, 2014.

Ö. Aydan (✉)

Department of Civil Engineering and Architecture, University of the Ryukyus, Nishihara, Okinawa, Japan
e-mail: aydan@tec.u-ryukyu.ac.jp

Ö. Aydan

Tokai University, Shizuoka, Japan

T. Ito

Department of Civil Engineering, Toyota National College of Technology, Toyota, Japan

U. Özbay

Department of Mining Engineering, Colorado School of Mines, Golden, CO, USA

M. Kwasniewski

Mining and Geology Faculty, Silesian University of Technology, Gliwice, Poland

K. Shariar

Department of Mining Engineering, Amirkabir University, Tehran, Iran

T. Okuno

Shimizu Corporation, Institute of Technology, Tokyo, Japan

A. Özgenoğlu

Engineering Faculty, Atılım University, Ankara, Türkiye

D. F. Malan

Department of Mining Engineering, Pretoria University, Pretoria, South Africa

T. Okada

Central Research Institute of Electrical Power Industry, Abiko, Japan

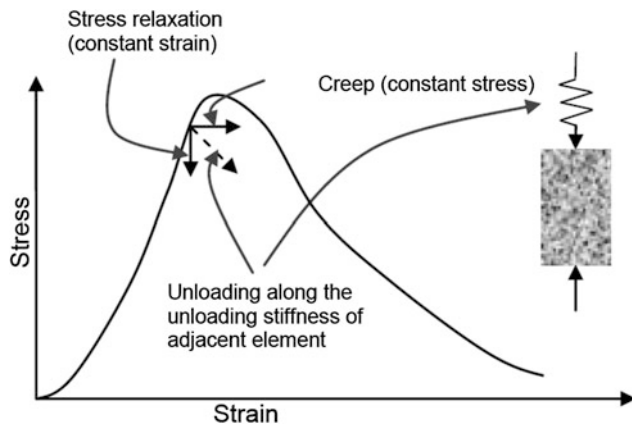


Fig. 1 Possible stress–strain paths during testing for the time-dependent characteristics of rocks (from Hagros et al. 2008)

Creep experiments are often used to determine the time-dependent strength and/or time-dependent deformation modulus of rocks. It has often been stated that creep of rocks does not occur unless the load/stress level exceeds a certain threshold value, which is sometimes defined as the long-term strength of rocks (Ladanyi 1974; Bieniawski 1970). Creep behavior is generally divided into primary, secondary, and tertiary, or accelerated, creep stages.

The creep characteristics of rocks are very important for assessing the long-term stability of rock engineering structures. These ISRM suggested methods have been developed for laboratory creep testing of rocks in the light of the available creep testing techniques used in rock mechanics as well as other disciplines of engineering.

2 Scope

The suggested methods for creep tests described herein concern the creep characteristics of intact rocks under the indirect tensile stress regime of the Brazilian test and the uniaxial and triaxial compression tests in the light of available creep testing techniques used in the field of rock mechanics as well as other disciplines of engineering under laboratory conditions. Three separate methods have been included because the reader may wish to establish the creep behavior in tension, uniaxial compression or triaxial compression.

3 Apparatuses

Apparatuses for creep tests can be of the cantilever type or the load/displacement-controlled type. Although the details of each testing machine may differ, the required features of apparatuses for creep tests are described in this section.

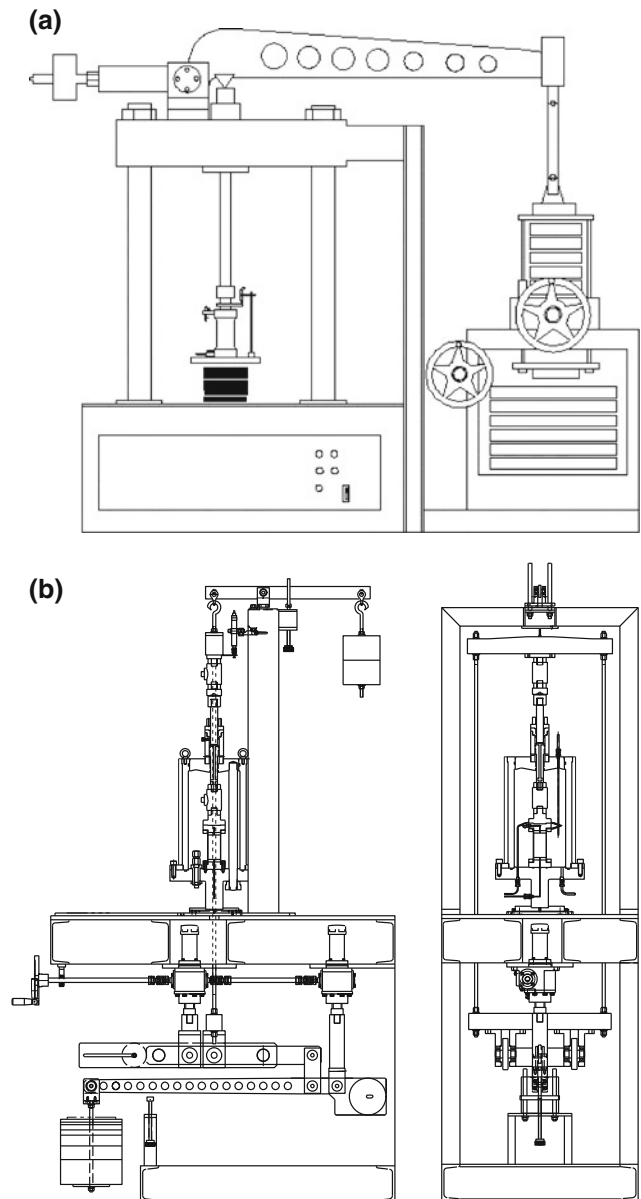
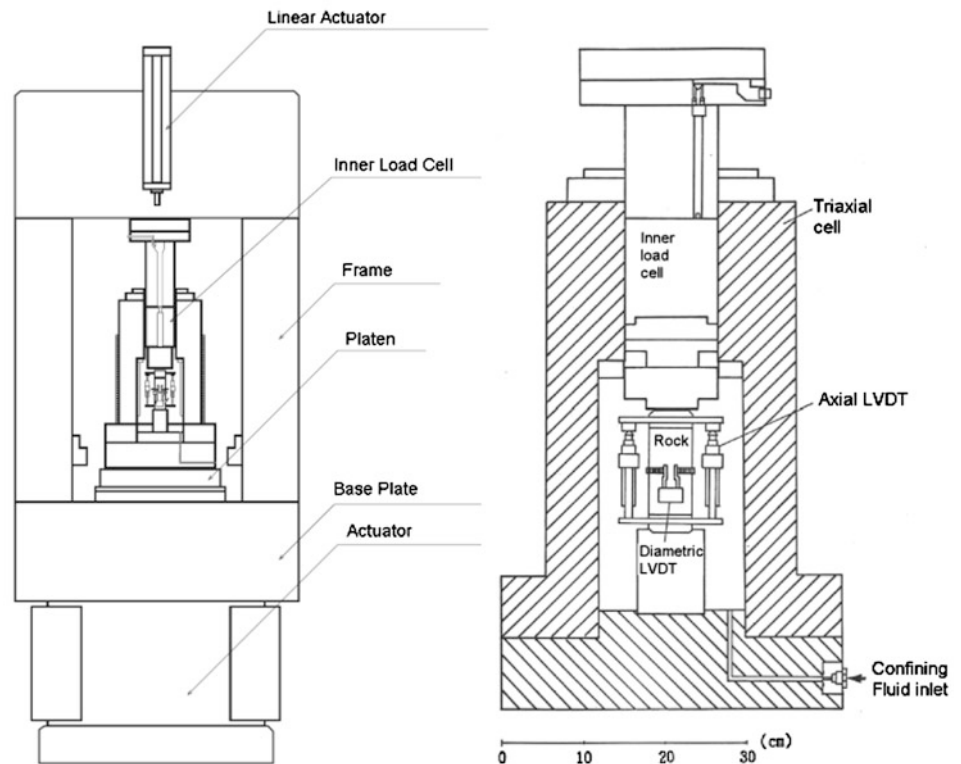


Fig. 2 Examples of cantilever-type creep apparatuses: **a** single-arm cantilever-type creep apparatus (from Ito and Akagi 2001), **b** multi-lever arm cantilever-type creep apparatus (from Okada 2006)

3.1 Cantilever-Type Apparatus

The cantilever-type apparatus has been used in creep tests since early times (Fig. 2). It is in practice the most suitable apparatus for creep tests because the load level can easily be kept constant with time. The greatest restrictions of this type of apparatus are the level of applicable load, which depends upon the length of the cantilever arm, and its oscillations during the application of the load. The cantilever-type apparatus utilizing a multi-arm lever overcomes the load limit restrictions (Okada 2005, 2006). The

Fig. 3 Load/displacement-controlled apparatus (from Ishizuka et al. 1993)



oscillation problem is also dealt with technically by the producers of such creep devices. If the load increase is done manually by placing dead-weights, as in some creep testing devices, utmost care must be taken during the loading procedure to prevent undesirable oscillations.

The load is applied onto samples by attaching dead-weights to the lever, which may be done manually for low-stress creep tests or mechanically for high-stress creep tests. In triaxial experiments, special load cells are required and the confining pressure is generally provided through oil pressure. Utmost care must be taken in keeping the confining pressure constant in terms of a continuous power supply to the compressor of the confining pressure system.

Deformation and strain measurements can be taken in several ways. The simple approach is to utilize a couple of linear variable displacement transducers (LVDTs). When a triaxial creep experiment is carried out, the LVDTs may be fixed onto the sample and inserted into the triaxial chamber. In such a case, special precautions must be taken to ensure accurate measurement of displacements. Strain gages may be used. However, strain gages glued onto samples should be capable of measuring strain over a long period of time without any debonding. For lateral deformation or strain measurements, diametric or circumferential sensors can be used.

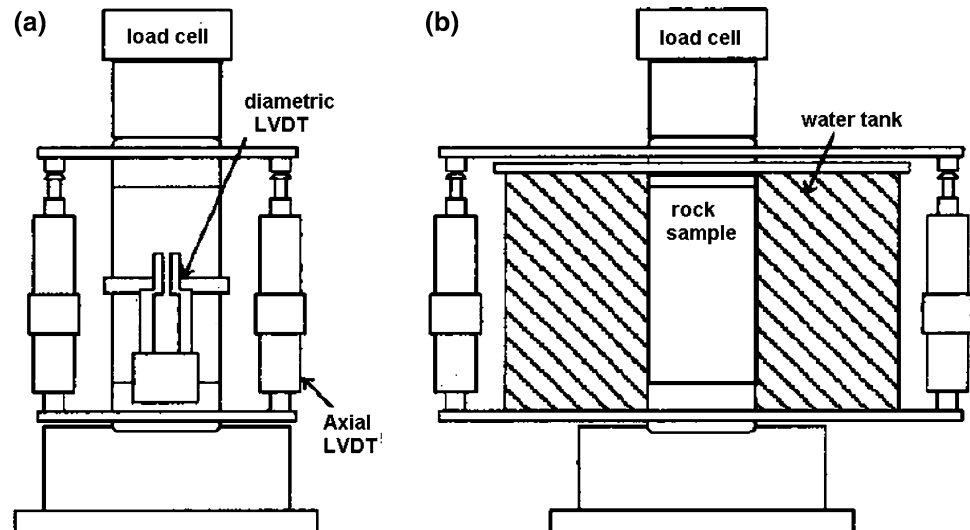
3.2 Load/Displacement-Controlled Apparatus

This type of apparatus is a servo-controlled testing machine that is capable of applying constant loads onto samples (Fig. 3). The most critical aspect of this experiment is to keep the axial stress acting on a sample constant, which requires continuous monitoring of the load and its automatic adjustment (i.e., Peng 1973). The load applied onto samples should be maintained to within $\pm 1\%$ of the specified load. When triaxial creep tests are carried out, a special triaxial cell is used as in the previous case. Deformation or strain measurements are carried out in the same way as in the previous type of experiments. This type of experiment is generally used for creep tests under a high stress state.

There has been some concern with the use of this type of machine that vibrations associated with the constant high-speed operation of the closed loop, which ensures that the chosen parameter (in this case, stress) is kept constant, could affect the results through a fatigue effect. However, the authors are not aware of any evidence to this effect.

There are also true triaxial testing apparatuses to perform creep tests under true triaxial stress conditions (Serata et al. 1968; Adachi et al. 1969). The three principal stresses can be controlled independently in such triaxial testing apparatuses. Recent technological advances have made such tests easier to perform.

Fig. 4 Special setups for testing under dry and saturated conditions (from Ishizuka et al. 1993)



4 Environmental Conditions

The creep responses of some rocks, particularly evaporitic rocks, mudstone, and tuff, may be influenced by the humidity conditions. Furthermore, the creep responses of all rocks are influenced by temperature. As the results of creep experiments are generally influenced by environmental conditions, special considerations must be given to the environmental conditions. When necessary, creep experiments are carried out in climate-controlled rooms or in environmental chambers that are specially constructed around individual or multiple specimens. The environmental conditions are closely monitored and controlled within close tolerances.

4.1 Temperature

Creep tests in a room-temperature environment are carried out in climate-controlled rooms. However, when the creep behavior of rocks at different temperature levels is required, special heating units with thermal insulation are used. The temperature of a specimen measured at mid-height under uniaxial condition and Brazilian tests or the inside temperature of the cell under triaxial stress condition should be maintained to within ± 1 °C of the required test temperature with a resolution of ± 0.1 °C.

4.2 Humidity

Some rocks, such as evaporitic rocks and clayey rocks, may be very sensitive to humidity conditions. According to the humidity requirement of creep tests, the humidity of climate-controlled rooms should be monitored and controlled within close tolerances of ± 5 % (Wawersik 1983). If the

humidity in the room cannot be controlled, the specimen should be sealed in a flexible membrane or coated with plastic or silicone rubber.

4.3 Saturation

The creep characteristics of many rocks are generally influenced by water saturation conditions. Special setups, shown in Fig. 4, may be used to achieve the appropriate saturation conditions. For performing creep experiments under different saturation conditions, the specimen should be sealed in a flexible membrane or coated with plastic or silicone rubber.

5 Preparation and Size of Samples

Specimen preparation for creep tests should follow the procedures of the ISRM suggested methods for the Brazilian, uniaxial compression, and triaxial compression tests (ISRM 2007). It is generally desirable to keep the size of samples as indicated in the suggested methods. However, the sample size may be smaller than the conventional sizes due to the loading limit of the device and the desired level of stress. In such circumstances, special care must be taken regarding the ratio of grain size to sample height, which should be less than 0.1.

6 Testing Procedures

6.1 Uniaxial Compression Creep Tests

The procedure described in the method suggested by the ISRM (2007) to test for uniaxial compressive strength should be followed unless the sample size differs from the conventional size. The displacement should be measured

continuously or periodically (seconds, minutes, hours or days depending upon the stress level applied on samples) as suggested in the ISRM suggested methods. The load application rate may be higher than that used in the ISRM suggested methods when a cantilever-type apparatus is used. Once the load reaches the designated load level, it should be kept constant. If the experiments are to be carried out under saturated conditions, the sample should be put in a special water-filled cell as illustrated in Fig. 4b.

6.2 Triaxial Compression Creep Tests

The procedure described in the method suggested by the ISRM (2007) to determine triaxial compressive strength should be followed unless the sample size differs from the conventional size. Utmost care should be taken to monitor the axial load when the confining fluid is supplied into the triaxial cell. The displacement should be measured continuously or periodically as suggested in the ISRM suggested methods. The load application rate may be higher than that used in the ISRM suggested methods when a cantilever-type apparatus is used. Once the load reaches the designated load level, it should be kept constant. If the experiments are to be carried out under saturated conditions, the saturated sample should be sealed in a flexible membrane or coated with plastic or silicone rubber.

6.3 Brazilian Creep Tests

The loading jigs and procedure used in the method suggested by the ISRM (2007) for Brazilian tests should be followed unless the sample size differs from the conventional size. The displacement should be measured continuously or periodically as suggested in the ISRM suggested methods. The load application rate may be higher than that used in the ISRM suggested methods when a cantilever-type apparatus is used. Once the load reaches the designated load level, it should be kept constant. If the experiments are to be carried out under saturated conditions, the jigs and sample should be put in a special water-filled cell.

6.4 Monitoring Irrecoverable Straining

Determination of the elastoviscoplastic constitutive behavior of rocks requires that irrecoverable strains be monitored. The applied load (differential load in triaxial tests) should be reduced to a load level of 1 % of the specified load, and the specimen should be reloaded at designated time intervals. The rate of loading during the reloading step should be the same as that used during the initial loading step.

7 Calculations

7.1 Uniaxial and Triaxial Compression Creep Tests

- (a) Axial strain, ε_a , and diametric strain, ε_d , can be recorded directly from equipment indicating strain or can be calculated from deformation readings depending on the type of instrumentation used and illustrated in Figs. 3 and 4.
- (b) Axial strain is calculated from the equation

$$\varepsilon_a = \frac{\Delta l}{l_0}, \quad (1)$$

where l_0 is the original measured axial length and Δl is the change in measured axial length (defined to be positive for a decrease in length).

- (c) Diametric strain can be determined either by measuring the changes in the diameter of the specimen or by measuring the circumferential strain. In the case of measuring changes in diameter, the diametric strain is calculated from the equation

$$\varepsilon_d = \frac{\Delta d}{d_0}, \quad (2)$$

where d_0 is the original undeformed diameter of the specimen and Δd is the change in diameter (defined to be negative for an increase in diameter). In the case of measuring the circumferential strain, ε_c , the circumference is $\Delta C = \pi \Delta d$, thus the change in circumference is $\Delta C = \pi \Delta d$. Consequently, the circumferential strain, ε_c , is related to the diametric strain, ε_d , by

$$\varepsilon_c = \frac{\Delta C}{C} = \frac{\Delta d}{d_0}, \quad (3)$$

so that

$$\varepsilon_c = \varepsilon_d,$$

where C and d_0 are the original circumference and the diameter of the specimen, respectively.

- (d) The compressive axial stress in the test specimen, σ_a , is calculated by dividing the compressive load P on the specimen by the initial cross-sectional area, A_0 , i.e.,

$$\sigma_a = \frac{P}{A_0}, \quad (4)$$

where compressive stresses and strains are considered positive in this test procedure. For a given stress level, the volumetric strain, ε_v , is calculated from the equation

$$\varepsilon_v = \varepsilon_a + 2\varepsilon_d. \quad (5)$$

7.2 Brazilian Creep Tests

The tensile strength of the specimen should be calculated using the following formula:

$$\sigma_t = \frac{2P}{\pi Dt}, \quad (6)$$

where P is the load at failure, D is the diameter of the test specimen (mm), and t is the thickness of the test specimen measured at its center (mm). The nominal strain of the Brazilian tensile test sample can be given as (see Hondros 1959 and Jaeger and Cook 1979 for details)

$$\varepsilon_t = 2 \left[1 - \frac{\pi}{4}(1 - \nu) \right] \frac{\sigma_t}{E} \text{ with } \varepsilon_t = \frac{\delta}{D}, \quad (7)$$

where δ , ε and E are diametrical displacement in the loading direction, strain and elastic modulus, respectively.

If the Poisson's ratio of the rock is not known or not measured, one may choose a Poisson's ratio of 0.25. Thus, the formula given above can be simplified to the following form (Aydan et al. 2011):

$$\varepsilon_t = 0.82 \frac{\sigma_t}{E}. \quad (8)$$

8 Reporting of Results

The report should include the following:

- Lithologic description of the rock;
- Source of the sample, including geographic location, depth and orientation, dates of sampling and storage history, and environment;
- Orientation of the axis of loading with respect to specimen anisotropy, e.g., bedding planes, foliation, grain size, etc.;
- Number of specimens tested;
- Specimen diameter and height;
- Water content and degree of saturation at the time of test;
- Test duration and/or stress rate;
- Date of testing and type of testing machine;
- Mode of failure, e.g., location and orientation of failure surface;
- Any other observations or available physical data, such as specific gravity, porosity, and permeability, citing the method of determination of each;
- The applied stress level for each specimen in the sample expressed to three significant figures together

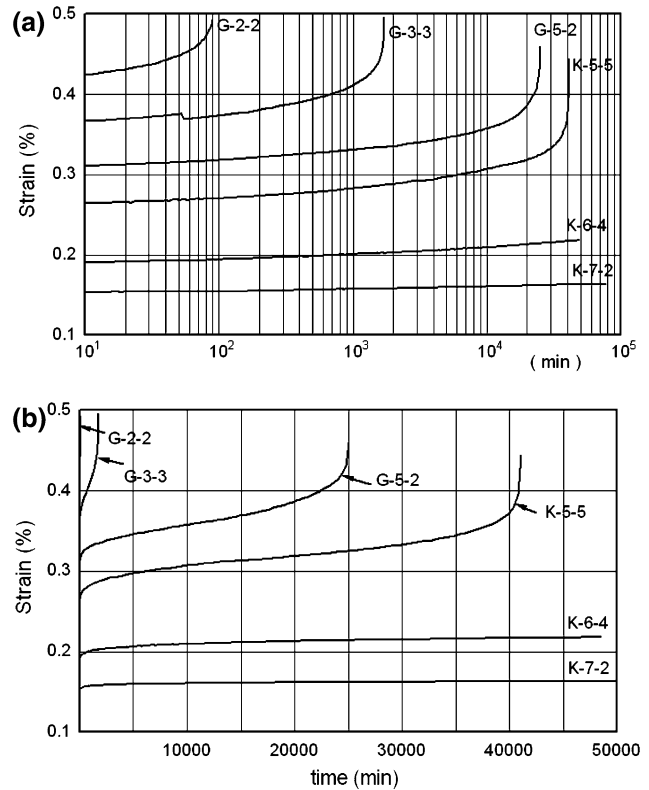


Fig. 5 Uniaxial compression creep response of Oya tuff (modified from Ito and Akagi 2001): **a** plot of experimental response on logarithmic scale, **b** plot of experimental results on linear scale

with the average result for the sample. Units of stress and strength must be given;

- If it is necessary in some instances to test specimens that do not comply with the above specifications, these facts should be noted in the test report;
- Results of creep experiments are generally presented in the space of time and strain for different combinations of experimental conditions (Fig. 5). Figure 6 shows the effect of saturation on the Brazilian and uniaxial compression creep responses of Cappadocian tuff samples from Zelve. Additional presentation may include failure time versus normalized applied stress by the short-term strength in both uniaxial and triaxial compression creep tests (Fig. 7). Figure 8 shows plots of responses during creep tests of Oya tuff and its failure time determined at different temperatures. Depending on the constitutive models chosen, the experimental results may be presented in different forms according to the user and his/her purpose. The “Appendix” included in the suggested methods provides some constitutive models for processing the results from creep experiments as advice to users.

Fig. 6 Responses of initially dry and later saturated tuff samples from Zelve during Brazilian and uniaxial compression creep tests (arranged from Ito et al. 2008): **a** responses during Brazilian creep test of an initially dry and later saturated sample, **b** responses during a uniaxial compression creep test of an initially dry and later saturated sample

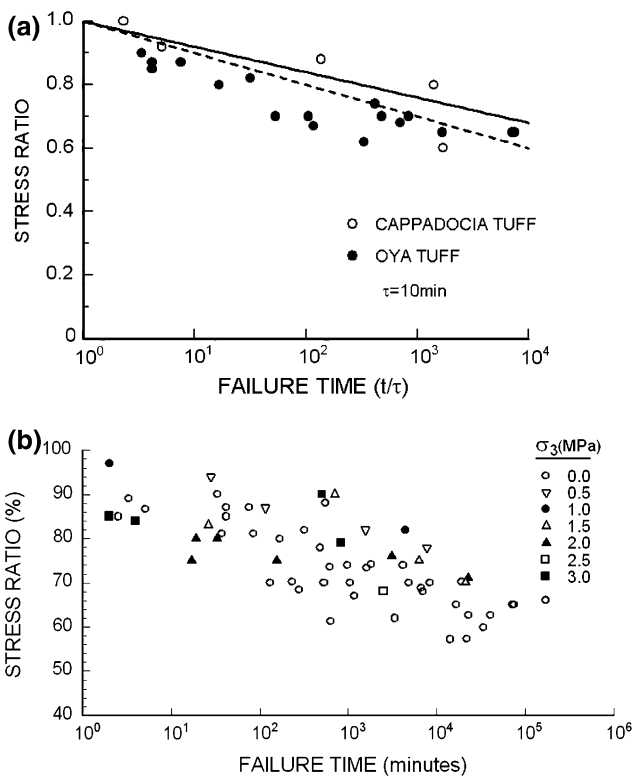
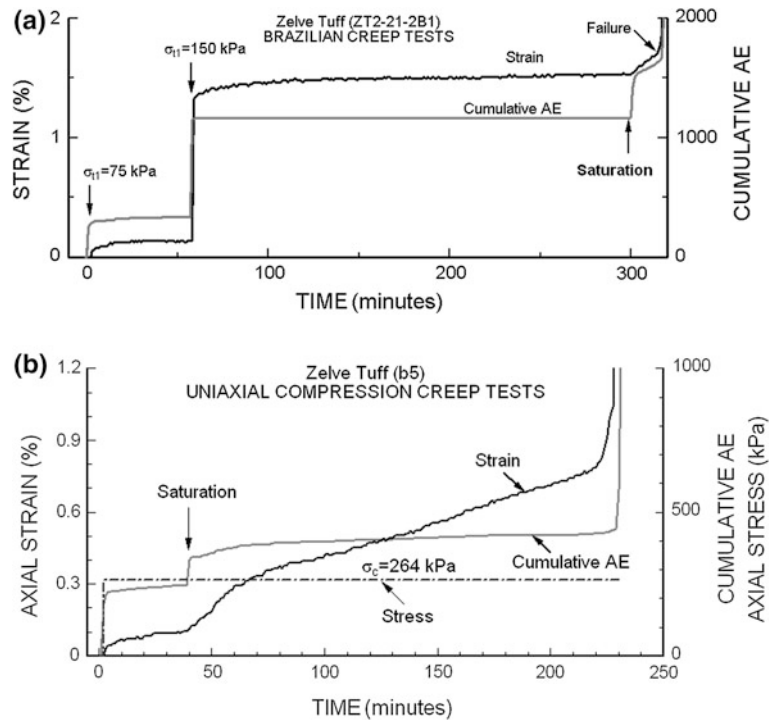


Fig. 7 **a** Creep failure time of Oya tuff and Cappadocia tuffs in uniaxial compression tests (from Ulusay et al. 1999). **b** Creep failure time of Oya tuff in triaxial compression tests (arranged from Ito et al. 1999; Shibata et al. 2007; Akai et al. 1979)

9 Notes and Recommendations

In this section some notes and recommendations are given. Some guidelines on how to utilize experimental results for modeling the time-dependent behavior of rocks are presented in the “Appendix.”

9.1 Power Backup

As creep experiments may involve very long durations, utmost care must be taken to avoid power supply failures.

9.2 Determination of Irrecoverable Strain

Determination of parameters in relation to elastoviscoplastic constitutive laws may require irrecoverable strain and strain rates. In such cases, use of loading and unloading cycles will be necessary. Extra precautions must be taken to ensure that the load level is not less than 1 % of the specified load level.

9.3 Stability of Confining Fluid

The confining pressure fluid should be stable at the temperature and pressure levels designated for the test.

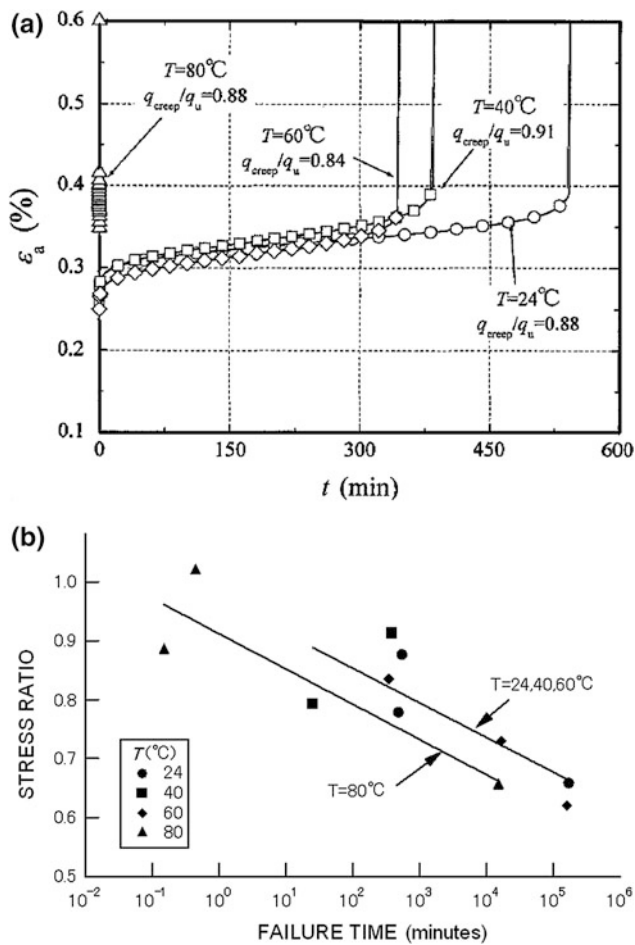
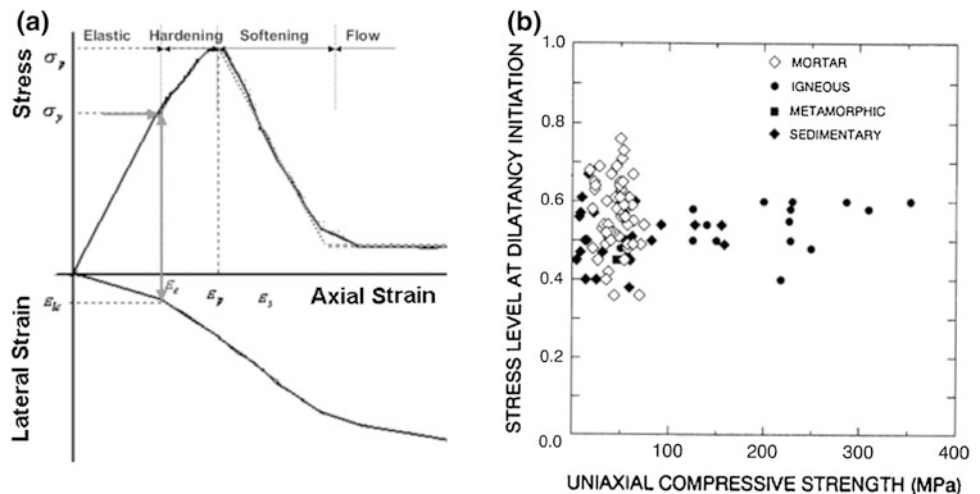


Fig. 8 a Creep response of Oya tuff. b Relationship between stress ratio and failure time at various temperatures (arranged from Shibata et al. 2007)

Fig. 9 Illustration of threshold value and experimental results (arranged from Aydan et al. 1993, 1994)



9.4 Stability of Measuring Devices

The measuring devices must remain stable at the temperature and pressure levels designated for the test.

9.5 Safety of Test System

Test systems under designated temperature and pressure levels must be compatible with the safety standards against system failure and fire. Furthermore, adequate protective shields should be used to protect people in the area from unexpected system failure.

Acknowledgments The members of this Working Group acknowledge the guidance and information given by Emeritus Prof. S. Sakurai, Japan and Emeritus Prof. J. A. Hudson (former presidents of the ISRM), Dr. N. Grossman (Portugal), Dr. W. R. Wawersik (USA), Dr. Eda Quadros (Brazil), Prof. P. Nawrocki (UAE), and Prof. R. Ulusay (Türkiye). Furthermore, Emeritus Professor John A. Hudson is thanked for his editorial assistance during the preparation of this document.

Appendix

Introduction

This “Appendix” is provided as supplementary material describing constitutive models available in the literature utilizing the experimental results of creep tests. As there have been numerous such models since the 1900s, it is impossible to cover all of them, and interested readers are recommended to consult textbooks, some of which are listed in the suggested methods reference list. Therefore, this

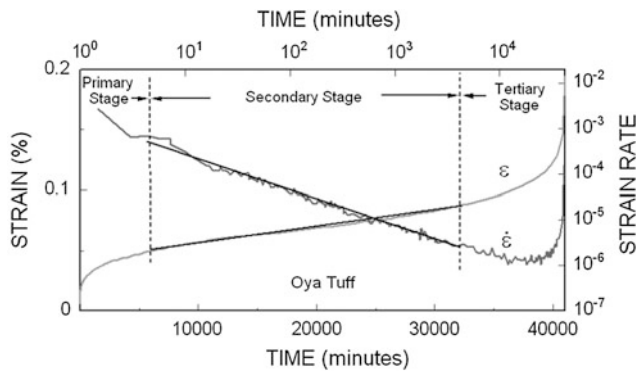


Fig. 10 Strain and strain rate response of a creep experiment on Oya tuff (Japan) shown in Fig. 5 in the main text

“Appendix” has been prepared with the purpose of serving as a guideline to users utilizing the suggested methods. As defined in the “Introduction” of the suggested methods, a creep test is an experiment carried out under sustained loading condition, and the constitutive models are presented for such a condition.

It is claimed that creep behavior is not observed if the level of applied stress is less than a certain threshold value (Ladanyi 1993) in a practical sense (in terms of days).

However, experiments carried out on igneous rock (granite, gabbro, etc.) beams by Ito (1991) for three decades show that a creep response definitely occurs even under very low stress levels. The threshold value suggested by Ladanyi (1993) may be associated with the initiation of dilatancy of volumetric strain as illustrated in Fig. 9. The initiation of dilatancy generally corresponds to 40–60 % of the stress level, and fracture propagation tends to become unstable when the applied stress level exceeds 70–80 % of the ultimate deviatoric strength for a given stress state (Aydan et al. 1994; Hallbauer et al. 1973). Therefore, the behavior below the threshold should generally correspond to viscoelastic behavior. The creep threshold according to Ladanyi (1974) should correspond to an elastoviscoplastic response, and it should not be possible to obtain viscoelastic properties directly from the measured responses.


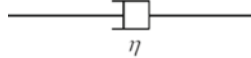
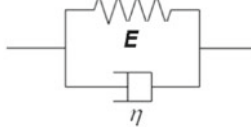

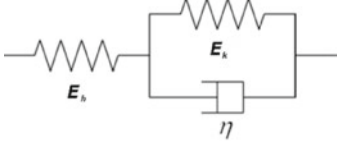
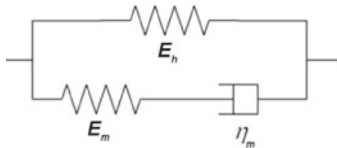
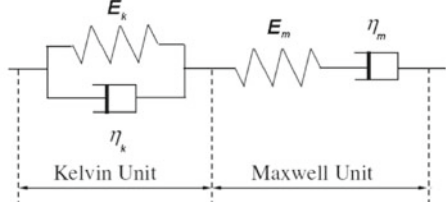
As noted from Fig. 5 in the suggested methods, some responses terminate with failure while others become asymptotic to certain strain levels. The responses terminating in failure are generally divided into three stages as shown in Fig. 10 using one of the response curves shown in Fig. 5. These stages are defined as the primary, secondary, and tertiary creep stages. The secondary stage appears to be a linear response in time (but in fact, it is not a linear

Table 1 Intuitive unidimensional creep models (except for Aydan et al. 2003 the references to the citations in this table can be found in Farmer 1983)

Proposed by	Formula	Comments
Andrade (1910, 1914)	$\varepsilon_c = Bt^{1/\beta}$	Applicable to primary stage; $\beta=3$;
Lomnitz (1956, 1957)	$\varepsilon_c = A \ln(1 + \alpha t)$	Applicable to primary stage
Modified Lomnitz law	$\varepsilon_c = A + B \log(t) + Ct$	Primary and secondary stages
Norton's law	$\varepsilon_c = A\sigma_a^n t$ or $\varepsilon_c = A\sigma_a^n$	Applicable to secondary stage and $n=4-5$
Modified Norton's law	$\varepsilon_c = B \left\langle \frac{\sigma_a}{\sigma_{ct}} - 1 \right\rangle^n t$ or $\varepsilon_c = B \left\langle \frac{\sigma_a}{\sigma_{ct}} - 1 \right\rangle^n$	Applicable to secondary stage and σ_{ct} is the stress threshold to induce steady state creep response.
Griggs and Coles (1958)	$\varepsilon_c = A + Bt^2$	Applicable to tertiary stage
Aydan et al. (2003)	$\varepsilon_c = A(1 - e^{-t/\tau_1}) + B(e^{t/\tau_2} - 1)$	Applicable to all stages creep leading to failure

$A, B, C, \alpha, \tau_1, \tau_2,$ and n are constants to be determined from experimental results. $\sigma_a, \varepsilon_c, \dot{\varepsilon}_c,$ and t are the applied stress, creep strain, strain rate, and time, respectively, hereafter

Table 2 Rheological models for unidimensional constitutive modeling

Model	Formula	Geometrical Illustration
Hooke	$\sigma_a = E\varepsilon$	
Newton	$\sigma_a = \eta\dot{\varepsilon}$	
Voigt-Kelvin	$\varepsilon = \frac{\sigma_a}{E} (1 - e^{-t/t_r}); t_r = \frac{\eta}{E}$	
Maxwell	$\varepsilon = \frac{\sigma_a}{E} + \frac{\sigma_a}{\eta} t$	
Generalized Voigt-Kelvin	$\varepsilon = \frac{\sigma_a}{E_h} + \frac{\sigma_a}{E_k} (1 - e^{-t/t_r}); t_r = \frac{\eta}{E_k}$	
Hill-Maxwell model	$\varepsilon = \frac{\sigma_a}{E_h} \left[1 - \frac{E_m}{E_h + E_m} e^{-t/t_r} \right]$	
Burgers	$\varepsilon = \frac{\sigma_a}{E_m} + \frac{\sigma_a}{E_k} (1 - e^{-t/t_k}) + \frac{\sigma_a}{\eta_m} t;$ $t_k = \frac{\eta_k}{E_k}$	

E are elastic and viscosity moduli, respectively. Suffixes “h,” “k,” and “m” indicate moduli of Hooke, Kelvin, and Maxwell units. ε is total strain

response). On the other hand, the tertiary stage is the stage in which the strain response increases exponentially, resulting in failure of the sample. Modeling of this stage in constitutive laws is an extremely difficult aspect as it also depends upon the boundary conditions.

The transitions from the primary to the secondary stage and from the secondary to the tertiary stage are generally determined from the deviation from a linearly decreasing or increasing strain rate plotted in logarithmic time space, as also shown in Fig. 10. Generally, it should, however, be noted that strain data must be smoothed before interpretation. Direct derivation of strain data containing actual responses as well as electronic noise may produce entirely different results. In this “Appendix,” the constitutive laws

are divided into two categories, namely unidirectional and multidimensional constitutive laws. These constitutive laws and available yield functions are briefly outlined and discussed together with some examples of applications.

Unidimensional Constitutive Models

Constitutive models are essentially based on responses obtained from experiments and fundamentally are fitting procedures of some functions to experimental results. Therefore, they cannot be purely derived from a certain theory. Nevertheless, they must satisfy certain rules established in constitutive modeling of material science. Unidimensional

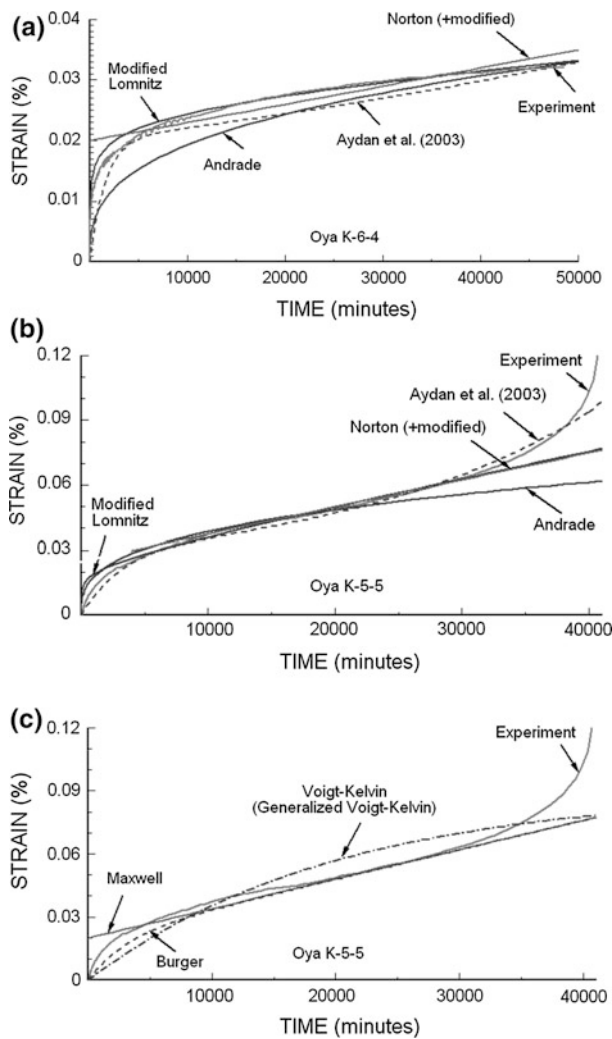


Fig. 11 Comparison of intuitive and rheological models with experimental responses: **a** asymptotic response (intuitive models), **b** response terminating with failure (intuitive models), and **c** response terminating with failure (rheological models)

constitutive models can also be broadly divided into two categories: intuitive models and rheological models. Table 1 summarizes some of the well-known intuitive models, while Table 2 summarizes linear rheological models (Mirza 1978; Doktan 1983; Farmer 1983). Figure 11 compares experimental responses with those from intuitive and rheological models. As can be noted from this figure, each model has its own merits and demerits, and the user should decide which one to adopt for his/her purpose.

When the behavior of rock includes irrecoverable (permanent) strain, nonlinear rheological models have also been developed, and some of them are listed in Table 3 and their responses compared in Fig. 12. Expressions for elastoviscoplastic models can be developed in a similar manner. However, they tend to be rather complicated. Also, it should be noted that such models require the determination of the irrecoverable

response from experiments, which definitely requires the implementation of loading and unloading procedures.

Multidimensional Constitutive Models

Some of the linear models are listed in Table 4. In particular, the rheological models presented in the previous section can be extended to the multidimensional situation. However, the algebra involved in developing the relations between total stress and total strain may become quite cumbersome. For an isotropic homogeneous rock material, if the coefficients to determine the lateral components for a given direction are time independent, it may be possible to develop constitutive relations between the total stress and total strain in analogy to those presented in the previous sections. However, the general situation would require some numerical integration and complex algebra.

Nonlinear behavior involving irrecoverable (permanent) responses is more difficult to model by constitutive models. Particularly, it is cumbersome to determine the parameters of constitutive models from experimental data. Therefore, it is quite common to introduce the effective stress (σ_e) and effective strain (ε_e) concepts (these are different concepts from that used for the effect of pore water pressure on the stress tensor) if the irrecoverable part of the strain tensor is independent of the volumetric component. They are defined as follows:

$$\sigma_e = \sqrt{\frac{3}{2} \mathbf{s} \cdot \mathbf{s}} \quad \text{and} \quad \varepsilon_e = \sqrt{\mathbf{e}_p \cdot \mathbf{e}_p}, \quad (9)$$

where \mathbf{s} and \mathbf{e} are the deviatoric stress and deviatoric strain tensors, respectively, as given below

$$\mathbf{s} = \boldsymbol{\sigma} - \frac{tr(\boldsymbol{\sigma})}{3} \mathbf{I} \quad \text{and} \quad \mathbf{e}_p = \boldsymbol{\varepsilon}_p - \frac{tr(\boldsymbol{\varepsilon}_p)}{3} \mathbf{I} \quad \text{with } tr(\boldsymbol{\varepsilon}_p) = 0. \quad (10)$$

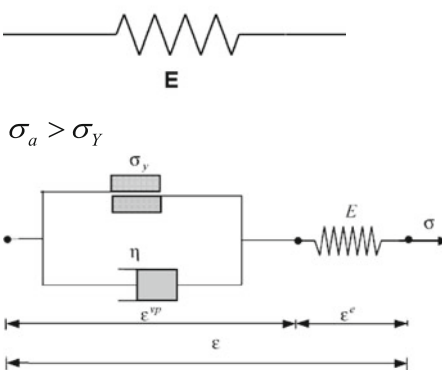
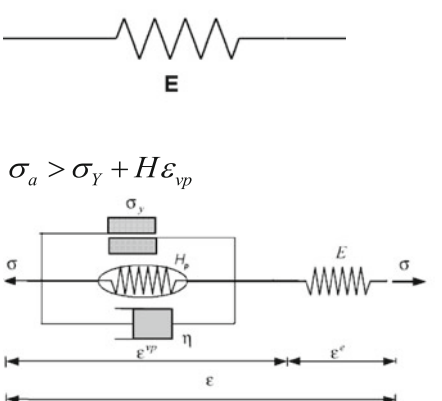
It is interesting to note that the effective stress and strain correspond to those in a uniaxial state, i.e.,

$$\sigma_e = \sigma_1 \quad \text{and} \quad \varepsilon_e = \varepsilon_1. \quad (11)$$

This leads to the very convenient conclusion that the nonlinear response can be evaluated under a uniaxial state and easily extended to the multidimensional state without any triaxial testing. However, it should be noted that this is only valid when the volumetric components are negligible in the overall mechanical behavior.

Some of the nonlinear models are listed in Table 5. The viscoelastoplastic model by Aydan and Nawrocki (1998) is illustrated in Fig. 13 for a one-dimensional situation.

Table 3 Rheological unidimensional nonlinear creep models

Model	Formula	Geometrical Illustration
Bingham model: Elastic-Perfectly Visco-plastic Model	$\varepsilon = \frac{\sigma_a}{E} \text{ if } \sigma_a \leq \sigma_Y$ $\varepsilon = \frac{\sigma_a - \sigma_Y}{\eta} t + \frac{\sigma_a}{E} \text{ if } \sigma_a > \sigma_Y$ $\sigma_Y : \text{yield threshold}$ $\gamma = \frac{1}{\eta} : \text{fluidity coefficient}$	$\sigma_a \leq \sigma_Y$ 
Elastic-Visco- Plastic Model of Hardening Type (Owen-Hinton 1980)	$\sigma_a = E\varepsilon \text{ if } \sigma_a \leq Y$ $Y = \sigma_Y + H\varepsilon_{vp}; \varepsilon = \varepsilon_e + \varepsilon_{vp}$ $\sigma_a = \sigma_Y + H\varepsilon_{vp} + C_p \frac{d\varepsilon_{vp}}{dt}$ $\varepsilon = \frac{\sigma_a}{E} + \frac{(\sigma_a - \sigma_Y)}{H} \left(1 - e^{-\frac{H}{C_p} t} \right)$	$\sigma_a \leq \sigma_Y + H\varepsilon_{vp}$ 

ε_e and ε_{vp} are elastic and viscoplastic components of strain. H and C_p are plastic hardening modulus and viscoplastic modulus, respectively

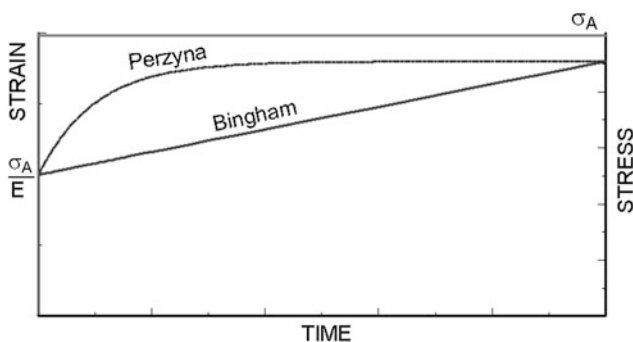


Fig. 12 Comparison of Bingham- and Perzyna-type viscoplastic responses

Yield Functions

There is no yield (failure) criterion directly incorporating the effect of creep experiments (Aydan and Nawrocki 1998;

Aydan et al. 2012), although the basic concept has been presented previously (Ladanyi 1974) for the time-dependent response of tunnels. Based on the yielding concept shown in Fig. 9, some of the yield criteria are listed in Table 6. The general form of the plastic potential functions is also assumed to be similar to yield criteria. If a plastic potential function is assumed to be the same as a yield criterion, it corresponds to the associated flow rule.

Aydan and Nawrocki (1998) discussed how to incorporate the results of creep experiments into yield functions on the basis of the results of rare triaxial creep experiments. On the basis of the experimental results on various rocks by several researchers (Ishizuka et al. 1993; Kawakita et al. 1981; Masuda et al. 1987; Aydan et al. 1995), Aydan and Nawrocki (1998) concluded that the time dependency of the friction angle is quite negligible and the time dependency of the cohesive component of

Table 4 Linear models

Model	Formula	Comments
Newton type	$\sigma_{ij} = C_{ijkl} \dot{\epsilon}_{kl}$ or $\sigma_{ij} = 2\mu^* \dot{\epsilon}_{ij} + \lambda^* \delta_{ij} \dot{\epsilon}_{kk}$	C_{ijkl} : viscosity tensor λ^* and μ^* are viscous Lame coefficients
Voigt-Kelvin type	$\sigma_{ij} = D_{ijkl} \epsilon_{kl} + C_{ijkl} \dot{\epsilon}_{kl}$ or $\sigma_{ij} = 2\mu \epsilon_{ij} + \lambda \delta_{ij} \epsilon_{kk} + 2\mu^* \dot{\epsilon}_{ij} + \lambda^* \delta_{ij} \dot{\epsilon}_{kk}$	D_{ijkl} : elasticity tensor λ and μ are elastic Lame coefficient
Maxwell type	$\dot{\epsilon}_{ij} = E_{ijkl} \sigma_{kl} + F_{ijkl} \dot{\sigma}_{kl}$	E_{ijkl} and F_{ijkl} are elasticity and viscosity compliance tensors

σ_{ij} , ϵ_{kl} , and $\dot{\epsilon}_{kl}$ are stress, strain, and strain rate tensors, respectively

Table 5 Nonlinear models

Model		Formula	Comment
Elastic-viscoplastic	Power Law	$\frac{d\mathbf{\epsilon}_{vp}}{dt} = \left(\frac{\sigma_{eq}}{\sigma_o} \right)^n \frac{\partial \sigma_{eq}}{\partial \boldsymbol{\sigma}}$ with $\mathbf{e}_{vp} = \boldsymbol{\epsilon}_{vp}$	
	Perzyna model	$\frac{d\mathbf{\epsilon}_{vp}}{dt} = \lambda \mathbf{s}$ and λ is determined from experimental response using the following relation $\lambda = \frac{\dot{\epsilon}_c}{\sigma}$ Flow rule $d\dot{\boldsymbol{\epsilon}}^p = \dot{\lambda} \frac{\partial G}{\partial \boldsymbol{\sigma}}$	λ is interpreted called as fluidity coefficient. Flow rule implies that any plastic straining is time-dependent
Elasto-viscoplastic	Aydan - Nawrocki model	$d\boldsymbol{\sigma} = \mathbf{D}^{rp} d\boldsymbol{\epsilon} + \mathbf{C}^{rp} d\dot{\boldsymbol{\epsilon}}$ $\mathbf{D}^{rp} = \mathbf{D}^r - \frac{\mathbf{D}^r \frac{\partial G}{\partial \boldsymbol{\sigma}} \otimes \frac{\partial F}{\partial \boldsymbol{\sigma}} \mathbf{D}^r}{h_{rp} + \frac{\partial F}{\partial \boldsymbol{\sigma}} \cdot \left(\mathbf{D}^r \frac{\partial G}{\partial \boldsymbol{\sigma}} \right) + \frac{\partial F}{\partial \boldsymbol{\sigma}} \cdot \left(\mathbf{C}^r \frac{\partial \dot{G}}{\partial \boldsymbol{\sigma}} \right)}$ $\mathbf{C}^{rp} = \mathbf{C}^r - \frac{\mathbf{C}^r \frac{\partial \dot{G}}{\partial \boldsymbol{\sigma}} \otimes \frac{\partial F}{\partial \boldsymbol{\sigma}} \mathbf{C}^r}{h_{rp} + \frac{\partial F}{\partial \boldsymbol{\sigma}} \cdot \left(\mathbf{D}^r \frac{\partial G}{\partial \boldsymbol{\sigma}} \right) + \frac{\partial F}{\partial \boldsymbol{\sigma}} \cdot \left(\mathbf{C}^r \frac{\partial \dot{G}}{\partial \boldsymbol{\sigma}} \right)}$ Flow rule $d\dot{\boldsymbol{\epsilon}}^p = \lambda \frac{\partial \dot{G}}{\partial \boldsymbol{\sigma}}$	Flow rule implies that the plastic potential function expands or shrinks in time domain and strain increments consists of time-dependent and time independent parts

F and G are yield and plastic potential functions, respectively. Indices “ r ” and “ p ” stand for adjectives “recoverable” and “permanent” respectively

Fig. 13 Illustration of viscoelastoplastic model by Aydan and Nawrocki (1998) for a one-dimensional situation

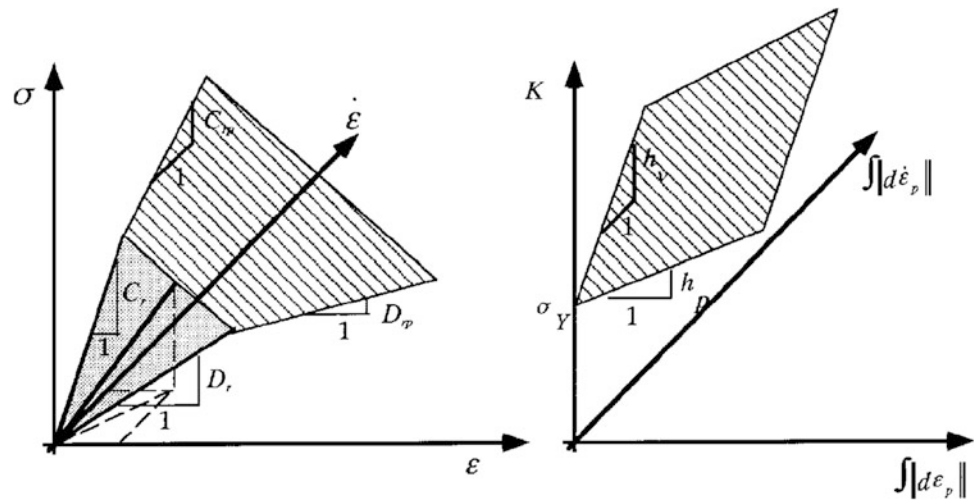


Table 6 Yield criteria (see Aydan et al. 2012 for details)

Model	Formula	Comments
Mohr-Coulomb	$\tau = c + \sigma_n \tan \phi$ or $\sigma_1 = \sigma_c + q\sigma_3$ $\sigma_c = \frac{2c \cos \phi}{1 - \sin \phi}$; $\sigma_t = \frac{2c \cos \phi}{1 + \sin \phi}$; $q = \frac{1 + \sin \phi}{1 - \sin \phi}$	c : cohesion ϕ : friction angle σ_t : tensile strength σ_c : uniaxial compressive strength
Drucker-Prager (Drucker and Prager 1952)	$\alpha I_1 + \sqrt{J_2} = k$ $I_1 = \sigma_1 + \sigma_2 + \sigma_3$ $J_2 = \frac{1}{6}((\sigma_1 - \sigma_2)^2 + (\sigma_2 - \sigma_3)^2 + (\sigma_3 - \sigma_1)^2)$	$\alpha = \frac{2 \sin \phi}{\sqrt{3}(3 \pm \sin \phi)}$ $k = \frac{6c \cos \phi}{\sqrt{3}(3 \pm \sin \phi)}$ -: outer apexes +: inner apexes
Hoek-Brown (1980)	$\sigma_1 = \sigma_3 + \sqrt{m\sigma_c\sigma_3 + \sigma_c^2}$	$m = \frac{\sigma_c^2 - \sigma_t^2}{\sigma_c\sigma_t}$
Aydan (1995)	$\sigma_1 = \sigma_3 + [S_\infty - (S_\infty - \sigma_c)e^{-b_1\sigma_3}]e^{-b_2T}$	σ_∞ : the ultimate deviatoric strength T : temperature b_1, b_2 : constants.

the yield criterion should be sufficient for incorporation of the results of creep experiments. Creep experiments would generally yield a decrease of the deviatoric strength in time in view of the experimental results shown in Fig. 6 of the suggested methods, which would correspond to shrinkage of the yield surface in time as shown in Fig. 14.

Based on the concept given above, the time-dependent uniaxial compressive strength $[\sigma_c(t)]$ of Oya tuff (Japan) and

Cappadocia tuff (Turkey) shown in Fig. 6 in the suggested methods can be represented in terms of their uniaxial compressive strength (σ_{cs}) and the duration (τ) of a short-term experiment by the following function (Aydan and Nawrocki 1998; Aydan and Ulusay 2013):

$$\frac{\sigma_c(t)}{\sigma_{cs}} = 1.0 - b \ln\left(\frac{t}{\tau}\right). \quad (12)$$

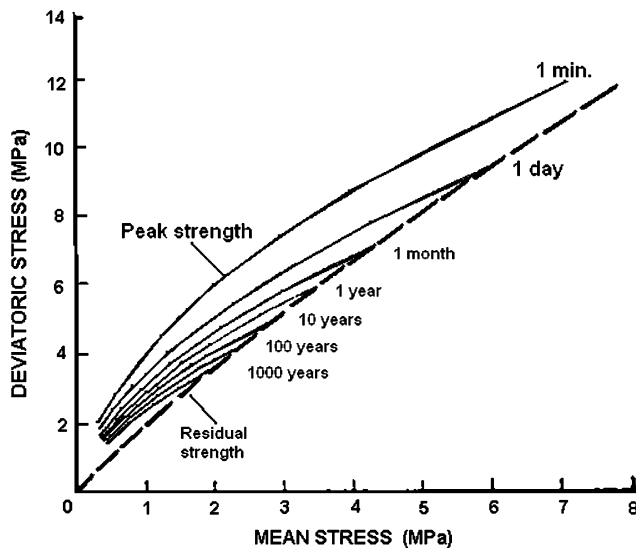


Fig. 14 Illustration of the failure criterion for fully saturated Oya tuff at various times estimated by Adachi and Takase (1981)

The value of b in Eq. 12 for Oya tuff and Cappadocia tuffs is 0.08 and 0.05, respectively. However, functions different from that given by Eq. 12 can be used provided that they fit the experimental results (Aydan et al. 2011).

References

- Adachi T, Takase A (1981) Prediction of long term strength of soft rocks. In: Proceedings of international symposium on weak rock, pp 99–104
- Adachi T, Sarata S, Sakurai S (1969) Determination of underground stress field based on inelastic properties of rocks. In: Proceedings of 11th symposium on rock mechanics, University of California, Berkeley, pp 293–328
- Akagi T (1976) An analytical research on the visco-elastic behaviour of civil engineering structures. Doctorate thesis, Nagoya University (in Japanese)
- Akagi T, Ichikawa Y, Kuroda T, Kawamoto T (1984) A non-linear rheological analysis of deeply located tunnels. *Int J Num Anal Meth Geomech* 8:107–120
- Akai K, Adachi T, Nishi K (1979) Time dependent characteristics and constitutive equations of soft sedimentary rocks (porous tuff). *Proc JSCE* 282–2:75–87 (in Japanese)
- Aydan Ö (1995) The stress state of the earth and the earth's crust due to the gravitational pull. The 35th US rock mechanics symposium, Lake Tahoe, pp 237–243
- Aydan Ö, Nawrocki P (1998) Rate-dependent deformability and strength characteristics of rocks. In: International symposium on the geotechnics of hard soils-soft rocks, Napoli, vol 1, pp 403–411
- Aydan Ö, Ulusay R (2013) Studies on Derinkuyu antique underground city and its implications in geo-engineering. *Rock Mech Rock Eng.* doi:10.1007/s00603-012-0301-7
- Aydan Ö, Akagi T, Kawamoto T (1993) Squeezing potential of rocks around tunnels; theory and prediction. *Rock Mech Rock Eng* 26(2):137–163
- Aydan Ö, Seiki T, Jeong GC, Tokashiki N (1994) Mechanical behaviour of rocks, discontinuities and rock masses. In: Proceedings of international symposium pre-failure deformation characteristics of geomaterials, Sapporo, vol 2, pp 1161–1168
- Aydan Ö, Akagi T, Ito T, Ito J, Sato J (1995) Prediction of deformation behaviour of a tunnel in squeezing rock with time-dependent characteristics. In: Proceedings of numerical models in geomechanics NUMOG V, pp 463–469
- Aydan Ö, Tokashiki N, Ito T, Akagi T, Ulusay R, Bilgin HA (2003) An experimental study on the electrical potential of non-piezoelectric geomaterials during fracturing and sliding. In: 9th ISRM congress, South Africa, pp 73–78
- Aydan Ö, Rassouli F, Ito T (2011) Multi-parameter responses of Oya tuff during experiments on its time-dependent characteristics. In: Proceedings of the 45th US rock mechanics/geomechanics symposium, San Francisco, ARMA, pp 11–294
- Aydan Ö, Tokashiki N, Geniş M (2012) Some considerations on yield (failure) criteria in rock mechanics ARMA 12-640. In: Proceedings of 46th US rock mechanics/geomechanics symposium, Chicago, 10 p (on CD)
- Berest P, Blum P, Charpentier J, Gharbi H, Vales F (2005) Very slow creep tests on rock samples. *Int J Rock Mech Min Sci* 42:569–576
- Bieniawski ZT (1970) Time-dependent behaviour of fractured rock. *Rock Mech* 2:123–137
- Boukharov GN, Chandi MW, Boukharov NG (1995) The three processes of brittle crystalline rock creep. *Int J Rock Mech Min Sci Geomech Abstr* 32 (4):325–335
- Chan KS (1997) A damage mechanics treatment of creep failure in rock salt. *Int J Damage Mech* 6:122–152
- Cristescu ND, Hunsche U (1998) Time effects in rock mechanics. Wiley, New York
- Doktan M (1983) The longterm stability of room and pillar workings in a gypsum mine. Ph.D. thesis, University of Newcastle Upon Tyne
- Drucker DC, Prager W (1952) Soil mechanics and plastic analysis for limit design. *Q Appl Math* 10(2):157–165
- Fabre G, Pellet F (2006) Creep and time-dependent damage in argillaceous rocks. *Int J Rock Mech Min Sci* 43(6):950–960
- Farmer I (1983) Engineering behaviour of rocks, 2nd edn. Chapman and Hall, London
- Hagros A, Johanson E, Hudson JA (2008) Time dependency in the mechanical properties of crystalline rocks: a literature survey. Possiva OY, Finland
- Hallbauer DK, Wagner H, Cook NGW (1973) Some observations concerning the microscopic and mechanical behaviour of quartzite specimens in stiff, triaxial compression tests. *Int J Rock Mech Min Sci Geomech Abstr* 10:713–726
- Hoek E, Brown ET (1980) Empirical strength criterion for rock masses. *J Geotech Eng Div, ASCE*, 106(GT9):1013–1035
- Hondros G (1959) The evaluation of Poisson's ratio and the modulus of materials of low tensile resistance by the Brazilian (indirect tensile) tests with particular reference to concrete. *Aust J Appl Sci* 10:243–268
- Hunsche U (1992) True triaxial failure tests on cubic rock salt samples—experimental methods and results. In: Proceedings of IUTAM symposium on finite inelastic deformations—theory and applications, Hannover, Springer, pp 525–538
- Hunsche U, Hampel A (1999) Rock salt—the mechanical properties of the host rock material for a radioactive waste repository. *Eng Geol* 52:271–291
- Ishizuka Y, Koyama H, Komura S (1993) Effect of strain rate on strength and frequency dependence of fatigue failure of rocks. In: Proceedings of assessment and prevention of failure phenomena in rock engineering, pp 321–327
- ISRM (2007) The complete ISRM suggested methods for rock characterization, testing and monitoring: 1974–2006. In: Ulusay R, Hudson JA (eds) Suggested methods prepared by the commission on

- testing methods, international society for rock mechanics, compilation arranged by the ISRM Turkish National Group, Ankara, Turkey
- Ito H (1991) On rheological behaviour of in situ rock based on long-term creep experiments. In: Proceedings of 7th ISRM congress, Aachen, Germany, vol 1, pp 265–268
- Ito T, Akagi T (2001) Methods to predict the time of creep failure. In: Proceedings of the 31st symposium on rock mechanics of Japan, pp 77–81 (in Japanese)
- Ito H, Sasajima S (1980) Long-term creep experiment on some rocks observed over three years. *Tectonophysics* 62(3–4):219–232
- Ito H, Sasajima S (1987) A ten year creep experiment on small rock specimens. *Int J Rock Mech Min Sci Geomech Abstr* 24:113–121
- Ito T, Fujiwara T, Akagi T (1999) Triaxial creep characteristics of soft rocks. In: Proceedings of the 29th symposium on rock mechanics of Japan, pp 126–130 (in Japanese)
- Ito T, Aydan Ö, Ulusay R, Kaşmer Ö (2008) Creep characteristics of tuff in the vicinity of Zelve antique settlement in Cappadocia region of Turkey. In: Proceedings of 5th Asian Rock Mechanics Symposium (ARMS5), Tehran, pp 337–344
- Jaeger JC, Cook NGW (1979) *Fundamentals of rock mechanics*, 3rd edn. Chapman & Hall, London, pp 79 and 311
- Kawakita M, Sato K, Kinoshita S (1981) The dynamic fracture properties of rocks under confining pressure. *Mem Fac Eng Hokkaido University* 15(4):467–478
- Ladanyi B (1974) Use of the long-term strength concept in the determination of ground pressure on tunnel linings. In: Proceedings of 3rd congress, international society for rock mechanics, Denver, vol. 2B, pp 1150–1165
- Ladanyi B (1993) Time-dependent response of rock around tunnels. In: Fairhurst C (ed). *Comprehensive rock engineering: principles, practice and projects*, vol 2, Analysis and design methods. Pergamon, Oxford, pp 77–112
- Lockner DA, Byerlee JD (1977) Acoustic emission and creep in rock at high confining pressure and differential stress. *Bull Seismol Soc Am* 67:247–258
- Masuda K, Mizutani H, Yamada I (1987) Experimental study of strain-rate dependence and pressure dependence of failure properties of granite. *J Phys Earth* 35:37–66
- Masuda K, Mizutani H, Yamada I, Imanishi Y (1988) Effects of water on time-dependent behavior of granite. *J Phys Earth* 36:291–313
- Mirza UA (1978) Investigation into the design criteria for underground openings in rocks which exhibit rheological behaviour. PhD thesis, University of Newcastle upon Tyne
- Mottahed P, Szeki A (1982) The collapse of room and pillar workings in a shaley gypsum mine due to dynamic loading symposium on strata mech. Newcastle, pp 260–264
- Okada T (2005) Mechanical properties of sedimentary soft rock at high temperatures (part 1) evaluation of temperature dependency based on triaxial compression test. Chiba, Japan: Central Research Institute of Electric Power Industry 04026, pp 1–26 (in Japanese)
- Okada T (2006) Mechanical properties of sedimentary soft rock at high temperatures (part 2)—evaluation of temperature dependency of creep behavior based on unconfined compression test. Central Research Institute of Electric Power Industry, Chiba, Japan 05057, pp 1–26 (in Japanese)
- Okubo S, Nishimatsu Y, Fukui K (1991) Complete creep curves under uniaxial compression. *Int J Rock Mech Min Sci Geomech Abstr* 28:77–82
- Okubo S, Fukui K, Nishimatsu Y (1993) Control performance of servocontrolled testing machines in compression and creep tests. *Int J Rock Mech Min Sci Geomech Abstr* 30:247–255
- Owen DRJ, Hinton E (1980) *Finite element in plasticity: theory and practice*. Pineridge Press Ltd, Swansea
- Passaris EKS (1979) The rheological behaviour of rocksalt as determined in an in situ pressurized test cavity. Fourth International Congress on Rock Mechanics, Balkema, Rotterdam, pp 257–264
- Peng S (1973) Time-dependent aspects of rock behavior as measured by a servo-controlled hydraulic testing machine. *Int J Rock Mech Min Sci Geomech Abstr* 10:235–246
- Perzyna P (1966) Fundamental problems in viscoplasticity. *Adv Appl Mech* 9(2):244–368
- Serata S, Sakurai S, Adachi T (1968) Theory of aggregate rock behavior based on absolute three-dimensional testing (ATT) of rock salt. In: Proceedings of 10th symposium on rock mechanics, University of Texas at Austin, pp 431–473
- Shibata K, Tani K, Okada T (2007) Creep behaviour of tuffaceous rock under high temperature observed in uniaxial compression test. *Soil Found* 47(1):1–10
- Slizowski J, Lankof L (2003) Salt-mudstones and rock-salt suitabilities for radioactive-waste storage systems: rheological properties. *Appl Energy* 75(1/2):137–144
- Ulusay R, Ito T, Akagi T, Seiki T, Yüzer E, Aydan Ö (1999) Long term mechanical characteristics of Cappadocia tuff. The 9th international rock mechanics congress, Paris, pp 687–690
- Wawersik WR (1983) Determination of steady state creep rates an activation parameters for rock salt. In: High pressure testing of rock, special technical publication of ASTM, STP86972-91
- Yang CH, Daemen JJK, Yin JH (1999) Experimental investigation of creep behavior of salt rock. *Int J Rock Mech Min Sci* 36(2): 233–242

ISRM Suggested Method for Laboratory Determination of the Shear Strength of Rock Joints: Revised Version

José Muralha, Giovanni Grasselli, Bryan Tatone, Manfred Blümel, Panayiotis Chryssanthakis, and Jiang Yujing

1 Introduction

The term ‘discontinuity’ refers to any mechanical break in a rock mass with negligible tensile strength (Priest 1993). Discontinuities can be geologic in origin (i.e., faults, bedding, schistosity, cleavage planes, and foliations) or anthropogenic in origin (i.e., blast-induced, stress-induced, or hydraulic-induced fractures).

Please send any written comments on this ISRM Suggested Method to Prof. Resat Ulusay, President of the ISRM Commission on Testing Methods, Hacettepe University, Department of Geological Engineering, 06800 Beytepe, Ankara, Turkey.

Originally published as an article in the journal *Rock Mechanics and Rock Engineering*, 47, J. Muralha, G. Grasselli, B. Tatone, M. Blümel, P. Chryssanthakis, J. Yujing, ISRM Suggested Method for Laboratory Determination of the Shear Strength of Rock Joints: Revised Version, 291–302, 2014.

J. Muralha (✉)

Departamento de Barragens de Betão, LNEC, Laboratório Nacional de Engenharia Civil, Av. Brasil, 101, 1700-066, Lisbon, Portugal
e-mail: j muralha@lnec.pt

G. Grasselli · B. Tatone
Department of Civil Engineering, University of Toronto, 35 St George Street, Toronto, ON M5S 1A4, Canada

M. Blümel
Institute for Rock Mechanics and Tunnelling, Geotechnical Group Graz, Graz University of Technology, Rechbauerstraße 12, 8010, Graz, Austria

P. Chryssanthakis
NGI, Norwegian Geotechnical Institute, Sognsveien 72, Ullevaal Hageby, P.O. Box 39300806, Oslo, Norway

J. Yujing
Department Civil Engineering, Faculty of Engineering, Nagasaki University, 1-14 Bunkyo-Cho, Nagasaki, 852-8521, Japan

Regardless of their origin, discontinuities play a significant role in the behavior of rock masses and, consequently, in the behavior of several rock engineering projects involving slopes, surface excavations and underground openings such as tunnels or caverns. Discontinuity-induced failures in rock masses are a major hazard in civil and mining engineering projects as they are responsible for many accidents and costly construction/production delays.

Assessing the risk posed by these blocky systems to a particular project requires the evaluation of the shear strength of the rock discontinuities. Estimates of shear strength can be obtained through shear testing. The best shear strength estimates are obtained from in situ direct shear tests as they inherently account for any possible scale effect (Barla et al. 2011; Alonso et al. 2011). However, due to the duration and cost of such tests, it is common practice to perform laboratory direct shear tests on relatively small discontinuity samples instead.

Conventionally, direct shear testing has been conducted with a constant normal load applied to the discontinuity plane. While this boundary condition is appropriate for a class of engineering problems involving the sliding of rock blocks near the ground surface (e.g., rock slope stability and surface excavation stability), there is class of problems where the normal stress may not remain constant as sliding occurs. Namely, any time the dilation of a discontinuity is constrained while sliding (e.g., around an underground excavation), the normal stress on the sliding surface may vary. For this class of problems, a constant normal stiffness boundary condition is more appropriate for direct shear testing (Johnston and Lam 1989; Lechnitz 1985).

2 Scope

- (a) This Suggested Method (SM) is a revision and an upgrade of Part 2. Suggested Method for laboratory determination of direct shear strength, included in the

Suggested Methods for determining shear strength (ISRM 2007), and was prepared with consideration of the technological advances since its initial publication and other existing standard methods, including ASTM D 5607–08 (ASTM 2008), USACE RTH 203-80 (USACE 1980), and JGS 2541-2008 (JGS 2008).

- (b) This SM intends to cover the requirements and laboratory procedures for performing direct shear strength tests of rock discontinuities using constant normal load and constant normal stiffness laboratory apparatuses. This type of test can also be referred to as a sliding friction test.
- (c) This SM is limited to the determination of the quasi-static shear strength of discontinuities under monotonic shear loading. Procedures for cyclic and dynamic shear loading are not addressed herein.
- (d) Discontinuities may be open or almost closed, and must display negligible tensile strength. This SM is not intended to cover direct shear tests of intact rock or other types of natural or artificial discontinuities that display tensile strength, such as rock–concrete interfaces or concrete lift joints.
- (e) Discontinuities may also be partially or completely filled with gouge or clay fillings. This SM is not intended to cover tests of discontinuities with gouge or clay fillings where in situ pore water pressure conditions have to be considered.
- (f) This SM proposes to measure peak and ultimate or residual direct shear strength in a selected direction as function of the normal stress applied to the sheared plane. Results can be implemented, for instance, in limit equilibrium analyses of rock blocks in slopes or sidewalls of underground excavations, and as input parameters for ‘joint’ elements in continuum and discontinuum numerical modeling of blocky rock masses.
- (g) Shear strength of rock discontinuities can be determined by tests under constant normal loading conditions (CNL), or under constant normal stiffness loading conditions (CNS). The use of constant normal load shear tests does not really test the joint strength, but the resistance to shear at a certain normal load, which may be appropriate for design purposes under certain boundary conditions. Constant normal stiffness testing procedures can be used to define the ultimate shear strength of a joint. Though they do not consider that the normal stiffness is likely to increase during dilatant shearing, CNS tests should be preferably used to reproduce the natural response to simple shearing of non-planar discontinuities.
- (h) Under constant normal loading conditions, shear strength determination usually includes the application of several different magnitudes of constant normal loads or stresses on multiple samples from the same joint or

test horizon, and measuring the shear stresses and respective shear and normal displacements resulting from a prescribed rate of shear displacement. At least three, but preferably five, specimens from the same joint or test horizon with similar characteristics must be sampled and tested along the same shear direction.

- (i) In cases where it is not possible to sample a large enough number of specimens, alternatively, the same specimen can be tested repeatedly under different constant normal loading conditions. For a single rock joint, at least three, but preferably five, different normal stresses should be used. This multi-stage approach is only applicable when breakage and degradation of joint surface asperities from subsequent shearing stages is minimal (e.g., under low normal stresses). To minimize the influence of damage and wear, each consecutive shear stage should be performed with an increasingly higher normal stress.
- (j) Under constant normal stiffness loading conditions, a single shear strength determination usually includes the testing of multiple samples from the same joint or tests horizon under differing initial normal loads and/or constant normal stiffnesses, and measuring the shear and normal stresses and respective displacements resulting from a prescribed rate of shear displacement. At least three, but preferably five, specimens from the same joint or test horizon must be sampled and tested along the same shear direction.

3 Apparatus

3.1 Testing Machine

- (a) Determination of shear strength of rock discontinuities is generally performed using direct shear apparatuses. Although there are many variations in the way specimens are prepared, mounted, and loaded, yet determinations of shear strength are usually similar (Boulon 1995; Blümel and Pötsch 2003; Jiang et al. 2004; Barla et al. 2010). Commonly, direct shear testing machines incorporate (Fig. 1):
 - i. A stiff testing system, including a stiff frame against which the loading devices can act and a stiff sample holder that is sufficiently rigid to prevent distortion during the test. A stiff system allows the prescribed shear displacement rate to be maintained and allows the post-peak behavior of the joint to be properly recorded.
 - ii. A specimen holder, such as a shear box, shear rings, or a similar device, where both halves of the specimen are fastened. It must allow relative shear and normal displacements of the two halves of the

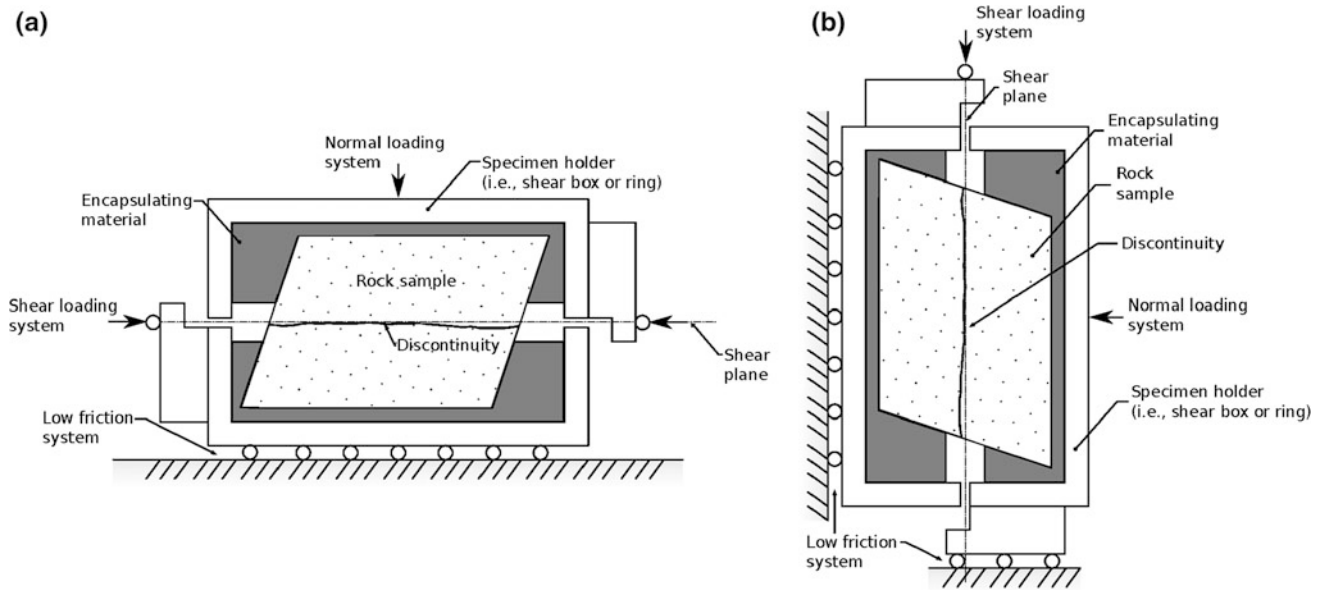


Fig. 1 Schematic illustrating arrangement of laboratory direct shear specimen: **a** conventional horizontal arrangement and **b** alternative vertical arrangement

discontinuity. Frictional forces on the perimeter of the sample holder must be minimized via rollers or other similar low friction devices.

- iii. Loading devices to apply the normal and shear loads on the specimens at adequate rates in such way that the resultant of the shear load goes through the centroid of the sheared area to minimize rotation of the specimen.
- iv. Devices to measure the normal and shear loads applied to the specimen and the normal and shear displacements throughout the test.

3.2 Loading

- (a) The applied shear forces are usually provided by actuators [hydraulic, pneumatic, mechanical (gear-driven), etc.] with or without closed-loop control. Shear force actuators and connecting parts should be designed to ensure that the shear load is uniformly distributed over the discontinuity plane to be tested with the resultant force acting parallel to the shear plane through its centroid.
- (b) The applied constant normal load or constant normal stiffness is usually provided by actuators (hydraulic, pneumatic, mechanical, etc.) with or without closed-loop control. Normal force actuators and connecting parts should be designed to ensure that the load is uniformly distributed over the discontinuity plane to be tested. They should accommodate travel greater than the amount of dilation expected in the test and

ensure the applied normal load is uniformly distributed over the test horizon with the resultant force acting perpendicular to the shear plane through its centroid.

- (c) A cantilever system can also be used to apply a constant normal dead-weight load for CNL tests under low normal stresses and null normal stiffness (Hencher and Richards 1982), while a spring can be used to maintain a constant normal stiffness condition for CNS tests (Indraratna et al. 1999).
- (d) Maintenance of the normal load or stiffness is important during shear tests. In accordance, the loading component of the apparatus must be devised to maintain the applied force or stiffness within a specified tolerance ($\pm 2\%$).

3.3 Recording Load and Displacement

- (a) The normal and shear forces are measured with accuracy better than $\pm 2\%$ directly by load cells, or indirectly by pressure gauges, transducers, or proving rings. Displacement transducers are used to measure the displacements.
- (b) A minimum of two transducers are required: one mounted parallel with the shear plane to measure the shear displacement and one mounted vertically at the centre of the specimen to measure normal displacement. Preferably, two transducers should be used to measure shear displacement such that yaw of the specimen is measured, and three to four transducers should be employed to measure horizontal

displacement, such that pitch and roll of the test specimen can be evaluated.

- (c) It is common practice to perform almost continuous measurements (sampling rate greater than 1 Hz) of these parameters using some kind of computer based data acquisition equipment, which is acceptable for quasi-static loading conditions considered under this SM.
- (d) To assure that the loads are effectively being applied to the shear surface, it may be convenient to measure the frictional forces or to perform a dummy test prior to real testing. If corrections are required, they should be reported.

4 Test Specimens

4.1 Sampling, Handling and Storage

- (a) The test horizon is selected and dip, dip direction, and other relevant geological characteristics are recorded. If possible, the absolute orientation of the sample relative to the test horizon should be marked on the sample (e.g., oriented core). In doing so, the shear direction in laboratory may be selected to correspond to a particular in situ displacement direction of interest.
- (b) Block or core samples containing the test horizon are collected using methods selected to minimize disturbance. The sample dimensions and the location of the test horizon within the block or core should, if possible, allow mounting without further trimming in the laboratory and provide sufficient clearance for adequate encapsulation.
- (c) No liquids other than water should come in contact with a test sample prior to testing. Discontinuity samples that appear to have been contaminated with mud produced by drilling or that show unnatural surface wear should be rejected.
- (d) Samples should be labeled and packaged to avoid damage in transit to the laboratory. Particular attention should be given to prevent differential movement from occurring along the sampled discontinuity. An option to prevent differential movement includes binding the walls of the discontinuity together with wire or tape, which is to be left in position until immediately before testing. If samples are not immediately transported to the laboratory they should be stored out of the weather to preserve their integrity. Because samples are to be tested near their natural moisture condition, they should be stored and transported in moisture-proof containers. Alternatively, tape, plastic wrap, wax, or other means may be utilized to preserve the in situ

moisture content along the test zone. Fragile samples require special treatment, for example packaging in polyurethane foam (Stimpson et al. 1970).

- (e) In the laboratory, sample handling and storage should follow the above mentioned measures to avoid any damage to the samples, and to preserve the in situ moisture content if required.

4.2 Size and Shape

- (a) Specimens with a regular (rectangular or elliptical) cross-sectional area are preferred. However, specimens may have any shape, such that the cross-sectional areas can be determined with a required accuracy.
- (b) The height of specimen shall be greater than the thickness of the shear (test) zone and sufficient to encapsulate the specimen in the specimen holder.
- (c) The length of the test plane (measured along the shear direction) should be at least 10 times the maximum asperity height.
- (d) The width of the test plane (measured perpendicularly to the shear direction) should have at least 48 mm, corresponding to discontinuities collected from NQ cores.
- (e) The width of the test plane should not change significantly over the shearing length. Minimum width should be greater than 75 % of the maximum width.
- (f) The sample half that remains fixed during shear tests should have a greater length than the moving half, so that the joint is always supported and the nominal area in contact remains constant. If this procedure is not feasible due to reduced length of the specimen, the nominal area reduction during shear has to be taken into account in the calculations.

4.3 Observations and Measurements on the Sample and Specimen

- (a) All characteristics of the discontinuity surface, that may influence its shear strength, including alteration, coatings, fillings, etc., should be assessed according to the methodology described in the ISRM Suggested Method for the quantitative description of discontinuities in rock masses (ISRM 2007).
- (b) Both walls of the test specimen should be photographed before and after the test. It is also important to measure the topography of both walls of the test specimen before and after the test to evaluate the surface roughness and roughness wear. For this purpose, two types of equipment can be used:

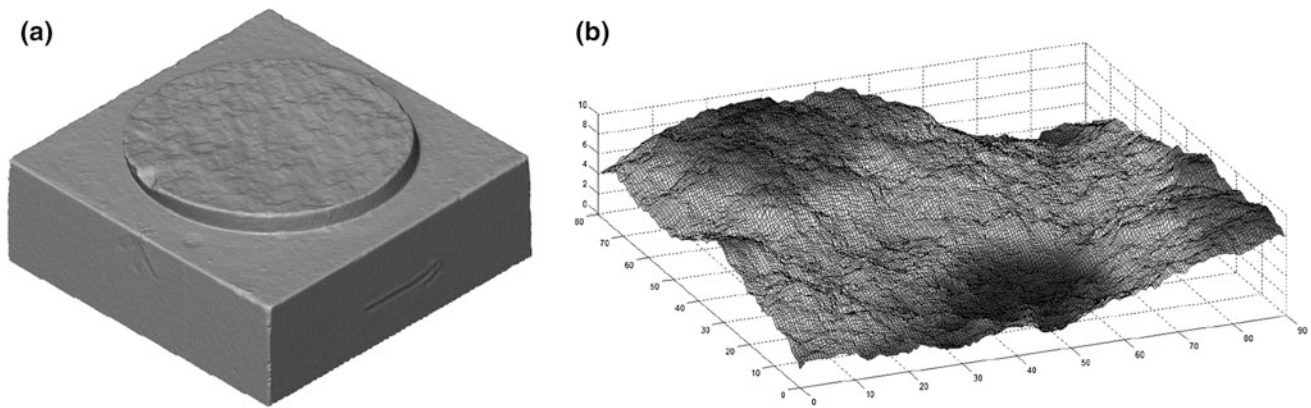


Fig. 2 Examples of the measurement of joint surfaces: **a** circular, **b** rectangular

- i. Profilometers are simple devices that produce a series of linear roughness profiles of the specimen surface along the shear and the transversal directions. The number of profiles depends on the surface dimension, but at least three along each direction should be mapped (Aydan et al. 1992; Grasselli 2001).
 - ii. If available, 3D non-contact measurement devices (e.g., laser scanner, slit scanner, photogrammetry or stereo-topometric camera) can be used to digitize the entire discontinuity surface (Fig. 2). Such systems are capable of obtaining point measurements with a nominal spacing <0.5 mm with a precision better than 0.025 mm (Tatone and Grasselli 2009).
 - (c) Measurement of the nominal cross-sectional area of the specimen shear plane shall be made before each test to the nearest 2.5 mm^2 . For regular geometrical shapes, the relevant dimensions required to calculate the nominal cross-sectional area can be measured using a calliper or micrometer. For irregular shapes, the outline of the cross-section can be traced on paper and the area measured using a planimeter or similar device. The area can also be measured using a 3D non-contact measurement device and CAD software.
- #### 4.4 Specimen Encapsulation
- (a) To test a discontinuity sample, each half of the sample must be secured in each half of the specimen holder (i.e., shear rings or shear boxes). As discontinuity samples are rarely cut to fit perfectly in the sample holder, they must be encapsulated in some other casting material (e.g., cement, resin, or similar) to ensure a tight fit. Encapsulation also allows the discontinuity plane to be aligned with the shear plane.
 - Specimens can be encapsulated directly inside the specimen holder of the test apparatus or, if several specimens are to be prepared simultaneously, a split mold(s) with identical dimension to the specimen holder can be used. Though some adaptations are allowed, encapsulation of a sample for testing should proceed as follows:
 - i. Remove sample from packaging.
 - ii. Position the lower half of the specimen centrally in the lower half of the specimen holder. Ensure that the shear horizon to be tested is secured and that it is parallel with the shear plane and oriented correctly with respect to the shear direction. Ensure the specimen position can be maintained while pouring and curing of the encapsulating material.
 - iii. Pour the encapsulating material, prepared in accordance with the directions of the manufacturer, carefully into the space between the lower half of specimen and the lower half of the specimen holder. Stop pouring just below the general plane of the test zone. Ensure a zone of about 5 mm around the sides of the shear plane remains free from encapsulating material. Do not disturb the specimen holding assembly after pouring until the encapsulating material is sufficiently cured.
 - iv. After the bottom encapsulating material is sufficiently cured, place a split spacer plate of specified thickness on the lower holder such that its cut-out edge encircles the encapsulated lower half of the specimen and encompasses the test zone thickness. Coarse sand or modeling clay can also be used for this purpose. If needed, apply a layer of silicon grease over the surface of the encapsulated material. Place the upper half of the test specimen onto the encapsulated lower half. Ensure a tight fit between the two halves is achieved. Lower the



Fig. 3 Encapsulate lower half of a rectangular shaped test specimen

upper half of the specimen holder onto the split spacer plate without disturbing the position of the top half of the specimen. Connect the two halves of the specimen holder. Pour encapsulating compound into the annular space between the top half of the specimen holder and the top half of the specimen. Do not disturb the assembly until the encapsulating compound cures.

- v. Remove the spacer plates, sand, or clay to expose the test horizon for shear testing (Fig. 3).
- (c) Following encapsulation, the average plane through the test horizon should be verified to be parallel to the top and bottom surface of the specimen holder (i.e., shear plane). Any angular deviation between the average plane and shear plane, measured in the shearing direction, should be measured and reported. This angular deviation should also be accounted for in the shear strength determination.

5 Testing Procedure

5.1 Preliminary Tasks

- (a) Prior to any set of tests, the loading conditions and the range of normal loads to be applied during shear have to be defined, according to the normal stresses expected to be acting on the joints in the project under consideration (e.g., slope, dam foundation, underground cavern, or tunnel).

- (b) If considered convenient, dummy tests with low deformability specimens, such as steel, with the same dimensions as the real specimens, and encapsulated following the same procedure can be run. Dummy tests of jointed specimens allow one to establish that all devices are operating correctly, and may enable calibration of measuring devices. Dummy tests of intact specimens also allow one to evaluate the normal and shear loading system stiffness, and eventually to correct accordingly (Chryssanthakis 2004).

5.2 Specimen Mounting

- (a) Mount and orient the encapsulated specimen within the moving and fixed specimen holders of the testing machine.
- (b) Ensure all measuring devices are calibrated according to the laboratory calibration procedures.
- (c) Test all monitoring devices to guarantee they are responding correctly and are properly connected to the data acquisition system.
- (d) Mount all displacement measuring devices perpendicularly to the shear surface such that they contact the perimeter of the moving half of the specimen holder to measure normal displacement during the test. Generally, four normal displacement measurement devices are used to assess the pitch and roll of the moving half of the specimen during the test. Although not recommended, fewer measurement devices can also be employed. In all cases, these devices must be distributed around the perimeter of the sample shear surface to provide the information necessary to evaluate the normal displacement at the centroid of the shear surface.
- (e) Mount displacement devices on the machine in such a manner to measure the shear displacement of the specimen during the test. A pair of devices symmetrically positioned with respect to the specimen cross-section should be used. For some machines, a single device positioned along the shear displacement axis may be sufficient. However, this latter option is not recommended, since eventual yaw movement of the specimen will not be detected.
- (f) Ensure all displacement monitoring devices have sufficient travel to accommodate the normal and shear displacements expected in the test. Moreover, ensure these devices maintain contact with specimen holder throughout the test to correctly measure the displacements.

- (g) If required, mount and position all other measuring devices, for instance load cells.

5.3 Load Application

5.3.1 Normal Load

- (a) Before any shear test, normal load application should consist of continuously increasing the load normal to the shear zone at a gradual rate until the specified normal stress is attained, and recording consequent normal displacements.
- (b) Normal load application should be applied continuously at selected rate of normal stress assuring that each loading or unloading paths takes about 5 min. In accordance, rates of 0.01 MPa/s or less are required.
- (c) Any normal loads imparted on the test horizon by the normal loading system should be accounted for when determining the apparent normal stress on the specimen especially under low normal stresses. For example, if the specimen is held in a horizontal position in the test apparatus, the weight of the upper half of the specimen should be considered.
- (d) For CNL tests ensure the testing apparatus maintains the specified constant normal load for the duration of the test. For CNS tests ensure the testing apparatus maintains the specified constant normal stiffness for the duration of the test.
- (e) If applicable, allow pore water pressure in the rock and filling material adjacent to the shear plane to dissipate before shearing. Do not apply the shear load until normal displacement has stabilized.

5.3.2 Shear Load

- (a) After the normal displacements stabilize under the applied normal load, invoke shear displacement continuously at the selected rate of shear displacement.
- (b) Shear displacement shall continue at the specified rate until ultimate or residual shear stress is reached. Generally, a shear displacement that ranges between 5 and 10 % of the length of the discontinuity is enough.
- (c) Shear displacement rates around 0.1–0.2 mm/min are usually suitable for the whole test, although it can be slightly increased up to values around 0.5 mm/min after peak shear strength. In special cases, such as joints with thin clay coatings, a slower rate (lower than 0.05 mm/min) may be required.

5.4 Alternative Procedures

- (a) Rock joint shear strength determination can follow two different types of procedures: single shear procedure and multi-stage shear procedure. Both types of procedures can be performed under CNL or CNS conditions (Muralha 2007; Blümel et al. 2003).
- (b) Single shear procedure includes the application of several constant normal stresses on multiple samples from the joint or test horizon and measuring the shear stresses and respective normal displacements resulting from a prescribed rate of shear displacement. At least three, and preferably five, specimens from the same test horizon can be obtained and each tested in the same direction.
- (c) Multi-stage shear procedure consists of testing repeatedly under different constant normal stresses the same specimen. For a single rock joint, at least three, and preferably five, different normal stresses should be applied, with shear testing in the same direction. Furthermore, two possible techniques for performing multi-stage shear tests can be followed: without repositioning of the joint in its initial natural position before each shearing stage (Fig. 4a), or with repositioning of the joint in its initial natural position before each shearing stage (Fig. 4b).

5.5 Measurements

5.5.1 Normal Displacement (δ_n)

- (a) Measure and record normal displacements of the specimen at each load observation to determine the normal displacement of the joint sample as previously defined in Sect. 3.

(b) It is recommended that four measuring devices are used to monitor the pitch and roll of the test sample. Fewer measuring devices can be used, but in all cases they should allow to determine the normal displacement at the centroid of the sample cross-section.

5.5.2 Shear Displacement (δ_s)

- (a) Measure shear displacements of the specimen at each load observation to determine the shear displacement of the joint sample as previously defined in Sect. 3.

(b) It is recommended that two measuring devices be used to monitor the pitch and roll of the test sample. Fewer measuring devices can be used, but in all cases they should

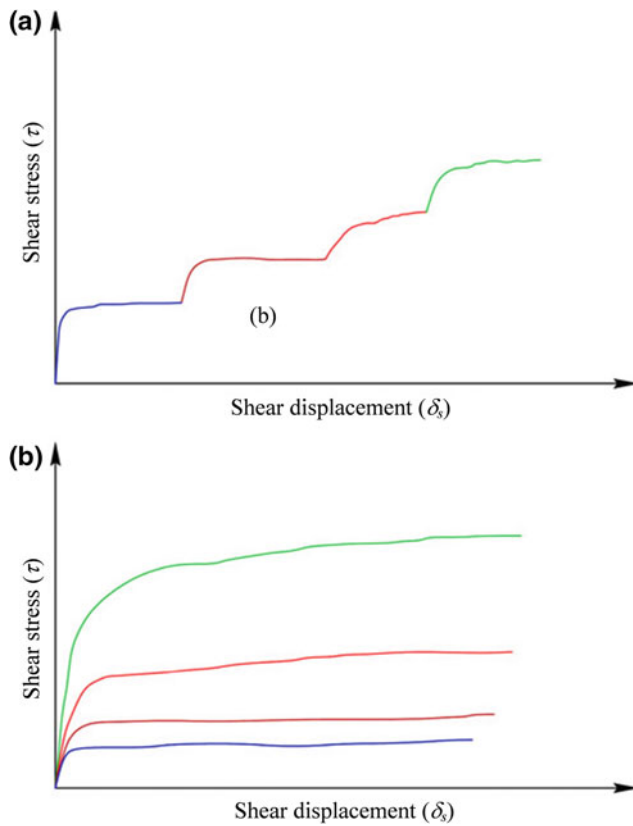


Fig. 4 Example of multi-stage shear tests under different normal loads, **a** without repositioning and **b** with repositioning

allow to determine the normal displacement at the centroid of the sample cross-section.

5.5.3 Normal Load (N)

- (a) If the normal loading mechanism is anything other than a dead-weight load (i.e., for CNL testing), measure the applied normal load at every shear load observation with a load measuring device. Normal load must be continuously monitored during testing.

5.5.4 Shear Load (T)

- (a) Measure the applied shear load with a load measuring device. The selected measurement frequency should be sufficient to fully capture the load displacement response of the specimen. This frequency depends on the nature of the specimen and shear displacement rate. Generally, a measurement every 1 s or less over the test duration should be adequate.

6 Calculations, Plots and Results

6.1 Data

- (a) Check the individual data records to check the consistency of all measurements.
 (b) If the nominal stresses are not provided directly by the data acquisition system, calculate the normal and shear stresses as:

$$\sigma_n = \frac{N}{A}, \quad (1)$$

$$\tau = \frac{T}{A}, \quad (2)$$

where N normal load, T shear load, A nominal area, σ_n normal stress, τ shear stress.

- (c) As referred in Sect. 4.2(f), if the nominal area decreases during shear displacement, it has to be taken in consideration for the calculation of the nominal stresses.
 (d) Calculate the normal and shear displacements if they are not provided directly by the data acquisition system.

6.2 Plots and Calculations

- (a) The following plots are required for the determination of the shear strength of the joint specimen (Fig. 5):
- i. Shear stress versus shear displacement graphs;
 - ii. Normal displacement versus shear displacement graphs;
 - iii. Normal load versus shear displacement graphs, in the case of CNS tests.
- (b) Normal load versus normal displacement graphs of the normal load application stages can also be provided.
- (c) Using the data records and the shear stress versus shear displacement graphs, evaluate the peak and ultimate or residual shear stresses for each sample of the same rock joint or test horizon in the case of single stage tests, or for all stages of multi-stage tests of the same rock sample (Fig. 6) (Wittke 1990).
- (d) Using the data records and the normal displacement versus shear displacement graphs, evaluate the peak

Fig. 5 Typical plots from a rock joint shear test, **a** under constant normal loading conditions (CNL), and **b** under constant normal stiffness conditions (CNS)

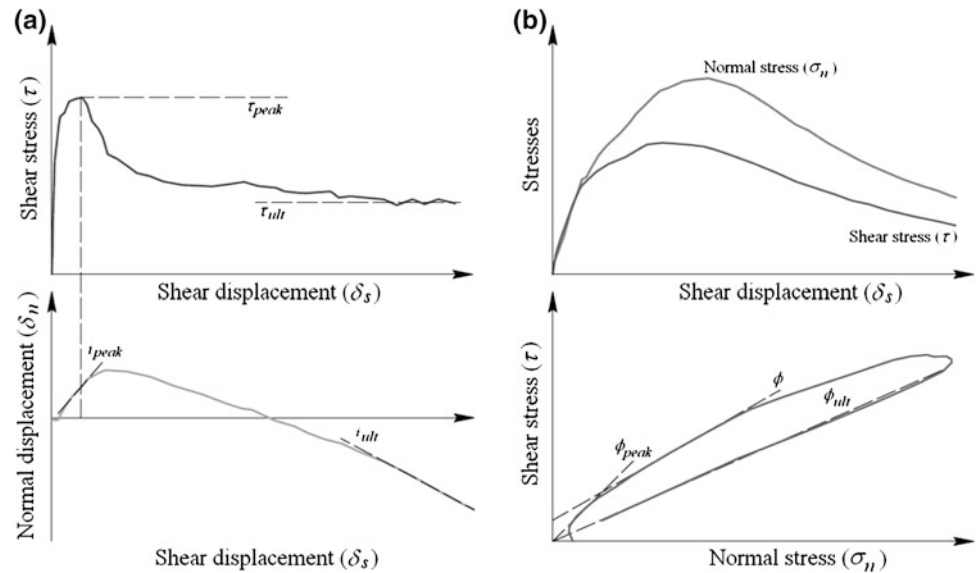
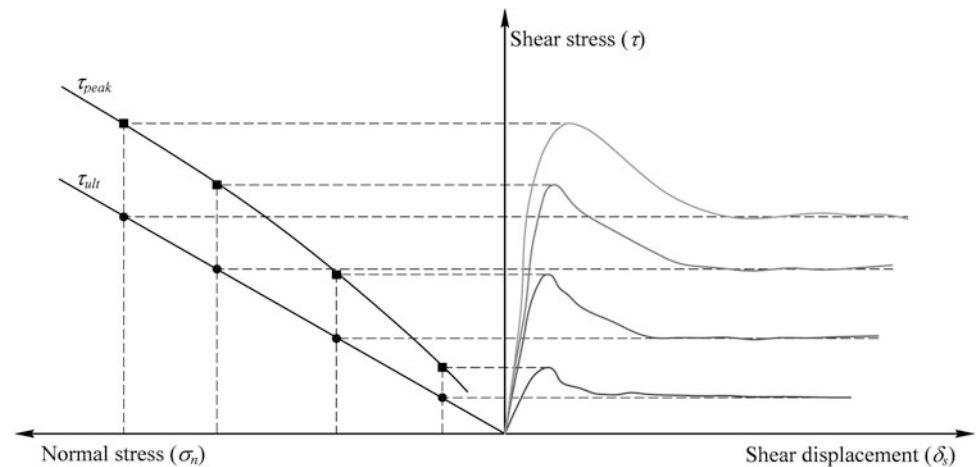


Fig. 6 Evaluation of the peak and ultimate or residual shear stresses



and ultimate or residual dilation angles for each sample of the same rock joint or test horizon in the case of single stage tests, or for all stages of multi-stage tests of the same rock sample.

- (e) Make plots that depict the relationships of peak shear stress versus normal stress and ultimate or residual shear stress versus normal stress.
- (f) Use these plots to evaluate the strength parameters of a prescribed failure criterion. Mohr–Coulomb criteria are usually suitable to adequately model the results of rock joint shear tests. In this case, parameters of this linear failure criterion are defined as follows:

$$\tau = c + \sigma_n \tan \phi \quad (3)$$

where c apparent cohesion, $\tan \phi$ friction coefficient, ϕ friction angle.

- (g) Particular care should be paid in using Mohr–Coulomb criterion strength parameters. Results should not be extrapolated beyond the range of the applied normal stresses during the tests, especially for low σ_n values, as illustrated in Fig. 6.
- (h) In the case of rough or non-planar joints, a non-linear shear strength envelope may be more representative of the test results. In these cases, it is possible to consider other well-established failure criteria, calculate the respective parameters, and deliver them also as results of the tests. Such criteria include: the i value of Patton (Barton 1976) or the JRC of Barton and Choubey (1977). The latter also allows addressing the issue of sample size effects (Bandis et al. 1981).
- (i) In the case of multi-stage tests, the apparent cohesion can be exaggerated due to accumulation of damage with successive shearing of the same joint specimen.

- (j) As shear and normal displacement measurements are available, deformability parameters such as normal and shear stiffness of the samples may also be derived from the tests.
- iii. Data tables with all values required to plot the graphs presented in the report.

7 Reporting of Results

(a) The report should include the following:

- i. A description of the test specimens, including:
 - identification of all samples and specimens;
 - the dates of sampling and testing;
 - the total number of test specimens;
 - the specimen dimensions, including nominal cross-sectional area;
 - the source of each specimen, including project name, location, and depth, drill hole number and inclination;
 - a geological description of each specimen, including a description of the intact rock, shear surface (e.g., roughness, aperture);
 - orientation of the samples and test horizons (dip and dip direction), including the relative angle between the dip direction and the shear direction, or, in the case of borehole samples, the angle between the samples and the borehole axis;
 - photographs of the specimens before and after the tests.
- ii. A set of plots including shear stress versus shear displacement graphs, normal displacement versus shear displacement graphs, and normal load versus shear displacement graphs, in the case of CNS tests. Normal stress versus normal displacement graphs depicting the normal load application can also be added.
- iii. Plots and tabulated values of peak and ultimate or residual shear stress versus normal stress, peak and ultimate or residual dilation angles, together with calculated values for the shear strength parameters.

(b) In the report, the following items may also be included. If not, they should be available upon request.

- i. A diagram and description of the test equipment and a description of the methods used for taking, packaging, transporting, storing, mounting and testing the specimen. Reference may be made to this ISRM Suggested Method stating only departures from the prescribed procedures.
- ii. Details of any special measuring devices employed to measure roughness, nominal areas or other specimen characteristics. For example, the name, type, resolution, and precision of any non-contact surface measurement device employed should be provided.

Appendix: Terminology

Aperture distance between discontinuity walls measured perpendicular to the average discontinuity plane.

Apparent stress nominal stress on the discontinuity surface, which is the external normal or shear load applied to the discontinuity per nominal unit area.

Asperity any surface irregularity or deviation with respect to the average discontinuity plane. Irregularities and deviations can range from sharp or angular to smooth or rounded.

Asperities the collection of surface irregularities that comprise the discontinuity surface roughness.

Closed-loop testing system a testing system in which the true response of the loading actuator(s) is continuously compared with the desired response of the loading actuator (i.e., a feedback loop) and corrected if required.

Constant Normal Load (CNL) direct shear test methodology whereby the applied normal loading is held constant throughout the test and the normal stiffness may vary.

Constant Normal Stiffness (CNS) direct shear test methodology whereby the applied normal stiffness is held constant throughout the test and the applied normal load varies.

Dilation angle arctangent of the ratio of normal displacement to the corresponding shear displacement

- i. *Peak dilation angle* (i_{peak}) arctangent of the ratio of the normal displacement at peak shear strength to the corresponding shear displacement.
- ii. *Ultimate dilation angle* (i_{ult}) arctangent of the ratio of the normal displacement at ultimate shear strength to the corresponding shear displacement.
- iii. *Residual dilation angle* (i_{res}) arctangent of the ratio of the normal displacement at residual shear strength to the corresponding shear displacement (Note that it is usually difficult to reach true residual strength, because of the limited shear displacement, and the term ‘ultimate strength’ should then be used).

Discontinuity any mechanical break in the integrity or physical properties of rock such as bedding planes, fractures, cleavage, cracks, joints, or faults. Discontinuities can be described as:

- i. tight (closed) (i.e., consisting of opposing rock surfaces in intimate and generally continuous contact);
- ii. gapped (open) (i.e., consisting of opposing rock surfaces separated by an open space);
- iii. partially or totally filled (i.e., consisting of opposing rock surfaces separated by a space, which is partially or totally filled by any type of filling material, such as clay, gouge, breccia, mylonite, thin coatings or veins);

and further characterized as a function of their geometry as:

- iv. planar to non-planar (undulating) (i.e., the level of deviation from the average discontinuity plane).
- v. Well matched to poorly matched (i.e., the degree of interlocking between the two walls of the discontinuity).

Friction angle arctangent of the ratio of the applied shear stress to the corresponding apparent normal stress (σ_n) which is equivalent to the arctangent of the ratio of applied shear load to the corresponding normal load.

- i. *Peak friction angle* (ϕ_{peak}) arctangent of the ratio of the peak shear strength to the corresponding apparent normal stress which is equivalent to the arctangent of the ratio of peak shear load to the corresponding normal load.
- ii. *Ultimate friction angle* (ϕ_{ult}) arctangent of the ratio of the ultimate shear strength to the corresponding apparent normal stress which is equivalent to the arctangent of the ratio of ultimate shear load to the corresponding normal load.
- iii. *Residual friction angle* (ϕ_{res}) equal to the residual friction angle if the apparatus is able to reach a large enough shear displacement.

Friction coefficient the ratio of the applied shear stress to the corresponding apparent normal stress which is equivalent to the ratio of applied shear load to the corresponding normal load.

- i. *Peak friction coefficient* (μ_{peak}) the ratio of the peak shear strength to the corresponding apparent normal stress which is equivalent to the arctangent of the ratio of peak shear load to the corresponding normal load.
- ii. *Ultimate friction coefficient* (μ_{ult}) the ratio of the ultimate shear strength to the corresponding apparent normal stress which is equivalent to the arctangent of the ratio of ultimate shear load to the corresponding normal load.
- iii. *Residual friction coefficient* (μ_{res}) equal to the residual friction coefficient if the apparatus is able to reach a large enough shear displacement.

Nominal area (A) area obtained by measuring or calculating the cross-sectional area of the projection of the discontinuity surface onto the shear plane.

Normal displacement (δ_n) relative displacement of the joint halves perpendicular to the shear plane.

Open-loop testing system a testing system in which the desired loading response is sent as input to the loading actuator without any feedback of the actual response to facilitate correction.

Peak shear load (T_{peak}) the highest recorded shear load corresponding to a specific initial normal load after which the shear load decreases until ultimate or residual shear loads are reached.

Peak shear strength (τ_{peak}) the highest recorded shear stress corresponding to a specific initial apparent normal stress after which the shear load decreases until ultimate or residual shear loads are reached.

Pitch angular rotation about an axis perpendicular to the shear direction and parallel to the shear plane.

Residual shear load (T_{res}) equal to the residual shear load if the apparatus is able to reach a large enough shear displacement.

Residual shear strength (τ_{res}) equal to the residual shear strength if the apparatus is able to reach a large enough shear displacement.

Roll angular rotation about an axis parallel to the shear direction.

Roughness a measure of the inherent unevenness and waviness of a discontinuity surface relative to its mean plane.

Shear displacement (δ_s) relative displacement of the joint halves measured along the direction of the shear load.

Shear stiffness the ratio of shear stress to the corresponding shear displacement prior to reaching the peak shear strength.

Ultimate shear load (T_{ult}) the shear load corresponding to a specific initial normal load, for which the shear load remains essentially constant with increasing shear displacement.

Ultimate shear strength (τ_{ult}) the shear stress corresponding to a specific initial apparent normal stress, for which the shear stress remains essentially constant with increasing shear displacement.

Yaw angular rotation about an axis perpendicular to the shear direction and to the shear plane.

References

- Alonso EE, Pinyol NM, Pineda JA (2011) Foundation of a gravity dam on layered soft rock. Shear strength of bedding planes in laboratory and large "in situ" tests. In: Anagnostopoulos A et al. (eds) Proc. 15th European Conf. Soil Mechanics and Geotechnical Engineering, Athens, Greece, IOS Press, Amsterdam
- ASTM (2008) Standard test method for performing laboratory direct shear strength tests of rock specimens under constant normal force. ASTM International, West Conshohocken, p 12
- Aydan Ö, Shimizu Y, Kawamoto T (1992) The anisotropy of surface morphology characteristics of rock discontinuities. *Rock Mech Rock Eng* 29(1):47–59
- Bandis S, Lumsden AC, Barton N (1981) Experimental studies of scale effects on the shear behaviour of rock joints. *Int J Rock Mech Min Sci Geomech Abstr* 18(1):1–21
- Barla G, Barla M, Martinotti ME (2010) Development of a new direct shear testing apparatus. *Rock Mech Rock Eng* 43:117–122
- Barla G, Robotti F, Vai L (2011) Revisiting large size direct shear testing of rock mass foundations. In: Pina C, Portela E, Gomes J

- (eds), 6th International Conference on Dam Engineering, Lisbon, Portugal. LNEC, Lisbon
- Barton N (1976) Shear strength of rock and rock joints. *Int J Rock Mech Min Sci Geomech Abstr* 13(9):255–279
- Barton N, Choubey V (1977) The shear strength of rock joints in theory and practice. *Rock Mech Rock Eng* 10:1–54
- Blümel M, Pötsch M (2003) Direct shear testing system. *Geotechnical Measurements and modelling*. In: Natau O, Fecker E, Pimentel E (eds), Karlsruhe, Germany, Swets and Zeitlinger, Lisse, pp 327–332
- Blümel M, Button EA, Pötsch M (2003) Stiffness controlled shear behavior of rock. 10th ISRM Congress, Technology roadmap for rock mechanics. Johannesburg, South Africa. South African Institute of Mining and Metallurgy, Johannesburg, vol 1, pp 121–124
- Boulon M (1995) A 3D direct shear device for testing the mechanical behaviour and the hydraulic conductivity of rock joints. In: Second Int. Conference on Mechanics of Jointed and Faulted Rock MJFR-2, Vienna, Balkema, Rotterdam, pp 407–413
- Chryssanthakis P (2004) Oskarshamn site investigation. Drill hole KSH01A. The normal stress and shear tests on joints. SKB Report No. P-04-185. SKB, Stockholm, p 38
- Grasselli G (2001) Shear strength of rock joints based on quantified surface description. PhD Dissertation. École Polytechnique Fédérale de Lausanne
- Hencher SR, Richards LR (1982) The basic frictional resistance of sheeting joints in Hong Kong granite. *Hong Kong Engineer*, pp 21–25
- Indraratna B, Haque A, Aziz N (1999) Shear behaviour of idealized infilled joints under constant normal stiffness. *Géotechnique* 49(3):331–355
- ISRM (2007) The complete ISRM suggested methods for rock characterization, testing and monitoring: 1974–2006. In: Ulusay R Hudson JA (eds), Suggested methods prepared by the Commission on Testing Methods, ISRM, Compilation arranged by the ISRM Turkish National Group, Kozan Ofset, Ankara
- JGS (2008) Method for direct shear test on a rock discontinuity. Japanese Geotechnical Society, Tokyo, p 8
- Jiang Y, Xiao J, Tanabashi Y, Mizokami T (2004) Development of an automated servo-controlled direct shear apparatus applying a constant normal stiffness condition. *Int J Rock Mech Min Sci* 41(2):275–286
- Johnston I, Lam T (1989) Shear behavior of regular triangular concrete/rock joints—analysis. *J Geotec Engng* 115(5):711–727
- Leichnetz W (1985) Mechanical properties of rock joints. *Int J Rock Mech Min Sci Geomech Abstr* 22(5):313–321
- Muralha J (2007) Stress paths in laboratory rock joint shear tests. In: Ribeiro Sousa L, Olalla C, Grossmann N (eds), 11th ISRM Congress The second half century of Rock Mechanics, Lisbon, Portugal, Taylor & Francis, London, vol 1, pp 431–434
- Priest SD (1993) Discontinuity analysis for rock engineering, 1st edn. Chapman & Hall, London
- Stimpson B, Metcalfe RG, Walton G (1970) A new field technique for sealing and packing rock and soil samples. *Q J Eng Geol* 3:127–133
- Tatone BSA, Grasselli G (2009) A method to evaluate the three-dimensional roughness of fracture surfaces in brittle geomaterials. *Rev Sci Instrum* 80:125110–125119
- USACE (1980) Method of test for direct shear strength of rock core specimens. United States Army Corps of Engineers, Vicksburg, p 9
- Wittke W (1990) *Rock mechanics: theory and applications with case histories*. Springer-Verlag, Berlin

ISRM Suggested Method for the Needle Penetration Test

Resat Ulusay, Ömer Aydan, Zeynal A. Erguler, Dominique J. M. Ngan-Tillard, Takafumi Seiki, Wim Verwaal, Yasuhito Sasaki, and Akira Sato

1 Introduction

Estimation of mechanical properties of intact rock is usually required for assessment of the stability of rock structures. They are also important elements of the rock classifications used in empirical assessment of rock masses. Measurement of

these properties requires laboratory testing, which must be performed on samples of certain dimensions to fulfill testing standards and/or suggested methods. Laboratory tests are also time-consuming due to sample preparation, as well as experimental procedures often require high-capacity loading devices. High-quality core samples recommended by standards and/or suggested methods for the laboratory tests cannot always be obtained, particularly from weak and clay-bearing rocks. For these reasons, some simple and inexpensive index test methods have been developed to indirectly estimate the mechanical properties of intact rock (ISRM 2007). However, even preparation of smaller samples from weak and clay-bearing rocks for some index tests is still troublesome. In addition, geo-engineering and/or restoration studies on natural and man-made historical rock structures and monuments or buildings built with masonry construction techniques may require the determination of mechanical properties of intact rock. Sampling from such ancient sites is not allowed due to preservation, and environmental and other concerns resulting in the lack of mechanical data for those studies.

To overcome the above-mentioned difficulties, a portable, lightweight and non-destructive testing device, called needle penetrometer, was developed in Japan and released as a suggested method by the Rock Mechanics Committee of the Japan Society of Civil Engineers (JSCE-RMC 1980). Similarly, Public Works Research Institute (PWRI 1987) published a draft manual of the test for weak rock mass classification of dam foundation. In the following years, JSCE (1991) revised the suggested method. Recently, JGS (2012) published the JGS standard for the needle penetration test, JGS 3431-2012.

According to the suggested method of Japan Society of Civil Engineers (JSCE 1991) and JGS (2012), the needle penetration test is applicable to soft rocks having uniaxial compressive strength (UCS) less than about 9.8 MPa.

The needle penetration test is a non-destructive index test applicable both in the field and laboratory to determine the needle penetration index (NPI) and does not require any

Please send any written comments on this ISRM Suggested Method to Prof. Resat Ulusay, President of the ISRM Commission on Testing Methods, Hacettepe University, Department of Geological Engineering, 06800 Beytepe, Ankara, Turkey.

Originally published as an article in the journal *Rock Mechanics and Rock Engineering*, 47, R. Ulusay, Ö. Aydan, Z. A. Erguler, D. J. M. Ngan-Tillard, T. Seiki, W. Verwaal, Y. Sasaki, A. Sato, ISRM Suggested Method for the Needle Penetration Test, 1073–1085, 2014.

R. Ulusay (✉)

Department of Geological Engineering, Hacettepe University, Ankara, Turkey
e-mail: resat@hacettepe.edu.tr

Ö. Aydan (✉)

Department of Civil Engineering and Architecture, University of the Ryukyus, Okinawa, Japan
e-mail: aydan@tec.u-ryukyu.ac.jp

Z. A. Erguler

Department of Geological Engineering, Dumlupınar University, Kutahya, Turkey

D. J. M. Ngan-Tillard · W. Verwaal

Department of Geoscience and Engineering, Delft University of Technology, Delft, The Netherlands

T. Seiki Department of Architecture and Civil Engineering, Utsunomiya University, Utsunomiya, Japan

Y. Sasaki

Public Works Research Institute, Geology Research Team, Tsukuba, Japan

A. Sato

Graduate School of Science and Technology, Kumamoto University, Kumamoto, Japan

special sample preparation. Several correlations between NPI values and other physico-mechanical properties of intact rock have been established by several authors for a number of rock types. The NPI value is mainly used to estimate the UCS of intact rock (e.g., Okada et al. 1985; Yamaguchi et al. 1997; Takahashi et al. 1988; Uchida et al. 2004; Aydan et al. 2006, 2008; Aydan 2012; Erguler and Ulusay 2007; Park et al. 2011; Ulusay and Erguler 2012). However, its use was also extended to allow assessing of other physico-mechanical properties of intact rock such as tensile strength, Young's modulus and P-wave velocity from NPI (Aydan 2012; Aydan and Ulusay 2013). Aydan et al. (2013) included also cohesion, friction angle and S-wave velocity in addition to the parameters previously covered by Aydan (2012). It should be stressed that that these correlations, though very helpful, comprise a high scatter. So, they are not intended to entirely replace proper evaluation of the aforementioned properties, but to easily provide estimates of their values.

The needle penetration test described in this suggested method is applied to rock specimens and rock exposures to determine the needle penetration index (NPI). In this suggested method, the device and operating procedure are described together with data evaluation. Documentation and presentation of the results are also explained. In addition, all possible uses of the NPI in practice, and other issues related to NP test such as rate of penetration, the effect of needle geometry, influence of grain size, degree of micro structural damage by needle, effect of water, variation of NPI with freezing–thawing and drying–wetting cycles and the possible use of different needle types are also presented in the last section.

2 Scope

The needle penetration test can be performed in the field on rock exposures or in laboratory on rock specimens. It uses a light portable device, called needle penetrometer that pushes a needle into the rock.

The needle penetration test is intended for the determination of the needle penetration index (NPI). This index value can be used to estimate other physico-mechanical properties of intact rock with which NPI is correlated, for example UCS.

3 Testing Device

The needle penetrometer (NP), a lightweight portable device (about 600–700 g), is used to make a needle penetrate into a rock surface (Fig. 1). The needle is a hardened steel, 0.84-mm-diameter rod terminated by a conical tip (Fig. 2). It is a sewing needle designated as JIS S 3008 (No. 2).

The device mainly consists of presser, chuck, penetration scale (0–10 mm, 1 mm graduation), load scale (0–100 N, 10 N graduation), load indicator ring, cap (removable; spare

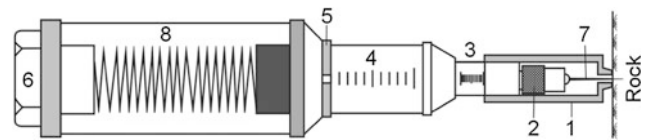


Fig. 1 Needle penetrometer and its parts: 1 presser, 2 chuck, 3 penetration scale, 4 load scale, 5 load indicating ring, 6 cap, 7 penetration needle and 8 spring

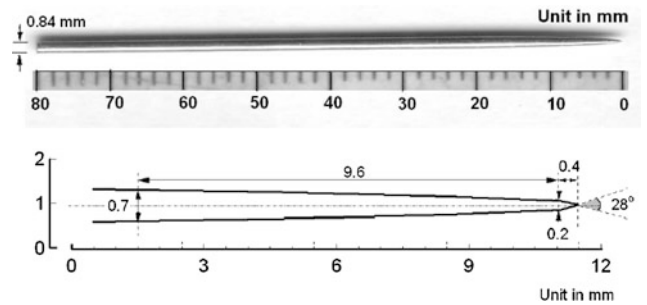


Fig. 2 Sewing needle designated as JIS S 3008 (No. 2) and its geometry (Aydan et al. 2013)

penetration needles contained in the grip), penetration needle and spring mounted in the penetrometer grip as shown in Fig. 1. To insert the needle, the presser (Fig. 1, part 1) is removed from the penetration scale (Fig. 1, part 3) using the vertical and horizontal notches, the chuck (Fig. 1, part 2) is turned counterclockwise and the penetration needle is inserted. Then the chuck is turned clockwise for fastening and fixing the needle and the presser is set using the co-axial notch for zero point adjustment of the penetration scale. The split-type load indicator ring (Fig. 1, part 5) is adjusted manually to zero. The device can measure the applied load up to 100 N and the penetration depth is up to 10 mm.

Based on data from needle penetration tests obtained from literature (i.e., Okada et al. 1985; Aydan 2012; Aydan et al. 2006, 2008, 2013; Erguler and Ulusay 2007; JSCE-RMC 1980; Takahashi et al. 1988; Yamaguchi et al. 1997; Ulusay and Erguler 2012), although this test has been used for rocks with UCS up to 35 MPa, it is generally recommended that it should be used for rocks with UCS lower than 20 MPa, in order to obtain realistic results the penetration of the needle should be more than 1 mm without causing any damage to the needle (Fig. 3).

4 Procedure

The needle penetrometer (NP) device can be used both on rock exposures in the field and on specimens with cylindrical, cubic or prismatic shapes prepared from cores or blocks. It does not require any special preparation of the rock surfaces or specimens. However, before testing, if the surface on which the test will be performed shows some

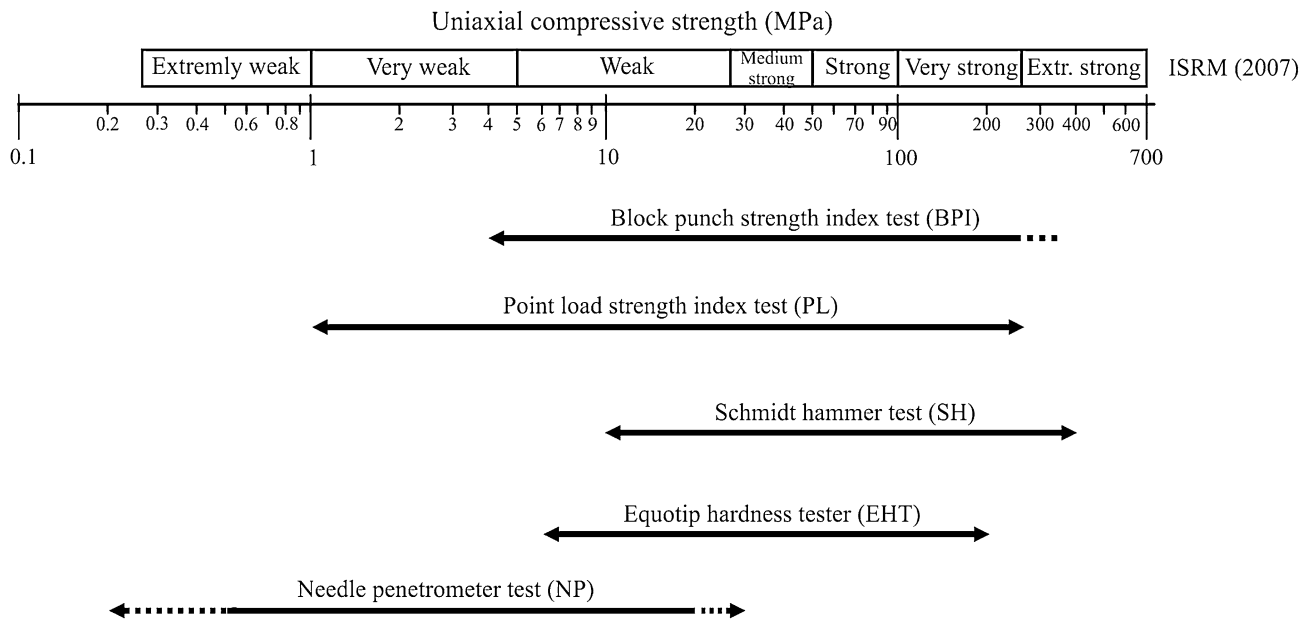


Fig. 3 Ranges of applicability of the most commonly used index tests in rock engineering and the needle penetration test for estimating the UCS (Ulusay and Erguler 2012)

asperities, they have to be removed. Since the test is only intended for weak/soft rocks, they can easily be grinded using common instruments such as files, sandpaper or pocketknives.

The size of samples should be such that no splitting of some samples occurs. Based on the experience, splitting may occur in laboratory samples having a size of $35 \times 35 \times 35$ mm. Therefore, sample size is suggested to be about $40 \times 40 \times 40$ mm for prismatic samples and 40–50 mm in diameter for cylindrical samples having a height greater than 15 mm. The NP test can be used in any direction.

The test is performed by holding tightly the truncated conical joint between load and displacement graduations with one hand and the main body with the other hand, and slowly pushing manually the penetrometer needle into the rock surface or specimen as shown in Fig. 4a, b. The load should be applied perpendicularly to the surface. It is recommended that users hold the needle penetrometer always in the same position, i.e., with both hands. It should be noted that if the operator becomes less focused and starts changing his/her usual *modus operandi* (e.g., holding the penetrometer with just one hand), the scattering of the NPI values will increase.

The needle is pushed into the rock until 100 N is reached; at this stage the penetration depth is measured from the position of the presser on the penetration scale (Fig. 1, part 3). Then, the needle is slowly pulled out. With softer and saturated rocks, it is possible that, before the maximum penetration force is reached, the maximum

penetration depth (10 mm) is attained. In this case, the test stops at this depth, the penetration load is read from the load scale (Fig. 1, part 4) and the needle is slowly pulled out.

The test is repeatedly carried out on the same surface between three to five times. However, if the results are not consistent or too scattered, the number of tests can be increased. At each time, the penetration point of the needle is shifted by at least 10 mm from the previous point.

During penetration, some fractures may develop and may create a radially fractured zone. It should be noted that when the needle is withdrawn, some inverted cones and associated fractures may also develop. If fractures develop during the penetration procedure, the results of such tests should be discarded (Fig. 5). However, if such fractures develop during the withdrawal of the needle, the test can be accepted as valid. In addition, if needle penetration causes tensile splitting of the specimen along a weakness plane, such as bedding or schistosity, the test should also be discarded.

5 Calculations

The needle penetration index (NPI) is calculated from the following equations:

$$\text{for } F = 100 \text{ N and } D \leq 10 \text{ mm,} \quad (1a)$$

$$\text{NPI} = 100/D$$

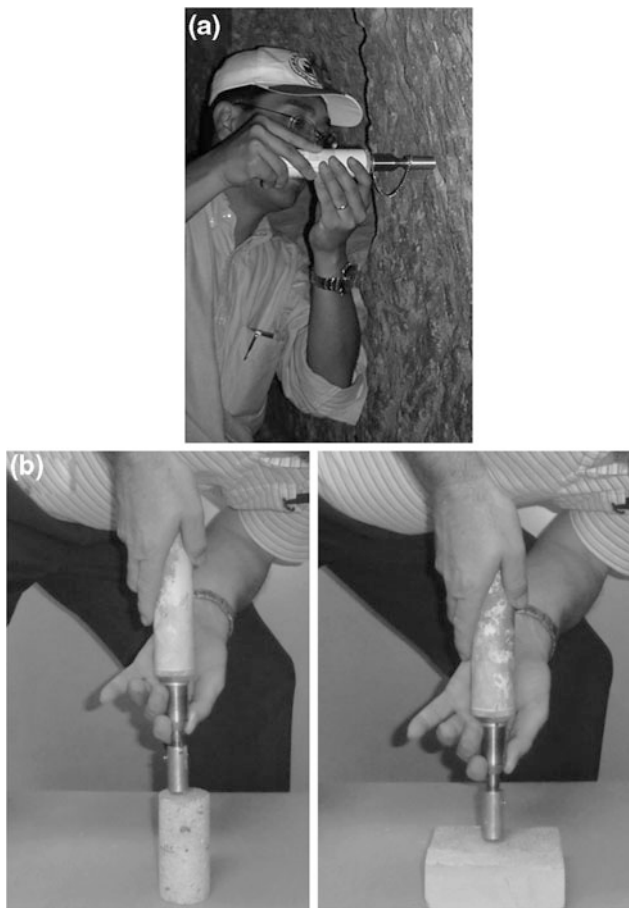


Fig. 4 Application of the needle penetrometer in **a** field on a rock exposure and **b** laboratory on core and prismatic samples

$$\text{for } D = 10 \text{ mm and } F < 100 \text{ N} \quad (1b)$$

$$\text{NPI} = F/10 \text{ (for } F \leq 100 \text{ N)}$$

where F is the applied load (N) and D is the depth of penetration (mm). The unit of NPI is N/mm.

The values of the NPI should be <100 N/mm and >1 N/mm, as the minimum graduation of the penetration scale is 1 mm and that of the load scale is 100 N.

The mean of the NPI values calculated using at least three points of measurement on the same testing surface is taken as the NPI value of the specimen or rock exposure.

Though the effect of the needle penetration rate on the NPI is negligible, each test should take around 30 s to perform.

In certain types of rocks displaying grain or porosity heterogeneity at the scale of the needle diameter (e.g., grains larger than 10 mm, uneven distribution of pores or a mixture of crushable with less crushable grains), a large scatter of the NPI values is expected. In the case of rocks with coarse hard grains in a soft cementing material, such as breccia or conglomerate, the NP test can be cautiously used to infer the properties of the soft matrix.

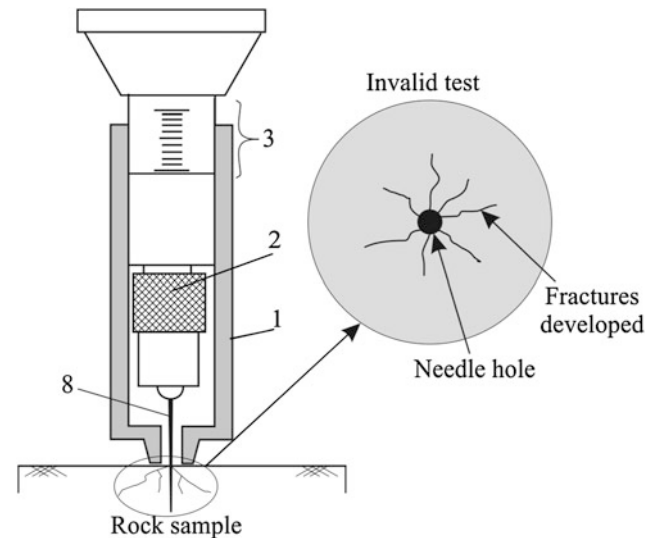


Fig. 5 Schematic illustration of an invalid NP test (Ulusay and Erguler 2012)

6 Reporting of Results

The report should contain at least the following information for each tested specimen or rock exposure:

- Lithological description of the rock.
- Orientation of the direction of penetration with respect to specimen anisotropy, e.g., bedding planes, schistosity, etc. (in degrees).
- Type of laboratory specimen or rock exposure.
- Identification of the laboratory specimen with sample number, source location and sampling depth and date, or identification of the rock exposure with description of the site.
- Number of tested specimens or rock exposures.
- Water content at the time of test (air dried, oven dried or value of water content in percent).
- Date of testing.
- A tabulation of the values of applied load and depth of penetration at each application point on the rock surface and the calculated mean NPI value.

7 Technical Issues Regarding Needle Penetration Test

The non-destructive nature of the NP test and the limited requirement for specimen preparation make it possible to perform both in laboratory and field. In addition, in geo-engineering or restoration studies conducted at historical rock structures or sites, where rock sampling for laboratory strength determinations is not allowed, the NP test can also

Table 1 Examples of empirical prediction equations to infer some mechanical properties of rocks from NPI*

Rock material property	Equation	Recommended by	Rock types tested
Uniaxial compressive strength, σ_c	σ_c (MPa) = 0.4 NPI ^{0.929} (N/mm)	Ulusay and Erguler (2012)	Marl, tuff, mudstone, siltstone, sandstone, greywacke, very stiff clay; data from Japan
	σ_c (MPa) = 0.2 NPI (N/mm)	Aydan (2012)	Tuff, sandstone, pumice, limestone, lignite measures (lignite, mudstone, siltstone, marl, loam)
	σ_c (kPa) = 27.3 NPI + 132 (N/cm)	Uchida et al. (2004)	Sandstone
	$\log \sigma_c$ (kgf/cm ²) = 0.978 log NPI + 1.599 (kgf/mm)	Okada et al. (1985)	Artificial cement-based samples and mudstone
	σ_c (MPa) = 1.539 NPI ^{0.9896} (N/mm)	Takahashi et al. (1988)	Sandstone, mudstone, conglomerate, greywacke, tuff
	$\log \sigma_c$ (kgf/cm ²) = 0.982 logNPI-0.209	Yamaguchi et al. (1997)	Pyroclastic flow and fall deposits
Tensile strength, σ_t (MPa)	$\sigma_t = 0.02$ NPI (NPI, N/mm)	Aydan (2012)	Tuff, pumice, lignite measures (lignite, mudstone, siltstone, marl, loam)
Young's modulus, E_i (GPa)	$E_i = 0.05$ NPI (NPI, N/mm)	Aydan (2012)	Tuff, sandstone, pumice, limestone, soapstone, lignite measures (lignite, mudstone, siltstone, marl, loam)
P-wave velocity, V_p (km/s)	$V_p = 0.33 + 0.3$ NPI ^{0.5} (NPI, N/mm)	Aydan (2012)	Tuff, sandstone, soapstone, pumice limestone, lignite measures (lignite, mudstone, siltstone, marl, loam)
Cohesion, c (MPa)	$c = 0.04$ NPI (NPI, N/mm)	Aydan et al. (2013)	Tuff, sandstone, soapstone, pumice limestone, lignite measures (lignite, mudstone, siltstone, marl, loam)
Friction angle ϕ (°)	$\phi = 54.9 (1 - \exp(-NPI/10))$ (for tensile stress regime)	Aydan et al. (2013)	Tuff, sandstone, soapstone, pumice limestone, lignite measures (lignite, mudstone, siltstone, marl, loam)
	$\phi = 13.375$ NPI ^{0.25} (for compressive stress regime) (NPI, N/mm)		
S-wave velocity, V_s (km/s)	$V_s = 0.1 + 0.18$ NPI ^{0.5} (NPI, N/mm)	Aydan et al. (2013)	Tuff, sandstone, soapstone pumice limestone, lignite measures (lignite, mudstone, siltstone, marl, loam)

* The diameter of the needle is 0.84 mm. Lignite measures of rocks are given in parentheses

be effectively used to provide estimates of the rock strength as well as other geomechanical properties.

This section summarizes a series of research studies addressing several technical issues regarding the tests, such as the correlations established with other rock strength parameters, the influence of some particular details and conditions of the tests, e.g., grain size, needle geometry and penetration rate, micro structural damage, environmental aspects (water content, freeze–thaw and wet–dry cycles), and relaxation and creep.

7.1 Correlations with Other Geomechanical Parameters and Estimation of the Weathering Degree

Several authors have presented results from their researches concerning the potential use of the needle penetration test to estimate other rock strength parameters, such as uniaxial

compressive strength, Young's modulus, tensile strength and elastic wave velocity, and shear strength parameters.

In Table 1, a wide variety of correlations are presented. It is strongly recommended to consult the original references before using the estimates they provide, to confirm that they can be applied and to assess the respective dispersions.

7.1.1 Correlations with Other Geomechanical Parameters

Empirical relationships between UCS and NPI have been recommended by several investigators from Japan and Turkey. In the establishment of these relationships, NP tests have been conducted using the same penetrometer and the needle manufactured in Japan. These empirical relations are recommended by: Okada et al. (1985) based on the test results from mudstone and artificial cement-based samples; Takahashi et al. (1988) from sandstone, mudstone, conglomerate, greywacke and tuff; Uchida et al. (2004) from

Ariake clay and sandstone separately; Yamaguchi et al. (1997) from pyroclastic flow and fall deposits; Aydan (2012) and Aydan et al. (2013) from tuff, sandstone, pumice, limestone and lignite measures. The empirical relations recommended by the above-mentioned researchers are given in Table 1, along with the corresponding rock types and the respective references. However, the equations based on utilizing data from artificial materials and soils (i.e., clay, embankment materials) are excluded from the table as this suggested method is only intended to cover NP test in weak and soft rock. Despite that some data come from artificial materials, Okada et al. (1985)'s equation fundamentally is based on mudstone and also used by the manufacturer of the testing device.

Empirical relationships between tensile strength, Young's modulus, P-wave velocity, cohesion, friction angle and S-wave velocity and NPI have also been recommended by Aydan (2012) and Aydan et al. (2013). In the establishment of these relationships, which are given in Table 1, NP tests have been conducted on different types of weak rock using the same penetrometer and needle manufactured in Japan.

7.1.2 Estimation of the Weathering Degree

Hachinohe et al. (1999) described the degree of weathering using the residual strength ratio (R_s), which is the ratio of NPI of the weathered part to that of fresh (unweathered) part of rock cores.

$$R_s = (NPI/NPI_{fp}) \times 100 \quad (2)$$

where NPI is the measured value and NPI_{fp} is an average value for the fresh part of each drill core. Based on the relationship between R_s and the depth from the bedrock surface, these researchers indicated that R_s decreases with increases in the weathering degree and that the longer the weathering time, the larger is the decrease in R_s . Hachinohe et al. (1999) determined R_s values from Tertiary sandstone and mudstone from the bedrock of marine terraces in Boso Peninsula, Japan. Recently, Aydan et al. (2013) correlated the degree of weathering of soft rocks utilizing the ratio of NPI values of weathered and unweathered soft rocks in a more quantitative manner.

7.2 Rate of Penetration

Various rates of penetrations have been adopted to record the data presented in this document. JGS suggests needle penetration rate of 20 ± 4 mm/min (0.33 ± 0.067 mm/s) (JGS 2012). Ulusay and Erguler (2012) conducted manual tests at rates of penetration ranging from 12 to 264 mm/min and showed that the rate of penetration had no effect on the

NPI. Aydan et al. (2013) performed well-controlled NP tests with the help of a compressive machine at 1.2–12 mm/min and observed that the NPI gradually increases as the penetration also increases. Nevertheless, the increase in NPI was small (always <5 N/mm). All these series of tests show that the effect of the needle penetration rate on the NPI is negligible.

7.3 Effect of Needle Geometry

Delft researchers (Ngan-Tillard et al. 2011) conducted five tests using six different types of needles on the same block sample and observed no trend in the peak resistance to penetration as function of needle diameter or cone angle. The tests were conducted on a calcarenitic sample composed of crushable grains of silt and fine sand with no mud between grains. The needles having a diameter varying between 1 and 1.4 mm and a short cone with an angle between 60° and 180° were pushed at a constant penetration rate and the required force was recorded. The peak resistance was defined as the maximum force registered during penetration divided by the cone area. The six needles progressed in the calcarenite by a punch through failure mechanism associated with grain crushing, which explains the insensitivity of the peak resistance to the needle shape and size.

Ngan-Tillard et al. (2012) conducted NP tests with needles with short and long tapered cones noticing a large influence of the slenderness of the needle on the degree of damage caused by the needle and its resistance to buckling. The comparison made by these researchers between the damage caused by the Maruto and modified Eijkelkamp needles is illustrated in Fig. 6; both (a) and (b) images are at the same scale. The modified Eijkelkamp needle with its short conical head at the extremity of a 1-mm-diameter rod had to fragment and open up strong aggregates (labels 1, Fig. 6b, c) to penetrate into the tuff. During testing, a very high penetration resistance (above 300 MPa) was measured and the needle shaft buckled. However, as the diameter of the Maruto's needle increases gradually from 0.38 to 0.84 mm over several millimeters, it might not have encountered any strong aggregates during penetration but gone through the weaker aggregates/cement/matrix by crushing them. Arrows highlight differences in the extent of the damaged zones. Nevertheless, it must be pointed out that micro cracking does occur when Maruto's needle is pushed adjacent to or near harder mineral grains. It is believed that the dilating cracks sub-parallel to the hole shaft (Fig. 6c) were formed during needle removal as high radial stresses caused by needle insertion were released.

Aydan et al. (2008) used three needles with diameters of 1, 2 and 3 mm with flat-circular ends and reported that there

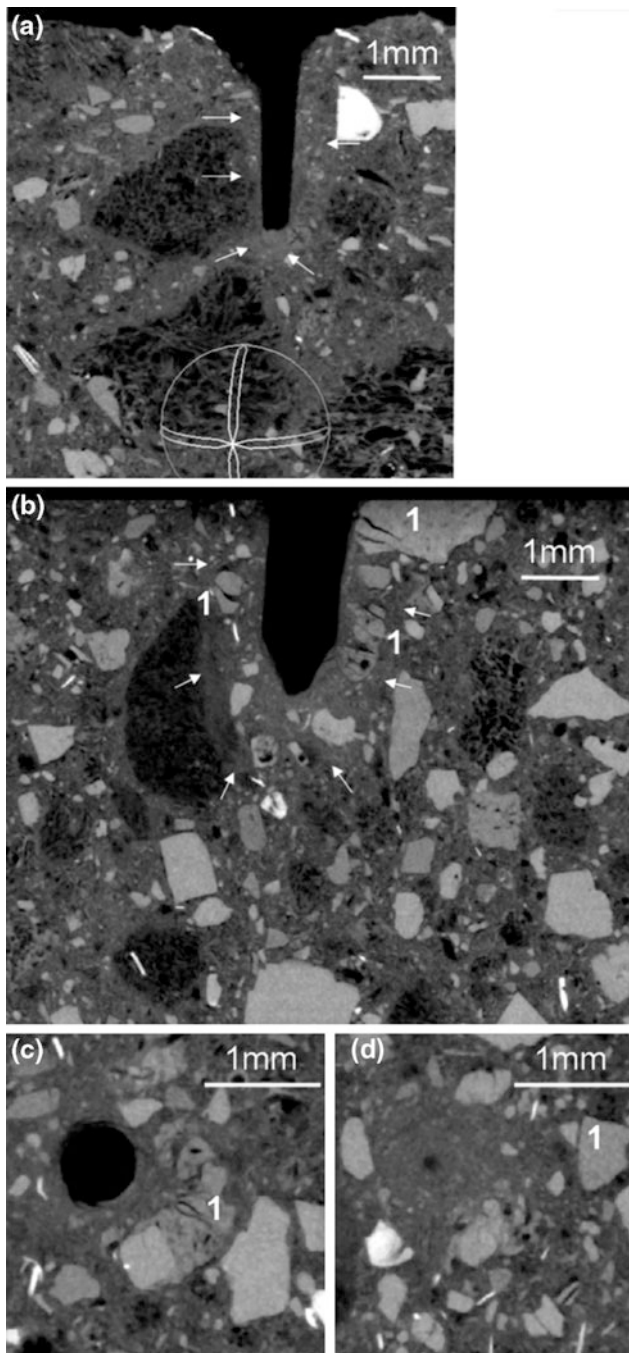


Fig. 6 Micro-CT scans with comparison of damage caused by different needles (*white circle* in the figure is an image rotating tool and was used to make a slice through the 3D micro-CT scanner dataset that passes through the axis of the needle) (Ngan-Tillard et al. 2012)

were some undesirable stress concentrations when the diameter was less than 1 mm and, in this case, non-tapered needles might buckle when high strength rock is tested. The JIS S 3008 (no. 2) needle with a diameter of 0.84 mm was also attached to the load cell and the response measured under the same circumstances. Figure 7 shows an example of measurements for a tuff from Cappadocia, Turkey. If the

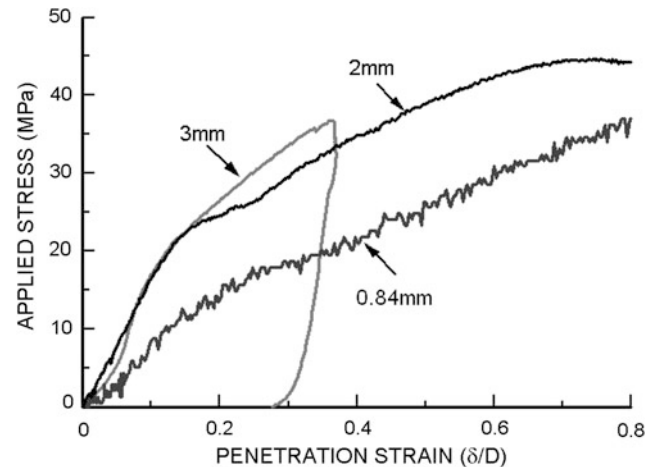


Fig. 7 Comparison of nominal strain versus applied pressure responses by a needle with a diameter of 0.84 mm and 2- and 3-mm flat-ended cylindrical needles (Aydan et al. 2008)

nominal strain is defined in terms of depth of penetration divided by rod diameter, the measured responses prove to be independent of rod diameter. As noted from the responses shown in Fig. 7, the gradient of the penetration curves recorded for both devices is different. The difference results from the plastic response occurring from the very beginning of penetration due to the configuration of the 0.84-mm needle, while the flat end needles initially show an elastic response followed by yielding behavior.

7.4 Influence of Grain Size

The needle penetration tests on various rock types with fine and/or coarse grains showed that scale effects are anticipated when the ratio of grain diameter to needle diameter is smaller than 6–10 (Ngan-Tillard et al. 2012). For these types of coarse-grained rocks, the scatter of NPI values reflects either a low needle diameter to mean grain size, an uneven pore space distribution, or a mixture crushable or less easily crushed grains.

As mentioned by Ngan-Tillard et al. (2009, 2011, 2012) and Ulusay and Erguler (2012), it should be kept in mind that the use of the NP test on rock types such as conglomerate and breccia consisting of coarse hard grains embedded in a cementing material, the test should be limited to infer the properties of the soft matrix.

7.5 Degree of Micro Structural Damage

The penetration of the needle results in a shallow hole at the location of the test. Although it is expected that the damage to rock would be of negligible level, the possible damage

Fig. 8 Views of damage zones in the vicinity of the needle: **a** soapstone; non-polished-no needle (*left*) and non-polished-with needle (*right*); **b** side views of plastic zone formation in split samples of various rocks

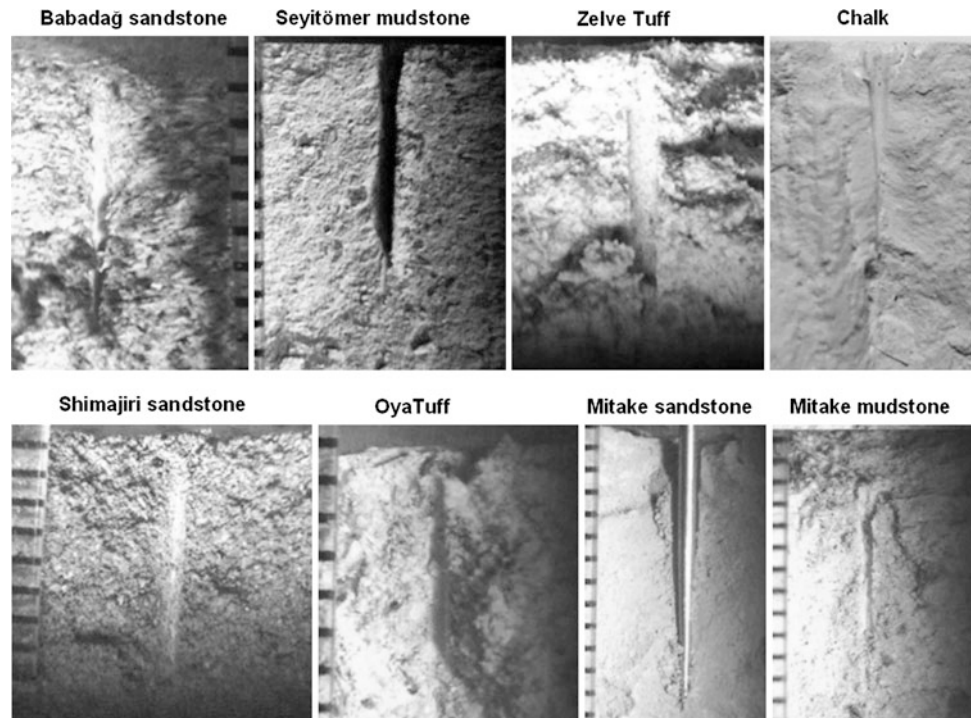
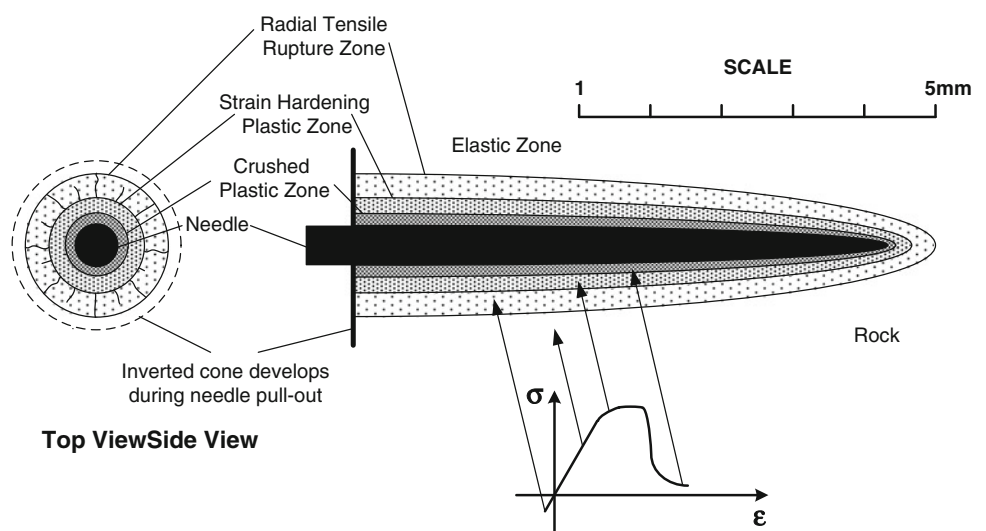


Fig. 9 Illustration of the damage zone around the needle (rearranged from Aydan et al. 2013)



caused by the needle has been investigated by some authors of this suggested method. These researches are briefly summarized in the following sub-sections.

7.5.1 Direct Observation on Damage Zones

Aydan et al. (2013) performed some needle penetration tests on samples of paraffin, chalk, mudstones, tuffs, marls, sandstones and soapstone collected from Turkey and Japan. During experiments, some samples were split so that it was possible to observe the damage zone around the needle. Figure 8 shows several views of damage zones formation in several rocks and materials. Particularly, the damage zones

around the needle are clearly differentiated with a sharp color difference in soapstone and paraffin. Aydan et al. (2013) depicted the damage zone as illustrated in Fig. 9. There is no doubt that a radially fractured zone occurs particularly in brittle rocks and expands until the penetration depth exceeds the diameter of the needle. However, a compressive (shear) stress-induced plastic zone (strain hardening and crushed zones) develops next to the needle, which is surrounded by a radial tensile fracture zone. Radial tensile fractures may sometimes be invisible when the needle is totally withdrawn. For example, when the plastic zone develops, the initially semi-transparent paraffin and

soapstone become whitish. The radius of the plastic zone seems to be about two to three times the radius of the needle. Furthermore, radial tensile fractures, which occur beforehand, are well distinguished during penetration and one can easily see the development of the inverted cone of material at the close vicinity of the surface. However, the formation and extension of tensile radial fractures gradually decrease as the penetration depth increases. When rocks have low density such as in mudstone, the formation of tensile fractures is almost suppressed. On the other hand when rocks become denser like soapstone whose unit weight is about 27 kN/m^3 and porosity $<1 \%$, the formation of tensile cracks becomes quite dominant in the overall process. Particularly, post-yielding behavior is also another major parameter in damage zone formation. If post-yielding is ductile, tensile fracture formation becomes suppressed while it is vice versa when the post-yielding is brittle.

7.5.2 CT Scanning Observations on Damage Zone

Ngan-Tillard et al. (2012) investigated the effect of damage caused by needle penetration using X-ray micro-tomography and environmental scanning electronic microscopy after the withdrawal of the needle (Figs. 10 and 11). They tested mudstone, marl and tuff samples from Turkey and calcarenite sample from the Netherlands. They showed that all failure patterns are concentrated around the needle hole. For all rocks the failure patterns consist of a compaction zone ahead and along the needle hole. For some rocks, other types of failure are also discerned. Densification around the hole is clearly visible in porous rocks containing crushable grains (marl, calcarenite and tuff). During needle penetration test, a punch-through mechanism associated with crushing rather than grain debonding takes place. Fine-grained materials (fines) are produced and compacted by the passage of the needle. In the tuff sample, while pumice is reduced to powder, less crushable grains made of quartz and plagioclase minerals are split in the radial direction. In the mudstone, the most brittle of the tested materials by Ngan-Tillard et al. (2012), dilating cracks initiating at the needle tip and propagating toward the free surface of the sample, away from the needle shaft, are also visible on micro-CT scans. They deepen the large crater observed at the point of impact on the core surface. The post-test observations do not allow the sequence of the different failure mechanisms taking place to be established. Spalling, i.e., detachment of plate-shaped slabs from the needle hole, is also observed. It is thought to have occurred during unloading and needle retrieval when the high radial confining stresses generated by needle penetration were released. Ideally, the sequence of events should have been tracked by conducting *in vivo* X-ray micro-tomography tests during needle loading, unloading and retrieval. Unfortunately, the needle creates metal artefacts on the micro-CT scans that hide subtle deformation patterns.

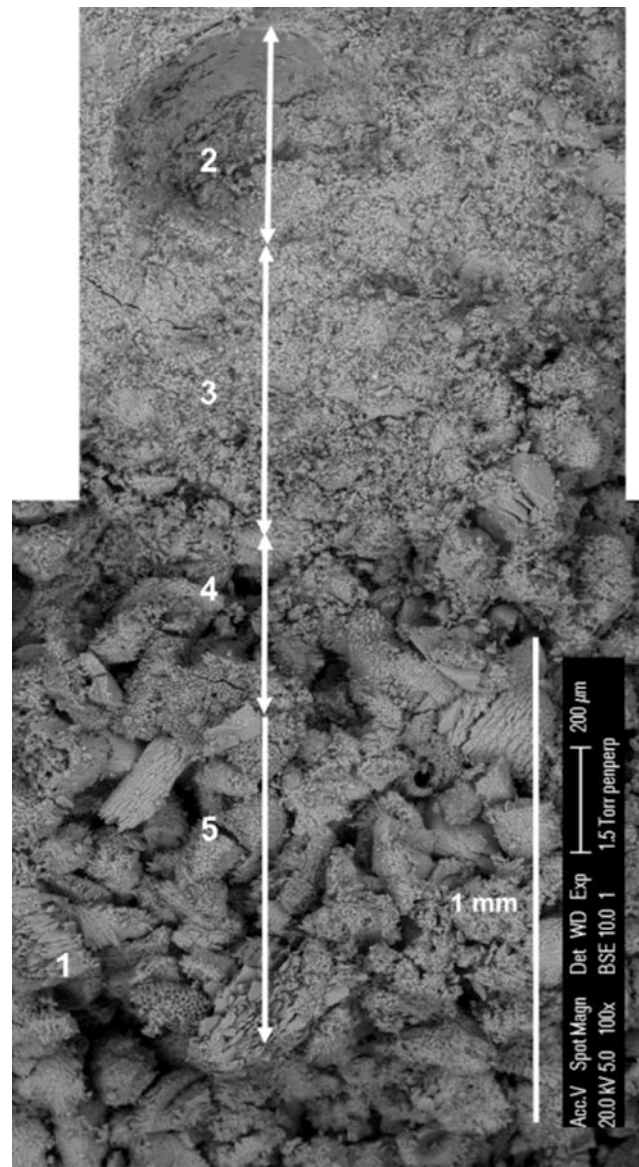


Fig. 10 ESEM photographs of the calcarenite nearby a hole at 100 magnification: 1 bioclast covered by a fringe of dog-teeth calcite cement, 2 imprint of needle tip, 3 crushed zone, 4 transition zone, 5 intact zone (after Ngan-Tillard et al. 2012)

Aydan et al. (2013) used the same X-ray micro-tomography technique to check the effect of additional damage zone formation by the withdrawal procedure. The penetration depths of the needle were set at 2.5, 5.0, 7.5 and 10.0 mm. For soapstone and mudstone samples, the formation of damage zones around the needle was investigated using the μ -focus X-ray CT Scanner System before and after the withdrawal of the needles. Figure 12 shows some selected images of these experiments. Aydan et al. (2013) concluded that the force to be applied to the needle might be up to 40–50 N during the withdrawal procedure, which reverses the stress conditions around the needle and

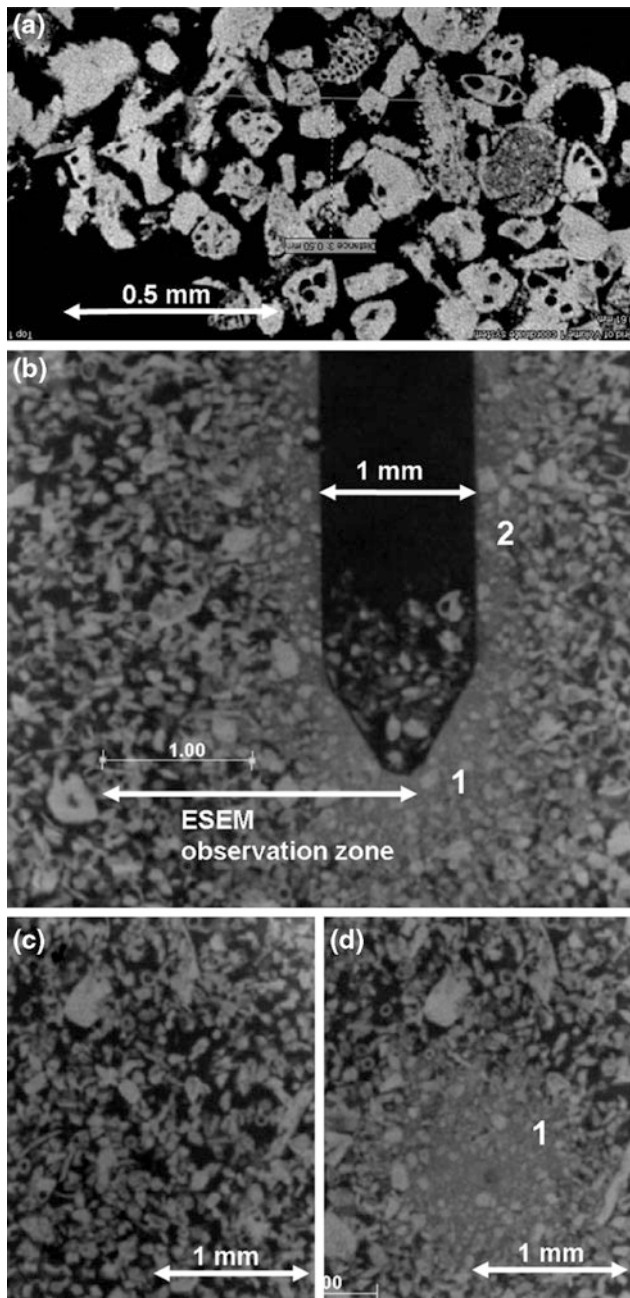


Fig. 11 Micro-CT images of the calcarenite: **a** details of the microstructure showing a large variety of bioclasts (resolution: 0.0018 mm), **b–d** micro-CT scans before and after testing with the modified Eijkelkamp NP in a 10-mm-diameter core (resolution: $0.007 \times 0.007 \times 0.007 \text{ mm}^3$; **b** section parallel to the needle shaft. Zone ahead of the needle tip: **c** before and **d** after needle penetration and retrieval (note the extent of the zone observed with the ESEM). 1, 2 crushed compacted zones (after Ngan-Tillard et al. 2011)

causes some additional damage around the needles. Some of the inverted cone-like cracking is a consequence of this process. Despite some interference caused by the needle, damage zones are observed mainly in the mudstone and tensile fractures are observed mainly in the soapstone.

As for the damaged zone of the mudstone, it occurs as shown in the schematic model in Fig. 8. It is also found that as expected, the damaged zone becomes larger around the tip of the needle. This is because of the large compression stress during the process of penetration. Furthermore, the withdrawal of the needle definitely caused formation of new fractures or extended the previously formed cracks. However, the tangential cracks close after needle withdrawal.

7.6 Influence of Water Content

Soft and weak rocks containing water-absorbing minerals are generally prone to water content variations, which can drastically change their mechanical properties (Aydan and Ulusay 2003, 2013). The value of needle penetration index (NPI) is expected to decrease as rock water content increases, as reported by Aydan (2012). He also examined the correlations among various engineering properties with needle penetration index (NPI) as a function of water content as shown in Fig. 13 for Oya tuff. The relations established for engineering properties of soft rocks as a function of saturation are basically found to be the same for NPI.

Nakamura and Sasaki (1991) reported a linear relationship between porosity of soft and weak rocks, such as the Tertiary mudstone, sandstone, tuff and conglomerate, and dry/saturated strength ratio (Fig. 14). Therefore, it would be possible to estimate the reduction of engineering properties of soft and weak rocks from the variation of needle penetration index with saturation.

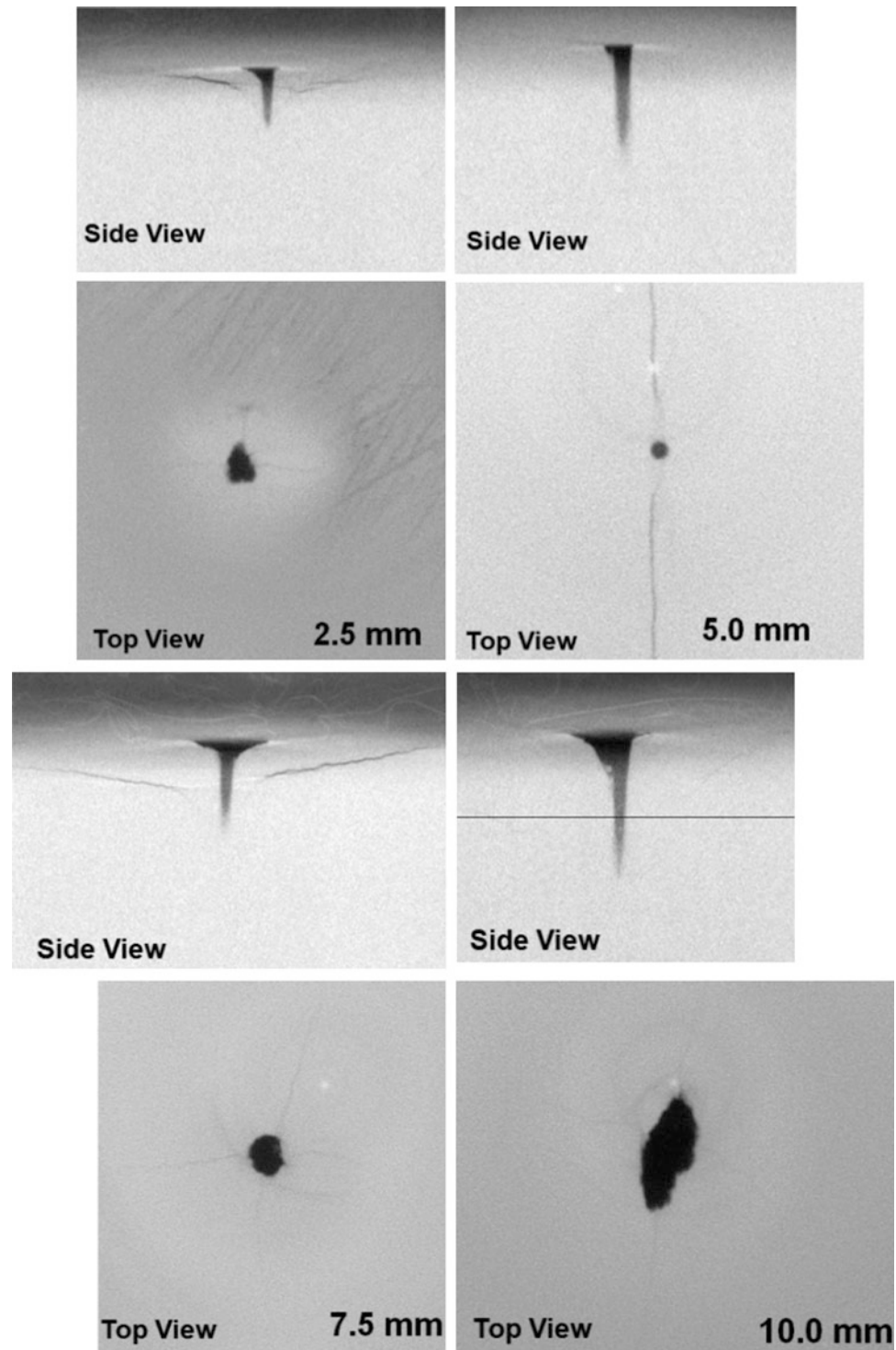
7.7 Variation of NPI with Thawing–Freezing and Drying–Wetting Cycles

It is well known that the properties of rocks deteriorate with the number of thawing–freezing and drying–wetting cycles. The needle penetration index value is expected to decrease with increasing number of these cycles. Figure 15 shows the variation of NPI with the number of drying–wetting cycles for Oya tuff. As noted from the figure, the value of NPI gradually decreases and, therefore, NPI may also be used to assess the degradation of soft rocks subjected to freezing and thawing and drying–wetting cycles.

7.8 Elasto-Plastic Characteristics

Aydan et al. (2008) also explored the use of flat-tip needles to infer the elasto-plastic characteristics of rocks from a single experiment. For this purpose, the diameter of flat-tip

Fig. 12 Some selected images obtained from X-ray micro-CT scanning of soapstone (Saitama and Gifu, Japan) at penetration depths of 2.5, 5.0, 7.5 and 10.0 mm. *Dark zones* correspond to fractures and permanent shape of hole after needle withdrawal. *Dark thin lines* in top views are tensile fractures. Dish-like truncated *dark lines* are induced by tensile stresses (Aydan et al. 2013)



needles varied and their responses investigated. Some theoretical and numerical methods were used to infer the properties of rocks from the responses measured by this special experimental technique. Using a theoretical model it

was possible to determine the yield function constants such as tensile strength, uniaxial compressive strength, friction angle and deformability parameters such as elastic modulus and Poisson's ratio from a single experiment (Fig. 16).

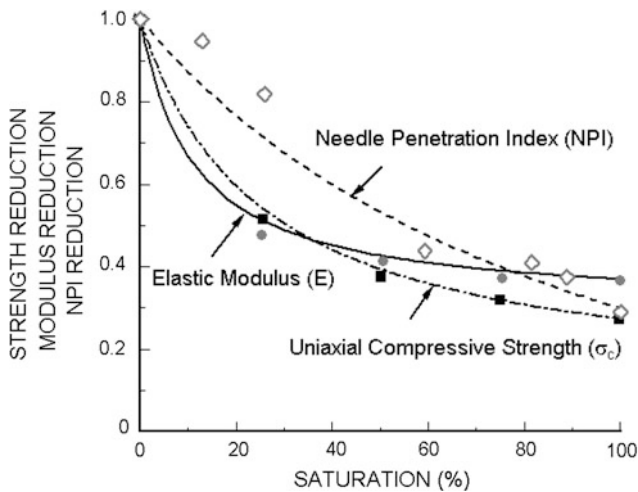


Fig. 13 Variation of normalized elastic modulus (black dots) and uniaxial compressive strength (black squares) and needle penetration index (NPI) (open diamonds) in relation to saturation (Aydan 2012)

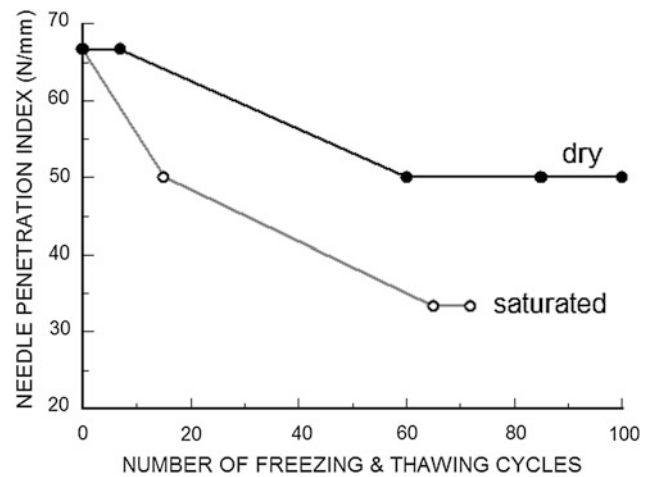


Fig. 15 The variation of NPI with the cycle number of thawing-freezing for Oya tuff (Aydan 2012)

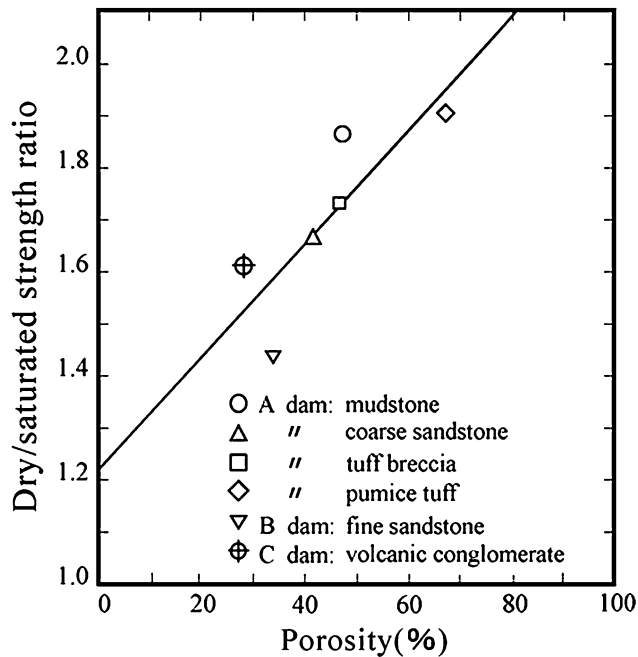


Fig. 14 Relationship between porosity or rocks and dry/saturated NPI strength ratio (Nakamura and Sasaki 1991)

7.9 Time-Dependent Properties

Aydan et al. (2011) devised an experimental setup with a 3-mm flat-tip needle to investigate creep characteristics of rocks. This type of creep experiments is also known as impression creep experiments and are relatively easy to perform; the capacity of loading equipment is relatively small compared to conventional creep experiments. Recently, Aydan et al. (2013) carried out needle penetration

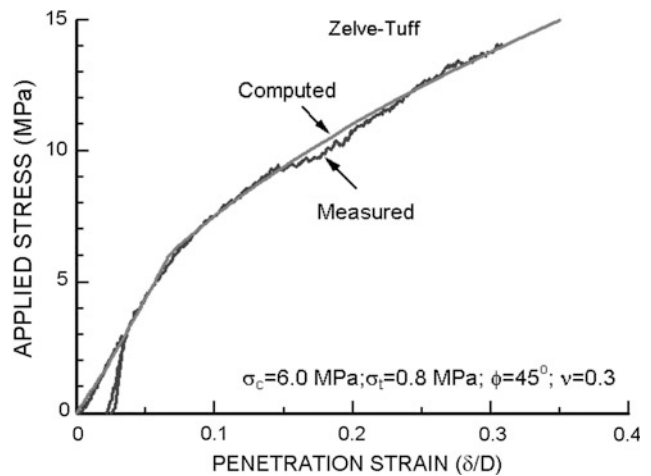


Fig. 16 Comparison of computed and measured nominal strain versus applied pressure responses (δ penetration; D diameter) (from Aydan et al. 2008)

tests to investigate both relaxation and creep characteristics of some soft rocks and found similar results to those from specific relaxation and creep experiments. Such experiments to investigate the time-dependent characteristics may be a further possible application of the needle penetration test. However, it should be noted that, for such purpose, the needle penetrometer has to be equipped with continuous monitoring devices for measuring both the load and penetration depth.

Acknowledgments The authors acknowledge the doctorate student of Ömer Aydan, M. Yagi from the Graduate School of Science and Engineering, Tokai University, for his help on the direct observation of damage in rock samples caused during the needle penetration tests. The authors also acknowledge the three reviewers (Prof. Hanifi Çopur, Dr. Yoshikazu Yamaguchi and Dr. Peter N.W. Verhoef) and the two members of the ISRM Commission on Testing Methods (Dr. Jose Muralha and

Prof. Hasan Gerçek) for their critical reviews and constructive comments that led to significant improvements to the Suggested Method. In addition, the authors sincerely thank Prof. Sergio Fontoura, the member of the Commission, for his kind help throughout the review process of the Suggested Method.

References

- Aydan Ö (2012) The inference of physico-mechanical properties of soft rocks and the evaluation of the effect of water content and weathering on their mechanical properties from needle penetration tests. Symposium of ARMA, Chicago, Paper No. ARMA12-639 (on CD)
- Aydan Ö, Ulusay R (2003) Geotechnical and geo-environmental characteristics of man-made underground structures in Cappadocia, Turkey. *Eng Geol* 69:245–272
- Aydan Ö, Ulusay R (2013) Geomechanical evaluation of Derinkuyu Antique underground City and its implications in geoengineering. *Rock Mech Rock Eng* 46:731–754
- Aydan Ö, Seiki T, Ito T, Ulusay R, Yüzer E (2006) A comparative study on engineering properties of tuffs from Cappadocia of Turkey and Oya of Japan. In: Proceedings of the Symposium on Modern Applications of Engineering Geology, Turkish National Group of Engineering Geology, Denizli, pp 425–433
- Aydan Ö, Watanabe S, Tokashiki N (2008) The inference of mechanical properties of rocks from penetration tests. In: Majidi A, Ghazvinian A (eds) Proceedings of the 5th Asian Rock Mechanics Symposium (ARMS5), Tehran, Iran, vol 1, pp 213–220
- Aydan Ö, Rassouli F, Ito T (2011) Multi-parameter responses of Oya tuff during experiments on its time-dependent characteristics. In: Proceedings of 45th US Rock Mechanics/Geomechanics Symp., San Francisco, ARMA 11-294
- Aydan Ö, Sato A, Yagi M (2013) The inference of geo-mechanical properties of soft rocks and their degradation from needle penetration tests. *Rock Mech Rock Eng*. doi:10.1007/s00603-013-0477-5
- Erguler ZA, Ulusay R (2007) Estimation of uniaxial compressive strength of clay-bearing weak rocks using needle penetration response. In: Proceedings of 11th Congress on Int. Soc. Rock Mechanics, Lisbon, vol 1, pp 265–268
- Hachinohe S, Hiraki N, Suzuki T (1999) Rates of weathering and temporal changes in strength of bedrock of marine terraces in Boso Peninsula, Japan. *Eng Geol* 55:29–43
- ISRM (2007) The complete ISRM suggested methods for rock characterization, testing and monitoring: 1974–2006. In: Ulusay R, Hudson JA (eds) Suggested methods prepared by the commission on testing methods, International Society for Rock Mechanics, Compilation Arranged by the ISRM Turkish National Group, Kozaan Ofset, Ankara, Turkey
- JGS (Japanese Geotechnical Society) (2012) Method for needle penetration test (JGS: 3431-2012). Japanese standards and explanations of geotechnical and geo-environmental investigation methods, no. 1, JGS Publication, Tokyo, pp 426–432 (in Japanese)
- JSCE (Japan Society of Civil Engineers) (1991) A suggested method for investigation and testing of soft rocks. Committee on Rock Mechanics of JSCE, p 124 (in Japanese)
- JSCE-RMC (1980) A suggested method for investigation and testing of soft rocks. In: Japan Society of Civil Engineers, Rock Mechanics Committee, The 4th Sub-committee, Tokyo (in Japanese)
- Nakamura Y, Sasaki Y (1991) Simple test for rock mass classification of dam foundation. *Eng Dams* 53:25–37 (in Japanese)
- Ngan-Tillard DJM, Verwaal W, Maurenbrecher PM, van Paassen LA (2009) Microstructural degradation of Maastrichtian limestones. In: Proceedings of Eurock 2009, engineering in difficult ground conditions soft rocks and Karst Leiden. CRC Press, pp 321–326
- Ngan-Tillard DJM, Verwaal W, Mulder A, Engin HK, Ulusay R (2011) Application of the needle penetration test to a calcarenite, Maastricht, the Netherlands. *Eng Geol* 123:214–224
- Ngan-Tillard DJM, Engin HK, Verwaal W, Mulder A, Ulusay R, Ergüler Z (2012) Evaluation of micro-structural damage caused by needle penetration testing. *Bull Eng Geol Environ* 71(3):487–498
- Okada S, Izumiya Y, Iizuka Y, Horiuchi S (1985) The estimation of soft rock strength around a tunnel by needle penetration test. *J Jpn Soc Soil Mech Found Eng* 33(2):35–38 (in Japanese)
- Park Y, Obara Y, Kang SS (2011) Estimation of uniaxial compressive strength of weak rocks using needle penetrometer. In: Qian Q, Zhou Y (eds) Proceedings of 12th ISRM International Congress on Rock Mechanics, Beijing, pp 795–798
- PWRI (Public Works Research Institute) (1987) Draft manual of simple tests for rock mass classification of dam foundation on soft rocks, Technical note of PWRI, No. 2506, p 31 (in Japanese)
- Takahashi K, Noto K, Yokokawa I (1988) Strength characteristics of Kobe formation in Akashi Strata (No. 1). In: Proceedings of 10th Japan National Conf. on Geotech. Eng., The Japanese Geotechnical Society, pp 1231–1232 (in Japanese)
- Uchida N, Etoh Y, Ono H, Miura N (2004) Strength evaluation of deep mixing soil–cement by needle penetration test. *J Jpn Soc Soil Mech Found Eng* 52(7):23–25 (in Japanese)
- Ulusay R, Erguler ZA (2012) Needle penetration test: evaluation of its performance and possible uses in predicting strength of weak and soft rocks. *Eng Geol* 149–150:47–56
- Yamaguchi Y, Ogawa N, Kawasaki M, Nakamura A (1997) Evaluation of seepage failure response potential of dam foundation with simplified tests. *J Jpn Soc Eng Geol* 38(3):130–144

Part II

Field Testing

ISRM Suggested Method for Rock Fractures Observations Using a Borehole Digital Optical Televiewer

S. J. Li, Xia-Ting Feng, C. Y. Wang, and J. A. Hudson

1 Introduction

Fractures in rock masses are important for the study of a whole range of rock mechanics and rock engineering issues including evaluation of the rock mass geometry, analysis of the Excavation Damaged Zone (EDZ), understanding the rock mass behaviour and response to excavation, numerical analyses, and reinforcement/support design.

A digital borehole camera records a continuous, magnetically orientated digital 360° colour image of the borehole wall, making it possible to directly observe lithological changes in the rock mass and its contained fractures (Paillet et al. 1990; Pusch 1998). Fractures display sinusoidal curves on the flattened image, enabling the strike and dip of the fractures to be determined directly from the images orientated to North (Kamewada et al. 1989; Wang et al. 2002; Williams and Johnson 2004). The technology has been widely applied in geological exploration, especially in petroleum (Maddox 1998; Tague 1999; Palmer and Sparks 1991), mining (Gochioco et al. 2002; Deltombe and Schepers 2000), Glacier (Engelhardt et al. 1978), geotechnical

and environmental engineering (Lau et al. 1987; Miyakawa et al. 2000; Lahti 2004; Cunningham 2004; Cunningham et al. 2004; Schepers et al. 2001; Roberson and Hubbard 2010; Uchita and Harada 1993; Li et al. 2012a). It has also been used to observe crack development and fracture evolution around underground excavations, contributing to the establishment of the EDZ characteristics (Li et al. 2012a, b; Yuji 1983).

There are two main types of digital borehole camera used: the first is a digital optical televiewer, such as the OPTV (Optical Televiewer), OTV (Optical Televiewer) and OBI-40 (Slimhole Optical Televiewer) (Williams and Johnson 2004; Lahti 2004; Cunningham 2004; Cunningham et al. 2004; Schepers et al. 2001; Roberson and Hubbard 2010); the other is a digital panoramic borehole camera, such as the DIPS (Borehole Image Processing System) and DPBCS (Digital Panoramic Borehole Camera System) (Wang et al. 2002; Wang and Law 2005; Williams and Johnson 2004; Uchita and Harada 1993; Li et al. 2012a). The main parameters of these two kinds of camera are listed in Table 1.

The first digital camera was developed as a stand-alone system in 1987 (Williams and Johnson 2004). Since then the tool has gradually become a standard tool. Although there are different types of digital camera system, the basic principle, components and operations of these test systems are almost the same. Thus, this Suggested Method describes the observation of fractures in a rock mass and the identification of EDZ. The apparatus and operating procedure are presented together with the possible ways of reporting the results. The recommendations are supported by case example data.

Please send any written comments on this ISRM Suggested Method to Prof. Resat Ulusay, President of the ISRM Commission on Testing Methods, Hacettepe University, Department of Geological Engineering, 06800 Beytepe, Ankara, Turkey.

Originally published as an article in the journal *Rock Mechanics and Rock Engineering*, 46, S.J. Lia, X.-T. Fenga, C.Y. Wanga, J.A. Hudson, ISRM Suggested Method for Rock Fractures Observations Using a Borehole Digital Optical Televiewer, 635–644, 2013

S. J. Li · X.-T. Feng (✉) · C. Y. Wang
State Key Laboratory of Geomechanics and Geotechnical Engineering, Institute of Rock and Soil Mechanics, Chinese Academy of Sciences, Wuhan, 430071, Hubei, China
e-mail: xtfeng@whrsm.ac.cn; xia.ting.feng@gmail.com

J. A. Hudson
Department of Earth Science and Engineering, Imperial College, London, SW7 2AZ UK

2 Scope

This Suggested Method is intended to directly observe fractures in a rock mass using a digital optical borehole camera through pre-drilled boreholes, with characteristics

Table 1 Technical specifications of representative borehole digital optical camera systems

Name	CCD pixels	Precision (mm)		Probe (mm)		Test velocity (m/min)	Colour (bits)	Borehole diameter (mm)
		Horizontal	Vertical	Diameter	Length			
OPTV	768 × 494	0.331	1.000	52 61	1,630	2.5	24	56–180
OBI 40	795 × 596	0.331	0.375	40	1,700	1.5	16/24	42–180
BIPS	795 × 596	0.331	0.250	42 50	1,540	0.9	16/24	55–180
DPBCS	795 × 596	0.325	0.160	45	350	1.5	16/24	48–91
				72	485			76–180

of the fractures being surveyed in both air and clear fluid-filled boreholes.

Based on the comparison of fractures observed at different times (Li et al. 2012a, b), the evolution characteristics of fractures, including initiation, propagation and closure, occurring in the rock mass are obtainable.

According to in situ observation of the evolution characteristics of fractures subject to excavation or rheological effect (Li et al. 2012a, b), the EDZ in the rock mass is identified based on the new fractures observable via the precision of the digital optical borehole camera.

This Suggested Method can also be adopted to detect possible stress induced damages in the borehole, and hence help to estimate in situ stress orientation.

3 Apparatus

3.1 Basic Components

The apparatus related to this in situ observation of rock mass fractures mainly consists of the probe, depth measuring device, integrating control box, data logger (portable media player or computer), cables, and alternative measuring rods for horizontal or inclined boreholes, as shown in Fig. 1.

3.2 Probe

The probe is the core component for the capture of borehole wall images. Probes in different diameter sizes are available as an option from 40 to 72 mm, and the diameter for test borehole should be in the range 42–180 mm, less than 110 mm for better quality of borehole wall images resulting in more effective identification of fractures and EDZ.

The key component of the digital optical borehole camera is a conical mirror installed in the probe as the reflector. The functions of the conical mirror are as follows.

1. Reflecting the light emitted from the probe light source used to illuminate the borehole wall.

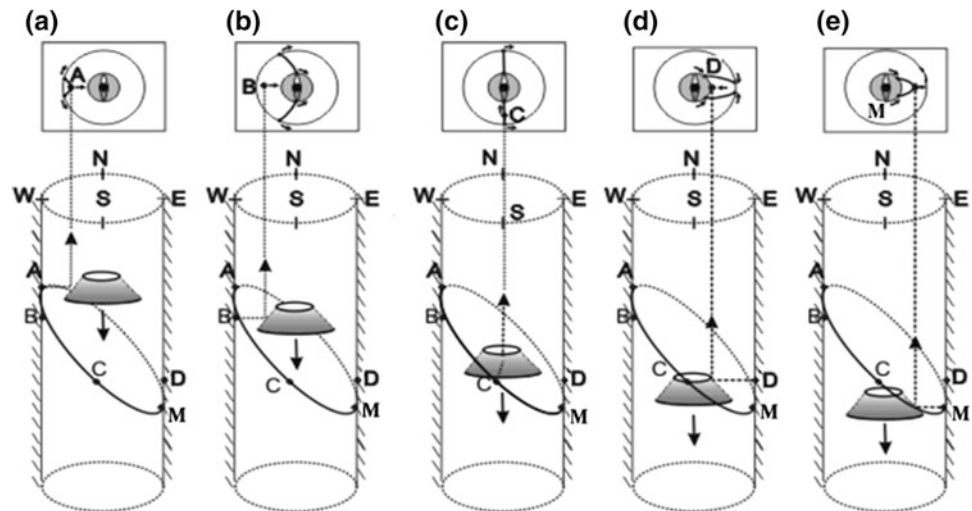


Fig. 1 The basic components of a typical borehole digital optical camera system. Note the photo of the components may change in case of the different borehole digital optical camera system

2. Reflecting the borehole wall information into the probe for the camera records.
3. Note that the radius of both the top and the bottom surfaces of the conical mirror determine the radius of the panoramic image. Also, the deformation mode of the conical mirror determines the changing manner of the borehole wall information in the panoramic image (Wang et al. 2002; Wang and Law 2005).

Fractures evident in the panoramic image are the projections of the fractures on the conical mirror. The borehole wall in the panoramic image is represented as a ring, in which the inner circle is the upper end of the borehole wall and the outer circle is the lower end. The position of a point on the borehole wall as displayed on the ring is related to the azimuth of this point. In the panoramic image, horizontal and vertical fractures display concentric circle and radial lines, respectively, whereas inclined fractures are like conic curves. Figure 2a–e indicate the changing nature of the eastward fracture in the panoramic image. Points A, C and M, shown in Fig. 2, are located on a fracture. Points B and D are located in the west and east directions,

Fig. 2 The changing appearance of the fracture in the panoramic image



respectively. As shown in Fig. 2a, the underside of the conical mirror is over the highest point A of the fracture; point A and parts of the fracture around it are in the outer circle, which appears as a conical curve. Point A is the cusp. Figure 2b shows that point B is in the same position as point A. The conical mirror is in the middle of the fracture, and point C is to the south of the fracture with an orientation of 180° , as shown in Fig. 2c. Figure 2d indicates that the topside of the conical mirror will be over the point D in the borehole wall. As presented in the panoramic image, point D is moving from the outer circle to the edge of the inner circle and ready to leave the ring. Also, as shown in Fig. 2e, the underside of the conical mirror is over the lowest point of the fracture. Point M is at an orientation of 90° , the fracture around which is displayed as a conical shape, and point M is the cusp.

3.3 Depth Measuring Device

There are two ways to test the depth of the probe in the borehole. One method is to record the length of each measuring rod manually, another method is to test the depth using depth measuring equipment installed at the borehole outlet. The data are displayed on the borehole wall images in real time and stored together with the image file. The depth measuring device mainly consists of the test wheel, photoelectric corner encoder and acquisition board. The test wheel is rotated by the friction between the rod/cable and wheel, and the depth measuring device records the depth in electronic pulse counting mode through a photoelectric corner encoder. The distance of the rod/cable moving through the test wheel is converted into an electronic signal by an acquisition board. Then, the depth is calculable according to the rotation angles of the test wheel and the

number of electronic pulses. The information is transferred to the interface board in the integrating control box and superimposed on panoramic images.

3.4 Integrating Control Box and Data Logger

The integrating control box is the power supply for the whole testing system, which controls the collection, input and output of the panoramic video signal and depth pulse signal. It is also used to connect the data logger and real-time image capture interface. The data logger is used for the storage of the borehole wall images and depth information in two different ways. One approach is through obtaining the video file in AVI format using video acquisition equipment and transferring the file into a personal computer for image process. In this case, portable media player is available, it can also be used as a video monitor. Another approach is connecting the personal computer through an interface in the integrating control box and obtaining the flattened borehole wall images directly in a specialized software platform.

3.5 Cables and Measuring Rods

The boreholes for this Suggested Method can be divided into three types namely vertical, horizontal and inclined boreholes. Cables are essential for signal transmission. For the in situ measurements of vertical or sub-vertical (inclination angle 75° – 90°) boreholes, some special carrying cables should be required to undertake the weight of probe and groundwater pressure in some deep boreholes. Whereas measuring rods should be taken for horizontal and inclined borehole with the inclination angle 0° – 75° .

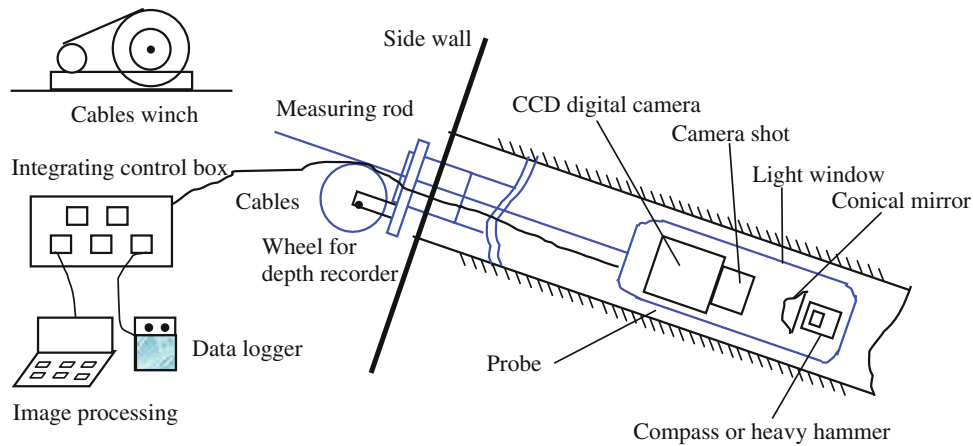


Fig. 3 Sketch of the installation and connection system for the borehole digital optical camera in situ testing system

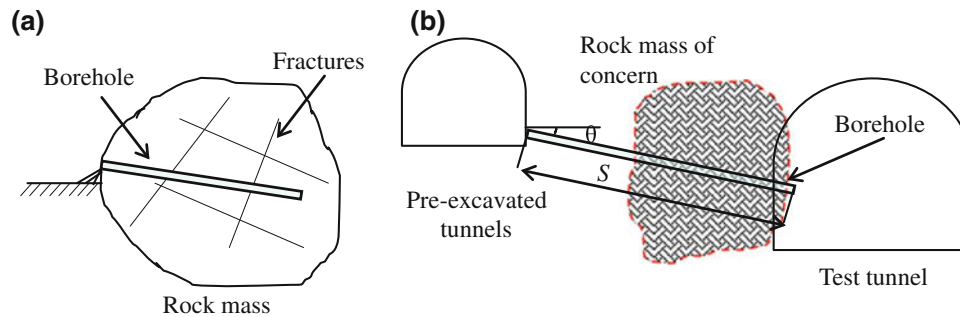


Fig. 4 Examples of borehole layouts for measurements of rock mass fractures. **a** Borehole configured directly into the rock mass in real time at any position and angle. **b** Borehole layouts determined by the pre-installed method

The installation and connection diagram for all the components of a borehole digital optical camera system are shown in Fig. 3.

3.6 Drilling Equipment

In order to conduct in situ borehole measurements of rock mass fractures, appropriate drilling equipment is required for the borehole drilling whatever with core or not. Any equipment capable of producing a stable hole to the required test depth and diameter may be used. Commonly, the drilling rig should have the properties of low weight, easy handling and vertical and inclined borehole double use.

In general, both percussive and rotative drilling methods are acceptable. However, the borehole wall should be well flushed by clean water when percussive drilling adopted. It is suggested that lining would be required in some circumstances. For instance, when the rock top is under a soil/decomposed rock layer.

4 Procedure

4.1 Layout of Boreholes

The layout of boreholes depends on the test goals concerned. Commonly, there are two approaches for borehole layout.

1. When the test objective is the understanding of rock mass structure, boreholes can be configured directly to the rock mass in real time at any position and angle, as shown in Fig. 4a.
2. When the test goal is to investigate the fracture evolution or zonal disintegration of rock mass (Qian et al. 2009), the boreholes should be pre-drilled before excavation of tunnels (Fig. 4b), so as to observe the entire process of fracture initiation, propagation and closure before, during and after tunnel construction.

In an underground construction project, taken as the example and as shown in Fig. 4b, borehole is drilled from

the pre-excavated underground tunnels to the test object. In order to fully reveal the characteristics of fractures and their evolutionary processes, the borehole diameter for fracture observation is suggested to be in the range 42–110 mm in view of the performance of the CCD digital camera and obtainable quality of borehole images. The length (S) and dip (θ) of the borehole are determined by the distance and spatial location between the test site and the object to be observed. Nevertheless, it is important that the length of borehole must pass through the rock mass around the test object. For example, the borehole needs to pass through the side wall of a test tunnel to be excavated.

4.2 Drilling and Inspection

Percussive and rotative drilling methods are acceptable as mentioned above. It is recommended that rock cores should be obtained during rotative drilling, and so diamond bit drilling should be adopted. Synthetic comparison of rock cores and images of borehole wall will lead to better understanding of geological conditions and rock mass fractures. The choices of borehole length and orientation are made taking into account the position of the object to be tested.

It is recommended that the drilling rig should be kept steady with the drilling speed less than 600 r/min, so that the borehole wall can be maintained smooth and straight without ridges or steps from the tunnels to the bottom of the borehole, as far as possible to make it easy for the probe's movement.

On the basis of rock cores, geological recording should be carried out during drilling, and the positions, orientations and apertures of geological discontinuities observed in the borehole should be estimated.

All of the boreholes to be observed should be flushed to remove debris or fractured rocks after drilling. It is also strongly recommended that the boreholes should be rinsed using clean water. However, in case of some severely weak or fractured stratum, drillers use bentonite or casing to prevent the collapse of the hole. The borehole wall can not be effectively observed by an optical camera. In this case, clean water should be used to flush some portions which the test mainly concerned and also the casing should be pulled out. If the borehole collapses seriously under this condition leading to the probe incapable of running through, drill pipes may be used to cope with the debris or fractured rocks. If all the remedial measures can not work, the borehole has to be scrapped and a new one should be drilled close to this position.

4.3 Observation of Rock Mass Fractures

- (a) Analyse the borehole drill records and associated histograms. If rotative drilling method is employed and rock cores are available, preliminarily analyse the characteristics of the stratum, geological defects and groundwater.
- (b) Flatten the test site to place all the monitoring facilities and relevant subsidiary equipment, connect water pump and water pipe, clean test boreholes to remove dust, mud and drilling waste slag.
- (c) Set and connect the test equipment, install and fix the depth measuring device near the borehole orifice, install the push rod through the depth measuring wheel and adjust it to the centre of the borehole orifice.
- (d) Choose a suitable probe with an appropriate diameter (according to the borehole diameter), put the probe into the borehole orifice and connect with the push rod tightly.
- (e) Connect the power cable, panorama probe signal cable, depth pulse signal cable, video signal cable and computer interface successively.
- (f) Connect the power, press the light switch and the zero depth switch.
- (g) Turn on the data logging and start to monitor and record depth and videos.
- (h) Let the probe run in the borehole slowly from top to bottom under the action of measuring rods or cables (length of each rod is 1.0 or 1.5 m), note that the advancing speed of the probe should be uniform and less than 1.5 m/min to obtain clear images.
- (i) According to observations of the borehole from the camera, write down the depth of probe advance in the borehole manually every 1.0 or 1.5 m and record the depth on the data logging monitoring screen at the same time. In brief, describe factors such as groundwater, rock mass integrity and fractures from the monitoring video in real time.
- (j) When the probe reaches the bottom of the borehole, the test is completed. Turn off the camera and the control box power, and save the video files. Disassemble the push rods and pull the probe out of the borehole slowly.
- (k) Check the state of the probe, clean and pack it in a dedicated box, and leave the test site after checking other equipment such as depth measuring device, integrating control box, computer, pump, and so on.

Based on the captured digital images stored in video file format, the digital image processing will be carried out in specially developed software so that fracture images in a

Fig. 5 Sketch diagram of the calculation co-ordinates of fracture occurrence

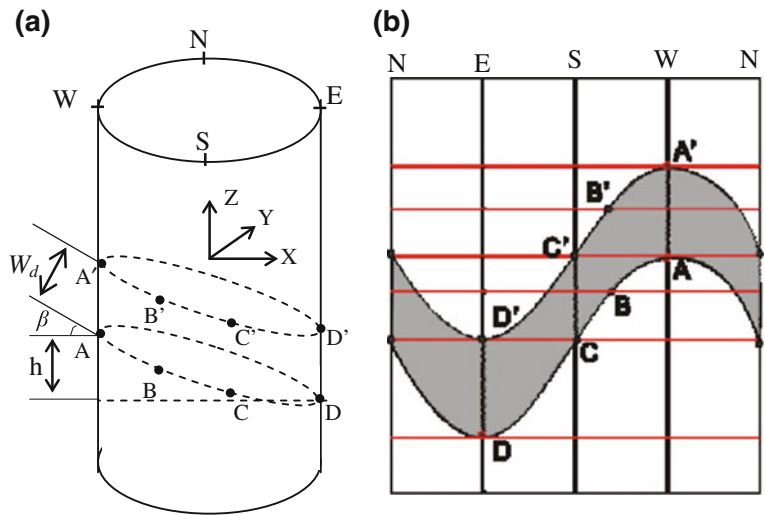
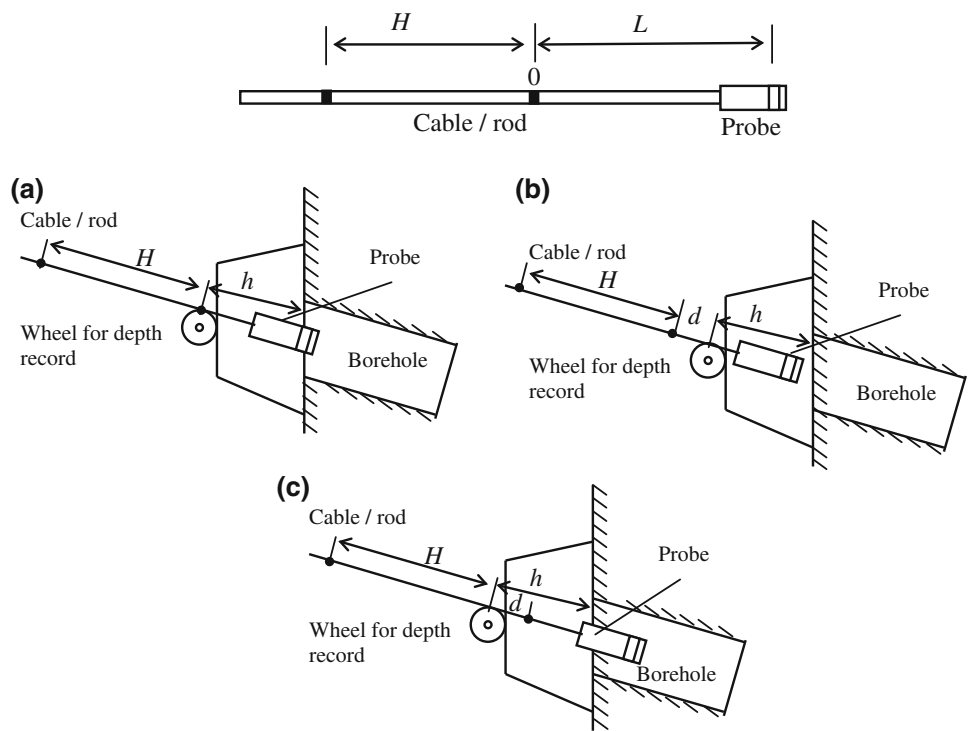


Fig. 6 The relation between the recorded depth by cumulative number of cable or measuring rods and the actual depth (a $L = h$, b $L > h$, c $L < h$)



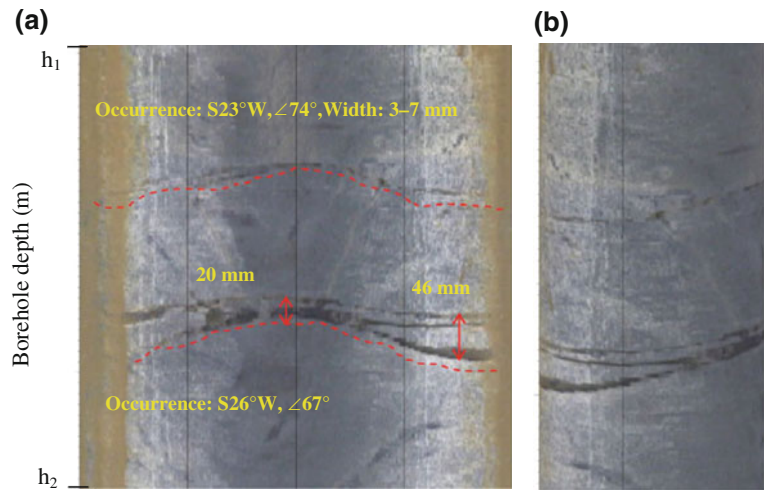
flattened mode and virtual core can be obtained. Further analysis involves rock lithology, fracture distribution, position, occurrence and width, evolution characteristics when the objective is to characterize the EDZ compared to construction progress.

4.4 Identification of EDZ

At present, there are several conceptions on the EDZ definition according to the project type, testing methods and research goals. Among them, the common content of EDZ is the region where the rock properties and conditions have

changed due to fracturing, stress redistribution and desaturation (Egger 1989; Martino and Chandler 2004). Many indirect methods have been taken to determine the EDZ of rock mass by measuring the decrease of acoustic velocity, change of hydraulic transport properties, etc. It indicates that direct observation of fracture changes is also an effective method which can reflect the permanent change of rock mass. The EDZ can be identified by directly observing fracture modifications via the precision of the borehole digital optical camera. The maximum resolution of the current borehole digital optical camera is 0.1–0.2 mm, while it will be continuously improved as the development of the CCD digital camera technology.

Fig. 7 Images of the borehole wall shown in **a** flattened pattern, **b** virtual core. (The *dashed lines* indicate the traces of the fractures; the *arrows* indicate the widths of fractures)



For this purpose, a series of flattened images of borehole wall observed in different time by borehole digital optical camera are needed. Evolutionary characteristics of width, length and occurrence of new and pre-existing fractures are to be analyzed. The EDZ of rock mass is identified by comparison of these flattened images observed in different time. The EDZ is determined to be the zone where new fractures are detected.

5 Calculations

5.1 Calculation of the Occurrence and Width of the Observed Rock Mass Fractures

When a complete fracture is at an angle to the borehole, the projection is displayed as a sinusoidal curve on the flattened image, as shown in Fig. 5.

It is assumed that the Z axis is the central axis of the borehole with the positive direction vertically upwards, and the plane fixed by axes X and Y is perpendicular to axis Z with the positive direction to the East and North, respectively (Fig. 5a). The calculation of the orientation of the rock mass fracture is described as follows.

Taking three non-collinear points A , C and D on a fracture shown in the flattened pattern, two vectors \bar{V}_1 and \bar{V}_2 in this plane can be obtained and described as:

$$\bar{V}_1 = \overline{AC}, \bar{V}_2 = \overline{AD} \quad (1)$$

The normal vector of this plane can be described as:

$$\bar{N} = \bar{V}_1 \times \bar{V}_2 \quad (2)$$

In order to represent the unit normal vector, Eq. (2) can be transformed as:

$$\bar{N}_u = \bar{N} / \|\bar{N}\| \quad (3)$$

If the Z -component of the unit normal vector is less than zero, the opposite vector $\bar{N}_0 = \{X_0, Y_0, Z_0\}$ will be expressed as:

$$\bar{N}_0 = -\bar{N}_u \quad (4)$$

So, the dip angle β of the fracture can be calculated as:

$$\beta = \cos^{-1} Z_0 \quad (5)$$

It can also be expressed as:

$$\beta = \tan^{-1}(h/d) \quad (6)$$

where h is the vertical distance of points A and D , d is the diameter of test borehole.

Assuming that $\bar{N}_p = \{X_p, Y_p\}$ is the projection of the unit normal vector \bar{N}_0 on the XY plane, then the dip azimuth α of the fracture can be calculated as:

$$\alpha = \begin{cases} 90^\circ - \tan^{-1} Y_p/X_p & \text{when } X_p > 0 \\ 90^\circ & \text{when } X_p = 0 \text{ and } Y_p > 0 \\ 270^\circ - \tan^{-1} Y_p/X_p & \text{when } X_p < 0 \\ 270^\circ & \text{when } X_p = 0 \text{ and } Y_p < 0 \end{cases} \quad (7)$$

According to the relationship between dip azimuth and orientation, the orientation of the fracture can be calculated as:

$$\theta = \begin{cases} \alpha + 90^\circ & \text{when } \alpha < 90^\circ \\ \alpha - 90^\circ & \text{when } \alpha \geq 90^\circ \end{cases} \quad (8)$$

The width of the fracture can be obtained by measuring the spatial distance of any relevant two points A and A' located on opposite sides of the fracture, which is described as:

$$W_d = \sqrt{(X_A - X_{A'})^2 + (Y_A - Y_{A'})^2 + (Z_A - Z_{A'})^2} \cdot \cos \beta \quad (9)$$

Fig. 8 Comparison of borehole wall images for fracture evolution studies: **a** original rock mass, **b** new fractures that have appeared due to time effect or excavation of rock mass. (*Dashed lines* are the traces of the fractures)

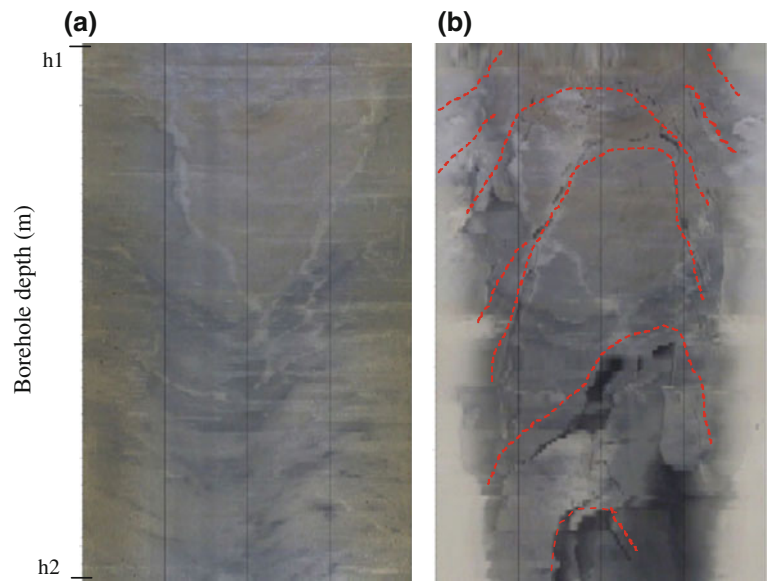
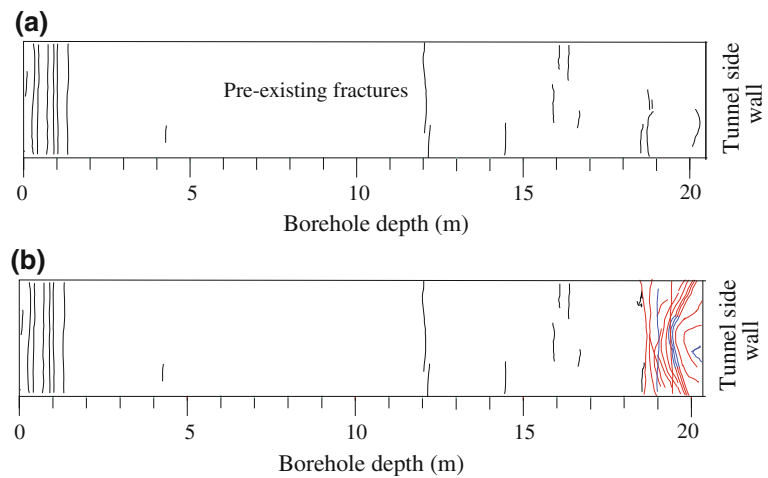


Fig. 9 Sketch plan of fracture distribution and evolution measured at different time of excavation steps: **a** pre-existing fractures, **b** abundant new fractures at another time due to time effect or excavation disturbance



5.2 Calculation of the Ratio Coefficient Between the Actual Depth and the Test Depth

Each image records a test depth (S_t), which is determined by a depth measuring wheel through an electronic pulse counting mode. Due to the friction of the measuring wheel and the sliding of the push rod, S_t is a little different from the actual probe depth (S_p) in the borehole. Therefore, it is necessary to obtain the ratio coefficient R between actual depth and test depth which is an important factor in the digital image processing software. Based on the proportional coefficient, the test depths of each segmental image can be calibrated.

As shown in Fig. 6, it is assumed that the distance between every two points of cable depth marks or length of

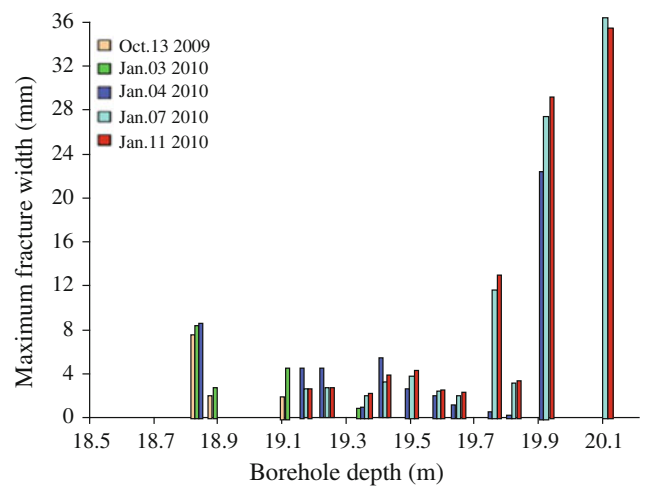


Fig. 10 Change of fracture width over time, as observed at different times

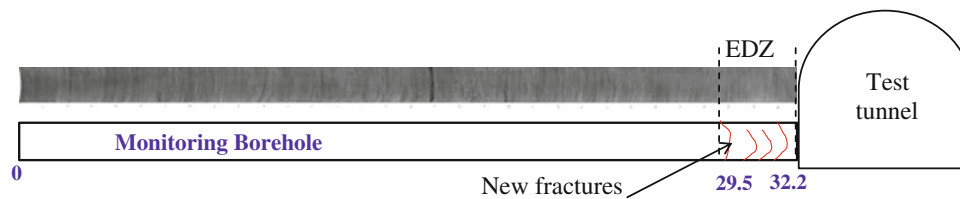


Fig. 11 Schematic diagram of the EDZ assessment based on the distribution of new fractures

each measuring rod is H , the distance from the zero point to the transparent window of the probe is L , the distance from the depth testing wheel and cable or testing rod tangent point to the orifice of the borehole is h , and the advancing distance of the probe is recorded as S .

$$\text{If } L = h, \text{ then } S_p = S.$$

$$\text{If } L > h, \text{ then } S_p = S - (h + d + L).$$

$$\text{If } L < h, \text{ then } S_p = S + (L + d - h).$$

The ratio coefficient R between the actual depth and the test depth is expressed as:

$$R = \frac{S_p^i - S_p^{i-1}}{S_t^i - S_t^{i-1}} \quad (10)$$

6 Reporting of Results

The report should include the following general information.

- A description of the test site and lithology.
- Description of the condition of groundwater in boreholes if there is groundwater in it, the depth of groundwater from the surface in borehole is needed to be given.
- Description of the lining located at some portion of the borehole when weak or fractured stratum exists.
- The location, diameter, length, direction and dip angle of the boreholes.
- The testing equipment, diameter of probe, cable depth marks and length of unique measuring rod.
- Testing date, total testing time of each borehole and depth records of borehole segments.

The report should also include the following detailed information of rock mass fractures:

- 360° RGB orientated images of the borehole wall for the whole length, shown in the flattened pattern and virtual core, as shown in Fig. 7.
- Statistics of the calculation results for fracture occurrence, location, width and properties.

- Description of construction scheme, excavation progress and geological sketching if EDZ identification is to be analyzed.
- Comparison of the borehole wall images with fracture changes due to the time effect or construction disturbance, including the evolution of fracture initiation, propagation and closure, as shown in Fig. 8.
- Sketch plan of fracture evolution and distribution displayed on flattened sides measured at different time or excavation steps, as shown in Fig. 9.
- Evolutionary characteristics of fracture width at different test times or excavation stage, as shown in Fig. 10.
- Identification of the EDZ according to the method previously mentioned in procedure. For the observation of the rock mass around tunnels, the results show the determination of the EDZ with new fractures being observed at the maximum resolution 0.1–0.2 mm of a borehole digital optical camera, as shown in Fig. 11.

References

- Cunningham KJ (2004) Application of ground-penetrating radar, digital optical borehole images, and cores for characterization of porosity hydraulic conductivity and paleokarst in the Biscayne aquifer, southeastern Florida, USA. *J Appl Geophys* 55:61–76
- Cunningham KJ, Carlson JI, Hurley NF (2004) New method for quantification of vuggy porosity from digital optical borehole images as applied to the karstic Pleistocene limestone of the Biscayne aquifer, southeastern Florida. *J Appl Geophys* 55(1–2):77–90
- Deltombe JL, Schepers R (2000) Combined processing of BHTV travel time and amplitude images. In: Proceedings from the seventh international symposium on minerals and geotechnical logging, Golden, Colorado, October 24–26, pp 1–13
- Egger P (1989) Study of excavation induced rock damage at the Grimsel underground rock laboratory. *Nucl Eng Ng Des* 116:11–19
- Engelhardt HF, Harrison WD, Kamb B (1978) Basal sliding and conditions at the glacier bed as revealed by bore-hole photography. *J Glaciol* 20(84):469–508
- Gochioco LM, Magill C, Marks F (2002) The borehole camera: an investigative geophysical tool applied to engineering, environmental and mining challenges. *Lead Edge Soc Explor Geophys* 21(5):474–477
- Kamewada S, Endo T, Kokubu H, Nishigaki Y (1989) The device and features of BIP system [A]. In: The 21st symposium on rock mechanics proceedings, committee on rock mechanics [C]. [sl.], Japanese Society of Civil Engineers, pp 196–200

- Lahti M (2004) Digital borehole imaging of the boreholes KR24 upper part and PH1 at Olkiluoto, Posiva Oy. Working Report 2004-28, p 21
- Lau JSO, Auger LF, Bisson JG (1987) Subsurface fracture surveys using a borehole television camera and acoustic televiewer. *Can Geotech J* 24:499–508
- Li SJ, Feng X-T, Li ZH, Chen BR, Zhang CQ, Zhou H (2012a) In situ monitoring of rockburst nucleation and evolution in the deeply buried tunnels of Jinping II hydropower station. *Eng Geol* 137–138:85–96
- Li SJ, Feng XT, Li ZH, Zhang CQ, Chen BR (2012b) Evolution of fractures in the excavation damaged zone of a deeply buried tunnel during TBM construction. *Int J Rock Mech Min Sci* 55(10):125–138
- Maddox SD (1998) Application of downhole video technology to multilateral well completions. *J Petrol Tech* 50(6):34–36
- Martino JB, Chandler NA (2004) Excavation-induced damage studies at the underground research laboratory. *Int J Rock Mech Min Sci* 41(8):1413–1416
- Miyakawa K, Tanaka K, Hirata Y, Kanauchi M (2000) Detection of hydraulic pathways in fractured rock masses and estimation of conductivity by a newly developed TV equipped flowmeter. *Eng Geol* 56(1–2):19–27
- Paillet FL, Barton C, Luthi S, Rambow F, Zemanek JR (1990) Borehole imaging and its application in well logging—an overview. *Borehole Imaging*, Society of Professional Well Log Analysts, Inc., 6001 Gulf Freeway, Suite C129, Reprint Series, Houston, Texas, pp 3–23
- Palmer ID, Sparks DP (1991) Measurement of induced fractures by downhole television camera in coalbeds of the Black Warrior basin. *J Petrol Tech* 43(3):270–275
- Pusch R (1998) Practical visualization of rock structure. *Eng Geol* 49(3–4):231–236
- Qian QH, Zhou XP, Yang HQ et al (2009) Zonal disintegration of surrounding rock mass around the diversion tunnels in Jinping II Hydropower Station, Southwestern China. *Theor Appl Fract Mec* 51:129–138
- Roberson S, Hubbard B (2010) Application of borehole optical televiewing to investigating the 3-D structure of glaciers: implications for the formation of longitudinal debris ridges, midre Lovénbreen, Svalbard. *J Glaciol* 56(195):143–156
- Schepers R, Rafat G, Gelbke C, Lehmann B (2001) Application of borehole logging, core imaging and tomography to geotechnical exploration. *Int J Rock Mech Min Sci* 38(6):867–876
- Tague JR (1999) Downhole video optimizes scale removal program. *Petrol Eng Int* 72(7):27–32
- Uchita Y, Harada T (1993) Behavior of discontinuous rock during large underground cavern excavation. In: *Proceedings of the International Symposium on Assessment and Prevention of Failure Phenomena in Rock Engineering*, Istanbul, Turkey, pp 807–816
- Wang CY, Law KT (2005) Review of borehole camera technology. *Chin J Rock Mech Engng* 24(19):3440–3448 (in Chinese)
- Wang CY, Law KT, Sheng Q, Ge XR (2002) Borehole camera technology and its application in the Three Gorges project. In: *Proceedings of the 55th Canadian geotechnical and 3rd joint IAHCNC and CGS groundwater specialty conferences*, Niagara Falls, Ontario, pp 601–608
- Williams JH, Johnson CD (2004) Acoustic and optical borehole-wall imaging for fractured-rock aquifer studies. *J Appl Geophys* 55(1–2):151–159
- Yuji K (1983) Observation of crack development around an underground rock chamber by borehole television system. *Rock Mech and Rock Eng* 16(2):133–142

ISRM Suggested Method for Measuring Rock Mass Displacement Using a Sliding Micrometer

S. J. Li, Xia-Ting Feng, and J. A. Hudson

1 Introduction

Displacement is the direct mechanical response of rock masses subjected to external disturbances such as excavation, blasting and vibration, and the other efforts. The measurement of displacement provides an important basis for understanding the rock mass behavior and evaluating the effectiveness of reinforcement to be used in the excavation.

There are many instruments available for geomechanical displacement measurement in the boreholes and they can be considered within two categories. The first is pointwise observation in which a displacement component is measured at isolated points within the rock mass. The multiple point borehole extensometer is a typical instrument for this purpose (Hansmire 1978). The other is linewise observation, the concept making it possible for the complete distribution of displacement values to be evaluated along a measuring line, e.g. along a borehole (Kovari and Amstad 1983). In order to perform linewise observation, inclinometer and sliding micrometers were developed. The borehole

inclinometer was suggested by Franklin and Benet for monitoring rock movements (ISRM 2007), and a horizontal borehole inclinometer had been developed by Hudson and Morgan (1974). Since the sliding micrometer was developed by Kovari and his co-workers in the 1970s (Kovari et al. 1979), it has been widely employed in site investigation for slopes, foundations, dams, tunnels, caverns, etc. (Kovari and Amstad 1982; Kovari and Peter 1983; Li and Huang 2001; Qin et al. 2008; Dong et al. 2006).

This Suggested Method describes the measurements of rock mass displacement using a sliding micrometer and the associated determination of the Excavation disturbed Zone (EdZ) induced by excavation in hard rock, and as a result of time dependency. The term EdZ is used here to encompass both the disturbed and damaged zones.

The apparatus and operating procedure are described together with the data recording and processing. There is an explanation of the possible ways of presenting and interpreting the results. The recommendations are supported by case example data.

2 Scope

The purpose of this Suggested Method is to describe a method of measuring rock mass displacement occurring as the result of surface and underground excavations, movement of natural and artificial slopes and foundation loading. The method can also be applied to measure settlement in earth or rock dams, and dam abutments or any other application where the main displacement follows the axial direction of the borehole.

The sliding micrometer enables displacement profiles to be determined with a high level of accuracy and precision up to ± 0.002 mm/m. The axial displacement at consecutive points along a borehole can be measured on a base length of 1.0 m.

The instrument is not suitable for those measurements with large displacement, the latest developed sliding micrometer has a maximum measuring range of 25 mm/m.

Please send any written comments on this ISRM Suggested Method to Prof. Resat Ulusay, President of the ISRM Commission on Testing Methods, Hacettepe University, Department of Geological Engineering, 06800 Beytepe, Ankara, Turkey.

Originally published as an article in the journal *Rock Mechanics and Rock Engineering*, 46, S. J. Li, Xia-Ting Feng, J. A. Hudson, ISRM Suggested Method for Measuring Rock Mass Displacement Using a Sliding Micrometer, 645–653, 2013.

S. J. Li · X.-T. Feng (✉)
State Key Laboratory of Geomechanics and Geotechnical Engineering, Institute of Rock and Soil Mechanics, Chinese Academy of Sciences, Wuhan, 430071 Hubei, China
e-mail: xtfeng@whrsm.ac.cn; xia.ting.feng@gmail.com

J. A. Hudson
Department of Earth Science and Engineering, Imperial College, London, SW7 2AZ, UK

According to the comparisons of displacement profiles measured at different times and, if required, the EdZ in the hard rock can be identified based on identifying the effective inflection point in the displacement profile via the precision of the sliding micrometer.

3 Apparatus

3.1 Components and Measuring Principle

Eight main components comprise a sliding micrometer: probe, probe guide, rod, measuring tube, measuring mark, cable, data controller and calibration device (Fig. 1). The basic principles of this instrument are described as follows.

Before the start of an in situ measurement of the axial displacement profile in the rock mass concerned, plastic tubes are introduced into a clean pre-drilled borehole and cemented in place (Fig. 2a). The diameter of the pre-drilled borehole should be larger than 110 mm. The measuring tubes are fitted with measuring marks at constant intervals of 1.0 m. As a result of firmly cementing the measuring marks to the rock, the displacement of the surrounding rock mass is transmitted to the measuring marks.

The measuring marks are constructed such that a probe, also of 1.0 m gauge length, may be placed in the same position at every time, allowing reproducible measurements to be made. The actual measurement is conducted after carrying out the initial zero measurement. The measurements are then carried out by sliding the probe along the tubes (Fig. 2b), inserting it stepwise into the measuring positions at 1.0 m intervals until all the sections defined by the measuring marks have been measured, as shown in Fig. 2c. If there is a difference between two readings taken at different times, such as different measuring date or excavation stages, this indicates that the relative displacements of adjacent reference points at a constant distance from each other can be measured. Accordingly, the differential displacements are obtained from the values of the zero measurement and the successive measurements, the integrated displacements can then be calculated by summing these values and possible measuring errors.

3.2 Probe

The probe uses the ball-and-cone positioning principle in the measuring marks of the measuring tube. The spherically shaped heads on the two sides of the probe and the circular cone shaped measuring marks ensure precise positioning of the 1 m long probe during measurement. By means of high precision sensors and regular calibration before and after each series of measurements, a high accuracy of measurement and long-term stability is achieved.

At present, the ideal maximum accuracy of measurement of the sliding micrometer is ± 0.002 mm/m, and the maximum measuring range is 25 mm/m. The practical measuring accuracy might be influenced by installation and testing procedure.

3.3 Probe Guide

The probe guide serves to rotate the probe within the measuring tubes. For this purpose, it has a swivel joint to rotate the probe from the sliding position to the measuring position. The probe guide is inserted above the probe as the first guide rod. It is usually made of flexible polyamide rod with a 45° swivel joint, the base length being 1.0 m.

3.4 Measuring Tube and Mark

The measuring line for the sliding micrometer is given by the measuring tubes that are installed in the borehole with a minimum diameter of 110 mm. Each individual measuring tube consists of a 1.0 m long connecting tube (aluminum or hard PVC) and the measuring marks with the conically shaped precision measuring stop. Measuring marks in the form of rings are telescopic couplings and are fixed at distances of 1.0 m apart in the tube by glueing. The probe measures the displacements at the measuring marks, which are firmly connected to the rock by means of cement.

3.5 LVDT

The linear variable differential transformer (LVDT) is an electrometric device that produces an electrical voltage proportional to the displacement of a movable magnetic core. It is often composed of a coil winding assembly, a cylindrical case, and a rod shaped magnetic core. When the probe is tensioned tightly between two close measuring marks through connected rods by manual, the LVDT will be activated and measurement data will be transferred to the data controller.

3.6 Data Controller

The data controller is connected to the measuring head at top of the probe by a cable. During the entire process of field measurement, the successive measuring information, consisting of both temperature and displacement data for each measuring unit, is directly transferred to the data controller. Then the data are displayed on a LED screen, and can be recorded manually or directly transferred to a personal computer via an interface.

Fig. 1 The components of a sliding micrometer

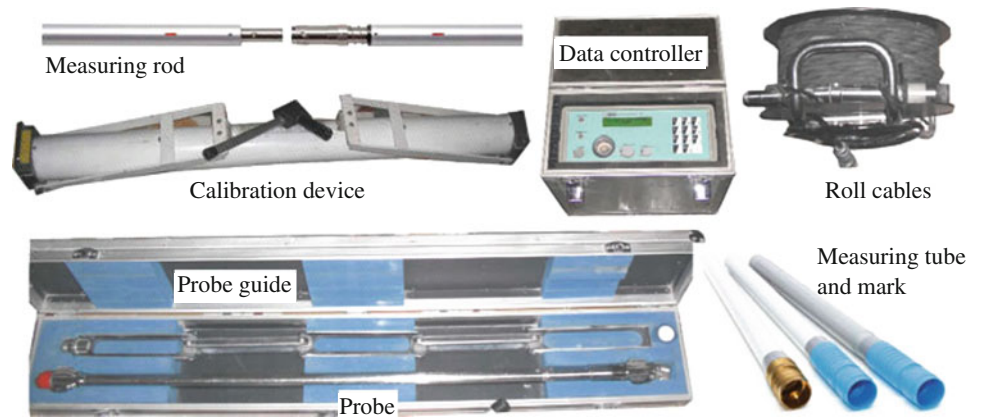
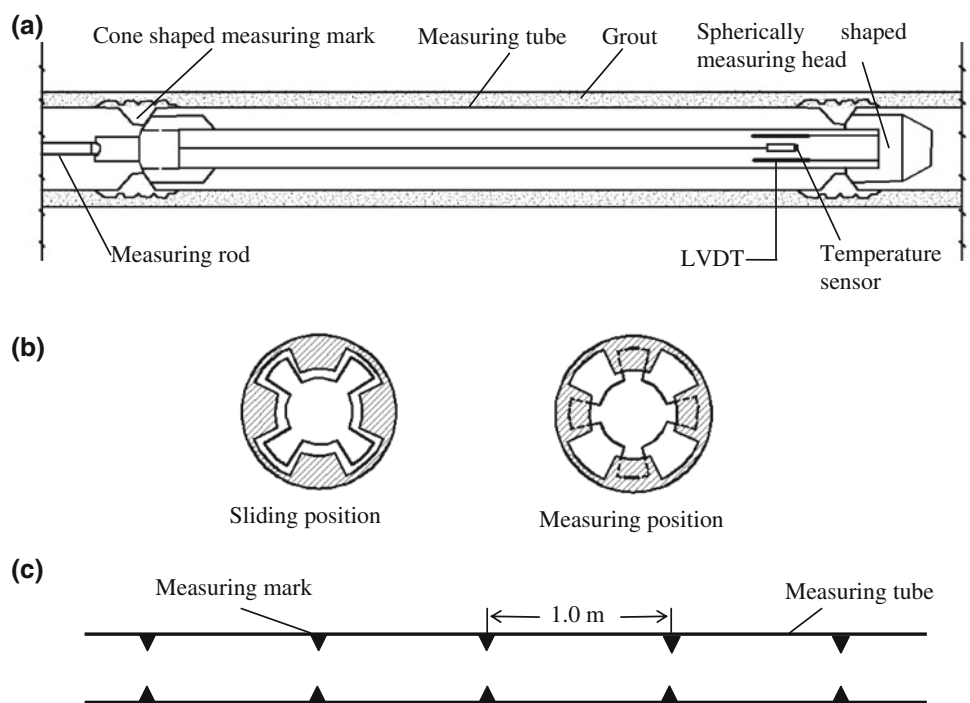


Fig. 2 Principle of the sliding micrometer: **a** schematic view of the sliding micrometer, **b** sliding and measuring positions of the instrument head, **c** interval between the measuring marks



3.7 Calibration Device

The sliding micrometer has a calibration device which serves to calibrate the zero reading and to check the calibration factor in the axis direction of the probes. The telescopic rod and separate temperature measuring device are the two essential accessories for this calibration device to be successfully used. The calibration of the probe should be carried out before and after each series of measurements. In this way, stable measuring accuracy of ± 0.002 mm/m and continuity are ensured.

3.8 Drilling and Inspection Equipment

Drilling equipment is, of course, essential for producing a stable borehole of the required test depth and diameter. In view of the variety of possible spatial configurations of test boreholes, the equipment must be capable of drilling at different trend and plunge angles. Percussion drilling equipment is usually present on site, but core drilling should be used unless it is unavailable.

The borehole axis should be maintained a straight line, the ratio of the designed borehole depth versus final

deviation distance should be less than 0.01. So that a special deviation measurement should be carried out to evaluation the borehole orientation and position at very 3–5 m of drilling footage. Measures should be taken to control the deviation during drilling. However, if there are some unexpected conditions leading to inevitable deviations, the borehole should be scrapped and another new borehole near the position is necessary. A borehole camera should be used to inspect the borehole condition and investigate the characteristics of the encountered joints and faults and any damage induced by drilling, particularly if the rock cores are significantly fractured with over 30 fractures per meter or when no core is retrieved in extreme cases due to poor geological conditions.

4 Procedure

4.1 Preparatory Investigations

The site, project scale and type, rock properties, and possible excavation methods should be considered in detail to specify the performance requirements of the displacement measuring equipment to be used.

The displacement measurements made before, during and after construction are all valuable, and recording of the geological conditions and construction events in the vicinity of the borehole measurements is essential to support the proper interpretation of the field data.

The location, length, and number of boreholes should be selected on the basis of a thorough review of both the geotechnical engineering and construction conditions, such as rock mass structure, rock properties, and excavation methods, taking into account the anticipated directions and magnitudes of potential rock movements by predictive numerical simulations and engineering analogies.

4.2 Layout of Boreholes

The layout of boreholes will depend on the purposes of the displacement measurements. Commonly, there are often three approaches to such borehole layout.

For slope engineering, boreholes are drilled directly into the slope body where there are concerns relating to slope surface, as shown in Fig. 3a.

For rock dams or dam abutments, boreholes are also drilled directly into the dam body and bedrock, an example is shown in Fig. 3b.

For underground excavations, there are two approaches to the establishment of the measuring boreholes. The first is the direct layout: boreholes are created within the surrounding rock mass by being drilled directly through the sidewalls, roof

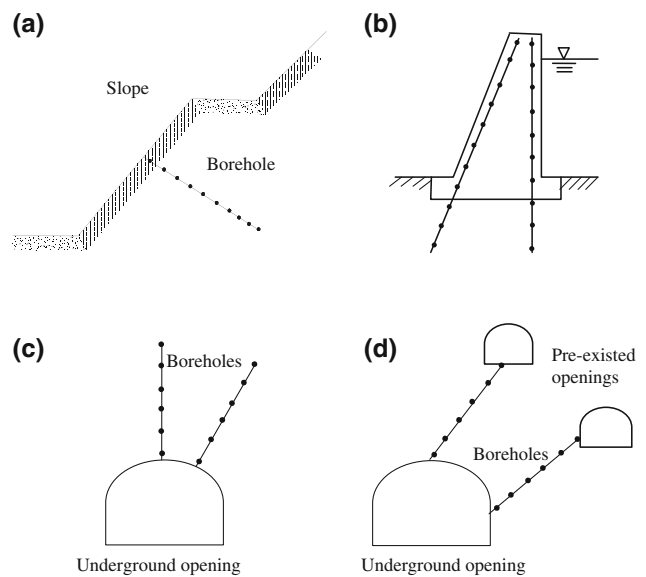


Fig. 3 Examples of borehole layouts for the measurement of rock mass displacement. **a** Slope engineering, **b** rock dam, **c** direct method from within an underground opening, **d** pre-installed borehole method from an adjacent underground opening

or floor of the underground opening after its excavation (Fig. 3c). The second is the pre-installed method: boreholes are drilled from one or more pre-existing adjacent openings, thus making it possible to measure the entire evolutionary process of rock mass displacement before during and after excavation of the underground opening, as shown in Fig. 3d.

The borehole length is important in terms of ensuring good measurement results. If identification of the EdZ is required, the determination of borehole length should take into consideration the EdZ development and the fixed reference point which should be established in a stable position sufficiently distant from the disturbed region. In some cases, to obtain a reliable identification of the EdZ, the length of the measurement boreholes should be at least twice the diameter of the underground opening to avoid the influence of excavation damage effect.

4.3 Drilling

The outer diameter of the telescope coupling often reaches 75 mm and the diameter of the grouting pipe is 20–30 mm, indicating that the diameter of the borehole should be larger than 110 mm.

As mentioned, although percussion drilling equipment may be available, diamond core drilling is much preferred and in many cases essential for providing the supporting geological information and for more reliable displacement measurements.

Special attention should be given to the drilling techniques that maintain the borehole wall straight and smooth

and ensure minimal induced damage to the rock core obtained.

The locations and orientations of the drillholes should be recorded. Also, the core should be well logged and described, including as a minimum the rock lithology, fracture occurrence and width, and any degree of weathering.

The complete borehole should be thoroughly cleaned immediately prior to installing the measuring tubes. However, in some poor ground conditions, special procedures involving grouting and temporary casing may be required to keep the borehole open sufficiently and long to allow installation, to guarantee both the borehole diameter and length.

A borehole camera is suggested to be adopted to inspect the completed borehole and investigate the strata and fractures, especially if no core is available. It is noted that camera is still available in those boreholes opened by percussive drilling method on condition that the boreholes maintain straight and can be thoroughly cleaned by water.

4.4 Installation

Installation plays a key role in the measurement of rock mass displacement by the sliding micrometer. A wrong installation out of the instructions listed as below will lead to rotation and dislocation of the measuring marks, causing difficulty in moving the probe in and out of the borehole. In some cases, if the measuring marks cannot be firmly connected to the surrounding rock mass, the relevant measuring points will not be viable, possibly resulting in scrapping of the entire measurement borehole.

1. The measuring tubes and telescope couplings must be inspected, any damage or breakage is not acceptable.
2. Clean the inner surfaces of the tubes and telescope couplings using cotton yarn, acetone may be used if there is oil on the telescope coupling surfaces.
3. Connect each numbered tube and telescope coupling using an adhesive material which can make plastic and steel firmly stuck. Note that the line marks on the surface of the tube and telescope coupling should be strictly aligned, and a special base tube installed at the bottom of the borehole should include a closure plug. All of the positions with the measuring marks should be sealed to prevent any ingress of grout.
4. A tremie pipe and a vent/drainage pipe are mandatory, they are fixed to the tubes and inserted into borehole together. The distance between the tremie pipe outlet and borehole bottom should be 1.0–1.5 m. The vent/drainage pipe can be fixed near the opening or at the middle of the borehole, permitting air or water to come out during the entire process of grouting.
5. Insert all the firmly connected tubes and measuring marks carefully, trying to maintain the tubes straight with no

rotation. 24 h after the solidification of the adhesive material, a trial measurement is needed to check the status of the tubes connections and insertion. If the probe and probe guide can run through all the measuring marks, the borehole opening should be plugged by cement.

6. Grouting: After the insertion of the tubes, the annular space between the measuring tubes and the borehole wall is grouted starting from borehole bottom. The maximum power of grouting pump should be at least 1.0 MPa. It is mandatory that the grouting should not be interrupted until the entire annular space within the borehole is completely grouted. The state of annular space grouting can be inferred by cement from vent/drainage pipe and cement volume.
7. After grouting, the interior of the tubes should be flushed with clean water. The water may be left in place or the tubes may be pumped dry after the grout has set.
8. A closure flange or cap should be installed over the exposed end of the measuring tubes.

4.5 Testing

1. Testing should be conducted by a person familiar with the equipment, and trained to recognize critical measurements and their relevance to the particular project.
2. The mechanical/electrical devices should be checked on site both before and after each day's testing. Instrument malfunction should be promptly investigated and corrected.
3. Before a measurement, the data controller should be switched on and warmed up for 20 min. The probe should be calibrated before and after each measurement, and the temperature of the test site must be recorded every five measuring positions during testing.
4. After the probe, probe guide, measuring rods and cables are connected, the 'downhole' (i.e. going into the borehole) measurement is to be carried out. The probe is inserted into the measuring tubes and pushed through to the bottom of the borehole. When the probe head is located at the measuring marks with 1.0 m intervals, it can be rotated at 45° to the measuring positions (Fig. 2b) and pulled to a stationary clamping position by the measuring rods, while recording the readings of depth and test data immediately at this time. It is necessary to repeat the testing at this measuring position at least three times until the differences of the consecutive data are acceptable. If the test data are always chaotic, there is likely to be a problem with the measuring position, so the values should be recorded and measured carefully again to establish whether the position is acceptable or should not be used.
5. When the probe guide reaches the bottom of the borehole, it is suggested that the 'uphole' (i.e. coming out of the borehole) measurements should be carried out at the

same measuring marks during the pullback of the probe, using the same testing method as described above.

5 Calculations and Data Processing

5.1 Calculation of Correction Factor and Measurement Data

As mentioned previously, the calibration should be carried out before and after each borehole measurement using the special calibration device. The calculation of the correction factor is described as follows.

$Val1$, $Val2$, and $Val3$ are assumed to be the three readings of each calibration. $E1$ and $E2$ are the mean values of the negative and positive readings, respectively, and can be expressed as:

$$E1 = (Val1 + Val2 + Val3)/3 \quad (1a)$$

$$E2 = (Val1 + Val2 + Val3)/3 \quad (1b)$$

$$\Delta E = E2 - E1 \quad (1c)$$

where ΔE is the difference of $E2$ and $E1$.

For the ‘downhole’ measurement (the probe runs from the borehole top to the bottom), the correction value of the zero point is calculated as:

$$Z_{01} = (E1 + E2)/2 \quad (2)$$

The correction factor can be expressed as:

$$K_1 = C/\Delta E \quad (3)$$

where C is a calibration constant provided by the manufacturer, it is often set to be 4.725 for most of the sliding micrometers.

Similarly, for the ‘uphole’ measurement (the probe runs back from the borehole bottom to the top), the correction value of the zero point (Z_{02}) and correction factor (K_2) can also be obtained. Thus, the final correction parameters can be determined using the following formula:

$$Z_0 = (Z_{01} + Z_{02})/2 \quad K = (K_1 + K_2)/2 \quad (4)$$

The measurement data can be corrected as:

$$m_c = K \times (m_a - Z_0) \quad (5)$$

where m_c is the corrected value for each measuring point, and m_a is the field measured data determined by mean value of three readings taken at each measuring mark.

5.2 Data Processing

Unless otherwise specified, all data should be processed within 24 h of the readings being taken so as to immediately respond to unusual displacement. The field data should again be scrutinized carefully and obvious errors clearly marked in the field data sheet (Table 1).

Corrected readings should be transferred to a computation and data summary sheet. An example taken from a measurement of tunnel displacement is shown in Table 1.

The method of calculating the displacement from the field data depends on the test objectives (slope cases, rock dams or underground openings) and borehole layouts. The key problem is assuming the fixed reference point. In general, the reference point located at the bottom of the borehole is set to be stationary, such as for slope engineering and direct method in underground opening cases, as shown in Fig. 3a, b. However, for the pre-installed method in underground opening shown in Fig. 3c, a certain point near the borehole orifice may be assumed to be the fixed reference point.

A plot of displacements at different borehole depths versus time is the best means of summarizing current data, and should be kept up to date. Figure 4 gives an example of measurements of a tunnel displacement by the pre-installed method (Li et al. 2012). The distance between point P01 and the sidewall of the test opening is 1.0 m. The relations among displacement, time, and construction are also illustrated in Fig. 4d.

Figure 5 shows an example of the determination of the EdZ for a tunnel with hard rock measured by the borehole pre-installed method. A graphical plot of total displacement versus depth should be prepared, as shown in Fig. 5a. The EdZ within the rock mass is identified by comparison of these displacements measured at different times during excavation. In most cases, it is easy to find the effective inflection point: this is defined as the position where displacement increases continuously in the subsequent test time. The zone between the effective inflection point and the slope surface or sidewall of the underground opening is regarded as the EdZ (Fig. 5b).

6 Reporting of Results

All reports of results should, unless otherwise specified, include general data, an installation report giving basic data on the instrumentation system at the time of installation, and monitoring reports presenting the results of routine measurements. For those projects with hard rock and high stress, identification of the EdZ might be included.

Table 1 Summary sheet for sliding micrometer data [the data listed in this sheet are taken from an example of measurements relating to tunnel displacement (Li et al. 2012)]

Sliding micrometer Summary data sheet					Borehole orientation	212°			
Project					Special test tunnels in Jinping II hydropower station				
Rock type					Marble				
Borehole no.					JPTSA-3-M2-SM01				
Measuring date					2010-01-10	Site temperature		12.7°	
Calibration parameters: $Z_0 = -0.06$ $K = 1.00$									
Depth (m)	Initial data	Measurement data			Calibrated	Relative	Total	Comments	
		Down	Up	Mean value					
1	-0.229	-0.288	-0.289	-0.289	-0.229	0.001	0.001		
2	0.988	0.929	0.930	0.930	0.990	0.002	0.002		
3	-3.588	-3.637	-3.636	-3.637	-3.577	0.012	0.014		
4	-0.023	-0.080	-0.082	-0.081	-0.021	0.002	0.015		
5	-0.375	-0.370	-0.372	-0.371	-0.311	0.064	0.079		
6	-0.287	-0.277	-0.277	-0.277	-0.217	0.070	0.149		
7	-0.281	-0.334	-0.332	-0.333	-0.273	0.008	0.158		
8	-0.243	-0.315	-0.316	-0.316	-0.256	-0.012	0.145		
9	-0.330	-0.453	-0.453	-0.453	-0.393	-0.063	0.082		
10	0.962	0.922	0.924	0.923	0.983	0.021	0.103		
11	0.090	0.055	0.055	0.055	0.115	0.025	0.128		
12	0.726	0.658	0.659	0.659	0.719	-0.008	0.120		
13	0.253	0.432	0.434	0.433	0.493	0.240	0.361		
14	-0.355	-0.426	-0.423	-0.425	-0.365	-0.010	0.351	Not stable	
15	-0.499	-0.177	-0.177	-0.177	-0.117	0.382	0.734		
16	-0.384	-0.366	-0.365	-0.366	-0.306	0.079	0.812		
17	0.303	0.523	0.525	0.524	0.584	0.281	1.094		
18	0.038	0.050	0.051	0.051	0.111	0.072	1.166		
19	0.150	0.240	0.241	0.241	0.301	0.151	1.317		
20	0.976	1.435	1.435	1.435	1.495	0.519	1.835		
21	0.807	1.071	1.073	1.072	1.132	0.325	2.161		

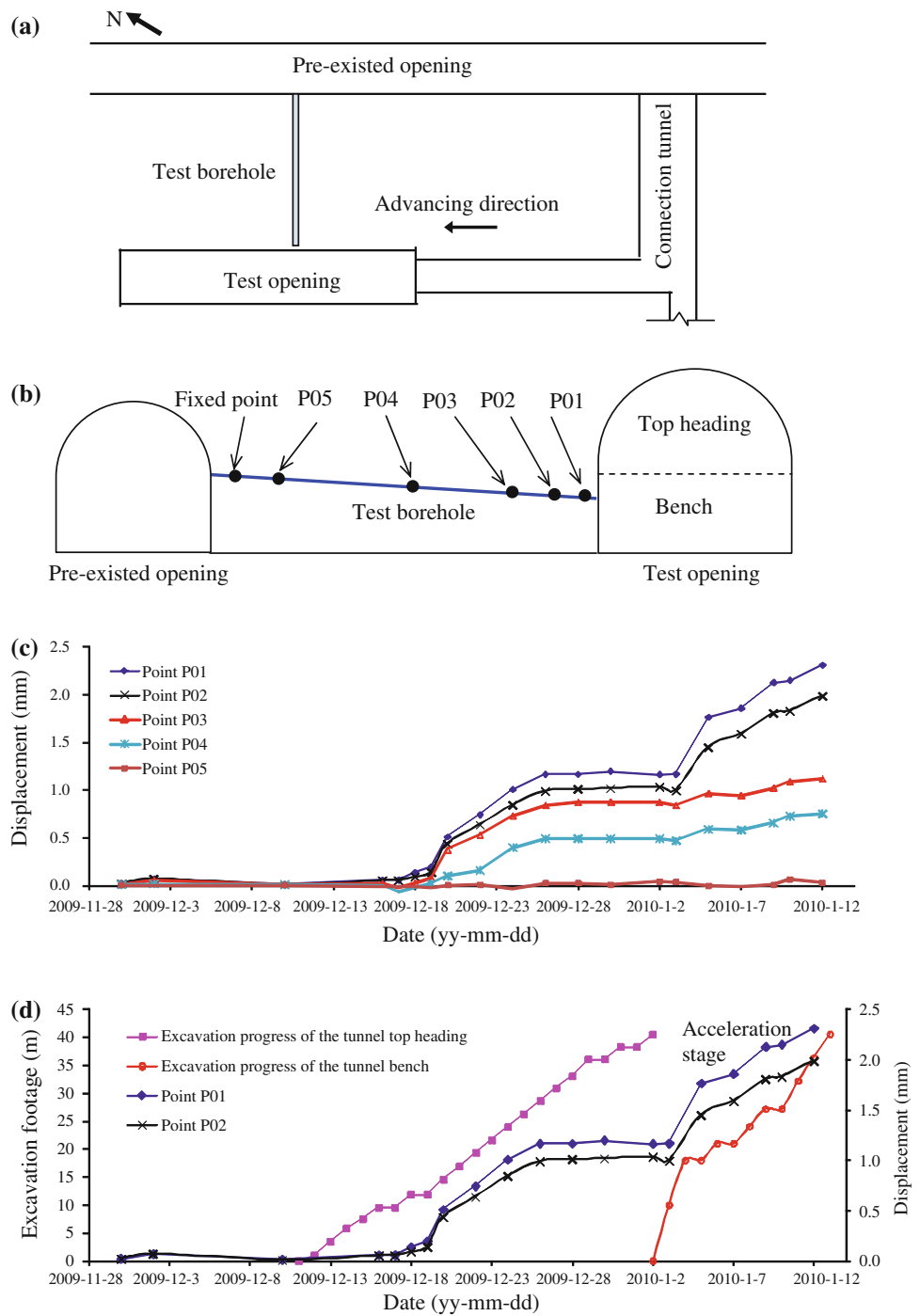
6.1 General Data Report

- A brief description of the test site, purpose of measurement, geological condition, rock lithology, and mechanics.
- The location, rock cores, length, direction, and dip angle of the boreholes.
- Testing date and time and abnormal readings of each borehole.
- Possible excavation method, progress and support during the entire measurement process if undertaken.
- Description of fracture distribution and groundwater condition in boreholes.

6.2 Content of the Installation Report

- A description and diagrams of all components of the sliding micrometer including procedures employed. Reference may be made to the present method.
- Record of type and details of drilling equipment used.
- Log of drilling. For cored holes, summary log to include the log of drilling and a log of the core. Inspection summaries of borehole camera when undertaken.
- Details and methods for installation, grouting, calibration and test measurements. Reference may be made to this ISRM Suggested Method stating only departures from the recommended procedures.

Fig. 4 Displacement–time plot and the relation between rock mass displacement and construction: **a** plan view of test borehole and underground openings, **b** locations of some typical measurement points, **c** relation between displacement and time, **d** comprehensive relation between displacement and excavation progress of an underground opening



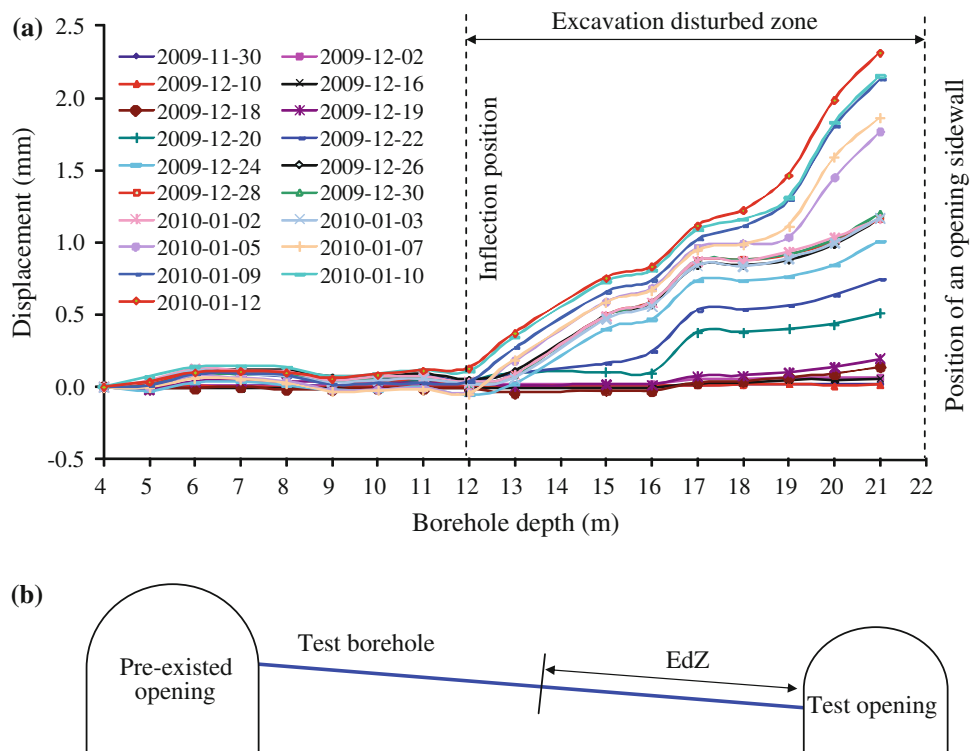
(e) For each borehole, a diagram that relates the specific instrument to the entire project showing the rock conditions and displacement evaluation by numerical simulation or analogy for such kind of ground condition. This should include: the station or co-ordinates and elevation of the borehole orifice, locations of measuring marks and the reference point.

6.3 Monitoring Report

This should include the following:

- (a) A set of field monitoring result tabulations containing information as shown in Table 1.
- (b) Graphs of displacement versus depth and time, sufficient to show clearly the locations, magnitudes, and

Fig. 5 An example of identification of the EdZ: **a** relation between displacement and depth for an underground opening, **b** schematic diagram of the identification of the EdZ corresponding to the effective inflection point of displacements as shown in (a)



- rates of all significant displacements, as shown in Figs. 4 and 5.
- (c) A plot of the relation between displacement and construction/time, as shown in Fig. 4c for a case of comparison of displacement and construction.
- (d) A brief commentary drawing attention to significant displacements compared to change of geological condition, groundwater, rainfall (for slopes and rock dams) and construction activities, and to any instrument malfunctions occurring since the preceding report.
- (e) Comparison to predicted displacements, if such exists. Discussion if major differences exist.
- (f) Comments on the practical accuracy of the measurements and possible recommendation for future measurements.
- (g) Possibly, for those projects excavated in hard rock or high stress, a schematic diagram of the determination of the EdZ can be included, interpreting the inflection position, identification method and comprehensive geological conditions, as shown in Fig. 5.

References

Dong ZR, Zhao H, Huang SJ (2006) Analysis of deformation in foundation excavation of Xiaowan high arch dam. *Chin J Underg Spac Eng* 2(6):1014–1018 (in Chinese)

Hansmire WH (1978) Suggested Methods for monitoring rock movements using borehole extensometers. *Int J Rock Mech Min Sci* 15(6):305–317

Hudson JA, Morgan J (1974) A horizontal inclinometer for measuring ground movements. Transport and Road Research Laboratory, UK, Report TRRL SR 92 UC, p 19

ISRM (2007) The complete ISRM suggested methods for rock characterization, testing and monitoring: 1974–2006. In: Ulusay R, Hudson JA (eds.) Suggested Methods prepared by the commission on testing methods, International Society for Rock Mechanics, Compilation Arranged by the ISRM Turkish National Group, Kozan Ofset, Ankara, Turkey

Kovari K, Amstad Ch (1982) A new method of measuring deformations in diaphragm walls and piles. *Geotechnique* 32(4):402–406

Kovari K, Amstad Ch (1983) Fundamentals of deformation measurements. Proceedings of international symposium on field measurements in geomechanics, Zurich, Vol. 1, pp 719–748

Kovari K, Peter G (1983) Continuous strain monitoring in the rock foundation of a large gravity dam. *Rock Mech Rock Eng* 16(3):55–59

Kovari K, Amstad Ch, Koppel J (1979) New developments in the instrumentation of underground openings. Proceedings of the 4th rapid excavation and tunnelling conference, Atlanta, USA, Vol. 1, pp 816–837

Li GY, Huang Y (2001) Linewise observation and portable instruments on strain monitoring in geomechanics. *Chin J Rock Mech Rock Eng* 20(1):99–109 (in Chinese)

Li SJ, Feng X-T, Li ZH et al (2012) *In situ* monitoring of rockburst nucleation and evolution in the deeply buried tunnels of Jinping II hydropower station. *Eng Geol* 137–138:85–96

Qin WM, Sun Y, Chen RF (2008) Application of total station instrument and sliding micrometer to monitoring Shuibuya underground powerhouse. *Rock and Soil Mech* 29(2):557–561 (in Chinese)

ISRM Suggested Method for Step-Rate Injection Method for Fracture In-Situ Properties (SIMFIP): Using a 3-Components Borehole Deformation Sensor

Yves Guglielmi, Frederic Cappa, Hervé Lançon, Jean Bernard Janowczyk, Jonny Rutqvist, C. F. Tsang, and J. S. Y. Wang

1 Introduction

It is commonly acknowledged that complex interactions among numerous pre-existing discontinuities determine primarily the potential instability of fractured rocks (Hoek and Bray 1974). This problem is of importance in many geotechnical (mining and slope stability, subsidence induced by drainage into a tunnel, etc.) and reservoir problems (loss of integrity of the reservoir/cap-rock system,

estimation of the efficiency of hydraulic stimulation tests, etc.). However, the stability analysis and monitoring of any rock structure face the major problem of determining properties at scales relevant to in situ conditions.

Several criteria have been proposed to identify the mechanical properties and strength of a natural rock joint (Patton 1966; Ladanyi and Archambault 1970; Barton and Choubey 1977; Plesha 1987; Saeb and Amadei 1992; Amadei et al. 1998). In practice, Barton's model is recognized and, in general, used through the joint morphological parameter called the joint roughness coefficient (JRC) and the joint compressive strength (JCS), both being measurable in the laboratory on jointed samples and in situ (ISRM 2007). Nevertheless, this method relies on the estimation of joint properties under unconfined conditions that do not reflect the in situ conditions of a very heterogeneous state of stress. Conversion of JRC numbers into ISRM roughness descriptions is subjective, and only for some roughness profiles it is possible without ambiguity (Barton and Bandis 1990; Hack 1993). Another key question is that there are very few in situ field techniques for estimating the parameters needed to calibrate hydromechanical analyses of fractured rocks at field scales. Indeed, mechanical and hydraulic properties of joints usually are estimated independently, and parameters describing joints' permeability variations with shear are poorly constrained.

This suggested method describes a method called step-rate injection method for fracture in-situ properties (SIMFIP) to quantify both discontinuities, hydraulic and mechanical properties in situ using coupled pressure/deformation measurements in boreholes. The method has been successfully applied to characterize fractures and fault zones in different underground environments (see for example <http://lsbb.oca.eu/>) and in jointed rock slopes, under different site conditions (20–500 m overburden, clay and carbonate rocks, joints saturated and unsaturated with water) showing acceptable levels of repeatability and reproducibility. The apparatus which is commercially available (www.sites.fr, for information about the apparatus

Please send any written comments on this ISRM Suggested Method to Prof. Resat Ulusay, President of the ISRM Commission on Testing Methods, Hacettepe University, Department of Geological Engineering, 06800 Beytepe, Ankara, Turkey.

Originally published as an article in the journal *Rock Mechanics and Rock Engineering*, 47, Y. Guglielmi, F. Cappa, H. Lançon, J. B. Janowczyk, J. Rutqvist, C. F. Tsang, J. S. Y. Wang, ISRM Suggested Method for Step-Rate Injection Method for Fracture In-Situ Properties (SIMFIP): Using a 3-Components Borehole Deformation Sensor, 303–311, 2014.

Y. Guglielmi (✉)
CNRS, IRD, CEREGE UMR6635, Aix-Marseille Université, 3
Place Victor Hugo, 13331, Marseille, France
e-mail: guglielmi@cerege.fr

F. Cappa
Geoazur, University of Nice Sophia-Antipolis, Côte d'Azur
Observatory, 250 rue Albert Einstein, 06560, Sophia-Antipolis,
France

H. Lançon
SITES S.A.S., Espace Européen, 4C Allée Claude Debussy,
69130, Ecully, France

J. B. Janowczyk
PETROMETALIC, 11 Rue des Ecluses de Selles, BP 287, 59405,
Cambrai cedex, France

J. Rutqvist · C. F. Tsang · J. S. Y. Wang
Earth Sciences Division, Lawrence Berkeley National
Laboratory, 1 Cyclotron Road, Berkeley, CA 94720, USA

C. F. Tsang
Department of Earth Sciences, Uppsala University, 75236,
Uppsala, Sweden

contact herve.lancon@sites.fr or jeremie.durand@sites.fr and operating procedure are described together with data recording and processing. The recommendations are supported by data from practical case examples.

2 Scope

The purpose of this suggested method is to use a step-rate injection of a given water volume to produce micro-scale elastic and inelastic deformations of a localized fractured rock mass volume to estimate elastic stiffness (normal and shear), strength (friction coefficient and cohesion) and hydraulic properties (hydraulic aperture and storage) of the fractures. This method can be applied for in situ estimations of fracture properties associated with a wide range of rock stability problems such as rock slope gravitational stability or fracture and fault reactivation induced by downhole industrial fluid injection or production, because one key idea is to focus on fractures favorably oriented for slip given the local stress state.

The scope is to induce a slight slip (few microns to millimeters) on fractures while synchronously and accurately measuring the injected fluid pressure, flow rate and the three-dimensional deformations of the borehole wall. The SIMFIP test allows to identify the elastic opening, the fracture extension pressure (FEP) and the stable slipping period of the tested fracture. Using simple equations relating pressures to deformations, hydraulic and elastic properties that control pre-slip and some strength properties that control slip hydromechanical responses of fractured rocks can be estimated.

3 Apparatus

The apparatus necessary for the SIMFIP tests is composed of surface equipment to conduct the test and acquire the data, and a probe. All the downhole equipment uses fiber-optic sensors with reflection of light at specific wavelengths (from fiber Bragg gratings mounted between inflatable packers, red lines in Fig. 1a), thus requires no down-hole electrical supply.

3.1 Surface Equipment is Composed of the Following Parts (Fig. 1):

- A tripod or drilling rig with a winch
- Three different hydraulic pumps (1) to provide oil pressure to the anchoring device of the probe deformation sensor (this pump must be servo-controlled to automatically maintain a constant anchoring pressure during the test), (2) to inflate the rubber packers of the

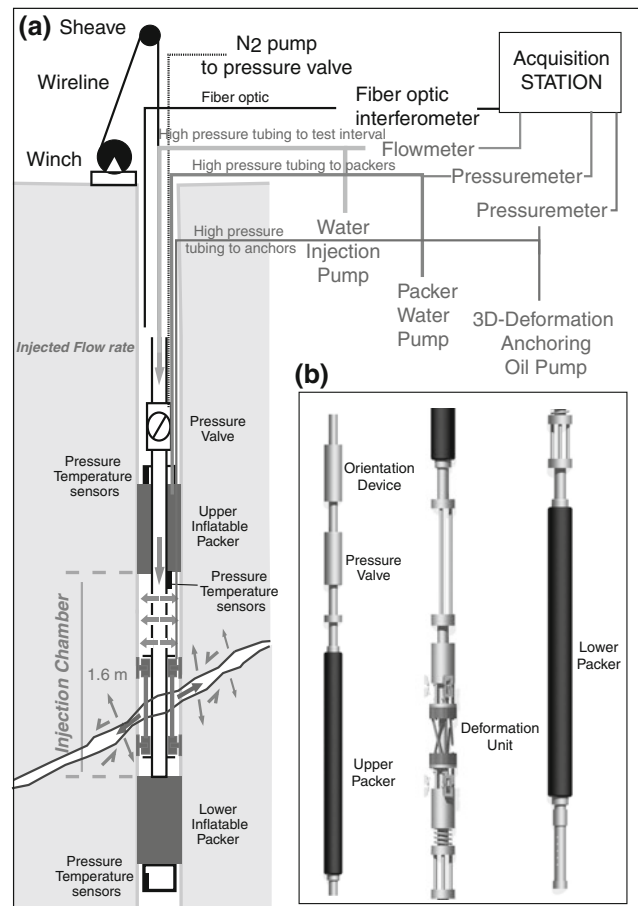


Fig. 1 a SIMFIP test equipment setup; b components of the SIMFIP downhole probe

probe, (3) to generate the water pressure for the test (this injection group must be equipped with high-accuracy flow-meters that allow to monitor 1–100 L/min flow rates with a 0.1 L/min accuracy)

- Multi-channel recording equipment with an interface that allows real-time reading of several test parameters (fluid pressures and temperatures, rock deformations, flow rate) at 1–500 Hz sampling frequencies. The system can easily be synchronized to a seismic acquisition system.

3.2 Downhole Equipment: The SIMFIP Probe

- Straddle packer:

Sealing of the borehole test interval is accomplished by use of two inflatable rubber packers, spaced apart a distance equal to at least six times the hole diameter. The two packers are connected mechanically as well as hydraulically to form one unit termed the straddle packer.

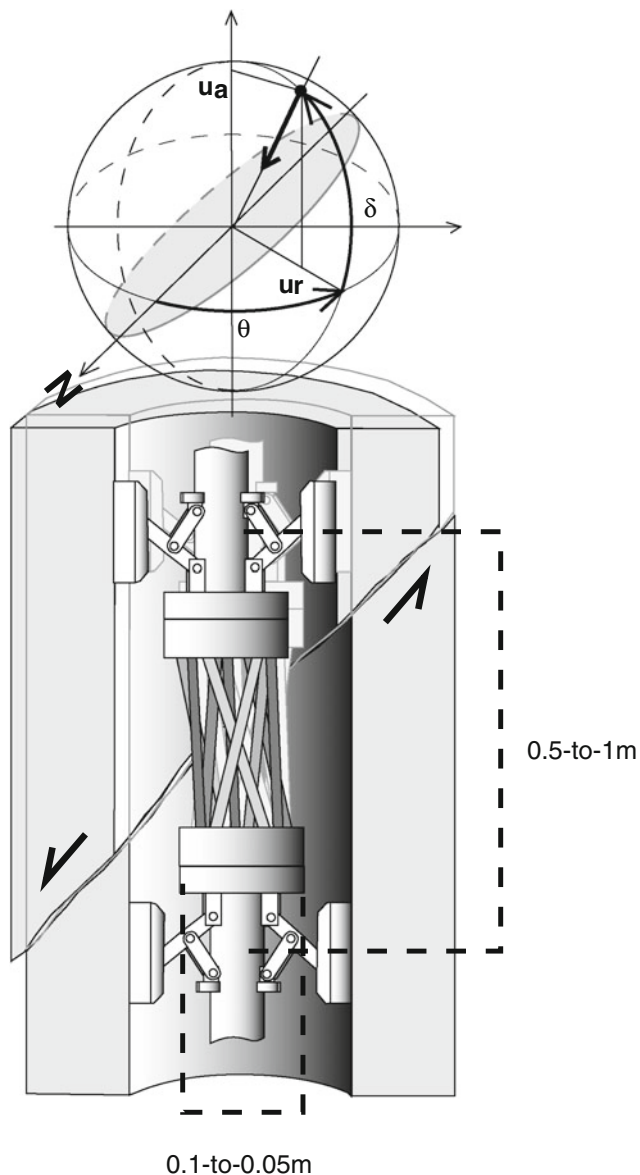


Fig. 2 Schematic view of the three-dimensional deformation unit. Tubes are differently colored to show that they display different deformations when there is a relative movement of the rings anchored to the borehole wall across the activated fracture. The sphere figures how the movement is oriented in the (u_r, u_a) plane of maximum shear strain (the tested fracture plane is shown in *gray*)

(e) Three-dimensional deformation unit

To capture the three-dimensional deformation of a fracture, a borehole extensometer must be centered along the axis connecting the two packers in the injection chamber (Fig. 2). Two un-deformable steel rings are coupled to the borehole wall by hydraulically placed keys which are running on precision-refined contact areas. Nine small diameter tubes made of deformable steel connect the two rings with varying oblique orientations. The nine tubes and the two rings are attached to each other to form the three-dimensional

deformation measuring unit. When the unit is anchored to the borehole wall, set across a fracture with each ring being anchored to each side, it is completely free to move from the straddle packer system. The unit size may be adjusted from 0.5 to 1 m length and 0.1–0.05 m diameter depending on the fracture geology (thickness, dip, and planarity). Several units can be put together to increase the interval testing length. Relative movements of the fracture walls induce a displacement of one ring relative to the other, and produce a deformation of the connecting tubes which is different depending on the tube orientation toward the movements' three-dimensional orientation. Tube deformations are captured with 10–15 fiber optic Bragg gratings that are attached to each tube and distributed along one single fiber that is also used to bring the Bragg sensors' signals to the surface acquisition system. An inversion algorithm is used to calculate the relative three-dimensional displacements of the ring units from the tube deformations that are permanently monitored during the test. The displacement range is 0.7 and 3.5 mm in the axial and radial directions of the borehole, respectively, and the accuracy is 10^{-6} m.

(f) Pressure and temperature measurements

Pressure sensors are installed to monitor independently the pressure variations in the test interval as well as above and below the straddle packer system to monitor the injection pressure build up in the interval and eventual leakage through fractures in the borehole outside the interval. Pressure sensors range must be high (0–10 MPa) to allow for high pressure step rate testing (STR), and accurate (0.001 MPa) to record small pressure variations related to fracture movements. Temperature sensors must also be installed in the interval and outside it to control and monitor the temperature evolution during the test. The equipment must handle temperatures of 20–80 °C (roughly corresponding to depths of 50–1000 m) and the accuracy of 0.1 °C. Both pressure and temperature measurements can be made with fiber Bragg gratings on the same fiber connecting the deformation unit.

(g) Orienting tool

Attached to the straddle packer system is an orienting tool, which can be magnetic, gyroscopic or an electrical imaging system. When an electrical imaging system is used, the same tool provides initial borehole reconnaissance, exact positioning at selected depth intervals, and in real time imaging of fracture movements that can be correlated to displacement data.

(h) Downhole valve, tubing and fiber optic

A downhole valve is recommended to control injections right at the entrance of the test interval, and to limit pressure loss effects mainly when conducting pressure pulse

injections. The valve may be operated from the surface using for example gas (N_2) pressure conveyed downhole through a flexible hose. Packer inflation and test interval pressurization are carried out hydraulically from the surface, using water conveyed in flexible hoses or high-pressure stainless steel tubings. The anchoring of the three-dimensional deformation unit to the borehole wall is also carried out hydraulically from the surface, using oil conveyed in flexible hose. Finally, the same optical fiber is used to interrogate the sensors distributed at depth and to convey the signal back to the acquisition system at the surface.

4 Test Procedure

4.1 Preparatory Investigation

(a) Drill borehole and fractures geology

The SIMFIP test may be installed in vertical, inclined or horizontal boreholes with a 140 mm diameter (diameter must not be lower than 120 mm since the probe diameter is 110 mm). Oriented borehole images are essential for selecting the fractures for testing. Since the 3D-displacement sensor of the SIMFIP probe that must be anchored on the two sides of the selected fracture is 0.5 m long, all fractures making an angle with the borehole axis ranging between 0 and 80° can be tested. Geophysical logs such as caliper, sonic, density and televiewer imaging are useful to characterize the fracture properties.

(b) Rock stress estimation

It is important for the SIMFIP test analyses that the state of in situ stress be estimated in or close to the borehole (it is simpler to perform stress analyses in a vertical hole). The hydraulic testing of pre-existing fractures method (HTPF), that yields a complete stress evaluation from an inversion of the normal stress measured on a set of fracture planes with different known orientations (Haimson and Cornet 2003), is recommended. Each HTPF test can be conducted with the SIMFIP probe and, a minimum of six tests must be performed on pre-existing non-parallel fractures for a complete stress tensor determination. Interestingly, the same pressure and flow rate data can be used for the HTPF and SIMFIP interpretations in the case where the HTPF tests are conducted with the SIMFIP probe.

4.2 Installation and Testing

The current SIMFIP test is a combination of short duration pulses and a long duration pressure “step-up” and “step-down” step-rate test. Test duration will depend on the injectivity of the formation. Once the SIMFIP probe has

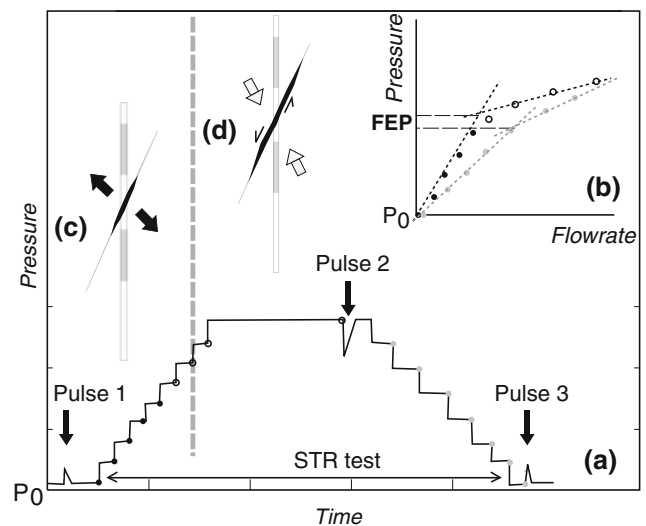


Fig. 3 SIMFIP test protocol—**a** pressure pulses and steps imposed in the interval test during the injection; **b** pressure-versus-flow rate correlation (points are taken at the time pressure stabilizes for each step); **c** initial mainly normal-to-the-fracture-plane opening at the beginning of the water injection; **d** fracture shear activation at the maximum pressure injection step

been installed in the selected borehole interval, each test sequence has the following segments (Fig. 3)

1. Inflation of the packers at the chosen depth and installation of the upper anchor followed by the installation of the lower anchor of the SIMFIP displacement sensor across a well-identified fracture.
2. A pressure pulse (shut-in pulse test type) is first applied with duration of a few seconds (pulse 1 in Fig. 3). The pulse pressure magnitude is chosen to be well below the “fracture extension pressure” to characterize the fracture initial hydromechanical elastic response.
3. The “step-up” step-rate test is initiated at a slow rate for a fixed amount of time, and the injection rate is then increased and again held for the same amount of time (STR in Fig. 3). A very small pressure increase at each step is recommended because inelastic deformations may occur very early in a highly heterogeneous fractured media. When the fracture extension pressure is achieved, a change in the pressure-versus-flow rate curve slope is observed (Fig. 3b). At that time, it is recommended to increase the pressure a little more (two-to-three more pressure steps at least), and then to maintain the injection for an amount of time at least ten times longer than the previous steps. This “post fracturing extension pressure step” (PFEP) is crucial to determine the failure and post-failure properties of the fracture.
4. Before the end of the PFEP step, the downhole gate is closed for a few seconds, and then reopened. This pulse of pressure decrease and recovery to the PFEP value is

used to estimate the activated fracture hydromechanical response.

5. Then, the test is terminated by a “step-down” step-rate test with at least three decreasing pressure steps.
6. A third pulse (pulse 3 in Fig. 3) is finally applied, with the same duration of testing conditions as the first pulse. This last pulse will estimate the permanently damage-induced changes in the fracture hydromechanical elastic properties.
7. Anchoring of deformation sensor is released from the borehole wall and packers are deflated.
8. A new borehole imaging is recommended to check the eventual changes in the tested fracture geometry.

5 Calculations and Data Processing

5.1 Estimation of the “Fracture Extension Pressure” (FEP)

Interpretation starts with the analysis of the differential pressure-versus-flow rate curve of the STR test. The curve can schematically be described by two straight lines corresponding to the evolution of the flow regime in the injected fracture, from an initially “closed” or “slightly open” to an “open” fracture with pressure increase (Fig. 3b). The “fracture extension pressure” (FEP) is the pressure value that is read at the intersection between the two lines. The step up and step down curves may be used to give a range of FEP values. Below the FEP, the tested fracture hydromechanical response is elastic and this time interval of the STR test will be used to estimate the initial elastic and hydraulic properties of the fracture. Above the FEP, the fracture has been damaged and this time interval of the STR test will be used to estimate strength properties of the fracture.

5.2 Determination of Fracture Transmissivity and Hydraulic Aperture

The pressure pulses conducted before, during and at the end of the experiment are interpreted following classical approaches from Cooper et al. (1967) that were validated for injected fractures that deform elastically (Schweisinger et al. 2009) giving:

$$T \approx 1.2 \times \frac{d_c^2}{t_{0.37}} \quad (1)$$

where d_c is the diameter of the casing attached to the upper packer and $t_{0.37}$ the time required for the head to decrease to 37 % of the maximum differential head.

The fracture hydraulic aperture (e) can be calculated using the following equation (Witherspoon et al. 1980):

$$e = \sqrt{[3] \frac{12 \times T \times \mu}{\rho \times g}} \quad (2)$$

where T is the hydraulic transmissivity, μ is the fluid viscosity, ρ is the fluid density and g is the gravitational constant.

Comparison of pulse analyses below and above the FEP allows estimating transmissivity variations with pressure increase.

5.3 Estimation of Fracture Normal Stiffness and Storativity

Following Rutqvist et al. (1998) the fracture normal stiffness is assumed to be:

$$k_n = \frac{dP}{du_n} \quad (3)$$

where dP is the pressure uniformly distributed over the face of the fracture and du_n is the normal displacement that is measured with the three-components sensor set across the fracture. The fracture storativity (s) can then be approximated to:

$$s \approx \frac{\gamma}{k_n} \quad (4)$$

where γ is the unit weight of water and k_n is the fracture normal stiffness.

Comparison of analyses below the FEP and during the pressure step-down allows estimating normal stiffness variations with pressure increase.

5.4 Estimation of the Fracture Friction Coefficient

The SIMFIP device gives the plane of maximum shear stress along the fracture plane (Arthaud 1969) and Fig. 2. The borehole axial-versus-radial movements measured at each of the stabilized pressure steps are plotted along the line corresponding to the intersection between this plane and the fracture plane. A linear correlation is conducted considering the displacement points of the pressure steps above the FEP, when there is inelastic fracture reactivation. The angle φ between the normal-to-the fracture plane and this line is related to the fracture friction angle ϕ using:

$$\varphi = 45 + \frac{\phi}{2} \quad (5)$$

5.5 Calculating the Tangential Stress and the Fracture Shear Stiffness

Whether the fracture surface will actually slip depends upon its cohesive strength, if any, and the coefficient of static friction, μ . For a cohesion-less fracture, taking the time the FEP is reached as the instant sliding is initiated; the static friction can be expressed as (Jaeger et al. 2007):

$$\mu_{sm} = \frac{\tau}{\sigma_n} \quad (6)$$

where σ_n which is the normal stress acting across the fracture plane, which can be approximated to the fracture extension pressure P_{FEP} , and the static friction μ_{sm} related to the friction angle ϕ estimated from Eq. (5). The shear stress and fracture shear stiffness are estimated using Eqs. (7), (8) and (9):

$$\mu_{sm} = \tan(\phi) \quad (7)$$

$$\tau = \tan(\phi) \times P_{FEP} \quad (8)$$

$$k_s = \frac{\tau}{du_{sFEP}} \quad (9)$$

where du_{sFEP} is the shear displacement measured when the fracture extension pressure is reached.

5.6 Integration with HTPF Stress Estimations

If the magnitudes and orientations of the principal effective stresses

$(\sigma'_1 = (\sigma_1 - P_f) > \sigma'_2 = (\sigma_2 - P_f) > \sigma'_3 = (\sigma_3 - P_f))$ and the fracture plane geometry are known from a HTPF test, the slip-tendency (T_s) defined as the ratio between the shear stress and the effective normal stress and the slip direction can be calculated on the fracture plane (Morris et al. 1996).

The comparison between the calculated static friction $\mu_{sc} = T_s$ and the measured static friction μ_{sm} related to the friction angle ϕ estimated from Eq. (7) gives an estimation of the fracture cohesion rearranging the Mohr–Coulomb failure criterion and considering that failure initiated at the FEP pressure (P_{fFEP}):

$$C = (T_s - \mu_{sm}) \times P_{fFEP} \quad (10)$$

The calculated and the measured slip directions may be plotted on the same stereogram to estimate the mismatch between the measured slip onto the fracture plane and the potential slip calculated from stresses estimated with the HTPF tests. By iteratively changing this initially proposed stress tensor, the stress tensor may be optimized using a misfit function that relies on the discrepancy between

observed and computed slip directions. We recommend for example the stress inversion algorithm based on minimizing the angular mismatch developed by McFarland et al. (2011). When coupled to a HTPF method, the SIMFIP test allows refining the stress tensor determination which may be useful when there are not enough different fractures attitudes to constrain the stress tensor with the HTPF method only.

6 Reporting of Results

6.1 Introduction

- Purpose of the tests.
- Details of site location, including a topographic and location map.
- Regional and site geological description. A careful description of the different joint families affecting the rock mass is recommended. Using the Q value method (ISRM 2007) will allow useful comparisons with joint properties estimation with the SIMFIP method.
- Regional stress description. If the stress state is unknown, HF or HTPF test is recommended to be conducted. HTPF tests can be included in the SIMFIP procedure.
- Diameter and length of the test borehole.
- Geological log of the test borehole (an oriented borehole wall image is necessary).
- Selected number and depth of individual tests.

6.2 Test Apparatus and Method

- Detailed description of the equipment and of its calibration.
- List of equations used to estimate fracture transmissivity, normal and shear stiffness, and friction coefficient. If the fracture properties have been estimated by a numerical model that considers coupled hydromechanical effects, the degree of coupling introduced in the model must be carefully described.
- Method for evaluating uncertainty of results should be specified.

6.3 Test Results

- Raw data must be presented with the following graphs (Fig. 4):
 - Pressure of the injection chamber and flow rate variations versus time.

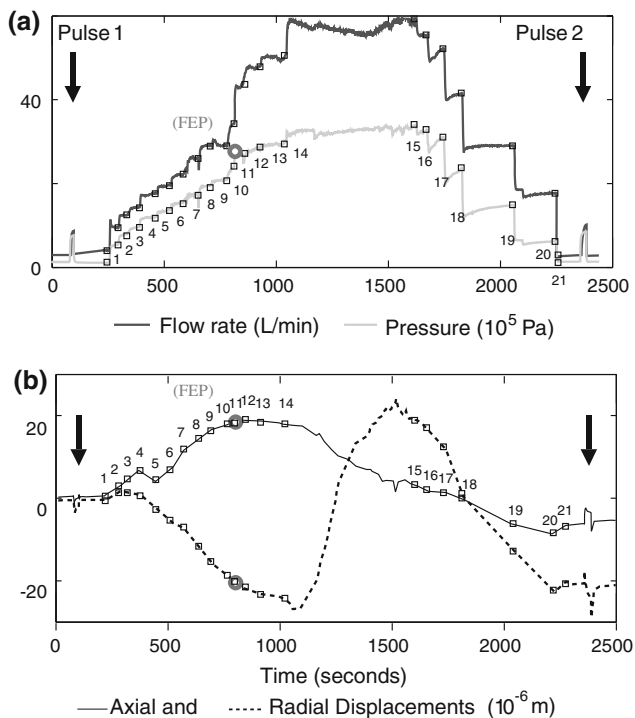


Fig. 4 Typical SIMFIP in situ raw data (numbers 1–21 correspond to the pressure steps operated during the test, FEP is the fracture extension pressure point)—**a** flow rate and water pressure time variations; **b** axial and radial displacements time variations in the plane of maximum shear strain perpendicular to the fault direction (see this plane in Fig. 2 upper sphere)

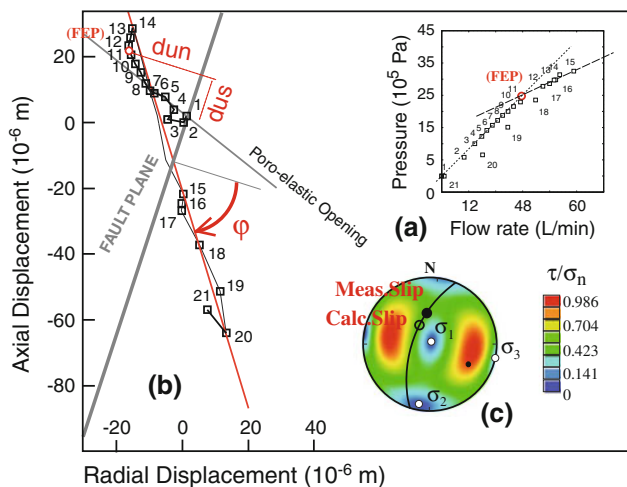


Fig. 5 SIMFIP test graphical analyses—**a** determination of the fracture extension pressure (FEP) on the pressure-versus-flow rate graph; **b** determination of fracture's du_n , du_s and ϕ from the analysis of the axial-versus-radial displacement of the fracture wall figured in the plane of maximum shear strain; **c** calculated (calc.slip) and measured (meas.slip) fracture slip considering a cohesion-less fracture and the fracture geometry in the state of principal stresses

7.2. Fracture hanging wall displacement versus time. Displacements are figured in the borehole axial and radial coordinates.

8. Graphical interpretations must be presented with the following figures (Fig. 5):

8.1. Pressure and flow rate values at each stabilized step are figured on the same pressure-versus-flow rate graph for the step-up and step-down values. The correlation lines and the FEP are plotted on the graph.

8.2. Stereographic view (lower hemisphere) of the fracture plane and pole, and of the three principal stress components (σ_1 , σ_2 , σ_3). The calculated slip and the measured slip are plotted on the trace of the fracture plane. The mismatch angle between the two is also plotted.

9. Tabulated values of the FEP, (σ_1 , σ_2 , σ_3), fracture strike and dip, fracture initial hydraulic aperture and normal and shear stiffness, fracture friction angle and cohesion, fracture damaged hydraulic aperture, total slip amplitude, slip average velocity are given for every test conducted.

7 Discussion of Results

10. Discussion of the uncertainties related to the FEP and friction coefficient determinations.
11. Discussion of the role of the heterogeneity/geology of the interval zone. Indeed, it may be difficult to isolate only one fracture in the interval zone or if the isolated discontinuity is a fault zone, some complexity in the fault architecture may influence the results.
12. Discussion of the volume influenced by the hydraulic injection and of the size of the slipping zone on the fracture.

8 Notes and Recommendations

8.1 Recommendations During Testing

13. A clean open hole is recommended before the test.
14. The SIMFIP test can be synchronized with seismic monitoring located in adjacent boreholes.
15. To simplify the analyses, it is recommended to operate pressure steps of same duration (duration will be fixed after the initial permeability of the tested fracture has been estimated).
16. The 1 Hz sampling rate is enough to well capture the signals (it may eventually be increased during the pulse tests).

17. With the current commercialized apparatus, SIMFIP tests are limited to depths of 300 m, 7 MPa pressure (3 MPa hydrostatic + 4 MPa in the injection chamber) and temperature differential of 60 °C. SIMFIP tests can be conducted in vertical, inclined (downward) or horizontal characterization wells (diameter of the SIMFIP probe is 0.11 m).

8.2 Recommendations During Test Interpretations

The data from the SIMFIP test sequence can be analyzed by various numerical methods. The following papers (Cappa et al. 2005, 2008; Guglielmi et al. 2008; Vasco 2009; Vasco and Minkoff 2009) are recommended. Data can be reproduced with the commercial codes FLAC^{3D} and 3DEC using the fully coupled hydromechanical algorithm and a Mohr–Coulomb model with strain softening constitutive behavior for the fractured rock mass. Such refined analyses of the in situ fracture pressure-elastic deformation response to a low amplitude pulse allow estimating the following properties with high accuracy (Cappa et al. 2008): hydraulic aperture, normal and shear stiffnesses of injected fractures, bulk modulus of the intact rock, permeability coefficient and bulk modulus of the surrounding rock. Numerical analyses of the STR data allow estimating the fracture permeability and friction evolution with effective stress and strain variations, by matching modeled to the measured deformations at the fracture extension pressure and during the pressure step-down.

Acknowledgments The SIMFIP method and probe developments were funded by the ANR “Captage de CO₂” through the “HPPP-CO₂” project and by the ADEME through the “mHPP” project. The contribution by LBNL authors in developing this report was funded by the US Department of Energy under contract No.DE-AC02-05CH11231. The authors thank the SITES S.A.S engineers Hervé Caron, Cédric Micollier, Régis Blin, Nicolas Bossard, Jérémie Durand and the Petrometalic S.A. engineers, who are employed by the two companies that develop and operate the probe instrument which allows the in situ pressure/displacement measurements.

References

- Amadei B, Wobowo J, Sture S, Price RH (1998) Applicability of existing models to predict the behavior of replicas of natural fractures of welded tuff under different boundary conditions. *Geotech Geo Eng* 16:79–128
- Arthaud F (1969) Méthode de détermination graphique des directions de raccourcissement, d’allongement et intermédiaire d’une population de failles. *Bull Soc Géol de France* 7(XI):729–737
- Barton N, Bandis S (1990) Review of predictive capabilities of JRC–JCS model in engineering practice. In: Barton N, Stephansson SG (eds) *Rock joints*, vol 5. Balkema, Rotterdam, pp 603–610 (ISBN:90 6191 109)
- Barton N, Choubey V (1977) Shear strength of rock joints in theory and practice. *Int J Rock Mech Sci Geomech Abstr* 10:1–54
- Cappa F, Guglielmi Y, Fénart P, Merrien-Soukatchoff V, Thoraval A (2005) Hydromechanical interactions in a fractured carbonate reservoir inferred from hydraulic and mechanical measurements. *Int J Rock Mech Min Sci* 42:287–306
- Cappa F, Guglielmi Y, Rutqvist J, Tsang C-F, Thoraval A (2008) Estimation of fracture flow parameters through numerical analysis of hydromechanical pulses. *Water Resour Res* 44(W11408):1–15
- Cooper HH, Bredehoeft JD, Papadopoulos IS (1967) Response of a finite-diameter well to an instantaneous charge of water. *Water Resour Res* 3(1):263–269
- Guglielmi Y, Cappa F, Rutqvist J, Tsang C-F, Thoraval A (2008) Mesoscale characterization of coupled hydromechanical behavior of a fractured-porous slope in response to free water-surface movement. *Int J Rock Mech Min Sci* 42:852–878
- Hack HRGK (1993) *Slopes in rock*. Proc An Overview of Engineering Geology in the Netherlands Ed DIG, Technical University Felft, The Netherlands, pp 111–119
- Haimson BC, Cornet FH (2003) ISRM suggested methods for rock stress estimation—Part 3: hydraulic fracturing (HF) and/or hydraulic testing of pre-existing fractures (HTPF). *Int J R Mech Min Sci* 40:1011–1020
- Hoek E, Bray J (1974) *Rock slope engineering*. Institution of Mining and Metallurgy, London
- ISRM (2007) The complete ISRM suggested methods for rock characterization, testing and monitoring: 1974–2006. In: Ulusay R, Hudson JA (eds) *Suggested methods prepared by the commission on testing methods*, International Society for Rock Mechanics, compilation arranged by the ISRM Turkish National Group, KozanOfset, Ankara, Turkey
- Jaeger JC, Cook NGW, Zimmerman R (2007) *Fundamentals of rock mechanics*, 4th edn. Blackwell, Oxford, p 475
- Ladanyi B, Archambault G (1970) Simulation of shear behaviour of a jointed rock mass. In: *Proceedings of the 11th Symp. On Rock Mech. (AIME)*, pp 105–125
- McFarland J, Morris A, Bichon B, Riha D, Ferrill D, McGinnis R (2011) Geological stress state calibration and uncertainty analysis. *Structural dynamics*, vol. 3. In: *Conference Proceedings of the Society for Experimental Mechanics Series*, pp 557–570
- Morris A, Ferrill DA, Henderson DB (1996) Slip-tendency analysis and fault reactivation. *Geology* 24(3):275–278
- Patton FD (1966) Multiple modes of shear of failure in rock. *Proceedings of 1st Cong Int Soc Rock Mech*, Lisbon, pp 509–513
- Plesha ME (1987) Constitutive models for rock discontinuities with dilatancy and surface degradation. *Int J Numer Anal Meth Geomech* 11:345–362
- Rutqvist J, Tsang CF, Stephansson O (1998) Determination of fracture storativity in hard rocks using high pressure testing. *Water Resour Res* 34:2551–2560
- Saeb S, Amadei B (1992) Modelling rock joints under shear and normal loading. *Int J Rock Mech Min Sci Geomech Abstr* 29:267–278
- Schweisinger T, Swenson EJ, Murdoch LC (2009) Introduction to hydromechanical well tests in fractured rock aquifers. *Groundwater* 47(1):69–79
- Vasco DW (2009) Modeling broad-band poroelastic propagation using an asymptotic approach. PDF from scholarship.org. *Geophys J Int Wiley Online Libr* 179(1):299–318
- Vasco DW, Minkoff SE (2009) Modelling flow in a pressure-sensitive, heterogeneous medium. *Geophys J Int* 179:972–989
- Witherspoon PF, Wang JSY, Iwai K, Gale JE (1980) Validity of cubic law for fluid flow in a deformable rock fracture. *Water Resour Res* 16(6):1016–1024

ISRM Suggested Methods for Rock Stress Estimation—Part 5: Establishing a Model for the In Situ Stress at a Given Site

Ove Stephansson and Arno Zang

1 Introduction

This contribution relates to the updated suggested method for rock stress estimation and concerns the final rock stress model (FRSM) of a site or an area. The previous four suggested methods are (1) Part 1: strategy for rock stress estimation (Hudson et al. 2003), (2) Part 2: overcoring methods (Sjöberg et al. 2003), (3) Part 3: hydraulic fracturing (HF) and/or hydraulic testing of pre-existing fractures (HTPF) (Haimson and Cornet 2003), and (4) Part 4: quality control of rock stress estimation (Christiansson and Hudson 2003).

The aim of a site or an area characterization for underground works is to produce a three-dimensional model containing information about topography, soils, rock mass lithology, structural geology, hydrogeology and mechanical data, including rock stress. Such a geological model is needed in analyzing the cause and effect on stresses from lithology boundaries, geological structures, faults and fracture zones intersecting the site or area. Although it is impossible to know all the details of the geological evolution of a site or an area, it is worth the effort of trying to ascertain the in situ stress state from the bulk knowledge of the site morphology, topography and geology, and if

possible, to verify this information with additional data from boreholes and drill cores. We advocate that stress measurements to be conducted after the best estimate stress model (BESM) has been compiled. Sometimes numerical models can be of assistance in estimating the effect of geological parameter variations in the establishment of a stress model for a site. In this contribution, a strategy and flow chart is presented to establish the FRSM from a combination of available stress data from the BESM, new stress data from stress measurement methods on site (SMM) and integrated stress determination (ISD) using previous data plus numerical modeling (see Fig. 1). We are aware that sometimes the economic constraints prevent application of all the steps in establishing the FRSM. However, the goal of a stress measurement campaign is to collate and harmonize the data in the best way to describe the in situ stress condition of a site or area.

2 Overview of the Final Rock Stress Model (FRSM)

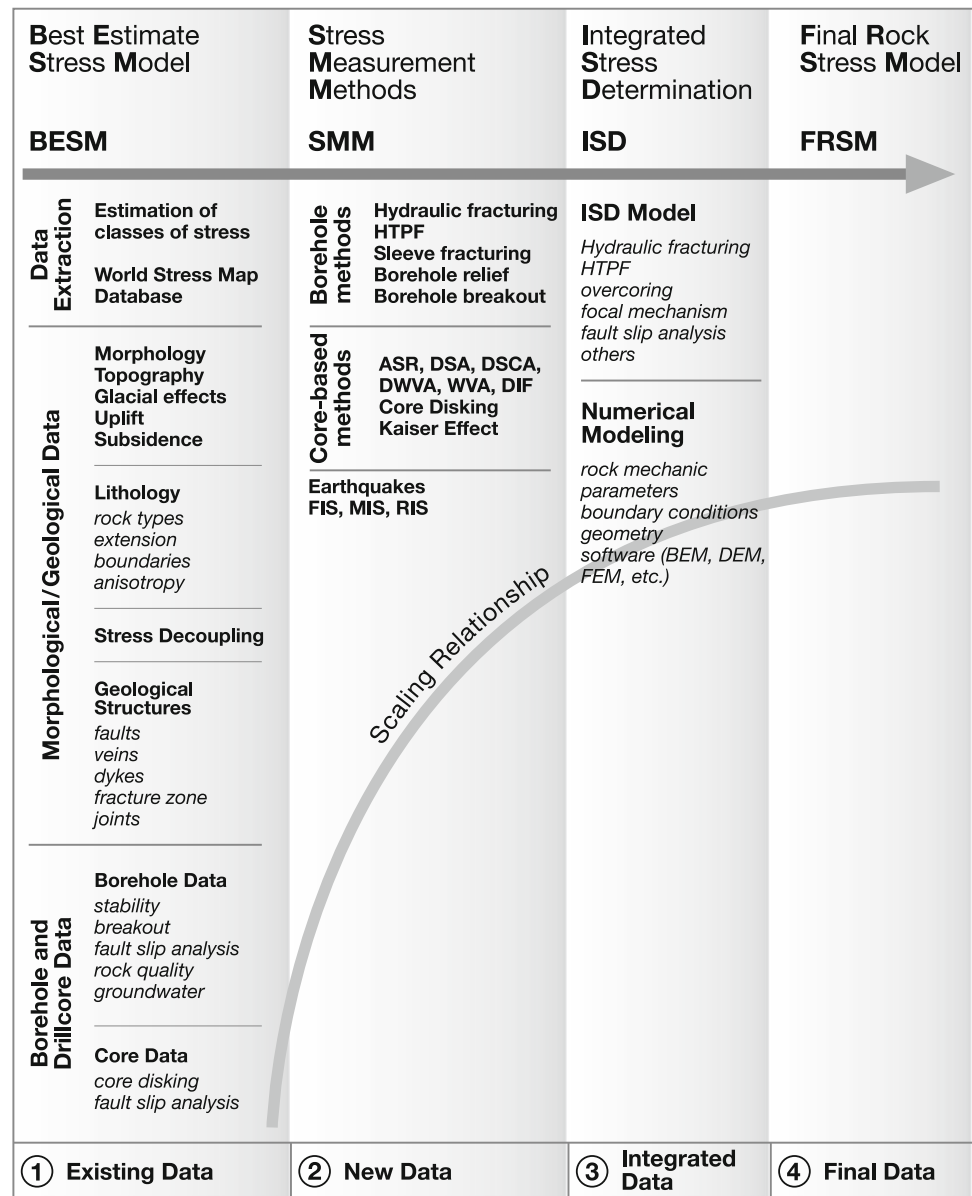
In situ stress exists in a rock mass prior to any manmade disturbances. Figure 1 presents the way forward for deriving the FRSM for a site or an area (Zang and Stephansson 2010). The BESM is established by collecting existing information from databases and analyzing field data on morphology, topography, geology, borehole and drill core information. Before any in situ stress measurements, the development of the BESM of the site or area is recommended. The established stress model should be used in selecting the appropriate stress measurement technique and assist in planning the measurements. After the BESM is established and stress measurement conducted, an integrated stress determination (ISD) should follow. In this last step, data from different stress sources (focal mechanism, fault slip analysis, borehole breakouts), information from the BESM and the results from

Please send any written comments on this ISRM Suggested Method to Prof. Resat Ulusay, President of the ISRM Commission on Testing Methods, Hecettepe University, Department of Geological Engineering, 06800 Beytepe, Ankara, Turkey.

Originally published as an article in the journal *Rock Mechanics and Rock Engineering*, 45, O. Stephansson, A. Zang, ISRM Suggested Methods for Rock Stress Estimation—Part 5: Establishing a Model for the In Situ Stress at a Given Site, 955–969, 2012.

O. Stephansson · A. Zang (✉)
Department 2: Physics of the Earth, Sect. 2.6: Seismic Hazard and Stress Field, GFZ German Research Centre for Geosciences, Telegrafenberg, 14473, Potsdam, Germany
e-mail: zang@gfz-potsdam.de

Fig. 1 Generation of the final rock stress model (FRSM) by combination of the best estimate stress model (BESM), new stress data from stress measurement methods (SMM) and integrated stress determination (ISD), after Zang and Stephansson (2010)



the different stress measurement methods are merged (e.g. Cornet and Buret 1992; Tonon and Amadei 2003; Wileveau et al. 2007). Numerical stress models can be of great help in predicting and validating the in situ stress and together with the results of the stress measurements and ISD, it supports the establishment of the final rock stress model (FRSM) as presented in Fig. 1. The scaling relationship is also illustrated in the figure. The scale of the problem is defined by the distribution of the available data and the objective of the BESM is to help identify if all data can be assumed to sample the same continuum, or if the data needs to be divided into subsets, which is then followed by the ISD phase. Once completed, the drastic change from the conventional single method approach concerns the precision and credibility of the in situ stress. A site with different single method interpretation of various locations in space and time now has to become one

ISD solution. This is the difficult task of the multiple-method, scaled, integrated approach. Geological field data and information from borehole and core data, together with old and new stress measurement data, are often point wise information. After performing the integrated stress determination (ISD) and stress modeling, the resulting stress data are relevant for larger rock volume and therefore are more adequate for the design and construction at a site or an area.

3 Best Estimate Stress Model

The data collection for establishing the best estimate stress model (BESM) can be divided into three main groups: (a) data extraction, (b) morphological/geological data, and (c) borehole and drill core data (Fig. 1).

The items listed in the left column of the boxes in Fig. 1 can serve as a checklist in performing the first step in a stress analysis for a site or an area. After collecting the data and performing the mapping and analysis, the BESM can be established and the model should result in the best estimate of stress orientation and magnitude versus depth. Before any in situ stress measurements at a site, establishment of BESM is recommended.

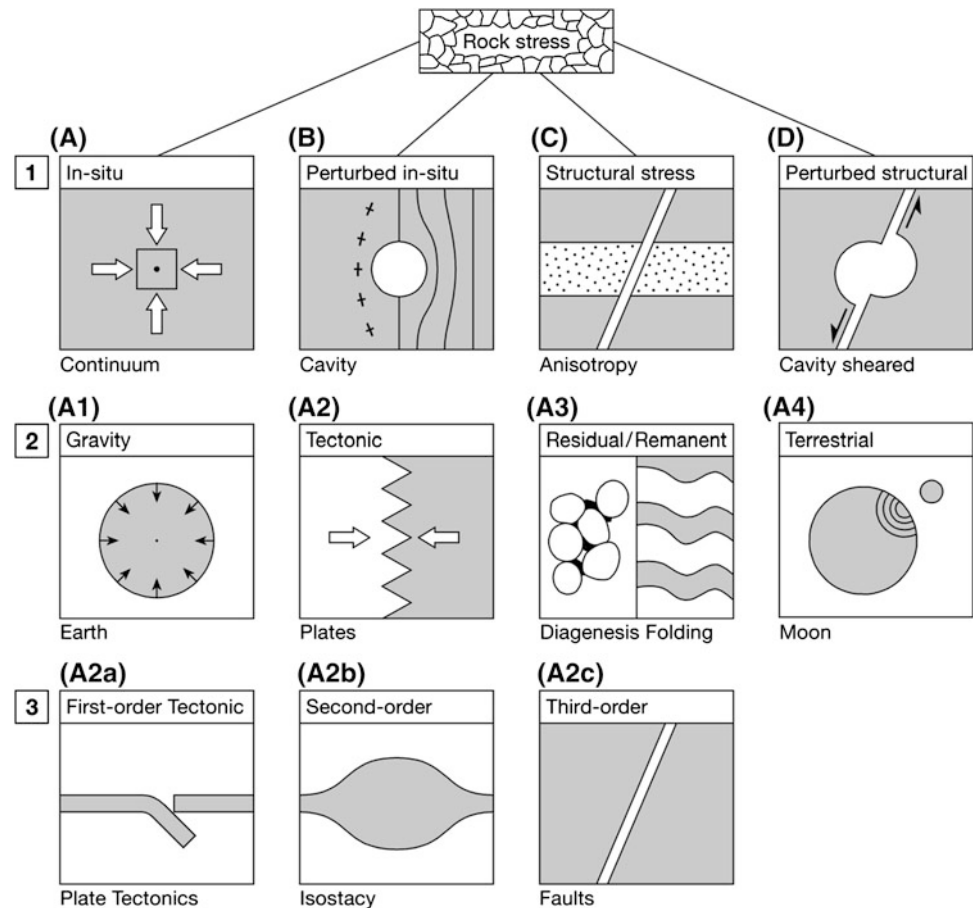
3.1 Data Extraction: Classes of Stresses

The first step in establishing the BESM, requires an assessment of the type of stresses that can exist at the site or in an area. There is no internationally agreed terminology and scheme for the different type of stresses existing in the Earth's crust. Recently, Zang and Stephansson (2010) presented a rock stress classification and terminology as shown in Fig. 2. The first level of stresses distinguish between in situ and perturbed in situ stresses and for anisotropic or heterogeneous rock material the term structural or perturbed structural stress has to be used. Note that depending on the distance from the heterogeneity we distinguish between near-field stresses, i.e. the local stress perturbation in the vicinity of the heterogeneity, and far-field stresses, i.e. the global stresses applied at infinity (regional). Near-field stresses decrease rapidly with distance from the defect (fault, heterogeneity). To separate out different components in the stress tensor (e.g. a regional horizontal stress which is locally perturbed by a fault), one has to operate at different scales, Sect. 2. The four second-level force contributors (A1–A4) to the in situ stress tensor are originating from different forces in the Earth's crust. On the third hierarchical level, active tectonic stresses due to present state straining of the Earth's crust are divided into first order (plate scale), second order (mountain range), and third order (fault scale) stresses. The different orders of tectonic stresses are scaled according to their coherent domain in the region in which a stress component is supposed to be uniform, both in magnitude and orientation. Figure 2 illustrates the broad scale and local active forces responsible for the stresses of first- and second order in the context of modern plate tectonics. The third-order stress patterns in Fig. 2 are explained by faults, seismic-induced stress changes due to large earthquakes and volcanic eruptions, as well as local density contrast, e.g. from salt diapers or detachment horizons (Heidbach et al. 2007, 2010). For applied rock mechanics and rock engineering purposes, gravitational and tectonic stresses are by far the most important (Fig. 2A1, A2).

3.2 Data Extraction: Stress Data and World Stress Map

Many authors have collected and summarized data on rock stresses and proposed expressions for the variation of the magnitude of the vertical and horizontal stresses with depth at specific sites and/or regions of the world. A summary of references to publications of horizontal and vertical stress versus depth, magnitude-depth profiles and stress orientation maps are presented in Amadei and Stephansson (1997) and Zang and Stephansson (2010), respectively. When estimating the state of stress at any depth in the rock mass, we make the assumption that the in situ stress can be described by three components: a vertical component due to the weight of the overburden at that depth and two horizontal components which are larger or smaller than the vertical stress. For the variation of vertical stress with depth, there has been a long series of in situ stress measurements conducted and several data compilations done (Herget 1974; Brown and Hoek 1978; Amadei and Stephansson 1997; Zang and Stephansson (2010)), that proofs that, in most cases, the magnitude of the vertical stress can be explained by the overburden weight only. Deviation from this rule exists and in particular in areas of young tectonics, volcanism, rough topography and near major discontinuities in the rock mass. Relationship between vertical and horizontal stress for simple, elastic, homogeneous Earth, and rock masses with transversely and orthotropic anisotropy are presented in Zang and Stephansson (2010), and in more details in Cornet and Burlet (1992). The authors, Amadei and Stephansson (1997) and Zang and Stephansson (2010) have pointed out that the generic, often linearly increasing stress magnitude versus depth relationships presented should be used with caution, as they are usually associated with scatter. The stresses at a site can vary locally due to topographical effect, geological unconformities, stratification, geological structures such as faults, dikes, veins joints, folds, etc. Therefore, in estimating the state of stress at a site or a region, these local perturbations need to be considered as they cause deviation from the often-assumed linearity of stress variations with depth. Measured variations of stress with depth have also demonstrated “stress decoupling” (Haimson 1980; Martin and Chandler 1993; Stephansson 1993; Roth and Fleckenstein 2001), where stresses at shallow depth might be entirely different from stresses at great depth. Stress decoupling is valid for both stress magnitude and orientation. The World Stress Map (WSM) is the global database for contemporary tectonic stress data from the Earth's crust (Zoback et al. 1989; Heidbach et al.

Fig. 2 Rock stress scheme and terminology at three hierarchical levels. Level 1 separates solid (AC) from excavated rock mass (BD). Level 2 separates in situ stress components according to their origin forces. Level 3 separates tectonic stresses according to their coherent domains, such as plate tectonics, isostasy and individual faults, after Zang and Stephansson (2010)



2008). Various academic and industrial institutions working in different disciplines of Earth sciences, such as geodynamics, hydrocarbon exploitations and rock engineering use the WSM. The uniformity and quality of the WSM is guaranteed through (1) quality ranking of the data according to international standards, (2) standardized regime assignment, and (3) guidelines for borehole breakout analysis and other methods. To determine the tectonic stress orientation, different types of stress indicators are used in the WSM. The 2008 release of WSM contains 21,750 data points and they are grouped into four major categories with the following percentage (<http://www.gfz-potsdam.de>) (Heidbach et al. 2010): (1) Earthquake focal mechanisms (72 %), (2) well-bore breakouts and drilling induced fractures (20 %), (3) in situ stress measurements [overcoring, hydraulic fracturing, borehole slotter (4 %)], and (4) young geologic data [from fault slip analysis and volcanic vent alignments (4 %)].

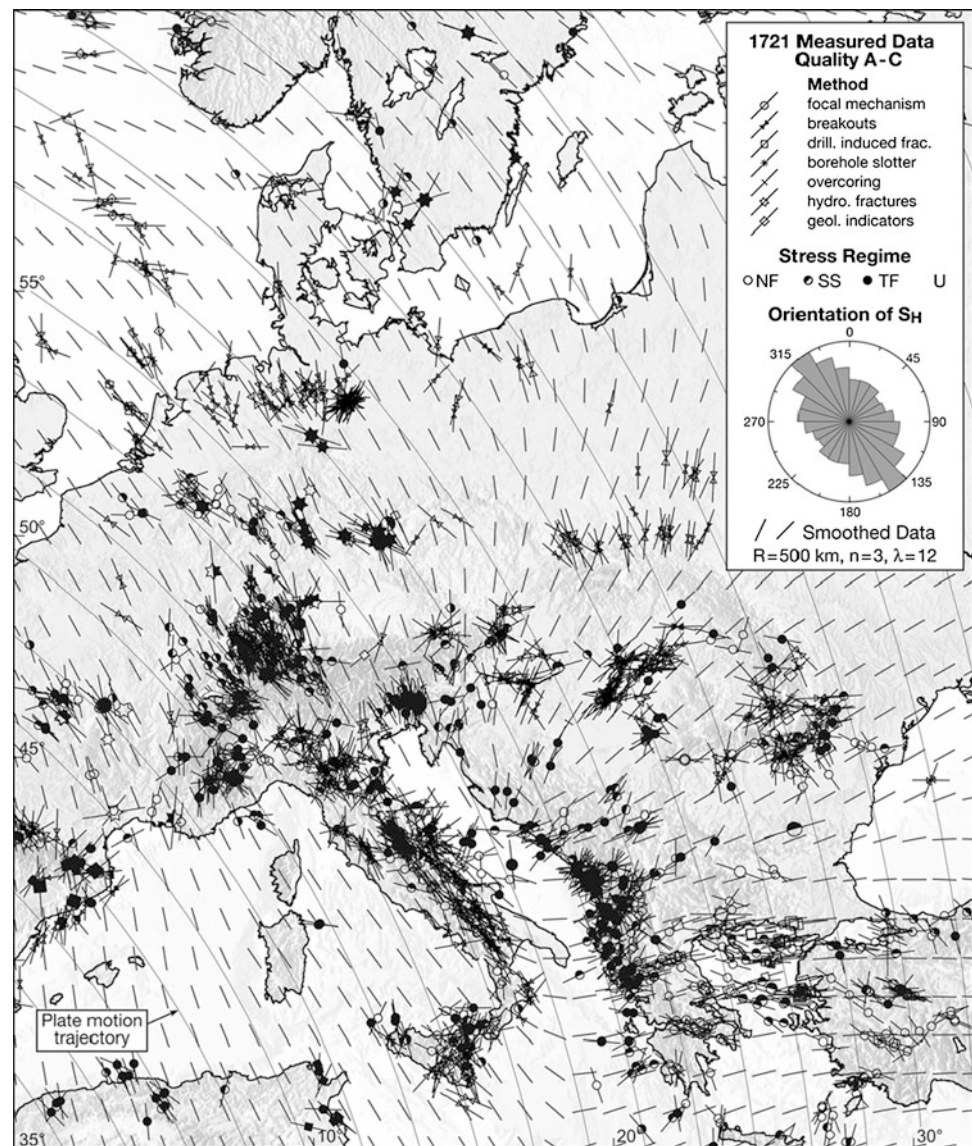
The seismologists and their analysis of the focal plane mechanisms related to large earthquakes (Angelier 2002) provide the majority of data to the WSM. The relatively small percentage of in situ stress measurements is due to the demanding quality ranking and the fact that many of the data are company owned. At the very first stage of estimating the

state of stress at a site or a region, consultation of the WSM is appropriate and often worthwhile. A detailed map of the area of interest can be provided free by the WSM. The delivered map contains a legend of the most likely type of stress regime (normal, strike slip and thrust faulting regime) in the area. Data can also be extracted from different depth interval and for different stress recording methods. If there is enough stress data from a region, a map of smoothed direction of maximum horizontal stress can be ordered (Fig. 3). In using stress data from the WSM, it is important to consider the depth for which the stress data are relevant.

3.3 Morphology and Geology

The issue of morphology and topography on estimating in situ stress is of particular interest in mountainous area, near valley slopes and at the top of high mountains and for mining projects, e.g. at the slopes of open pit mines. The slopes and valley sides can create stress perturbations of underground excavations located at the toe of the slopes and valleys and cause rock burst and spalling and other types of rock failure. It is a difficult task to determine analytically the in situ stress field in a rock mass or a region with an

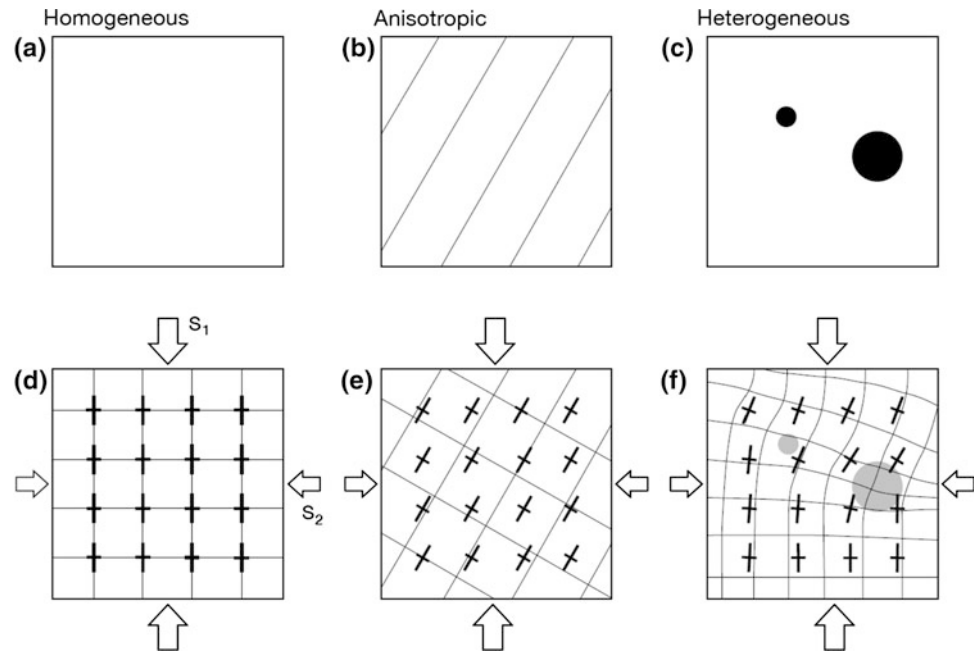
Fig. 3 Smoothed maximum horizontal stress direction map of Western Europe (*short bars*) based on the 1,721 stress entries from the World stress map. *Thin grey lines* show the relative plate motion trajectories of the African plate with respect to the Eurasian plate, modified from Heidbach et al. (2007) and after Zang and Stephansson (2010)



irregular surface using the theory of linear elasticity. The difficulty of determining stresses in regions with rough topography is due to the fact that the Earth's surface is a principal stress plane where shear stress is zero. A summary of the developments and their application to different topography and gravity and tectonic loadings and rock mass anisotropy is presented in Amadei and Stephansson (1997). All the derived analytical expressions predict tensile stress in the valley bottom and this is supported by the observations from the field in terms of a zone of fractured and loose rock masses and tendencies of up-warping phenomena in the bottom of valleys. In steep mountainous areas or rock slopes, the gravity loading alone cause high stress concentrations parallel with the surface of the slope. In rock engineering, the stress deflection caused by these slopes has a tendency to cause spalling in the walls of a tunnel

(Myrvang 1993). Spalling is a common phenomenon in valley tunnels across the fjords in Norway and in valleys of young mountainous areas where topography is steep and rough. The simplifying assumption that the principal rock stresses are vertical and horizontal with depth and that the vertical stress is equal to the weight of the overburden is not valid for areas with gentle to strong topography. The influence of morphology and topography has to be included in establishing the best-estimate stress model (BESM). Glacial effects, uplift and subsidence very often cause a more intense fracturing and faulting in the uppermost parts of the Earth's crust. This disturbs the stress field so that for example in glaciated terrains like Scandinavia and Canada one often finds an excess of horizontal stresses and thrust faulting conditions in the uppermost couple of hundred meters of the rock (Stephansson 1993).

Fig. 4 Homogeneous (a), anisotropic (b), and heterogeneous (c) material affect principal stress orientation and magnitude (d–f), after Zang and Stephansson (2010)



3.4 Geological Data

Understanding the geological history of a site or an area is essential as it can be used to determine the evolution of the stress regime in which the site or area of interest is located. No one should run a stress estimation campaign and produce a model without studying the geology carefully and understanding its ramifications. Such an approach has been applied recently to the area at Äspö Hard Rock Laboratory in Sweden (Hakami et al. 2002). A methodology for building a stress model has been suggested that involves different steps, starting with preliminary stress estimation, followed by steps for interpreting site-specific information. Factors that might influence the regional stresses and the in situ stresses at the site are listed. Because the Fennoscandian Shield, where Äspö is located, is a part of the Eurasian plate its geological history is presented in the context of plate tectonics. The role of current plate motion for the present day state of stress in the NW European sub-plate is highlighted (see also Fig. 3). The report by Hakami et al. (2002) is one of the very first attempts ever made to present a plan for a complete stress model of a specific site and where the tectonics and structure geology play an important part. With respect to determination, the magnitude of the stresses with reasonable certainty, the authors (Hakami et al. 2002) advocate that in situ stress measurements should be used. Estimating in situ stresses requires a detailed characterization of the site geology like lithology and lithological boundaries, its tectonic history, critical structures, erosion, uplift, influence of glaciation, hydrogeology, neo-tectonic and others. In the following sections, a few of the most important geological factors to rock stress estimation are considered.

3.5 Lithology and Lithological Boundaries

In situ stresses can vary significantly from one lithological unit to the next depending on the relative stiffness and strength between the individual rock masses. Abrupt changes are likely to appear at the contacts between different lithological units (e.g. Tonon and Amadei 2003; Wileveau et al. 2007). Therefore, it is of utmost importance to perform a correct geological mapping and characterization of the site or area. The influence of lithology on the distribution of horizontal stress at depth has been demonstrated by a large number of stress measurements conducted in sedimentary and volcanic rocks. A list of references is presented by Amadei and Stephansson (1997). In general, one expects to find larger stress magnitudes in the more competent strata as stresses tend to concentrate in hard rocks surrounded by less competent rocks and subjected to the same far-field stress field. However, there have been reported results from hydraulic stress measurements where instantaneous shut-in pressure was found to be lower in layers with high Young's modulus and low Poisson's ratio and higher in layers with low Young's modulus and high Poisson's ratio (Amadei and Stephansson 1997). Similar results have also been reported for sedimentary rocks in tectonically relaxed areas. However, these are exceptions and in general, higher modulus rock types are more likely to carry higher than average stresses. The term structural stress (see Sect. 3.1) was introduced by Jaeger and Cook (1979). Structural stresses are caused by anisotropy and heterogeneity of rock mass and are depicted from Zang and Stephansson (2010) with and without externally applied loads in Fig. 4. Principal stress orientation at selected points are oriented parallel to

the applied load for the homogeneous material (Fig. 4a, d). In the case of anisotropic material, the applied far-field stress is perturbed by the planes of anisotropy and principal stress orientation in the material is rotated towards the orientation of the rock anisotropy (Fig. 4b, e). In case of heterogeneous material (Fig. 4c, f) orientation and magnitude of stresses are perturbed in the vicinity of the defect. As a rule of thumb, far-field stresses can be treated as undisturbed at distances of about three times the diameter of the defect.

3.6 Different Stress Regimes and Stress Decoupling (Near-Field and Far-Field Stress)

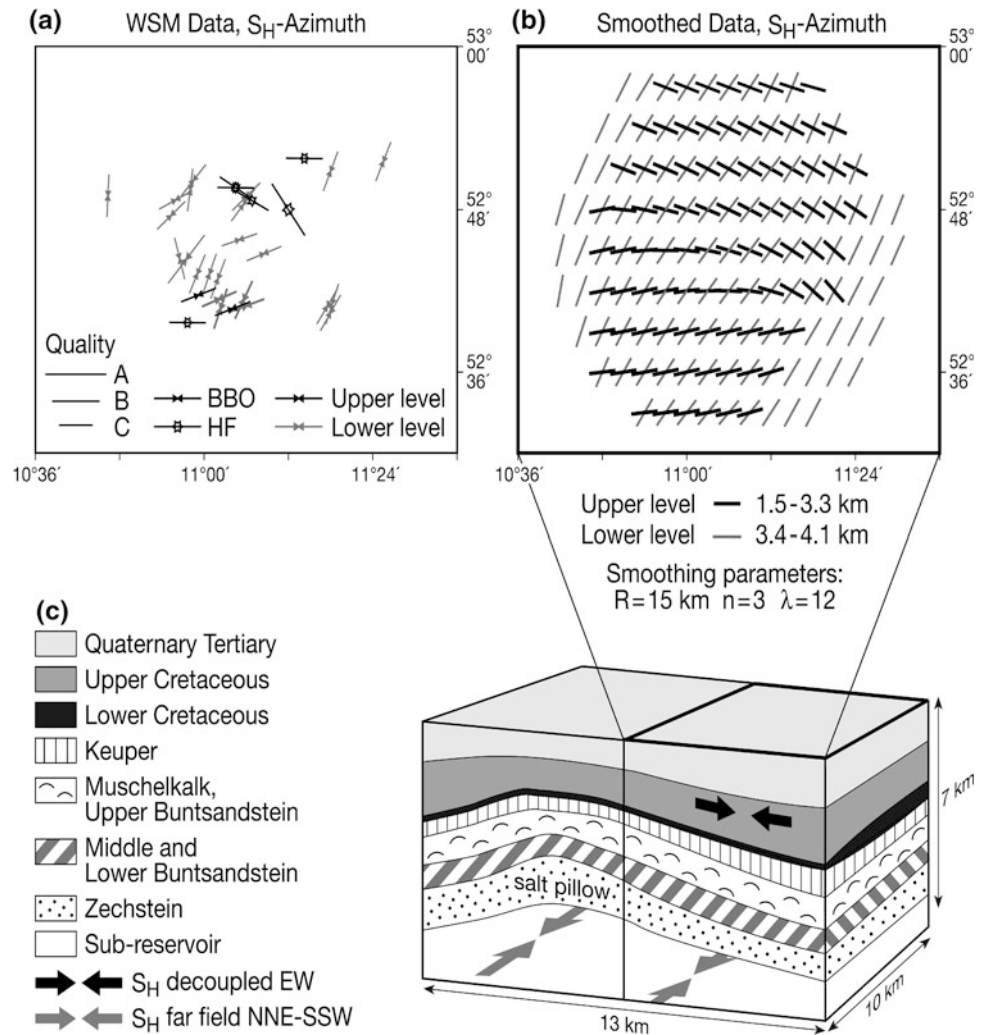
From the results of stress measurements in vertical boreholes, it has been demonstrated that the type of stress regime at shallow depth may be entirely different from the stress regime at great depth. A recent example is described from the stress measurements for the Björkö geothermal project in the vicinity of Stockholm, Sweden (Ask and Stephansson 2003). Here, the stresses in the uppermost 400–500 m are characterized by a thrust faulting stress state, where the vertical stress is the minimum principal stress. Below ca. 500 m depth, the stress state corresponds to a strike slip stress regime where the vertical stress is the intermediate principal stress. The stress measurements were conducted in the centre of the Björkö meteoritic impact with an estimated diameter of 10 km. The granitic rocks are severely fractured due to the impact. Another of the Swedish meteoritic impacts, the Siljan impact structure in central-north Sweden shows a similar stress change with depth (Lund and Zoback 1999). Both impact structures indicate somewhat lower stress magnitudes as compared to the general situation in Fennoscandia. A similar stress change with depth to that observed at Siljan and Björkö in Sweden has been shown among others for the site investigations of the geothermal project in the Carnmenellis granite, Cornwall, UK (Cooling et al. 1988). These types of different stress regimes with depth are referred to as stress decoupling and can occur for various reasons, e.g. a marked hiatus in the stratigraphy like a basement-cover situation, different lithology in a rock sequence, non-persistent far-field boundary stresses, post-glacial lithosphere flexure and major discontinuities intersecting the area. Post-glacial lithosphere flexure and the transition from more fractured rock mass to less fractured rock of the glaciated terrains is the most likely explanation for the stress change with depth for the three mentioned sites. An interesting study related to stress decoupling in the Perm-Triassic rocks of the eastern part of the North German Basin (ENGB) is presented by Roth and Fleckenstein (2001). From the data collected in

the WSM project, it is known that central Western Europe is dominated by a NW–SE to NNW–SSE orientation of the maximum horizontal compressive stress (cf. Fig. 3), the result of ridge push from the North Atlantic and the northward drift of Africa (Müller et al. 1992). From a new analysis of four-arm-dipmeter data and televiwer loggings at intervals from 1,500 to 6,700 m in deep boreholes and comparison with hydraulic fracturing stress measurements from the region, the substrata below the more than 1,000 m thick Zechstein salt formation is dominated by a NNE–SSW striking orientation of the maximum horizontal stress. The 45°–90° difference in stress orientation above and below the detachment of the Zechstein salt formation is explained by decoupling of stresses (Fig. 5). Roth and Fleckenstein (2001) have suggested three hypotheses for this stress decoupling: (1) the influence of the large ancient suture zones, a trans-European fault zone and the Elbe fault system, with a NW–SE strike and bordering the basin; (2) dominance of local stresses due to postglacial lithosphere flexure where the compressive stresses outside the edge of the Weichselian and earlier Fennoscandian ice sheets might have caused the reorientation of the stress field in the sub-saline formations; (3) a strong lithosphere barrier below the northern margin of the basin, derived from rheology/depths profiling and modeling, which proves that stresses are attracted and reoriented to the observed N–S orientation. In conclusion, as there is no indication for stress differences from the plate boundaries, the stress decoupling in ENGB is likely to be due to contrast in competence (rigidity) between sedimentary rocks in North German Basin and the more competent basement of Fennoscandian rocks.

3.7 Stress Perturbation from Fault (Near-Field and Far-Field Stress, Continued)

Geological structures, such as faults, folds, dikes, veins, sills, fault striation or slickensides have long been used by structural geologists to indicate the paleo-stress, i.e. the state of stress prevailing at the time of genesis of the structure. Since the stresses that created the structure may have been modified due to later tectonic events, erosion, uplift, and glaciation, etc. the structure and petrography fabric might not be correlated at all with the current stress field. To determine the contemporary stress field, one has to seek out the most recent geological structures and use as stress orientation indicators. As an example, different volcanic vent alignments and inversion of fault-slip data are used for stress orientation in the WSM database (Heidbach et al. 2008). Fault-slip analysis, as developed by Angelier (1989) and others for stress analysis of recent geological formations or inversion of data from slickensides on

Fig. 5 Decoupling of stress in the eastern part of the North German Basin: **a** stress data entries from World Stress Map, **b** smoothed maximum horizontal stress orientations, **c** block diagram of geology and far-field stress orientation in the sub-reservoir rock and decoupled stress in the overburden, after Heidbach et al. (2007) and modified by Zang and Stephansson (2010)

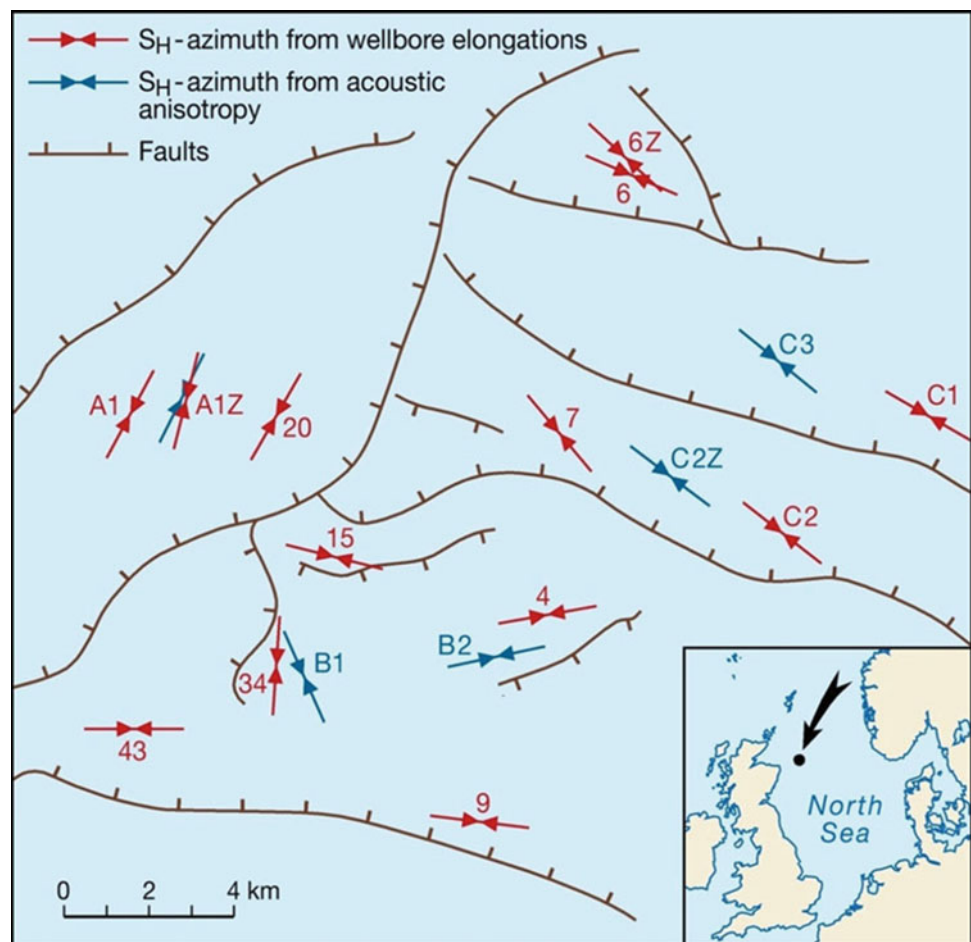


fracture surfaces in oriented drill core samples (Hayashi and Masuoka 1995) are powerful tools in stress determination of a site or an area. The existence of geological structures and heterogeneities will affect the distribution and magnitude of in situ stresses and make the local stress field different from the regional stress field. When a regional stress field is approaching a major discontinuity, the stress transfer across the stress perturbation from the discontinuity is very much dependent upon the material property of the discontinuity. If it happens to be an open structure the stresses cannot transect it. If the structure has the same properties as the surrounding rocks, the stresses are unaffected. If the material in the discontinuity is more rigid than the surrounding rock mass the maximum principal stress is diverted perpendicular to the discontinuity and if it is less rigid the maximum stress will tend to divert parallel with the discontinuity. The classical example of the second situation is the stress field in the surrounding of the San Andreas Fault system often referred to as a weak fault in a strong crust (Hickman and Zoback 2004). The ongoing San Andreas Fault Observatory at Depth (SAFOD) project in the central

part of the fault is motivated by the need to answer fundamental questions about the physical processes, including rock stresses, controlling faulting and earthquake generation within a major plate-bounding fault. In Japan, at a somewhat smaller scale, Sugawara and Obara (1995) demonstrated using overcoring that the least principal stress acted perpendicular to the Atotsugawa fault plane, in an area otherwise dominated by thrust faulting. Lin et al. (2010) found the localized rotation of principal stress around faults and fractures from borehole B of the Taiwan Chelungpu-fault drilling project. In this study, borehole breakouts and drilling-induced tensile fractures were used together with electrical images and photographs of the borehole wall to determine the relationship between faults and fractures and stress orientation changes. It is reported that the stress field is frequently distorted in the vicinity of faults, fractures and lithological boundaries.

Local stresses close to fault systems are also most critical to characterizing hydrocarbon reservoirs. Fracture orientation, well stability, well orientation, and permeability anisotropy are all strongly affected by variations in the local

Fig. 6 Correlation of the direction of the maximum horizontal stress and the strike orientation of faults in the northern British North Sea sector, from Yale (2003)



near-field stresses. Figure 6 shows a map view of a field in the northern part of the British North Sea sector, and is located in the WNW–ESE extensional basin called the Witch Ground Graben. Data are taken from Yale (2003), and display acoustic anisotropy measurements on core from Piper Sands and wellbore elongation data from the overlying Kimmerage shale and the Piper Sands. The WNW trending faults are interpreted as normal faults and lie roughly parallel to the major Witch Ground Graben faults. The NNE trending fault through the centre of the field is interpreted as a wrench fault. The throw on faults is generally between 250 and 400 m. The regional stress trend in this area is considered to be maximum compression in a NNE direction (Müller et al. 1992). However, the data in Fig. 6 show significant variations from this general trend and significant variations between individual fault blocks. Maximum horizontal stress parallel to the strike of the faults is consistent with the normal faulting seen in the field (far-field stress). However, 30°–50° variation between the far-field and the near-field stress strongly suggests a rotation of the in situ stress field by the local fault structure. The very large throws on these faults and the strong segmentation of

the field may be the cause of the observed in situ stress rotation in this area (Yale 2003).

Stress relief from neotectonic faulting in the northern parts of the Fennoscandian Shield has been reported by Amadei and Stephansson (1997) and Bjarnason et al. (1989). Measured stresses with hydraulic fracturing method in a borehole adjacent to the neotectonic, postglacial Landsjärv fault show a marked stress magnitude anomaly compared to the average state of stress in Fennoscandia (Fig. 7). Magnitude of both minimum and maximum horizontal stress is reduced to half the expected value close to the fault at about 500 m depth. Faults, fracture zones and dikes intersecting the rock mass at a site or region cause perturbation of the regional stress state. The amount of perturbation is very much governed by the strength and deformability of the discontinuity. Here, we are faced with the problem of lack of strength and stiffness data about large structures and sometimes the difficulty in determining their orientation in space. Sometimes, the application of simple numerical models of generic type can be of great value in analyzing the stress perturbation from planar structures (Su and Stephansson 1999).

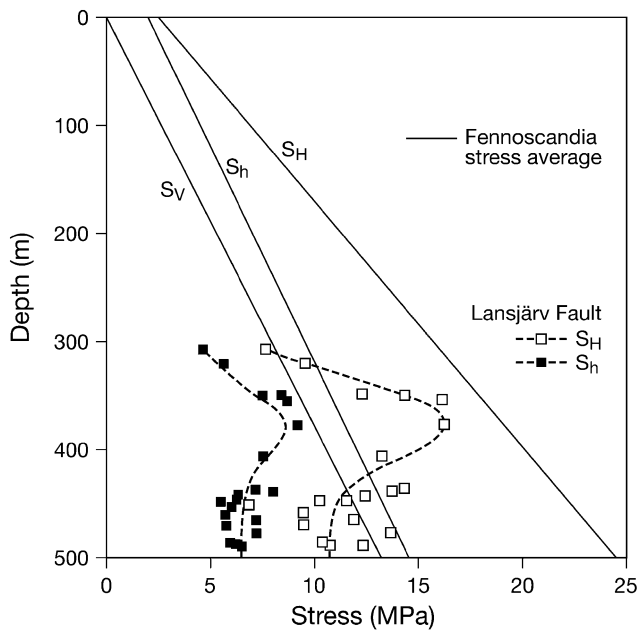


Fig. 7 Hydraulic stress measurements adjacent to the Lansjärv neotectonic fault, northern Sweden. Average hydrofracturing stress data from Fennoscandia (solid lines) are shown to illustrate the anomaly of stress magnitudes at the fault, after Bjarnason et al. (1989) and modified by Zang and Stephansson (2010)

3.8 Borehole and Drill Core Data

Information from borehole and drill core data is important for the establishment of BESM. Borehole instabilities and breakouts and fault slip developed in the wall of the borehole give information about orientation of stresses. Sometimes the magnitude of stresses can be estimated from the shape of the breakout in combination with numerical modeling (Shen 2008). Observation of the geometry of core dinking and fault slip on drill cores provide data relating to the magnitude and orientation of the stresses in the plane perpendicular to the drill core axis. Borehole breakout is now an established method to estimate the orientation of the maximum and minimum principal stresses in the plane perpendicular to the borehole axis. The breakouts are enlargements of the borehole wall occurring 180° apart, caused by stress-induced failure of the wells. In vertical wells, the diametrically positioned zones of broken or fall-out rock material occur at the azimuth of minimum horizontal compressive stress and typically have a consistent orientation in a given well or field. The shape and depth of the breakouts depend on the type of rock and the magnitude of in situ stress. Hard rocks and high stresses tend to generate deep breakouts with relatively small breakout angle. Breakouts can have a length of between centimeters up to several hundred meters. Borehole breakouts in a well can be visualized using optical (camera), mechanical (caliper) or electrical resistivity (formation micro-scanner) and ultrasonic image (borehole televiewer)

tools (Ellis and Singer 2007). A summary of theories of breakout formation, laboratory studies, techniques, equipment and evaluation procedures are presented in Amadei and Stephansson (1997) and Zang and Stephansson (2010). If data of borehole breakouts exist from a site, the information is of great value for the delineation of the stress orientation of the BESM.

Once drill cores are available from a site or an area, the search for and analysis of core dinking should be included in the stress estimation program. Core dinking is often an indication of high horizontal stresses and the geometry of the disks and the orientation of the disk saddle are indicators of stress orientation. The core breaks up into disks that are usually curved with the centre of curvature oriented towards the bottom of the borehole. The orientation of the crest line of the curved disk surface tends to coincide with the direction of the maximum principal stress. Laboratory testing and later numerical modeling has shown that once the radial stress in the core trunk during drilling exceeds the compressive strength of the rock core, dinking starts to develop. Haimson and Lee (1995), in their study on core dinking, proposed that thinner disks are indicative of higher horizontal stresses and that the through axis of saddle-shaped core disks often is aligned with the orientation of the maximum horizontal in situ stress. Less regular core dinking might also develop due to existing discontinuities or fabrics in the rock mass. The application of high thrust during the drilling operation can form horizontal tensile stress at the root of the drill core which is sufficiently large to generate extensile micro-cracks that coalesce to cause core dinking (Kutter 1993; Hakala 1999). Matsuki et al. (2004) estimated the directions of three-dimensional in situ stresses from the height at the periphery of the end surface of the core disks investigated. They applied the method to rock disks of diorite and granite from a vertical borehole (SB1) at Sakuma, Shizuoka prefecture, Japan where hydraulic fracturing was carried out to measure horizontal stress. Lim and Martin (2010) investigated the phenomenon of dinking, and its relationship with stress magnitudes, in cores from 75-mm diameter boreholes in the Canadian Underground Research Laboratory (URL). The data suggests that dinking in Lac du Bonnet granite initiates when the maximum principal stress normalized to the Brazilian tensile strength exceeds 6.5.

4 Stress Measurement Methods (SMM)

It is our recommendation that rock stress measurements should be performed after the establishment of the best estimate rock stress model. Data and information collected for BESM can also be used in selecting the best suited method for in situ stress measurement(s) and/or core-based stress measurement(s). The authors (Amadei and Stephansson 1997)

and more recently (Ljunggren et al. 2003; Zang and Stephansson 2010) have presented overviews of the most important stress measurement methods. Rock stress measurements in the Earth's crust can be classified according to their underlying physical principle, or according to the rock volume involved in the measurement technique. Crustal stress measurement techniques can be grouped into five different categories according to physical mechanism, experimental technique and ultimate borehole depth (see Table 7.1 in Zang and Stephansson (2010)). Category (1) mechanism is related to rock fracture as applied to boreholes. The most important method of this category is hydraulic fracturing (HF) (Haimson 1978; Amadei and Stephansson 1997; Zang and Stephansson 2010) where the minimum stress and the orientation of the maximum stress perpendicular to the borehole axis is determined. One modification of the HF test is hydraulic tests on pre-existing fractures (HTPF) (Cornet and Valette 1984; Haimson and Cornet 2003). The fluid pressure in HTPF balances exactly the normal stress across the pre-existing fracture. By combining pressure data from six or more fractures along the length of the borehole the 3D state of stress can be determined. When compared with HF, HTPF has the advantage of less limitation as regards geologic structures and the method does not require the determination of rock tensile strength. Another crucial issue with the HTPF technique is that it does not require that the borehole is aligned with a principal stress. Sleeve fracturing (Stephansson 1983), drilling-induced tensile fractures (Brudy and Zoback 1999) and borehole breakouts (Bell and Gough 1979) also belong to category (1) in the classification scheme.

Category (2) mechanisms are related to elastic strain relief due to coring. The technique can be further subdivided to surface relief methods, borehole relief methods and techniques that involve relief of large rock volumes with subsequent analysis of re-equilibrium deformation. Borehole relief methods can be further sub-classified according to the type of strain analysis at the borehole wall (see Zang and Stephansson 2010). Strains can be measured diametral (e.g. US Bureau of Mines USBM) or circumferential [e.g. Borre probe (Sjöberg et al. 2003)], at the flat end of the borehole (doorstopper), and at the surface of a conical or hemispherical end of a borehole (Obara and Ishiguro 2004). The Borre probe, the CSIR and CSIRO hollow inclusion cell are the most common tools applied in relief stress measurements (Sjöberg et al. 2003). Relief methods are the most widely used techniques in the engineering application of stress measurements for underground works.

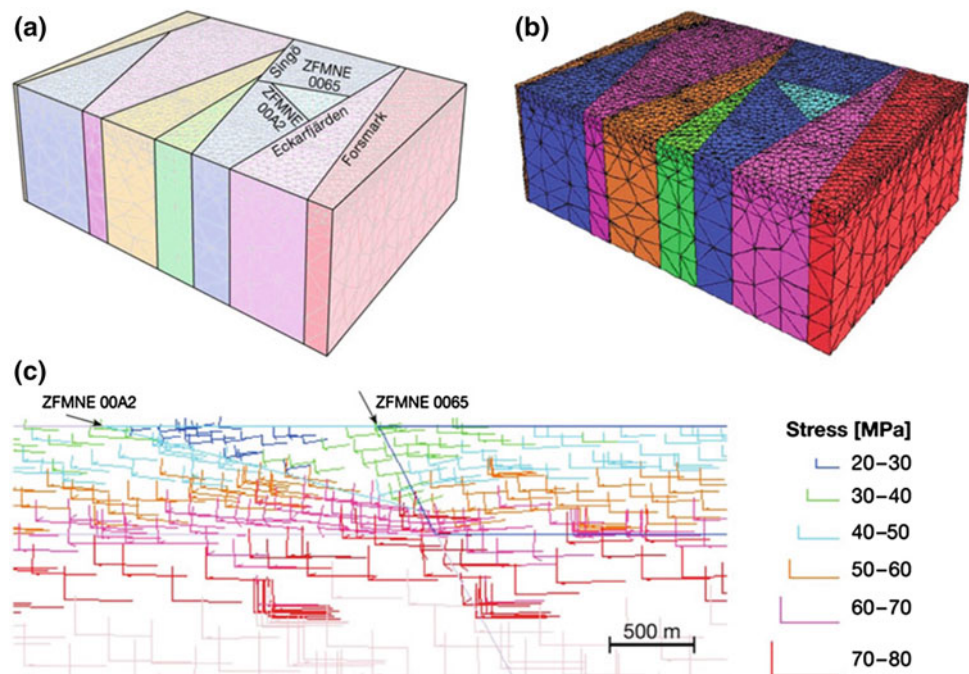
Category (3) mechanism in the classification recommended by Zang and Stephansson (2010) is related to crack-induced strain relief in drill cores. Micro-cracking is generated in stress relief when the rock is cut from the in situ stress field at the bottom or the wall of a borehole. Core-based methods can be further sub-divided into the analysis of

strain data like anelastic strain recovery (ASR), differential strain rate analysis (DRA), differential strain analysis (DSA), analysis of wave velocity data like differential wave-velocity analysis (DWVA) and wave velocity analysis (WVA). Cracking phenomena in drill cores and monitoring of related acoustic emissions by means of the Kaiser effect also belongs to this category (see Fig. 1, SMM).

Category (4) techniques, also called borehole seismic logging or indirect methods, combine the variation of physical rock properties with stress. Shear-wave polarization, shear wave splitting and analysis of Stonely waves are examples of wave propagation methods for stress analysis (Zang and Stephansson 2010). Finally, Category (5) techniques for stress estimates are concerned with physical properties of pre-existing fault zones in the Earth's crust and related earthquakes. The end members are fault plane solutions (FPS). Focal mechanisms of earthquakes provide the orientation of principal stresses and this information dominates the overall entries of stress data in the World Stress Map (WSM) described in Sect. 3.2. Guidelines for stress derivation from earthquake focal mechanisms are supplied on the WSM homepage (<http://www.dc-app3-14.gfz-potsdam.de>). Stress inversion from focal mechanisms can be separated into natural seismicity (NS) and induced seismicity (IS). In contrast to NS, the term IS refers to typically minor earthquakes and tremors that are caused by human activities that perturb the crustal stress field. Induced events are refined into mining-induced seismicity (MIS) and fluid-induced seismicity (FIS). MIS includes seismic events and related rock bursts arising from stress changes associated with mining activities. FIS is caused by injection of fluids in liquid waste disposal, or in the fracturing of hydrocarbon and geothermal reservoirs. Impoundment of large water reservoirs can generate FIS, and in this case are called RIS (reservoir induced seismicity). Stress inversions from induced seismic events, together with stress inversions from background natural seismicity, are useful tools to identify stress perturbations triggered by human activity (see Fig. 1, SMM).

By far the most extensive stress measurements campaigns and improvement of stress measurement techniques have been conducted for site investigations of underground laboratories and sites for final disposal of radioactive waste and spent nuclear fuel. One of the most important lessons learned from these site investigations is that it takes relatively long time and usually application of several different methods to obtain a reliable stress field of a site to host a deep geological repository of the size of about 1 km² located at a depth of 400–500 m below the ground surface. For the case of the Forsmark site for final disposal of spent nuclear fuel, the Swedish waste handling organization SKB came to the conclusion after six years of site investigations (2002–2008) from the ground surface that the stress field and in particular the magnitude of stresses at repository

Fig. 8 Numerical stress modeling with distinct element code 3DEC: **a** the model showing the orientation of the major fracture zones at the Forsmark site for spent nuclear fuel, Sweden, **b** overview of 3DEC model at the site, **c** principal stresses above and below a major shallow inclined deformation zone ZFMNE00A2 overlaying the rock mass for a future repository at ~ 420 m depth, after Hakami (2006)



level has to be defined in conjunction with the future tunneling and underground works. SKB started to use overcoring measurements with the Borre probe (Sjöberg et al. 2003) in deep boreholes later followed by hydraulic fracturing and HTPF (Haimson and Cornet 2003). The overcoring measurements gave core diskings below the depth of ca. 200 m and the successful measurements above were recorded in exfoliated rock mass and therefore not relevant for the depth of the repository. Despite the problems with the overcoring method, the presented stress model for Forsmark is based on the overcoring data, core diskings and the absence of borehole breakouts (SKB 2008). The hydraulic methods resulted in stress magnitudes about half the values of overcoring.

5 Integrated Stress Determination Method (ISD) and Numerical Analyses

The method of integrating the results of various stress measurement data obtained from applying different techniques to obtain a more reliable assessment of the in situ state of stress was introduced in the mid-1980 s and is still under development. In the early days, the integration method was based on a least square criterion (Tarantola and Valette 1982) where all measurements were assumed to obey a Gaussian distribution. In 1993, Cornet (1993) presented the HTPF stress determination method together with the Integrated Stress Determination Method. Data from hydraulic fracturing (HF) and hydraulic testing on

pre-existing fractures (HTPF) were integrated in order to obtain a better indication of the regional stress field (far-field). Integration of the hydraulic fracturing (HF) and HTPF data at the Äspö Hard Rock Laboratory in Sweden was presented in Ask et al. (2001). The same type of integration was carried out at two sites in southern France (Ask et al. 2003) and for the geothermal project on Björkö, Sweden (Ask and Stephansson 2003). The integration of CSIR and CSIRO overcoring stress data from Äspö Hard Rock Laboratory was presented in Ask et al. (2001) and integration of HF, HTPF and overcoring data on each side of the major fracture zone NE-2 in Ask (2006).

Today the integration method ISD uses a variety of algorithms, although least-squares are dominating. There are also numerous sites where this type of integration (ISD) has been applied. For example, Cornet and Burel (1992) applied the integration of HF-HTPF at eight different sites (four crystalline, four sedimentary rock) in France. Further, Yin and Cornet (1994) and Scotti and Cornet (1994) used information on induced seismicity and focal mechanisms to determine the in situ stress field in central France. A recent example for the “complete” determination of the in situ stress near the possible repository site for radioactive waste at Bure, NE France is given in Wileveau et al. (2007). In here, a combination of four different techniques; namely, HF, HTPF, sleeve fracturing and the analysis of en-echelon cracks were used in ISD to determine the in situ stresses within an argillite formation interbedded between two stiffer limestone layers, for the development and design of an underground research facility.

Numerical analyses employing a variety of simulation techniques (FEM, BEM, DEM, etc.) have been used in an attempt to predict or explain the in situ stress field and to illustrate the effect on the in situ stress of topography (Sturgul et al. 1976), stress distribution in a blocky rock mass subjected to a 2-D stress field (Stephansson et al. 1991), and the influence of large scale structures like faults (te Kamp et al. 1999). Inside and in the vicinity of faults and major fractures zones, both the stress magnitude and orientation will vary from point to point (Sect. 3.7). Stress prediction in these areas is more uncertain and even if it is possible to perform any stress measurements in these areas of poor rock quality, the variation in stresses will be larger. The numerical stress modeling shall help in obtaining an overall understanding of the state of stress between two points of stress measurements. The modeling results shall also contribute to the estimation of the variability of in situ stress magnitude and orientation in predicting the stresses in points or regions and uncertainty in presenting the final rock stress model. An example of stress modeling from the completed site investigations for the final repository of spent nuclear fuel at Forsmark, Sweden is illustrated in Fig. 8 (Hakami 2006). The site will host the Swedish repository of spent nuclear fuel. The 3DEC model shown in Fig. 8a consists of blocks with the same rock properties within a block surrounded by major deformation zones (faults). When equilibrium is obtained in the model the stress distribution is presented as a result, Fig. 8b. A detail of the orientation and magnitude of the maximum and minimum principal stresses for a region at a slightly inclined major deformation zone, called ZFMNE00A2, is presented in Fig. 8c. Notice the rotation and reduction of the principal stresses in the hanging wall of the deformation zone. The final repository at Forsmark will be located ~420 m below surface and at the footwall side of ZFMNE00A2.

6 Summary

To reach the final rock stress model (FRSM) at the site or area in question (see Fig. 1), it is necessary to proceed in steps. (1) Define classes of likely stresses and collect all available stress data of the location and its surroundings. (2) Include topography, lithology and faults as well as borehole and drill core stress data (BESM). (3) Measure stresses at the site and determine vertical and horizontal stresses versus depth (SMM). (4) Combine available and measured in situ stress data with earthquake and fault related stresses and perform an integrated stress analysis (ISD). (5) Validate the results of the integrated stress analysis and generate a 2-D/3-D stress model with rock parameters measured, appropriate boundary conditions defined and solve the resulting momentum equations with appropriate

numerical techniques and software. (6) Perform a sensitivity analysis, and (7) calibrate the model. Finally, it is necessary to consider the final near-field rock stress model in the context of the far-field stress pattern and present the stress model as principal or horizontal stresses versus depth (8) with clear indications of variability and uncertainty in magnitude and orientation. More detailed information on the procedures plus examples can be obtained from Zang and Stephansson (2010), and will be of major supplementary benefit to the readers of the SM—Part 5.

Acknowledgments For constructive comments and thorough review of the manuscript we thank Daniel Ask (Pöyry SwedPower AB, Luleå, Sweden), John W. Cosgrove (Imperial College, London, Great Britain), John A. Hudson (ISRM President), and Resat Ulusay (President of the ISRM Commission on Testing Methods).

References

- Amadei B, Stephansson O (1997) Rock stress and its measurement. Chapman & Hall, London
- Angelier J (1989) From orientation to magnitudes in paleostress determinations using fault slip data. *J Struct Geol* 11:37–50
- Angelier J (2002) Inversion of earthquake focal mechanism to obtain the seismotectonic stress IV—a new method free of choice among nodal planes. *Geophys J Int* 150:588–609
- Ask D (2006) New development of the integrated stress determination method and application to rock stress data at the Äspö HRL, Sweden. *Int J Rock Mech Min Sci* 43:107–126
- Ask D, Stephansson O (2003) Hydraulic stress measurements in borehole BJO01, Björkö impact structure, Lake Mälaren, Sweden. In: Sugawara K, Obara Y, Sato A (eds) International symposium rock stress, RS Kumamoto'03, Japan. Balkema, Rotterdam, pp 115–121
- Ask D, Stephansson O, Cornet FH (2001) Integrated stress analysis of hydraulic and overcoring rock stress data in the Äspö region. Analysis of hydraulic fracturing stress measurements and HTPF in boreholes KAS02, KAS03, and KLX02. Swedish Nuclear Fuel and Waste Management Co, SKB International Progress Report, IPR-01-26, Stockholm
- Ask D, Stephansson O, Cornet FH (2003) Integration of CSIR- and CSIRO-type of overcoring rock stress data at the Zedex Test Site, Äspö HRL, Sweden. In: Proceedings of tenth ISRM Congress, Johannesburg, Balkema, Rotterdam
- Bell JS, Gough DI (1979) Northeast-southwest compressive stress in Alberta: evidence from oil wells. *Earth Planet Sci Lett* 45:475–482
- Bjarnason B, Klasson H, Leijon B, Strindell L, Öhman T (1989) Rock stress measurements in boreholes KAS02, KAS03 and KAS05 on Äspö. Swedish Nuclear Fuel and Waste Management Co, SKB Progress Report 25-89-17, Stockholm
- Brown ET, Hoek E (1978) Trends in relationships between measured in situ stresses and depth. *Int J Rock Mech Min Sci Geomech Abstr* 15:211–215
- Brudy M, Zoback MD (1999) Drilling-induced tensile well-fractures: implications for determination of in situ stress orientation and magnitude. *Int J Rock Mech Min Sci* 36:191–215
- Christiansson R, Hudson JA (2003) ISRM suggested methods for rock stress estimation—part 4: quality control of rock stress estimation. *Int J Rock Mech Min Sci* 40:1021–1025
- Cooling CM, Hudson JA, Tunbridge LW (1988) In situ rock stresses and their measurement in the UK—part II. Site experiments and

- stress field interpretation. *Int J Rock Mech Min Sci Geomech Abstr* 25:371–382
- Cornet FH (1993) The HTPF and the integrated stress determination method. In: Hudson JA (ed) *Comprehensive rock engineering*, vol 3, Pergamon Press, Oxford, pp 413–432
- Cornet FH, Buret D (1992) Stress field determination in France by hydraulic tests in boreholes. *J Geophys Res* 97:11829–11849
- Cornet FH, Valette B (1984) In situ stress determination from hydraulic injection test data. *J Geophys Res* 89:11527–11537
- Ellis DV, Singer JM (2007) *Well logging for earth scientists*. Springer, Dordrecht
- Haimson BC (1978) The hydrofracturing stress measurement method and recent field results. *Int J Rock Mech Min Sci Geomech Abstr* 15:167–178
- Haimson BC (1980) Near surface and deep hydrofracturing stress measurements in the Waterloo quartzite. *Int J Rock Mech Min Sci Geomech Abstr* 17:1–88
- Haimson BC, Cornet FH (2003) ISRM suggested methods for rock stress estimation—part 3: hydraulic fracturing (HF) and/or hydraulic testing of pre-existing fractures (HTPF). *Int J Rock Mech Min Sci* 40:1011–1020
- Haimson BC, Lee CF (1995) Estimating in situ stress conditions from borehole breakouts and core diskings. In: Matsuki K, Sugawara K (eds) *Proceedings of international workshop on rock stress measurement at great depth*, Tokyo, Japan, 8th ISRM Congress. Balkema, Rotterdam, pp 19–24
- Hakala M (1999) Numerical study on core damage and interpretation of in situ state of stress. *Posiva Rep* 99–25, p 234
- Hakami H (2006) Numerical studies on spatial variation of the in situ stress field at Forsmark a further step. Site descriptive modeling Forsmark—stage 2.1. Swedish Nuclear Fuel and Waste Management Co, SKB R-06-124 (downloadable from <http://www.skb.se>), Stockholm
- Hakami E, Hakami H, Cosgrove J (2002) Strategy for a rock mechanics site descriptive model—development and testing of an approach to modeling the state of stress. Swedish Nuclear Fuel and Waste Management Co, SKB Research Report R-02-03 (downloadable from <http://www.skb.se>), Stockholm
- Hayashi K, Masuoka M (1995) Estimation of tectonic stress from slip data from fractures in core samples. In: Matsuki K, Sugawara K (eds) *Proceedings of international workshop on rock stress measurement at Great Depth*, Tokyo, Japan, 8th ISRM Congress. Balkema, Rotterdam, pp 35–39
- Heidbach O, Reinecker J, Tingay M, Müller B, Sperner B, Fuchs K, Wenzel F (2007) Plate boundary forces are not enough: second- and third-order stress patterns highlighted in the World Stress Map database. *Tectonics* 26:TC6014. doi:10.1029/2007TC00213
- Heidbach O, Tingay M, Barth A, Reinecker J, Kurfeß D, Müller B (2008) The 2008 release of the World Stress Map. doi:10.1594/GFZ.WSM.Rel2008
- Heidbach O, Tingay M, Barth A, Reinecker J, Kurfeß D, Müller B (2010) Global stress pattern based on the World Stress Map database release 2008. *Tectonophysics* 482:3–15
- Herget G (1974) Ground stress conditions in Canada. *Rock Mech* 6:53–74
- Hickman SH, Zoback MD (2004) Stress orientations and magnitudes in the SAFOD pilot hole. *Geophys Res Lett* 31, L15S12. doi:10.1029/2004GL020043
- Hudson JA, Cornet FH, Christiansson R (2003) ISRM suggested methods for rock stress estimation—Part 1: strategy for rock stress estimation. *Int J Rock Mech Min Sci* 40:991–998
- Jaeger JC, Cook NGW (1979) *Fundamentals of rock mechanics*, 3rd edn. Chapman & Hall, London
- Kutter HK (1993) Influence of drilling method on borehole breakouts and core diskings. In: Wittke W (ed) *Proceedings of 7th ISRM Congress*, Aachen. Balkema, Rotterdam, pp 1659–1664
- Lim SS, Martin CD (2010) Core diskings and its relationship with stress magnitude for Lac du Bonnet granite. *Int J Rock Mech Min Sci* 47:254–264
- Lin W, Yeh C-H, Hung J-H, Haimson B, Hirono T (2010) Localized rotation of principal stress around faults and fractures determined from borehole breakouts in hole B of the Taiwan Chelungpu-fault Drilling Project (TCDP). *Tectonophysics* 482:82–91
- Ljunggren C, Chang Y, Janson T, Christiansson R (2003) An overview of rock stress measurement methods. *Int J Rock Mech Min Sci* 40:975–989
- Lund B, Zoback MD (1999) Orientation and magnitude of in situ stress to 6.5 km depth in the Baltic Shield. *Int J Rock Mech Min Sci* 36:169–190
- Martin CD, Chandler NA (1993) Stress heterogeneity and geological structures. *Int J Rock Mech Min Sci Geomech Abstr* 30:993–999
- Matsuki K, Kaga N, Yokoyama T, Tsuda N (2004) Determination of the three-dimensional in situ stress from core diskings based on the analysis of principal tensile stress. *Int J Rock Mech Min Sci* 41:1167–1190
- Müller B, Zoback ML, Fuchs K, Mastin L, Gregersen S, Pavoni N, Stephansson O, Ljunggren C (1992) Regional patterns of tectonic stress in Europe. *J Geophys Res* 97:11783–11803
- Myrvang A (1993) Rock stress and rock stress problem in Norway. In: Hudson JA (ed) *Comprehensive rock engineering*, vol 3, Pergamon Press, Oxford, pp 461–471
- Obara Y, Ishiguro Y (2004) Measurements of induced stress and strength in the near-field around a tunnel and associated estimation of the Mohr–Coulomb parameters for rock mass strength. *Int J Rock Mech Min Sci* 41:761–769
- Roth F, Fleckenstein P (2001) Stress orientations found in North-East Germany differ from the West European trend. *Terra Nova* 13:289–296
- Scotti O, Cornet FH (1994) In situ stress fields and focal mechanism solutions in central France. *Geophys Res Lett* 21:2345–2348
- Shen B (2008) Borehole breakouts and in situ stresses. In: Potvin Y, Carter J, Dyskin A, Jeffrey J (eds) *SHIRMS 2008*. Australian Centre for Geomechanics, Perth, pp 407–418
- Sjöberg J, Christiansson R, Hudson JA (2003) ISRM suggested methods for rock stress estimation—Part 2: overcoring methods. *Int J Rock Mech Min Sci* 40:999–1010
- SKB (2008) Site description of Forsmark at completion of the site investigation phase. SDM-Site Forsmark. Swedish Nuclear Fuel and Waste Management Co, SKB Technical Report, TR-08-05 (downloadable from <http://www.skb.se>), Stockholm
- Stephansson O (1983) Rock stress measurement by sleeve fracturing. In: *Proceedings of 5th ISRM Congress*, Melbourne. Balkema, Rotterdam, pp F129–F137
- Stephansson O (1993) Rock stress in the Fennoscandian shield. In: Hudson JA (ed) *Comprehensive rock engineering*, vol 3, Pergamon Press, Oxford, pp 445–459
- Stephansson O, Ljunggren C, Jing L (1991) Stress measurements and tectonic implications for Fennoscandia. *Tectonophysics* 189:317–322
- Sturgul JR, Scheidegger AE, Greenspan Z (1976) Finite element model of a mountain massif. *Geology* 4:439–442
- Su S, Stephansson O (1999) Effect of a fault on in situ stresses studied by the distinct element model. *Int J Rock Mech Min Sci* 36:1051–1056
- Sugawara K, Obara Y (1995) Rock stress and rock stress measurements in Japan. In: Matsuki K, Sugawara K (eds) *Proceedings of international workshop on rock stress measurement at Great Depth*, Tokyo, Japan, 8th ISRM Congress. Balkema, Rotterdam, pp 1–8
- Tarantola A, Valette V (1982) Generalized non-linear inverse problem solved using the least squares criterion. *Rev Geophys Space Phys* 20:219–232

- te Kamp L, Konietzky H, Blümling P (1999) Three-dimensional modelling of the planned Wellenberg repository site in Switzerland. In: Editors missing. Numerical methods in geomechanics—NUMOG VII. Balkema, Rotterdam, pp 385–390
- Tonon F, Amadei B (2003) Stresses in anisotropic rock masses: an engineering perspective building on geological knowledge. *Int J Rock Mech Min Sci* 40:1099–1120
- Wileveau Y, Cornet FH, Desroches J, Blümling P (2007) Complete in situ stress determination in the argillite sedimentary formation. *Phys Chem Earth* 32:866–878
- Yale DP (2003) Fault and stress magnitude controls on the variations in the orientation of in situ stress. In: Ameen (ed) *Fracture and in situ stress characterization of hydrocarbon reservoirs*. Geological Society London, Special Publications 209, pp 55–64
- Yin FM, Cornet FH (1994) Integrated stress determination by joint inversion of hydraulic tests and focal mechanisms. *Geophys Res Lett* 21:2645–2648
- Zang A, Stephansson O (2010) *Stress field of the Earth's crust*. Springer Science and Business Media BV, Dordrecht
- Zoback ML, Zoback MD, Adams J, Assumpcao M, Bell S, Bergman EA, Blümling P, Brereton NR, Denham D, Ding J, Fuchs K, Gay N, Gregersen S, Gupta HK, Gvishiani A, Jacob K, Klein R, Knoll P, Magee M, Mercier JL, Mueller BC, Paquin C, Rajendran K, Stephansson O, Suarez G, Suter M, Udias A, Xu ZH, Zhizhin M (1989) Global patterns of tectonic stress. *Nature* 341:291–298

Part III
Monitoring

ISRM Suggested Method for Monitoring Rock Displacements Using the Global Positioning System (GPS)

Norikazu Shimizu, Shinichiro Nakashima, and Tomohiro Masunari

1 Introduction

Monitoring rock displacements is important to understanding the behavior of a rock mass and to assessing its stability. The Global Positioning System (GPS) is a satellite-based positioning system developed in the USA; it was established as a navigation system and then as a method for long baseline surveys (e.g., Hoffman-Wellenhof et al. 2001; The Survey Advisory Board and the Public Land Survey Office for State of Washington Department of Natural Resources 2004; Misra and Enge 2006). GPS has the potential to monitor three-dimensional displacements over an extensive area with high accuracy. It began to be used for displacement monitoring in the mid-1980s in the fields of civil and mining engineering, and other related fields (e.g., Chrzanowski and Wells 1988; Burkholder 1988, 1989). Since then, practical applications have been performed by many researchers (e.g., Hudnut and Behr 1998; Gili et al. 2000; Malet et al. 2002; Kim et al. 2003; Taşçi 2008), and some guidelines have been published for displacement (deformation) monitoring (e.g., US Army Corps of Engineers 2002; Vermeer 2002; Bond 2004).

This Suggested Method describes a method for monitoring rock displacements using GPS, focusing on baselines which are <1 km in length. The devices, the procedure, and examples of applications are illustrated, together with methods of data correction for improving the measurement results. The terminology (glossary) about GPS used in this Suggested Method is listed in Appendix “Terminology”.

Originally published as an article in the journal “Rock Mechanics and Rock Engineering”, 47, N. Shimizu, S. Nakashima, T. Masunari, ISRM Suggested Method for Monitoring Rock Displacements Using the Global Positioning System (GPS), 313–328, 2014.

N. Shimizu (✉) · S. Nakashima · T. Masunari
Department of Civil and Environmental Engineering,
Yamaguchi University, 2-16-1 Tokiwadai, Ube,
755-8611, Japan
e-mail: nshimizu@yamaguchi-u.ac.jp

2 Scope

There are two methods for using GPS. One method is point positioning for navigation. The three-dimensional absolute coordinates of latitude, longitude, and height of a measurement point are obtained. The accuracy of the point positioning is approximately a few meters to ten meters or more.

The other method is relative positioning. Relative positioning using carrier phase measurements was established for precise surveying. It provides the three-dimensional relative coordinates between two points with an accuracy of millimeters to centimeters. Therefore, relative positioning is used for monitoring rock displacements. By continuously observing the coordinates of measurement points, the displacements are obtained as changes in the coordinates. The standard deviation of the measurement can be a few millimeters, when the baseline length is <1 km, and the installation and data corrections are conducted carefully.

The conventional geotechnical measurement devices, i.e., extensometers, inclinometers, etc., are usually available only for limited areas of several tens of meters at most. Besides, it is difficult to measure three-dimensional displacements with them. The advantage of GPS is that it can easily provide three-dimensional displacements with high accuracy over an extensive area.

3 Outline of GPS

GPS was firstly developed as a navigation system in the early 1970s. It was also established as a method for precise long baseline surveying in the late 1970s to early 1980s. The U.S. Department of Defense controls the system (Hoffman-Wellenhof et al. 2001; Misra and Enge 2006).

GPS is composed of three segments, namely, (1) the space segment, (2) the control segment, and (3) the user segment (Fig. 1). The space segment is composed of

Fig. 1 System architecture of GPS

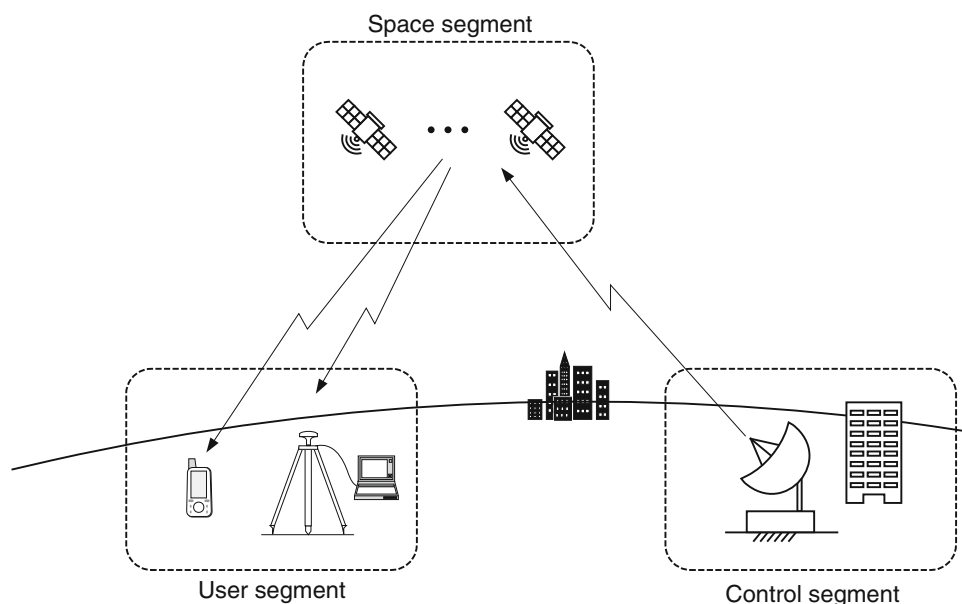
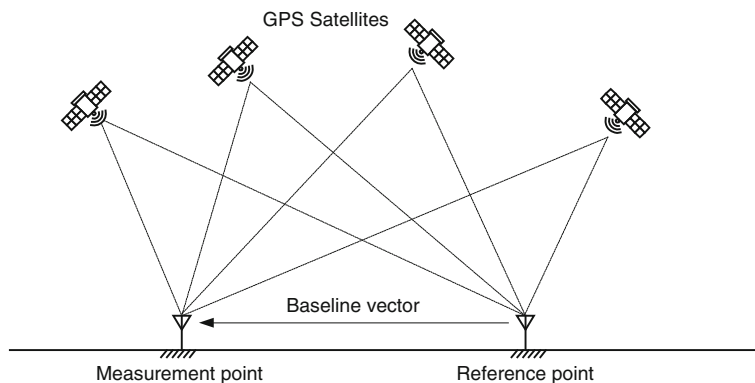


Fig. 2 Relative positioning of GPS



artificial satellites. Currently, 31 satellites are in operation. The satellites fly in nearly circular orbits for periods of sidereal hours (11 h and 58 min). Each satellite continuously transmits the signals for positioning. The control segment consists of a worldwide network of ground facilities. Its tasks are to track the satellites in orbit, to time the synchronization of the satellites, to upload the data messages from the satellites, etc. Both the space and the control segments are managed by the USA. The user segment consists of receiver equipment and a related system. Anyone who prepares the receiver can use GPS at any time.

When users conduct relative positioning for monitoring rock displacements, an antenna with its receiver is set on the reference point and a second antenna is set on the measurement point (Fig. 2). If users set antennas at a number of measurement points, the displacements are simultaneously obtained at each point.

The static method, which is one method of relative positioning, will yield the most reliable and precise results in GPS positioning, and, thus, is the method that is

recommended for monitoring quasi-static (not dynamic) rock displacements.

4 Devices

4.1 General

In order to conduct displacement monitoring with the static method of relative positioning, which uses the carrier phase of the signal, at least two sets of antennas and receivers, data downloading software and baseline analysis (post-processing) software, and a computer are needed.

4.2 Antennas and Receivers

The antennas and receivers for the relative positioning, using the carrier phase, are commercially available (Fig. 3). Figure 3a shows an antenna set, consisting of an antenna, a

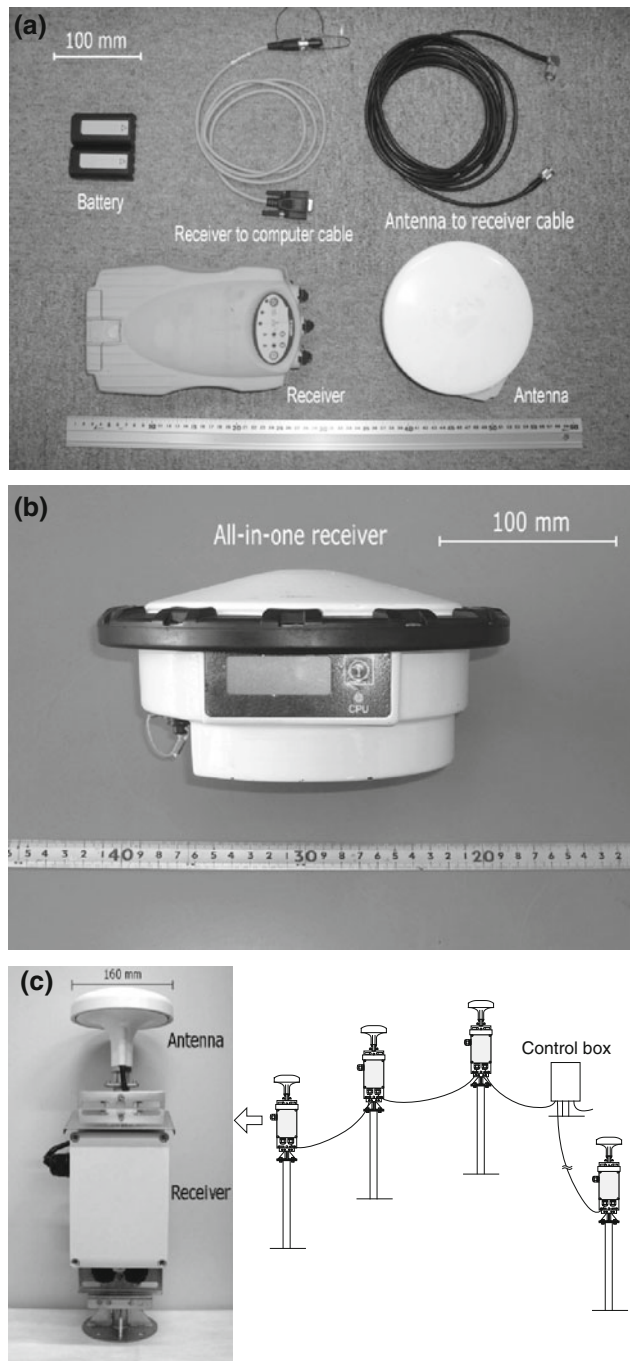


Fig. 3 Antenna and receiver: **a** separate type, **b** all-in one type, **c** system for displacement monitoring

receiver, and cables, which were originally developed for precise surveying or geodesy use, but they can also be applied for monitoring displacements. An all-in-one type of antenna and receiver is shown in Fig. 3b, while an automatic monitoring system is shown in Fig. 3c.

The L1 phase receiver is selected for monitoring displacements of short baseline length less than a few kilometers. It is desirable to use antennas designed to mitigate the multipath effect. The standard accuracy (root mean squares) of the positioning is at least $5 \text{ mm} + 1 \text{ ppm} \times D$ and $10 \text{ mm} + 1 \text{ ppm} \times D$ for horizontal and height directions, respectively. D is the distance of the baseline length in kilometers. Standard commercial receivers satisfy this accuracy. Better accuracy can be expected under good observation conditions.

The receiver continuously measures the carrier phase of the signal and receives the navigation data transmitted from the satellites and saves them in the memory. Stable electric power must be supplied to the receivers by an AC power supply and/or a 12 V DC battery.

4.3 Software and Computer

Software for downloading, logging, and processing the GPS data is needed for retrieving the data files from the receivers. Baseline analysis software is also required for determining the three-dimensional relative coordinates between two points. The software is provided by the manufacturer of the receiver. The software is generally not difficult to operate.

The format for the GPS data usually depends on the type of receivers or the manufacturers. GPS observation data can be converted to the Receiver INdependent Exchange (RINEX) format. If users are going to analyze data obtained from the receivers of different manufacturers during the same observing session, all the data should be converted to the RINEX format. Almost all GPS processing software provided by manufacturers can convert the received data to the RINEX format.

Computer equipment (standard personal computer) is used to run the software for data downloading and the baseline analysis.

4.4 Automatic Monitoring System

When standard receivers for surveys are used for monitoring displacements, the users are usually required to download the GPS data from the receivers, analyze the data to obtain the coordinates of the measurement points, and calculate the displacements for each session. If such a process is conducted manually, it is inconvenient and ineffective for continuous monitoring. In order to overcome this troublesome process, automatic monitoring systems can be designed and applied for monitoring displacements (e.g., Shimizu et al. 1996; Manetti and Glisic 2003; Masunari et al. 2003; Zhang et al. 2012).

5 Procedure

5.1 General

Before starting the fieldwork of the monitoring procedure, the number of visible satellites is predicted by the software provided by the manufacturer of the receiver. Each receiver must simultaneously observe at least four satellites.

The epoch interval (measurement interval or logging rate of the carrier phase) and the session length (the observing duration of the carrier phase measurements) are important user-defined parameters for precise monitoring (Table 1). The elevation mask (or mask angle) is another user-defined parameter (see Sect. 5.3).

The outline of the procedure for monitoring displacements by the static method is given as follows:

1. Set up the receiver(s) at the measurement point(s) and the reference point (Fig. 2).
2. Measure the carrier phase of the signal every epoch interval and receive the navigation data at every measurement point(s) and the reference point from the same satellites simultaneously. The measured carrier phase and data are saved automatically in the memory of the receivers. The receivers perform this process automatically.
3. Download data from all the receivers to a computer.
4. Select the downloaded data of the reference point and the measurement point(s) at which the user would like to know the displacements, and conduct a baseline analysis to obtain the relative coordinates of the measurement point(s) from the reference point.
5. Repeat Steps (3) and (4) for the succeeding observation session.
6. Calculate the changes in the coordinates at each measurement point between the two sessions, and then obtain the displacements.

5.2 Installation of Antennas and Receivers

The locations of the measurement points are determined according to the purpose of the monitoring project, i.e., monitoring the stability of slopes and structures, etc. The reference point should be selected on firm ground.

Antennas are set up above the measurement point(s) and the reference point by a tripod/pillar (Fig. 4). It is noted that GPS provides the coordinates of the antenna phase center. If an antenna is firmly fixed at a measurement point on the ground surface by a tripod/pillar and anchors, the displacement of the antenna can be supposed to coincide with

Table 1 Typical values of user-defined parameters for displacement monitoring

Observation parameters	Value
Epoch interval	5–30 s
Session length	45 min to 3 h
Elevation mask (mask angle)	15°

one of the measurement points. It is recommended that the antennas be firmly fixed on the ground to mitigate errors due to the uncertainty of the antenna phase center. This is very important for precise monitoring with millimeter accuracy. When the height of the measurement point on the ground is needed, the antenna height must be measured in order to adjust the difference in height between the antenna phase center and the measurement point.

Multipath and signal disturbances can be significantly reduced by carefully selecting the site for each antenna in order to avoid reflective objects and signal obstructions, i.e., walls, fences, trees, etc.

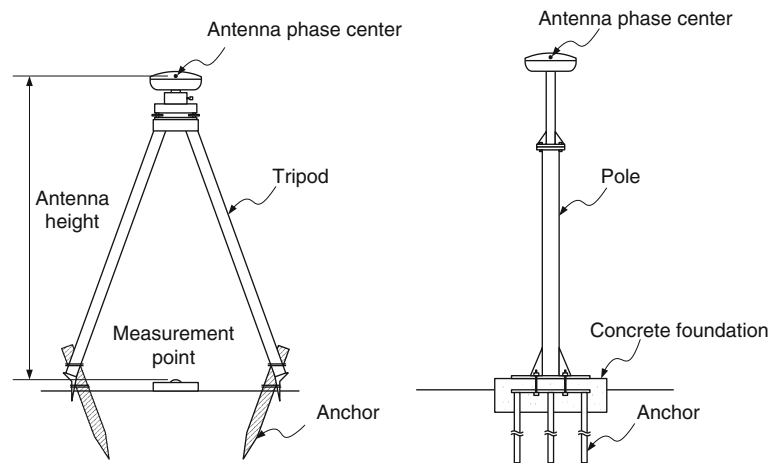
5.3 Observation

The epoch interval and the session length affect the accuracy of the positioning. The epoch interval is typically 5–30 s, and the session length is normally 45 min to 3 h (The Survey Advisory Board and the Public Land Survey Office for State of Washington Department of Natural Resources 2004). If users take a 30-s epoch and a 1-h session under 5–6 observable satellites, the accuracy (the standard deviation) will be 2–3 and 3–4 mm or better in horizontal and height directions, respectively, for a short baseline of <1 km in length. Since a baseline analysis is conducted every session, displacements are obtained every session period. When the observation session is 1 h, the displacements are measured every hour.

The elevation mask (or mask angle) is another user-defined parameter. Signals transmitted from low-elevation satellites are strongly affected by tropospheric delays due to water vapor in the troposphere, multipath effects, and signal disturbances due to objects (walls, trees, mountains, etc.) near the earth's surface. In order to reduce such influences, the elevation mask is typically set to 15° from the horizontal plane so that the receiver cuts the signals from the low-elevation satellites.

Setting the user-defined parameters (Table 1), receivers continuously track the GPS signals and measure the carrier phase at every epoch. The data are saved in the memory of each receiver and downloaded into a computer for a baseline analysis.

Fig. 4 Examples of the installation of an antenna at a measurement point by a tripod or pole



5.4 Analysis

The relative coordinates of the measurement point(s) from the reference point are determined by a baseline analysis using the GPS data collected from the receivers. The three-dimensional relative coordinates of a measurement point, i.e., latitude, longitude, and height, are provided in the 1984 World Geodetic System (WGS84), which is a coordinate system used in GPS. If users need to represent the coordinates in another system, they can convert them to the other coordinate system.

Repeating the baseline analysis for the succeeding observation session, displacements at a measurement point are obtained by taking the difference in the coordinates between the two sessions by supposing that the reference point does not move.

If users need to monitor displacements continuously, it is recommended that the data be downloaded and a baseline analysis conducted automatically.

In order to achieve precise monitoring, error-correction methods should be applied to improve the monitoring results.

5.5 Error Correction

Measurement results generally include random errors (noise) and bias errors. Random errors arise from random fluctuations in the measurements. On the other hand, typical bias errors in GPS monitoring are tropospheric delays, multipath effects, and other signal disturbances (Appendix “Sources of Error”). Since both random and bias errors affect the monitoring quality, it is recommended that appropriate error-correction methods be applied to reduce such errors.

5.5.1 Random Errors

Figure 5 shows the three-dimensional displacements originally obtained by the baseline analysis in the local coordinate system (the horizontal X and Y directions, and the

height direction) as an example of GPS displacement monitoring results. The results denoted by the circles are scattered due to random errors. The standard deviations (denoted by σ in Fig. 5) are 2.4, 1.2, and 3.5 mm in the directions of X , Y , and height, respectively. The baseline length and the height difference between the two antennas were 142 and 13 m, respectively. The epoch interval and the session length were 30 s and 1 h, respectively.

The solid lines are drawn as smoothing results, which were obtained by applying the trend model (Kitagawa and Gersch 1984; Appendix “Fundamental Equations for Relative Positioning”) to the original results. It is found that the trend model can yield good estimates from the original measurement results including random errors (Shimizu 1999; Shimizu and Matsuda 2002). It is recommended that users adopt an adequate method to reduce random errors.

5.5.2 Bias Errors

In the case of a short baseline length, tropospheric models using meteorological data (atmospheric pressure, temperature, and humidity), which are measured near the measurement points, are effective in reducing the bias due to tropospheric delays in the monitoring results. The tropospheric models, for example, the Saastamoinen model and the modified Hopfield model (Misra and Enge 2006; Hoffman-Wellenhof et al. 2001), are usually installed in the baseline analysis software. Users can select a model and input the measured meteorological data around the measurement area for this purpose.

Figure 6 shows the originally monitored three-dimensional displacements for a complete year. The baseline length and the height difference between the two antennas were 252 and 106 m, respectively. The epoch interval and the session length were 30 s and 1 h, respectively. The displacement in height increased from May to August and then decreased from August to October, although the monitoring area was stable and there must not have been any displacements during the monitoring period.

Fig. 5 Example of original monitoring results and estimated displacements using the trend model (baseline length: 142 m and height difference: 13 m) (Matsuda et al. 2012)

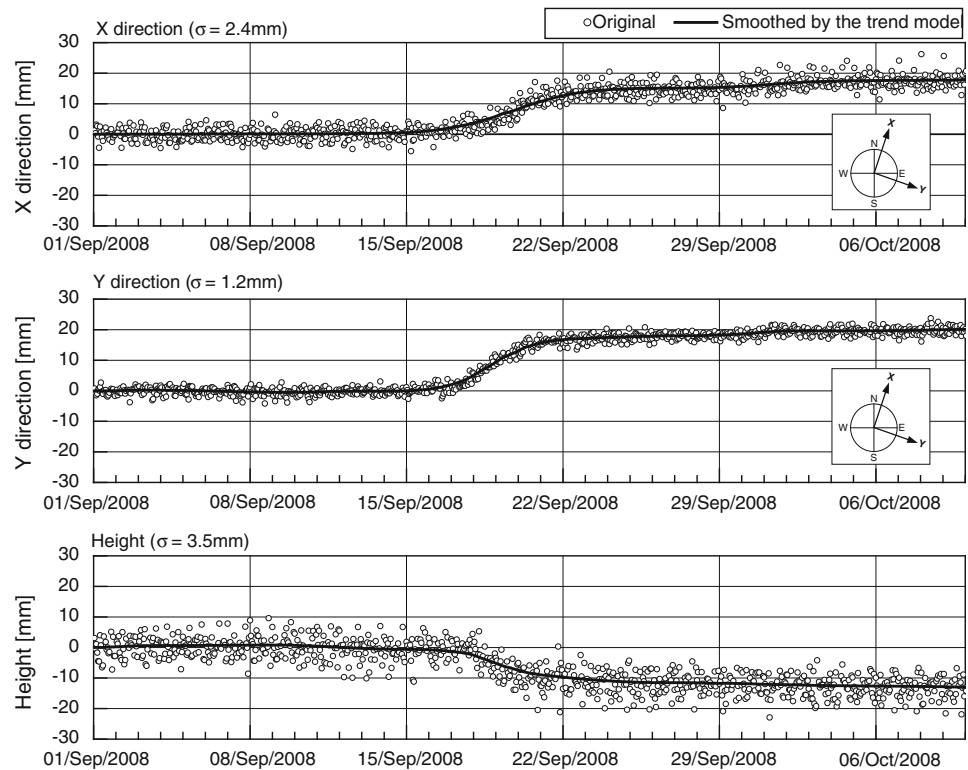
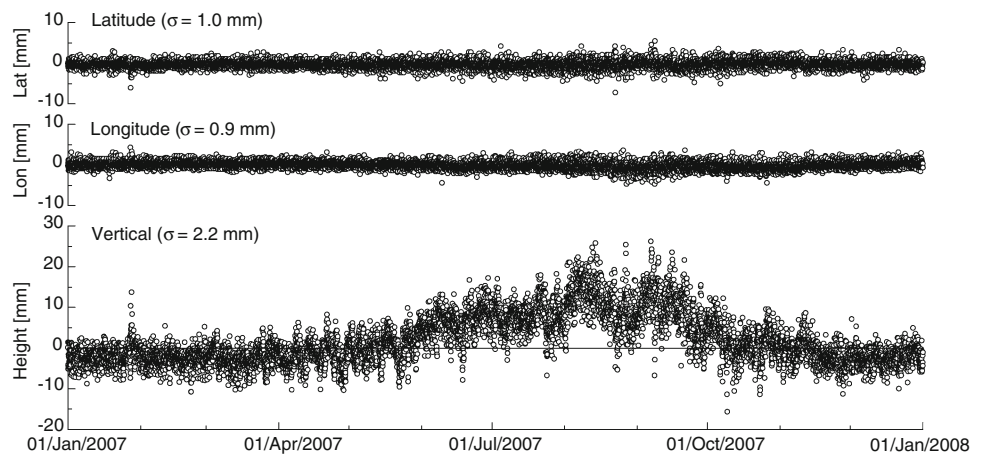


Fig. 6 Example of displacement monitoring results affected by tropospheric delay (baseline length: 252 m and height difference: 106 m) (Nakashima et al. 2012)



The above phenomenon is usually seen in cases where the height difference between the reference and the measurement points is large.

Figure 7 shows the measured temperature, the relative humidity, the atmospheric pressure, the estimated partial pressure of the water vapor, and the zenith tropospheric delay (per unit height difference) using the modified Hopfield model (Appendix “Tropospheric Model”). It is found that the transition in tropospheric delay over a year is quite similar to that of the displacements in height. This might indicate that the tropospheric delay affects the displacement in height.

In order to correct the tropospheric delay, the modified Hopfield model was adopted for the baseline analysis using the measured temperature, the relative humidity, and the atmospheric pressure. The corrected results are shown in Fig. 8. Figure 9 shows a comparison between the original and the corrected monitoring results, which are smoothed by the trend model. It is clear that the movement in the original displacements in height from May to November 2007, as well as daily scatters, have been almost eliminated (Nakashima et al. 2012). On the other hand, the horizontal displacements are hardly subjected to the influence of the tropospheric delay (see Figs. 7, 8). The bias caused by the tropospheric delay

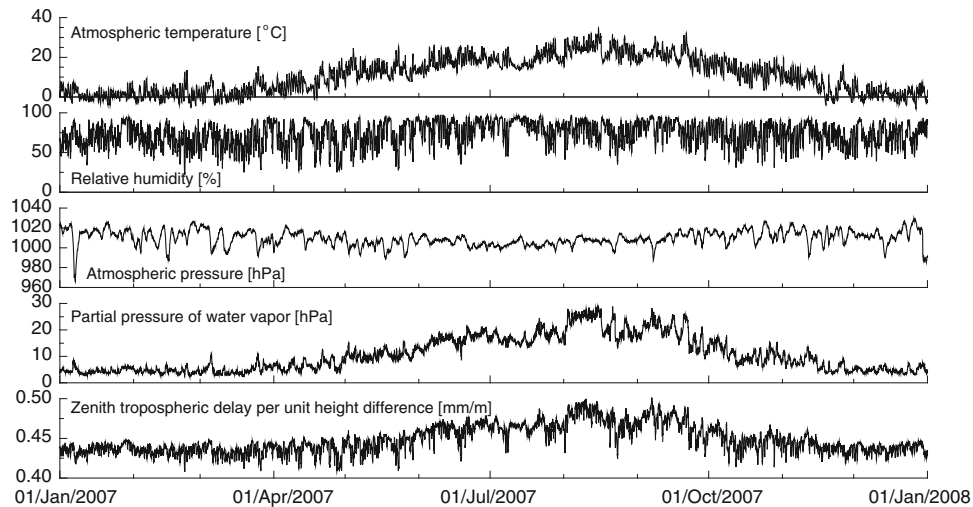


Fig. 7 Measured temperature, relative humidity and atmospheric pressure, and estimated partial pressure of water vapor and zenith tropospheric delays (Nakashima et al. 2012)

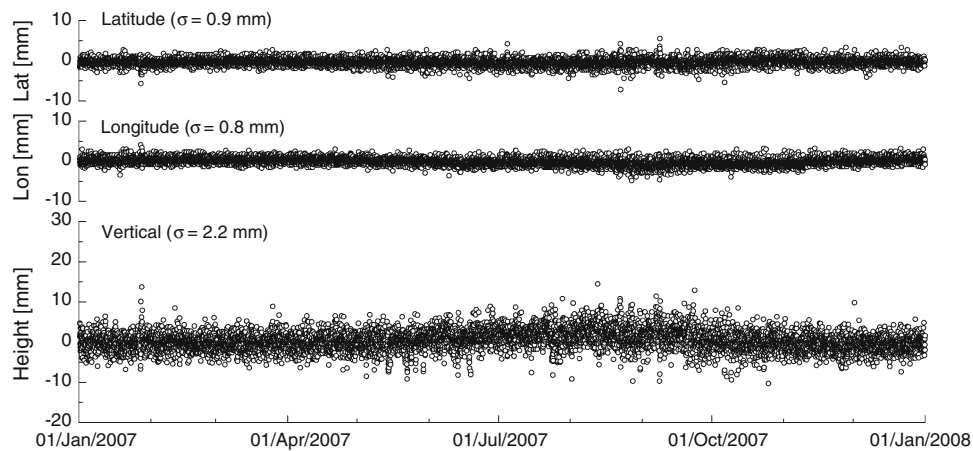


Fig. 8 Displacement monitoring results corrected by tropospheric delays using the modified Hopfield model (Nakashima et al. 2012)

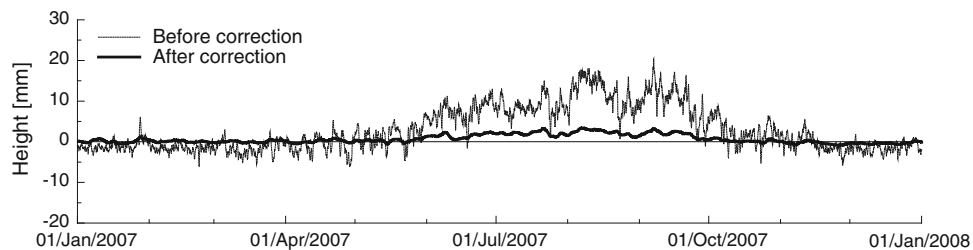


Fig. 9 Comparison between original and corrected monitoring results for tropospheric delay (Nakashima et al. 2012)

tends to be proportional to the height difference between the reference and the measurement points. The amount of bias is 10–20 mm for a height difference of about 100 m during a period of a year, as shown in Fig. 6. It is recommended that users correct the bias due to the tropospheric delays.

Another source of bias is the signal disturbance due to obstructions above antennas. When there are unavoidable obstructions (mainly trees) above the antennas, it is a good practice to analyze the data without the signals transmitted from the satellites behind the obstructions.

Fig. 10 Example of original and corrected monitoring results without using the data from the satellites moving behind the trees (baseline length: 266 m and height difference: 7 m) (Shimizu et al. 2011)

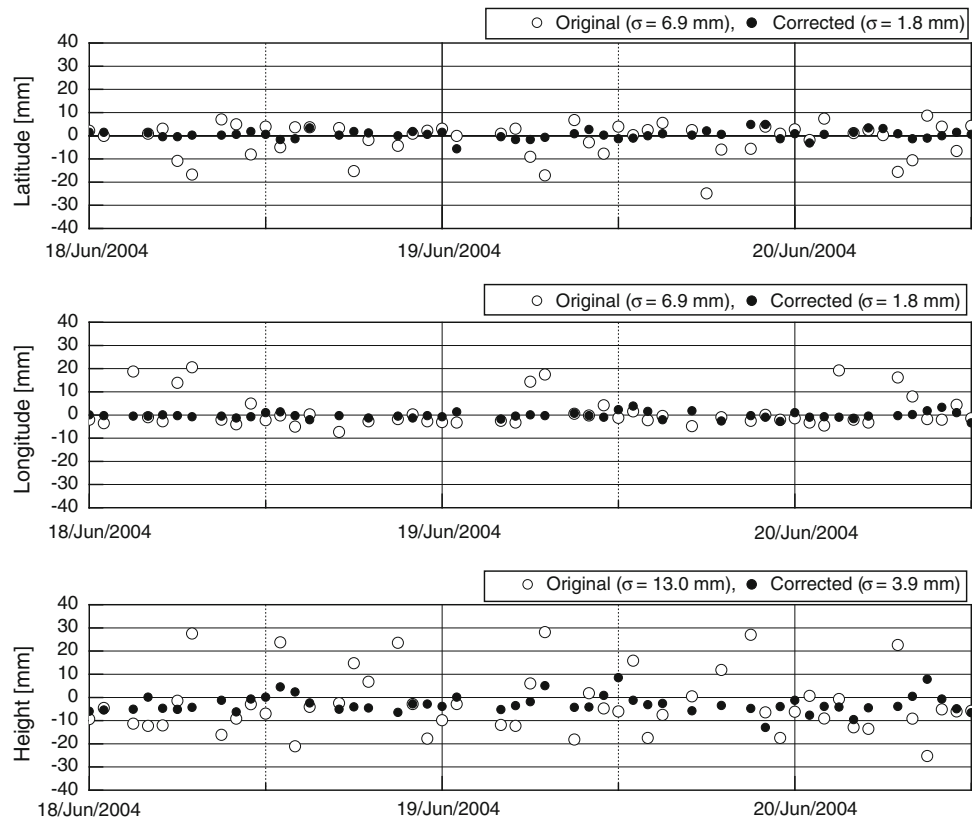


Figure 10 shows the monitoring results at a point on a slope where there were trees on the upper parts of the slope as obstructions. The baseline length and the height difference were 266 and 7 m, respectively. The epoch interval and the session length were 30 s and 1 h, respectively. The circles in Fig. 10 represent the original results obtained from the baseline analysis. They are seen to scatter periodically.

Figure 11 shows satellite paths, drawn in the sky photo above the antenna, for a session in which the monitoring results were largely scattered. The numerals represent the satellite numbers. The antenna received signals from all the satellites, except no. 24, which was moving behind the slope (its signal could not reach the antenna). The signals of satellite nos. 4 and 20 came through the trees and were disturbed. Therefore, the baseline analysis was conducted without using the data from satellite nos. 4, 20, and 24 moving behind the trees or the slope during the whole monitoring period.

The corrected results were obtained as the bullets shown in Fig. 10. The scattered results were significantly improved. The standard deviations in the horizontal and height displacements improved from 6.9 and 13.0 mm to 1.8 and 3.9 mm, respectively. It is clear that the analysis without the data from the satellites moving behind the obstructions is effective in reducing errors and in improving

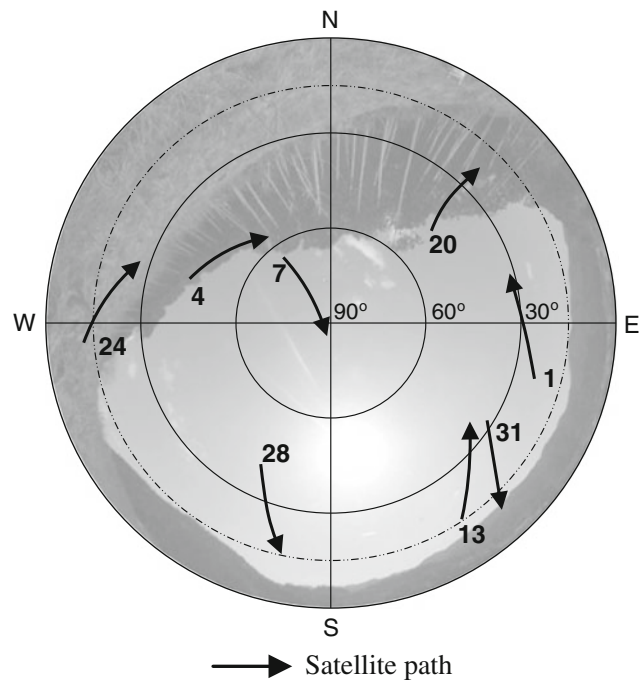


Fig. 11 Satellite paths on a sky photo above the antenna during a session (1 h) for scattered results (Shimizu et al. 2011)

the accuracy of the GPS displacement measurements (Shimizu et al. 2011). Users can conduct the process in a baseline analysis.

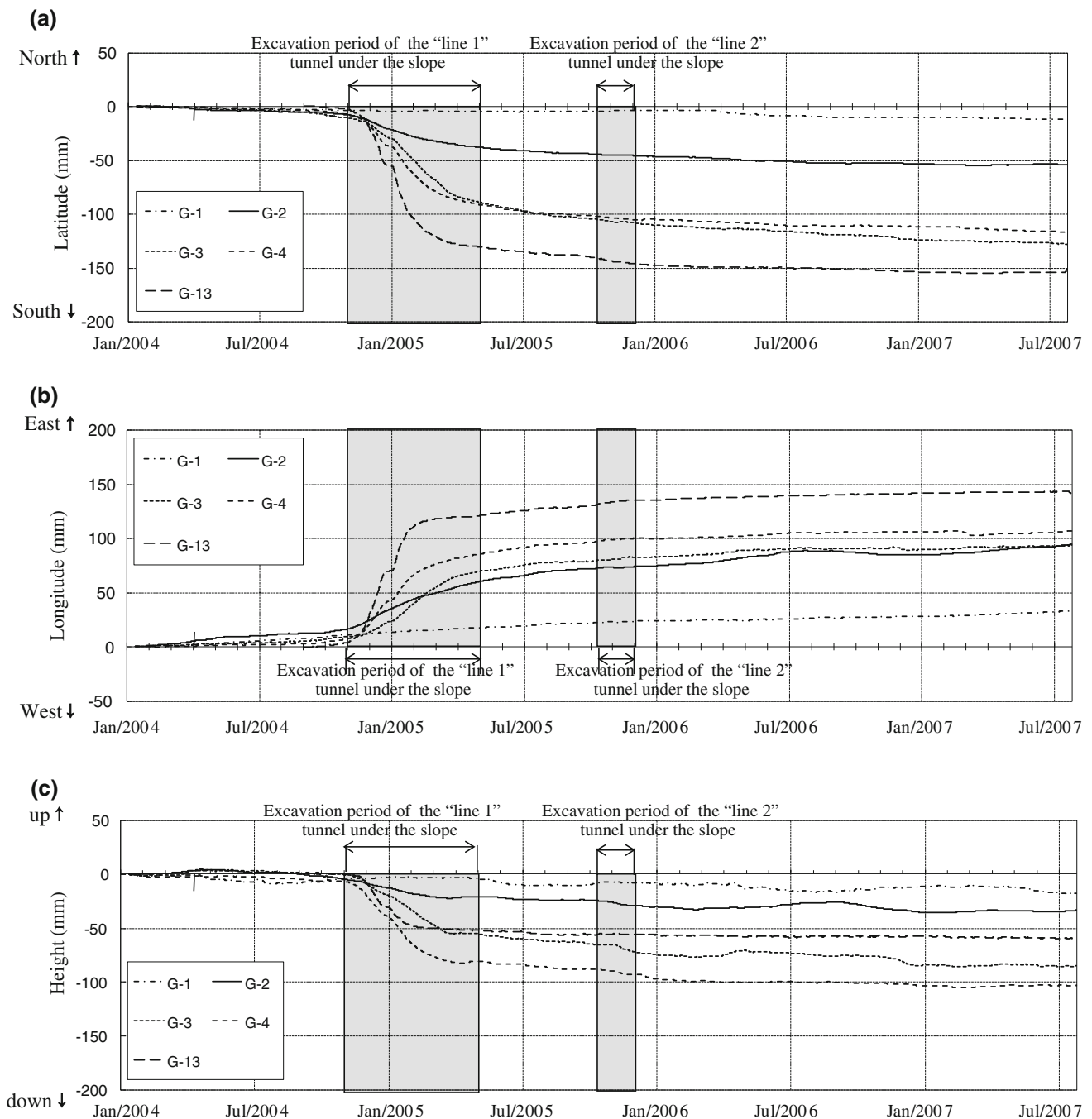


Fig. 12 Measurement results of displacements on a landslide slope due to tunnel excavations (Hirano et al. 2011)

5.6 Examples of Practical Application

Examples from practical applications of GPS to monitoring landslide displacements due to tunnel excavations are shown in Figs. 12 and 13. Two tunnels, "line 1" and "line 2", were constructed just beneath a landslide slope. Five

measurement points, G-1 to G-4 and G-13, were installed on the slope. The reference point was located on stable ground about 400 m away from the slope. An automatic monitoring system was used in this case. The epoch interval and the session length were 30 s and 1 h, respectively. The mask angle was given as 15° .

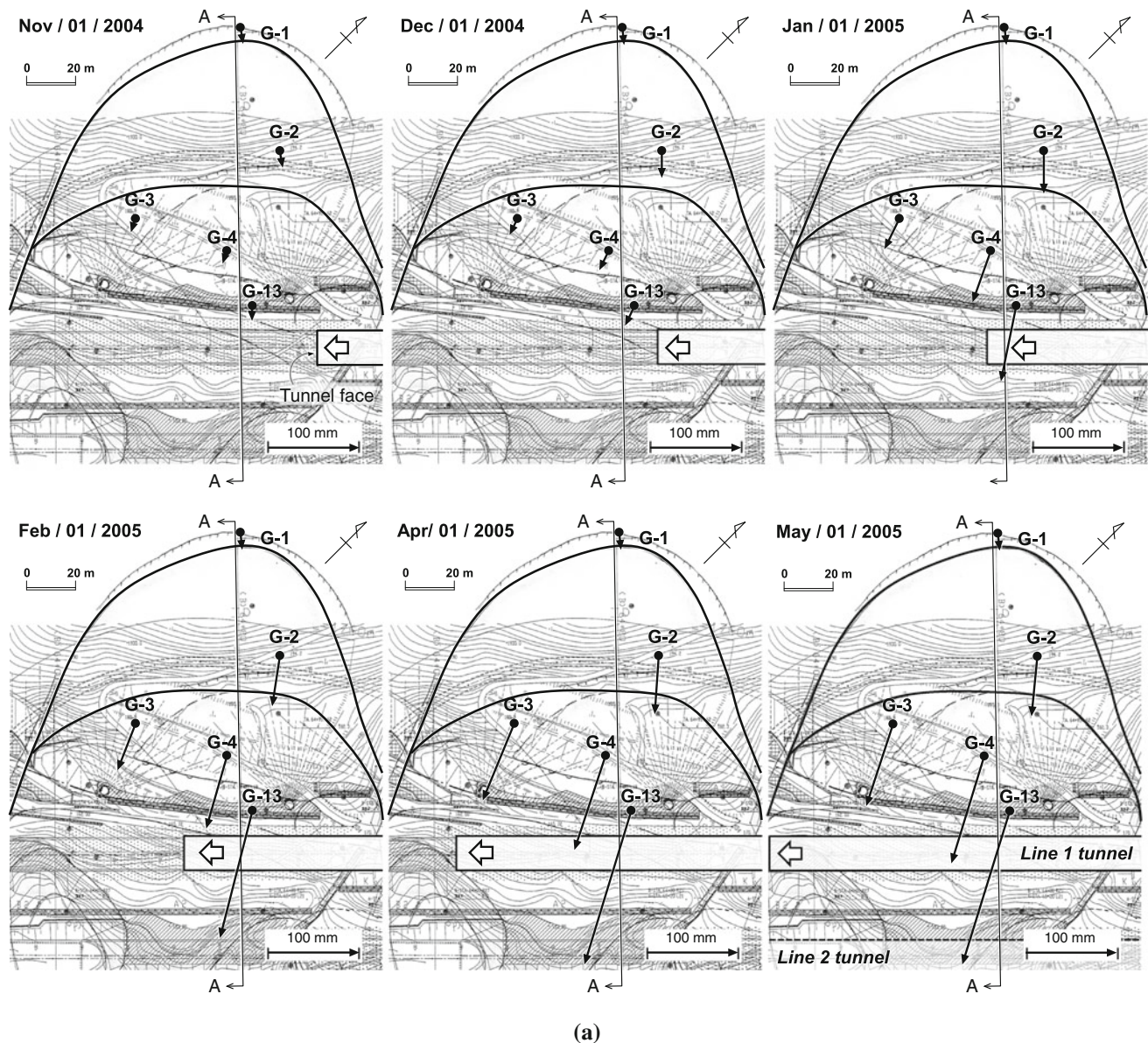


Fig. 13 Displacement vectors on a landslide slope due to tunnel excavations: **a** plane view and **b** vertical section (Hirano et al. 2011)

The three-dimensional displacements were automatically and continuously monitored for 4 years, as shown in Fig. 12. The displacements of all the measurement points, except G-1 located outside the landslide block, increased as the “line 1” tunnel was approaching. The “line 2” tunnel did not affect the displacement behavior of the slope much in comparison to the “line 1” tunnel. Figure 13 shows the transition in the displacement vectors in the plane view and in the vertical section. It is easy to recognize how the tunnel excavations influenced the landslide behavior and how the slope became stable after the tunnels passed through this area.

6 Report

6.1 General

Reports on GPS monitoring are important for evaluating the quality of the measurements, for interpreting the monitoring results, and for accumulating experience. Since the results of GPS monitoring depend on the equipment, the observation parameters, the software, and the error-correction methods, details of those items should be reported. Reports may be prepared in hard copy or by means of an electronic medium.

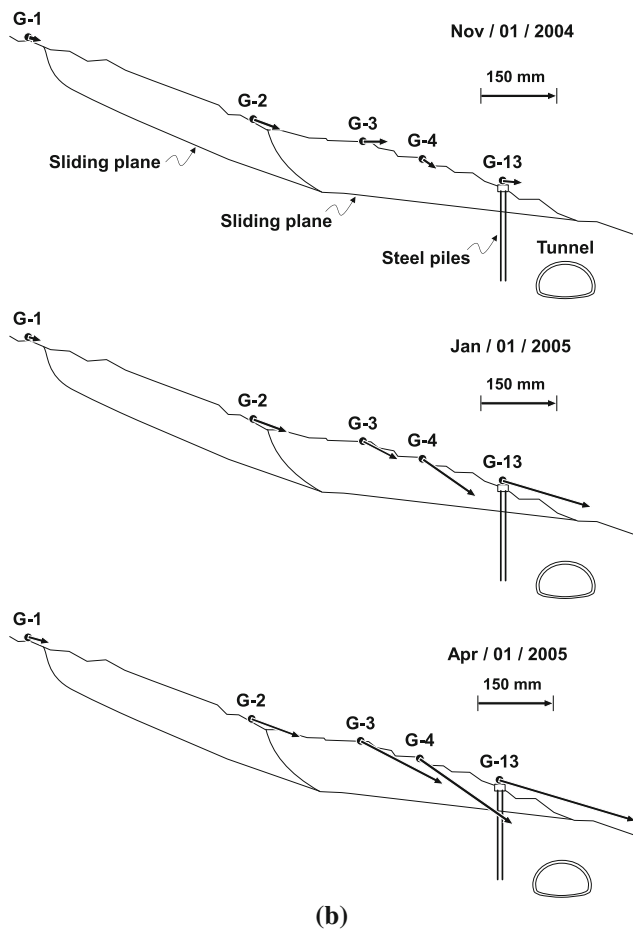


Fig. 13 continued

6.2 Installation Reports

Installation reports should contain the following items:

- Antennas and receivers (type and manufacturer)
- Method of mounting antenna(s) at measurement and reference point(s) (pole, tripod, foundations, etc.)
- Antenna heights (if needed)
- Environment (objects around antenna(s) and obstructions above antenna(s))
- Baseline analysis software (name and version and manufacturer or developer)
- Format of the GPS data
- Any additional comments.

6.3 Monitoring Reports

Monitoring reports should contain the following items:

- Location of measurement points
- Observation parameters: epoch interval (seconds), session duration (hours), and mask angle (degrees)
- Observing times (start and finish)

- Monitoring results (displacements represented in time series, vectors, etc.)
- Coordinate system (WGS84 and others)
- Error-correction methods (name of statistical methods, tropospheric models, and other methods)
- Meteorological measurement results (measurement place, atmospheric pressure, temperature, and humidity, if needed)
- GPS observational data files (save in DVD or other type of medium)
- Output files of baseline analysis (save in DVD or other type of medium)
- Any additional comments.

Acknowledgments The authors referred to several texts, guidelines, and home pages, in addition to those listed in the references here, for the fundamental and applied GPS, in order to prepare this Suggested Method. They wish to express their sincere appreciation to the authors of all the referenced publications.

Appendix

Sources of Error

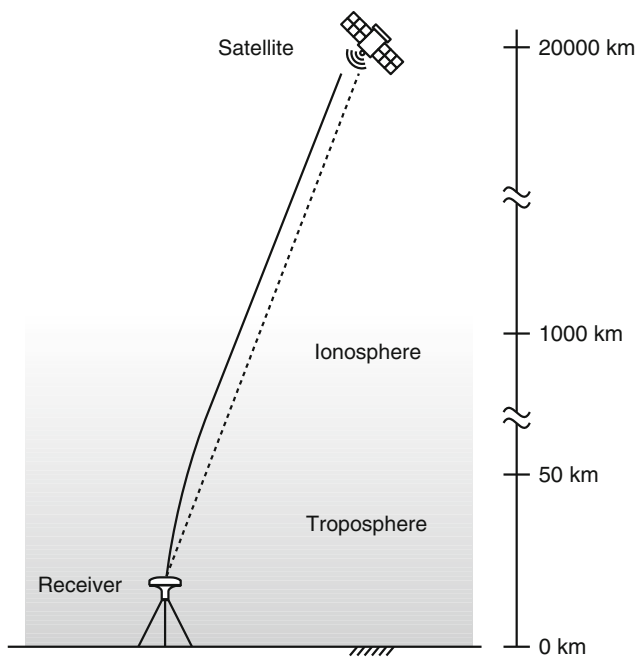
For any measurement device, it is important to know the source of the errors and the corresponding correction methods. Sources of errors in positioning by GPS are summarized in Table 2. The errors can be classified into three groups, namely, errors related to satellites, errors associated with the propagation medium of the signal from the satellites to the receivers, and errors occurring in the vicinity of the antenna by receiver noise and signal disturbances.

Errors related to satellites are satellite ephemeris and clock parameters, which are broadcast by satellites in the navigation message. The control segment, managed by the USA, is responsible for correcting these errors.

The GPS signals are affected by the ionosphere and the troposphere through which they travel from the satellites to a receiver (Fig. 14). Ionospheric delays occur as a result of refractive effects, due to the total electron content, when signals propagate through the ionosphere extending from a height of about 50 to 1,000 km above the earth. These errors can be substantially removed by using a dual-frequency (L1/L2) receiver in the relative positioning. When a baseline length between two antennas is less than a few kilometers, it will be mitigated by taking the difference in carrier phases at two points to eliminate their common-mode errors (Appendix “Fundamental Equations for Relative Positioning”). A single-frequency (L1) receiver is enough, therefore, for use with a short baseline length, as described in this Suggested Method.

Table 2 Sources of errors

Sources
Satellite clock errors
Satellite ephemeris errors
Ionospheric propagation delays
Tropospheric propagation delays
Multipath
Receiver noise
Electrical phase center of antennas
Obstructions

**Fig. 14** Refraction of GPS signals in the atmosphere

Tropospheric delays occur as a result of refractive effects, due to the air density, when signals propagate through the troposphere extending from a height of about 0 to 11 km above the earth. The air density is a function of the pressure of dry gases and water vapor. This means that the measurement results are subject to the influence of the meteorological conditions along the signal propagation path. When the difference in height between antenna points is more than a few tens of meters, the bias of the tropospheric delays may not be able to be ignored in precise monitoring with an accuracy at the millimeter level, even for short baseline lengths. It is recommended that users employ an appropriate model (modified Hopfield model, Saastamoinen model, etc., Hoffman-Wellenhof et al. 2001; Misra and Enge 2006) to correct such tropospheric delays in order to realize precise monitoring. Tropospheric models

are usually installed in the baseline analysis software. Users can select a model with the measured meteorological data for reducing these errors.

Multipath and signal disturbances, caused by the obstruction around antennas, and receiver noise affect the measurement results in the vicinity of the antenna.

Multipath is the phenomenon of a signal reaching an antenna via two or more paths; it is mainly caused by signal reflections from objects (buildings, walls, fences, etc.) and from the ground surface in the vicinity of the antennas. GPS antennas are designed to reduce the effect of multipath, and antenna/receiver manufacturers have developed and implemented proprietary techniques for dealing with it. Naturally, the primary defense against multipath is to position the antennas away from any reflective objects and to set a mask angle for cutting multipath signals.

Obstructions above an antenna (trees, slopes, etc.) may block the antenna signal reception or may cause a disturbance to the signals, and then overhead obstructions become error sources in GPS displacement monitoring. Antennas should be located in areas with a sufficiently open sky. When there are unavoidable obstructions (mainly trees) above the antennas, it is a good practice to analyze the data without the signals transmitted from the satellites behind the obstructions.

Carrier phase measurements are affected by random measurement errors due to receiver noise. Generally, receivers can measure the carrier phases of signals with a precision of 0.5–1 % of a cycle. Since the wavelength of L1 is about 19 cm, measurement errors due to receiver noise will be estimated at 1–2 mm. Users can adopt an adequate method (e.g., statistical model) to reduce this type of random error.

Fundamental Equations for Relative Positioning

The fundamental equation for relative positioning is described as follows (Misra and Enge 2006). The carrier phase of the signals transmitted from satellite k at measurement point mi is expressed as follows (Fig. 15):

$$\phi_{mi}^k = \frac{r_{mi}^k + I_\phi + T_\phi}{\lambda} + \frac{c(\delta t_{mi} + \delta t^k)}{\lambda} + N_{mi}^k + \varepsilon_{\phi_{mi}^k} \quad (1)$$

where r_{mi}^k is the distance between measurement point mi and satellite k as follows:

$$r_{mi}^k = \sqrt{(x_{mi} - X_k)^2 + (y_{mi} - Y_k)^2 + (z_{mi} - Z_k)^2} \quad (2)$$

(x_{mi}, y_{mi}, z_{mi}) and (X_k, Y_k, Z_k) are the coordinates of measurement point mi and satellite k , respectively. I_ϕ is the ionospheric delay, T_ϕ is the tropospheric delay, and λ is the wavelength of the signal. δt_{mi} and δt^k are the biases of

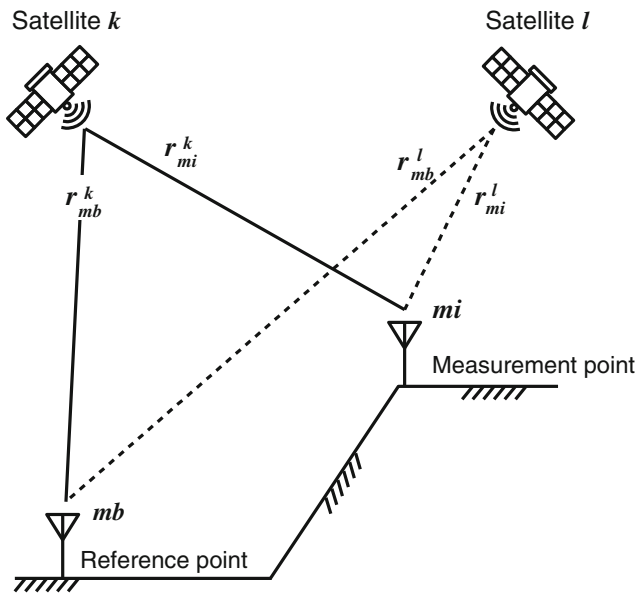


Fig. 15 Satellites, measurement point, and reference point

the receiver clock and the satellite clock, respectively. c is the velocity of light, N_{mi}^k is the unknown integer ambiguity of the carrier phase, and $\varepsilon_{\phi_{mi}}^k$ is an observation error.

The single-phase difference between measurement point mi and reference point mb for satellite k , $\phi_{mi}^k - \phi_{mb}^k$, is taken. In the same manner, another single-phase difference, $\phi_{mi}^l - \phi_{mb}^l$, is taken for satellite l . The double-phase difference, $(\phi_{mi}^k - \phi_{mb}^k) - (\phi_{mi}^l - \phi_{mb}^l)$, is obtained by using the above two single-phase differences as follows:

$$\phi_{mi-mb}^{k-l} = \frac{r_{mi-mb}^{k-l}}{\lambda} + N_{mi-mb}^{k-l} + \varepsilon_{mi-mb}^{k-l} + \frac{T_{\phi_{mi-mb}}^{k-l}}{\lambda} \quad (3)$$

Equation (3) is the fundamental equation for relative positioning. It is noted that the biases of the receiver clock and the satellite clock are eliminated as their common errors during the process of deriving the double-phase difference. In addition, the ionospheric delay is also eliminated when the baseline length between the measurement point and the reference point is short, as in the Suggested Method, less than a few km in length.

On the other hand, tropospheric delay $T_{\phi_{mi-mb}}^{k-l}$ remains when the difference in height between the measurement point and the reference point is more than a few tens of meters, even for such a short baseline length.

The observation equations for the relative positioning method are obtained from Eq. (3). The double-phase difference on the left side of Eq. (3) is observed by a GPS sensor. Then, the three-dimensional coordinates of the measurement point appearing in r_{mi-mb}^{k-l} , and integer ambiguity N_{mi-mb}^{k-l} , are determined by means of the least squares method for residual $\varepsilon_{mi-mb}^{k-l}$.

Trend Model: Model for Improving Measurement Results with Random Errors

The trend model is a smoothing technique for estimating the real values from scattered measurement data (Kitagawa and Gersch 1984). It is composed of a system equation and an observation equation, as follows:

$$\begin{aligned} \Delta^k u_n &= v_n \\ y_n &= u_n + w_n \end{aligned} \quad (4)$$

where u_n represents the estimates for the exact values of the displacements and y_n is the measured displacement. The measurement interval is Δt and subscript n denotes progressing time t ($t = n\Delta t$). Δ is the operator for the finite difference ($\Delta u_n = u_n - u_{n-1}$) and Δ^k means the rank “ k ” difference.

Equation (4) is a kind of probability finite difference equation for rank k . v_n and w_n are white noises with an average value of 0, a standard deviation of τ , and an observation error with a standard deviation of σ .

The trend model can yield good estimates for exact displacements from scattered data obtained from the GPS monitoring system. Through experiments and practical applications, it was proven that the system can detect displacements of 1–2 mm and displacement velocities of 0.1 mm/day (Shimizu and Matsuda 2002).

Tropospheric Model

Modified Hopfield model (Hoffman-Wellenhof et al. 2001)

Tropospheric delays are defined by the following equation:

$$\Delta R^{\text{Trop}} = 10^{-6} \int N^{\text{Trop}} ds \quad (5)$$

where N^{Trop} is the refractivity.

Hopfield showed the possibility of separating N^{Trop} into dry and wet components. The dry part results from the dry atmosphere, while the wet part results from water vapor. Equation (5) becomes:

$$\Delta R^{\text{Trop}} = 10^{-6} \int N_d^{\text{Trop}} ds + 10^{-6} \int N_w^{\text{Trop}} ds \quad (6)$$

Using real data covering the whole earth, Hopfield empirically found a presentation of the refractivity of the dry component as a function of height h above the surface:

$$N_d^{\text{Trop}} = N_{d,0}^{\text{Trop}} \left(\frac{h_d - h}{h_d} \right)^4 \quad (7)$$

where the height of dry component h_d is assumed to be the following equation:

$$h_d = 40136 + 148.72(T - 273.16) \text{ (m)} \quad (8)$$

where T is the absolute temperature (K). Similarly, the refractivity of the wet component is assumed to be:

$$N_w^{\text{Trop}} = N_{w,0}^{\text{Trop}} \left(\frac{h_w - h}{h_w} \right)^4 \quad (9)$$

where the average value, $h_w = 11,000$ (m), is used as the height of the wet component.

Models for dry and wet refractivity at the earth's surface have been used for some time. The corresponding dry and wet components are:

$$N_{d,0}^{\text{Trop}} = c_1 \frac{p}{T} \quad c_1 = 77.64 \text{ (K/hPa)} \quad (10)$$

$$N_{w,0}^{\text{Trop}} = c_2 \frac{e}{T} + c_3 \frac{e}{T^2} \quad c_2 = -12.96 \text{ (K/hPa)}, \quad (11)$$

$$c_3 = 3.718 \times 10^5 \text{ (K}^2\text{/hPa)}$$

where p is the atmospheric pressure and e is the partial pressure of the water vapor, namely:

$$e = 6.112 \cdot \left(\frac{RH}{100} \right) \cdot \exp\left(\frac{17.62T - 4813}{T - 30.03} \right) \quad (12)$$

where RH is the relative humidity (%).

Terminology

Antenna Phase Center

The electronic center of the antenna often does not correspond to the physical center of the antenna. The radio signal is measured at the antenna phase center. The phase center cannot be physically measured. The offset of the physical phase center from an external point on the antenna can be known commonly by referring to the base/bottom of antenna.

Baseline

It is the length of the three-dimensional vector between a reference point and a measurement point (or between a pair of measurement points) for which simultaneous GPS data are collected.

Baseline Analysis (Post-Processing)

The act of using a computer program to compute baseline solutions from measured data (i.e., carrier phase and navigation data) by receivers at both a reference point and a measurement point is a baseline analysis. The three-

dimensional relative coordinates (latitude, longitude, and height) of a measurement point from the reference point are provided in the 1984 World Geodetic System (WGS84).

Carrier

It is the radio frequency sine wave signal. In the case of GPS, there are two transmitted carrier waves, namely, L1 and L2. The L1 carrier frequency is 1,575.42 MHz and the L2 carrier frequency is 1,227.60 MHz.

Dual-Frequency (L1/L2) Receiver

A type of receiver that uses both L1 and L2 signals from the GPS satellites is a dual-frequency receiver. A dual-frequency receiver can compute more precise position fixes over longer distances and under more adverse conditions by compensating for ionospheric delays.

Elevation Mask (Mask Angle)

Satellites are tracked from above this angle. Users can avoid interference and multipath errors from under this angle. It is normally set to 15°.

Epoch

It is a measurement interval used by a receiver when measuring and recording the carrier phase.

Ionospheric Delay

Ionospheric delays occur as a result of refractive effects due to the total electron content when signals propagate through the ionosphere. The errors can be substantially removed by using a dual-frequency receiver. When a baseline length is less than a few kilometers, it will be mitigated by taking the difference in carrier phases at two points (Appendix “[Fundamental Equations for Relative Positioning](#)”).

L1/L2 Carriers

The frequencies of the L1 and the L2 carriers are transmitted by the GPS satellites.

Multipath

Interference, similar to ghosting on television, is called a multipath error. It occurs when the GPS signals traverse different paths before arriving at the antenna, typically as refracting from structures or other refractive surfaces (e.g., the ground, walls, fences, etc.) near the antenna.

Navigation Data

Data messages, containing the satellite's broadcast ephemeris, the satellite clock (bias) correction parameters,

constellation almanac information, and satellite health constitute the navigation data. They are transmitted from satellites.

Observing Session

A period of time over which GPS data are collected simultaneously by two or more receivers is called the observing session (length).

Point Positioning

Point positioning is a method of obtaining the absolute coordinates (longitude, latitude, and height in WGS84) of a point in an instant by one receiver. The receiver measures the transit time of the signal from satellites to the receiver and receives the navigation data. The standard accuracy is around 30 m.

Relative Positioning

The determination of the relative positions between two or more receivers, simultaneously tracking the GPS signals, is the relative positioning. One receiver is set on the reference point, while the second receiver is set on a measurement point. Three-dimensional relative coordinates of the measurement point are provided in WGS84.

RINEX

RINEX is the Receiver INdependent Exchange format. It is a set of standard definitions and formats to promote the free exchange of GPS.

Single-Frequency (L1) Receiver

A single frequency receiver is a device that can receive signals (L1 wave) and navigation data; it can measure the L1 carrier phase during a specific time period. It is used for the relative positioning of short length baselines.

Static Method

This belongs to relative positioning. It is commonly used due to its reliability and ease of data collection. It is performed by setting up antennas at two or more points for a predetermined observing session length.

Tropospheric Delay

Tropospheric delays occur as a result of refractive effects due to the air density when signals propagate through the troposphere. These errors can be reduced by using an appropriate model to correct tropospheric delays for a short baseline length.

WGS84

WGS84 is the World Geodetic System 1984. It is a global geodetic datum defined and maintained by the U.S. Department of Defense. A mathematical model (or

reference ellipsoid) of the earth, whose dimensions were chosen to provide a “best fit” with the earth as a whole, is used. Descriptions of the GPS satellite orbits in the navigation message are referenced in WGS84.

References

- Bond J (2004) An investigation on the use of GPS for deformation monitoring in open pit mines. Technical Report No. 222, Department of Geodesy and Geomatics Engineering, University of New Brunswick, Fredericton, Canada
- Burkholder EF (ed) (1988) Special issue: GPS88. *J Surv Eng (ASCE)* 114(4)
- Burkholder EF (ed) (1989) Special issue: GPS88. *J Surv Eng (ASCE)* 115(1)
- Chrzanowski A, Wells W (eds) (1988) Proceedings of the 5th international (FIG) symposium on deformation measurements and the 5th Canadian symposium on mining surveying and rock deformation measurements, Fredericton, Canada, June 1988
- Gili JA, Corominas J, Rius J (2000) Using Global Positioning System techniques in landslide monitoring. *Eng Geol* 55:167–192
- Hirano H, Usuda Y, Kanzawa K, Miyata K, Shimizu N (2011) Application of the GPS monitoring system to measuring the three dimensional displacements of a landslide slope during tunnel construction and its interpretation. *J Jpn Landslide Soc* 48(2):81–92 (in Japanese)
- Hoffman-Wellenhof B, Lichtegger H, Collins J (2001) *GPS: theory and practice*, 5th revised edition. Springer, Berlin
- Hudnut KW, Behr JA (1998) Continuous GPS monitoring of structural deformation at Pacoima Dam, California. *Seismol Res Lett* 69(4):299–308
- Kim D, Langley RB, Bond J, Chrzanowski A (2003) Local deformation monitoring using GPS in an open pit mine: initial study. *GPS Solut* 7:176–185
- Kitagawa G, Gersch W (1984) A smoothness priors–state space modeling of time series with trend and seasonality. *J Am Stat Assoc* 79(386):378–389
- Malet JP, Maquaire O, Calais E (2002) The use of global positioning system techniques for the continuous monitoring of landslides: application to the Super-Sauze earthflow (Alpes-de-Haute-Provence, France). *Geomorphology* 43:33–54
- Manetti L, Glisic B (2003) Monitoring a harbor structure during reinforcement using a GPS-based monitoring system. In: Proceedings of the 6th international symposium on field measurements in geomechanics, FMGM03, Oslo, Norway, September 2003, pp 531–536
- Masanari T, Tanaka K, Okubo N, Oikawa H, Takechi K, Iwasaki T, Shimizu N (2003) GPS-based continuous displacement monitoring system. In: Proceedings of the 6th international symposium on field measurements in geomechanics, FMGM03, Oslo, Norway, September 2003, pp 537–543
- Matsuda H, Tsutsui T, Ikeda K, Shimizu N (2012) Application of GPS displacement measurements for monitoring slope displacements at a tunnel entrance. *J Jpn Soc Civil Eng Ser F1 (Tunn Eng)* 68(2):21–28 (in Japanese)
- Misra P, Enge P (2006) *Global positioning system: signals, measurements, and performance*, 2nd edn. Ganga-Jamuna Press, Lincoln
- Nakashima S, Shimizu N, Hirabayashi K, Masanari T, Iwasaki T, Ono M (2012) Effects of correction of atmospheric delay on GPS displacement measurements in large slopes. *J Min Mater Process Inst Jpn* 128(6):255–264 (in Japanese)

- Shimizu N (1999) Displacement monitoring by using Global Positioning System for assessment of rock slope stability. In: Proceedings of the 9th international congress on rock mechanics, Paris, France, August 1999, pp 1435–1438
- Shimizu N, Matsuda H (2002) Practical applications of the global positioning system for the assessment of slope stability based on the displacement monitoring approach. In: Proceedings of the 3rd Korea–Japan joint symposium on rock engineering, ISRM Regional Symposium, Seoul, Korea, July 2002, pp 57–70
- Shimizu N, Kondo H, Ono H, Mizuta Y (1996) A new GPS real-time monitoring system for deformation measurements and its application. In: Proceedings of the 8th FIG international symposium on deformation measurements, Hong Kong, June 1996, pp 47–54
- Shimizu N, Masunari T, Iwasaki T (2011) GPS displacement monitoring system for the precise measuring of rock movements. In: Proceedings of the 12th international congress on rock mechanics, Beijing, China, October 2011, pp 1117–1120
- Taşçi L (2008) Dam deformation measurements with GPS. *Geod Cartogr* 34(4):116–121
- The Survey Advisory Board and the Public Land Survey Office for State of Washington Department of Natural Resources (2004) GPS guidebook—standards and guidelines for land surveying using global positioning system methods. Washington State Department of Natural Resources
- US Army Corps of Engineers (2002) Monitoring structural deformations using the global positioning system. In: Structural deformation surveying, Engineer Manual EM 1110-2-1009, Chapter 8, pp 8-1–8-42
- Vermeer M (2002) Review of the GPS deformation monitoring studies. STUK-YTO-TR 186. STUK, Finland
- Zhang L, Stange M, Schwieger V (2012) Automatic low-cost GPS monitoring system using WLAN communication. FIG Working Week 2012, TS03F—Deformation Monitoring I, 5801

Part IV

Failure Criteria

Suggested Methods for Rock Failure Criteria: General Introduction

R. Ulusay and J. A. Hudson

In the application of rock mechanics to rock engineering design, one of the most important issues is the failure of rock: we wish to fail the rock during the excavation process; and then avoid failure of the completed structure. For this reason, the failure of rock has been one of the most important research subjects since the formation of the ISRM in 1962. However, over the years it has become difficult to decide on the best failure criterion to use in specific situations. The ‘Mohr–Coulomb’ and ‘Hoek–Brown’ are the most frequently used failure criteria—but both of these incorporate only the major and minor principal stresses, and not the intermediate principal stress. However, other criteria have been suggested over the years. The ISRM Commission on Testing Methods set out to prepare this document to provide guidance on the characteristics of the several existing failure criteria and suggest circumstances when they should be employed.

In the ISRM Suggested Methods published to date (Ulusay and Hudson 2007), there is explicit guidance on testing procedures. However, such explicit guidance is not appropriate for the application of a failure criterion because of all the many factors that can be involved in a particular potential rock failure circumstance, plus the individual requirements of the researcher or engineer. Accordingly, the Suggested

Methods for failure criteria report on six failure criteria, presenting the background, formulation, related experimental data, advantages and limitations, plus recommendations. In addition, there is an extensive suite of key references. In this way, we hope that the publication of the Suggested Methods for Failure Criteria will assist readers’ understanding of the failure criteria and hence enable them to make more informed and hence appropriate choices concerning which criterion to utilise in any given circumstances.

The individual Suggested Methods have been both written and reviewed by international authorities. We are especially grateful to Professors Bezalel Haimson and Antonio Bobet for taking the lead in the Working Group and to all the individual authors who are named in each Suggested Method.

Reference

Ulusay R, Hudson JA, ISRM (2007) The complete ISRM suggested methods for rock characterization, testing and monitoring: 1974–2006. In: Ulusay R, Hudson JA (eds) Commission on testing methods. International Society of Rock Mechanics. Compilation arranged by the ISRM Turkish National Group, Ankara, Turkey, 628 p

Please send any written comments on these ISRM Suggested Methods to Prof. R. Ulusay, President of the ISRM Commission on Testing Methods (Hacettepe University, Geological Engineering Department, 06800 Beytepe, Ankara, Turkey, E-mail: resat@hacettepe.edu.tr).

Originally published as an article in the journal *Rock Mechanics and Rock Engineering*, 45, R. Ulusay, J. A. Hudson, Suggested Methods for Rock Failure Criteria: General Introduction, 971, 2012.

R. Ulusay (✉) · J. A. Hudson
Geological Engineering Department, Hacettepe University,
06800 Beytepe, Ankara, Turkey
e-mail: resat@hacettepe.edu.tr

Introduction to Suggested Methods for Failure Criteria

Bezalel Haimson and Antonio Bobet

Accurate assessment of rock strength is necessary for the rational design of underground structures, for the evaluation of wellbore stability, for the determination of in situ stresses (e.g., hydraulic fracturing, borehole breakouts, drilling-induced cracks), and as part of geophysical research such as faulting and earthquake mechanics. In engineering fields, the stress condition by which ultimate strength is reached is referred to as the “failure criterion”. Failure criteria are often expressed in terms of the major principal compressive stress σ_1 that rocks can sustain for given values of the other two principal stresses, σ_2 and σ_3 . In its most general form, this can be expressed as $\sigma_1 = f_1(\sigma_2, \sigma_3)$ or $f_2(\sigma_1, \sigma_2, \sigma_3) = 0$ (Scholz 1990) where f_1 or f_2 are functions that vary with the selected criterion and can be determined theoretically, empirically or from laboratory tests (in some failure criteria, the effect of σ_2 is not considered and in that case the functions f_1 or f_2 are independent of σ_2). The convention used is positive for compression, and it is implied that failure is expressed in terms of effective stresses; correspondingly, expressions such as $f_2(\sigma_1, \sigma_2, \sigma_3) = 0$ and $f_2(\sigma'_1, \sigma'_2, \sigma'_3) = 0$ are used interchangeably.

Laboratory experiments should be aimed at characterizing deformation and strength behavior under stress conditions simulating those encountered in situ. However, most laboratory tests are conducted on cylindrical specimens

subjected to uniform confining pressure. Such conventional triaxial tests simulate only a special field condition where intermediate and minor principal stresses, σ_2 and σ_3 , are equal. Triaxial tests have been widely used for the study of mechanical characteristics of rocks because of equipment simplicity and convenient specimen preparation and testing procedures. The underlying assumption is that the intermediate principal stress has negligible effect on rock strength.

A growing number of in situ stress measurements at shallow to intermediate depths has shown that rock stresses are almost always anisotropic, i.e., $\sigma_1 \neq \sigma_2 \neq \sigma_3$ (Haimson 1978; McGarr and Gay 1978; Brace and Kohlstedt 1980). Additional evidence based on borehole breakout dimensions in crystalline rocks (Vernik and Zoback 1992) and on calculations for the critical mud weight necessary to maintain wellbore stability (Ewy 1998) unequivocally show that rock failure criteria should account for the effect on the strength of the intermediate principal stress.

The first extensive true triaxial compressive tests in rocks, in which $\sigma_1 \neq \sigma_2 \neq \sigma_3$, were conducted by Mogi (1971). He subjected Dunham dolomite and other rocks to different intermediate principal compressive stresses for the same minor principal stress, and then raised the major principal stress to failure. Mogi demonstrated experimentally that for the rocks tested, strength was a function of σ_2 in a manner similar to that predicted theoretically by Wiebols and Cook (1968). Although Wiebols and Cook and Mogi demonstrated independently that the intermediate principal stress has a major effect on rock strength, their work has been largely ignored for over 20 years. Recently, the interest in the true triaxial strength of rocks has been rekindled in part by the need to employ appropriate failure criteria for the design of structures in rock under complex loading. Haimson and Chang (2000) and Chang and Haimson (2000) designed and built a true triaxial testing apparatus and conducted an exhaustive series of tests on Westerly granite (Rhode Island, USA) and on KTB

Originally published as an article in the journal *Rock Mechanics and Rock Engineering*, 45, B. Haimson, A. Bobet, Introduction to Suggested Methods for Failure Criteria, 973–974, 2012.

B. Haimson (✉)
Department of Materials Science and Engineering, University of Wisconsin-Madison, Madison, WI 53706, USA
e-mail: haimson@engr.wisc.edu; bhaimson@wisc.edu

A. Bobet
School of Civil Engineering, Purdue University, West Lafayette, IN 47905, USA
e-mail: bobet@purdue.edu

amphibolite (Germany). Their results largely confirmed those obtained by Mogi (1971). Additional true triaxial testing also supported previous findings regarding the effect of the intermediate principal stress on the compressive strength of Long Valley, California, hornfels and metapelite, a Korean rhyolite, and several Taiwanese sandstones and siltstones (Chang and Haimson 2005, 2007; Oku et al. 2007; Haimson and Rudnicki 2010).

Following a keynote lecture by Professor Haimson on “A three-dimensional strength criterion based on true triaxial testing of rocks” at the SinoRock 2009 Symposium in Hong Kong, Professors Hudson and Ulusay, President of ISRM and President of the ISRM Commission on Testing Methods, respectively, approached him regarding the need to standardize the different failure criteria used in practice and make the ISRM members aware of new developments. As a result, a new working group on “Suggested Methods for Failure Criteria” was established, co-chaired by Bezalel Haimson and Antonio Bobet. The co-chairs invited seven internationally known rock mechanics experts to join the working group. They all accepted the challenge. Their names are listed in the following table.

The working group agreed to prepare suggested methods for the most known failure criteria applied to rock and to make recommendations about when each criterion may be applied, highlighting wherever possible the extent to which the effect of the intermediate principal stress is accounted for. The scope of work is restricted to isotropic and homogeneous rock without discontinuities. Failure criteria of rock mass were left for later consideration. Suggested methods were completed for the following failure criteria:

Criterion	Working group members
Mohr–Coulomb	J. Labuz and A. Zang
Hoek–Brown	E. Eberhardt
3D Hoek–Brown	S. Priest
Drucker–Prager	L. Alejano and A. Bobet
Lade and modified Lade	S. Fontoura
Based on true triaxial testing	Ch. Chang and B. Haimson

In preparing each suggested method, the Jaeger and Cook (1979) notation was followed to the extent possible.

The publication of these suggested methods is an attempt to standardize the use of failure criteria in rock mechanics practice enabling the practitioner to employ the most appropriate criterion for the project at hand.

References

- Brace WF, Kohlstedt DL (1980) Limits on lithospheric stress imposed by laboratory experiments. *J Geophys Res* 85:6248–6252
- Chang C, Haimson BC (2000) True triaxial strength and deformability of the KTB deep hole amphibolite. *J Geophys Res* 105:18999–19014
- Chang C, Haimson BC (2005) Nondilatant deformation and failure mechanism in two Long Valley Caldera rocks under true triaxial compression. *Int J Rock Mech Min Sci Geomech Abstr* 42:402–414
- Chang C, Haimson B (2007) Effect of fluid pressure on rock compressive failure in a nearly impermeable crystalline rock: implication on mechanism of borehole breakouts. *Eng Geol* 89:230–242
- Ewy RT (1998) Wellbore stability predictions using a modified Lade criterion. In: *Proceedings of the Eurock 98: SPE/ISRM Rock Mechanics in Petroleum Engineering*, vol 1, pp 247–254
- Haimson B (1978) The hydrofracturing stress measurement technique—method and recent field results. *Int J Rock Mech Min Sci Geomech Abstr* 15:167–178
- Haimson B, Chang C (2000) A new true triaxial cell for testing mechanical properties of rock, and its use to determine rock strength and deformability of Westerly granite. *Int J Rock Mech Min Sci Geomech Abstr* 37:285–296
- Haimson B, Rudnicki JW (2010) The effect of the intermediate principal stress on fault creation and angle in siltstone. *J Struct Geol* 32:1701–1711
- Jaeger JC, Cook NGW (1979) *Fundamentals of rock mechanics*. Chapman and Hall Ltd., London
- McGarr A, Gay NC (1978) State of stress in the earth’s crust. *Annu Rev Earth Planet Sci* 6:405–436
- Mogi K (1971) Fracture and flow of rocks under high triaxial compression. *J Geophys Res* 76:1255–1269
- Oku H, Haimson B, Song SR (2007) True triaxial strength and deformability of the siltstone overlying the Chelungpu fault (Chi–Chi earthquake), Taiwan. *Geophys Res Lett* 34:L09306
- Scholz CH (1990) *The mechanics of earthquake and faulting*. Cambridge University Press, New York
- Vernik L, Zoback MD (1992) Estimation of maximum horizontal principal stress magnitude from stress-induced well bore breakouts in the Cajon Pass scientific research borehole. *J Geophys Res* 97:5109–5119
- Wiebols GA, Cook NGW (1968) An energy criterion for the strength of rock in polyaxial compression. *Int J Rock Mech Min Sci Geomech Abstr* 5:529–549

Mohr–Coulomb Failure Criterion

Joseph F. Labuz and Arno Zang

List of Symbols	Description
a	$(m - 1)/(m + 1)$
b	$1/(m + 1)$
c	Cohesion
C_0	Uniaxial compressive strength
m	$(1 + \sin \phi)/(1 - \sin \phi)$
S_0	Inherent shear strength (cohesion)
T	Uniaxial tensile strength
T_0	Theoretical MC uniaxial tensile strength
ϕ	Angle of internal friction
$\mu = \tan \phi$	Coefficient of internal friction
σ	Normal stress on plane
τ	Shear stress on plane
$\sigma_1, \sigma_2, \sigma_3$	Principal stresses, with no regard to order
$\sigma_I, \sigma_{II}, \sigma_{III}$	Major, intermediate, minor principal stresses
σ_m	$(\sigma_I + \sigma_{III})/2$
τ_m	$(\sigma_I - \sigma_{III})/2$
σ_I^*	$C_0 - mT$
σ_{III}^*	$-T$

Originally published as an article in the journal *Rock Mechanics and Rock Engineering*, 45, J. F. Labuz, A. Zang, Mohr–Coulomb Failure Criterion, 975–979, 2012.

J. F. Labuz (✉)
Department of Civil Engineering, University of Minnesota,
Minneapolis, MN 55455, USA
e-mail: jlabuz@umn.edu

A. Zang
Section 2.6 Seismic Hazard and Stress Field, GFZ German
Research Centre for Geosciences, Telegrafenberg,
14473, Potsdam, Germany
e-mail: zang@gfz-potsdam.de

1 Description

The Mohr–Coulomb (MC) failure criterion is a set of linear equations in principal stress space describing the conditions for which an isotropic material will fail, with any effect from the intermediate principal stress σ_{II} being neglected. MC can be written as a function of (1) major σ_I and minor σ_{III} principal stresses, or (2) normal stress σ and shear stress τ on the failure plane (Jaeger and Cook 1979). When all principal stresses are compressive, experiments demonstrate that the criterion applies reasonably well to rock, where the uniaxial compressive strength C_0 is much greater than the uniaxial tensile strength T , e.g. $C_0/T > 10$; some modification is needed when tensile stresses act, because the (theoretical) uniaxial tensile strength T_0 predicted from MC is not measured in experiments. The MC criterion can be considered as a contribution from Mohr and Coulomb (Nadai 1950). Mohr's condition is based on the assumption that failure depends only on σ_I and σ_{III} , and the shape of the failure envelope, the loci of σ, τ acting on a failure plane, can be linear or nonlinear (Mohr 1900). Coulomb's condition is based on a linear failure envelope to determine the critical combination of σ, τ that will cause failure on some plane (Coulomb 1776). A linear failure criterion with an intermediate stress effect was described by Paul (1968) and implemented by Meyer and Labuz (2012).

2 Background

Coulomb, in his investigations of retaining walls (Heyman 1972), proposed the relationship

$$|\tau| = S_0 + \sigma \tan \phi \quad (1)$$

where S_0 is the inherent shear strength, also known as cohesion c , and ϕ is the angle of internal friction, with the coefficient of internal friction $\mu = \tan \phi$. The criterion

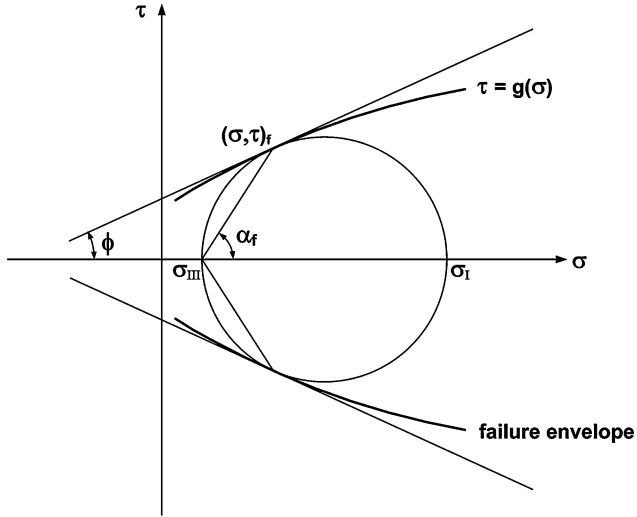


Fig. 1 Mohr diagram and failure envelopes

contains two material constants, S_0 and ϕ , as opposed to one material constant for the Tresca criterion (Nadai 1950). The representation of Eq. (1) in the Mohr diagram is a straight line inclined to the σ -axis by the angle ϕ (Fig. 1). By constructing a Mohr circle tangent to the line (a stress state associated with failure) and using trigonometric relations, the alternative form of Eq. (1) in terms of principal stresses is obtained:

$$(\sigma_I - \sigma_{III}) = (\sigma_I + \sigma_{III}) \sin \phi + 2S_0 \cos \phi \quad (2)$$

One form of Mohr's failure criterion is

$$\tau_m = f(\sigma_m) \quad (3)$$

where $\tau_m = (\sigma_I - \sigma_{III})/2$, $\sigma_m = (\sigma_I + \sigma_{III})/2$. Knowing the relationship given by Eq. (3), the Mohr envelope can be constructed on the σ , τ plane (Fig. 1), and failure occurs if the stress state at failure, the circle of diameter $(\sigma_I - \sigma_{III})$, is tangent to the failure envelope, $\tau = g(\sigma)$. Thus, from Eq. (2), Coulomb's criterion is equivalent to the assumption of a linear Mohr envelope.

Coulomb's and Mohr's criteria are notable in that an effect of σ_m , the mean stress in the σ_I , σ_{III} plane, is considered, which is important for materials such as rock and soil; i.e., experiments on geomaterials demonstrate that τ_m at failure increases with σ_m . However, the additional claim that the point of tangency of the critical stress circle with the failure envelope, as constructed on the Mohr diagram, represents the normal and shear stresses $(\sigma, \tau)_f$ on the failure plane with normal inclined to σ_I at an angle α_f is not always observed in experiments. Nonetheless, Mohr's criterion allows for a curved shape of the failure envelope, and this nonlinear behavior is exhibited by many rock types (Jaeger and Cook 1979).

3 Formulation

With no order implied by the principal stresses σ_1 , σ_2 , σ_3 , the MC criterion can be written as

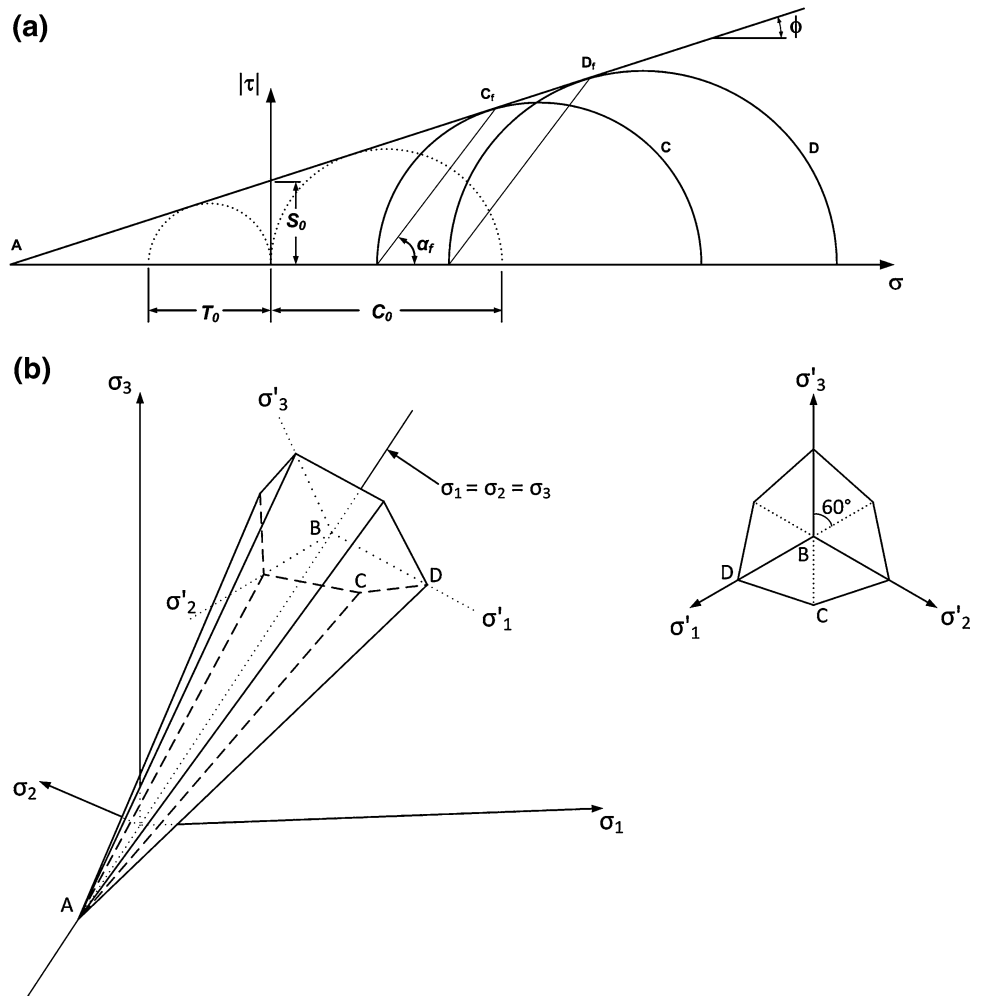
$$\begin{aligned} \pm \frac{\sigma_1 - \sigma_2}{2} &= a \frac{\sigma_1 + \sigma_2}{2} + b, \quad \pm \frac{\sigma_2 - \sigma_3}{2} \\ &= a \frac{\sigma_2 + \sigma_3}{2} + b, \quad \pm \frac{\sigma_3 - \sigma_1}{2} = a \frac{\sigma_3 + \sigma_1}{2} + b \end{aligned} \quad (4)$$

where $a = \frac{m-1}{m+1}$, $m = \frac{C_0}{T_0} = \frac{1+\sin \phi}{1-\sin \phi}$, $b = \frac{1}{m+1}$, $C_0 = \frac{m}{m+1} T_0 = \frac{C_0}{2}(1 - \sin \phi)$, and $0 \leq a < 1$. T_0 is the theoretical MC uniaxial tensile strength (Fig. 2a) that is not observed in experiments; rather, a much lower strength T is measured ($\sigma_I = 0$, $\sigma_{III} = -T$), with the failure plane being normal to σ_{III} . C_0 is the theoretical MC uniaxial compressive strength (Fig. 2a) that is usually close to the measured value (so another symbol is not introduced).

The shape of the failure surface in principal stress space is dependent on the form of the failure criterion: linear functions map as planes and nonlinear functions as curvilinear surfaces. As shown in Fig. 2b, the six equations in (4) are represented by six planes that intersect one another along six edges, defining a hexagonal pyramid. Also presented in Fig. 2b is the failure surface on the equipressure ($\sigma_1 + \sigma_2 + \sigma_3 = \text{constant}$) or π -plane perpendicular to the hydrostatic axis, where MC can be described as an irregular hexagon with sides of equal length (Shield 1955). Isotropy requires threefold symmetry because an interchange of σ_1 , σ_2 , σ_3 should not influence the failure surface for an isotropic material. Note that, the failure surface need only be given in any one of the 60° regions (Fig. 2b).

Consider the transformation from principal stress space ($\sigma_1, \sigma_2, \sigma_3$) to the Mohr diagram (σ, τ). Although the radial distance from the hydrostatic axis to the stress point is proportional to the deviatoric stress, a point in principal stress space does not directly indicate the value of shear stress on a plane. However, each point on the failure surface in principal stress space corresponds to a Mohr circle tangent to the failure envelope (Fig. 2a). For the particular case where σ_2 is the intermediate principal stress in the order $\sigma_1 \geq \sigma_2 \geq \sigma_3$, the failure surface is given by the side ACD of the hexagonal pyramid (Fig. 2b). The principal stresses at point D represent the stress state for a triaxial compression test ($\sigma_1, \sigma_2 = \sigma_3$) $_D$, and point D is given by circle D in the Mohr diagram. Similarly, for point C with principal stresses ($\sigma_3, \sigma_1 = \sigma_2$) $_C$ associated with a triaxial extension test, Mohr circle C depicts the stress state. Points D and C can be viewed as the extremes of the intermediate stress variation, and the normal and shear stresses corresponding to failure are given by points D_f and C_f . Points lying on the

Fig. 2 Mohr–Coulomb failure criterion: **a** linear envelope in the Mohr diagram; **b** pyramidal surface in principal stress space and cross-section in the equipressure plane



line CD (Fig. 2b) will be represented by circles between C and D (Fig. 2a).

For negative (tensile) values of the minor principal stress, experiments show that the failure plane is perpendicular to $\sigma_{III} = -T$. Indeed, the tensile failure mode is completely different from the shear failure mode that occurs with compressive normal stresses, although failure under uniaxial compression is also different, usually observed as axial splitting (Vardoulakis et al. 1998). To account for tensile failure, Paul (1961) introduced the concept of tension cut-offs and a modified MC failure criterion requiring three material constants: Eq. (3) is valid when

$$\sigma_I > (C_0 - mT) = \sigma_I^* \tag{5}$$

but MC is modified as

$$\sigma_{III} = -T \text{ when } \sigma_I < \sigma_I^* \tag{6}$$

The representation of tension cut-offs on the Mohr diagram is shown in Fig. 3a. Note that, the stress state depicted by the broken circle, defined by $\sigma_I = \sigma_I^* = (C_0 - mT)$,

$\sigma_{III}^* = -T$, is not part of the failure envelope. Rather, all Mohr circles with $\sigma_I < \sigma_I^*$ are tangent to the envelope at the point $\sigma_{III}^* = -T$. In principal stress space, the modified MC criterion with tension cut-offs involves the MC pyramid intercepted by a second pyramid with three planes perpendicular to the principal stress axes (Fig. 3b).

4 Experimental Data

Typically, laboratory results are evaluated using the MC failure criterion, as axisymmetric loading imposes a representation where the intermediate stress σ_{II} is equal to the minor σ_{III} or major σ_I principal stress. Few tests independently control σ_{II} because of experimental challenges, although conventional triaxial compression ($\sigma_I > \sigma_2 = \sigma_3$) and extension ($\sigma_I = \sigma_2 > \sigma_3$) tests offer simple approaches to evaluate an influence of the intermediate stress. However, a true triaxial apparatus is needed to investigate stress states between the axisymmetric conditions represented by points C and D in Fig. 2b (Meyer and Labuz 2012).

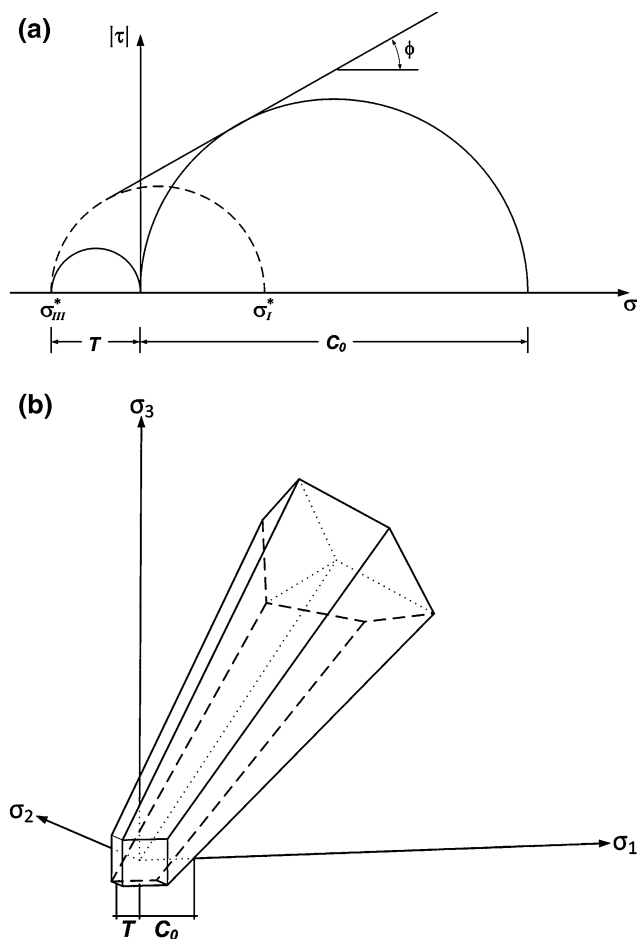


Fig. 3 Tension cut-offs for the modified Mohr-Coulomb failure criterion: **a** failure envelope in the Mohr diagram; **b** representation in principal stress space

Various researchers (Mogi 1971, 1974; Takahashi and Koide 1989; Chang and Haimson 2000; Al-Ajmi and Zimmerman 2005) have performed true triaxial testing, and the intermediate stress effect appears to depend on rock type, although anisotropy and experimental conditions may also influence the results. In fact, anisotropy can cause a reserve intermediate-stress effect, where the friction angle appears larger in compression than extension (Dehler and Labuz 2007). In addition, boundary conditions can play a substantial role in experiments with rock, where a uniform state of stress is a basic assumption of element testing that is often violated (Labuz and Bridell 1993; Paul and Gangal 1967).

Several references can be found dealing with the application of the MC failure criterion (Vutukuri et al. 1974; Andreev 1995; Paterson and Wong 2005). In a treatise on rock properties (Landolt-Börnstein 1982), a chapter by Rummel (pp. 141–238) gives an overview of failure parameters for various types of rock, and Mogi (2007) summarized results on a number of rocks. Generally, it is

claimed that MC well describes the stress state at failure over a limited range of mean stress. Statistical treatment of various failure criteria applied to experiments on intact rock can be found in the literature (Colmenares and Zoback 2002; Hoek et al. 2002; Pincus 2000; Al-Ajmi and Zimmerman 2005; Pariseau 2007; Benz and Schwab 2008; Das and Basudhar 2009).

5 Advantages and Limitations

The advantages of the MC failure criterion are its mathematical simplicity, clear physical meaning of the material parameters, and general level of acceptance. A limitation surrounds the numerical implementation of a failure criterion containing corners in the π -plane (Fig. 2b), as opposed to a smooth function, e.g., Drucker-Prager (1952) failure criterion. Deformation analysis requires a flow rule, a relationship between strain increments and stress, such that the flow rule determines the orientation of the strain-increment vector with respect to the yield condition, e.g., normal for an associative flow rule. Thus, the orientation of the strain-increment vectors is unique along the sides of the MC pyramid. However, along the edges of the pyramid (corners in the π -plane), there is some freedom in the orientation (Drescher 1991).

6 Recommendations

Among the various failure criteria available, both linear and nonlinear equations dependent on the major σ_1 and minor σ_{III} principal stresses are attractive because the geometric representation of laboratory data can be either in the principal stress plane or the Mohr diagram, which is often convenient. Triaxial compression and extension testing is suggested as a standard procedure to evaluate an intermediate-stress effect, although true triaxial testing is needed to describe the failure surface between the axisymmetric stress states. Nonetheless, as a first order approximation to the behaviour of rock, the Mohr–Coulomb failure criterion is recommended when the three principal stresses are compressive and when considering a limited range of mean stress.

References

- Al-Ajmi AM, Zimmerman RW (2005) Relation between the Mogi and the Coulomb failure criteria. *Int J Rock Mech Min Sci* 42:431–439
- Andreev GE (1995) *Brittle Failure of Rock Material*. Balkema, Rotterdam
- Benz T, Schwab R (2008) A quantitative comparison of six rock failure criteria. *Int J Rock Mech Min Sci* 42:1176–1186

- Chang C, Haimson BC (2000) True triaxial strength and deformability of the German Continental deep drilling program (KTB) deep hole amphibolite. *J Geophys Res* 105:8999–9013
- Colmenares LB, Zoback MD (2002) A statistical evaluation of intact rock failure criteria constrained by polyaxial test data for five different rocks. *Int J Rock Mech Min Sci* 39:695–729
- Coulomb CA (1776) Sur une application des regles maximis et minimis a quelques problems de statique, relatives a l'architecture. *Acad Sci Paris Mem Math Phys* 7:343–382
- Das SK, Basudhar PK (2009) Comparison of intact rock failure criteria using various statistical methods. *Acta Geotech* 4:223–231
- Dehler W, Labuz JF (2007) Stress path testing of an anisotropic sandstone. *J Geotech Eng* 133(1):116–119
- Drescher A (1991) *Analytical Methods in Bin-Load Analysis*. Elsevier Science, Amsterdam
- Drucker DC, Prager W (1952) Soil mechanics and plastic analysis or limit design. *Q Appl Mech* 10(2):157–164
- Heyman J (1972) *Coulomb's Memoir on Statics*. Cambridge University Press, London
- Hoek E, Carranza-Torres C, Corkum B (2002) Hoek-Brown failure criterion—2002 Edition. *Proc 5th N Am Symp NARMS-TAC*, Toronto
- Jaeger JC, Cook NGW (1979) *Fundamentals of Rock Mechanics*, 3rd edn. Chapman & Hall, London
- Labuz JF, Bridell JM (1993) Reducing frictional constraint in compression testing through lubrication. *Int J Rock Mech Min Sci Geomech Abstr* 30(4):451–455
- Landolt-Börnstein (1982) Numerical data and functional relationships in science and technology. In: Angenheister G (ed) *Physical properties of rocks*. Springer, Berlin, p 1b
- Meyer JP, Labuz JF (2012) Linear failure criteria with three principal stresses. *Int J Rock Mech Min Sci*, Submitted
- Mogi K (1971) Fracture and flow of rocks under high triaxial compression. *J Geophys Res* 76(5):1255–1269
- Mogi K (1974) On the pressure dependence of strength of rocks and the Coulomb fracture criterion. *Tectonophysics* 21:273–285
- Mogi K (2007) *Experimental rock mechanics*. Taylor & Francis Group, London
- Mohr O (1900) Welche Umstände bedingen die Elastizitätsgrenze und den Bruch eines Materials? *Zeit des Ver Deut Ing* 44:1524–1530
- Nadai A (1950) *Theory of flow and fracture of solids*. McGraw Hill, New York
- Pariseau WG (2007) Fitting failure criteria to laboratory strength tests. *Int J Rock Mech Min Sci* 44:637–646
- Paterson MS, Wong T-f (2005) *Experimental rock deformation—the brittle field*, 2nd edn. Springer-Verlag, Berlin
- Paul B (1961) Modification of the Coulomb–Mohr theory of fracture. *J Appl Mech* 28:259–268
- Paul B (1968) Generalized pyramidal fracture and yield criteria. *Int J Solids Struct* 4:175–196
- Paul B, Gangal M (1967) Initial and subsequent fracture curves for biaxial compression of brittle materials. In: Fairhurst C (ed) *Failure and breakage of rock*, *Proc 8th Symp Rock Mech*. University of Minnesota, MN, pp 113–141
- Pincus H (2000) Closed-form/least-squares failure envelopes for rock strength. *Int J Rock Mech Min Sci* 37:763–785
- Shield RT (1955) On Coulomb's law of failure in soils. *J Mech Phys Sol* 4:10–16
- Takahashi M, Koide H (1989) Effect of intermediate principal stress on strength and deformation behavior of sedimentary rocks at the depth shallower than 2000 m. In: Maury V, Fourmaintraux D (eds) *Rock at Great Depth*, vol 1. Balkema, Rotterdam, pp 19–26
- Vardoulakis I, Labuz JF, Papamichos E, Tronvoll J (1998) Continuum fracture mechanics of uniaxial compression of brittle materials. *Int J Solids Struct* 35:4313–4335
- Vutukuri VS, Lama RD, Saluja D (1974) *Handbook on the mechanical properties of rocks*. Trans Tech Pub, Clausthal

The Hoek–Brown Failure Criterion

Erik Eberhardt

List of Symbols

σ_1	Major principal stress
σ_3	Minor principal stress
C_o	Uniaxial compressive strength
m_i	Hoek–Brown material constant (intact rock)
m_b	Hoek–Brown material constant (rock mass)
s	Hoek–Brown material constant
a	Hoek–Brown material constant
GSI	Geological Strength Index
D	Disturbance factor
T_o	Uniaxial tensile strength
$\sigma'_{3\max}$	Upper limit of confining stress
r^2	Coefficient of determination

1 Description

The Hoek–Brown failure criterion is an empirically derived relationship used to describe a non-linear increase in peak strength of isotropic rock with increasing confining stress. Hoek–Brown follow a non-linear, parabolic form that distinguishes it from the linear Mohr–Coulomb failure criterion. The criterion includes companion procedures developed to provide a practical means to estimate rock mass strength from laboratory test values and field observations. Hoek–Brown assumes independence of the intermediate principal stress.

Originally published as an article in the journal *Rock Mechanics and Rock Engineering*, 45, E. Eberhardt, The Hoek–Brown Failure Criterion, 981–988, 2012.

E. Eberhardt (✉)
Geological Engineering, EOAS, University of British Columbia,
Vancouver, Canada
e-mail: erik@eos.ubc.ca

2 Background and Formulation

The Hoek–Brown criterion was developed as a means to estimate rock mass strength by scaling the relationship derived according to the geological conditions present. The criterion was conceived based on Hoek's (1968) experiences with brittle rock failure and his use of a parabolic Mohr envelope derived from Griffith's crack theory (Griffith 1920, 1924) to define the relationship between shear and normal stress at fracture initiation. By associating fracture initiation with fracture propagation and rock failure, Hoek and Brown (1980) proceeded through trial and error to fit a variety of parabolic curves to triaxial test data to derive their criterion. Accordingly, the Hoek–Brown criterion is empirical with no fundamental relationship between the constants included in the criterion and any physical characteristics of the rock (Hoek 1983).

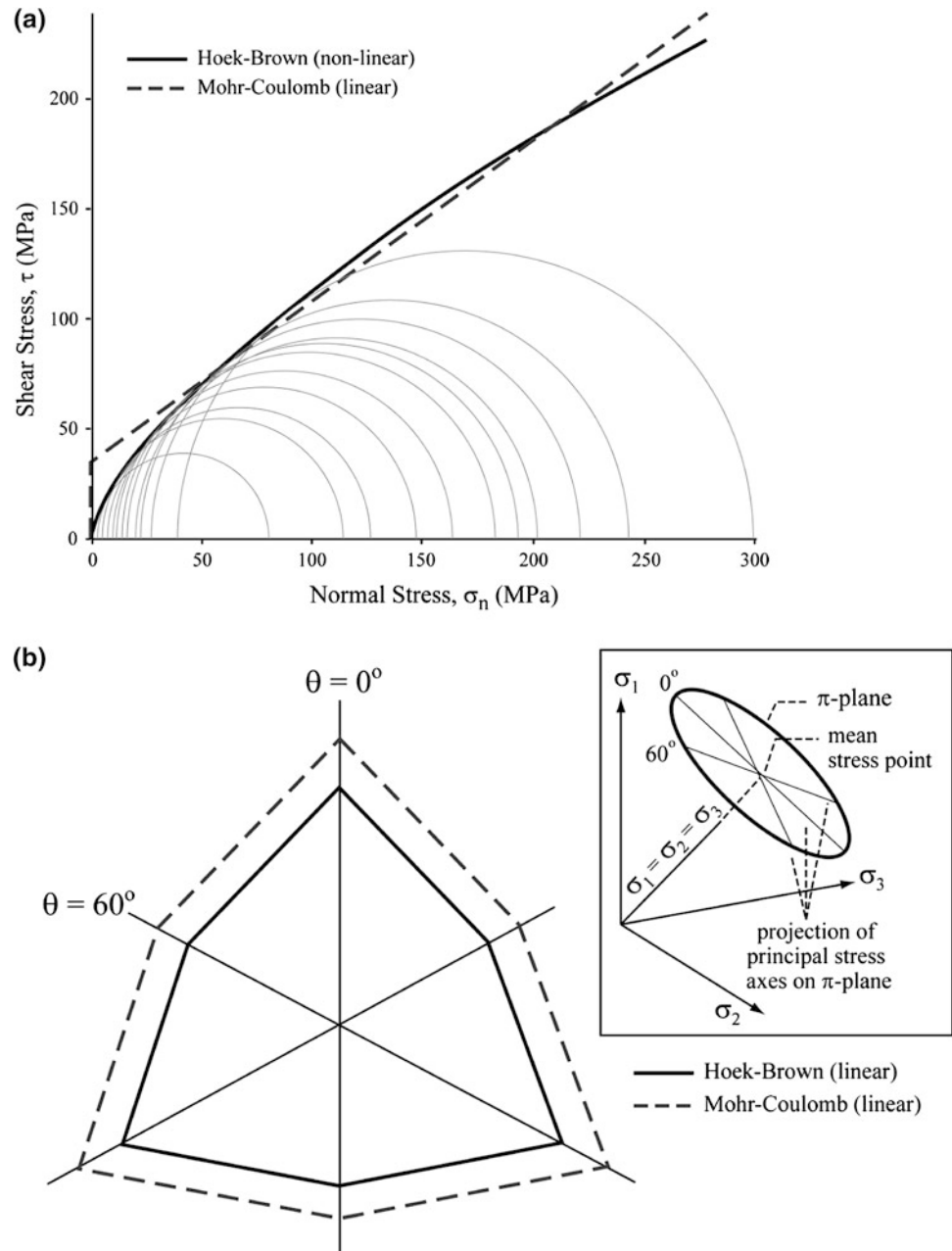
The original non-linear Hoek–Brown failure criterion for intact rock (Hoek and Brown 1980) was introduced as:

$$\sigma_1 = \sigma_3 + \sqrt{m C_o \sigma_3 + s C_o^2} \quad (1)$$

where σ_1 and σ_3 are the major and minor principal stresses at failure, C_o is the uniaxial compressive strength of the intact rock, and m and s are dimensionless empirical constants. The criterion is non-linear in the meridian plane (defined as the plane which passes through the hydrostatic axis and cuts the failure envelope) and linear in appearance in the π -plane (defined as the plane perpendicular to hydrostatic axis and cuts the failure envelope; see Fig. 1). The criterion is also linear in the biaxial ($\sigma_1 - \sigma_2$) plane (e.g., see Fig. 6).

The non-linear form of the Hoek–Brown criterion distinguishes it from the linear Mohr–Coulomb failure criterion (Fig. 1a). In terms of equivalencies, the parameter m is analogous to the frictional strength of the rock and s , which is a measure of how fractured the rock is, is related to the rock mass cohesion. Large values of m give steeply inclined

Fig. 1 a Comparison of the linear Mohr–Coulomb and non-linear Hoek–Brown failure envelopes plotted against triaxial test data for intact rock and **b** similar comparison but projected onto the π -plane. *Inset* shows definition of π -plane (i.e., plane perpendicular to hydrostatic stress axis)



Mohr envelopes and high instantaneous friction angles at low effective normal stresses, as is generally found for strong brittle rocks; lower m values give lower instantaneous friction angles as observed for more ductile rocks (Hoek 1983). This is demonstrated in Fig. 2. The constant s varies as a function of how fractured the rock is from a maximum value of 1 for intact rock to zero for heavily fractured rock where the tensile strength has been reduced to zero.

As can be seen in Eq. (1), the Hoek–Brown criterion assumes that rock failure is controlled by the major and minor principal stress, σ_1 and σ_3 ; the intermediate principal stress, σ_2 , does not appear in the equations except insofar as

$\sigma_2 = \sigma_3$ (i.e., conventional triaxial compression test) or $\sigma_2 = \sigma_1$. This assumption is later discussed in more detail in the treatment of the advantages and limitations of the criterion.

3 Rock Mass Properties

As the primary focus of this Working Group report is failure criterion for intact rock, the application of Hoek–Brown to rock mass strength is only briefly discussed here. By adjusting the m and s parameters according to the rock mass conditions, the criterion can be applied to the estimation of

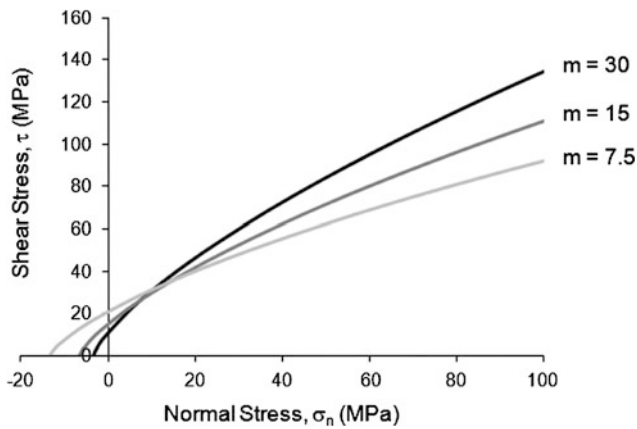


Fig. 2 Change in Hoek–Brown failure envelope as a function of m plotted in shear versus normal stress space. Note how larger values of m give more steeply inclined Mohr envelopes and higher equivalent friction angles than lower m values

rock mass strength properties. This requires the assumption that any fractures present are numerous enough that the overall strength behavior has no preferred failure direction; i.e., the rock mass responds as an isotropic, equivalent continuum.

As an empirical criterion, the Hoek–Brown criterion has been updated several times in response to experience gained with its use and to address certain practical limitations (Hoek and Brown 1988; Hoek et al. 1992, 1995, 2002). These primarily involve adjustments to improve the estimate of rock mass strength. One key update was the reporting of the ‘generalised’ form of the criterion (Hoek et al. 1995):

$$\sigma'_1 = \sigma'_3 + C_o \left(m_b \frac{\sigma'_3}{C_o} + s \right)^a \quad (2)$$

The term m_b was introduced for broken rock. The original m_i value had been reassessed and found to depend upon the mineralogy, composition and grain size of the intact rock (Hoek et al. 1992). The exponential term a was added to address the system’s bias towards hard rock and to better account for poorer quality rock masses by enabling the curvature of the failure envelope to be adjusted, particularly under very low normal stresses (Hoek et al. 1992). The Geological Strength Index (GSI) was subsequently introduced together with several relationships relating m_b , s and a , with the overall structure of the rock mass (or blockiness) and surface conditions of the discontinuities (Hoek et al. 1995). The principal stress terms in the original equation had been replaced earlier with effective principal stress terms as it was assumed that criterion was valid for effective stress conditions (Hoek 1983).

In 2002, Hoek et al. (2002) re-examined the relationships between the GSI and m_b , s and a , and introduced a new factor D to account for near surface blast damage and stress relaxation. This edition of the criterion represents the last major revision of the Hoek–Brown system. The rock mass scaling relationships for m_b , s and a were reported as:

$$m_b = m_i \exp\left(\frac{\text{GSI} - 100}{28 - 14D}\right) \quad (3)$$

$$s = \exp\left(\frac{\text{GSI} - 100}{9 - 3D}\right) \quad (4)$$

$$a = \frac{1}{2} + \frac{1}{6} \left(e^{-\frac{\text{GSI}}{15}} + e^{-\frac{20}{3}} \right) \quad (5)$$

From above, m_i is a curve fitting parameter derived from triaxial testing of intact rock. The parameter m_b is a reduced value of m_i , which accounts for the strength reducing effects of the rock mass conditions defined by GSI (Fig. 3). Adjustments of s and a are also done according to the GSI value. GSI is estimated from the chart of Marinos et al. (2005); Sönmez and Ulusay (2002) discuss the sensitivity of the Hoek–Brown strength envelope to GSI. Although relationships exist to convert RMR₈₉ and Q to GSI (see Hoek et al. 1995), Hoek (2007) recommends that GSI be estimated directly by means of the charts published on its use.

For practicing engineers, the Hoek–Brown and GSI procedures (see Hoek et al. 2002) provide a straight forward means to scale laboratory test values to obtain isotropic rock mass properties. However, it must first be decided whether the representation of the engineered rock mass as an equivalent continuum is appropriate or not. The criterion should not be used where discontinuities have a significant influence on the mobilization of failure and failure kinematics, for example where the discontinuity spacing is large compared with the dimensions of the underground opening or when a rock slope is being analyzed and stability is more governed by the shear strength of individual discontinuities. Where the rock mass is more moderately to heavily jointed and the rock mass strength is approximately isotropic, then the GSI and Hoek–Brown treatment of the rock mass as an equivalent continuum are applicable.

Hoek (2007) recommends, where possible, the Hoek–Brown criterion be applied directly. However, given that many geotechnical design calculations are written for the Mohr–Coulomb failure criterion, it is often necessary to calculate equivalent rock mass cohesion, c , and friction angle, ϕ , values from the Hoek–Brown parameters. Moreover, most practitioners have an intuitive feel for the physical meanings of cohesion and friction, which is not the

Fig. 3 Scaling of Hoek–Brown failure envelope for intact rock to that for rock mass strength. See Marinou et al. (2005) for full details on use of the GSI chart

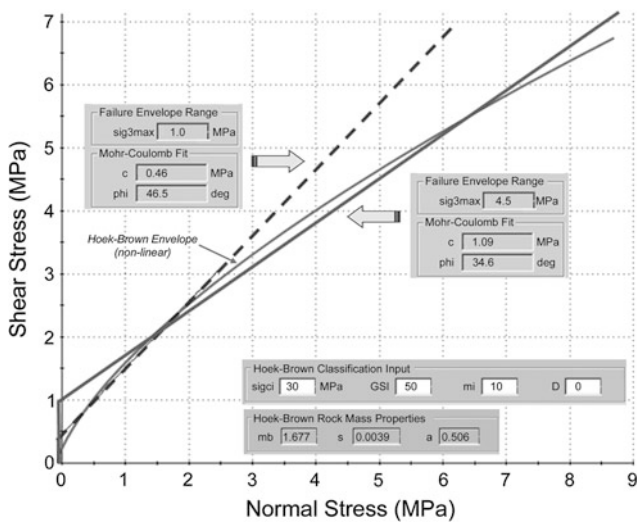
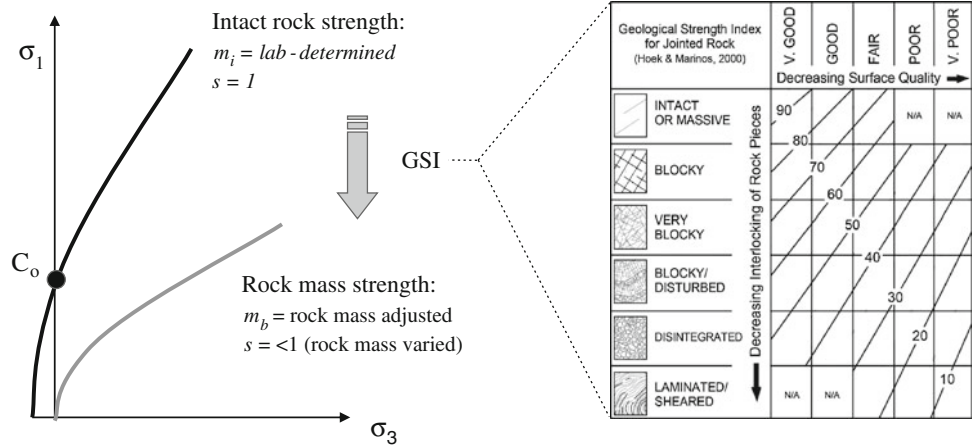


Fig. 4 Fitting of linear Mohr–Coulomb failure envelopes (blue solid and dashed lines) along two different stress ranges of a non-linear Hoek–Brown failure envelope (red curve). Note the change in equivalent cohesion and friction angle values for the two different stress ranges specified. Failure envelopes plotted using Rocscience’s (2007) RocLab (color figure online)

case for m_b , s and a . The quantitative conversion of Hoek–Brown to Mohr–Coulomb parameters is done by fitting an average linear relationship to the non-linear Hoek–Brown envelope for a range of minor principal stress values defined by $T_0 < \sigma_3 < \sigma'_{3max}$ (Hoek et al. 2002). Note that the value of σ'_{3max} , the upper limit of confining stress over which the relationship between the Hoek–Brown and Mohr–Coulomb criteria is considered, has to be determined for each individual case (Fig. 4). Brown (2008) warns against applying programs that calculate equivalent Mohr–Coulomb

parameters too automatically without thinking clearly about the range of effective normal stress that applies to the case being considered. If high values of σ'_{3max} are used, then the equivalent effective cohesion value may be too high and the equivalent effective friction angle too low.

4 Experimental Data on Intact Rock

There are several laboratory testing procedures from which the peak strength of intact rock can be measured. These include uniaxial compression, conventional triaxial compression ($\sigma_2 = \sigma_3$) and true triaxial compression. Empirical strength criteria have been developed based on fitting the best line or curve to these data. The accuracy of a criterion’s fit to the data is generally evaluated based on the biaxial plane-stress condition ($\sigma_1 - \sigma_2$ plane) and any meridian cross section ($\sqrt{2}J_2 - I_1/\sqrt{3}$ plane for $0^\circ \leq \theta \leq 60^\circ$), including the $\sigma_1 - \sqrt{2}\sigma_3$ plane (conventional triaxial test condition, where $\sigma_2 = \sigma_3$ or $\theta = 0^\circ$).

In developing the Hoek–Brown criterion, Hoek and Brown (1980) analyzed published conventional triaxial test data for more than 14 intact rock types covering a range of igneous, sedimentary and metamorphic rocks, with peak strengths ranging from 40 MPa for a sandstone to 580 MPa for a chert. This analysis included multiple tests for the same rock type carried out in different laboratories and only considered data sets containing a minimum of five tests covering a range of confining stresses. The choice of a non-linear criterion was based on this review and the m_i parameter was derived from best-fit linear regression to these data. The coefficient of determination, r^2 , for these fits ranged from 0.68 to 0.99, with most being >0.9 .

Zhao (2000) compared Mohr–Coulomb and Hoek–Brown fits to experimental data from a series of dynamic uniaxial and triaxial compression, uniaxial tension and unconfined shear tests performed on Bukit Timah granite from Singapore (average UCS approximately 190 MPa). This comparison showed that the intact rock strength under dynamic loads, at both low and high confining pressures, was better represented by the non-linear Hoek–Brown criterion. Similarly, Ghazvinian et al. (2008) found that the non-linear form of the Hoek–Brown criterion gave a better fit to their experimental data than the linear Mohr–Coulomb, in this case for weak marlstones (average UCS approximately 12 MPa).

Pariseau (2007) compared Mohr–Coulomb, Hoek–Brown and Drucker–Prager fits to triaxial experimental data of several intact rock types using the unconfined compressive and tensile strength intercepts as common reference points between the different criteria (it was assumed that the criteria are independent of the intermediate principal stress). Based on data from a sandstone, a high-strength norite, an Indiana limestone and a Dunham dolomite, the non-linear Hoek–Brown envelope provided a significantly better fit over the entire data range (i.e., low to high confining pressures) than Mohr–Coulomb and Drucker–Prager. Pariseau (2007) concluded, based on added comparisons involving other non-linear criteria, that a non-linear failure criterion is required to address the shortcomings of linear failure criteria.

A similar comparison was reported by Benz and Schwab (2008), assessing six different criteria: Mohr–Coulomb, Lade–Duncan, an approximation to Wiebols–Cook, Mogi, Hoek–Brown and a combined Hoek–Brown Matsuoka–Nakai criterion proposed by Benz et al. (2008), which accounts for the influence of the intermediate principal stress, σ_2 . These criteria were fitted to true triaxial test data for eight different intact rocks taken from previously published studies: Dunham dolomite, Solnhofen limestone, Shirahama sandstone, Yuubari shale, KTB amphibolite, Mizuho trachyte, a dense marble and Westerly granite. Again, in each case, the non-linear Hoek–Brown envelope gave either an equal or better fit than the linear Mohr–Coulomb criterion. Comparisons between Hoek–Brown and the other criteria were variable, though in six out of the eight cases, a clear reduction in the misfit between criteria and data was found when the intermediate principal stress was considered in the failure criterion.

It should be emphasized that the relevance of these comparisons and the level of fit achieved are dependent, in part, on the confining stress range (i.e., regression range) and the coordinate system in which the data and criterion are compared (e.g., σ_1 – σ_3 plane). Fitting of criteria near the origin of a normal stress–shear stress plot, including tensile strength, is typically more important for engineering

excavations in rock; the closeness of fit in this region may thus be of more concern than that at high confining pressures.

5 Advantages and Limitations

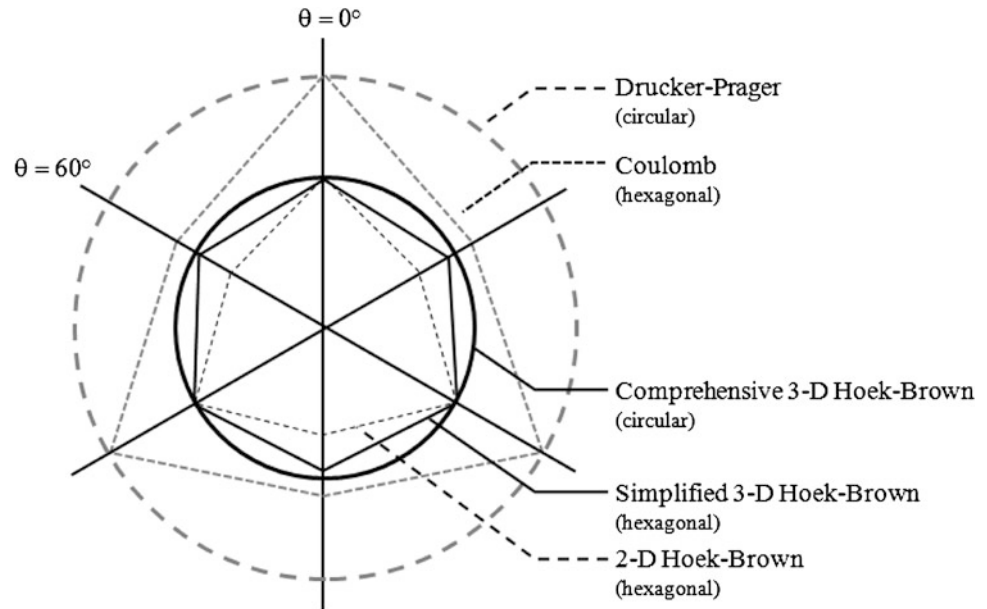
The main advantages of the Hoek–Brown criterion are:

- It is non-linear in form (in the meridian plane), which agrees with experimental data over a range of confining stresses;
- It was developed through an extensive evaluation of laboratory test data covering a wide range of intact rock types;
- It provides a straight forward empirical means to estimate rock mass properties;
- There is almost three decades worth of experience with its use by practitioners on a variety of rock engineering projects.

Considerable progress has also been made in applying the Hoek–Brown criterion to the assessment and prediction of brittle fracture damage in overstressed massive rock. Martin et al. (1999) provide an empirical depth of spalling failure relationship using the Hoek–Brown criterion, setting $m = 0$ and $s = 0.11$. The fundamental assumption made by the authors is that the stress-controlled failure process around the tunnel is dominated by cohesion loss. Hence the m_b parameter, which can be equated to frictional strength, is set to zero. It should be emphasized that this treatment (i.e., $m = 0$) differs from that which would be used for an elasto-plastic yielding failure mechanism where the frictional strength component mobilizes and dominates the behavior of the rock mass, requiring the m value to be set to a typical value for the rock type in question. These findings and the empirical relationship suggested by Martin et al. (1999) have since been repeated and confirmed in other studies on tunnel stability in highly stressed rock (e.g., Kaiser et al. 2000; Diederichs et al. 2004). Diederichs (2007) also uses the Hoek–Brown relationship to develop a reliable procedure for modelling the depth and extent of brittle spalling for deep tunnels in blocky to massive rock ($GSI > 65$). His procedure introduces a bi-linear failure criterion that accounts for different stress thresholds under which brittle fractures initiate and propagate during spalling. Considering the influence of confinement on self-stabilization of the spalling process at some distance into the rock mass, this criterion captures the dependence of fracture propagation on confinement and can be incorporated into a non-elastic numerical model using modified Hoek–Brown parameters.

Limitations in the Hoek–Brown criterion have been documented through detailed discussions on the simplifying assumptions made in deriving the criterion (Hoek and

Fig. 5 π -Plane plot comparing Priest's (2005) comprehensive and simplified 3-D Hoek–Brown criteria relative to other commonly used criteria. See Fig. 1b inset for definition of the π -plane projection (modified after Priest 2005)



Brown 1980; Hoek 1983; Brown 2008). One of the most important of these is the independency of the criterion from the intermediate principal stress, σ_2 . Hoek and Brown (1980) justified this by pointing to triaxial extension and compression tests by Brace (1964) that showed no significant variation between results when $\sigma_2 = \sigma_3$ and $\sigma_2 = \sigma_1$. Brace concluded that σ_2 had a negligible influence on failure. True triaxial testing by others (for e.g., Mogi 1971) shows that a more pronounced influence of σ_2 was discounted as involving brittle/ductile transitions in the failure process.

Subsequent experimental studies have since suggested that the intermediate principal stress has a substantial influence on rock strength (e.g., Takahashi and Koide 1989; Colmenares and Zoback 2002; Haimson 2006). This has led to the development of several 3-D versions of the Hoek–Brown failure criterion (Pan and Hudson 1988; Priest 2005; Zhang and Zhu 2007; Zhang 2008; Melkounian et al. 2009). Figure 5 compares the comprehensive and simplified 3-D Hoek–Brown envelopes developed by Priest (2005) to other commonly used criteria for a given hydrostatic stress. Melkounian et al. (2009) explain that despite the capacity of the Hoek–Brown criterion for modelling a wide range of intact and fractured rock types, its use has not been widely adopted in the petroleum industry, partly because it does not take into account the intermediate principal stress. A stress state where the intermediate principal stress is substantially larger than the minor principal stress can occur adjacent to boreholes drilled for petroleum and gas extraction and thus

the strength of the rock is higher than what the criterion predicts. Figure 6 compares the fit of the Hoek–Brown criterion to true triaxial test data for five different intact rock types as reported by Colmenares and Zoback (2002).

Another limitation of the Hoek–Brown criterion, as discussed by Pariseau (2007), is with respect to its mathematical characteristics. He noted that the parabola form of the criterion is not centered on the hydrostatic stress axis. However, this does not have any influence on the practical application of Hoek–Brown. The underlying assumption in the development of the Hoek–Brown criterion is $\sigma_1 \geq \sigma_2 \geq \sigma_3$ (or $0^\circ \leq \theta \leq 60^\circ$ in the π -plane), which implies a positive mean shear stress $\tau_m \geq 0$. Therefore, Hoek–Brown is actually a segment of the parabola in the meridian plane which starts from the hydrostatic stress axis, I_1 (Fig. 7).

6 Recommendations

As a peak strength criterion for intact rock, the Hoek–Brown criterion has the advantage of describing a non-linear increase in strength with increasing confinement that agrees with extensive laboratory triaxial test data covering a wide range of intact rock types. Its use can be recommended for most rock types (igneous, sedimentary, metamorphic) under both low and high confining pressures. Similarly, its use can be recommended for problems involving a varying range of confining stress magnitudes (from low to very high

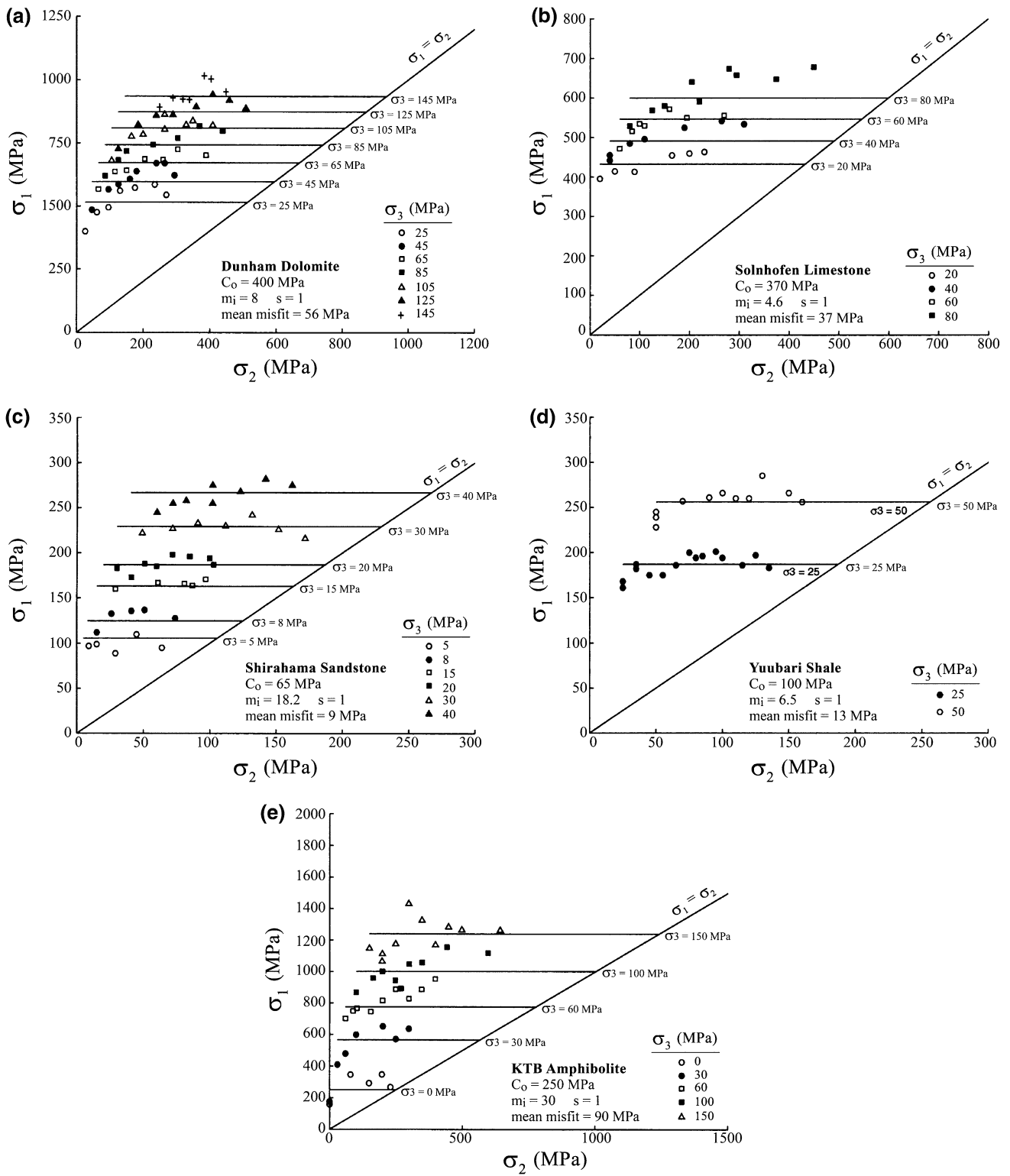


Fig. 6 Best-fit comparison of the Hoek–Brown criterion to true triaxial ($\sigma_1 > \sigma_2 > \sigma_3$) tests of intact rock for: **a** Dunham dolomite, **b** Solnhofen limestone, **c** Shirahama sandstone, **d** Yuubari shale, and **e** KTB amphibolite. The Hoek–Brown criterion is represented by *straight lines* in σ_1 versus σ_2 space, extending laterally from each σ_3 value (after Colmenares and Zoback 2002)

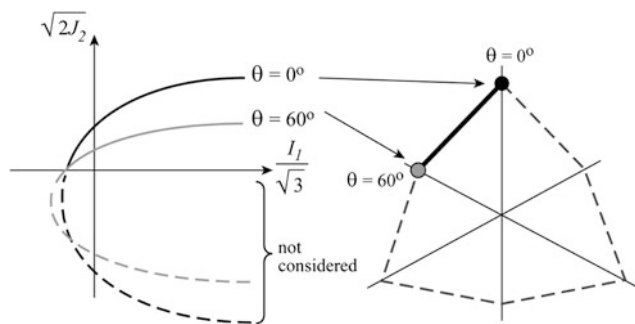


Fig. 7 Illustration of underlying assumption in the development of the Hoek–Brown criterion in which $\sigma_1 \geq \sigma_2 \geq \sigma_3$ (or $0^\circ \leq \theta \leq 60^\circ$ in the π -plane). This forces a positive mean shear stress. The Hoek–Brown criterion is a segment of the parabola which starts from the hydrostatic stress axis

confinement). Where rock mass strength is more appropriate, empirical procedures, which provide an important and straight forward means to estimate rock mass properties, are also available. These are not discussed in detail here as the scope of the Working Group's report is dedicated to reporting on failure criteria for isotropic intact rock (see WG Introduction).

Acknowledgments The author would like to thank Dr. Evert Hoek, Masoud Rahjoo and Prof. Bill Pariseau, together with the reviewers of the Working Group's report for their constructive review comments and suggestions.

References

- Benz T, Schwab R (2008) A quantitative comparison of six rock failure criteria. *Int J Rock Mech Min Sci* 45(7):1176–1186
- Benz T, Schwab R, Kautner RA, Vermeer PA (2008) A Hoek–Brown criterion with intrinsic material strength factorization. *Int J Rock Mech Min Sci* 45(2):210–222
- Brace WF (1964) Brittle fracture of rocks. In: Judd WR (ed) *State of stress in the Earth's crust: Proceedings of the International Conference*. American Elsevier Publishing Co., New York, pp 110–178
- Brown ET (2008) Estimating the mechanical properties of rock masses. In: Potvin Y, Carter J, Dyskin A, Jeffrey R (eds) *Proceedings of the 1st Southern Hemisphere International Rock Mechanics Symposium*, Australian Centre for Geomechanics, Perth, pp 3–22
- Colmenares LB, Zoback MD (2002) A statistical evaluation of intact rock failure criteria constrained by polyaxial test data for five different rocks. *Int J Rock Mech Min Sci* 39(6):695–729
- Diederichs MS (2007) Mechanistic interpretation and practical application of damage and spalling prediction criteria for deep tunnelling. *Can Geotech J* 44(9):1082–1116
- Diederichs MS, Kaiser PK, Eberhardt E (2004) Damage initiation and propagation in hard rock tunnelling and the influence of near-face stress rotation. *Int J Rock Mech Min Sci* 41(5):785–812
- Ghazvinian AH, Fathi A, Moradian ZA (2008) Failure behavior of marlstone under triaxial compression. *Int J Rock Mech Min Sci* 45(5):807–814
- Griffith AA (1920) The phenomena of rupture and flow in solids. *Philos Trans R Soc Lond Ser A Math Phys Sci* 221(587):163–198
- Griffith AA (1924) The theory of rupture. In: Biezeno CB, Burgers JM (eds) *Proceedings of the First International Congress for Applied Mechanics*. Delft. J. Waltman Jr, Delft, pp 55–63
- Haimson B (2006) True triaxial stresses and the brittle fracture of rock. *Pure Appl Geophys* 163(5–6):1101–1130
- Hoek E (1968) Brittle failure of rock. In: Stagg KG, Zienkiewicz OC (eds) *Rock mechanics in engineering practice*. Wiley, New York, pp 99–124
- Hoek E (1983) Strength of jointed rock masses, 23rd Rankine Lecture. *Géotechnique* 33(3):187–223
- Hoek E (2007) *Practical Rock Engineering*. e-book
- Hoek E, Brown ET (1980) *Underground excavations in rock*. The Institution of Mining and Metallurgy, London
- Hoek E, Brown ET (1988) The Hoek–Brown failure criterion—a 1988 update. In: Curran J (ed) *Proceedings of the 15th Canadian Rock Mechanics Symposium*. University of Toronto, Toronto, pp 31–38
- Hoek E, Wood D, Shah S (1992) A modified Hoek–Brown criterion for jointed rock masses. In: Hudson JA (ed) *Rock characterization: ISRM Symposium, Eurock '92*, Chester, UK. Thomas Telford, London, pp 209–213
- Hoek E, Kaiser PK, Bawden WF (1995) Support of underground excavations in hard rock, A.A. Balkema, Rotterdam
- Hoek E, Carranza-Torres CT, Corkum B (2002) Hoek–Brown failure criterion—2002 edition. In: Hammah R, Bawden W, Curran J, Telesnicki M (eds) *Proceedings of the Fifth North American Rock Mechanics Symposium (NARMS-TAC)*, University of Toronto Press, Toronto, pp 267–273
- Kaiser PK, Diederichs MS, Martin D, Sharpe J, Steiner W (2000) Underground works in hard rock tunnelling and mining. In: *GeoEng2000, Proceedings of the International Conference on Geotechnical and Geological Engineering*, Melbourne, Technomic Publishing Company, Lancaster, pp 841–926
- Marinos V, Marinos P, Hoek E (2005) The geological strength index: applications and limitations. *Bull Eng Geol Environ* 64(1):55–65
- Martin CD, Kaiser PK, McCreath DR (1999) Hoek–Brown parameters for predicting the depth of brittle failure around tunnels. *Can Geotech J* 36(1):136–151
- Melkounian N, Priest SD, Hunt SP (2009) Further development of the three-dimensional Hoek–Brown yield criterion. *Rock Mech Rock Eng* 42(6):835–847
- Mogi K (1971) Fracture and flow of rocks under high triaxial compression. *J Geophys Res* 76(5):1255–1269
- Pan XD, Hudson JA (1988) A simplified three-dimensional Hoek–Brown yield criterion. In: Romana M (ed) *Rock mechanics and power plants*, A.A. Balkema, Rotterdam, pp 95–103
- Pariseau WG (2007) Fitting failure criteria to laboratory strength tests. *Int J Rock Mech Min Sci* 44(4):637–646
- Priest SD (2005) Determination of shear strength and three-dimensional yield strength for the Hoek–Brown criterion. *Rock Mech Rock Eng* 38(4):299–327
- Rocscience (2007) *RocLab*. 1.031 edn. Rocscience Inc., Toronto
- Sönmez H, Ulusay R (2002) A discussion on the Hoek–Brown failure criterion and suggested modifications to the criterion verified by slope stability case studies. *Yerbilimleri* 26:77–99
- Takahashi M, Koide H (1989) Effect of the intermediate principal stress on strength and deformation behavior of sedimentary rocks at the depth shallower than 2000 m. In: Maury V, Fourmaintraux D (eds) *Rock at great depth*, A.A. Balkema, Rotterdam, pp 19–26
- Zhang L (2008) A generalized three-dimensional Hoek–Brown strength criterion. *Rock Mech Rock Eng* 41(6):893–915
- Zhang L, Zhu H (2007) Three-dimensional Hoek–Brown strength criterion for rocks. *J Geotech Geoenviron Eng ASCE* 133(9):1128–1135
- Zhao J (2000) Applicability of Mohr–Coulomb and Hoek–Brown strength criteria to the dynamic strength of brittle rock. *Int J Rock Mech Min Sci* 37(7):1115–1121

Three-Dimensional Failure Criteria Based on the Hoek–Brown Criterion

Stephen Priest

List of symbols

m_b	Hoek–Brown material constant
s	Hoek–Brown material constant
a	Hoek–Brown material constant
C_o	Uniaxial compressive strength
I'_1	First invariant of the effective stress tensor
σ'_1	Major principal effective stress
σ'_2	Intermediate principal effective stress
σ'_3	Minor principal effective stress
τ_{oct}	Octahedral shear stress
$\sigma'_{1\text{hb}}$	Major principal effective stress at failure for the 2D Hoek–Brown criterion
$\sigma'_{3\text{hb}}$	Minor principal effective stress at failure for the 2D Hoek–Brown criterion
α	Simplified Priest material constant
β	Simplified Priest material constant
w	Simplified Priest material constant

1 Description

There is a growing body of experimental evidence (Takahashi and Koide 1989) to suggest that the intermediate principal stress has a substantial influence on the strength of rock materials. Widely adopted failure criteria, such as the Coulomb and Hoek–Brown criteria, ignore the influence of the intermediate principal stress and therefore may not

Originally published as an article in the journal *Rock Mechanics and Rock Engineering*, 45, S. Priest, Three-Dimensional Failure Criteria Based on the Hoek–Brown Criterion, 989–993, 2012.

S. Priest (✉)
School of Civil, Environmental and Mining Engineering, The University of Adelaide, Adelaide, SA, Australia
e-mail: stephen.priest@adelaide.edu.au

provide a reliable prediction of rock strength under true triaxial stress conditions. Although a number of three-dimensional failure criteria have been developed, such as the Drucker and Prager (1952) criterion and Lade criterion (Kim and Lade 1984), these criteria were not primarily developed for the application to rocks.

The widespread adoption of the empirical two-dimensional Hoek–Brown failure criterion (2DHB) (Hoek and Brown 1997; Hoek et al. 2002) for rock engineering applications has prompted a number of researchers to develop three-dimensional versions, in which the predicted major effective principal stress at failure is dependent on the intermediate effective principal stress, in addition to the parameters in the existing 2DHB failure criterion. Three-dimensional versions of the 2DHB failure criterion have been proposed by Pan and Hudson (1988), Priest (2005) and Zhang and Zhu (2007). Zhang (2008) presented a generalised version of the Zhang–Zhu criterion. Melkounian et al. (2009) presented an explicit version of the ‘comprehensive’ Priest criterion. Conventionally, in the literature, each criterion has been named after the author(s) who first described the criterion; this convention will be adopted here. It is likely that additional new three-dimensional versions of the Hoek–Brown criterion will be developed over the next few years.

2 Background

The most recent generalised version of the 2DHB failure criterion is introduced by Eberhardt and Rahjoo (this volume). This version of the Hoek–Brown criterion is here referred to as ‘generalised’ because the key parameters m_b , s and a can take any general values to allow the application to intact rock and to rock masses. The paper explains how the parameters m_b , s and a for a fractured rock mass can be estimated from empirical expressions.

For intact rock, the parameters m_b , s and a are m_i , 1.0 and 0.5, respectively. A number of authors, including Hoek and Brown (1997), provide tabulations of suggested values of m_i for a range of rock types. Alternatively, the parameters m_i , s and a can be determined from a series of conventional triaxial tests on intact rock, as explained by Eberhardt and Rahjoo (this volume).

In the following section, three-dimensional versions of the Hoek–Brown criterion have been expressed in terms of the parameters m_b , s and a , in order to provide a generalised formulation. However, since these criteria have not been shown to be, nor indeed claimed to be, applicable to fractured rock masses, the parameters m_b , s and a should be replaced by m_i , 1.0 and 0.5, respectively, and the criteria limited to the application to intact rock materials.

3 Formulation

3.1 Generalised Zhang–Zhu (GZZ) Criterion

The Zhang–Zhu criterion was first presented by Zhang and Zhu (2007). A generalised version of this criterion, based on the generalised Hoek–Brown criterion, was presented by Zhang (2008) as follows:

$$s C_o = C_o^{(1-\frac{1}{a})} \left(\frac{3\tau_{\text{oct}}}{\sqrt{2}} \right)^{\frac{1}{a}} + \frac{3m_b\tau_{\text{oct}}}{2\sqrt{2}} - \frac{m_b(3I'_1 - \sigma'_2)}{2} \quad (1)$$

where σ'_3 is the minor effective principal stress at failure, σ'_2 is the intermediate effective principal stress at failure, σ'_1 is the major effective principal stress at failure, and the other Hoek–Brown parameters are as defined earlier.

$$\tau_{\text{oct}} = \frac{\sqrt{(\sigma'_1 - \sigma'_2)^2 + (\sigma'_2 - \sigma'_3)^2 + (\sigma'_3 - \sigma'_1)^2}}{3} \quad (2)$$

and I'_1 is given by

$$I'_1 = \frac{\sigma'_1 + \sigma'_2 + \sigma'_3}{3} \quad (3)$$

In Eq. (1),

$$\frac{m_b(3I'_1 - \sigma'_2)}{2} = \frac{m_b(\sigma'_3 + \sigma'_1)}{2}.$$

Unfortunately, this failure criterion cannot easily be formulated to express σ'_1 explicitly in terms of the input data. It is, however, a relatively straightforward matter to apply a numerical strategy to determine the value of σ'_1 that satisfies Eqs. (1)–(3).

3.2 Generalised Pan–Hudson (GPH) Criterion

Zhang and Zhu (2007) demonstrated that the only difference between their yield criterion and the one proposed by Pan and Hudson (1988) is the absence of the intermediate principal stress in the third term of Eq. (1). The generalised form of the Pan–Hudson criterion can be written as

$$s C_o = C_o^{(1-\frac{1}{a})} \left(\frac{3\tau_{\text{oct}}}{\sqrt{2}} \right)^{\frac{1}{a}} + \frac{3m_b\tau_{\text{oct}}}{2\sqrt{2}} - m_b I'_1 \quad (4)$$

where the parameters are as defined earlier. Again, a numerical strategy is required to determine the value of σ'_1 in Eq. (4). Although there is apparently only a minor difference between the GZZ and GPH criteria, these criteria predict very different strength values.

3.3 Generalised Priest (GP) Criterion

A three-dimensional version of the Hoek–Brown yield criterion was developed by Priest (2005) by combining the two-dimensional Hoek and Brown (1997) and the three-dimensional Drucker and Prager (1952) criteria. The nomenclature ‘Priest criterion’ has been adopted following Zhang (2008). The term ‘comprehensive’ three-dimensional Hoek–Brown criterion was adopted by Priest (2005) to distinguish this failure criterion from the ‘simplified’ version described below. The term ‘comprehensive’ is somewhat misleading, since this criterion is no more comprehensive than the other criteria outlined above. This criterion will therefore be referred to as the generalised Priest criterion (Priest 2009). The formulation presented by Priest (2005) required a numerical solution strategy. Melkounian et al. (2009) addressed this problem by developing an explicit version of this three-dimensional Hoek–Brown criterion involving the 2DHB minimum effective stress at failure $\sigma'_{3\text{hb}}$, as summarised below:

$$C = s + \frac{m_b(\sigma'_2 + \sigma'_3)}{2 C_o} \quad (5)$$

$$E = 2 C^a C_o \quad (6)$$

$$F = 3 + 2 a C^{a-1} m_b \quad (7)$$

$$\sigma'_{3\text{hb}} = \frac{\sigma'_2 + \sigma'_3}{2} + \frac{-E \pm \sqrt{E^2 - F(\sigma'_2 - \sigma'_3)^2}}{2F} \quad (8)$$

Equation (8) gives two values for σ'_{3hb} , one of which can be negative and the other positive. In a compressive stress regime, σ'_{3hb} will be positive, so Melkounian et al. (2009) recommended that the greater or positive root in Eq. (8) should be adopted.

$$P = C_o \left\{ \left(\frac{m_b \sigma'_{3hb}}{C_o} \right) + s \right\}^a \quad (9)$$

Finally,

$$\sigma'_1 = 3\sigma'_{3hb} + P - (\sigma'_2 + \sigma'_3). \quad (10)$$

3.4 Simplified Priest (SP) Criterion

Priest (2005) proposed a ‘simplified’ three-dimensional version of the Hoek–Brown criterion, which has the merit of providing an easily computed estimate for the three-dimensional effective failure stress σ'_1 .

$$\sigma'_1 = \sigma'_{1hb} + 2\sigma'_{3hb} - (\sigma'_2 + \sigma'_3) \quad (11)$$

where, as before, σ'_{3hb} is the minimum 2DHB effective stress at failure, and σ'_{1hb} is the maximum 2DHB effective stress at failure, calculated from Eq. (2), and

$$\sigma'_{3hb} = w\sigma'_2 + (1-w)\sigma'_3 \quad (12)$$

where w is a weighting factor in the range 0–1, which governs the relative influence of σ'_2 and σ'_3 on the strength of the rock. Priest (2005) suggested that for a wide range of rock types, w can be estimated from the following simple power law.

$$w \approx \alpha \sigma_3^\beta \quad (13)$$

Preliminary studies by Priest (2005) suggest that, as a first approximation, $\alpha = \beta = 0.15$.

4 Experimental Data on Rock

True triaxial rock test data published by Chang and Haimson (2000) for the KTB amphibolite and by Haimson and Chang (2000) for Westerly granite were selected to compare the predictions of the four three-dimensional Hoek–Brown failure criteria. Data published in these papers include uniaxial and ‘conventional’ triaxial test data for these rocks (where $\sigma'_2 = \sigma'_3$), so it was possible to determine the experimental values of the Hoek–Brown parameter m_i and the uniaxial compressive strength of the intact rock

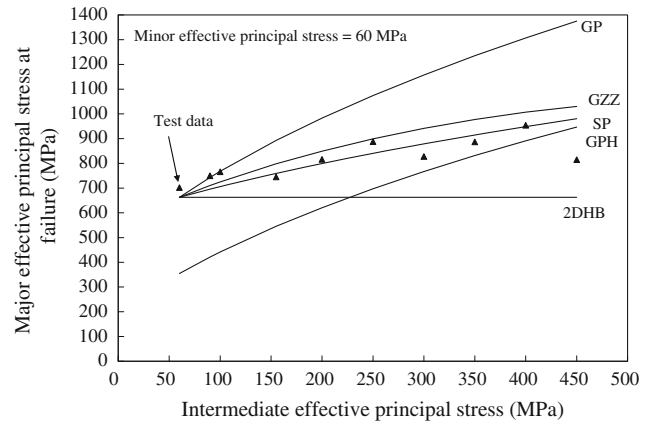


Fig. 1 Four three-dimensional Hoek–Brown failure criteria and also the two-dimensional Hoek–Brown failure criterion for KTB amphibolite, $m_i = 35.4$, $\sigma_{ci} = 159.1$ MPa

material C_o , on the assumption that the Hoek–Brown parameters s and a are 1.0 and 0.5, respectively, for the intact rock specimens. Simple curve fitting against the data presented for these two rock types gave the following best estimates for the key parameters: KTB amphibolite $m_i = 35.4$, $C_o = 159.1$ MPa; Westerly granite $m_i = 40.5$, $C_o = 191.0$ MPa. Although the test data can be compared with the predictions of the yield criteria in a number of different ways, including, for example, plots of failure envelopes in the deviatoric plane, the primary focus here will be to examine how well the failure criteria model the influence of the intermediate principal stress σ'_2 .

Figure 1 shows the four three-dimensional Hoek–Brown failure criteria and also the 2DHB failure criterion for a minor principal effective stress σ'_3 of 60 MPa and an intermediate effective principal stress at failure σ'_2 ranging from 60 to 450 MPa for KTB amphibolite. This figure shows that the 2DHB failure criterion is, as expected, insensitive to the intermediate principal stress. All criteria, except the GPH, diverge from the common point where $\sigma'_2 = \sigma'_3 = 60$ MPa and $\sigma'_1 = 662.9$ MPa. This somewhat anomalous behaviour of the GPH criterion merits further investigation. The generalised Priest criterion (GP) is the most sensitive to the influence of the intermediate principal stress, predicting substantially higher values of σ'_1 than the other criteria and the test data. The simplified Priest criterion (SP), adopting Eq. (13) to calculate the weighting factor w , is the least sensitive, with the GZZ lying between these two. These latter two criteria appear to model the test data reasonably well. This same general pattern is repeated for the test data at other values of intermediate principal stress, presented by Chang and Haimson (2000), with the simplified Priest (SP) and the GZZ criteria offering the best

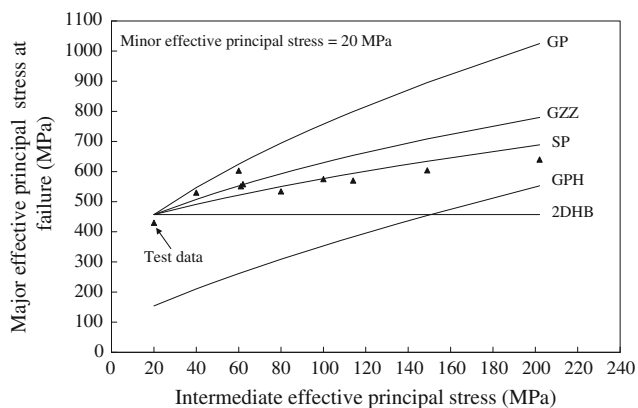


Fig. 2 Four three-dimensional Hoek–Brown failure criteria and also the two-dimensional Hoek–Brown failure criterion for Westerly granite, $m_i = 40.5$, $\sigma_{ci} = 191.0$ MPa

models for the test data. The test data do, however, indicate that the sensitivity of σ'_1 to σ'_2 reduces at higher values of σ'_3 .

Figure 2 shows the four three-dimensional Hoek–Brown failure criteria and also the 2DHB failure criterion for a minor principal effective stress σ'_3 of 20 MPa and an intermediate effective principal stress at failure σ'_2 ranging from 20 to 202 MPa, for Westerly granite. This figure again shows that the 2DHB failure criterion is, as expected, insensitive to the intermediate principal stress. Again, all criteria, except the GPH, diverge from the common point where $\sigma'_2 = \sigma'_3 = 20$ MPa and $\sigma'_1 = 457.1$ MPa. Again, the generalised Priest criterion (GP) is the most sensitive to the influence of the intermediate principal stress, predicting substantially higher values of σ'_1 than the other criteria and the test data. The simplified Priest criterion (SP), adopting Eq. (13) to calculate the weighting factor w , is the least sensitive, with the GZZ again lying between these two. These latter two criteria appear to model the test data reasonably well. This same general pattern is repeated for the test data at other values of intermediate principal stress, presented by Haimson and Chang (2000), with the simplified Priest and the GZZ criteria offering the best models for the test data. As for the KTB amphibolite, the test data for Westerly granite indicate that the sensitivity of σ'_1 to σ'_2 reduces at higher values of σ'_3 .

5 Advantages and Limitations

The generalised Priest criterion seems to overestimate the experimentally determined true triaxial rock strength for KTB amphibolite and Westerly granite by around 10–30 % for σ'_2 in the approximate range $2\sigma'_3$ to $4\sigma'_3$. This overestimate rises to more than 50 % at higher values of σ'_2 . Clearly, the generalised Priest criterion (GP) should be used

with some caution at this stage, particularly at higher levels of intermediate principal stress.

The simplified Priest criterion (SP), adopting Eq. (13) to calculate the weighting factor w , and the GZZ criterion both provide a reasonably good model of the experimentally determined true triaxial rock strength for KTB amphibolite and Westerly granite. The generalised and simplified Priest criteria (GP, SP) do, however, have the benefit of being amenable to direct explicit evaluation and so are more suitable for incorporation into numerical modelling software. The simplified Priest criterion substantially underestimates the experimentally determined true triaxial rock strength for KTB amphibolite and Westerly granite when the minor principal stress is zero. Under these conditions the weighting factor w in Eq. (13) is zero, which creates a negative slope for the graph of σ'_1 versus σ'_2 for this failure criterion.

None of the criteria examined, with the exception of the simplified Priest criterion, require additional input parameters beyond σ'_2 and the parameters required for the 2DHB criterion. It is, of course, possible to obtain a close fit to almost any experimental data by incorporating additional parameters (or ‘fudge factors’) into the formulation of a criterion. Adoption of a criterion with one or more additional parameters would necessitate the determination of these parameters for the particular rock type from a series of true triaxial tests. Such testing facilities are not generally available to rock mechanics practitioners, so existing and future three-dimensional Hoek–Brown failure criteria with additional parameters are likely to be of limited practical use.

A potential advantage of three-dimensional failure criteria based on the Hoek–Brown criterion is that, theoretically, it would be possible to adopt values of m_b , s and a that reflect the properties of a fractured rock mass. Consideration of the strength of fractured rock masses is, however, beyond the scope of these suggested methods.

6 Recommendations

A significant obstacle to recommending which, if any, of the above three-dimensional Hoek–Brown failure criteria should be applied to rock materials and rock masses is the relative paucity of rock strength test data for specimens loaded under uniaxial, conventional triaxial and true triaxial conditions for a range of rock types.

It is recommended that a substantial amount of further research and rock testing should be conducted before any of the three-dimensional Hoek–Brown failure criteria can be applied with confidence. This testing, which should cover a wide range of rock types and rock strengths, should follow the testing strategy adopted by Chang and Haimson (2000)

for the KTB amphibolite and by Haimson and Chang (2000) for Westerly granite, as follows:

- (a) A series of conventional uniaxial and triaxial tests should be conducted on intact rock specimens to determine the uniaxial compressive strength and the Hoek–Brown parameter m_i for the rock material, following the relevant ISRM Suggested Methods. It is also recommended that this series of conventional uniaxial and triaxial tests should be repeated in the true triaxial testing apparatus to assess if there is any specimen geometry or testing machine influence on the strength results.
- (b) A series of true triaxial tests should be conducted on specimens of the same intact rock, covering a range of minor and intermediate effective principal stresses. If it is assumed that the geological strength index (GSI) is 100 for intact rock, it will then be possible to assess the predictions of the published three-dimensional Hoek–Brown failure criteria over a range of rock types and stress levels.

Evaluation of the three-dimensional Hoek–Brown failure criteria for fractured rock masses presents a substantial challenge. The sampling and testing of undisturbed specimens of fractured rock of a size sufficient to represent in situ rock mass conditions presents a significant technical and financial difficulty. Furthermore, true triaxial testing equipment is currently only capable of testing relatively small specimens of intact rock. One promising strategy might be in situ pressuremeter tests in boreholes coupled with testing of recovered core and/or chips and detailed downhole surveys.

References

- Chang C, Haimson BC (2000) True triaxial strength and deformability of the German Continental Deep Drilling Program (KTB) deep hole amphibolite. *J Geophys Res* 105:18999–19014
- Drucker D, Prager W (1952) Soil mechanics and plastic analysis or limit design. *Q Appl Math* 10:157–169
- Haimson BC, Chang C (2000) A new true triaxial cell for testing mechanical properties of rock, and its use to determine rock strength and deformability in Westerly granite. *Int J Rock Mech Min Sci* 37:285–296
- Hoek E, Brown ET (1997) Practical estimates of rock mass strength. *Int J Rock Mech Min Sci Geomech Abstr* 34:1165–1186
- Hoek E, Carranza-Torres S, Corkum B (2002) Hoek–Brown failure criterion—2002 version. *Rockscience*. <http://www.rockscience.com/highlights>
- Kim MK, Lade PV (1984) Modelling rock strength in three dimensions. *Int J Rock Mech Min Sci Geomech Abstr* 21:21–33
- Melkounian N, Priest SD, Hunt SP (2009) Further development of the three-dimensional Hoek–Brown yield criterion. *Rock Mech Rock Eng* 42:835–847
- Pan XD, Hudson JA (1988) A simplified three-dimensional Hoek–Brown yield criterion. In: Romana M (ed) *Rock mechanics and power plants*. Balkema, Rotterdam, pp 95–103
- Priest SD (2005) Determination of shear strength and three-dimensional yield strength for the Hoek–Brown criterion. *Rock Mech. Rock Eng* 38:299–327
- Priest SD (2009) Comparisons between selected three-dimensional yield criteria applied to rock. *Rock Mech Rock Eng* 43:379–389
- Takahashi M, Koide H (1989) Effect of the intermediate principal stress on strength and deformation behavior of sedimentary rocks at the depth shallower than 2000 m. In: Maury V, Fourmaintraux D (eds) *Rock at great depth*, vol 1. Balkema, Rotterdam, pp 19–26
- Zhang L (2008) A generalized three-dimensional Hoek–Brown strength criterion. *Rock Mech Rock Eng* 41:893–915
- Zhang L, Zhu H (2007) Three-dimensional Hoek–Brown strength criterion for rocks. *J Geotech Geoenviron Eng ASCE* 133:1128–1135

Drucker–Prager Criterion

Leandro R. Alejano and Antonio Bobet

List of Symbols

λ	Drucker–Prager material constant
κ	Drucker–Prager material constant
J_2	Second invariant of the stress deviator tensor
I'_1	First invariant of the effective stress tensor
σ'_1	Major principal effective stress
σ'_2	Intermediate principal effective stress
σ'_3	Minor principal effective stress
τ_{oct}	Octahedral shear stress
σ'_{oct}	Octahedral effective normal stress
C_0	Uniaxial compressive strength
T_0	Uniaxial tensile strength
θ	Lode angle
b	MSDP _u parameter that defines the shape of the criterion in the π -plane (usually, $b \cong 0.75$)
a_1	MSDP _u parameter
a_2	MSDP _u parameter
ϕ	Angle of internal friction
c	Cohesion

Originally published as an article in the journal *Rock Mechanics and Rock Engineering*, 45, L. R. Alejano, A. Bobet, Drucker–Prager Criterion, 995–999, 2012.

L. R. Alejano (✉)
Department of Natural Resources and Environmental
Engineering, University of Vigo, Campus Lagoas
Marcosende s/n, Vigo, Spain
e-mail: alejano@uvigo.es

A. Bobet
School of Civil Engineering, Purdue University,
550 Stadium Mall Drive, West Lafayette, IN 47907, USA

1 Description

The Drucker–Prager failure criterion is a three-dimensional pressure-dependent model to estimate the stress state at which the rock reaches its ultimate strength. The criterion is based on the assumption that the octahedral shear stress at failure depends linearly on the octahedral normal stress through material constants.

2 Background

The Drucker–Prager failure criterion was established as a generalization of the Mohr–Coulomb criterion for soils (Drucker and Prager 1952). It can be expressed as:

$$\sqrt{J_2} = \lambda I'_1 + \kappa \quad (1)$$

where λ and κ are material constants, J_2 is the second invariant of the stress deviator tensor and I'_1 is the first invariant of the stress tensor, and are defined as follows:

$$\begin{aligned} I'_1 &= \sigma'_1 + \sigma'_2 + \sigma'_3 \\ J_2 &= \frac{1}{6} [(\sigma'_1 - \sigma'_2)^2 + (\sigma'_1 - \sigma'_3)^2 + (\sigma'_3 - \sigma'_1)^2] \end{aligned} \quad (2)$$

σ'_1 , σ'_2 , and σ'_3 , are the principal effective stresses.

The criterion, when expressed in terms of octahedral shear stress, τ_{oct} , and octahedral normal stress, σ'_{oct} , takes the form:

$$\tau_{\text{oct}} = \sqrt{\frac{2}{3}} (3\lambda \sigma'_{\text{oct}} + \kappa) \quad (3)$$

where $\sigma'_{\text{oct}} = 1/3 I'_1$ and $\tau_{\text{oct}} = \sqrt{\frac{2}{3}} J_2$. The Drucker–Prager criterion can thus be considered as a particular case of Nadai's criterion that states that the mechanical strength

of brittle materials takes the form $\tau_{\text{oct}} = f(\sigma'_{\text{oct}})$, where f is a monotonically increasing function (Nadai 1950; Addis and Wu 1993; Chang and Haimson 2000; Yu 2002). It can be also considered as an extension of the Von Mises failure criterion, which is recovered when $\lambda = 0$.

The original Drucker–Prager criterion has been modified to incorporate tension cut off or a cap model (e.g. Lubarda et al. 1996), which allows yield under hydrostatic pressure. Extended Drucker–Prager models have been proposed where the criterion is expressed in linear (i.e. the original criterion), general exponent, or hyperbolic form (e.g. Pariseau 1972 or Hadjigeorgiou et al. 1998).

The modified Drucker–Prager criterion includes the generalized Priest criterion (GP) (Priest 2005), which is discussed in detail in this issue, and the MSDP_u (Mises–Schleicher and Drucker–Prager unified) criterion. The MSDP_u has been proposed to approximate the short-term laboratory strength of low-porosity rocks (Aubertin and Simon 1996; Aubertin et al. 1999; Li et al. 2000) and provides for a non-circular surface in the π -plane, which allows for different strength values in triaxial compression and extension. The MSDP_u criterion is expressed as:

$$\sqrt{J_2} = b \sqrt{\frac{\alpha^2 (I_1^2 - 2 a_1 I_1) + a_2^2}{b^2 + (1 - b^2) \sin^2(45^\circ - 1.5 \theta)}} \quad (4a)$$

$$\alpha = \frac{2 \sin \phi}{\sqrt{3} (3 - \sin \phi)} \quad (4b)$$

$$a_1 = \frac{1}{2} (C_o - T_o) - \frac{C_o^2 - (\frac{T_o}{b})^2}{6 \alpha^2 (C_o + T_o)} \quad (4c)$$

$$a_2 = \sqrt{\left[\frac{C_o + \frac{T_o}{b^2}}{3(C_o + T_o)} - \alpha^2 \right] C_o T_o} \quad (4d)$$

where C_o and T_o are the uniaxial compression and tension strengths, respectively; ϕ is the internal friction angle of the rock, θ is the Lode angle and b is a parameter that defines the shape of the criterion in the π -plane (usually, $b \cong 0.75$).

3 Formulation

The original criterion, i.e. Eq. (1), describes a right-circular cone in the stress space when $\lambda > 0$, or a right circular cylinder when $\lambda = 0$; hence the intersection with the π -plane is a circle (Fig. 1).

The parameters λ and κ can be determined from triaxial tests by plotting the results in the I'_1 and $\sqrt{J_2}$ space. Alternatively, the parameters can be obtained from standard compression triaxial tests and can be expressed in terms of internal friction angle and cohesion intercept (Colmenares and Zoback 2001, 2002; Yi et al. 2005, 2006):

$$\lambda = \frac{2 \sin \phi}{\sqrt{3} (3 - \sin \phi)} \quad (5a)$$

$$\kappa = \frac{6 c \cos \phi}{\sqrt{3} (3 - \sin \phi)} \quad (5b)$$

where c and ϕ are the cohesion intercept and internal friction angle of the rock, respectively. The Drucker–Prager failure cone is circumscribed to the Mohr–Coulomb hexagonal pyramid. There is also the option of obtaining the values of λ and κ that match results from triaxial extension tests. The failure cone passes through the interior vertices of the pyramid, resulting in the middle cone shown in Fig. 1. As a result, and considering only triaxial loading conditions, the circumscribed cone overestimates strength when the stress field evolves from triaxial compression ($\sigma'_1 > \sigma'_2 = \sigma'_3$) to triaxial extension ($\sigma'_1 = \sigma'_2 > \sigma'_3$), and the middle cone underestimates strength, with increasing errors, as the stress state moves from triaxial extension to triaxial compression.

For plane strain, assuming that the dilation angle of the rock is equal to the internal friction angle, i.e. an associated flow rule (inscribed cone in Fig. 1):

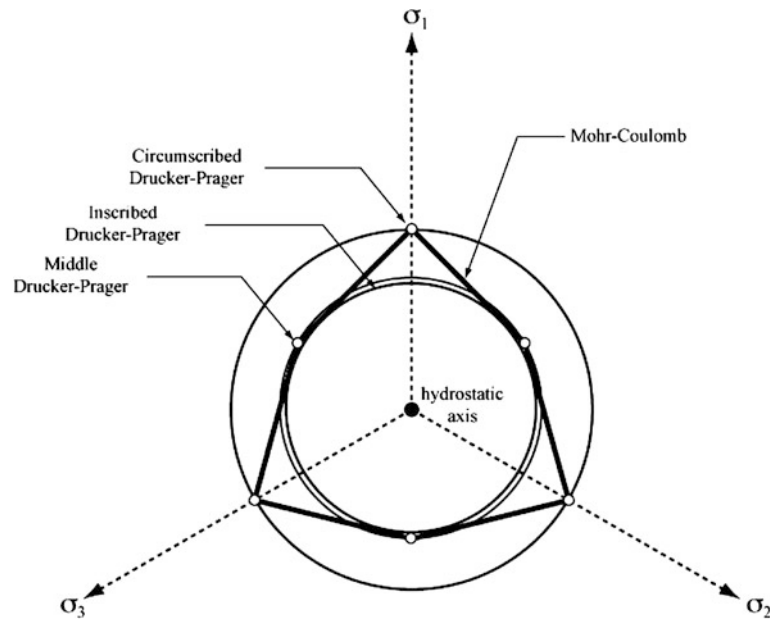
$$\lambda = \frac{\tan \phi}{\sqrt{9 + 12 \tan^2 \phi}} \quad (6a)$$

$$\kappa = \frac{3 c}{\sqrt{9 + 12 \tan^2 \phi}}. \quad (6b)$$

4 Experimental Data

The difficulties of the Drucker–Prager criterion in predicting polyaxial strength data of intact rock have been documented in the technical literature. It was perhaps Mogi (1967) who first recognized the inability of the criterion to match experimental observations when plotted in the $\tau_{\text{oct}}-\sigma_{\text{oct}}$ space, as the data showed different results in triaxial compression than in triaxial extension. Later, Vermeer and De Borst (1984) indicated that the Drucker–Prager approximation was useful for stiff clays with low friction angles but not for sand, rock or concrete. Comparisons between

Fig. 1 Drucker–Prager and Mohr–Coulomb failure criteria in stress space



laboratory results and predictions from the criterion have consistently shown that Drucker–Prager criterion tends to overestimate the strength of rock. This was the conclusion reached by Colmenares and Zoback (2002) when they compared the suitability of the criterion with the strength of the following five rocks, obtained from laboratory results reported by others: KTB amphibolite (laboratory results obtained from Chang and Haimson 2000), Dunham dolomite (Mogi 1971), Solnhofen limestone (Mogi 1971), Shirahama sandstone (Takahashi and Koide 1989) and Yuubari shale (Takahashi and Koide 1989). Colmenares and Zoback (2002) observed that Drucker–Prager yielded errors larger than other criteria including Mohr–Coulomb, Hoek–Brown, Modified Lade, Modified Wiebols and Cook, Mogi (1967) and (1971). Similar conclusions were reached by Al-Ajmi and Zimmerman (2005, 2006) who added to the Colmenares and Zoback (2002) rock database laboratory results from Mizuho trachyte (Mogi 1971), coarse-grained dense marble (Michelis 1985, 1987) and Westerly granite (Haimson and Chang 2000).

The shortcomings of the Drucker–Prager failure criterion in reproducing polyaxial laboratory experiments are illustrated in Fig. 2, which is a plot of laboratory strength tests on Dunham dolomite (Mogi 1971).

Figure 2a shows the strength of the rock in π -stress plane for tests where I'_1 ranges between 800 and 1,000 MPa, together with the corresponding failure envelopes of Mohr–Coulomb and Drucker–Prager inscribed and circumscribed. The Mohr–Coulomb and Drucker–Prager parameters are obtained from triaxial compression tests results, i.e. $\sigma'_1 > \sigma'_2 = \sigma'_3$. As expected, the figure shows a good match between results and predictions of Mohr–Coulomb

and Drucker–Prager around the triaxial compression stresses. The errors, however, increase as the differences between σ'_2 and σ'_3 increase. These errors are highlighted in Fig. 2b, which is a plot of two sets of results, each at a different confining stress, $\sigma'_3 = 25$ and 105 MPa, and for different intermediate principal stresses, σ'_2 .

In Fig. 2b, Mohr–Coulomb plots as a horizontal line for each value of the minor principal stress σ'_3 , as the criterion does not depend on the intermediate principal stress. The predictions match results for the triaxial compression tests results, i.e. for $\sigma'_2 = \sigma'_3$, but the errors increase as σ'_2 increases. A similar trend is observed for the predictions from Drucker–Prager, but with a much larger increase of the errors as the intermediate principal stress σ'_2 increases. This is because in Drucker–Prager the contribution of σ'_2 to strength is the same as that of σ'_3 , while in Mohr–Coulomb there is no contribution. The final result is that Mohr–Coulomb underestimates the strength of the rock with increasing intermediate principal stress and Drucker–Prager overestimates it.

Statistical and theoretical considerations also show that the Drucker–Prager criterion provides inaccurate predictions of rock strength and tends to overestimate the magnitude of σ'_1 at failure. Pariseau (2007) proposed the use of the Euclidean or distance norm, defined as the square root of the sum of the squares of the differences between estimated and maximum shear stress at failure, to evaluate different criteria, including Drucker–Prager. Laboratory data from a sandstone (results obtained from Pariseau 2007), norite (Pariseau 2007), Indiana limestone (Schwartz 1964) and Dunham dolomite (Mogi 1971) were used for the comparisons. The Drucker–Prager criterion resulted in the

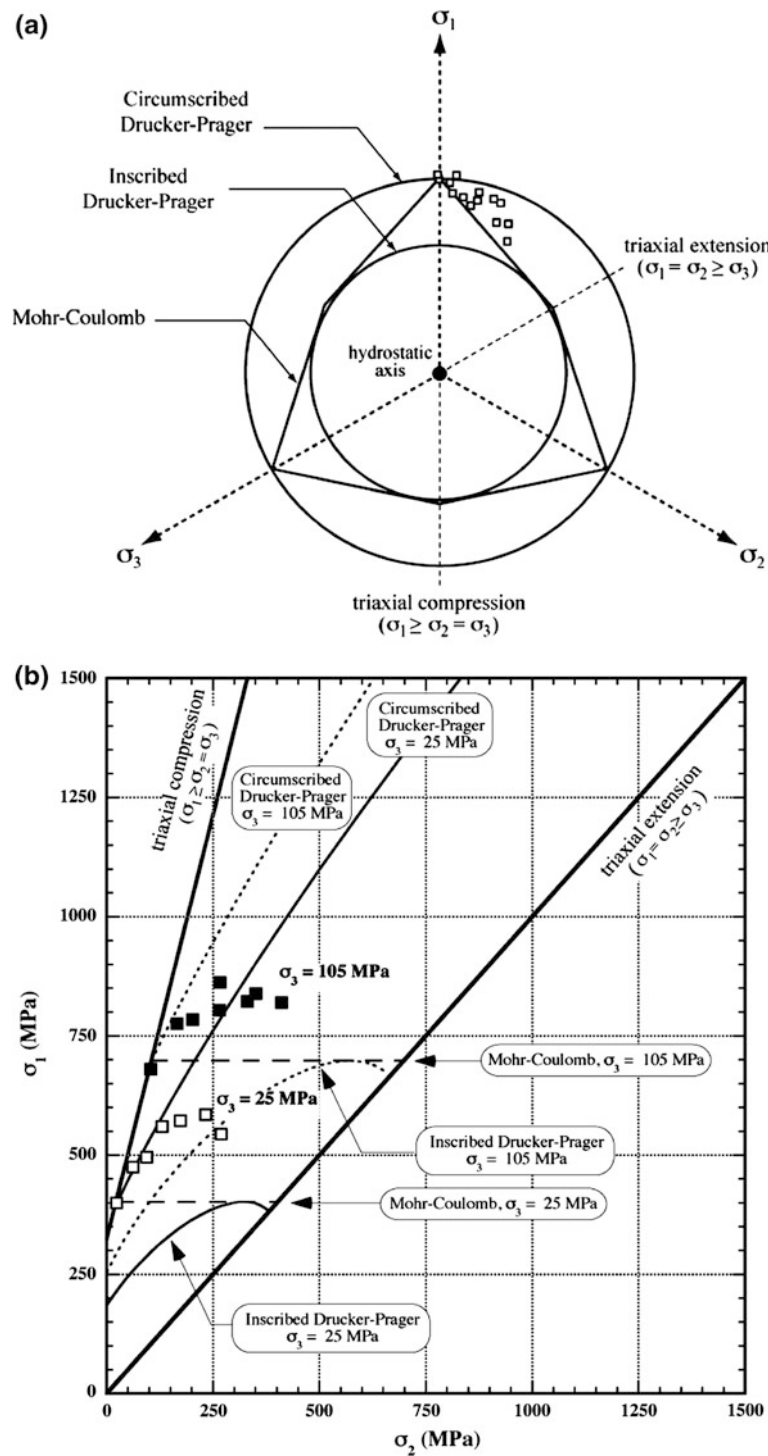


Fig. 2 Polyaxial compression tests results of Dunham dolomite (Mogi 1971). **a** π -Plane and **b** predictions from Mohr–Coulomb and Drucker–Prager failure criteria

worst predictions, revealing increasing errors with increasing confining pressure. Theoretical considerations by Ewy (1999) and Priest (2010) highlighted the disproportionate

sensitivity of the criterion on the intermediate principal stress σ_2 , resulting in an overestimation of the rock strength.

5 Advantages and Limitations

The advantages of the Drucker–Prager criterion are its simplicity and its smooth and, with the exception of some of the modified criteria, symmetric failure surface in the stress-space, which facilitate its implementation into numerical codes (Cividini 1993). The criterion gives as much weight to σ'_2 as it does to σ'_1 and σ'_3 . While it is certain that σ'_2 has a strengthening effect, it is not as profound as that predicted by Drucker–Prager. The main limitation of the criterion is that it tends to overestimate rock strength for general stress states (Ewy 1999) and produces significant errors in triaxial extension, i.e. $\sigma'_1 = \sigma'_2 > \sigma'_3$. In addition, while the parameters of the criterion can be chosen to match the uniaxial tensile strength of the rock through Eqs. (4), (5) or (6), the criterion does not produce accurate predictions when one or more principal stresses are tensile.

6 Recommendation

Comparisons between laboratory results and predictions from the Drucker–Prager failure criterion consistently show that the criterion tends to overestimate the strength of intact rock. This is because the strengthening effect of σ'_2 is the same as that of σ'_3 in the criterion, which is not supported by laboratory observations. Because the criterion parameters are typically obtained from triaxial tests results, where the intermediate and the minor principal stresses are identical, i.e. $\sigma'_2 = \sigma'_3$, the errors between predictions and results rapidly increase as the values of σ'_2 differ from σ'_3 . The Drucker–Prager failure criterion is easy to use and implement in numerical models, but due to the potentially large errors that can occur in estimating intact rock strength, its use should be limited to a narrow range of stresses in the vicinity of the intermediate and minor principal stresses from which the parameters of the criterion are obtained.

References

- Addis MA, Wu B (1993) The role of the intermediate principal stress in wellbore stability studies: evidence from hollow cylinder tests. *Int J Rock Mech Min Sci Geomech Abstr* 30(7):1027–1030
- Al-Ajmi AM, Zimmerman RW (2005) Relation between the Mogi and the Coulomb failure criteria. *Int J Rock Mech Min Sci* 42(3):431–439
- Al-Ajmi AM, Zimmerman RW (2006) Stability analysis of vertical boreholes using the Mogi–Coulomb failure criterion. *Int J Rock Mech Min Sci* 43(8):1200–1211
- Aubertin M, Simon R (1996) A multiaxial failure criterion that combines two quadratic surfaces. In: Aubertin M, Hassani F, Mitri H (eds) *Rock mechanics—tools and techniques*. Proceedings of second North American rock mechanical symposium, Montreal. A.A. Balkema, Rotterdam, pp 1729–1736
- Aubertin M, Li L, Simon R, Khalfi S (1999) Formulation and application of a short-term strength criterion for isotropic rocks. *Can Geotech J* 36(5):947–960
- Chang C, Haimson B (2000) True triaxial strength and deformability of the German Continental Deep Drilling Program (KTB) deep hole amphibolite. *J Geophys Res* 105(B8):18999–19013
- Cividini A (1993) Constitutive behaviour and numerical modelling. In: Hudson J (ed) *Comprehensive rock engineering*, vol 1. Pergamon Press, Oxford, pp 395–426
- Colmenares LB, Zoback MD (2001) Statistical evaluation of six rock failure criteria constrained by polyaxial test data. In: Elsworth D, Tinucci JP, Heasley KA (eds) *Rock mechanics in the national interest*. Proceedings of 38th US rock mechanics symposium, Washington DC. A.A. Balkema, Lisse, pp 1251–1258
- Colmenares LB, Zoback MD (2002) A statistical evaluation of intact rock failure criteria constrained by polyaxial test data for five different rocks. *Int J Rock Mech Min Sci* 39(6):695–729
- Drucker DC, Prager W (1952) Soil mechanics and plastic analysis or limit design. *Q Appl Math* 10:157–165
- Ewy RT (1999) Wellbore-stability predictions by use of a modified Lade criterion. *SPE Drill Compl* 14(2):85–91
- Hadjigeorgiou J, Ghanmi A, Paraszczak J (1998) 3-D numerical modelling of radial-axial rock splitting. *Geotech Geol Eng* 16(1):45–57
- Haimson B, Chang C (2000) A new true triaxial cell for testing mechanical properties of rock, and its use to determine rock strength and deformability of Westerly granite. *Int J Rock Mech Min Sci* 37(1–2):285–296
- Li L, Gamache M, Aubertin M (2000) Parameter determination for nonlinear stress criteria using simple regression model. *Can Geotech J* 37(6):1332–1347
- Lubarda VA, Mastilovic S, Knap J (1996) Brittle–ductile transition in porous rocks by cap model. *J Eng Mech* 122(7):633–642
- Michelis P (1985) Polyaxial yielding of granular rock. *J Eng Mech* 111(8):1049–1066
- Michelis P (1987) True triaxial cyclic behavior of concrete and rock in compression. *Int J Plas* 3(2):249–270
- Mogi K (1967) Effect of the intermediate principal stress on rock failure. *J Geophys Res* 72(20):5117–5131
- Mogi K (1971) Fracture and flow of rocks under high triaxial compression. *J Geophys Res* 76(5):1255–1269
- Nadai A (1950) *Theory of flow and fracture of solids*, vol 1. McGraw-Hill, New York
- Pariseau WG (1972) Plasticity theory for anisotropic rocks and soils. In: Grey KE (ed) *Basic and applied rock mechanics*. Proceedings of the tenth US rock mechanics symposium, NY SME/AIME, pp 267–295
- Pariseau WG (2007) Fitting failure criteria to laboratory strength tests. *Int J Rock Mech Min Sci* 44(4):637–646
- Priest SD (2005) Determination of shear strength and three-dimensional yield strength for the Hoek–Brown criterion. *Rock Mech Rock Eng* 38(4):299–327
- Priest SD (2010) Comparisons between selected three-dimensional yield criteria applied to rock. *Rock Mech Rock Eng* 43(4):379–389
- Schwartz AE (1964) Failure of rock in the triaxial shear test. In: Spokes EM, Christiansen CR (eds) *Proceedings of sixth US symposium on rock mechanics*. University of Missouri, Rolla, pp 109–151
- Takahashi M, Koide H (1989) Effect of the intermediate principal stress on strength and deformation behavior of sedimentary rocks at the depth shallower than 2000 m. In: Maury V, Fourmaintraux D (eds) *Rock at great depth*, vol I. A.A. Balkema, Rotterdam, pp 19–26
- Vermeer PA, De Borst R (1984) Non associated plasticity for soils, concrete and rock. *Heron* 29:3–64

- Yi X, Valkó PP, Russell JE (2005) Effect of rock strength criterion on the predicted onset of sand production. *Int J Geomech* 5(1):66–73
- Yi X, Ong S, Russell JE (2006) Quantifying the effect of rock strength criteria on minimum drilling mud weight prediction using polyaxial rock strength test data. *Int J Geomech* 6(4):260–268
- Yu M-H (2002) Advances in strength theories for materials under complex stress state in the 20th century. *App Mech Rev* 55(3):169–218

Lade and Modified Lade 3D Rock Strength Criteria

Sergio A. B. da Fontoura

List of Symbols

a, m, η_1	Parameters of original Lade formulation
c	Cohesion
C_0	Uniaxial compressive strength
I'_1	First invariant of the effective stress tensor
I'_3	Third invariant of the effective stress tensor
I''_1	Modified first invariant of effective stresses tensor in modified Lade
I''_3	Modified third invariant of effective stresses tensor in modified Lade
p_a	Atmospheric pressure
P_p	Pore fluid pressure
S_a, η	Parameters of modified Lade formulation
T_0	Uniaxial tensile strength
α	Biot's parameter
ϕ	Angle of internal friction
σ'_1	Major principal effective stress
σ'_2	Intermediate principal effective stress
σ'_3	Minor principal effective stress

1 Description

This part describes the failure criterion known as Lade criterion (LC) and its variation, the so-called modified Lade criterion (MLC) as proposed by Ewy (1999). The two failure criteria are described first, including the material parameters involved. Next is shown how to determine these parameters from laboratory experiments conducted on rock samples. Then follows a section on the validation of each criterion. In the same section, there is a discussion on how to evaluate the stresses at failure knowing the material parameters. Advantages and disadvantages of these two criteria are highlighted at the end of this report, followed by suggestions of when these two failure criteria should be applied for evaluating rock strength.

2 Background

The strength of isotropic rocks is a function of the three principal effective stresses acting upon the material and may be represented by a surface in the principal stress space, as described by Eq. (1), and the indexes 1, 2 and 3 refer to the principal directions of the stress field. For porous, saturated rocks, the effective stresses follow the definition by Terzaghi and later modified by Biot, Eq. (2), where α is the so-called Biot's parameter, and P_p is the pore fluid pressure, and σ is the total stress.

$$f(\sigma'_1, \sigma'_2, \sigma'_3) = 0 \quad (1)$$

$$\sigma' = \sigma - \alpha \cdot P_p \quad (2)$$

Figure 1 shows the results of stresses at failure obtained from different tests and plotted on the octahedral plane characterized by a given value of the first stress invariant, I_1 . The curve displayed and adjusted to the test results

Originally published as an article in the journal *Rock Mechanics and Rock Engineering*, 45, S. A. B. da Fontoura, Lade and Modified Lade 3D Rock Strength Criteria, 1001–1006, 2012.

S. A. B. da Fontoura (✉)
Department of Civil Engineering, Pontifical Catholic University
of Rio de Janeiro, Rio de Janeiro, Brazil
e-mail: fontoura@puc-rio.br

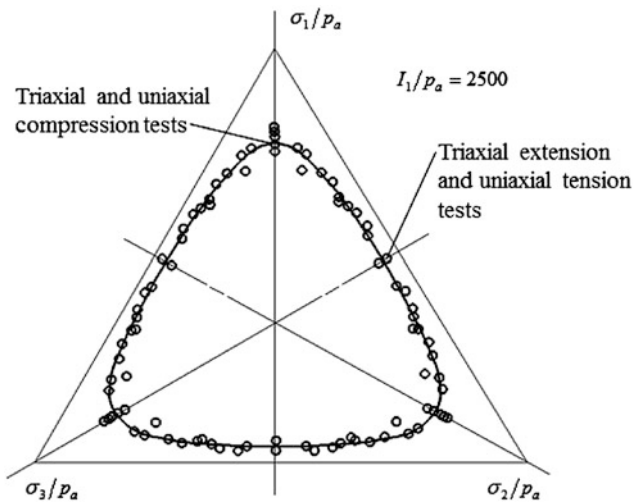


Fig. 1 Results of triaxial, biaxial and cubical triaxial compression tests on sandstone by Akai and Mori (1970) displayed on a given octahedral plane (Lade 1993)

represents the intersection between the failure surface and the octahedral plane.

It is common practice in geotechnical engineering to use a particular form of Eq. (1) such as Mohr–Coulomb and Hoek–Brown failure criteria, that do not recognize the importance of the intermediate principal effective stress, σ'_2 , on the ultimate rock failure load. However, small-scale laboratory experiments have proven that rock strength depends on all three principal stresses and several failure criteria have been developed to describe such a dependency. Lade (1993) presents a review of several 3D failure criteria for evaluating strength of materials, in particular of soils and rocks, and concludes that none of these criteria represent, with reasonable accuracy, the 3D nature of rock failure.

Lade’s failure criterion was initially developed for soils which present very low to no cohesion, Lade (1977), and later on modified to include materials such as concrete and rocks (Lade 1982; Kim and Lade 1984). Differently from other 3D failure criteria that relate the first stress invariant with the second deviatoric stress invariant, Lade’s failure criterion uses a special relationship between the first and the third stress invariants. Ewy (1999) proposed a failure criterion based upon Lade’s criterion, and named modified Lade criterion, which is forced to coincide with the Mohr–Coulomb failure criterion under the conditions of triaxial compression test, i.e., $\sigma_1 > \sigma_2 = \sigma_3$. Ewy’s motivation was to develop a simple methodology to take into account the effect of the intermediate principal stress on wellbore stability calculations.

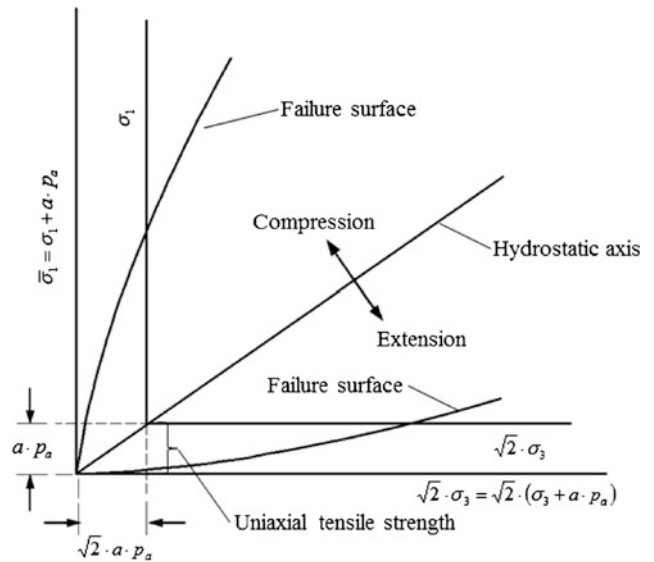


Fig. 2 Translation of principal stress space along hydrostatic axis to include effect of tensile strength in failure criterion (Lade 1993)

3 Formulation, Parameters and Validation

3.1 Original Lade Criterion

3.1.1 Formulation

The original form of Lade’s criterion for rocks is expressed as:

$$\left(\frac{I_1^3}{I_3} - 27\right) \left(\frac{I_1}{p_a}\right)^m = \eta_1 \quad (3)$$

In Eq. (3), I_1' and I_3' are, respectively, the first and the third invariants of the effective stress tensor at failure, modified by a translation of axes of ap_a in the space of principal stresses along its hydrostatic axis in order to accommodate tensile strength, see Fig. 2, as discussed by Kim and Lade (1984). Equations (4) and (5) describe the stress invariants and the stresses are defined in Eq. (6). In these equations, p_a is the atmospheric pressure in the same unit system as the stresses. For instance, if the stresses are expressed in MPa, p_a is 10^{-1} MPa.

$$I_1' = \bar{\sigma}_1 + \bar{\sigma}_2 + \bar{\sigma}_3 \quad (4)$$

$$I_3' = \bar{\sigma}_1 \cdot \bar{\sigma}_2 \cdot \bar{\sigma}_3 \quad (5)$$

$$\bar{\sigma}_1 = \sigma'_1 + ap_a; \quad \bar{\sigma}_2 = \sigma'_2 + ap_a; \quad \bar{\sigma}_3 = \sigma'_3 + ap_a \quad (6)$$

For intact rocks there are three parameters to be determined in order to describe the 3D nature of the failure criterion: a , m and η_1 . The evaluation of these parameters is explained next. As should be expected, these three parameters, a , m and η_1 , influence the shape and location of the failure surface as discussed by Kim and Lade (1984).

3.1.2 Evaluating Rock Parameters from Experiments

Lade failure criterion describes failure of rocks subjected to three different effective principal stresses, even though the most common test is the so-called compression, axisymmetric triaxial test, where $\sigma'_1 > \sigma'_2 = \sigma'_3$. True triaxial tests are less common ($\sigma'_1 > \sigma'_2 > \sigma'_3$) but can also be interpreted through this failure criterion.

Parameter a The value of a can be estimated by considering that ap_a is equal or very close to the tensile strength of the rock, T_0 . If the tensile strength is not determined directly or indirectly through the Brazilian tensile test, the empirical formulation, proposed by Lade (1993), Eq. (7), can be used, where C_0 is the unconfined compressive strength and T and t are material parameters. Lade (1993) suggests values of T and t as a function of rock type based on a large set of tests. Average values for T and t , are, respectively, -0.219 and 0.825 .

$$T_0 = Tp_a \left(\frac{C_0}{p_a} \right)^t \tag{7}$$

Parameters m and η_1 Using the value of a determined as explained above, each data point corresponding to failure, and obtained experimentally, can generate a pair of values of A and B , Eqs. (8) and (9). These two numbers, plotted in a log–log diagram, generate a theoretical linear relationship, Eq. (10), and the parameters m and η_1 can be obtained by linear regression.

$$A = \left(\frac{I_1^3}{I_3} \right) - 27 \tag{8}$$

$$B = \left(\frac{p_a}{I_1} \right) \tag{9}$$

In a log–log space, Eq. (3) may be expressed as Eq. (10).

$$\log A = m \log B + \log \eta_1 \tag{10}$$

The parameters m and η_1 can be obtained by least-square fitting Eq. (10) through the experimental data. Figure 3 indicates a typical example.

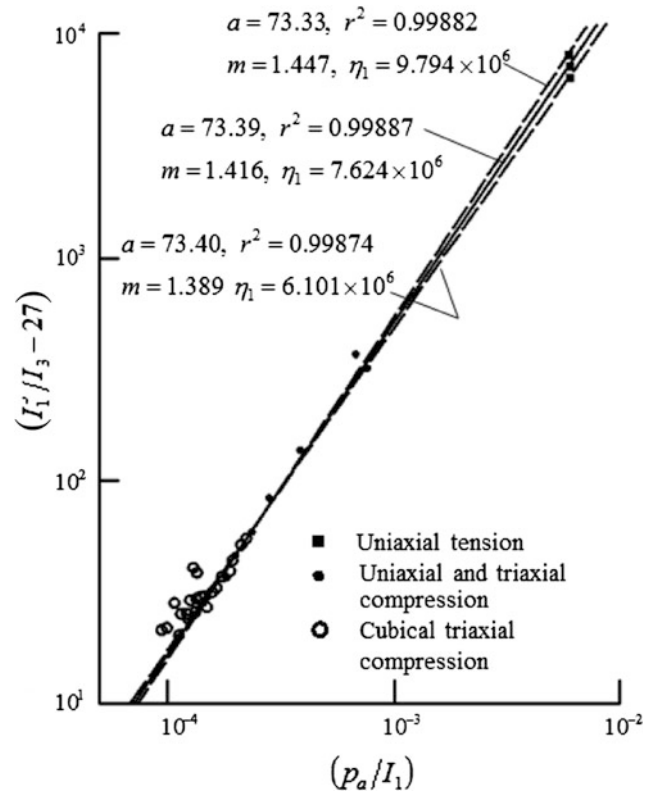
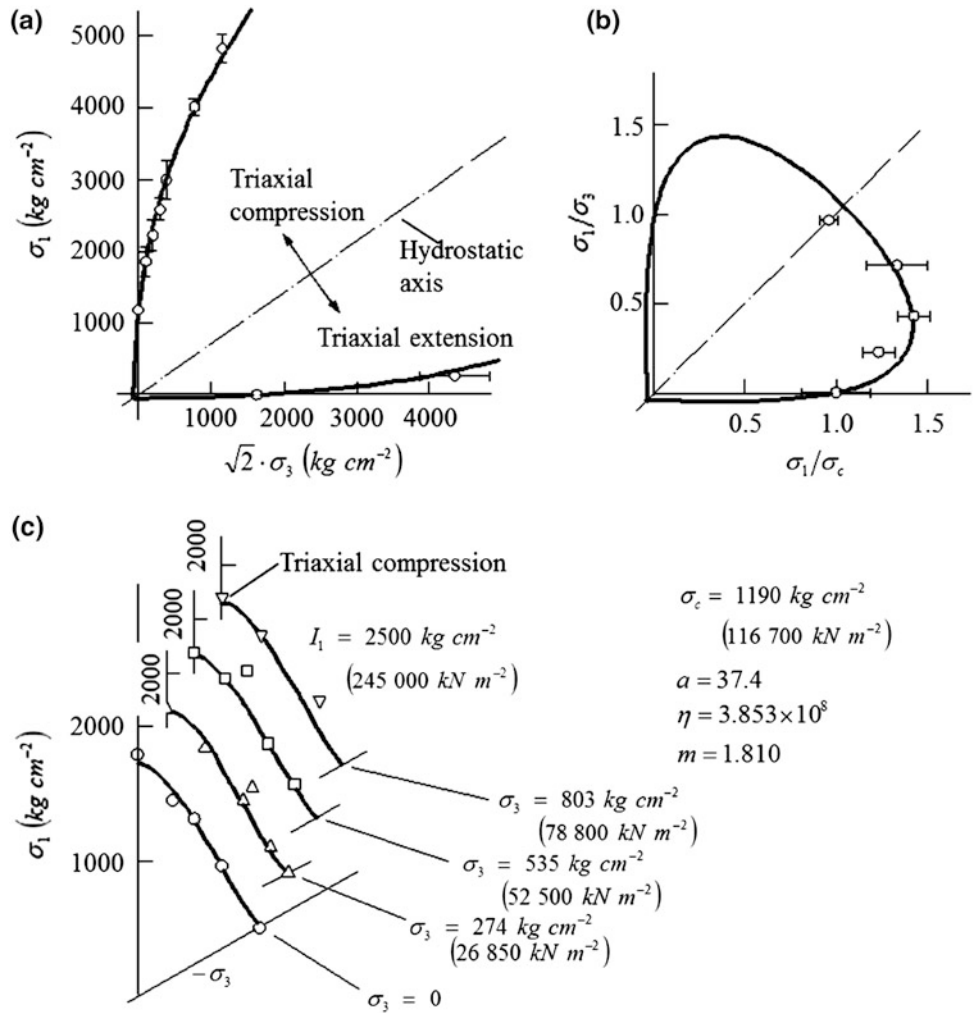


Fig. 3 Determination of material parameters involved in the failure criterion for Mizuho Trachyte tested by Mogi (1971) and (Lade 1993)

3.1.3 Validation of the Lade Failure Criterion: Applications

Lade (1993) describes the interpretation of about 90 data sets obtained from the literature and covering different types of igneous, metamorphic and sedimentary rocks. Different types of tests were used to obtain the data including the simple ones such as unconfined compression test, uniaxial tension test, triaxial compression test and the less common ones such as triaxial extension test, biaxial compression test, cubical triaxial test, and torsion shear test on hollow cylinder with axial loading. Two types of tests were considered to be unreliable for the purpose of obtaining data set for interpretation: internal and external pressure on hollow cylinders combined with axial loading and torsional tests on solid samples. The validation of the failure criterion proposed was acceptable and, as it should be expected, the range of values of the parameters was very wide. Only in few cases the regression coefficient was low in the range of 0.1–0.40 mainly in coals, suggesting that anisotropy may play a role in the application and validation of the failure criterion.

Fig. 4 Comparison of failure criterion with results of tests on sandstone performed by Akai and Mori (1970) in **a** triaxial plane, **b** biaxial plane and **c** octahedral plane (Lade 1993)



3.1.4 Evaluating Stresses at Failure

An important issue is the evaluation of the stress at failure knowing the material parameters and two principal stresses at failure. This is the operation to be carried out when plotting the failure surface knowing the material parameters, i.e., for each pair of values of two principal stresses, the third one must be determined (Fig. 4). Equation (3) must be solved but it does not end up being a simple matter since the final equation is of the transcendental type and must be solved numerically or graphically.

is the translation of axis. The term S_a proposed by Ewy (1999) is related to both the cohesion and friction angle as defined by the Mohr–Coulomb failure criterion.

$$\left(\frac{I_1''}{I_3''}\right)^3 = 27 + \eta \tag{11}$$

$$I_1'' = (\sigma_1 + S_a - P_p) + (\sigma_2 + S_a - P_p) + (\sigma_3 + S_a - P_p) \tag{12a}$$

$$I_3'' = (\sigma_1 + S_a - P_p)(\sigma_2 + S_a - P_p)(\sigma_3 + S_a - P_p) \tag{12b}$$

3.2 Modified Lade Criterion

3.2.1 Formulation

Ewy (1999) presented a simplified version of the Lade criterion that can be expressed by Eq. (11). Comparing Eqs. (11) with (3) one can observe both the similarity and the difference: the non-linear dependence upon I_1 to the power m was removed which is equivalent to make m equal to zero. Another important difference between the two criteria

3.2.2 Material Parameters

As presented in Eqs. (11) and (12a), (12b), the MLC requires two parameters to describe the rock strength: S_a and η . The parameter S_a , that represents the axis translation, is made equal to $c/\tan\phi$, (c is the cohesion and ϕ is the friction angle in the Mohr–Coulomb failure criterion), which is equivalent to translate the τ axis, in the σ – τ space,

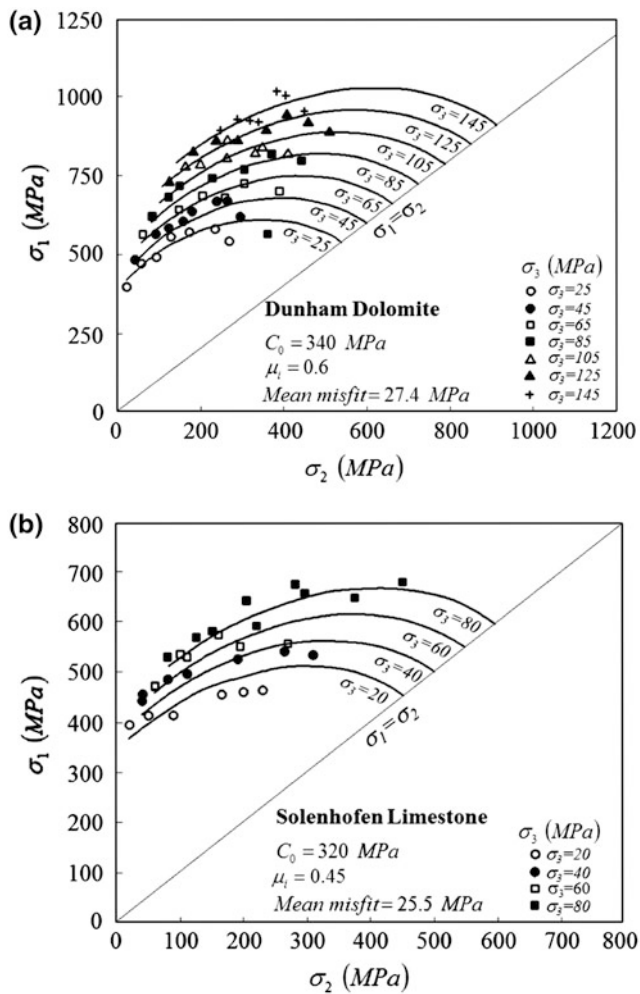


Fig. 5 Fitting modified Lade criterion through polyaxial test carried out on **a** Dunham dolomite and **b** Solnhofen limestone (Colmenares and Zoback 2002)

in order to make a cohesive material appear like a cohesionless one. In order to obtain the material parameter η , as described by Eq. (14), the MLC is forced to coincide with the Mohr–Coulomb failure criterion when the stress state coincides with the triaxial compression test ($\sigma_1 > \sigma_2 = \sigma_3$), and that means that the MLC is linear in the space $\sigma_3 - \sigma_1$ (or $\sqrt{2} \sigma_2 - \sigma_1$ or $p - q$).

$$S_a = \frac{c}{\tan \phi} \quad (13)$$

$$\eta = 4 \cdot (\tan \phi)^2 \left\{ \frac{9 - 7 \sin \phi}{1 - \sin \phi} \right\}. \quad (14)$$

3.2.3 Validation of MLC: Applications

Ewy (1999) presents some numerical experiments generating strength envelopes using the MLC for a given set of

c and ϕ and demonstrates that the results are similar, in trend, to experimental results of polyaxial tests described in the literature. Several investigators have tested the MLC in their experiments and concluded that the criterion represented well the test results. Colmenares and Zoback (2002) investigated the application of MLC to five different types of rocks, all of high strength and of very brittle nature (Dunham dolomite: $C_0 = 450$ MPa and $\phi = 33^\circ$, Shiva-hama sandstone: $C_0 = 95$ MPa and $\phi = 38.6^\circ$, Yuubari shale: $C_0 = 120$ MPa and $\phi = 26.5^\circ$, Solnhofen limestone: $C_0 = 375$ MPa and $\phi = 28.8^\circ$, KTB amphibolite: $C_0 = 300$ MPa and $\phi = 50.1^\circ$). Figure 5 displays the use of MLC to the experimental data from Dunham dolomite and Solnhofen limestone suggesting a very good fit when minimizing the mean standard deviation misfit to the test results.

3.2.4 Evaluating Stresses at Failure

An important issue is the evaluation of the stress at failure knowing the material parameters and two principal stresses at failure. This is the operation to be carried out when plotting the failure surface knowing the material parameters. For each pair of values of principal stresses, the third one must be determined. Equation (11) is to be solved and that leads to a 3rd degree equation in the unknown stress that has to be obtained numerically and the appropriate solution, of the three possible ones, selected.

4 Advantages and Disadvantages

The 3D strength criteria, LC and MLC, proposed do not generate sharp corners in the failure surface allowing the continuity of the first derivative with respect to the stresses. The LC requires the determination of three parameters but imposes no restrictions to the experimental data neither assumes any special shape of the strength envelope. There are indications that the criterion suits well a very large range of rocks tested under different stress conditions as presented by Lade (1993). Very important, the parameters can be determined using data set obtained from very simple unconfined compression tests and triaxial compression tests. An important limitation of LC is that the parameters associated with this criterion do not have a clear relationship with the most commonly used c and ϕ from the Mohr–Coulomb failure criterion. This somehow limits the application of Lade’s criterion in practice.

The MLC was devised with the possibility of application in mind and therefore has components that make the method attractive. The parameters can be determined as a function of the well known c and ϕ from the Mohr–Coulomb failure which increases its attractiveness for applications in the oil industry since there are hardly any samples available for

experiments and the shear strength parameters are obtained through correlations with well logs. Implicit in the MLC is the linear nature of the shear strength envelope when interpreting the results of compression triaxial test. This implies that the MLC cannot handle experimental data from rocks that behave in a non-linear manner, which is the case of high pressure, high temperature applications. The LC does not offer this restriction.

5 Recommendations

The use of both criteria is restricted to cases where the intact rock behavior is representative of the problem. The wellbore behavior problem in the oil industry is a natural candidate for the application of both LC and MLC. Ewy (1999) and Yi et al. (2006) have reported the application of MLC to investigate the effect of the intermediate stress in the wellbore stability and Yi et al. (2005) have also used the MLC to study the onset of sand production around producing wells.

References

- Akai K, Mori H (1970) Ein versuch uber Bruchmechanismus von Sandstein unter mehrachsigen Spannungszustand. In: ISRM Proc. 2nd Int Congress Rock Mech. ISRM, Belgrad, vol 2, Paper 3–30
- Colmenares LB, Zoback MD (2002) A statistical evaluation of intact failure criteria constrained by polyaxial test data for five different rocks. *Int J Rock Mech Min Sci Geom Abstr* 29:695–729
- Ewy RT (1999) Wellbore stability prediction by use of a modified Lade criterion. *SPE Drill Complet* 14:85–91
- Kim MK, Lade PV (1984) Modeling rock strength in three dimensions. *Int J Rock Mech Min Sci Geom Abstr* 21:21–33
- Lade PV (1977) Elasto-plastic stress–strain theory for cohesionless soils with curved yield surfaces. *Int J Solids Struct* 13:1019–1035
- Lade PV (1982) Three-parameter failure criterion for concrete. *J Eng Mech DivAm Soc Civ Eng* 108:850–863
- Lade PV (1993) Rock strength criteria: the theories and the evidence. In: Hudson J, Brown ET (eds) *Comprehensive rock engineering*. Elsevier Inc, London, pp 225–284
- Mogi K (1971) Fracture and flow of rocks under high triaxial compression. *J Geophys Res* 76:1255–1269
- Yi X, Valkó PP, Russell JE (2005) Effect of rock strength criterion on the predicted onset of sand production. *Int J Geomech ASCE* 5(1):66–73
- Yi X, Ong S, Russell JE (2006) Quantifying the effect of rock strength criteria on minimum drilling mud weight prediction using polyaxial rock strength test data. *Int J Geomech ASCE* 6(4):260–268

A Failure Criterion for Rocks Based on True Triaxial Testing

Chandong Chang and Bezalel Haimson

List of Symbols

σ_1, σ_2 and σ_3	Major, intermediate, and minor effective principal stresses, respectively
τ_{oct}	Octahedral shear stress
σ_{oct}	Octahedral effective normal stress
$\sigma_{\text{m},2}$	Mean effective normal stress acting on the failure plane
c	Cohesion
ϕ	Angle of internal friction
A, n, a, b	Material constants

1 Description

The failure criterion based on true triaxial testing considers the effect of all three principal stresses on rock compressive strength, and is entirely based on true triaxial tests conducted on rectangular prismatic specimens subjected to three independent principal stresses. The failure criterion is commonly expressed in terms of the octahedral shear stress as a monotonically increasing function of the mean effective normal stress acting on the plane of failure. In tests

Originally published as an article in the journal *Rock Mechanics and Rock Engineering*, 45, C. Chang, B. Haimson, A Failure Criterion for Rocks Based on True Triaxial Testing, 1007–1010, 2012.

C. Chang (✉)

Department of Geology, Chungnam National University,
Daejeon, 305-764, South Korea
e-mail: cchang@cnu.ac.kr

B. Haimson

Geological Engineering Program, Department of Materials
Science and Engineering, University of Wisconsin, Madison, WI
53706, USA
e-mail: bhaimson@wisc.edu

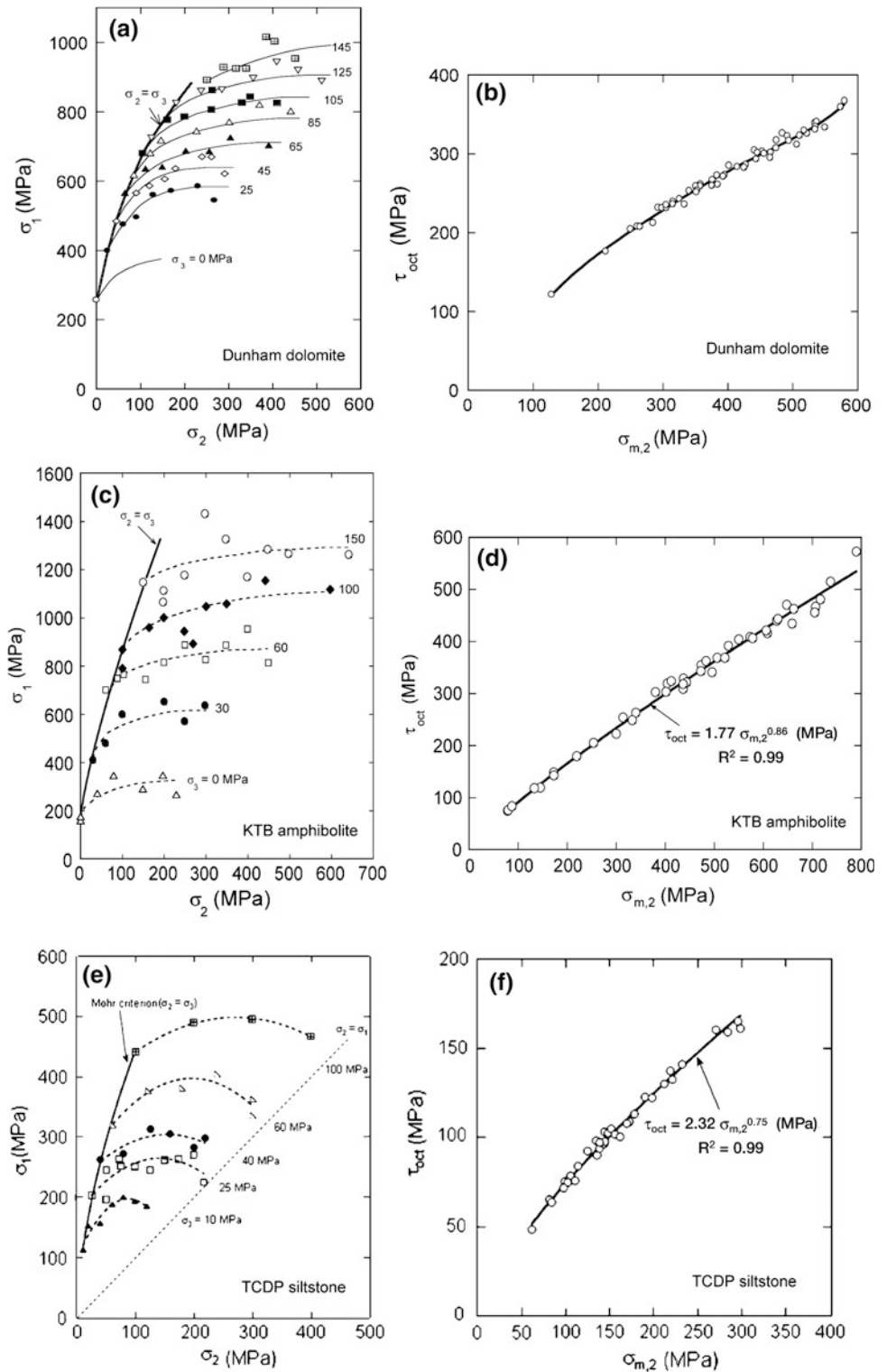
conducted thus far the function best fitting experimental data is the one obeying the power law. This criterion was first derived by Mogi (1971) and confirmed for several other rocks by Haimson and Chang (2000), Chang and Haimson (2000), Oku et al. (2007) and Lee and Haimson (2011).

2 Background

The significant observation by Murrell (1963) and Handin et al. (1967) that rock compressive strength in experiments conducted in conventional triaxial extension ($\sigma_1 = \sigma_2 > \sigma_3$) is higher than in conventional triaxial compression ($\sigma_1 > \sigma_2 = \sigma_3$), provided convincing evidence that the effect of the intermediate principal stress on rock failure cannot be ignored and should be further studied.

In a 1971 seminal paper, Mogi (1971) reported the results of tests conducted in a true triaxial testing apparatus that enabled the application of three independent and unequal orthogonal compressive loads to each pair of faces of a rectangular prismatic rock sample. His experiments demonstrated the systematic variation of rock strength as a function of σ_2 for constant σ_3 . He produced the first comprehensive set of rock true triaxial strength data for Dunham dolomite (Fig. 1a) and other rocks, which unequivocally demonstrated the strong dependence of rock strength on σ_2 for given σ_3 magnitudes. Mogi attempted to find a simple relationship that would satisfy all his true triaxial experimental results. Nadai (1950) had propounded as early as 1950 a 3D failure criterion for brittle materials by which failure occurs when the octahedral shear stress
$$\left(\tau_{\text{oct}} = \frac{1}{3} \sqrt{(\sigma_1 - \sigma_2)^2 + (\sigma_2 - \sigma_3)^2 + (\sigma_3 - \sigma_1)^2} \right)$$
 has reached a critical value in terms of the octahedral effective normal stress [$\sigma_{\text{oct}} = (\sigma_1 + \sigma_2 + \sigma_3)/3$]. Mogi, however, observed in his experiments that brittle failure in rocks occurs along a 2D inclined plane striking in the σ_2 direction,

Fig. 1 True triaxial strength for various rock types: **a** Dunham dolomite (Mogi 1971), **c** KTB amphibolite (Chang and Haimson 2000), and **e** TCDP siltstone (Oku et al. 2007), and the experiment-based true triaxial failure criteria for the respective rocks (**b**, **d**, **f**)



rather than in the entire specimen volume as implied by σ_{oct} . Thus, he adjusted the Nadai criterion (1950) by replacing σ_{oct} with $\sigma_{m,2} = (\sigma_1 + \sigma_3)/2$.

Some 25 years later, Haimson and Chang (2000) tested the strength and deformability of Westerly granite in a newly designed true triaxial cell, which was similar in principle to

Mogi's, but considerably more portable and servo-controlled. They derived an experiment-based true triaxial failure criterion for the granite which was similar to Mogi's. Following this initial series of tests, true triaxial failure criteria were obtained for rocks extracted from three scientific deep drilling projects, KTB (the ultra deep scientific hole,

Bavaria, Germany) (Chang and Haimson 2000), Taiwan Chelungpu-fault Drilling Project (TCDP) (Oku et al. 2007), and San Andreas Fault Observatory at Depth (SAFOD), USA (Lee and Haimson 2011) (Fig. 1c–f). In all these experiments, rock strength data as a function of σ_2 for a constant σ_3 follow a similar pattern to that in the Mogi's tests, and are fitted along single curves in the $\tau_{\text{oct}}-\sigma_{m,2}$ domain.

3 Formulation

The best fitting curves for all true triaxial failure criteria, τ_{oct} , obtained to date are power functions of the mean stress acting on the plane of failure, $\sigma_{m,2}$ (Mogi 1972; Haimson and Chang 2000; Chang and Haimson 2000; Oku et al. 2007; Lee and Haimson 2011):

$$\tau_{\text{oct}} = A\sigma_{m,2}^n \quad (1)$$

where A and n are material constants. Since Eq. (1) is purely empirical, there is no obvious direct correlation between the two constants and known rock mechanical properties. Based on existing true triaxial test results on various rock types (dolomite, limestone, trachyte, sandstone, siltstone, amphibolite, marble, shale, and granite), however, n is generally <1 and A is >1.5 (Al-Ajmi and Zimmerman 2005). These constraints on the two empirical constants are subject to change as more true triaxial rock strength data become available. As these empirical constants are not parameterized with any other known material properties, the true triaxial failure criterion has to be determined strictly from true triaxial experiments.

Although true triaxial strength data in various rocks are best modeled by power-law relationships between τ_{oct} and $\sigma_{m,2}$, it has been suggested that they can be approximated by linear relationships (Al-Ajmi and Zimmerman 2005):

$$\tau_{\text{oct}} = a + b\sigma_{m,2}. \quad (2)$$

The merit of linearizing the criterion is that the material parameters a and b can be linked to known rock mechanical properties. However, this assumes that these parameters are constants of the materials. By comparing the formulations of the Coulomb failure criterion and Eq. (2), the following correlation can be made:

$$a = \frac{2\sqrt{2}}{3} c \cos\phi \quad (3a)$$

$$b = \frac{2\sqrt{2}}{3} \sin\phi \quad (3b)$$

where c is cohesion and ϕ is the angle of internal friction, or alternatively,

$$a = \frac{2\sqrt{2}}{3} \frac{C_o}{q+1} \quad (4a)$$

$$b = \frac{2\sqrt{2}}{3} \frac{q-1}{q+1} \quad (4b)$$

where C_o is uniaxial compressive strength and $q = (1 + \sin\phi)/(1 - \sin\phi)$. Thus, the linearized true triaxial failure criterion allows the construction of a three-dimensional criterion that incorporates the three principal stresses through relatively simple rock mechanics experiments such as conventional triaxial compression tests.

There is, however, one major over-simplification in this approach. The dip angle of the shear fracture that develops upon failure is not constant, but varies with σ_2 for constant σ_3 under true triaxial testing, increasing by up to 20° in some rocks as the intermediate principal stresses are raised beyond the base value of $\sigma_2 = \sigma_3$ (Mogi 1971, 1972; Chang and Haimson 2000; Oku et al. 2007). Hence ϕ , which is directly related to the fracture dip angle is also not a constant of the material, contrary to the requirement of the Mohr–Coulomb criterion.

4 Advantages and Limitations

The true triaxial failure criterion is entirely based on true triaxial experiments. The criterion is obtained from strength data recorded during true triaxial tests for a wide range of σ_3 values and σ_2 varying from equal to much larger than σ_3 . All test results plotted in the form of τ_{oct} as a function of $\sigma_{m,2}$ are best fitted by a power function that defines the true triaxial failure criterion for the rock.

A practical limitation of the criterion is that it requires the use of a true triaxial testing apparatus. At this time only a few such devices are available. As the advantages of the experiment-based true triaxial failure criteria gain more recognition, it is foreseen that standardized equipment will soon become available.

A perceived shortcoming of Eq. (1) is that when applied to individual plots of σ_1 at failure as a function of σ_2 for constant σ_3 (Fig. 1a, for example), it predicts that the strength when $\sigma_2 = \sigma_1$ is the same as when $\sigma_2 = \sigma_3$, which is not in agreement with previous conventional triaxial test results, in which strength in triaxial extension was shown to be generally higher by some 10–20 % than that in triaxial compression (Murrell 1963; Handin et al. 1967). Two counter arguments are noted: (1) the failure criterion represented by Eq. (1) is strictly empirical, i.e. a best fitting curve to experimental data in the $(\tau_{\text{oct}} - \sigma_{m,2})$ domain, and

the appropriateness of its use in the $(\sigma_1 - \sigma_2)$ domain is unclear, and (2) in most realistic field conditions, σ_2 is seldom larger than about 5 times the magnitude of σ_3 , and for this condition, the criterion is clearly correct even in the $(\sigma_1 - \sigma_2)$ domain.

5 Recommendations

When selecting an appropriate failure criterion, it is important that it represents correctly the rock strength under generalized compressive stress conditions prevailing in the earth's crust. This means that a failure criterion should be based on rock strength data obtained under controlled true triaxial stress conditions. The true triaxial failure criterion is backed up by such experimental data. Thus, the use of the experiment-based true triaxial failure criterion is recommended for a variety of conditions of compressive stresses whenever comprehensive true triaxial strength data are available.

True triaxial failure criteria are particularly needed in situations where all three principal stresses are widely differential, as is the case in the vicinity of a borehole wall. The experiment-based criterion was successfully employed in two major international research projects in conjunction with in situ stress measurements using a hybrid method involving hydraulic fracturing and borehole breakouts (Vernik and Zoback 1992). The true triaxial failure criteria and the logged breakout spans were used to derive the in situ maximum principal stress in the KTB amphibolite, Germany (Haimson and Chang 2002), and in the siltstone adjacent to Chelungpu Fault in Taiwan (Haimson et al. 2010).

References

- Al-Ajmi AM, Zimmerman RW (2005) Relation between the Mogi and the Coulomb failure criteria. *Int J Rock Mech Min Sci* 42:431–439
- Chang C, Haimson BC (2000) True triaxial strength and deformability of the German Continental deep drilling program (KTB) deep hole amphibolite. *J Geophys Res* 105:18999–19013
- Haimson BC, Chang C (2000) A new true triaxial cell for testing mechanical properties of rock, and its use to determine rock strength and deformability of Westerly granite. *Int J Rock Mech Min Sci* 37:285–296
- Haimson B, Chang C (2002) True triaxial strength of the KTB amphibolite under borehole wall conditions and its use to estimate the maximum horizontal in situ stress. *J Geophys Res* 107:2257–2271
- Haimson B, Lin W, Oku H, Hung J-H, Song S-R (2010) Integrating borehole breakout dimensions, strength criteria, and leak-off test results to constrain the state of stress across the Chelungpu Fault, Taiwan. *Tectonophysics* 482:65–72
- Handin J, Heard HC, Magouirk JN (1967) Effect of the intermediate principal stress on the failure of limestone, dolomite, and glass at different temperature and strain rate. *J Geophys Res* 72:611–640
- Lee H, Haimson B (2011) True triaxial strength, deformability, and brittle failure of granodiorite from the San Andreas Fault Observatory at Depth. *Int J Rock Mech Min Sci* 48:1199–1207
- Mogi K (1971) Fracture and flow of rocks under high triaxial compression. *J Geophys Res* 76:1255–1269
- Mogi K (1972) Effect of the triaxial stress system on fracture and flow of rocks. *Phys Earth Planet In* 5:318–324
- Murrell SAF (1963) A criterion for brittle fracture of rocks and concrete under triaxial stress, and the effect of pore pressure on the criterion. In: Fairhurst C (ed) *Proceedings of the 5th Symposium on Rock Mechanics*. University of Minnesota, Minneapolis, pp 563–577
- Nadai A (1950) *Theory of flow and fracture of solids*, vol 1. McGraw-Hill, New York
- Oku H, Haimson B, Song S-R (2007) True triaxial strength and deformability of the siltstone overlying the Chelungpu fault (Chi-Chi earthquake), Taiwan. *Geophys Res Lett* 34:L09306
- Vernik L, Zoback MD (1992) Estimation of maximum horizontal principal stress magnitude from stress-induced well bore breakouts in the Cajon Pass scientific research borehole. *J Geophys Res* 97:5109–5119

Part V

**Additional Article on
Rock Characterization**

A Survey of 3D Laser Scanning Techniques for Application to Rock Mechanics and Rock Engineering

Quanhong Feng and Kennert Röshoff

1 Foreword

The work resulting in this report “A survey of 3D laser scanning techniques for application to rock mechanics” commenced in 2007 and was conducted during the 2007–2011 ISRM Presidential period. The motivation for the work was to produce a comprehensive report explaining the techniques and advantages of laser scanning for rock mechanics/rock engineering use. 3D laser techniques have been used in many engineering fields over the last twenty years and show great promise for characterising rock surfaces. Thus, it was considered that a report concentrating on a description of the laser scanning capabilities plus the actual and potential rock mechanics applications would be of great benefit to the ISRM members and the rock engineering community at large.

The project began as an ISRM–Swedish National Group project, stimulated by Professor John A Hudson (then ISRM President), with the work being undertaken by Dr. Quanhong Feng, latterly of the MultiInfo 3D Laser Scan Solution AB company but also while formerly working with Kennert Röshoff in the employment of BBK AB and ÅF-Infrastructure AB. The work was funded by BeFo, the Swedish Rock Engineering Foundation in three different stages. The first stage was in 2008 for the pre-study of both laser scanning and photogrammetry, the second stage in 2010 for the further pre-study of laser scanning, and then the third stage in 2011 for the case study and final report. Financial support for these three stages, were arranged by Mr. Mikael Hellsten, the BeFo Director of Research. BeFo’s aim is to support research which will have broad support among takers in industry, academia and society in general and that the results should be useful in practical applications. Thus, the overview of laser scanning

techniques fitted well within this BeFo objective. For the 2011 latter stage of the project, BeFo set up a reference group, comprised of the following: John A. Hudson (ISRM), Mikael Hellsten (BeFo), Ulf Håkansson (Skanska), Tommy Ellison (Besab), Anders Boberg (Tyrens), Peter Lund (Swedish Traffic authority) and Peter Hultgren (SKB).

We are pleased to report that the project has been brought to an extremely successful conclusion with the Dr. Feng’s production of the following document published in this ‘Orange Book’ of the ISRM. Readers will find that the successive main report sections (of Introduction, Current Development, Special Features, Capturing Procedure, Application Examples, and Rock Exposure Characterisation) are both comprehensive and lucid. The report does exactly what was originally intended: to alert readers to the significant potential of laser scanning capabilities and to illustrate its use with examples.

We are grateful to Dr. Feng for his commitment to the project throughout the four-year period and congratulate him on its most satisfactory outcome. We hope that readers will be as impressed by the report as we are. We are also grateful to Professor Resat Ulusay, the Editor of ISRM’s ‘Orange Book’, for graciously agreeing to include this report in its contents.

*Professor John A. Hudson, ISRM President, 2007–2011
Mr. Mikael Hellsten, Director of Research, BeFo, Sweden*

2 Introduction

2.1 Background

In rock mechanics, on-site characterisation of a rock exposure for a project is one of the important steps, which is required to collect the input data for further rock mechanics analysis, rock engineering design and numerical modelling. The quality and quantity of the on-site mapping data play an important role for the results of the following steps. However, traditional methods have some drawbacks in capturing

Q. Feng (✉)

MultiInfo 3D Laser Scan Solution AB, Stockholm, Sweden
e-mail: quanhong.feng@gmail.com

K. Röshoff

ÅF-Infrastructure AB, Stockholm, Sweden

enough data for further analysis, which then affects the results for the whole project. Therefore, efforts to improve on-site mapping data with new techniques have continued, and different techniques have been tested in order to make on-site mapping successful.

A typical set of parameters often suggested for capturing in practice include fracture orientation, spacing, trace length and aperture etc. (Hudson 1989; Priest 1993; ISRM 2007). However, in current practice, much of these data is still obtained by hand, including using compass and inclinometer for fracture mapping, measurement with a ruler, and documentation by recording information in a notebook and photographing with a camera. These so-called traditional methods are now still used in most of rock engineering projects, so the quality and quantity of the data are sometimes unable to meet the necessary requirements for rock engineering projects. The most well-known drawback in traditional methods is that too much personal work is involved in the in situ data acquisition procedure, which is time-consuming, not accurate enough, and sometimes difficult and can be dangerous when reaching the rock faces physically. In addition, the method of data recording and storing cannot make full use of modern IT and computer technology to speed up the data processing, and then provide the input data in a required format for further analysis and designing. Therefore, the quality and quantity of the drawbacks inherent in the traditional method have great impact on the quantity and quality of mapping data, and will inevitably affect our understanding of the rock mass behaviour.

In this case, it has been recently realised that applying a new method for in situ data acquisition is the key point in solving the bottleneck problem for improving rock face mapping data, in terms of both quality and quantity. Especially with the development of IT technology, the digital data must be used as the input for computer-aided work. Therefore, interest in new methods for acquisition of digital data has greatly increased in recent years.

To avoid these problems, a new method should have the following benefits:

- (a) quickly capturing the data in the field;
- (b) digitally collecting the data in order to utilise modern computer resources to speed up the procedure of data capturing and processing;
- (c) having the access to visually operate the data so that the operator's background knowledge and experiences can be fully utilised to observe any complicated phenomena observed in the jointed rock mass, and then obtain the required information for rock engineering applications;
- (d) keeping the necessary level of accuracy for different rock engineering applications; and

- (e) having the possibility to capture the data in 3D without physically contacting rock faces at a range of distances.

Through the literature review for this project, it has been found that different digital techniques have been tested, including the following.

(1) Digital image analysis:

Several research groups have tested the utility of image processing techniques for automatic measurement of fracture geometry on rock surfaces. The research work done by Reid and Harrison (2000), Post and Kemeny (2001) have shown successfully applied different image segmentation techniques for automatically extracting and recognising trace lines of fractures. Roughness measurement was also performed using image processing techniques (Maerz et al. 1990). To perform the automatic 3D mapping, automatic image matching is another important step. Due to the complexity of the features in the rock face images, it seems difficult now to successfully achieve 3D fracture mapping by image processing techniques.

(2) Geodetic total station:

Total station (TS) is a geodetic method usually used for surveying and mapping. It also has been employed for determining the trace length of fractures on inaccessible rock slopes by Bulut and Tüdes (1996). With the TS method, discontinuity traces can be determined through the co-ordinates of a set of points, but the co-ordinates of the points must be captured by the help of a reflector. In addition, TS has also been tested by Feng et al. (2001) for measurement of fracture orientation. However, it is time-consuming for a large amount of measurements.

(3) Photogrammetry:

There are different photogrammetry techniques. Analytical photogrammetry techniques have been already used before for measuring fracture geometry at exposed rock faces by Ross-Brown et al. (1973), Harrison (1993), and Coe (1995). With this method, each pair of photographic hard copies is used to create a stereoscopic view of target areas of the rock face using a stereoscopic plotter or stereo-comparator. Geometrical parameters of fractures, such as orientation, spacing and trace length, can then be determined by capturing co-ordinates of several target points. With the latest development of digital photogrammetry technology, the rock surface is recorded as the images from a digital camera, and the procedure (similar to that of analytical photogrammetry) for capturing 3D data can be conducted in a PC with suitable software by using a pair of digital images of the rock faces, instead of the hard copies of six photos. This method has been applied for fracture mapping in tunnelling by Beer et al. (1999), and more applications have been continuously developed in recent years.

2.2 Purpose of the Study

In addition to the items mentioned above, a new technique, 3D laser scanning, has become more and more popular in recent years for on-site mapping, and shows more potential as a digital method for on-site characterisation of a rock exposure in rock mechanics.

3D laser scanning techniques have developed since the late 1990s, and these enable us to capture 3D digital data and associated images with high speed and accuracy. It has also now become more and more popular for use in capturing 3D digital data for 3D documentation and measurement in the processing industry for 3D virtual design, documentation in architecture and archaeology, and also 3D surveying and mapping in civil and infrastructure fields. In addition, these techniques have also been tested in some rock engineering projects, such as 3D digital fracture mapping (Feng 2001; Feng and Röshoff 2004; Slob et al. 2005), detecting water leakage via laser images (Feng and Röshoff 2004), identifying rock types based upon image analysis (Wang 2005; Feng et al. 2006), input data for numerical modelling (Bäckström et al. 2009a), deformation monitoring (Hesse and Stramm 2004; Schneider 2006) and 3D roughness analysis (Fardin et al. 2004) which shows the potential benefits for rock mechanics and rock engineering applications.

In order to investigate the practical possibility, the 2007–2011 ISRM (International Society of Rock Mechanics) President, Professor John A. Hudson, established a ‘National Task’ with the Swedish National Group in 2007. The purposes of this study were:

- (i) Investigate the current development for hardware and software for 3D laser scanning,
- (ii) Summarise the existing applications to rock mechanics,
- (iii) Evaluate the laser scanning benefits for rock mechanics, compared to other methods, and
- (iv) Identify the limits and needs for further development.

In this report, the purpose of this study is further described first and then the current development of laser scanning techniques, both hardware and software, is summarised. Based on the literature review and some case studies, the current status of the application of laser scanning techniques to rock mechanics is presented. Finally, the limits of current development and the needs for further development are discussed.

3 Current Development of 3D Laser Scanning Techniques

3.1 State-of-the-Art of 3D Laser Scanning Hardware

Laser scanning, often also referred to as *LiDAR* (light detection and ranging), is a new technique to obtain the digital data of an object—rather than making a single measurement like a laser rangefinder, but capturing millions of measurements by rotating mirrors, so the unit can cover a large area of an object. The 3D scanner is a type of a device that records the as-built situation with the data on its shape and possibly its appearance (i.e. intensity or colour), by emitting light and detecting the reflection of the light in order to accurately determine the distance to the reflected object. This technique has been developed since the late 1990s, and has now been applied to different fields for 3D measurement, surveying, documentation and modelling.

There are different scanning systems used for capturing different sized objects (i.e. from a small tool to a large building), with a wide range of scales (i.e. from few mm up to tens of hundreds of metres), and so can be divided into different scanning systems according to range:

- (a) Airborne Laser Scanning (ALS)
- (b) Terrestrial Laser Scanning (TLS)
- (c) Micro-Laser scanning (MicroLS)

ALS is the scanning system used on an aircraft to capture 3D data of large areas, such as agricultural or forestry sites, urban areas, industrial plants, etc. MicroLS are those 3D scanning devices used to scan an object over a short distance (from millimetre to a few metres), and mainly applied to reverse engineering and prototyping, quality control/inspection and documentation of cultural artifacts, etc. These two types of scanning systems are not typically applied to rock engineering. So, in this report, the focus is on TLS which is now mostly applied to rock engineering projects in practice.

There are many different types of laser scanners on the market and they have different specifications for different applications. However, the specifications of different scanners are designed with different scanning principles. Almost all of these scanners are designed according to three different scanning principles: (1) Pulse-based; (2) Phase-based; and (3) Triangulation-based. Most of the hand-held

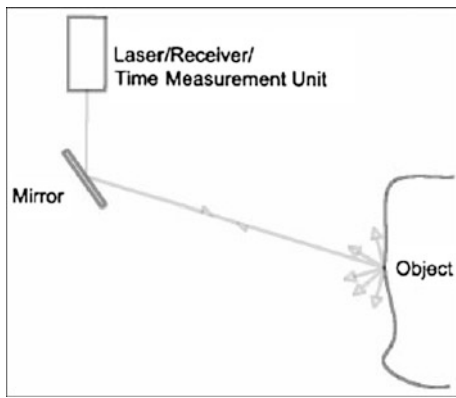


Fig. 1 Principle of time-of-flight laser scanner (http://en.wikipedia.org/wiki/3D_scanner)

and short-range scanners or MicroLS are designed with triangulation-based techniques, but all TLS scanners are designed with either pulse-based or phase-based techniques, and the scanning principles can be described simply as the following:

(1) Pulse-based scanner:

The pulse-based scanner is also called the time-of-flight (TOF) scanner, which is an active scanner that uses laser light to probe the subject. At the heart of this type of scanner is a time-of-flight laser rangefinder. The laser rangefinder finds the distance of a surface by timing the round-trip time of a pulse of light, see Fig. 1 (Wolfgang and Andreas 2003). A laser is used to emit a pulse of light and the amount of time before the reflected light is seen by a detector is timed. Since the speed of light c is a known quantity, the round-trip time determines the travel distance of the light, which is twice the distance between the scanner and the surface. When t (the round-trip time) is recorded, then the distance can be calculated with the following equation.

$$\text{Distance} = (\text{Speed of Light} * \text{Time of Flight})/2 \quad (1)$$

Clearly the accuracy of a time-of-flight 3D laser scanner depends on how precisely we can measure the t time. The laser rangefinder only detects the distance of one point in its direction of view. Thus, the scanner scans its entire field of view one point at a time by changing the range finder's direction of view to scan different points. The view direction of the laser rangefinder can be changed by either rotating the range finder itself, or by using a system of rotating mirrors. The latter method is commonly used because mirrors are much lighter and can thus be rotated much faster and with greater accuracy. The typical time-of-flight 3D laser scanners can measure is the distance of 1,000–150,000 points every second (http://en.wikipedia.org/wiki/3D_scanner).

(2) Phase-based scanner:

Compared to the TOF scanner, this type of scanner has a high speed scanning rate and better accuracy, but a short distance in the range of tens of metres. In this case, the transmitted beam is modulated by a harmonic wave and the distance is calculated using the phase difference between the transmitted and received wave. The Phase-based scanner has a higher precision, in the domain of millimetres, and higher measurement rates up to one million points per second, can be obtained applying the phase shift measurement principle. A c/w (continuous wave) laser is used as the carrier for a signal modulated onto it, typically using amplitude modulation. The phase of the emitted and the received signal are compared. The relation between phase differences, $\Delta\phi$, given in radians, and the one-way range is:

$$\gamma = \Delta\phi / (2 * \pi) * \lambda / 2 + \lambda / 2 * n \quad (2)$$

where λ is the wavelength in metres, and n is the unknown number of full wavelengths between the sensor system and the reflecting object surface. Choosing, e.g., $\lambda = 100$ m, means that there is a unique measurement range of 50 m. All measurements to objects further away will be folded into the first 50 m interval. The precision of the measurement is in the order of one per cent of the phase and can even be better. With the values from above, this would result in a measurement precision of ± 50 cm. This problem can be solved by using more than one modulation wavelength, i.e. two or three wavelengths (Fig. 2). Then, the longest wavelength defines the uniqueness range and the shortest wavelength defines the precision that can be obtained.

Comparing these two different types of scanners, their main features can be presented as follows.

- (1) The TOF scanner is a long-range scanner. It has a large range of scanning field, up to several hundreds of metres, but lower accuracy and scanning speed compared to the phase-based scanner. The maximum scanning range is now about 6,000 m;
- (2) The phase-based scanner is a middle-range scanner, up to the maximum of 187 m. Its accuracy is between the TOF and Triangulation scanners, but it has a high scanning speed and wide field of scanning view by rotation in both the vertical and horizontal through 360°.

Table 1 shows the most of the TLS scanners on the current market, and Fig. 3 shows some pictures of the TLS scanners.

3.2 Current Development of Software

Software for terrestrial laser scanning actually comprises several software modules of different types. Considering the whole procedure of a scanning project from data collection to the final model, a rough division may be made as follows:

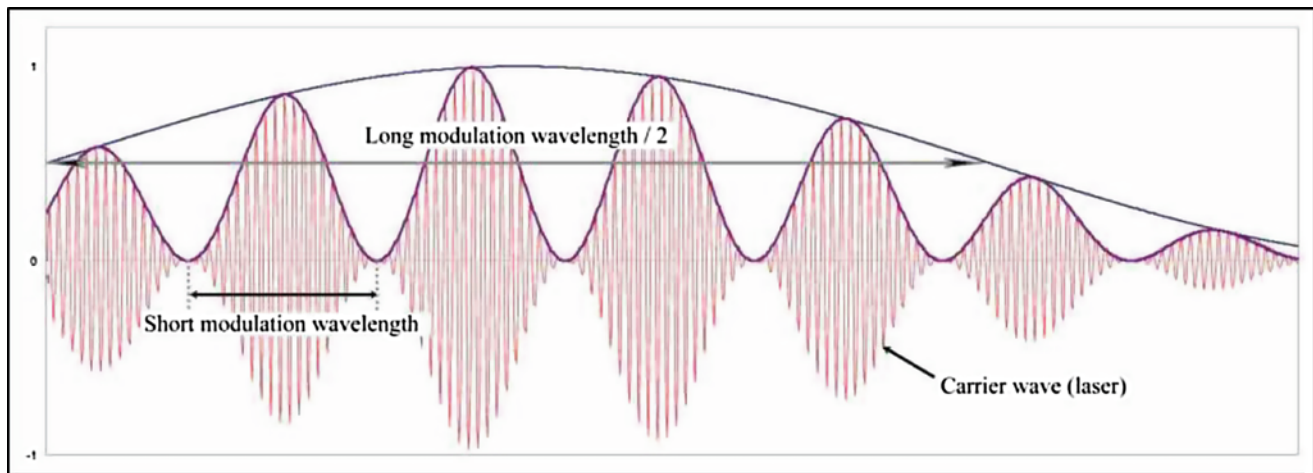


Fig. 2 Schematic drawing of two modulation wavelengths and carrier wave for phase-based laser ranging (http://en.wikipedia.org/wiki/3D_scanner)

Table 1 Terrestrial laser scanner existing on the current market

TLS scanner	Company	Date of introduction	Scanning principle
DeltaSphere-3000IR	3rdTech	2005	Phase-based
Surphaser 25HSX	Basis Software	2006	Phase-based
Surphaser 25HS	Basis Software	2005	Phase-based
LS 420	Faro	2005	Phase-based
LS 840	Faro	2005	Phase-based
LS 880	Faro	2005	Phase-based
Imager 5006/HDS6000	Z + F/Leica	2006	Phase-based
Imager 5010/HDS7000	Z + F/Leica	2010	Phase-based
Faro Focus 3D	Faro	2010	Phase-based
CPW 8000	Callidus	2007	TOF /Phase-based
CP 3200	Callidus	1997–2006	TOF
4400-LR	I-Site	2006	TOF
4400-CR	I-Site	2006	TOF
ScanStation 2	Leica Geosystem	2007	TOF
ILRIS-3DER	Optech	2006	TOF
ILRIS-3D	Optech	2000	TOF
LMS-Z420i/LMS-Z390i	Riegl	2003/2007	TOF
LPM-321	Riegl	2007	TOF
GX	Trimble	2005	TOF
VX	Trimble	2007	TOF

- (a) Software for scanning control
- (b) Software for registration of individual scans together or into the global co-ordinate system
- (c) Software for point cloud treatment
- (d) Software for CAD modelling
- (e) Software for texture and image mapping
- (f) Software for data and project management
- (g) Software to integrate scanning data to another existing program, e.g. CAD and GIS systems

The software described above is more general for scanning and modelling. Some special software is needed as follows:

- (i) Software for converting between scanning data and CAD or other software; and

Fig. 3 Examples of TLS scanners on the current market (updated to September, 2011, and US Federal Highway Administration (2008))



(ii) Software for special applications, i.e. architecture documentation, rock surface mapping.

The development of the software is advancing rapidly, and becoming more and more studied by the users-because the quality of these software modules has a considerable influence on the quality of the final modelling results, and also on the time needed to achieve the results. Thus, a smoothly performing software product is the basic requirement for the acceptance of 3D laser scanning techniques.

For laser scanning data, the most important software is the one for point cloud processing, and indeed most of the scanner manufacturers have developed their own point cloud processing software. In addition, several other companies have developed point cloud processing software. By exporting the point clouds in the xyz file format, point clouds from any scanner can be analysed with any of the software packages. Point cloud processing software includes:

- (1) Luposcan (Lupos3D)
- (2) Cyclone and Cyclone Cloudworx (Leica)

- (3) Polyworks (Innovmetric)
- (4) Riscan Pro (Riegl)
- (5) Isite Studio (Isite)
- (6) LFM Software (Zoller + Fröhlich)
- (7) Split FX (Split Engineering)
- (8) RealWorks Survey (Trimble)
- (9) Pointools (Pointools)

Furthermore, much research work has also focused on development and improvement of the algorithms in order to provide good quality software, including:

- (i) Error analysis and control of the whole scanning procedure from scanner calibration to modelling; and
- (ii) Matching and segmentation of 3D point clouds in order to make the modelling more effective and automatic.

3.3 New Trend for Further Development

Through more than ten years of development, hardware and software have been greatly improved for their basic functions as a new technique for 3D surveying, such as scanning

speed, range and resolution. However, compared to other surveying techniques, laser scanning has its own special features, and therefore cannot only be taken as a surveying tool, but also as a new 3D technique for documentation, design and visualisation. Some of its new features, such as too much data flow (in the unit of MB and GB), all the information being in 3D (3D image, point clouds and model), inevitably there are some problems in its applications: for example, incompatibility with existing software, difficulties in processing so much data, and transformation between 2D and 3D.

So, laser scanning provides us with much more information than any other surveying techniques, but at the same time introduces difficulties in use if no good solutions for the afore-mentioned problems are found. Fortunately, the recent developments in both hardware and software are focused more on practical applications. The development focus can be summarised as described in the following text.

3.3.1 Developing a Unique System for Special Applications

In order to make the whole procedure simple, new development is focusing now on the key-door solution, which develops a system, including both scanning hardware and software for data processing, and also the data formats, for the results to be compatible for exchange with the existing software. Such systems have their own special applications, and both hardware and software are developed for special application situations and standards.

A typical example is the tunnel scanning system, TMS, developed by Amberg AG, and it is specially applied to tunnelling projects in order to control the geometry of a tunnel. In this package, the hardware consists of, not only a phase-based scanner, but also associated tools for positioning of each scan, and the software is also specially designed for scanning control in the tunnel situation. It enables the creation of standard products, such as cross-section and difference models for tunnel dimension measurement and documentation. The export results have a standard format for input to other software, such as AutoCAD.

Another example is the cavity scanning system, which has been developed by Optech (www.optech.com) and MDL (www.mdl.com).

3.3.2 Much More Development has Taken Place with the Associated Tools and Scanners

As the scanner is applied to many different projects, it is not enough only to use the scanner, but some associated tools are needed to perform the scanning tasks. Scanning examples are scanning a shaft or borehole by running the scanner up and down, or inserting the scanning system into an



Fig. 4 A prototype of remote-control scanning system developed by Faro (www.faro.com)

enclosed building through a small hole (e.g. 200 mm diameter) due to the high radiation, or mobile-scanning on the railway or on the road surface. Therefore, the scanner is also developed by being associated with some tools to load and run the scanning, so as to make the scanning more effective and applicable.

A typical example of recent developments is to use remote-control for the scanning in order to run the scanning in an area where it is dangerous or inaccessible. Figure 4 illustrates a remote-control scanning system developed by Faro (www.faro.com). A special scanning system which can run on the railway has been developed by Amberg (www.amberg.com) and is shown in Fig. 5.

3.3.3 Integration of Colour Photography

In addition, and compared to photogrammetry, the greatest disadvantage is that the laser scanner cannot provide a colour image. It is not easy to develop a true colour 3D laser scanner with high scanning speed and accuracy, so one of the alternatives, which is now often used, is to integrate colour photography with the laser scanning. Much more development has been undertaken by different vendors, and can make scanning systems semi- and fully-automatic through both scanning and photographing. A 'semi-automatic' system means that the scanning is made automatically first, and then the scanner is replaced by a digital camera at the same position (i.e. on a tripod) for taking a series of colour photos manually. But, the 'fully-automatic' system has both scanning and photographing automatically controlled by the software, and there is no need to replace the scanner by the camera because they are installed together. Figure 6 shows the integrated system both from Faro (www.faro.com) and Z + F (www.zf-laser.com).



Fig. 5 Amberg GRP scanning system developed for railway scanning (www.amberg.com)

3.3.4 Mobile Scanning System

In recent years, mobile scanning systems have been significantly developed. These mobile scanning systems are grouped as follows:

- (1) car-borne mobile scanning systems (Fig. 7)
- (2) train-borne mobile scanning systems (Fig. 8) and
- (3) small-vehicle-borne mobile scanning systems (Fig. 9)

Compared to a normal TLS scanning system, the mobile scanning system consists of several units with integration of the different techniques, including:

- (1) GPS positioning system
- (2) Profile laser scanning system
- (3) Video camera
- (4) Associated tools for anti-vibration and data transferring etc.

3.3.5 Hand-Held Scanner

This type of scanner is based on the triangulation scanning principle and is often used for scanning a small object a short distance away, e.g. few metres. Compared to both pulse-based and phase-based scanners, it has higher resolution and high accuracy, but normally a lower scanning-speed. So, it is not recommended for application to scanning large objects.

However, the updated developments show potential for scanning large objects. A new hand-held scanning system, called Mantis Vision, can quickly scan an object with high resolution up to less than 1 mm (Fig. 10).

Compared to other hand-held scanners, it has some advantages:

- (a) Longer scanning range: 0.3–5 m with a resolution of 0.5 mm
- (b) Large scanning view field: 38–40°

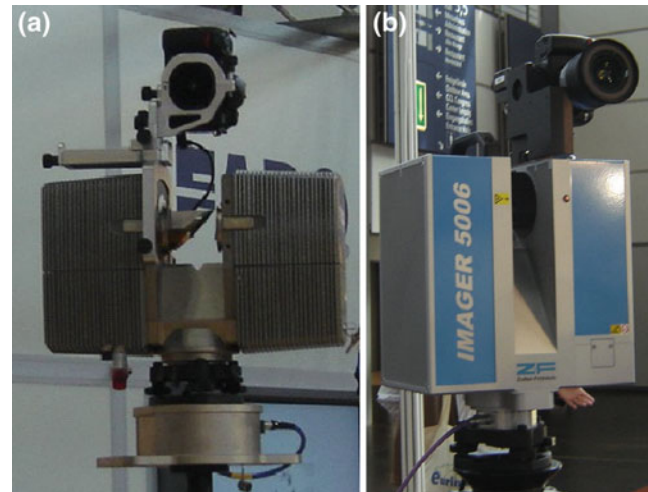


Fig. 6 Integration of laser scanner and digital camera: **a** Faro system (www.faro.com), **b** Z + F system (www.zf-laser.com)

- (c) Higher scanning speed: few seconds per scan
- (d) No need for reference targets

3.3.6 Software Suitable for Multiple Data Format

Software has been developed for more compatibility in exchanging the scanning data with other existing software, and it is now focusing on:

- (i) Scanning raw data to be directly imported to different software or converted as the standard format (e.g. ASCII) to be processed in other software;
- (ii) Developing interface programs to exchange the scanning data with the existing software; now it is much more developed in CAD software.

3.3.7 Development for 3D Analysis

In recent years, laser scanning has not been only limited to 3D surveying and documentation, but also has been combined with other parameters (e.g. stress, temperature and radioactivity) to make 3D analyses of some physical features in 3D. As laser scanning can provide an accurate as-built 3D model, 3D modelling of physical parameters become more realistic. For example, stress distribution and deformation monitoring in rock masses can be modelled in a more realistic environment; also 3D analysis of radioactivity distribution has been used for nuclear decommissioning through a combination of the 3D as-built mode from laser scanning and the 3D distribution model from radioactivity measurements.

4 Special Features from 3D Laser Scanning Data

Compared to traditional methods for rock mass characterisation, laser scanning has more advantages, with the following features:

Fig. 7 Topcon mobile scanning system (www.topcon.com)



Fig. 8 Z + F Railway mobile scanning system (www.zf-laser.com)

- (a) Capturing a large coverage of a rock surface with high resolution (up to mm) in a short time (in a few minutes depending on the resolution selection)
- (b) All the data are digital and in 3D, both image and co-ordinates
- (c) After reference surveying, all scanning data are registered in a global co-ordinate system, and the rock mass is referenced to its real position in space
- (d) The rock mass can be recorded by remote control and so there are no adverse personal safety issues
- (e) No need for illumination for a high resolution digital image
- (f) By combining scanning and photographing in the software, a rock mass can be recorded in real colour.



Fig. 9 S + H trolley mobile scanning system (www.intergeo.com)

Through these advantages, laser scanning can avoid the drawbacks of the traditional method, and improve the quality and quantity of the data for rock mass mapping. So, via the laser scanning, a rock mass can be quickly recorded and the following useful information obtained.

- (i) Position of a rock mass with 3D co-ordinates in a global co-ordinate system
- (ii) Geometrical features, e.g. length between points, orientation of a fracture, etc.
- (iii) Visual information, e.g. 2D and 3D digital image, 3D virtual model

Fig. 10 Hand-held scanner of Mantis Vision



- (iv) Physical features, e.g. water leakage and different rock type by different intensity

Those features have great potential for rock mass characterisation in a rock mechanics project.

5 Procedure for Capturing 3D Digital Data by 3D Laser Scanning

A typical scanning procedure and the associated data can be described as the following. For a typical scanning job in the field, both reference surveying and scanning are needed.

5.1 Control Surveying

Reference surveying is often carried out by using a total station to set up a local co-ordinate system around the scanning area, and link the local co-ordinate system to a global co-ordinate system, and then the surveying data are applied for positioning of each scanning set into the global reference co-ordinate system.

5.2 Scanning

The operation of each different scanning system is different, because it depends upon the requirements of scanning software and reference surveying. But some basic parameters must be correctly selected for different applications: (1) scanning resolution; (2) scanning range; (3) position of each scanning; (4) number and location of reference targets. In addition, some scanning systems are also sensitive to the environment, such as temperature, moisture, density of particles in the air, and even the reflectivity of the object. These parameters and factors must be carefully considered in order to obtain good quality scanning data.

The typical raw data from laser scanning is the so-called point cloud, which is a set of vertices in a 3D co-ordinate system. These vertices are usually defined by x-y-z co-

ordinates, and typically intended to be digitally representative of the external surface of the rock mass.

For most of the phase-based scanners, the raw scanning data is combined as both point and intensity, so the corresponding intensity image in both 2D and 3D can be obtained, which is useful for documentation and identification of objects in detail. Figure 11 shows the raw scanning data typically captured from a phase-based scanner.

The true colour scanner is still under development, and it is only possible now to scan some small objects, but not possible in practice to scan the rock mass over a large area. However, another alternative, through combining scanning data with colour photos in software, is now possible. When scanning at the location, the colour photos are captured by a digital camera at the same time and then the colour photos are registered to the scanning data in the software; the true colour 3D model of a rock mass can be obtained (Fig. 12).

5.3 Pre-processing Data

The on-site captured scanning data, also termed raw scanning data, are necessary to make pre-processing before any further modelling and calculation. The reasons are:

- (1) Each individual scan obtains the scanning data in the local co-ordinate system, and mostly several scans are needed to cover the whole object. Therefore, each individual scan needs to be registered into a common co-ordinate system; and
- (2) Not all points in the raw scanning data can be used because there are always some noise points captured, especially there are more noise points from the phase-based scanner. So, these noise points need to be filtered out from the raw scanning data.

In this case, the raw scanning data need to be pre-processed mostly by two steps:

Step 1. Register each individual scan into a common co-ordinate system; and

Step 2. Filter out noise points from the raw scanning data.

Fig. 11 Presentation of raw scanning data from scanning of the same object (Feng et al. 2011): **a** point cloud; **b** 3D laser image; **c** 2D laser image

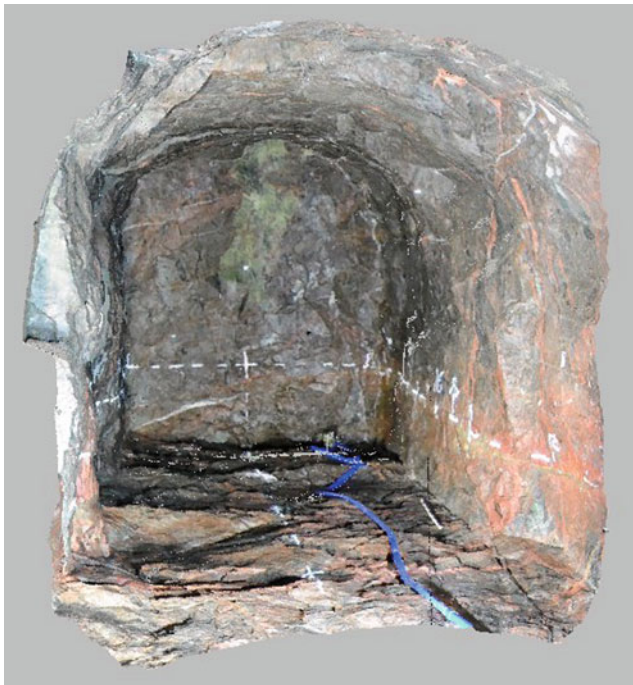
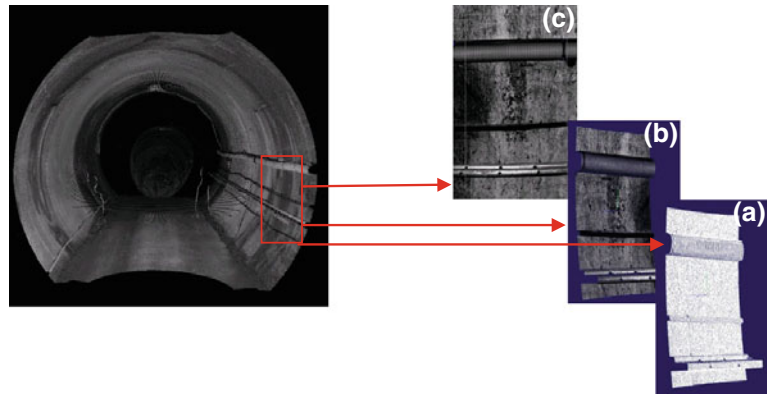


Fig. 12 3D colour model of scanning in a tunnel (Feng et al. 2011)

In addition, there are different data formats for the raw scanning data from different scanner producers, so it is sometimes necessary to convert the raw scanning data into another format, depending upon which modelling software is used for the post-processing.

5.4 Post-processing Data

After pre-processing of the raw scanning data, the point clouds are positioned and oriented in a certain co-ordinate system, and all scanning points are correctly located in a

known co-ordinate system, so the post-processing can be performed. The post-processing is done by two different situations or software, as follows.

(1) By special developed software:

As the scanning data are quite substantial, compared to other data, and also have a special data format, special software has been developed. These software methods can process large amounts of scanning data, and create different results, including support for a CAD model, mesh-model, cross-section, etc. And then, the results can be exported into other existing systems, such as CAD, GIS or other user-familiar systems for different applications.

(2) Input into existing software:

This was difficult in the earlier period of the development, but now many types of so-called 'plug-in' software have been developed, and this plug-in software makes it possible to import a large scanning data file into user-familiar software, such as CAD, GIS and so on.

In addition, many hardware producers will now attract more users, so they allow their special data formats to be converted into a neutral format, the ascii format, to be available for post-processing in many different software programs.

6 Application Examples to Rock Mechanics

To evaluate the potential application of laser scanning to rock face mapping, it is important to establish what is the typical procedure for site mapping in a rock engineering project, and then find out if laser scanning can help to improve or solve the problems of the traditional methods.

For a site mapping project, a typical procedure is given below.

(1) Collect the raw data in the field:

The raw data consist of different types, which depends upon the different projects, but all projects must collect some data, such as location, geometry (of fracture, rock surface etc.), through measurement, photographs, taking notes of the observations, etc. Digital methods can make this step much faster and accurate than the traditional approaches. More detailed description in relation to this subject will be presented in the later sections.

(2) Calculate and analyse the raw data:

After the field data collection, the raw data must be processed for different purposes, such as calculation of fracture orientation and plotting on a stereogram for fracture analysis and stability analysis, importing the fracture parameters for numerical modelling, and also for the design of a dam or tunnel. All of the data processing is now computer-aided, so the raw data must be digitised, which is time-consuming with the traditional recording method.

(3) Present and transform the processed data:

The processed data and results, either in table or in graphical form, should be presented in a way, or exported to other software, to enable further analysis, modelling or design, which might be in digital form and computer-aided.

(4) Store and archive the raw data and results:

With the development of computer science, the data and results are now mostly stored and archived in a digital way on CD/DVD, band or external/internal hard disk, so it is important to convert all the data to digital form.

So, in order to avoid the drawbacks of the traditional methods, a new method must have the following important features: (i) quickly capturing the data in the field; (ii) digitally collecting the data in order to utilise the computer resources to speed up the procedure of data capturing and processing; (iii) having the ability to visually operate the data so that the operator's background knowledge and experiences can be fully utilised to observe the complicated phenomena related to a jointed rock mass, and then obtain the required information for rock engineering applications; (iv) keeping a certain level of accuracy for different rock engineering applications; (v) possibility to capture the data in 3D without physically contacting rock faces-over a range of distances.

As 3D laser scanning has many advantages for 3D measurement and documentation, it shows great potential for application to different projects in rock engineering and rock mechanics. Some typical examples are summarised in this section.

6.1 Site Characterisation of a Rock Exposure

The most typical application for 3D laser scanning is applied to site characterisation of a rock exposure. Currently, rock surface mapping is still mainly performed by

traditional methods, which is well known as by a geological compass with inclinometer to measure dip and strike, and taking notes in a notebook, and also taking some photos for documentation etc. Obviously, the traditional methods have some drawbacks, including:

- (a) Physical contact with the rock face, which inevitably leads to some problems, such as danger in reaching the rock face in some cases, and the impossibility or difficulty in obtaining the mapping data;
- (b) Uncertainty and inaccuracy. Mapping results are very dependent upon personal experience, and the related difficult in making sure or checking out whether the mapping data are reliable, and, if not, why not;
- (c) Time-consuming-not only for the field work but also in transferring data into the computer for further modelling and analysis.

But with 3D laser scanning, there is a great potential to avoid some drawbacks of the traditional methods, and also to improve the quantity and quality of the raw data and the results.

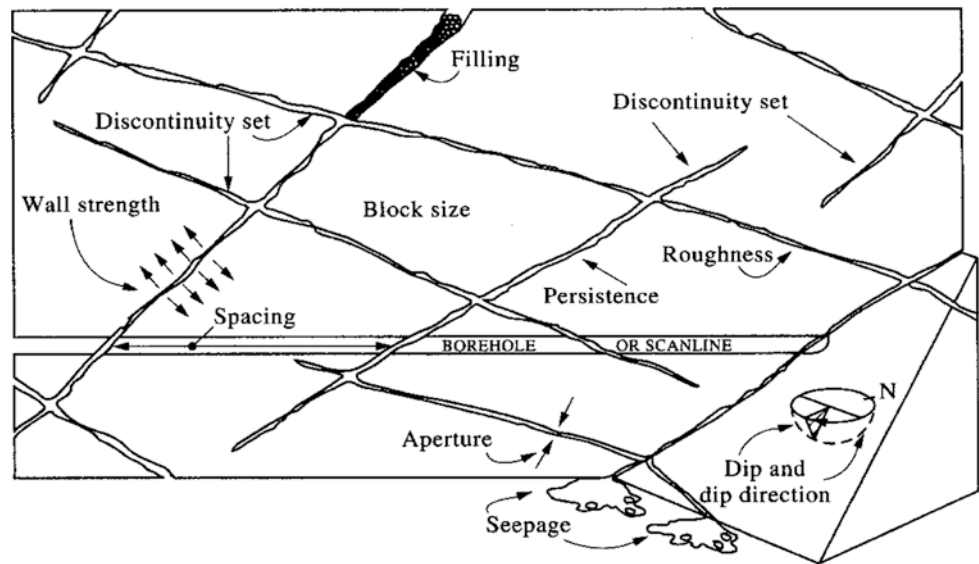
Based upon the literature review and our project experiences, the potential application of laser scanning to rock surface mapping can be summarised as the following:

- (1) Laser scanning is a non-contact technique, so it is not necessary to reach the rock surface, and there is thus no risk to the person in this regard;
- (2) It can capture the rock surface with its geometry and position much more quickly and accurately than traditional methods;
- (3) It collects the data in digital form and in 3D, so 3D digital mapping is possible, and the raw data can be directly processed by a computer, and so possible to utilise computer-aided resources to speed up the data processing. Both semi-automatic (Feng and Röshoff 2004) and fully-automatic methods (Slob et al. 2005) are possible and have been tested for fracture mapping;
- (4) All the data, from the raw data to the processed results, can be stored and archived within a digital medium, and also transferred (i.e. input and output) between different software;
- (5) In particular, the data and the results can be checked because the raw data and the processing methods are retrievable, which make the data quality more reliable and controllable.

To characterise the features of exposed rock faces, the International Society for Rock Mechanics (ISRM) proposed ten parameters (ISRM 2007), namely: orientation, spacing, persistence (or trace length), roughness, aperture, wall strength, filling, seepage, number of fractures sets, and block size (as shown in Fig. 13), to describe the geometrical, mechanical and hydraulic features of fractures.

To be able to characterise the features of a rock surface, the methods must provide the enough information in order

Fig. 13 Primary characteristics of discontinuities in rock mass (from Hudson 1989)



to replace the personal observation and measurement obtained by the traditional methods, and be even better in some ways. In general, this information is as follows.

(1) Geometrical information:

This is necessary for obtaining relevant geometrical parameters, i.e. fracture orientation (dip and strike or dip direction), block size, spacing, roughness and aperture. Digital methods are able to capture 3D digital data, and can provide 3D geometrical information for rock face mapping.

(2) Physical information:

Rock face mapping also needs to obtain particular information, such as rock types, mechanical properties of a rock, wall strength, mineral fillings, etc. It is possible to identify the rock types, perhaps also the mineral fillings from the colour photos and laser intensity images, but has limited value for estimating the mechanical properties, e.g. wall strength.

(3) Visual information:

Visual information, like photo and images, are needed for a mapping mission in order to identify the rock types, discontinuity sets and water leakage (seepage). The colour photos and laser intensity images make this possible.

(4) Spatial information:

Spatial information can provide the location and orientation of a rock surface in space, which can also be captured by the digital methods through measurement of some reference points, and then transformed into a global co-ordinate system.

As in the description of laser scanning features in Sect. 4, laser scanning can be applied to obtain significant information for a rock exposure characterisation. From the literature review, laser scanning techniques have been applied to different situations at rock exposures, from roadcuts, open-pits, tunnels and even boreholes (Fig. 14a–d).

For site mapping of a rock exposure, it is possible to apply laser scanning for different purposes, and here we present some application examples.

(5) Fracture orientation:

The orientation of a fracture plane is traditionally measured by a compass and inclinometer. By using laser scanning, the fracture orientation can be measured semi-automatically or full-automatically. Both semi-automatic (Feng and Röshoff 2004) and full-automatic (Slob et al. 2005) methods have been tested. By using the semi-automatic method, the orientation of a fracture plane (e.g. dip and strike) can be determined interactively or semi-automatically from the 3D laser scanning data. The presented method aims to not only make use of the advantages of modern computer techniques, but also enables the operators to utilise their geological background knowledge to control the mapping results.

A typical mapping procedure by this method is not only taken by computer software as a virtual mapping platform, but is also interactively performed between the computer and the operator: (1) select a part of rock surface from the whole 3D scanning model by the operator; (2) choose a fracture exposed on the scanned rock surface, and mark the exposed fracture surface interactively by the operator; (3) automatically calculate the best-fit fracture plane by the computer program, and then calculate the fracture orientation. Figure 15 shows an example for fracture mapping based on 3D laser scanning data from an exposed rock face.

The automatic method (Slob et al. 2005) is based upon some segmentation approaches for processing of the scanning point clouds, and then the best-fit plane of fracture surfaces can be automatically calculated, so the fracture orientation can be determined (Fig. 16).

(6) Roughness:

Fracture roughness is mostly characterised in the laboratory on small specimens of a natural fracture surface. In situ determination of fracture roughness at the large-scale is important for understanding the scale effect of fracture roughness, large-scale deformation of rock masses, and

Fig. 14 Scanning of different types of rock exposures (US Federal Highway Administration 2008)

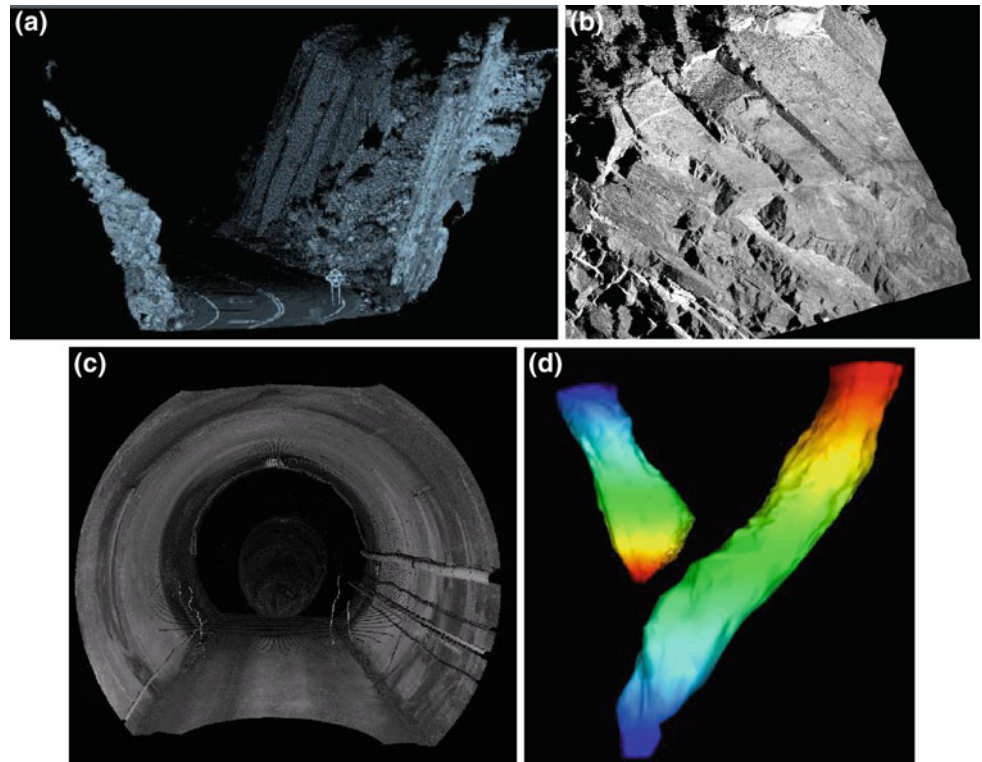
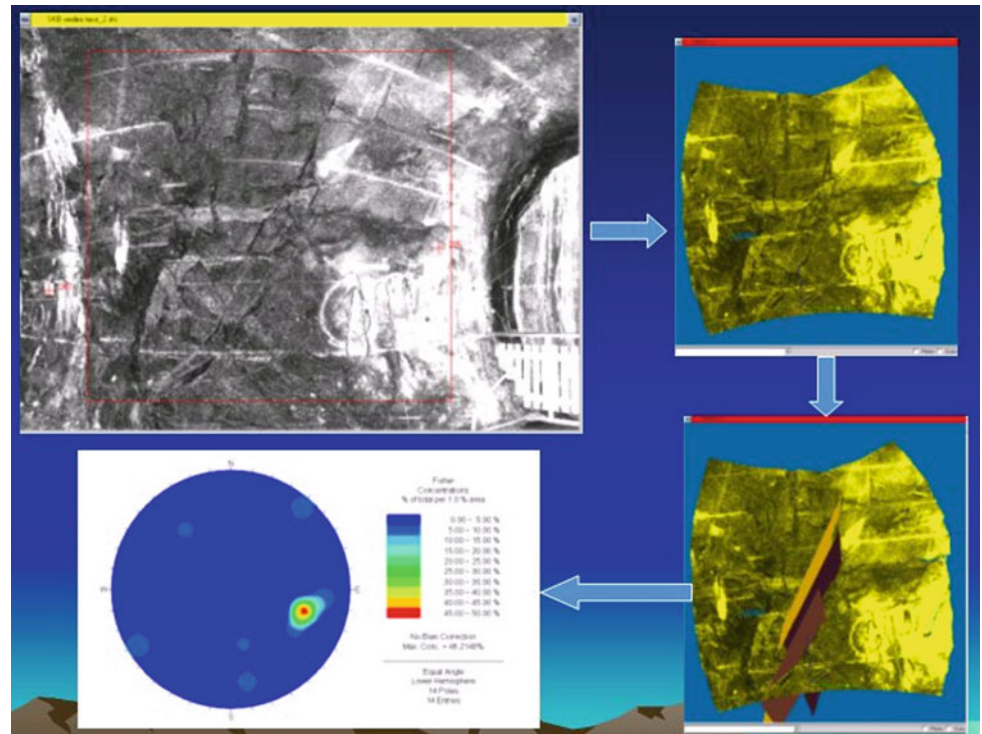


Fig. 15 Semi-automatic fracture mapping (Feng et al. 2011)



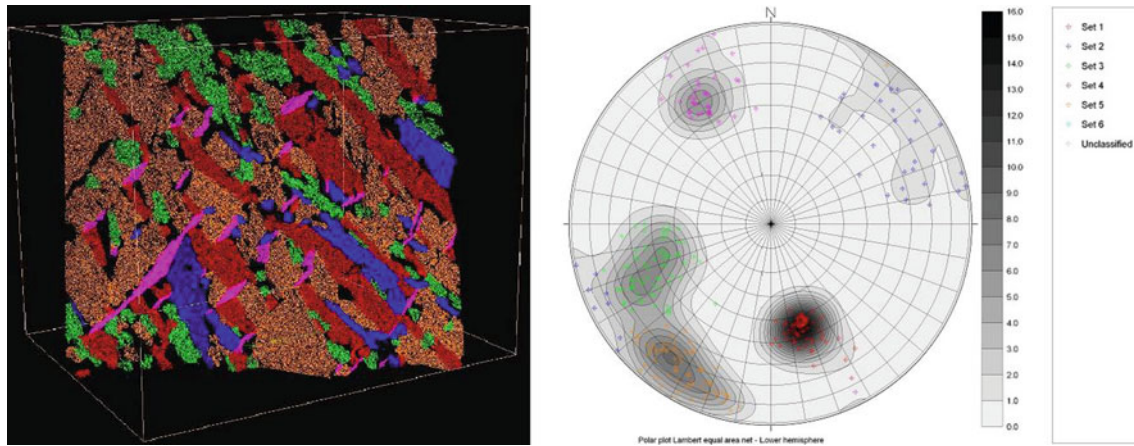
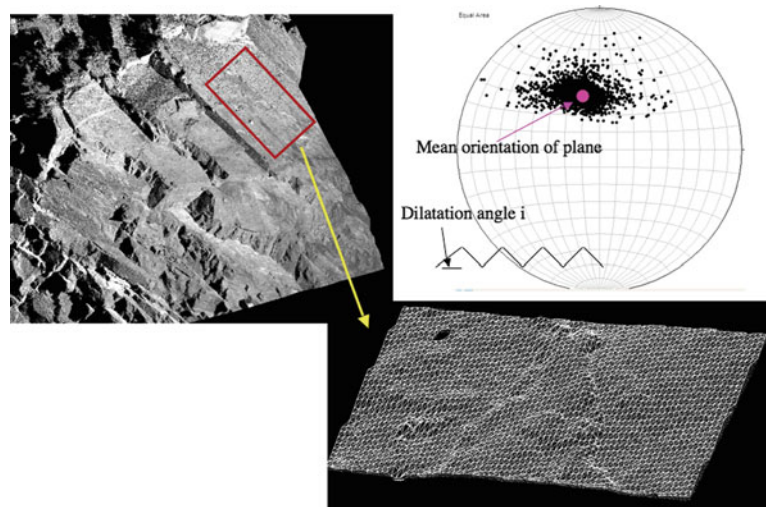


Fig. 16 Full-automatic fracture mapping (Slob et al. 2005)

Fig. 17 Schematics from one method of analysing fracture roughness using scanning data by a triangulated mesh of a fracture and plotting the pole for each triangle on a stereonet (US Federal Highway Administration 2008)



hydro-mechanical behaviour of fractured rocks. By using laser scanning, fracture roughness can be quantitatively described in several different ways, and show more advantages.

(6.1) Using a triangulated mesh created from scanning point clouds:

The first technique is to use a triangulated mesh of a fracture, as illustrated in Fig. 17 (US Federal Highway Administration 2008). If the orientation of each triangle is plotted on a stereonet, then the scatter about the mean orientation of the fracture gives information on the dilatation angle. In the classic saw-toothed fracture analyzed by Patton (1966), the dilatation angle is defined as the rise angle of the saw teeth compared with the mean orientation, as shown in Fig. 17. The dilatation angle is directly related to the additional friction angle due to roughness (Goodman 1989), and on a stereonet, the dilatation angle can be directly

determined by the angle between the mesh triangle orientation and the mean orientation of the fracture. The example in Fig. 17 shows a scatter of triangle orientations, with the mean fracture orientation at the centre of the scatter. The stereonet in Fig. 17 is marked off in degree increments of 10° , and indicates dilatation angles ranging from a few degrees to over 30° . Also the shape of the scatter in the stereonet is elliptical, indicating roughness anisotropy (dilatation angle varies with direction). By varying the triangle size of the mesh, scale-dependent roughness can be determined. As an important note, the triangle size needs to be greater than the scanner error, or else roughness due to measurement error will be calculated.

(6.2) Cross-sectional profile with a direction:

The second way (US Federal Highway Administration 2008) to obtain information about roughness is to make cross-sections through a fracture at different angles (a cross-

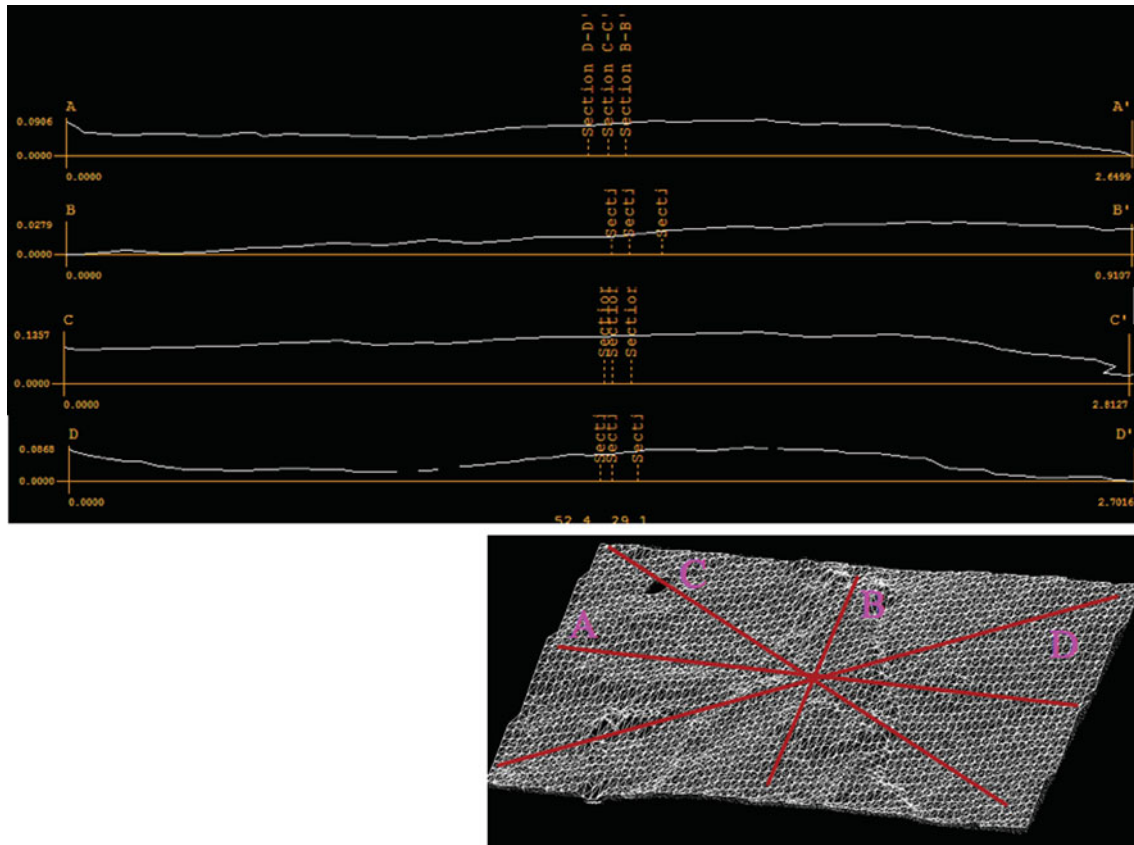


Fig. 18 A second method of analysing fracture roughness, by making topographic profiles of the fracture in different directions, and processing the roughness profile to extract roughness parameters such as JRC (US Federal Highway Administration 2008)

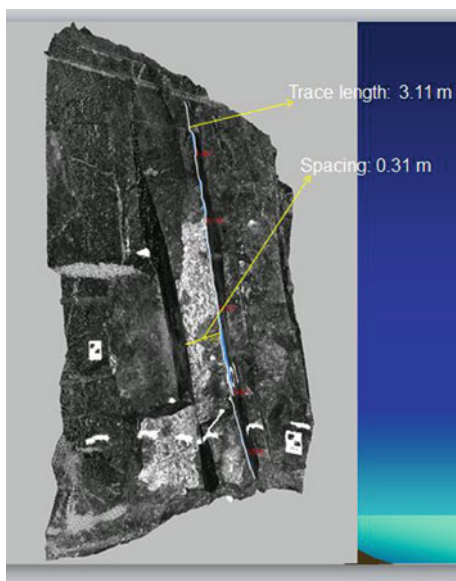


Fig. 19 Measuring fracture length and spacing in 3D scanning point clouds

section in the direction of the dip vector, for instance, would be relevant for slope stability purposes). Figure 18 illustrates the procedure.

Compared to traditional methods, laser scanning can not only describe the fracture roughness quantitatively, but also give its orientation in a known direction when the scanning area is registered in a known co-ordinate system. This is important for rock mechanics, not only to calculate the shear strength, but also to determine the slipping direction.

(7) Length and spacing:

Fracture exposure length and spacing between different fracture sets can also be measured, either in the laser image or in 3D point clouds (Fig. 19).

(8) Rock type:

Laser scanning can not only measure the position but also the reflex intensity at every point, so the laser image is created based upon the intensity difference of different objects. As different rocks have different intensities, the intensity of the laser image has been tested to identify different rock types. In this study, several image processing methods have been tested, such as texture analysis, image classification. Figure 20 shows different rock types in the pseudo-colour laser image by image processing methods.

(9) Identify water leakage:

Water leakage is an important hydrological parameter in site characterisation. Based upon the reflex intensity difference between water leakage and the dry rocks, the laser

Fig. 20 Rock type comparison between laser image (*left*) and pseudo colour image (*right*) (Wang 2005)

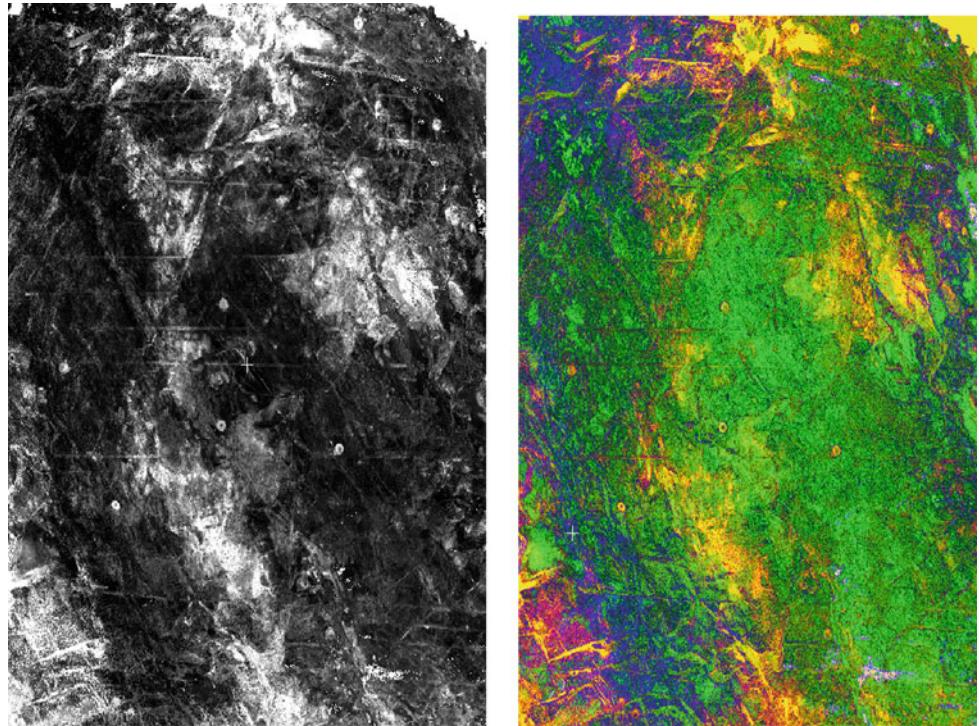
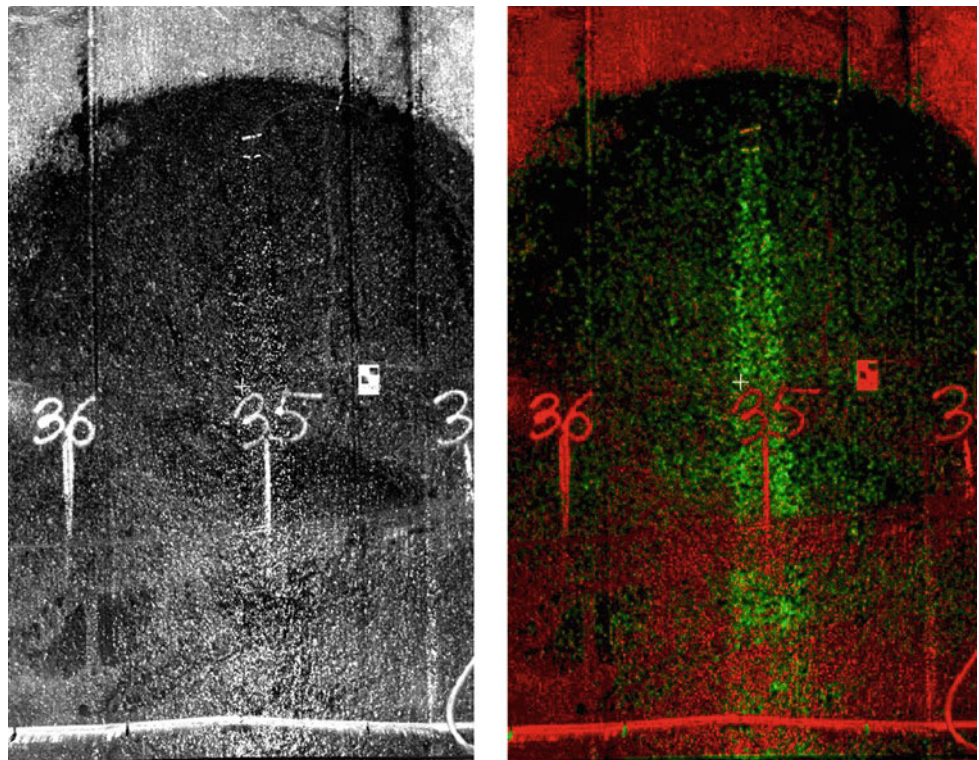


Fig. 21 Identification of water leakage from laser images by image processing analysis (Wang 2005)



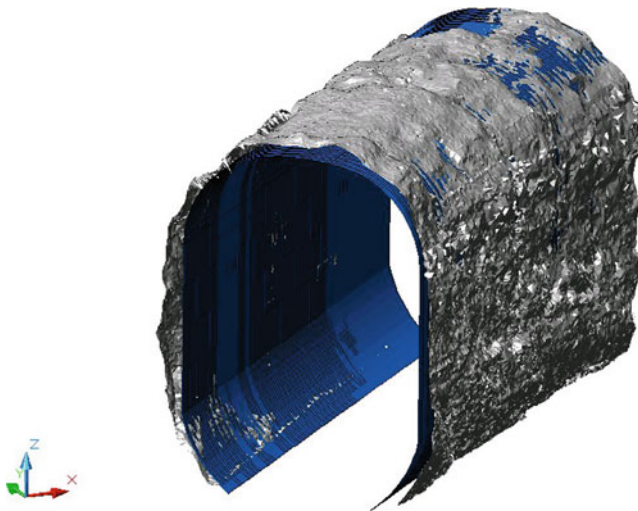


Fig. 22 Difference model for profile comparisons between designed and blasted tunnel

image can be used, not only to detect the position and area of the water leakage, but also to quantify the amount of the water leakage (Fig. 21).

6.2 Quality Control of Tunnel Blasting

(1) Controlling the quality of tunnel blasting:

For a new tunnel and during the construction period, it is important to control the over- or under-break as compared to the theoretical design. By using the full-coverage laser scanning data, the quality of the blasting can be accurately presented, by either a 3D model (Fig. 22), a cross-section or an unfolded difference model (Fig. 23).

(2) Controlling the thickness of sprayed-concrete:

The thickness of sprayed concrete is important for tunnel enforcement. Traditionally, it is just checked by a stick at randomly selecting some points. Using the full-coverage laser scanning data, the thickness of the sprayed concrete can be accurately calculated and presented in the unfolded tunnel map and even in the 3D model (Fig. 24).

6.3 Deformation Monitoring

A rock mass can be deformed by both artificial and natural forces, such as in tunnelling, mining and earthquakes, which may result in a disaster for both human beings and facilities. Therefore, one of the important concerns for rock mechanics is to monitor the deformation of a rock mass, e.g. a tunnel, underground storage facility, or road slope.

Traditionally, the rock mass is monitored by measuring the displacement of several points at some defined

positions, so the monitoring is limited to those selected parts, with no control of the rock mass as a whole. Therefore, it is risky because of missing some unstable parts.

With laser scanning, the surface of a rock mass can be scanned at a full coverage with a high density of scanning points at the millimetre level, so the rock mass can be monitored as a whole, and it is possible to control the deformation of the whole surface. Compared to the traditional methods, the laser scanning has some advantages for deformation monitoring:

(1) Full coverage of the complete monitored part, not only limited to some selected points:

Traditionally, the deformation is monitored by the relative displacement between some selected points, which are limited to some points, so this is risky because of missing the unstable parts due to the points being selected subjectively or randomly. By laser scanning, the disturbed parts can be fully covered and quickly scanned at high resolution up to few millimetres, so there is much less risk of missing unstable portions, and it is possible to monitor the complete area of interest. Figure 25 shows the deformation at a section of a tunnel by scanning before and after blasting, and the deformation variation at different parts is shown in different colours, so the deformation can be monitored and displayed across the whole area.

(2) By using the laser image, the deformation can be visualised in 3D and recognised in the laser image:

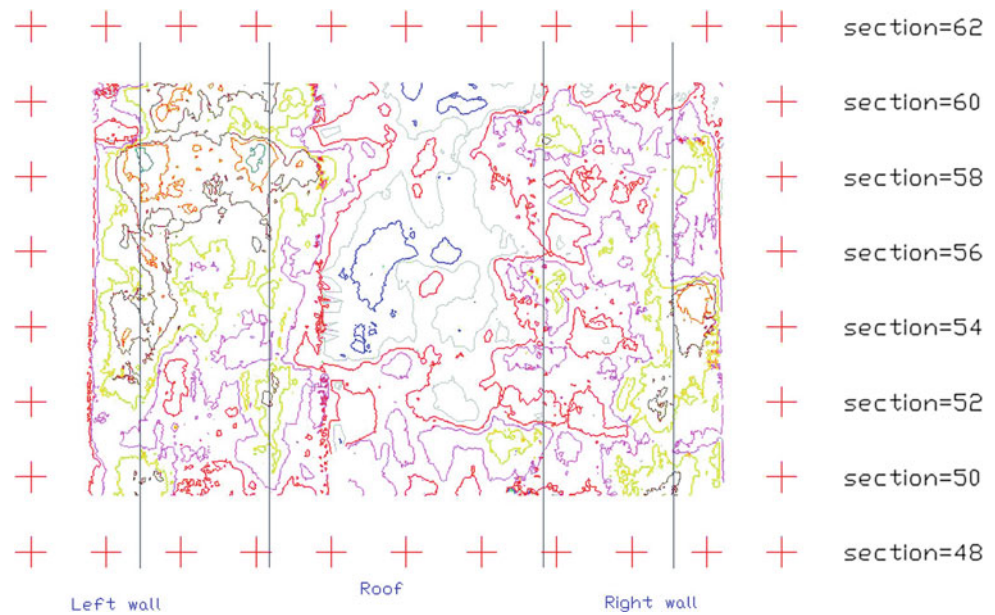
As mentioned before, the scanning data consists of both point clouds and an intensity laser image so, if some particular objects are of interest, then the deformation and its corresponding objects can be visualised in both 3D and laser image. Figure 26 shows the location of a special object and its deformation after blasting.

(3) Deformation of a rock mass can be evaluated by more parameters:

As the rock mass can be scanned, so its deformation can be evaluated in different ways, not just the relative displacement between points. For example, if a section of a tunnel is deformed due to blasting, by scanning before and after blasting, the deformation can be investigated by the difference of the volume and the surface area. In addition, by creating some profiles from scanning point clouds, the deformation can be identified by the length of the profile, or easily recognised by comparing two profiles before and after blasting.

In addition, a case study by Monserrat and Crosetto (2008) has applied a long-range scanner to land deformation. In this study, several parameters are tested to show the potential application by laser scanning for 3D deformation measurement, including 3D displacement vectors, 3D rotations. Moreover, the least squares 3D surface matching was used to check the quality of the estimated deformation parameters.

Fig. 23 Control of tunnel blasting by laser scanning data



Although laser scanning techniques show the potential for deformation monitoring, it is still difficult to monitor small deformations, and the system is limited to a few millimetres for both long-range and short-range scanners. There are some problems and uncertainty concerning deformation monitoring, so we must pay more attentions to them as follows.

- (4) Accuracy of control surveying related to the real deformation:

In order to monitor the absolute movement of a rock mass, control surveying is important, which is linking the deformed part to the stable part, or transforming the deformed area to the global co-ordinate system. In this case, it is important to know the accuracy of the control surveying with respect to the real deformation. In many case studies and publications, the accuracy of control surveying is not mentioned. So it is uncertain if the displacement comes from the error of control surveying or the real deformation. This is very sensitive if the deformation is small, in the range of few millimetres, because the control survey often has an accuracy of just a few millimetres.

- (5) Resolution of a scanner related to the accuracy of deformation measurement:

In general, high resolution scanning is possible for identifying the minor deformation of an object. However, the object scanned by a high resolution scanner may not provide a high accuracy of deformation measurement. This often causes misunderstanding in practice. As mentioned before, a rock mass sometimes needs to be scanned from several positions, or a large area of rock mass needs to be covered by several scans. In this case, all of the scans must be registered into the same co-ordinate system. Normally, the more scans to be registered, the more errors can be propagated in registration.

- (6) Accuracy of the parameters created from scanning points:

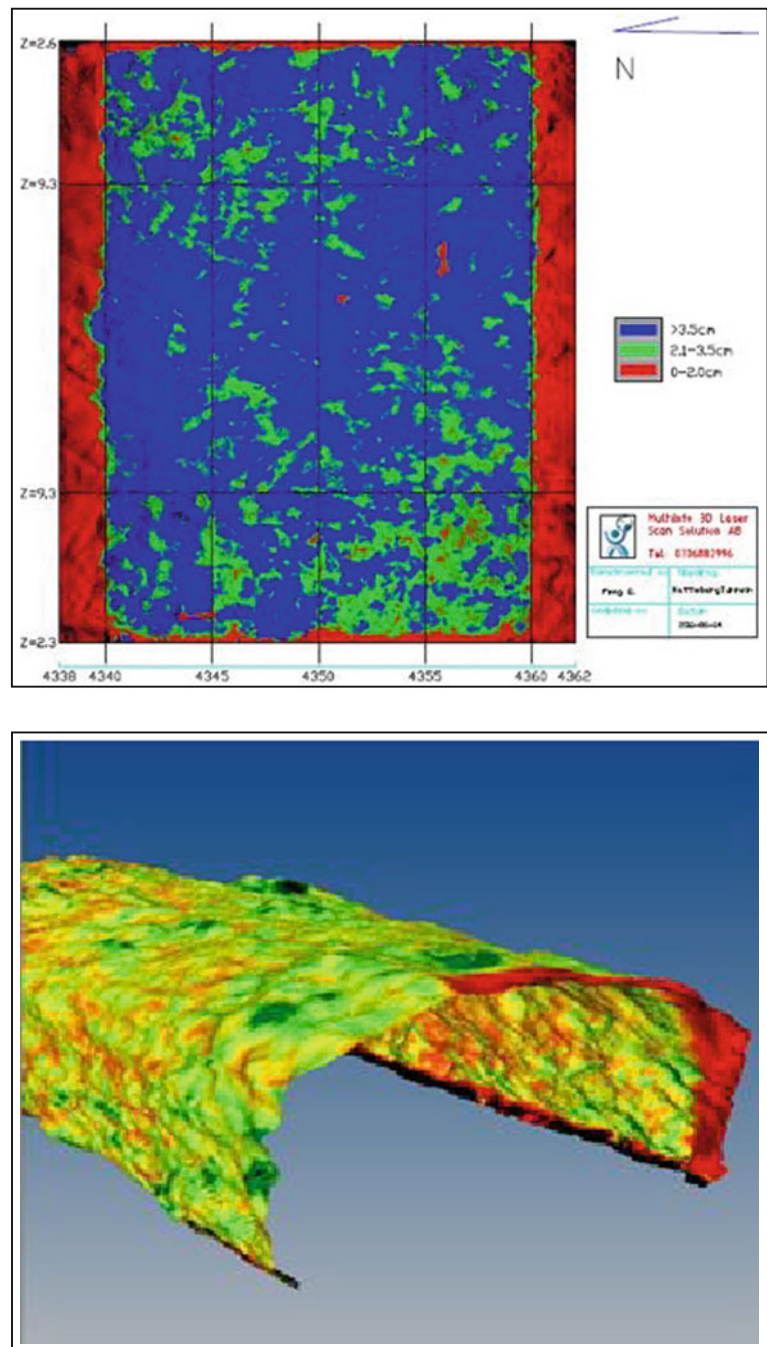
By laser scanning, the deformation can be evaluated through different parameters, e.g. changes of volume, surface area, rotation and length of a profile, etc. However, it is also necessary to analyse the accuracy for creating those parameters from scanning points. If the error to create the parameters is larger than the deformation, no deformation is discovered.

6.4 Improve Input Data for Numerical Modelling

In rock mechanics, numerical modelling is often used to estimate and simulate the behaviour of a rock mass under certain conditions in geometrical, geological and hydrological boundaries. The results of numerical modelling with respect to the reality depend upon the parameters that represent the boundaries of the rock mass. Therefore, it is important for numerical modelling to input the parameters that closely describe the real conditions of a rock mass. By laser scanning, the input data can be improved, and then the results of numerical modelling can be closer to the rock reality. Some case studies have tested laser scanning techniques to create the input data for numerical modelling, and to show the potential applications.

A case study by Bäckström et al. (2009b) applied the input data from laser scanning, e.g. the as-built 3D model and profile of a tunnel, to evaluate the factors that affect and control the EdZ/EDZ (Excavation Disturbed/Damaged Zone), and compare the results with the designed data, which are traditionally applied for the numerical modelling.

Fig. 24 Thickness of the sprayed concrete created from scanning data in an unfolded tunnel map (*upper*) and 3D model (*lower*)



By using the irregular as-built profile of the tunnel, the stress distribution around the tunnel shows interesting results. Figure 27 shows that the irregular shape of the tunnel walls in the as-built sections, as well as their bumpiness, generate asymmetry in the stress redistribution around the tunnel. “Bumpy” type irregularities (convex) tend to distress the area because of being able to generate high tension locally. On the contrary, cavity type irregularities (concave) tend to increase the compressive stress locally. The larger the irregularity of the tunnel contour, the larger such heterogeneity is found in the boundary stresses

at the tunnel contour. The localised high stresses caused by the tunnel wall irregularity could induce local fracturing and asymmetry in the EdZ/EDZ.

In this study, it was also shown that the current developed software for numerical modelling has some limits for inputting the ‘heavy’ 3D model and profile with a high resolution up to few mm. However, it does show the potential application of laser scanning data to numerical modelling. With the further development of the numerical modelling software, more interesting results may develop which could not be obtained from the traditional methods.

Fig. 25 Deformation of a section of a tunnel by laser scanning analysis (Feng et al. 2011)

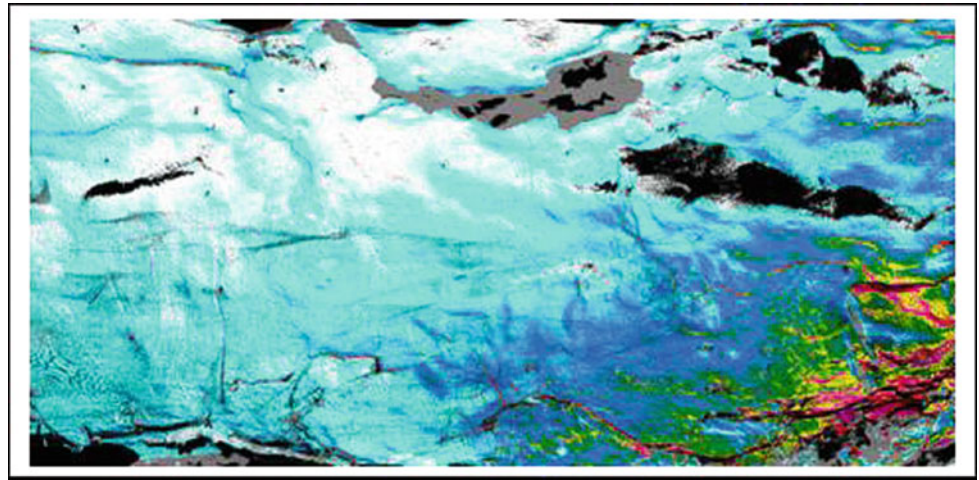
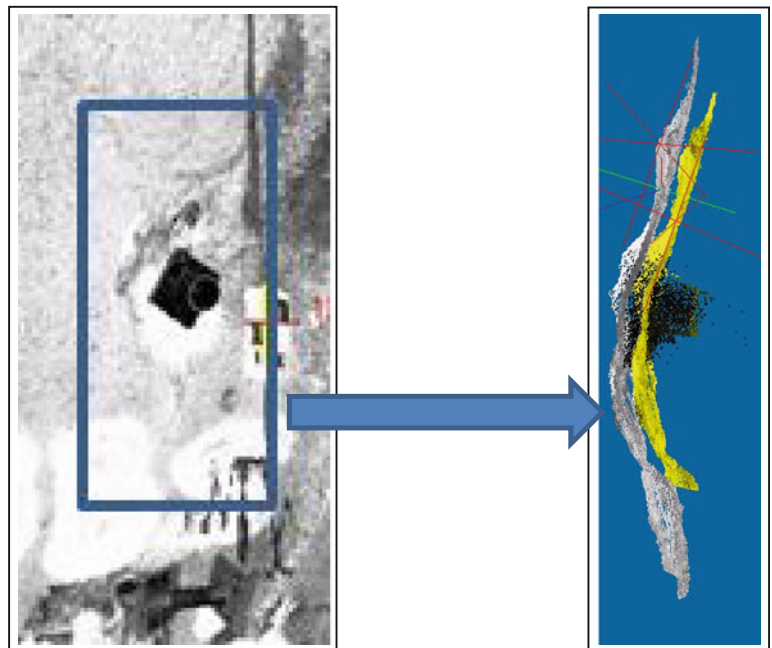


Fig. 26 Identifying the deformation of an object in both the laser image and 3D model



Another case study example was undertaken by Abellan et al. (2006), which applied a long-range terrestrial laser scanner for the detailed study of rockfall. In this study, the authors applied the laser scanning method to obtain some input data for rockfall analysis, such as orientation of joints, the slope, block geometry and volume. Accordingly, one of the most important input data for rockfall simulation is the slope itself (Hoek 2000). But in the earlier studies (Piteau Associated Limited 1980), the slope was represented by a bi-dimensional profile. By using laser scanning, the topography can be described in a 3D model with a DEM (Digital Elevation Model), and the presence of 3D variations in slope morphology (e.g. ridges, convex talus cones and micro-topography) may exert a considerable influence on rockfall trajectories (Giani et al. 2004; Crosta and Agliardi 2004).

If an accurate DEM can be generated by laser scanning data, the results of the rockfall simulation (e.g. trajectories, energy and rebound height) can bear a closer resemblance to the rock reality. The results of this study show that accurate input data are important for a rockfall hazard assessment. Laser scanning appears to have great potential in the characterisation and monitoring of landslides.

6.5 Documentation and Visualisation

In rock engineering, the in situ documentation and visualisation is important for observing the situation around a rock exposure. Traditionally, a notebook with some numbers and drawings, together with a camera, is the common

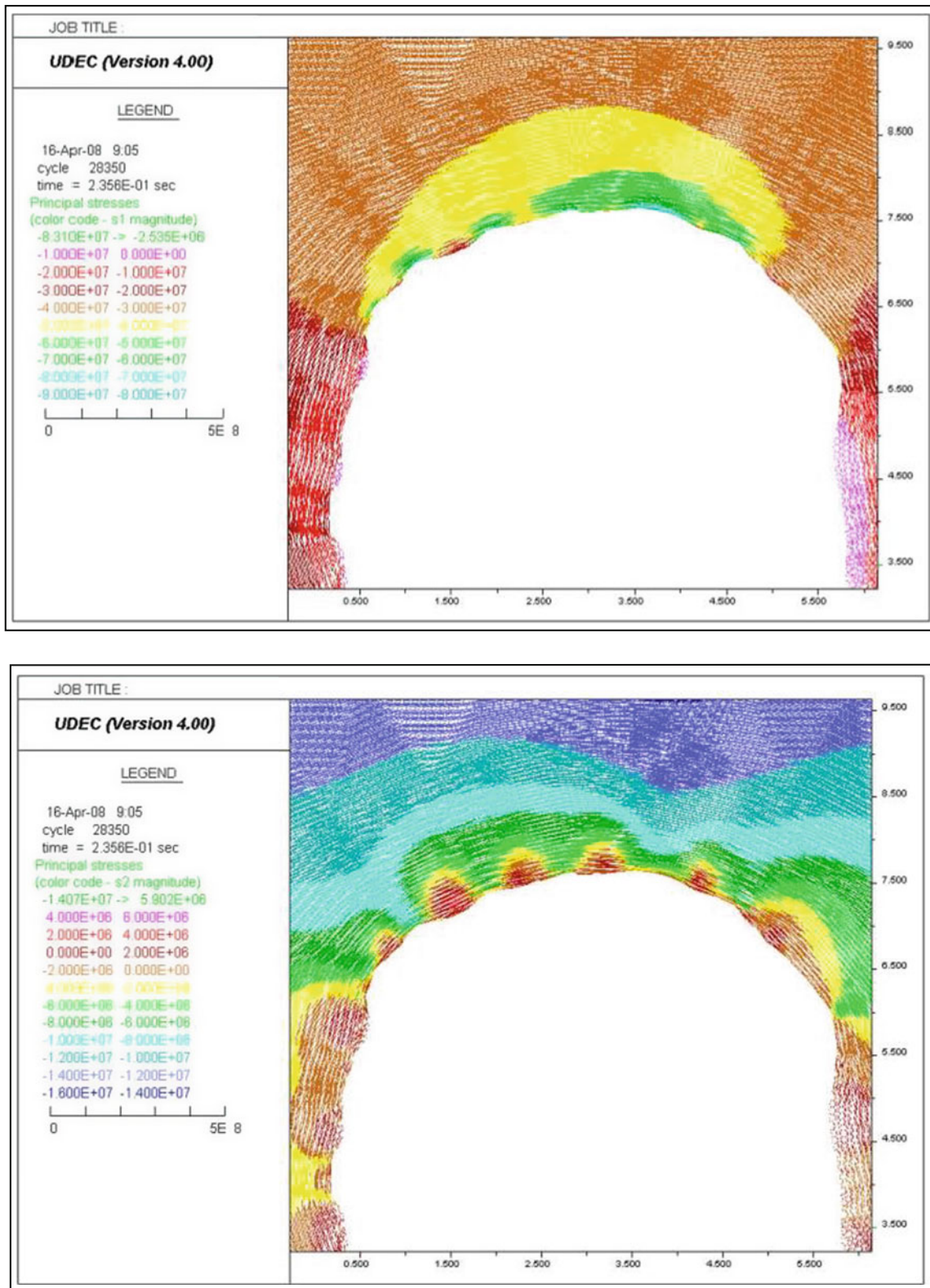


Fig. 27 Stress tensor plots at Sect. 47 with the borehole seismic data after excavating the heading; Model with $E = 65$ GPa. Upper maximum compressive stress = 83 MPa, Lower maximum tensile stress = 5.9 MPa (Bäckström et al. 2009b)

Fig. 28 Intensity image from high resolution laser scanning



way for on-site documentation, which has some drawbacks, such as the following.

- (a) The notes and drawings made by the person can be wrong or subjective, and difficult to check;
- (b) Pictures taken by a camera need to have illumination, and have a small coverage;
- (c) Particularly, the pictures taken by a camera are only 'visible', not measurable. If using photogrammetry techniques, extra work is needed;
- (d) All the information is separately recorded, and it is difficult to combine them in terms of their location, so it is difficult to understand the relations between them.
- (e) Some of the data are not digital, so an extra job is needed if the information is required to be processed by a computer.

Compared to the traditional methods, laser scanning techniques have some advantages for on-site documentation, as follows.

- (1) A high resolution intensity image can be recorded by scanning without illumination:

The best resolution of a high speed scanning can now be up to less than 1 mm with the intensity image. Figure 28 shows a part of an intensity laser image with high resolution, and the boundary line of the paper target is about 0.8 mm, so it can be identified. In addition, as the scanner utilises an infrared laser, so illumination is not necessary, which means a high resolution digital image can be quickly captured in the dark, so it is especially useful for underground rock engineering projects.

- (2) Integration of both visualisation and position:

As in the above-mentioned, laser scanning data consists of both position information with the co-ordinates for each point and the visual information with the laser image or intensity image. So, an object in the laser scanning intensity image cannot only be visualized but also measured in 3D

(Fig. 29) with the co-ordinates of the head of a rock bolt in an intensity laser image. This is a unique feature compared to the photos from a still camera or film from a video camera.

- (3) Provide relational information:

As we know, the on-site documentation by traditional methods, e.g. written notes and pictures from a camera, has no exact positional information, so it is difficult to inter-relate the data. By laser scanning, the scanning data can be registered into the same co-ordinate system, so the laser scanning image has the exact location, and any objects shown on the image can be positioned in space, and the relationship between them can be obtained.

One of the examples is the trace map of fractures overlaid on the laser scanning image (Fig. 30) (Wang et al. 2009). Compared to a traditional trace map, it is easy to see what is presented by the fracture trace line, and also each trace line can be tracked to its position in a 3D model. In addition, a 3D trace line is also possible to be obtained, and it will be interesting to see how to use such a 3D trace line in rock mechanics in the future.

In addition, when a scanner is scanning, it can rotate through 360° both horizontally and vertically. So, normally, a rock face is often recorded together with its surroundings. Moreover, even a whole tunnel, e.g. a 42 km long tunnel, can be scanned and registered in the same co-ordinate system, and each scan, together with the laser image, shown by its exact position in space. In this case, the relation between a rock face and its surroundings can also be obtained, which shows good potential application for design and project planning in both rock mechanics and rock engineering.

- (4) Retrievability:

By laser scanning, a rock face or a tunnel can be accurately recorded in a certain co-ordinate system, and visible

Fig. 29 Co-ordinates of a rock bolt shown in the laser scanning intensity image

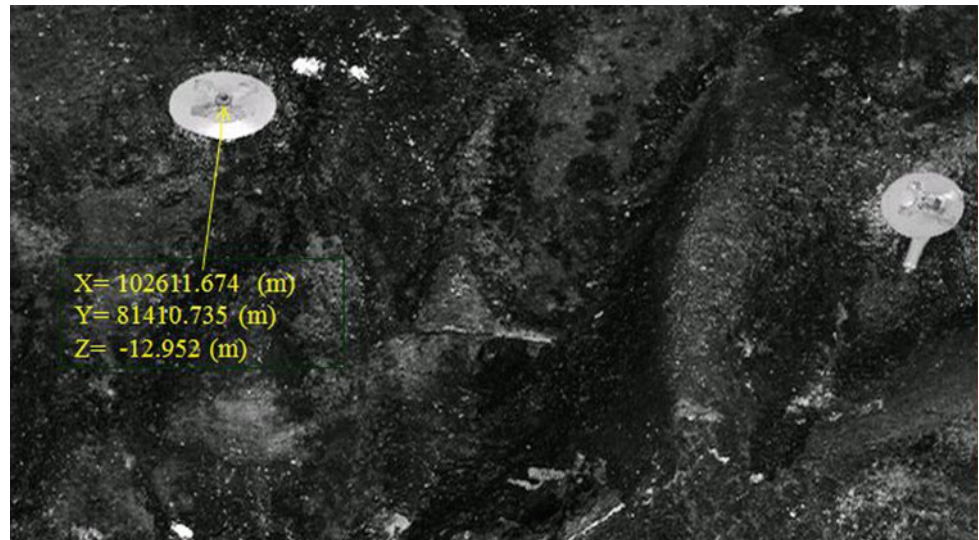
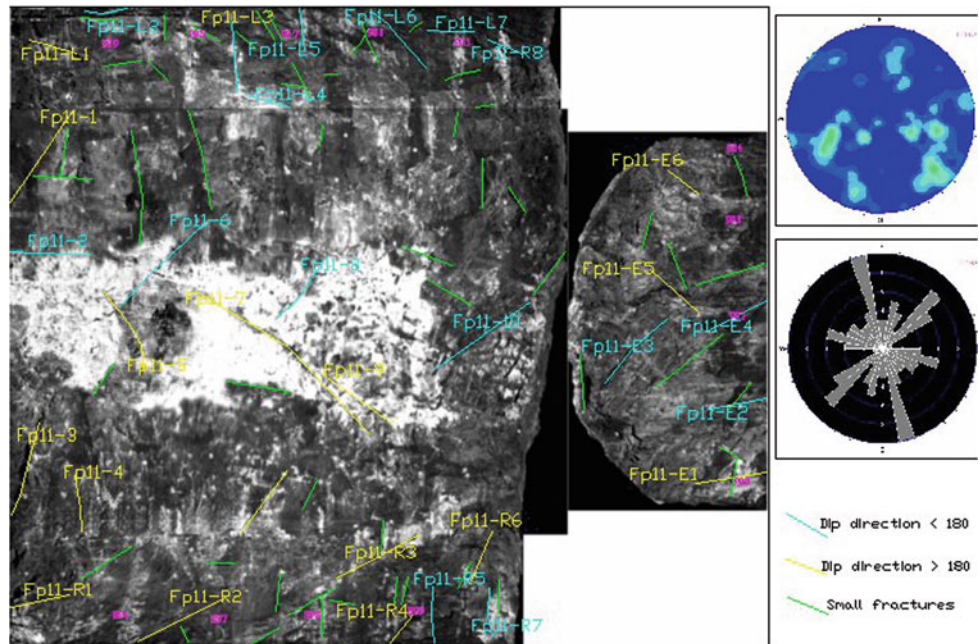


Fig. 30 Fracture trace line map created from a laser scanning intensity image (Wang et al. 2009)



in laser scanning image, which means that the rock mass can be virtually stored in a computer in 3D. This indicates potential applications to rock mechanics in at least two cases.

- (a) If something is uncertain or wrong, it is possible to be tracked back to the original virtual model, and one can find out the reasons. For example, if the measurements of the on-site mapping, e.g. fracture orientation and slope geometry, are uncertain, it is possible to check these out by the 3D scanning virtual model, and to establish the correction.
- (b) If some information is missing, this is also possible to be obtained from the virtual model, and there is no

need to visit the site again. Even if the original rock face has disappeared, e.g. a tunnel section is blasted out or collapsed, the required data can be retrieved from the scanning model. This is useful for both quality control and accident investigation.

- (5) Large and wide coverage:

Comparing to a camera, the laser scanning has a large and wide coverage, even in the dark. In particular, each scan can be registered into the same co-ordinate system, so a large 3D model, up to a tens of kilometres long tunnel, and a large laser scanning image (e.g. an unfolded tunnel image several hundred metres long) can be obtained, which is impossible by a camera. In addition, a high resolution laser

image can be captured in difficult conditions, such as a vertical, small (about a half-metre in diameter) shaft.

(6) Generate different types of ways for visualisation from the same data resources:

Based upon the same scanning data, a rock surface or a tunnel can be visualised in several different ways by data processing with different software, including: (1) 2D unfolded laser image with the same format as the photos from a camera (e.g. jpg or tiff); (2) 3D panoramic image, which can 'see' all around in a tunnel; (3) A video film or movie with the usual format (e.g. *.avi) can also be created, so one can fly through or walk through a tunnel in a 3D virtual model; (4) The scanning data, e.g. point clouds, can also be converted as 3D model (e.g. CAD model, mesh model), and then be animated or be used for simulation in some software for further analysis.

7 Discussions

Laser scanning techniques have been developed for more than 10 years since the late 1990s. They show significant potential applications in rock mechanics and rock engineering. However, there are still some uncertainties for rock mechanics application for some reasons, including (1) there is usually no detailed description of the scanners from the scanner developers or manufactures in terms of all the information required by the rock mechanics user; (2) scanning is carried out by surveyors, and the users in rock mechanics receive the scanning data from the surveyors, but the users have no detailed information how the scanning data are captured, and hence no idea about the quality of the scanning data. Therefore, it is important to clarify some points in order to apply this method correctly and effectively in practice.

7.1 How to Select a Suitable Type of Laser Scanner for a Certain Application

On the market, there are many different types of 3D laser scanners, and about 90 % of them utilise pulse-based scanning and about 9 % of them by phase-based scanning. They are quite different in their specifications, such as scanning speed, maximum scanning range, resolution, accuracy, limit for working temperature, etc. Normally, the pulse-based scanner has a long scanning range, but the phase-based scanner has a short range. However, the pulse-based scanner has a slower scanning speed than the phase-based scanner. For different applications in rock mechanics, it is important to select the most suitable type of scanner in order to apply this technique in the best way.

7.2 How to Use the Specification Parameters of the Scanner

Each scanner has a list of its specification parameters, such as the resolution, accuracy, scanning speed and maximum scanning range etc. It is necessary to understand exactly what the real meaning is for each specification parameter which is important for a user to use the scanner correctly. For example, the maximum scanning range is related to the reflex intensity. If the object has very low or very strong reflex, the scanner cannot receive the return signal, so the scanning data cannot be collected. So, it is not only important to know the maximum scanning range for a scanner, but also there is a need to confirm what the reflex limit of the scanner is. In addition, the maximum scanning range can be affected by some factors. For example, the scanning range of a pulse-based scanner can be affected by weather. If it is cloudy or sunny, there is no substantial difference, but there is a shorter range if the sun shines too strongly. Light rain or fog also affects the scanning range, depending on their intensity. Day and night conditions also affect the scanning range. When scanning at night, the noise is less, but the scanning spot is larger, and the scanning range is longer. For a phase-based scanner, it is difficult to obtain the return signal if the object has a reflex less than 5 % or stronger than 95 %.

7.3 Difference Between Resolution and Accuracy

Although 'accuracy' is quite different from 'resolution' in terms of their definitions, it is easy to confuse the real meaning of these two terms in practice when laser scanning is applied to some practical projects. With the experience of the authors, there are two main problems in practice.

(1) Misunderstanding the difference between resolution and accuracy:

By using the scanning control software, the scanning resolution can be selected according to the requirement of a project. Different scanners have different maximum resolutions as well. However, the scanning resolution of an object not only depends upon the defined resolution parameters while scanning, but is also related to other factors, including the distance and incidental angle to the scanned object, the reflex intensity of the object or rock surface, etc., and even the transformation between different co-ordinate systems by a software can affect the final resolution. So, the effective resolution of the scanning data can be quite different to the defined resolution parameters in the scanner. On the other hand, even if the object cannot be scanned with a high resolution, this does not mean that one cannot achieve high accuracy of the final results. For

example, the accuracy of deformation monitoring on a rock mass depends upon several factors, including the accuracy of control surveying from the stable area to the deformed area, the resolution of each individual scan, the registration accuracy of each scan into the same co-ordinate system, and also the calculation accuracy of parameters or models to monitor the deformation. So, there can be confusion by the users caused by the difference between resolution and accuracy, and it is not so easy to check out in practice.

- (2) Confusing the meaning of the accuracy between the scanner specification and the accuracy of the final results:

The manufacturer often provides a specification of a scanner with different parameters, including the instrument accuracy. It is then a simple step for some users to use the instrument accuracy as the accuracy of their final results or the reference for their projects. This is quite dangerous in practice. The instrument accuracy is often carefully or simply illustrated by the manufacture under some specific and perhaps advantageous conditions, e.g. within a certain distance and incidental angle, or for some object surface, and with some working temperature, etc. Moreover, the instrument accuracy is often given separately by its linear and angular accuracy, which is quite different to the accuracy of the co-ordinates of a point, or a 3D model, etc. The accuracy of a final result for a project depends upon many factors, such as: (1) Control surveying; (2) Instrument accuracy and setting of scanning parameters; (3) Methods and procedures for registration of scanning point clouds with different software; (4) How to present the final results, e.g. the cross-section with a point line or a 'polyline', and a 3D model with a mesh or a solid model. Nowadays, it is difficult for the clients to check out the final accuracy; even some consultants may confuse the instrument accuracy with the final accuracy for a project. This must be improved in the future.

7.4 Data Format

There are different data formats in the whole procedure of laser scanning, but these can be categorised in three main groups.

- (1) Raw scanning data from a scanner:

There are several different formats for raw scanning data as captured by different scanners, e.g. FLS, FWS, ZFS, ZFC, IXF, 3DD, RSP, PTB, PTG, etc. At the beginning of the technique development, these raw data format could only be opened by some special software for each type of scanner, but now the situation is much better, and the data can be imported directly by the so-called third-party software for different applications.

- (2) Processed data from the raw data:

The raw data can be processed by different software, and exported as point clouds, laser images, etc. For the point clouds, there are many different formats, e.g. XYZ, PTS, PTX, DXF, ASC, etc., and for a laser scanning image with formats including BMP, TIFF, JPG, PNG, COE, etc. These formats of the data are often more neutral than the raw data, which can be imported and processed in many application software types.

- (3) Final model or parameters for applications:

The 3D model or parameters generated from the scanning data can be saved and then exported in some formats which are compatible to the application software for design and further analysis, e.g. SAT, DWG, DXF, STL, etc.

In practice, it is often required to convert among these different data formats during the whole procedure of a laser scanning project. The situation is now much improved compared to the beginning of the development of this technique. However, it is still not fully satisfactory. Information converted from one format to another can be lost, and not be mutually exchangeable. In addition, even the same format of the data can be displayed in different ways after importing into different software due to reasons such as the different structures of the layers in different CAD software, etc.

7.5 Data Back-up and Storage

The safety of the data back-up and storage is important for a laser scanning project because the data can be reused and retrieved, and sometimes it is impossible to go back to scan again, for example, a section of a tunnel can be removed by blasting, or the rock surface be covered by the shotcrete. Two questions on this subject are often asked: (1) which media type is the safest way to back up? (2) how long can the data be stored? Actually, this is the same challenge for back-up and storing the digital information in computer science as well. For laser scanning, it is special because of the large amount of data, from several GB up to several TB. However, thanks to the development of the hard disk techniques, this is now overcome. It was just a several GB hard disk ten years ago, but now an external hard disk can contain TBs. Just now, it is not 100 % clear just how long the data can be stored, and which storage medium is the best for laser scanning data. But the scanning data stored on a CD for about ten years are still readable if the CD is kept carefully. Alternatively, extra work is necessary to check out the data regularly and to make several backup in different media. Also, the technology is changing rapidly, as we have experienced over recent years, and so it may be

necessary to upload the data into new systems in a case where longevity is required, e.g. the scanned data of an historical building made of stone.

8 Conclusions

Traditional methods for site characterisation of rock exposures have several drawbacks which can affect further analysis, numerical modelling and design in rock mechanics. Many efforts have been made to improve the quality and quantity of site mapping and documentation. In this context, 3D laser scanning has been developed for more than 10 years since the late of 1990s, and shows potential application for site mapping and documentation in rock mechanics, and so has become an interesting subject in recent years.

By reviewing the state-of-the-art for 3D laser scanning techniques as reported in this article, it is clear that there has been much development and improvement in both hardware and software since the late 1990s, and the new developmental trends are focusing on improving scanning quality (e.g. scanning speed, resolution and accuracy, and scanning with colour), easy and simple operation for the users' hardware, and data format and processing is becoming more compatible and standard. Especially, there has been more development on the interfacing to and integration with the existing application software which make the data from laser scanning more compatible with other data and hence useable for more applications.

3D laser scanning has significant advantages compared to other characterisation methods because it enables quick capture of an object in 3D with large coverage and high resolution without illumination. The scanning data consist of different information, including geometrical, spatial, visible and physical information. In particular, the data can be retrievable and reusable, which make it possible to improve the quality control and reduce the cost for a site investigation. Comparing to the photos and videos from a camera or video camera, the laser scanning images in both 2D and 3D can not only be visualised but also measured, which indicates the potential application for site characterisation in rock mechanics and rock engineering.

Case studies show the potential applications in rock mechanics for using scanning data with both co-ordinates and images, which make it possible to measure and view the rock surface in 3D at high resolution and accuracy. In recent years, laser scanning techniques have been applied to different projects in rock mechanics and rock engineering, including site characterisation of rock exposures (e.g. fracture mapping, identifying water leakage and rock types

from laser images), measurement of over- and under-break for tunnel blasting, quality control of sprayed shotcrete, deformation monitoring, improving input data for numerical modelling, documentation and visualisation, etc. These case studies show the potential application of laser scanning techniques to rock mechanics and rock engineering.

However, there are some issues while using laser scanning techniques in practice, such as selecting the most suitable scanner for the required application, not misunderstanding the specification parameters provided by the manufactures, establishing the difference between resolution and accuracy, etc. The user should pay attention to the function of each scanning system, and control the whole procedure from filed data capture to office data processing in order to apply laser scanning data in the correct and effective way. In addition, there are still some limits with current development, such as the fact that colour scanning still, by definition, limited to circumstances with a good illumination, it is difficult to process a large amount of scanning data having a high resolution, and especially that there has not been so much development for specific application software to rock mechanics. These problems will be solved with further development underway.

9 Suggestions for Further Development

3D laser scanning techniques indicate the potential applications in rock mechanics and rock engineering. For better application to our field, the current development on both hardware and software should be continued. The following aspects are suggested, based upon the users' feedback and investigation of current developments.

(1) Improvement in hardware:

Up-to-date reviewing of the hardware development indicates the following improvement in hardware: (1) scanning range extending longer for both pulse-based and phase-based scanners; (2) scanning resolution is being improved, especially the phase-based scanner can reach up to less than 1 mm, but this is taking a longer time and it is difficult to process the data by a normal computer; (3) scanning speed is improved, but related to the resolution; (4) scanning noise is a big problem, specially for the phase-based scanner, which is improved, but hopefully will be effectively solved by both hardware and software; (5) WiFi and Bluetooth are now used for remote control of the scanning, but limited to a short distance. The scanning needs to be remotely controlled, even for a considerable distance for some situations; (6) hardware needs to be improved for some rock mechanics working conditions (e.g. working temperature) and for stability.

- (2) Integration of other sensors and associated tools with the laser scanning system:

Control survey is one of the important steps in the whole scanning procedure, which determines the location of each individual scan, and then registers all the scans into the same co-ordinate system. There are different ways to stitch each scan together, but improvement is needed to make the registration more accurate and simple by integration of other sensors (e.g. GPS). In addition, other associated tools are necessary to be improved in order to make the field scanning safer and easier and to operate, such as built-in tilting and bearing measurement, on-board camera with high resolution, built-in motion compensators, etc.

- (3) Mobile scanning:

Mobile scanning on a train, car or other terrestrial vehicles have been developed significantly in recent years, but the associated resolution and accuracy need to be improved for some rock mechanics applications.

- (4) Colour scanning:

Scanning with the true colour is required for some projects, like rock type mapping, which can be solved by either using a real colour scanner or the texture mapping of colour pictures on the scanning point clouds. The former solution is difficult, but possible in the future. The latter is often used now in other fields such as architectural and archaeological documentation. However, illumination is necessary. A simple and easy way to provide sufficient illumination for a camera needs to be developed, and the software for texture mapping needs to be improved.

- (5) Registration of each scan into the common co-ordinate system:

For further modelling and data processing, one of the important steps is to register each individual scan into the same co-ordinate system. The registration accuracy depends upon not only the control surveying but also on the software or algorithms to perform the registration. Different algorithms have been developed but a more accurate and robust solution is needed.

- (6) Development of software for rock mechanics applications:

Special software used by laser scanning for rock mechanics applications is not well-developed. Existing software, e.g. software for numerical modelling, needs to be improved for compatibility, both for data format and for the limits of large amounts of data.

- (7) Standardisation of data formats:

There are so many types of data formats in the whole procedure of a scanning project which need to be converted, involving extra work. So, standardisation of different data formats is important for better application.

- (8) Evaluation of the accuracy for rock mechanics applications:

Laser scanning has potential applications in a variety of rock mechanics projects, e.g. site mapping, deformation monitoring, quality control of tunnelling, etc. It is often confusing for the users to distinguish between the instrument accuracy and the final result accuracy. Moreover, it is not so simple for the users to evaluate the actual accuracy and the associated influential factors. More case studies are needed to evaluate the influential factors for different applications in the future.

Acknowledgements This study was stimulated by the ISRM through Professor John A. Hudson during his presidential period in 2007–2011, and financially funded by BeFo, Swedish Rock Engineering Research Foundation with the support by Mr. Mikael Hellsten, Research Director of BeFo. Special thanks go to Dr. Kennert Röshoff for his suggestions, support and efforts related to this study. The authors would like to acknowledge the users in giving us the opportunities to test the laser scanning techniques in different projects related to rock mechanics applications, including SKB (Swedish Nuclear Fuel and Waste Management Company), Trafikverket (Swedish Road and Railway authority), Fortum, Vattenfall, SP Technical Research Institute of Sweden, Besab, RTC (Rock Tech Centre in Sweden), SL (Stockholm Local Traffic Management Company). Thanks also go to BBK and ÅF for allowing time to carry out some parts of this study. We are indebted to the reference group including Professor John A. Hudson (ISRM), Mikael Hellsten (BeFo), Anders Boberg (Tyrens), Ulf Håkansson (Skanska), Tommy Ellison (Besab), Peter Lund (Trafikverket) and Peter Hultgren (SKB) for their suggestions and critical inputs to improve both the contents and English of this report. The final version of this report was checked for English and editorial aspects by Professor Hudson.

References

- Abellan A, Vilaplana JM, Martinez J (2006) Application of a long-range terrestrial laser scanner to a detailed rockfall study at Vall de Nuria (Eastern Pyrenees, Spain). *Engineering Geology* 88:136–148.
- Bäckström A, Berglund J, Mas Ivars D, Olsson M, Johansson M, Johansson M, Feng Q (2009a) Studies of factors that affect and control the EDZ (Excavation Damaged/Disturbed Zone). SKB Report, 311 p.
- Bäckström A, Jonsson M, Christiansson R, Mas-Ivars D (2009b) Analysis of factors that affect and control the excavation disturbance/deformation zone in crystalline rock. Abstracts Book of SinoRock 2009, JA Hudson, LG Tham, XT Feng, AKL Kwong (eds.), Hong Kong, Paper No. 111, p. 173 (on CD).
- Beer G, Oppiessnig G, Golser H, Fasching A, Gaich A (1999) Geotechnical data acquisition, numerical simulation and visualisation on site. Proceedings of the 9th ISRM Congress, Paris, A.A. Balkema, Rotterdam, pp 1333–1338.
- Bulut F, Tüdes S (1996) Determination of discontinuity traces on inaccessible rock slopes using electronic tacheometer: an example from the İkizdere (Rize) Region, Turkey. *Engineering Geology* 44: 229–233.
- Coe JA (1995) Close-range photogrammetric geological mapping and structural analysis. Master Thesis, Colorado School of Mines, USA.
- Crosta, GB, Agliardi F (2004) Parametric evaluation of 3D dispersion of rockfall trajectories. *Natural Hazards and Earth System Sciences* 4 (4): 583–598.

- Fardin N, Feng Q, Stephansson O (2004) Application of a new in situ 3D laser scanner to study the scale effect on rock joint surface roughness. *Int J Rock Mech Min Sci* 41: 329–335.
- Feng Q (2001) Novel methods for 3-D semi-automatic mapping of fracture geometry at exposed rock surfaces. KTH Doktorsavhandling, Sweden.
- Feng Q, Röshoff K (2004) In situ mapping and documentation of rock faces using full coverage 3D laser scanning techniques. *Int J Rock Mech Min Sci, Special Issue for SinoRock 2004*, p 379.
- Feng Q., Wang G, Röshoff K (2006) Detection of water leakage using laser images from 3D laser scanning data, Proceedings of IAEG 10th Congress, Nottingham, UK, M Culshaw, H Reeves, T Spink, I Jefferson (eds), Taylor & Francis Group, London, p 87.
- Feng Q, Sjögren P, Stephansson O, Jing L (2001) Measuring fracture orientation at exposed rock faces by using a non-reflector total station. *Engineering Geology* 59: 133–146.
- Feng Q, Wang G, Röshoff K (2011) Investigation of 3D terrestrial laser scanning techniques for potential application to rock mechanics. Proceedings of the 12th ISRM Congress 2011, Q Qian, Y Zhou (eds), Beijing, China. Taylor & Francis Group, London, pp 963–968.
- Giani GP, Giacomini A, Migliazza M, Segalini A (2004) Experimental and theoretical studies to improve rock fall analysis and protection work design. *Rock Mechanics and Rock Engineering* 37 (5): 369–389.
- Goodman R (1989) *Introduction to Rock Mechanics*. 2nd Edition, John Wiley & Sons, N. York.
- Harrison JP (1993) Improved analysis of rock mass geometry using mathematical and photogrammetric methods. PhD Thesis, Imperial College, London, UK.
- Hesse C, Stramm H (2004) Deformation measurements with laser scanners-possibilities and challenges. Proceedings of the International Symposium on Modern Technologies, Education and Professional Practise in Geodesy and Related Fields, Sofia, pp 228–240.
- Hoek E (2000) Analysis of rockfall hazard. *Rock Engineering: Course Notes*, Rocscience, pp. 115–136 (Available at www.rocsience.com).
- Hudson JA (1989) *Rock Mechanics Principles in Engineering Practice*. CIRIA/Butterworths, London,
- ISRM (2007) *The Complete ISRM Suggested Methods for Rock Characterization, Testing and Monitoring: 1974-2006*. Suggested Methods Prepared by the Commission on Testing Methods, International Society for Rock Mechanics, R Ulusay and JA Hudson (eds.), Compilation Arranged by the ISRM Turkish National Group, Ankara, Turkey.
- Maerz NH, Franklin JA, Bennett CP (1990) Joint roughness measurement using shadow profilometry. *Int J Rock Mech Min Sci & Geomech* 27 (5): 1073–1089.
- Monserrat O, Crosetto M (2008) Deformation measurement using terrestrial laser scanning data and least squares 3D surface matching. *ISPRS Journal of Photogrammetry and Remote Sensing* 63: 142–154.
- Patton FD (1966) Multiple modes of shear failure in rock. *Proc. First Cong. Int. Soc. Rock Mech., Lisbon, Vol 1*: pp 509–513.
- Piteau Associated Limited (1980) Slope stability analysis for rockfall problems: The computer rockfall model for simulating rockfall distribution. *Rock Slope Engineering*. Department of Transportation, Washington DC, pp 62–68.
- Post RM, Kemeny JM (2001) Image processing for automatic extraction of rock joint orientation data from digital images. *Proc. of the 38th US Rock Mechanics Symposium*, Washington DC, USA, AA Balkema, Rotterdam, pp 58–62.
- Priest SD (1993) *Discontinuity Analysis for Rock Engineering*. Chapman & Hall, London, UK.
- Reid TR, Harrison JP (2000) A semi-automated methodology for discontinuity trace detection in digital images of rock mass exposures. *Int J Rock Mech Min Sci* 37: 1073–1089.
- Ross-Brown DM, Wickens EH, Markland JT (1973) Terrestrial photogrammetry in open pits: 2-an aid to geological mapping. *Trans Inst Min Metall, Section A, Min Industry* 82: 115–130.
- Schneider D (2006) Terrestrial laser scanner for area-based deformation analysis of towers and water dams. Proceedings of the 3rd IAG Symposium of Geodesy for Geotechnical and Structural Engineering and 12th FIG Symposium on Deformation Measurements, Baden, Austria (on CD).
- Slob S, Hack HRGK, van Knapen B, Turner K, Kemeny J (2005) A method for automated discontinuity analysis of rock slopes with three-dimensional laser scanning. In: *Transportation Research Record: Journal of the Transportation Research Board*, pp 187–194. U.S. Federal Highway Administration (2008) Report: Ground-Based LIDAR, Rock Slope Mapping and Assessment.
- Wang G (2005) Applications of 3D laser scanning data for tunnel geological mapping. MSc Thesis. Royal Institute of Technology, Stockholm, Sweden.
- Wang G, Feng Q, Röshoff K (2009) A new approach to tunnel digital geological mapping using 3D terrestrial laser scanning technique. Abstracts Book of SinoRock 2009, Hong Kong, JA Hudson, LG Tham, XT Feng, AKL Kwong (eds.), Hong Kong, Paper No. 315, p. 101 (on CD).
- Wolfgang B, Andreas M (2003) 3D scanning instruments. *Instruments and Methods*, 12, 9–12.